ONCOTHERMIA JOURNAL

A publication of Oncotherm® ISSN 2191-6438

Volume 31 - March 2022

Imprint

Editorial

Dear Reader, Dear Fellow Researchers, Dear Colleagues,

You are reading now the 31st volume of Oncothermia Journal, the first in 2022. We are pleased to recognize that the popularity of our Journal grows as we have a rapid increase in the number of Oncothermia users worldwide, and the acceptance of this method gradually rises. The Oncothermia Journal became a regular resource for many physicians and an excellent option to publish new results. We follow the existing recently published literature and reprint them.

We are presenting some important preclinical studies of modulated electro-hyperthermia (mEHT) in this volume. Prof. Hamar's (Schwarcz et al. Semmelweis University Budapest, Hungary) group published results on the apoptosis and the genetic variation of mEHT at breast cancer model.

We are pleased to see the extending number of clinical studies in modulated electro-hyperthermia. Prof. Kanamori's research group (Nagata et al., Toyama University, Japan) shows case reports with successful treatments on advanced breast cancers.

Prof. Kim's group (Kim et al. Ewha Womans University Mokdong Hospital, Seoul, S.Korea) shows the first results of KGOG3030 clinical trial with mEHT complementary application to chemotherapies for gynecology patients.

Prof. Fiorentini's group (Fiorentini at al., Azienda Ospedaliera "Ospedali Riuniti Marche Nord", Pesaro, Italy) shows important clinical results on esopharus, colorectal and pancreatic cancers.

New biophysical results were published on various aspects of bioelectromagnetic applications by Prof. Szasz's group (Szasz et al., The Hungarian University of Agriculture and Life Sciences, Godollo, Hungary) that compares the various technical solutions of capacitive couplings and shows the therapeutic basis of electromagnetic resonances. The same group showed some specialties of fractal physiology and bioscaling and a hypothesis about the bioelectromagnetics without fields; only potentials are active.

We hope this volume also provides relevant and up-to-date information for your daily practice. I would like to draw your attention to the importance of reading the Oncotherm Newsletter as well. This monthly summary provides information of the most recent articles published on international domains and brings all the news about events and actualities related to hyperthermia in oncology. These newsletters also highlight such clinical information like Oncothermia Journal. We would be happy to hear your opinions or critical remarks and initiate open communication regarding the Journal or published articles. Your help and attention is highlyappreciated.

We would like to wish you a successful and prosperous 2022. Enjoy this 31th volume of the Oncothermia Journal. Follow us in the new year as well.

Dr. Andras Szasz
Professor, Chair, Biotechnics Department of St. Istvan University

Liebe Leserinnen und Leser, liebe Forscherkollegen, liebe Kolleginnen und Kollegen,

Sie lesen nun die 31. Ausgabe des Oncothermia Journal, die erste im Jahr 2022. Wir stellen erfreut fest, dass die Popularität unseres Journals wächst, da die Zahl der Oncothermie-Anwender weltweit rapide zunimmt und die Akzeptanz dieser Methode allmählich steigt. Das Oncothermia Journal ist für viele Ärzte zu einer regelmäßigen Quelle geworden und eine hervorragende Möglichkeit, neue Ergebnisse zu veröffentlichen. Wir verfolgen die bestehende, kürzlich veröffentlichte Literatur und drucken sie nach.

Die Gruppe von Prof. Hamar (Schwarcz et al. Semmelweis Universität Budapest, Ungarn) veröffentlichte Ergebnisse über die Apoptose und die genetische Variation von mEHT im Brustkrebsmodell.

Wir freuen uns über die wachsende Zahl klinischer Studien zur modulierten Elektro-Hyperthermie. Die Forschungsgruppe von Prof. Kanamori (Nagata et al., Toyama University, Japan) zeigt Fallberichte mit erfolgreichen Behandlungen von fortgeschrittenem Brustkrebs.

Die Gruppe von Prof. Kim (Kim et al. Ewha Womans University Mokdong Hospital, Seoul, Südkorea) stellt die ersten Ergebnisse der klinischen Studie KGOG3030 vor, bei der die mEHT ergänzend zur Chemotherapie bei gynäkologischen Patienten eingesetzt wird.

Die Gruppe von Prof. Fiorentini (Fiorentini at al., Azienda Ospedaliera "Ospedali Riuniti Marche Nord", Pesaro, Italien) zeigt wichtige klinische Ergebnisse bei Speiseröhren-, Dickdarm- und Bauchspeicheldrüsenkrebs.

Die Gruppe von Prof. Szasz (Szasz et al., Ungarische Universität für Landwirtschaft und Biowissenschaften, Godollo, Ungarn) hat neue biophysikalische Ergebnisse zu verschiedenen Aspekten bioelektromagnetischer Anwendungen veröffentlicht, die verschiedene technische Lösungen für kapazitive Kopplungen vergleichen und die therapeutische Grundlage elektromagnetischer Resonanzen aufzeigen. Dieselbe Gruppe zeigte einige Spezialitäten der fraktalen Physiologie und Bioskalierung sowie eine Hypothese über die Bioelektromagnetik ohne Felder; nur Potentiale sind aktiv.

Wir hoffen, dass dieser Band auch für Ihre tägliche Praxis relevante und aktuelle Informationen enthält. Ich möchte Sie darauf aufmerksam machen, wie wichtig es ist, auch den Oncotherm Newsletter zu lesen. Diese monatliche Zusammenfassung enthält Informationen über die neuesten Artikel, die auf internationaler Ebene veröffentlicht wurden, und bringt alle Neuigkeiten über Ereignisse und Aktualitäten im Zusammenhang mit der Hyperthermie in der Onkologie. In diesen Newslettern werden auch klinische Informationen wie das Oncothermia Journal hervorgehoben. Wir würden uns freuen, Ihre Meinungen oder kritischen Anmerkungen zu hören und eine offene Kommunikation bezüglich des Journals oder der veröffentlichten Artikel zu initiieren. Wir wissen Ihre Hilfe und Aufmerksamkeit sehr zu schätzen.

Wir wünschen Ihnen ein erfolgreiches Jahr 2022. Viel Spaß mit dieser 31. Ausgabe des Oncothermia Journals. Folgen Sie uns auch im neuen Jahr.

Dr. Andras Szasz
Professor und Vorsitzender der Fakultät für Biotechnik an der St. Istvan Universität

Rules of submission

As the editorial team we are committed to a firm and coherent editorial line and the highest possible printing standards. But it is mainly you, the author, who makes sure that the Oncothermia Journal is an interesting and diversified magazine. We want to thank every one of you who supports us in exchanging professional views and experiences. To help you and to make it easier for both of us, we prepared the following rules and guidelines for abstract submission.

Als redaktionelles Team vertreten wir eine stringente Linie und versuchen, unserer Publikation den höchst möglichen Standard zu verleihen. Es sind aber hauptsächlich Sie als Autor, der dafür Sorge trägt, dass das Oncothermia Journal zu einem interessanten und abwechslungsreichen Magazin wird. Wir möchten allen danken, die uns im Austausch professioneller Betrachtungen und Erfahrungen unterstützen. Um beiden Seiten die Arbeit zu erleichtern, haben wir die folgenden Richtlinien für die Texterstellung entworfen.

1. **Aims and Scope**

   The Oncothermia Journal is an official journal of the Oncotherm Group, devoted to supporting those who would like to publish their results for general use. Additionally, it provides a collection of different publications and results. The Oncothermia Journal is open towards new and different contents but it should particularly contain complete study-papers, case-reports, reviews, hypotheses, opinions and all the informative materials which could be helpful for the international Oncothermia community. Advertisement connected to the topic is also welcome.

   - Clinical studies: regional or local or multilocal Oncothermia or electro cancer therapy (ECT) treatments, case-reports, practical considerations in complex therapies, clinical trials, physiological effects, Oncothermia in combination with other modalities and treatment optimization
   - Biological studies: mechanisms of Oncothermia, thermal- or non-temperature dependent effects, response to electric fields, bioelectromagnetic applications for tumors, Oncothermia treatment combination with other modalities, effects on normal and malignant cells and tissues, immunological effects, physiological effects, etc.
   - Techniques of Oncothermia: technical development, new technical solutions, proposals
   - Hypotheses, suggestions and opinions to improve Oncothermia and electro-cancer-therapy methods, intending the development of the treatments

   Further information about the journal, including links to the online sample copies and content pages can be found on the website of the journal: www.oncothermia-journal.com

   Umfang und Ziele

   Das Oncothermia Journal ist das offizielle Magazin der Oncotherm Gruppe und soll diejenigen unterstützen, die ihre Ergebnisse der Allgemeinheit zur Verfügung stellen möchten. Das Oncothermia Journal ist neuen Inhalten gegenüber offen, sollte aber vor allem Studienarbeiten, Fallstudien, Hypothesen, Meinungen und alle weiteren informativen Materialien, die für die internationale Oncothermie-Gemeinschaft hilfreich sein könnten, enthalten. Werbung mit Bezug zum Thema ist ebenfalls willkommen.

   - Klinische Studien: regionale, lokale oder multilokale Oncothermie oder Electro Cancer Therapy (ECT) Behandlungen, Fallstudien, praktische Erfahrungen in komplexen Behandlungen, klinische Versuche, physiologische Effekte, Oncothermie in Kombination mit anderen Modalitäten und Behandlungsoptimierungen
   - Biologische Studien: Mechanismen der Oncothermie, thermale oder temperaturunabhängige Effekte, Ansprechen auf ein elektrischesFeld, bioelektromagnetische Anwendungen bei Tumoren, Kombination von Oncothermie und anderen Modalitäten, Effekte auf normale und maligne Zellen und Gewebe, immunologische Effekte, physiologische Effekte etc.
   - Oncothermie-Techniken: technische Entwicklungen, neue technische Lösungen
   - Hypothesen undMeinungen, wie die Oncothermie- und ECT-Methoden verbessert werden können, um die Behandlung zu unterstützen

   Weitere Informationen zum Journal sowie Links zu Online-Beispielen und Inhaltsbeschreibung sind auf der Website zu finden: www.oncothermia-journal.com

2. **Submission of Manuscripts**

   All submissions should be made online via email: info@oncotherm.org

   Manuskripte einreichen

   Manuskripte können online eingereicht werden: info@oncotherm.org

3. Preparation of Manuscripts

Manuscripts must be written in English, but other languages can be accepted for special reasons, if an English abstract is provided.

Texts should be submitted in a format compatible with Microsoft Word for Windows (PC). Charts and tables are considered textual and should also be submitted in a format compatible with Word. All figures (illustrations, diagrams, photographs) should be provided in JPG format.

Manuscripts may be any length, but must include:

- Title Page: title of the paper, authors and their affiliations, 1-5 keywords, at least one corresponding author should be listed, email address and full contact information must be provided
- Abstracts: Abstracts should include the purpose, materials, methods, results and conclusions.
- Test: unlimited volume
- Tables and Figures: Tables and figures should be referred to in the text (numbered figures and tables). Each table and/or figure must have a legend that explains its purpose without a reference to the text. Figure files will ideally be submitted as a jpg-file (300dpi for photos).
- References: Oncothermia Journal uses the Vancouver (Author-Number) system to indicate references in the text, tables and legends, e.g. [1], [1-3]. The full references should be listed numerically in order of appearance and presented following the text of the manuscript.

Manuskripte vorbereiten

Manuskripte müssen in englischer Sprache vorliegen. Andere Sprachen können in Ausnahmefällen akzeptiert werden, wenn ein englisches Abstract vorliegt.

Texte sollten in einem mit Microsoft Word für Windows (PC) kompatiblen Format eingereicht werden. Tabellen sollten in einem Word-kompatiblen Format eingefügt werden. Alle Graphiken (Illustrationen, Diagramme, Photographien) sollten im jpg Format vorliegen.

Manuskripte können jede Länge haben, müssen aber die folgenden Punkte erfüllen:

- Titelseite: Titel der Arbeit, Autor, Klinikzugehörigkeit, 1-5 Schlüsselworte, mindestens ein Autor muss genannt werden, E-Mail-Adresse und Kontaktdetails des Autors
- Abstracts: Abstracts müssen Zielsetzung, Material und Methoden, Ergebnisse und Fazit enthalten.
- Text: beliebige Länge
- Abbildungen und Tabellen: Abbildungen und Tabellen sollten im Text erläutert werden (nummeriert). Jede Abbildung / Tabelle muss eine erklärende Bildunterschrift haben. Bilder sollten als jpg eingereicht werden (300 dpi).
- Zitate: Das Oncothermia Journal verwendet die Vancouver Methode (Autornummer), um Zitate auszuweisen, z.B. [1], [1-3]. Die Bibliographie erfolgt numerisch in Reihenfolge der Erwähnung im Text.

4. Copyright

It is a condition of publication that authors assign copyright or license the publication rights in their articles, including abstracts, to the publisher. The transmitted rights are not exclusive, the author(s) can use the submitted material without limitations, but the Oncothermia Journal also has the right to use it.

Copyright

Es ist eine Publikationsvoraussetzung, dass die Autoren die Erlaubnis zur Publikation ihres eingereichten Artikels und des dazugehörigen Abstracts unterschreiben. Die überschriebenen Rechte sind nicht exklusiv, der Autor kann das eingereichte Material ohne Limitation nutzen.

5. Electronic Proofs

When the proofs are ready, the corresponding authors will receive an e-mail notification. Hard copies of proofs will not be mailed. To avoid delays in the publication, corrections to proofs must be returned within 48 hours, by electronic transmittal or fax.

Elektronische Korrekturfahne

Wenn die Korrekturfahnen fertig gestellt sind, werden die Autoren per E-Mail informiert. Gedruckte Kopien werden nicht per Post versandt. Um Verzögerungen in der Produktion zu verhindern, müssen die korrigierten Texte innerhalb von 48 Stunden per E-Mail oder Fax zurückgesandt werden.

6. Offprints and Reprints

Author(s) will have the opportunity to download the materials in electronic form and use it for their own purposes.
Offprints or reprints of the Oncothermia Journal are not available.

Sonderdrucke und Nachdrucke

Die Autoren haben die Möglichkeit, das Material in elektronischer Form herunterzuladen, Sonderdrucke und Nachdrucke des Oncothermia Journals sind nicht erhältlich.

7. **Advertisement**

The Oncothermia Journal accepts advertising in any language but prefers advertisements in English or at least partially in English. The advertising must have a connection to the topics in the Oncothermia Journal and must be legally correct, having checked that all information is true.

Werbung

Das Oncothermia Journal akzeptiert Werbeanzeigen in allen Sprachen, bevorzugt, aber die zumindest teilweise Gestaltung in englischer Sprache. Die Werbung muss eine Beziehung zu den Themen des Oncothermia Journals haben und der Wahrheit entsprechende Inhalte aufweisen.

8. **Legal responsibility**

Authors of any publications in the Oncothermia Journal are fully responsible for the material which is published. The Oncothermia Journal has no responsibility for legal conflicts due to any publications. The editorial board has the right to reject any publication if its validity has not been verified enough or the board is not convinced by the authors.

Haftung

Die Autoren aller im Oncothermia Journal veröffentlichten Artikel sind in vollem Umfang für ihre Texte verantwortlich. Das Oncothermia Journal übernimmt keinerlei Haftung für die Artikel der Autoren. Die Redaktion hat das Recht Artikel abzulehnen.

9. **Reviewing**

The Oncothermia Journal has a special peer-reviewing process, represented by the editorial board members and specialists, to whom they are connected. To avoid personal conflicts the opinion of the reviewer will not be released and her/his name will be handled confidentially. Papers which are not connected to the topics of the journal could be rejected without reviewing.

Bewertung

Die Texte für das Oncothermia Journal werden durch die Redaktion kontrolliert. Um Konflikte zu vermeiden, werden die Namen des jeweiligen Korrektors nicht öffentlich genannt. Artikel, die nicht zu den Themen des Journals passen, können abgelehnt werden.

Contents

Modulated Electro-Hyperthermia Induces a Prominent Local Stress Response and Growth Inhibition in Mouse Breast Cancer Isografts

Csaba András Schvarcz, Lea Danics, Tibor Krenács, Pedro Viana, Rita Béres, Tamás Vancsik, Ákos Nagy, Attila Gyenesei, József Kun, Marko Fonovi´c , Robert Vidmar, Zoltán Benyó, Tamás Kaucsár and Péter Hamar*

Institute of Translational Medicine, Semmelweis University, 1094 Budapest, Hungary
1st Department of Pathology and Experimental Cancer Research, Semmelweis University, 1085 Budapest, Hungary
Molecular Oncohematology Research Group, 1st Department of Pathology and Experimental Cancer Research, Semmelweis University, 1085 Budapest, Hungary
Bioinformatics Research Group, Genomics and Bioinformatics Core Facility, János Szentágothai Research Centre, University of Pécs, H-7624 Pécs, Hungary
Department of Pharmacology and Pharmacotherapy, Medical School & Szentágothai Research Centre, Molecular Pharmacology Research Group, Centre for Neuroscience, University of Pécs, H-7624 Pécs, Hungary
Department of Biochemistry and Molecular and Structural Biology, Jožef Stefan Institute, 1000 Ljubljana, Slovenia

* Correspondence: hamar.peter@med.semmelweis-univ.hu

Cite this article as:
Schvarcz, C. A. et al. (2021): Modulated Electro-Hyperthermia Induces a Prominent Local Stress Response and Growth Inhibition in Mouse Breast Cancer Isografts, Cancers 13, no. 7: 1744. https://doi.org/10.3390/cancers13071744

Oncothermia Journal 31, 2022 March: 8-31
www.oncotherm.com/sites/oncotherm/files/2022-03/Schvarcz_Modulated.pdf

Simple Summary: Here we investigated the most aggressive type of breast cancer (triple negative breast cancer (TNBC)) for which no effective therapies exist. Modulated electro-hyperthermia (mEHT) utilizes the altered bioelectric properties of tumors to implement a selective energy-transmission of an electromagnetic field and induce thermal and non-thermal anti-tumor effects. In our present study, repeated mEHT treatment effectively inhibited growth and proliferation and caused significant, destruction of TNBC tumors when applied alone without any other therapy in mice. Immunohistochemistry and multiplex analysis revealed that mEHT treatment induced protective mechanisms, like upregulation of heat shock proteins and other stress-related genes. Inhibition of these factors may serve as therapeutic approach to enhance the efficacy of mEHT.We were able to inhibit one of these protective proteins in cell culture. We aim to study the possibility of enhancing mEHT and other cancer therapies by inhibiting the identified protective stress response.
Abstract: Modulated electro-hyperthermia (mEHT) is a selective cancer treatment used in human oncology complementing other therapies. During mEHT, a focused electromagnetic field (EMF) is generated within the tumor inducing cell death by thermal and nonthermal effects. Here we investigated molecular changes elicited by mEHT using multiplex methods in an aggressive, therapyresistant triple negative breast cancer (TNBC) model. 4T1/4T07 isografts inoculated orthotopically into female BALB/c mice were treated with mEHT three to five times. mEHT induced the upregulation of the stress-related Hsp70 and cleaved caspase-3 proteins, resulting in effective inhibition of tumor growth and proliferation. Several acute stress response proteins, including protease inhibitors, coagulation and heat shock factors, and complement family members, were among the most upregulated treatment-related genes/proteins as revealed by next-generation sequencing (NGS), Nanostring and mass spectrometry (MS). pathway analysis demonstrated that several of these proteins belong to the response to stimulus pathway. Cell culture treatments confirmed that the source of these proteins was the tumor cells. The heat-shock factor inhibitor KRIBB11 reduced mEHT-induced complement factor 4 (C4) mRNA increase. In conclusion, mEHT monotherapy induced tumor growth inhibition and a complex stress response. Inhibition of this stress response is likely to enhance the effectiveness of mEHT and other cancer treatments.

Keywords: modulated electro-hyperthermia; triple negative breast cancer isograft; tumor growth inhibition; antiproliferative effect; stress response

1. Introduction

In our previous study we demonstrated that modulated electro-hyperthermia (mEHT) induced Hsp70 upregulation, and exhaustion of this defense mechanism resulted in apoptotic cell death of the mouse 4T1 triple negative breast cancer (TNBC) model. Hsp70 inhibition synergistically enhanced the tumor-killing effect of mEHT [1]. In the present study, our aim was to investigate the molecular effects of mEHT using multiplex methods.

Loco-regional deep hyperthermia (mEHT) is a type of medical hyperthermia usually used as supplementary treatment for cancer patients [2]. mEHT is applied together with conventional modalities like chemo, radio or immunotherapy to enhance their effect and tumor-specificity [3]. mEHT can also boost the effect of targeted therapies, e.g., angiogenesis inhibition by Bevacizumab (Avastin®) in different types of malignancies, including breast cancer [4]. Hyperthermia decreases the activity of hypoxia-inducible factor 1 (HIF-1) and contributes to the vascular endothelial growth factor (VEGF)-mediated angiogenesis inhibition of Bevacizumab [5]. mEHT's potential as a monotherapy is currently under investigation [1,6]. mEHT uses a 13.56 MHz frequency capacitively coupled electromagnetic field that transmits energy to the tumor. mEHT utilizes the bioelectrical difference between the tumor tissue and healthy tissues [7]. The difference in bioelectrical properties results from the higher aerobic glycolysis of cancer cells, known as the Warburg-effect, that causes higher lactate and ion levels in the cancer cells and thus elevates electric conductivity of the tumor [8]. Due to these factors, the energy of the electromagnetic field is absorbed mainly by the tumor.

mEHT can effectively induce caspase-dependent apoptosis as demonstrated by elevated cleaved caspase 3 (cC3) expression in mEHT-treated tumors [1,9]. mEHT induces a heat shock response and subsequent heat

shock protein (Hsp70) upregulation in treated tumors [1,10]. In addition, mEHT potently inhibits tumor cell proliferation indicated by the attenuation of Ki67-positive cell nuclei [11,12], a widely used proliferation marker.

Breast cancer is the most frequently occurring cancer type among women worldwide [13]. Fifteen percent of all breast cancers are triple negative, with no hormone— (estrogen, progesterone) and human epidermal growth factor (HER2) receptors on the surface of the cells. Consequently, hormone and anti-HER2 therapies are ineffective and, as TNBC is the most aggressive breast cancer type, prognosis is poor [14]. Thus, complementary therapies are needed to improve the outcome.

The most commonly used mouse TNBC models utilize cell lines derived from mouse mammary carcinoma cell line 410.4 isolated from a single spontaneous tumor in the BALB/c mouse. Cell lines 4T1 and 4T07 are the most aggressive and invasive subclones derived from the 4104 cell line [15,16]. Implantation of these cell lines creates isografts in BALB/c mice. Thus, after the inoculation of syngeneic cells, immune mechanisms can be investigated under conditions very similar to those of human TNBC [17,18].

In the present study we investigated the molecular effects of mEHT using multiplex methods at the RNA (NGS RNA seq, Nanostring) and the protein level (mass spectrometry). The multiplex data revealed that one of the most significant responses to mEHT was the upregulation of acute stress response proteins. These proteins are part of the innate immune system's nonspecific humoral response as an ancient defense mechanism and have been reported to participate in the immunomodulation of cancer [19], as well as in supporting cancer cells by the formation of extracellular matrix of the tumor microenvironment (protease inhibitors, fibrinogens, haptoglobin, pentraxin). These stress proteins are induced by several forms of tissue injuries, inflammation and in different chronic diseases. They are also often upregulated in cancer patients' serum [20]. These proteins are regarded collectively as acute phase proteins (APPs). However, according to the generally held concept, the major source of APPs is the liver, and only scarce literature demonstrates local production of these proteins upon tissue injury. However, these factors can be induced by different forms of cell stress, like ischaemia [21] or heat [22], and they can contribute to disease elimination and the restoration of homeostatic conditions via different mechanisms [23,24]. The local production of these stress proteins (protease inhibitors, coagulation and complement factors, as well as heat shock proteins) in tumors has been reported to contribute to tumor progression by supporting carcinogenesis, tumor growth, proliferation and angiogenesis [25], and their elevation is considered as a poor prognostic factor [20]. Therefore, inhibition of some of these stress-response proteins such as heat shock proteins [1,9], complement [26], haptoglobin [27] or fibrinogen [28], has recently been proposed as a promising new direction for cancer treatment. However, this is the first report comprehensively demonstrating the local production of several stress-induced proteins in TNBC as a defense to treatment, using multiplex methods. Furthermore, we demonstrate that the specific heat shock inhibitor KRIBB11 abrogates complement upregulation (C4). Thus, our data support that besides inhibition of the heat-shock response, complement inhibition may be utilized in cancer therapy and may synergistically improve the therapeutic effectiveness of mEHT.

Results

2.1. mEHT Reduced Tumor Growth

Follow-up measurements of the tumors by ultrasound (US) and a digital caliper demonstrated a decline in the tumor growth rate in the mEHT-treated group (Figure 1) Tumor volume significantly decreased after three treatments in the mEHT-treated group as measured both by caliper ($p = 0.0363$) and US ($p < 0.0001$) (Figure 1A). Further (4–5) treatments were able to reduce tumor size. The difference in volume became even larger after five treatments (US: $p < 0.0001$, caliper: $p = 0.0003$) (Figure 1B). Comparison of the final and initial tumor volumes demonstrated a higher growth ratio in sham-treated (three treatments: US: 5.0, caliper: 2.7; 5 treatments: US: 4.7, caliper: 6.0), than in mEHT-treated (three treatments: US: 2.1, caliper: 1.8; 5 treatments:

US: 2.0, caliper: 3.0) tumors. The weights of the excised tumors were also significantly smaller in the mEHT-treated than in the sham group after three (p = 0.0091) and five treatments (p = 0.0206) (Figure 1C,D). The excised tumors were significantly smaller in the mEHT-treated versus sham-treated mice (Figure 1E,F). After five treatments in one mEHT-treated mouse, ultrasound demonstrated a small tissue at the site of the tumor. However, by dissection and histological analysis, this tissue was shown to contain no tumor cells, only fat and connective tissue. Therefore, this tumor was regarded as treated (Figure 1F) and its data were included in the tumor growth (Figure 1B) but not in the tumor weight (Figure 1D) data.

2.2. mEHT Induced Caspase-3-Positive Tumor Tissue Destruction

The tumor destruction ratio (TDR), evaluated in hematoxylin and eosin (H&E) sections, demonstrated remarkable tumor tissue destruction in the mEHT-treated tumors (TDR: mEHT: 78.9 _ 5.1% vs. sham: 52.8 _ 10.3%) (Figure 2A,B). Besides the three small tumors in the sham group, TDR was not significantly smaller in the sham-treated animals than in the mEHT group (Figure 2C). The destroyed area identified on the H&E sections stained cleaved caspase-3 (cC3) positive on consecutive cC3-stained sections, confirming a caspasedependent manner of tumor destruction (Figure 2D–F). The complete set of all tumors (H&E and cC3 staining) is presented in the Supplementary Material (Figure S1). 410.4-derived tumors developed a necrotic core after reaching a certain size [29]. In the present study TDR strongly correlated with tumor size (Figure 2G). Comparison of TDR in tumors of similar size (sham vs. mEHT, Figure 2H) demonstrated a significant increase (p = 0.0167) in TDR by mEHT treatments, corroborating that in the sham group TDR elevation was size-dependent, whereas in the mEHT group it was size-independent but treatment-related (Figure 2I).

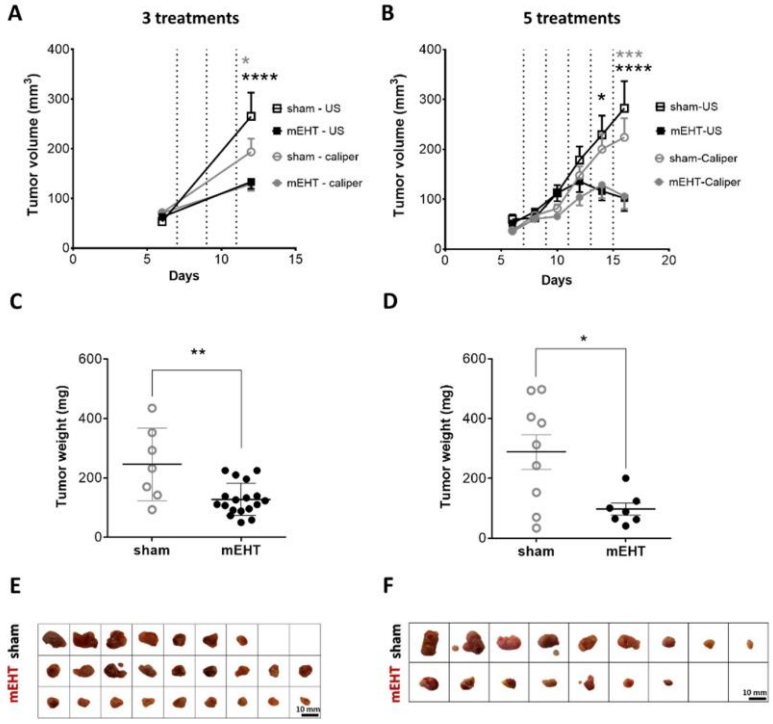

Figure 1. Effect of repeated modulated electro-hyperthermia (mEHT) treatments on tumor size and weight. Digital caliper and ultrasound data after three (A,C,E) and five (B,D,F) treatments (dotted lines, A,B). Tumor weight (C,D), scale images of the excised tumors (E,F). (A–E) n(sham) = 7, mEHT) = 18. sham) 9, n(mEHT) = 7. Mean _ SEM, (A,B) two-Bonferroni correction, (C,D) Mann-Whitney test, *: p < 0.05, ***: p < 0.001, ****: p < 0.0001. Cell line: 4T07, 3–5_ treated.

2.3. mEHT Induced Heat Shock Protein 70 (Hsp70) Accumulation

Specific Hsp70 immunostaining in mEHT-treated animals was intense brown (DAB) in the living cells around the damaged core are of the tumor. Such intense (specific) staining was absent in sham-treated tumors (p=0.0008) (Figure 3A-C).

2.4. mEHT Reduced Ki67 Expression

Most cell nuclei in sham tumors were intensely positive for the Ki67 proliferation marker in the living tumor area (Figure 4A,B). mEHT treatment significantly decreased Ki67 positivity (p = 0.0120) (Figure 4C). The number

of total cell nuclei counted in the living tumor area was also significantly lower in the mEHT-treated compared to the sham-treated group, with a significantly less dense tissue structure due to mEHT treatments ($p = 0.0048$) (Figure 4D).

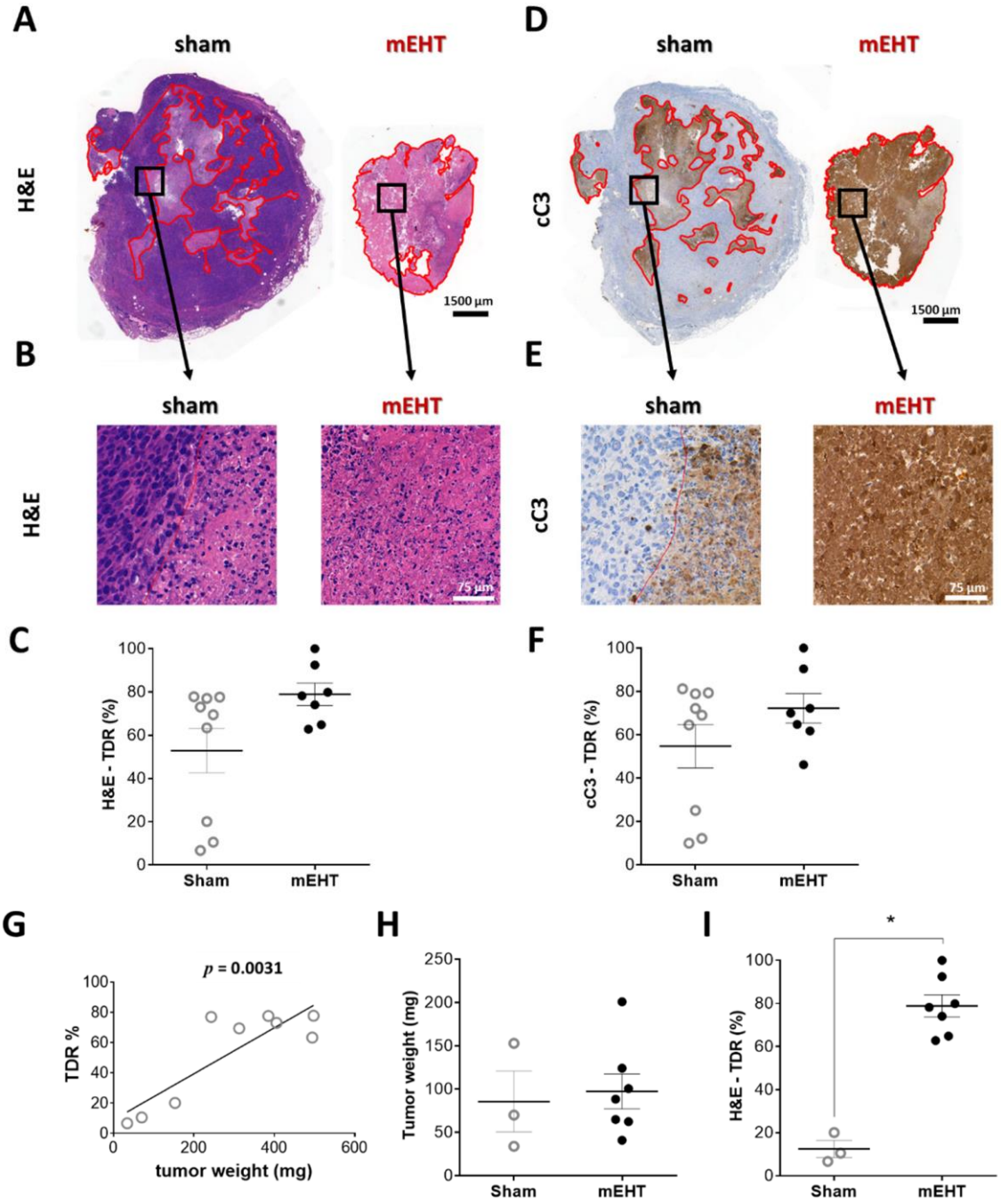

Figure 2. Effect of mEHT treatment on tumor destruction ratio (TDR) in hematoxylin-eosin-(H&E)-stained, and cleaved caspase-3 (cC3) immunohistochemistry-stained sections 24 h after the 5th mEHT treatment. Representative H&E-stained tumors from sham and mEHT-treated groups with 0.9× (A) and 40× (B) magnification. Destructed area is annotated (red). TDR (%) evaluated on H&E (A–C) and cC3 (D–F) sections. Representative cC3 (D,E) stained tumors with low (0.9×, D) and high (40×, E) magnification. Correlation between tumor weight and TDR (%) in sham animals (G). Three smallest sham tumors with weights similar to those of mEHT tumors (H). Comparison of TDR (%) of sham and mEHT tumors of similar weight (I). Mean ± SEM, Mann-Whitney test, n = 7–9/group, *: $p < 0.05$. Cell line: 4T07, 5× treated.

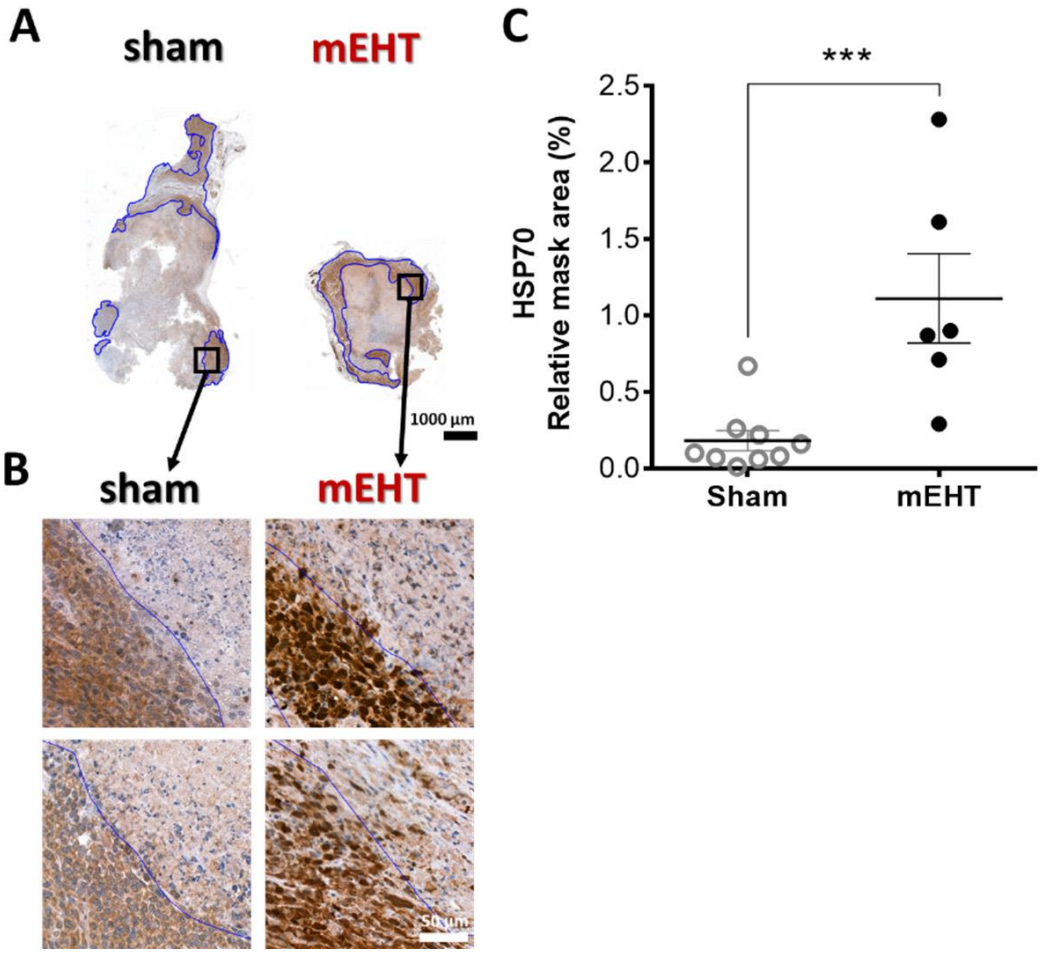

Figure 3. Effect of mEHT treatment on Hsp70 expression 24h after the 5th mEHT treatment. Representative tumors from sham and mEHT-treated mice with Hsp70 staining (0.9× magnification), black rectangles magnified at 'B' (A). Representative sections of Hsp70 express ion near the damaged tumor area (blue annotation), 40× magnification (B). Expression of Hsp70 evaluated in the intact tumor tissue (blue annotations) significantly increased in mEHT-treated tumors (C). In one case, TDR appeared to be 100% and no living area remained to be evaluated for Hsp70 expression. Mean ± SEM, Mann-Whitney test, n = 6–9/group, ***: $p < 0.001$. Cell line: 4T07, 5× treated.

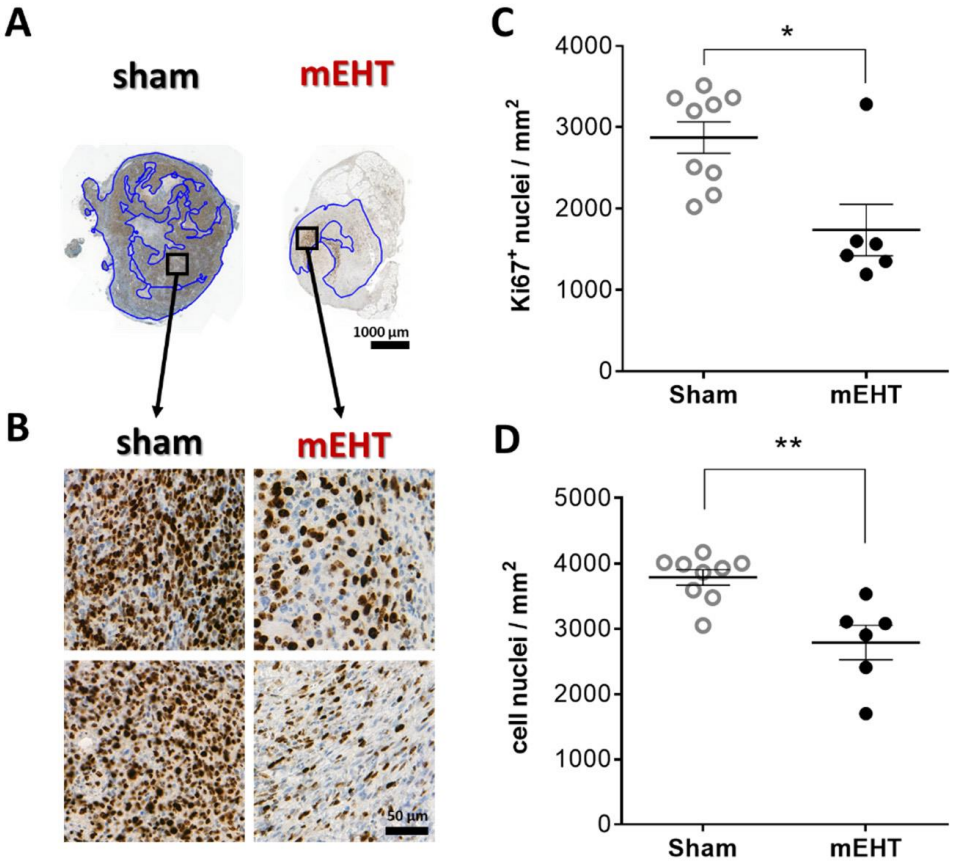

Figure 4. Effect of mEHT treatment on Ki67 expression 24h after the 5th mEHT treatment. Representative tumor sections from sham and mEHT-treated mice with Ki67 staining (A,B). Blue annotations: intact area where Ki67+ nuclei were evaluated (0.9× magnification, bla ck rectangles magnified at 'B' (A), 40× magnification (B)). Area-proportional number of strongly Ki67 positive (C) and all nuclei in the intact tumor area (D). Mean ± SEM, Mann-Whitney test, n = 6–9/group, *: $p < 0.05$, **: $p < 0.01$. Cell line: 4T07, 5× treated.

2.5. Multiplex Analysis of mEHT Effects on Gene Expression

Next-generation sequencing of RNA (NGS RNA Seq) was performed from 4T1 tumor samples 24 h after the third mEHT treatment to investigate gene changes induced by mEHT. Two hundred ninety genes were differentially expressed (DE, criteria: $p < 0.05$ or $\log10(p) < 1.30103$; Fold Change (FC) > 2 or logFC > 1). Heat map visualization clustered with Kendall's Tau distance measurement clearly showed that the vast majority of DE genes were upregulated due to the treatments: one hundred eighty-five upregulated and one hundred five downregulated genes appeared (Figure 5A) A dendogram labeled with gene names is presented in our Supplementary Material (Figure S2). A Volcano plot visualization of gene logFC and $-\log10(p)$ values is presented in Figure 5B. For validation of gene expression at the mRNA level, individual mRNA molecular counting was performed with Nanostring nCounter® Technology (Nanostring Technologies, Seattle, WA, USA). One hundred and thirty-four DE target genes from NGS data were sorted to create a custom Nanostring gene panel. One hundred and four target genes were identified with Nanostring. All of the target genes' direction of change (up or downregulation) was the same as that detected by NGS. Three genes didn't fulfill the DE criteria (Figure 5C).

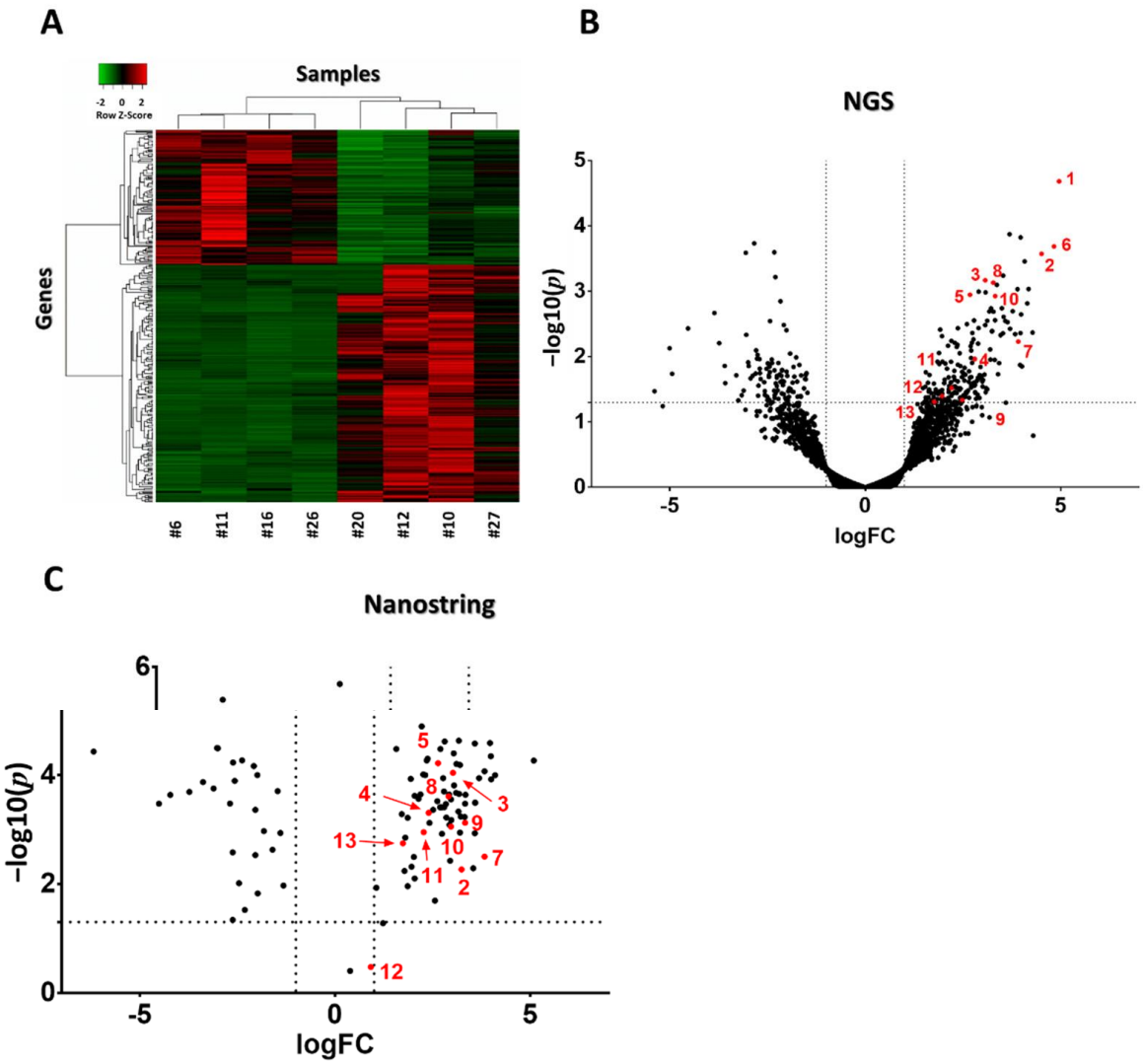

Figure 5. Heat map and volcano plot visualization of DE genes after three mEHT treatments. Heat map clusterization with dendograms (Kendall tau's method, dendogram details: Figure S2) of differentially expressed (DE) genes according to the next generation sequencing (NGS) RNA seq data. Columns represent samples, rows represent genes. Red = upregulation, green = downregulation (A). Volcano plot of all genes according to the NGS RNA seq data (B). Volcano plot of DE genes from the Nanostring data (C). (B,C) −log10(p) values plotted against fold changes (logFC). Vertical dotted line: logFC = 1, horizontal dotted line: −log10(p) = 1.30103. n = 4–6/group. Red dots with numbers mark genes identified in Table 1. Cell line: 4T1, 3× treated.

Table 1. Absolute mRNA Count of cellular stress response factors from the Nanostring data. Individual data of sham and mEHT group members and group averages**. Bold letters:** genes with highest mRNA absolute count and fold-change between the two groups. Background values measured in negative, synthetic probe RNA counts were between 0–16. Cell line: 4T1, 3x treated.

RNA Count	Sham							mEHT						
Genes	#5	#6	#11	#14	#16	#26	Avg.	#4	#10	#12	#15	#20	#27	Avg.
Itih2	2	3	6	9	1	2	3.8	7	54	63	7	27	27	30.8
Itih4	48	9	9	13	2	4	14.2	196	42	60	20	158	40	86.0
Serpina3n	**109**	**62**	**186**	**110**	**25**	**96**	**98.0**	**1265**	**614**	**565**	**444**	**1016**	**352**	**709.3**
Serpina3c	69	37	78	47	12	18	43.5	284	191	216	64	251	111	186.2
Serpina3m	17	13	16	15	7	8	12.7	85	49	30	19	75	34	48.7
Fgb	2	7	21	3	4	5	7.0	7	278	116	18	61	118	99.7
Fgg	7	16	9	19	4	5	10.0	4	103	121	18	19	170	72.5
Hp	**7782**	**3082**	**4825**	**7449**	**1505**	**1632**	**4379.2**	**48,983**	**25,954**	**16,208**	**11,680**	**56,174**	**16,738**	**29,289.5**
Ptx3	**244**	**87**	**180**	**100**	**15**	**107**	**122.2**	**2024**	**568**	**983**	**566**	**2202**	**185**	**1088.0**
Cfd	**3224**	**975**	**1846**	**2293**	**260**	**402**	**1500.0**	**22,431**	**7571**	**7408**	**2341**	**16,311**	**4961**	**10,170.5**
C4b	**1242**	**1081**	**997**	**1244**	**166**	**1443**	**1028.8**	**9234**	**4573**	**3806**	**2930**	**5258**	**1794**	**4599.2**
Hc	17	28	16	32	6	33	22.0	2	77	47	6	6	49	31.2
C1s1	493	479	744	233	141	345	405.8	2036	1638	1390	841	979	672	1259.3

We focused on the upregulated DE genes. These genes were sorted into nineteen functional categories created by us, based on a literature search. Gene ontology (GO) pathway analysis of upregulated genes (DEListEnrichment_upR) revealed that most upregulated genes (38 genes) clustered into the response to stimulus pathway (GO:0050896; pathway p value: 0.00012, Figure 6). Tabular display of the pathway is presented in our Supplementary Material (Table S1). Various types of stress-related genes (coagulation factors, protease inhibitors, complement factors) are included in this pathway. Therefore, we investigated these genes further.

mEHT treatment induced innate immune-response reactions, among others, in the tumor. Thirteen stress-related genes were observed to be significantly upregulated, including protease inhibitors (Itih2, Itih4, Serpina3n, Serpina3c, Serpina3c), coagulation factors (Fbg, Fgg), the free hemoglobin-binding haptoglobin (Hp), and complement cascade-related genes including secreted pattern recognition receptor (PRR), pentraxin-related protein 3 gene (Ptx3), classical pathway (C1s1, C4b), alternative pathway (Cfd) and terminal pathway (Hc) complement components. Fold-changes and p values of the aforementioned significantly upregulated genes, detected with NGS RNA Seq and Nanostring, are presented in Table 2. To investigate if APP upregulation appears not just at the mRNA but also at the protein level, mass spectrometry (MS) examination was performed fromwith the same samples. Eight out of thirteen APPs detected with NGS also appeared at the protein level, and demonstrated significantly upregulated levels when examined by MS. Four heat shock proteins were detected as significantly upregulated by MS, but not by NGS. Label-free quantification intensity difference (LFQ Int. Diff.) values of the given proteins detected by MS are shown in Table 2.

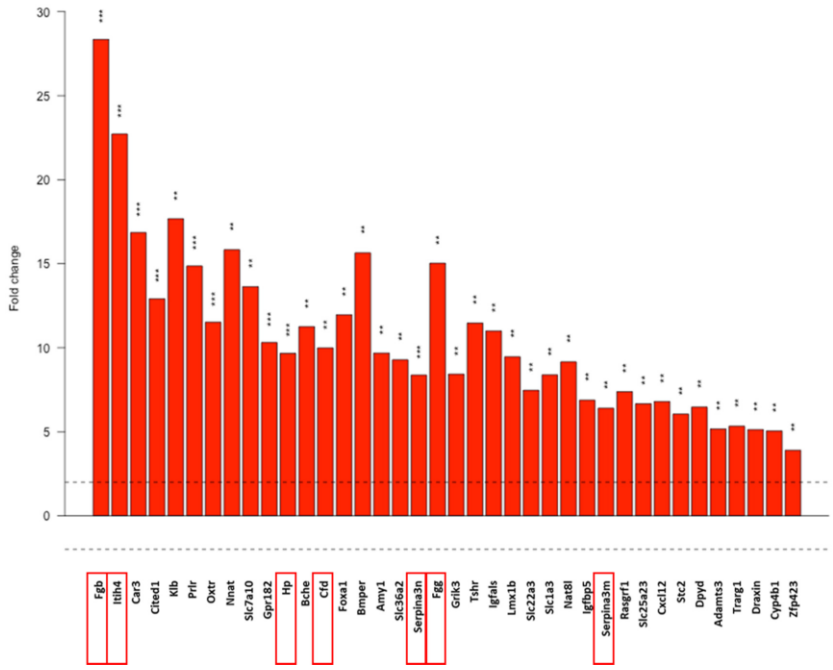

Figure 6. Response to stimulus pathway based on the gene-ontology (GO) analysis of the NGS data. Dotted line: FC = 2. Red frames: further analyed genes. Gene names, p values and further pathways containing stress-related genes analyzed with the DEListEnrichment_up R module are presented in Table S2. **: p < 0.01, ***: p < 0.001. Cell line: 4T1, 3× treated.

Table 2. Cellular stress response upregulated by mEHT treatment. Genes (official name abbreviations as used in all multiplex platforms and descriptions of the coded proteins) detected as upregulated with all three multiplex methods (NGS RNA Seq, Nanostring, MS) are designated with bold letters. Nanostring validated all NGS hits with a similar FC value. Hspa1a and Hspa1b are the most common isoforms of Hsp70. Cell line: 4T1, 3× treated.

Table 2. *Cont.*

Nr.	Gene Name	Description	NGS		Nanostring		MS	
			FC	*p*	FC	*p*	LFQ Intensity Difference	*p*
11	C4b	**complement component 4B (Chido blood group)**	**4.6**	**0.03**	**4.8**	**0.001**	**3.1**	2.9×10^{-4}
12	Hc	hemolytic complement	3.9	0.04	1.9	0.335	1.2	1.7×10^{-4}
13	C1s1	complement component 1. s subcomponent 1	3.4	0.049	3.3	0.002	Not detected	Not detected
		Heat shock factors						
	Hspb1	Heat shock protein beta-1	3.8	0.075	not investigated		2.7	1.1×10^{-5}
	Hspa1a	Heat shock 70 kDa protein 1A	2.0	0.551	not investigated		2.1	1.3×10^{-5}
	Hspa1b	Heat shock 70 kDa protein 1B	2.4	0.362				
	Hsph1	Heat shock protein 105 kDa	1.8	0.761	not investigated		1.3	0.023
		Complement factors						
9	Ptx3	pentraxin related gene	5.6	0.046	10.1	7.5×10^{-4}	Not detected	Not detected
10	Cfd	**complement factor D (adipsin)**	**10.0**	**0.001**	**7.8**	$\mathbf{8.8 \times 10^{-4}}$	**2.0**	**0.001**

* uniquely expressed in mEHT-treated samples but not in the sham-treated tumors, no FC applies by the nanostring evaluation.

Nanostring data provided absolute RNA count cellular stress response factors (Table 1). These data further oriented our research, since those targets that demonstrated low absolute expression despite fulfilling DE criteria ($p < 0.05$, FC > 2) were excluded from further investigation. Thus, we focused on Serpina3n, haptoglobin (Hp), pentraxin (Ptx)3, and the complement factors (Cfd, C4b) with high absolute RNA counts and high FC without overlapping values between the groups (bold letters in Table 1).

2.6. The Heat-Shock Factor-1 Inhibitor KRIBB11 Reduced C4b Expression In Vitro

One of the most upregulated genes/proteins with significant upregulation on all three screens was the mouse C4 complement C4b. C4b mRNA was measurable by qPCR from in vitro 4T1 cell culture, demonstrating that 4T1 tumor cells produce C4b. mEHT treatment in monotherapy induced a significant upregulation of C4b mRNA 2 h after treatment in vitro ($p < 0.0001$; Figure 7A). We demonstrated in our earlier paper [1] that KRIBB11 (N(2)-(1H-indazole-5-yl)-N(6)-methyl-3-nitropyridine-2,6-diamine) reduced the cellular heat shock response of 4T1 cancer cells through inhibiting the heat-shock factor (Hsf)-1. Therefore, we hypothesized that heat shock-related complement production can be targeted by KRIBB11. KRIBB11 significantly reduced baseline C4b mRNA compared to Dimethyl sulfoxide (DMSO)–treated cells in the 37 °C control group ($p = 0.0256$; Figure 7A). After mEHT treatment, the mEHT-induced C4b elevation was also significantly inhibited by KRIBB11 compared to DMSO treatment ($p < 0.0001$; Figure 7A). Moreover, C4b correlated significantly with Hsp70 expression ($p < 0.0001$; Figure 7B)

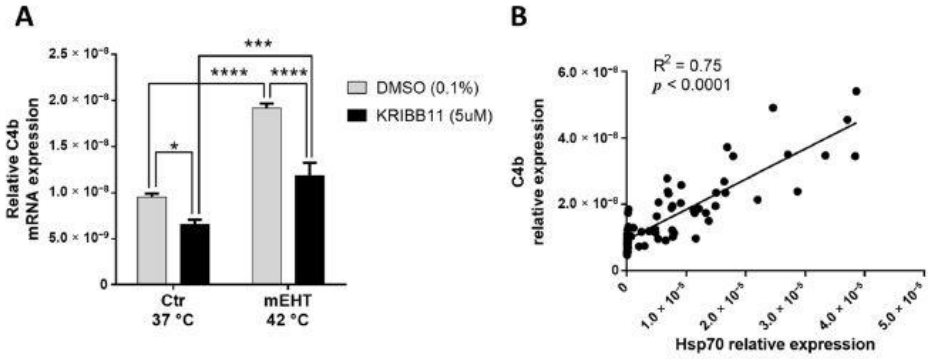

Figure 7. KRIBB11 effect on mEHT-induced C4b production. C4b mRNA relative expression, 2 h post-mEHT, normalized to 18S, with KRIBB11 treatment, vs. DMSO (A). Correlation between C4b and Hsp70 expression (B). Mean SEM, Two-way ANOVA, n = 5–15/group, *: $p < 0.05$, ***: $p < 0.001$, ****: $p < 0.0001$. Cell line: 4T1.

Discussion

In our previous paper [1] we presented the LabEHY200 treatment apparatus with newly developed electrodes, able to perform selective mEHT treatment in a TNBC mouse model. It clearly demonstrated the antitumoral effects of mEHT, which resulted in elevated tumor tissue destruction and reduced cell viability in vivo, even after a short-term protocol (1× or 2× mEHT). Our current paper describes the long-term effects of repeated mEHT treatments on tumor progression in a triple negative mouse breast cancer model for the first time. This is the first comprehensive, multiplex analysis-based investigation of the overall anticancer effects of mEHT at both the gene and protein level. Here, we report that mEHT, even in monotherapy, was able to reduce the growth rate of the highly aggressive triple negative 4T07 isografts. In the background of this strong tumor-inhibitory effect of mEHT we observed reduced proliferation of tumor cells, and heat shock-induced caspase-mediated tumor tissue damage. Multiplex analysis of the mEHT-treated 4T1 tumors revealed massive, local upregulation of protease inhibitors and coagulation and complement factors as a response to cellular stress. These factors are part of the innate immune system's acute phase reaction. However, being produced locally in tumors, they have a more complex role, depending on the tumor microenvironment and cellular source [23].

Tumor growth was significantly inhibited by mEHT as demonstrated by digital caliper and ultrasound measurements and confirmed by the dramatically smaller weights of the excised tumors in mEHT-treated mice. Moreover, mEHT-treated tumors began to shrink only after the fifth treatment. Tumor shrinkage was not observed after only two treatments, despite a significant induction of tumor cell damage [1]. The tumor growth inhibitory effects of mEHT monotherapy in other tumors were quite similar in previously published studies.: A single (colorectal cancer (CT26) isografts [30,31]) or three (squamous cell carcinoma (SCCVII) isografts [32]) mEHT treatments induced slower tumor growth, but no decline in tumor volume. In our experimental design

we applied noninvasive temperature detection during the experiments. Animals were randomized based on tumor size (Table S1) before treatment initiation, overcoming some shortagescomings of previous experiments [30,31]. Similar to our study, five mEHT treatments induced a measurable tumor shrinkage of HepG2 hepatic cancer xenografts [33] and U87-MG rat glioma xenografts [34]. One possible explanation for the lack of measurable tumor shrinkage after three treatments, despite obvious tumor destruction, is a delayed clearance of the apoptotic tumor cells. APPs have a major role in apoptosis, e.g., Pentraxin 3 (PTX3) binds to apoptotic cells and facilitate their clearing by macrophages via the Fcγ receptor [35] and dendritic cells [36]. An immunologically silent clearance of apoptotic tumor cells was reported to be mediated by an opsonizing effect of complement factors [37]. Thus, the detected upregulation of PTX3 and C4 may contribute to the clearance of apoptotic cancer cells and tumor shrinkage after five treatments.

As we demonstrated in our previous paper [1], Hsp70 is a reliable marker of mEHT treatment effects and, similar to two treatments, in our current paper five mEHT treatments resulted in strong upregulation of Hsp70. The MS study demonstrated the upregulation of several heat shock proteins (Hspβ1, Hsp70-1A, Hsp70-1B, Hsp105), corroborating our IHC data. These proteins were also detected at the RNA level by NGS, but there was no significant difference between the two groups. This finding is in accordance with our previous findings, demonstrating that 24 h after mEHT treatment the Hsp70 response returns to baseline at the mRNA level but not at the protein level [1].

In this study we observed a significant tumor size reduction by mEHT treatment, but the damaged area (tumor destruction ratio, TDR) in the mEHT-treated tumors did not differ significantly from the TDR in large sham-treated tumors. The explanation for the extensive destruction in sham tumors is spontaneous necrosis due to their large size. Spontaneous necrosis, due to low oxygen and nutrient supply, is well-known in fast progressing tumors such as the 4T1/4T07 [38,39,40,41]. Consequently, the degree of destruction is consistent with tumor size [42,43,44]. As sham tumors in our study were very large, a central necrosis developed. In contrast, mEHT-treated tumors were much smaller, but their TDR was comparable to that of sham tumors. This implies that the increase of tumor tissue destruction was only size-related in the sham group, but treatment-related in the mEHT group.

Furthermore, mEHT was able to diminish Ki67+ proliferation of this highly proliferative tumor. Ki67 is strongly correlated with aggressiveness and worse prognosis, especially in breast carcinomas, where it is a prognostic marker and one of the molecular features of disease classification [45,46,47]. In our study, not only the proliferative activity, but also the cell density of the tumor tissue was reduced. Only one laboratory reported similar results after a single mEHT treatment of C26 colorectal cancer isografts, but they detected loss of Ki67 expression in the already damaged and early apoptotic areas, while the living tumor around the destructed area seemed to be strongly Ki67-positive [11]. In the present study we demonstrated the loss of proliferating activity of viable tumor cells, which may have led to the diminished tumor growth rate in the mEHT-treated mice.

mEHT activated the local production of several stress-related factors (protease inhibitors: Itih2, Itih4, Serpina3n, Serpina3c, Serpina3m, coagulation related factors: Fgb, Fgg, Hp, and complement related factors (Cfd, C4b, Hc, C1s1, Ptx3)) both at the mRNA and protein level. In fact, induction of these proteins was most significant, with the highest fold-change values in our multiplex next generation sequencing (NGS RNA seq), Nanostring and mass spectrometry (MS) study. Despite the different methods, fold-change mRNA values were very similar with NGS and nanostring, demonstrating good reliability of these methods. A great advantage of the nanostring method is that it detects the absolute copy number of the RNA molecules directly, without reverse transcription and amplification. Moreover, gene ontology (GO) analysis revealed that the most differentially expressed (DE) upregulated genes were related to the response to stimulus pathway (GO:0050896). Thus, in our further studies, we focused on the abundant genes (high RNA copy number) with significant induction by mEHT (no overlap in RNA copy number and FC > 4). The lack of detection of some genes

with mass spectrometry may be due to the time lapse between mRNA (as detected by NGS, nanostring) and protein (MS) expression. Here we would like to emphasize that we detected messenger RNA and protein from the tumor tissue, indicating local production of these stress related proteins by the tumor, contrary to the general view about the liver-driven acute phase response [48]. Extra-hepatic synthesis of these proteins has been documented before [49]. Often these genes are regulated by mechanisms different from those acting in hepatocytes [50]. Production of these proteins as a cellular stress-response has been demonstrated before by us [21] and others [51,52], and in the case of cancer cells [53,54]. Similar to our results, photodynamic therapy of fibrosarcoma induced production (mRNA) of other acute phase proteins (serum amyloid-P (SAP) mannose binding lectin (MBL) and c-reactive protein (CRP)) [53]. A recent review demonstrated association of different patterns of acute phase protein production with various types of cancers [54]. A possible interpretation of this finding is that the different patterns are due to protein production by the cancer itself, and not by the liver.

The genes we found massively upregulated by mEHT are all related to cellular stress response and appear to have a general, tumor-protective role in different types of cancer.

The protease inhibitors (serpins and ITIHs) have been described as ancient markers of cell stress [55]. Serine protease inhibitor family A member 3 (Serpina3) was reported as an antiapoptotic factor in trophoblast cells [56]. Furthermore, high expression of Serpina3 was reported in colon [57] and endometrial [58] cancers, and in melanoma [59]. Serpina3n was described as a cellular stress response gene in different types of stress and has been associated with a wide range of diseases such as photoreceptor cell loss in a retinal degeneration mouse model [60], and muscle atrophy in mice and humans [61]. The other members of these protease inhibitors detected, namely Itih2,4 and SerpinA3c,m, had very low absolute mRNA copy numbers, especially in the sham animals, hardly exceeding background values. Even in the mEHT-treated animals, copy numbers were low. Thus, we did not investigate these factors further.

The association of coagulation factors and cancer was first described in 1865 [62]. Fibrinogen (especially Fgg) production by breast cancer cells has been demonstrated before [63]. The production of fibrinogen without fibrin formation contributed to extracellular matrix (ECM) production in breast cancer [64]. Fibrin(ogen) surrounding tumor cells may protect them by acting as a barrier [65]. Thus, fibrinogen synthesized by tumor cells promoted tumor growth [63]. Inhibition of fibrinogen (Fgg) production reduced chemotherapy resistance [28] and growth [63] of breast cancer. Thus, inhibition of mEHT-induced fibrinogen upregulation may have tumor inhibitory effects through diminishing the supportive tumor microenvironment and could synergize with mEHT.

Taken together, the upregulation of both protease inhibitors and fibrinogens seem to contribute to stability of the tumor microenvironment (TME). Thus, the inhibition of these proteins may aid several cancer-treatment forms by inhibiting the formation of a protective tumor microenvironment and facilitating the access of the therapy to the tumor cells.

The primary role of haptoglobin (Hp) is the binding of free Hb released by erythrocytes upon hemolysis. As cell-free hemoglobin is an oxidant, Hp protects from oxidative stress [66]. However, in breast cancer, the Hp mRNA level was significantly higher in the tumor tissue compared to normal breast tissue. Hp production was also reported to be tumor promoting by inducing glycolysis, whereas Hp inhibition by siRNA was antiproliferative and reduced tumor size [27]. Thus, Hp inhibition should be antiproliferative and could synergize with mEHT.

The complement system has been considered for a long time as a simple lytic cascade, aimed at killing bacteria. Nowadays, it is well accepted that complement is a complex innate immune surveillance system, playing a key role in host homeostasis, inflammation, and defense [37]. In the tumor microenvironment, complement factors can perform nocanonical functions [23], such as stimulation of angiogenesis, inflammation, proliferation and

migration, and they can even attenuate immunotherapy [25,67]. The therapeutic inhibition of complement components for cancer treatment has been well described [26], and the angogenesis-stimulating role of complements advocates the concept of applying mEHT in combination with angiogenesis inhibitors like Bevacizumab, which has been demonstrated to be beneficial for patients [4]. In our multiplex studies of isolated tumor tissue, the mouse complement C4 (C4b) gene was detected as one of the most upregulated genes/proteins with all three methods (NGS, Nanostring, MS). The complement factor C4 has two isotypes encoded by the C4A and C4B genes in humans, as well as in mice (C4a, C4b). The C4A/C4a (Rodgers blood group) gene encodes the acidic form, whereas the C4B/C4b (Chido blood group) encodes the basic form. Their role in the complement cascade is identical [68]. Production of C4 by nonhepatic (endothelial cells, fibroblasts) cells in the TME has been well described [23,69]. However, we detected C4 in cultured 4T1 cells, demonstrating that C4 was produced by the tumor cells themselves. Production of C4 by 4T1 cells has not been described before. mEHT treatment further upregulated the production of C4, 2 h after treatment in vitro, corroborating our in vivo multiplex data. As mEHT induced a heat shock response, as demonstrated by Hsp70 upregulation, inhibition of HSR by the specific heat-shock factor-1 inhibitor KRIBB11 synergized with mEHT, as demonstrated in our previous paper. Here, we demonstrated that KRIBB11 significantly decreased C4 mRNA. This is a newly described effect of KRIBB11. C4 has been reported to be important for the growth of cervical (TC-1) tumors [70]. Moreover, serum C4 levels may have a prognostic value [71] correlating with tumor size [72]. Finally, inhibition of C4 along with VEGFA inhibition inhibited tumor progression [73]. C4 may act by activating C3 and C5 into their active forms. Furthermore, the alpha chain may be cleaved to release C4 anaphylatoxin [37]. Taken together, the C4-inhibiting effects of KRIBB11 may be beneficial in anticancer therapies and can synergize with mEHT in clinical practice.

Pentraxin 3 (PTX3) is another ancient molecule involved in various cell stress responses, such as oxidative stress [74], a key player in the innate immunity involved in inflammatory responses and wound healing and is a component of the extra-cellular matrix (ECM). Most cell types, including tumor cells, are able to produce PTX3. The PTX3 interactome includes complement [75] and ECM components and apoptotic cells [76]. In breast cancer, PTX3 was induced by hypoxia and correlated with poor prognosis, inducing stem-cell-like characteristics and metastasis formation [76]. Although, antitumoral effects have been also reported, overexpression of PTX3 accelerated metastasis [77], whereas knockdown suppressed tumorigenicity [78]. Thus, PTX3 inhibition may synergize with anti-tumor therapies, including mEHT.

In conclusion, modulated electro hyperthermia (mEHT) has effective antitumor effects, even in monotherapy, in our highly aggressive and rapidly growing 4T1/4T07 triple negative breast cancer in vivo mouse model. The mEHT-induced significant tissue stress was indicated by the upregulation of Hsp70 and cleaved/activated caspase-3, and by the local production of other ancient stress response proteins. The exhaustion of these protective mechanisms resulted in diminished cancer proliferation and caspase-mediated apoptotic tumor cell death. Inhibition of the protective heat shock response and complement C4 production by a specific heat-shock factor inhibitor, KRIBB11, suggests that inhibitors of such stress response proteins may synergize with antitumor therapies such as mEHT.

4. Materials and Methods

4.1. Tumor Model

410.4 cell-line derived triple negative murine breast cancer cells (4T1/4T07) were grown in cell culture and processed for inoculation as described previously by Ostrand- Rosenberg et al. [79]. Previously [1], we demonstrated significant tumor inhibition after 2 mEHT treatments enhanced by simultaneous inhibition of the heat-shock response by KRIBB11. In the present studies we investigated the proteomic response after three treatments and long-term effects on tumor progression after five treatments. The experiments investigating mEHT effects on tumor progression after three or five treatments were performed on the more immunogenic

4T07 tumors. However, the multiplex and in vitro studies were performed from the more commonly used and more aggressive 4T1 cell line to obtain results which are more generally applicable.

Six- to eight-week-old female BALB/c mice were kept under 12 h dark/light cycles with ad libitum access to food and water in the animal department of Basic Medical Center, Semmelweis University. For tumor-cell inoculation, animals were narcotized with isoflurane (Baxter International Inc., Deerfield, IL, USA), 4–5% for induction, 1.5–2% to maintain anesthesia, with compressed air (0.4–0.6 L/min). Cells were inoculated in standard, 1 106 cells /50 L PBS (Phosphate Buffered Saline without Calcium and Magnesium #17- 516F, Lonza A. G., Basel, Switzerland). Inoculations were performed subcutaneously by a Hamilton syringe (Hamilton Company, Reno, NV, USA) into the inguinal mammary fat pad of each mouse. On the sixth day after inoculation, tumor size was measured by digital caliper and ultrasound as described earlier by Danics et al. [1] (Figure 8). In the short-term experiment (3 mEHT), measurements were made at the sixth day after inoculation and at the day of termination, while in the long-term experiment (5 mEHT) tumor size was measured on every other day beginning on day six after inoculation until the termination of the experiment. Animals were randomized into mEHT-treated and sham-treated groups according to tumor size (Figure S3). Tumors were treated three or five times. Tumors were removed 24 h after the last treatment. Multiplex analyses were performed after three treatments, whereas long-term effects of repeated treatment were investigated after five treatments. Mice were euthanized by cervical dislocation, tumors were resected, cleaned and precisely cut in half along the longest diameter. One half was fixed in 4% formaldehyde solution (Molar Chemicals Ltd., Halásztelek, Hungary) and transferred for histological processing. The other half was stored in liquid nitrogen for molecular analysis (RNA isolation). Interventions and housing of the animals conformed to the Hungarian Laws No. XXVIII/1998 and LXVII/2002 about the protection and welfare of animals, and the directives of the European Union. All animal procedures were approved by the National Scientific Ethical Committee on Animal Experimentation under the No. PE/EA/50-2/2019, date of approval: 01 November 2019.

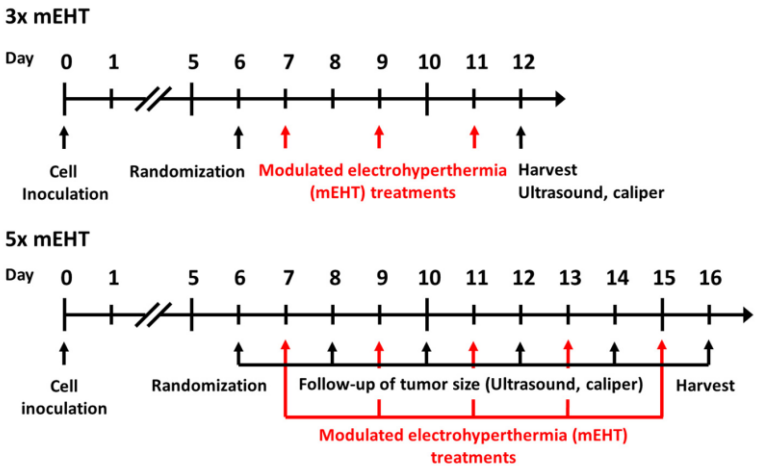

Figure 8. Timeline of in vivo experiment protocols. Cell inoculation was performed at day zero, randomization at day six in both short- and long- term experiments. Modulated electrohyperthermia treatments were performed at day 7, 9, 11 in the short and at day 7, 9, 11, 13, 15 in the long-term experiment. Ultrasound, caliper measurements were performed at day 6 and 12 in the short-term, and at day 6, 8, 10, 12, 14, 16 in the long-term experiment. Harvests were performed in the short- and long-term experiments at day 12 and 16, respectively.

4.2. In Vivo Treatments

Tumors were treated 3–5 times with the newly developed rodent modulated electro hyperthermia device as described in detail in our previous paper [1]. The principle of the treatment is a capacitively coupled, amplitude-modulated, 13.56 MHz electromagnetic field which transfers energy to the tumors. The electromagnetic field was established between two electrodes in the inguinal region. The mobile (upper) electrode was a 2 mm diameter column-shaped plastic case filled with stainless steel rods, covered with 3.1 cm2 silver-plated textile, positioned on the tumor. Animals were placed on a heating pad (in vivo applicator), functioning as the lower electrode, and connected to the LabEHY modulated electro hyperthermia 200 device with heating and

radiofrequency (RF) cable. The abdominal area below the mobile electrode and the back of the mice was shaved before the treatments to enable electric coupling. Treatments were performed with a LabEHY 200 device in a temperature-driven way, for 30 min with 0.7 _ 0.3 watts after a 5-min-long warmup. Temperature monitoring was performed with a four-channel TM-200 thermometer (Oncotherm Ltd., Budaörs, Hungary). Temperature sensors were placed (1) on the skin above tumor, (2) in the rectum for core temperature monitoring, (3) on the heating pad and (4) nearby the treatment setup for room temperature monitoring. Skin temperature was kept at 40 _ 0.5 _C during the treatments, as it assured the required 42 _C inside the tumor. Rectal temperature was kept in the physiologic range (37.5 _ 0.5 _C), and the lower electrode's temperature was set at the same temperature. Room temperature was at 25 _ 1 _C. During sham treatments, the electromagnetic field was turned off but all other conditions (heat pad temperature, upper electrode position) were similar to the mEHT treatment. A schematic illustration of the treatment procedure is presented in Figure 9. Numbers of animals in the three-time treatment experiments were n_{sham} = 7, n_{Meht} = 18, and n_{sham} = 9, n_{mEHT} = 7 in the five-time treatment experiment.

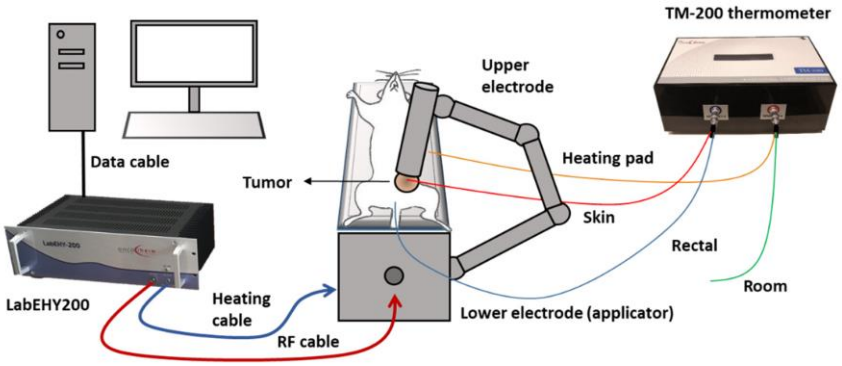

Figure 9. Schematic illustration of mEHT treatment setup. Mice were placed on the lower electrode (in vivo applicator) in isoflurane anesthesia. The upper electrode was positioned on the tumor in the inguinal region. The LabEHY200 was connected with the lower elect rode with a radiofrequency (RF) and a heating cable. Temperature monitoring of tumor surface (red: skin temp. sensor), rectum (blue), heating pad (yellow) and room temperature (green) was performed by a TM-200 thermometer and the data were registered with a computer during the treatment.

As demonstrated in the H&E and cC3 stained sections, five treatments had such a strong effect on the tumors that RNA isolation was troublesome, and we were not able to isolate sufficient quality RNA or protein from tumors treated three times. Thus, mRNA and proteomic studies were performed after three mEHT treatments, when tumor size reduction was already significant, but RNA and protein isolations were still possible.

4.3. In Vitro Treatments

In vitro treatments were performed as described by us earlier [1]. Briefly, 1 × 106 4T1 cells were pretreated in cell culture with 5 µM KRIBB11 (#385570, Sigma-Aldrich Co., St. Louis, MO, USA) or 0.01% DMSO (#D2438, Sigma-Aldrich Co., St. Louis, MO, USA) for 1h before mEHT. The cell suspension was transferred into a plastic bag for treatment with the LabEHY 200 in vitro applicator. A thermosensor (TM-200 thermometer, Oncotherm Ltd., Budaörs, Hungary) was inserted into the bag for temperature follow-up. The unit was placed in glass cuvette (filled with distilled water), which was inserted between the two electrodes of the in vitro applicator (Oncotherm Ltd., Budaörs, Hungary). An average of 4 ± 1 Watts was applied with the same amplitude-modulation (AM) as in the in vivo experiments. The temperature rise of the cell suspension was around 2.3 ± 0.8 °C/min. Cells were treated for 30 min in a temperature-driven way to maintain 42 °C in the cell suspension. Cells were collected 2 h after mEHT treatment, lysed with Tri-Reagent (#TR118/200, Molecular Research Center, Inc., Cincinnati, OH, USA) and processed for RNA isolation.

4.4. Histopathology and Immunohistochemistry

Formalin-fixed tumor samples were dehydrated and embedded in paraffin. Serial sections (2.5 _m) were cut for hematoxylin-eosin (H&E) staining or dewaxed and rehydrated for immunohistochemistry (IHC) using a polymer-peroxidase system (Histols, Histopathology Ltd., Pécs, Hungary). Evaluation of Tumor Destruction Ratio (TDR%) on H&E and cC3 and digital evaluation of Hsp70 and Ki67 stainings was performed as described earlier [1]. The antibodies used are listed in Table 3.

Table 3. Antibodies and conditions used for immunohistochemistry and immunofluorescence. pAb: polclonal antibody, Hsp70: heat shock protein-70, Ki67: marker of proliferation.

Antigen	Type	Reference No.	Dilution	Vendor [1]
Hsp70	Rabbit, pAb	#4872	1:200	Cell Signaling
Ki67	Rabbit, pAb	#RM-9106	1:400	Thermo

[1] Vendor specifications: Cell Signaling (Danvers, MA, USA), Thermo (Waltham, MA, USA).

4.5. RNA Isolation and RT-PCR

RNA isolation was performed with TRI reagent (Molecular Research Center Inc.,Cincinatti, OH, USA) according to the manufacturer's instructions. Isolated RNA was reverse transcribed by a High-Capacity cDNA Reverse Transcription Kit (Applied Biosystems, Carlsbadm, CA, USA). The amplified cDNA was used as a template for RT-PCR. Messenger RNAs were detected in the samples by SYBER Green based RT-PCR with SsoAdvanced™ Universal SYBER® Green Supermix and the CFX96 Touch Real-Time PCR Detection System (Bio Rad, Hercules, CA, USA). Expressions were normalized to 18S. The primers used are listed in Table 4.

4.6. Next-Generation Sequencing and Bioinformatic Analysis

Table 4. Primers used for RT-PCR.

Gene Symbol	Gene Name	Primer Pairs
18S	18S [Mus musculus]	Fwd: CTCAACACGGGAAACCTCAC Rev: CGCTCCACCAACTAAGAACG
C4b	Complement component 4b [Mus musculus]	Fwd: AACCCCTCGACATGAGCAAG Rev: TGGAACACCTGAAGGGCATC

Five sham and five mEHT-treated samples were chosen based on the quality and quantity of the isolated RNA and the relative Hsp70 expression (used as a marker of effective treatment), measured by immunohistochemistry. RNA integrity and RNA concentration were assessed by the RNA ScreenTape system with the 2200 Tapestation (Agilent Technologies, Santa Clara, CA, USA) and the RNA HS Assay Kit with the Qubit 3.0 Fluorometer (Thermo Fisher Scientific, Waltham, MA, USA). The DNaseI treatment (Thermo Fisher Scientific, Waltham, MA, USA), the Ribo-Zero rRNA removal (Illumina, San Diego, CA, USA) and the KAPA Stranded RNA-Seq libraries (Roche Diagnostics, Indianapolis, IN, USA) were prepared according to manufacturer's protocols. The quality and quantity of the libraries were determined by the High Sensitivity DNA1000 ScreenTape system with the 2200 Tapestation (Agilent Technologies, Santa Clara, CA, USA) and dsDNA HS Assay Kits with Qubit 3.0 Fluorometer (Thermo Fisher Scientific,Waltham, MA, USA). Pooled libraries were diluted to 1.6 pM for 2 80 bp paired-end sequencing with 150-cycles of the High Output v2 Kit on the NextSeq 550 Sequencing System (Illumina, San Diego, CA, USA) according to the manufacturer's protocol. Raw sequenced reads >50 M per sample were demultiplexed and adapter-trimmed by using the NextSeq Control

Software, whilst the FastQ Toolkit (Illumina, San Diego, CA, USA) was applied to trim bases at the 30- and the 50-ends with a quality score <30. Reads with mean quality score <30 and shorter than 32 bp were filtered out.

Reads were compared with the Mus musculus reference genome (GRCm38 Ensembl release, STAR v2.6.1c) [80]. After alignment, the reads were associated with known proteincoding genes and the number of reads aligned within each gene was counted using the HTSeq tool v0.6.1p1 [81]. Gene count data were normalized using the trimmed mean of M values (TMM) normalization method of the edgeR R/Bioconductor package (v3.28, R v3.6.0, Bioconductor v3.9) [82]. For statistical testing, the data were further log transformed using the voom approach [83] in the limma package [84]. TMM normalized counts were represented as transcripts per million (TPM) values. Fold-change (FC) values between the compared groups, resulting from a linear modeling process and modified t-test p-values, were produced by the limma package. FC > 2.0 and p-value < 0.05 thresholds were used for filtering the differentially expressed (DE) genes. Based on intensive literature search on PubMed, UniProt, Protein Atlas, nonprotein-coding genes, previously unidentified (no literature search possible) genes and those that had no/insufficient literature (lack of information on expression, function, and regulation) were excluded from further analysis. Remaining DE genes were grouped into functional categories created by us. Functional analysis was performed to consider the functional annotations of genes using the gene ontology (GO) database. Detection of functional enrichment was performed in the differentially expressed gene list (DE list enrichment) and towards the top of the list when all genes were ranked according to the evidence for being differentially expressed (ranked list enrichment) applying the topGO v2.37.0 packages. We show results of the GO analysis of significant upregulated genes (DEListEnrichment_upR). A heat map was created from the normalized NGS RNA Seq data with Kendall tau's method at heatmapper.ca (Wishart Research Group, University of Alberta, Canada) [85]. Raw RNA-Seq data sets generated as part of this study will be publicly available at the European Nucleotide Archive (https://www.ebi.ac.uk/ena, accessed on 19 March 2021), under study accession number PRJEB43813.

4.7. Mass Spectrometry Analysis

Mass spectrometry analysis of the same samples used for NGS was performed as described earlier by Róka et al. [19]. Briefly, liquid chromatography with tandem mass spectrometry (LC-MS/MS) analysis was done using an EASY-nanoLC II HPLC unit (Thermo

Fisher Scientific, Waltham, MA, USA) coupled with an Orbitrap LTQ Velos mass spectrometer (Thermo Fisher Scientific, Waltham, MA, USA). Samples containing 0.1% FA were loaded onto a C18 trapping column (Proxeon Easy-column, Thermo Fischer Scientific, West Palm Beach, FL, USA) and separated on a C18 PicoFrit Aquasil analytical column (New Objective, Inc.,Woburn, MA, USA). The peptides were eluted using a 5–40% (v/v) 90 min linear gradient of acetonitrile in a 0.1% formic acid solution at a constant flow rate of 300 nL/min. The full MS mass spectra were acquired with the Orbitrap mass analyzer in the mass range of 300 to 2000 m/z at a resolution of 30,000. The MS/MS spectra were obtained by higher-energy collisional dissociation (HCD) fragmentation of the nine most intense MS precursor ions and recorded at a resolution of 7500. Only the precursor ions with assigned charge states (>1) were selected for MS/MS fragmentation. The dynamic exclusion was set to a repeat count of 1, repeat duration of 30 s, and exclusion duration of 20 s. For data analysis, the MaxQuant proteomics software (version 1.6.0.13; Max-Planck Institute for Biochemistry, Martinsried, Germany) was used for database search and quantification by spectral counting [86]. The database search was performed against a Mus musculus Uniprot database (database date 15.10.2017, 16,923 entries). For the database searches, methionine oxidation (+15995 Da) and protein N-terminal acetylation (+45011 Da) were set as variable modifications. Carbamidomethylation of cysteines (+57021 Da) was set as a fixed modification. Trypsin cleavage at arginine and lysine residues was used as enzyme specificity. For the database search, one missed cleavage was allowed. In addition, precursor ion and fragment ion mass tolerances were set to 20 ppm and 0.5 Da, respectively. A reversed database search was performed, and the false discovery rate was set to 1% for peptide

and protein identifications. Raw data and database search files are available at ProteomeXchange (identifier PXD024150) [87]. Relative quantification of identified proteins was performed by label-free quantification (LFQ) algorithm in MaxQuant.

4.8. Nanostring Analysis

RNA samples from the same tumors used for sequencing (NGS), and two further samples per group, were chosen for gene expression validation by nanostring. RNA concentrations measured by a Qubit 4 Fluorometer (Thermo Fisher Scientific, USA). RNA samples with adequate concentrations were hybridized to the customized nCounter® gene panel (NanoString, Redwood, CA, USA). The applied custom gene panel was composed of 134 genes identified by NGS as differentially expressed with the highest FC and lowest p values. Genes with no or deficient information according to the literature were excluded. Samples were transferred to the nCounter Prep Station for further processing. The gene expression profiles of the samples were digitized with the nCounter Digital Analyzer. Results were quantified using the nSolver 4.0 Analysis Software (NanoString, Redwood, CA, USA). Background was determined with synthetic negative probes provided by the Nanostring company, calculating the background level at maximum negative control count number.

4.9. Statistical Analysis

GraphPad Prism software (v.6.01; GraphPad Software, Inc., La Jolla, CA, USA) was applied for statistical analysis. Unpaired Mann-Whitney nonparametric tests were performed in the comparison of sham and mEHT treated groups. Follow-up examinations were statistically evaluated with two-way ANOVA with Bonferroni correction. Differences were considered statistically significant as * $p < 0.05$, ** $p < 0.01$, *** $p < 0.001$, **** $p < 0.0001$. Data are presented as mean ± SEM.

5. Conclusions

Here, we demonstrated that modulated electro-hyperthermia (mEHT) effectively inhibited tumor growth and proliferation. Moreover, mEHT activated several stress response genes such as members of the heat shock response, complement factors such as C4, fibrinogens, haptoglobin and pentraxin, locally in the tumor. Applying KRIBB11 + mEHTin combination may have a synergistic effect in vivo, potentiating mEHT's antitumor effects. Therefore this will be the focus of our future work. Inhibition of these protective mechanisms has the potential to enhance the effectivity of anticancer therapies, including mEHT and other clinically applied, traditional treatment modalities like chemo, radio and immunotherapy.

Supplementary Materials: The following are available online at https://www.mdpi.com/article/10.3390/cancers13071744/s1, Figure S1. Hematoxylin-eosin (HE) and cleaved caspase-3 (cC3) immunohistochemistry stained sections of all tumors by groups, 24 h after the fifth mEHT treatment. Figure S2. Heat map dendogram of the differentially expressed (DE) genes with labels after 3 mEHT treatments. Figure S3. Tumor volumes measured by ultrasound at randomization (day 6 after inoculation). Table S1. Upregulated genes in the response to stimulus pathway as identified by the gene ontology (GO) analysis. Table S2. Upregulated genes in stress response related pathways as identified by the gene ontology (GO) analysis.

Author Contributions: L.D., C.A.S., T.K. (Tamás Kaucsár) and P.H. conceived and designed the experiments. L.D., C.A.S., T.K. (Tamás Kaucsár), T.V., P.V. and T.K. (Tibor Krenács) performed the experiments and analyzed the results. L.D., R.V., M.F., A.G., J.K. and Á.N. performed the multiplex studies and bioinformatical analysis. R.B., Á.N., P.V., J.K. and C.A.S. analyzed the multiplex results. L.D., C.A.S., T.K. (Tibor Krenács) and P.H. discussed the results and wrote the manuscript. P.H. and Z.B. provided the financial contribution. All authors have read and agreed to the published version of the manuscript.

Funding: This work was funded by the Hungarian National Research, Development and Innovation Office (NVKP_16-1-2016-0042, K-112964, K-125174, ANN-110810, SNN-114619) as well as by the Higher Education Institutional Excellence Program of the Ministry of Human Capacities in Hungary, within the framework of the Molecular Biology Thematic Program of the Semmelweis University, the EFOP-3.6.3-VEKOP-16-2017-00009 grant, András Korányi Foundation, Semmelweis Fund for Science and Innovation (139610/TMI/2020) and Cooperative Doctoral Program of National Research, Development and Innovational Office, Hungary. Further support was provided by GINOP-2.3.4-15-2020-00010, GINOP-2.3.1-20-2020-00001 and Educating Experts of the Future: Developing Bioinformatics and Biostatistics competencies of European Biomedical Students (BECOMING, 2019-1-HU01-KA203-061251). The bioinformatics infrastructure was supported by ELIXIR Hungary (http://elixir-hungary.org/, accessed on 15 March 2021).

Institutional Review Board Statement: The study was conducted according to the Hungarian Laws No. XXVIII/1998 and LXXVIII/2018 about the protection and welfare of animals, and the direc-tives of the European Union. All animal procedures were approved by the National Scientific Ethical Committee on Animal Experimentation and Semmelweis University's AnimalWelfare Committee under the No. PE/EA/50-2/2019 (date of approval: 1 November 2019).

Informed Consent Statement: Not applicable because here we report the results of animal studies, patients were not involved.

Data Availability Statement: Data available in a publicly accessible repository that does not issue DOIs. Publicly available datasets were analyzed in this study. This data can be found here: NGS: https: //www.ebi.ac.uk/ena, accession number: PRJEB43813; MS: http://www.proteomexchange.org/, identifier: PXD024150.

Acknowledgments: The authors wish to thank Erzsébet Fejes for careful language editing of the text, Éva Mátrainé Balogh for her expert technical assistance and Oncotherm Ltd. (Budapest, Hungary) for making available the LabEHY-200 device and accessories. The research was performed in collaboration with the Genomics and Bioinformatics Core Facility at the Szentágothai Research Centre of the University of Pécs.

Conflicts of Interest: The authors declare no conflict of interest. The funders had no role in the design of the study; in the collection, analyses, or interpretation of data; in the writing of the manuscript, or in the decision to publish the results.

Abbreviations

APPs	Acute phase proteins
C4	Complement component 4
cC3	Cleaved caspase-3
DE	Differentially expressed
EMF	Electromagnetic field
FC	Fold change
H&E	Hematoxylin and eosin
HER2	Human epidermal receptor growth factor receptor 2
Hsp70	Heat shock protein 70
IHC	Immunohistochemistry
LFQ	Label-free quantification
mEHT	Modulated electro-hyperthermia
mRNA	Messenger ribonucleic acid
MS	Mass spectrometry
NGS RNA seq	Next-generation sequencing ribonucleic acid sequencing
RF	Radio frequency
RT-qPCR	Real-time quantitative polymerase chain reaction
TDR	Tissue damage ratio
TNBC	Triple-negative breast cancer

References

1. Danics, L.; Schvarcz, C.A.; Viana, P.; Vancsik, T.; Krenács, T.; Benyó, Z.; Kaucsár, T.; Hamar, P. Exhaustion of protective heat shock response induces significant tumor damage by apoptosis after modulated electro-hyperthermia treatment of triple negative breast cancer isografts in mice. Cancers 2020, 12, 2581.
2. Szasz, A.M.; Minnaar, C.A.; Szentmártoni, G.; Szigeti, G.P.; Dank, M. Review of the clinical evidences of modulated electrohyperthermia (mEHT) method: An update for the practicing oncologist. Front. Oncol. 2019, 9, 1012.
3. Lee, S.Y.; Lee, N.R.; Cho, D.-H.; Kim, J.S. Treatment outcome analysis of chemotherapy combined with modulated electrohyperthermia compared with chemotherapy alone for recurrent cervical cancer, following irradiation. Oncol. Lett. 2017, 14, 73–78.
4. Ranieri, G.; Ferrari, C.; Di Palo, A.; Marech, I.; Porcelli, M.; Falagario, G.; Ritrovato, F.; Ramunni, L.; Fanelli, M.; Rubini, G.; et al. Bevacizumab-based chemotherapy combined with regional deep capacitive hyperthermia in metastatic cancer patients: A pilot study. Int. J. Mol. Sci. 2017, 18, 1458.
5. Ranieri, G.; LaFace, C.; Laforgia, M.; De Summa, S.; Porcelli, M.; Macina, F.; Ammendola, M.; Molinari, P.; Lauletta, G.; Di Palo, A.; et al. Bevacizumab plus FOLFOX-4 combined with deep electro-hyperthermia as first-line therapy in metastatic colon cancer: A pilot study. Front. Oncol. 2020, 10, 590707.
6. Minnaar, C.A.; Szigeti, G.P.; Kotzen, J.A.; Baeyens, A. Modulated electro-hyperthermia as a monotherapy: A potential for further research? Oncothermia J. 2018, 24, 303–317.
7. Blad, B.; Wendel, P.; Jonsson, M.; Lindstrom, K. An electrical impedance index to distinguish between normal and cancerous tissues. J. Med. Eng. Technol. 1999, 23, 57–62.
8. Vander Heiden, M.G.; Cantley, L.C.; Thompson, C.B. Understanding the Warburg effect: The metabolic requirements of cell proliferation. Science 2009, 324, 1029–1033.
9. Meggyesházi, N.; Andocs, G.; Balogh, L.; Balla, P.; Kiszner, G.; Teleki, I.; Jeney, A.; Krenács, T. DNA fragmentation and caspaseindependent programmed cell death by modulated electrohyperthermia. Strahlenther. Onkol. 2014, 190, 815–822.
10. Szasz, A.; Szasz, N.; Szasz, O. Oncothermia: Principles and Practices; Springer: Dordrecht, The Netherlands, 2011.
11. Vancsik, T.; Kovago, C.; Kiss, E.; Papp, E.; Forika, G.; Benyo, Z.; Meggyeshazi, N.; Krenacs, T. Modulated electro-hyperthermia induced loco-regional and systemic tumor destruction in colorectal cancer allografts. J. Cancer 2018, 9, 41–53.
12. Thomas, M.J.; Major, E.; Benedek, A.; Horváth, I.; Máthé, D.; Bergmann, R.; Szász, A.M.; Krenács, T.; Benyó, Z. Suppression of metastatic melanoma growth in lung by modulated electro-hyperthermia monitored by a minimally invasive heat stress testing approach in mice. Cancers 2020, 12, 3872.
13. Ahmad, A. breast cancer statistics: Recent trends. Adv. Exp. Med. Biol. 2019, 1152, 1–7.
14. Foulkes, W.D.; Smith, I.E.; Reis-Filho, J.S. Triple-negative breast cancer. N. Engl. J. Med. 2010, 363, 1938–1948.
15. Le, M.T.N.; Hamar, P.; Guo, C.; Basar, E.; Perdigão-Henriques, R.; Balaj, L.; Lieberman, J. miR-200–containing extracellular vesicles promote breast cancer cell metastasis. J. Clin. Investig. 2014, 124, 5109–5128.
16. DuPre, S.A.; Redelman, D.; Hunter, K.W., Jr. The mouse mammary carcinoma 4T1: Characterization of the cellular landscape of primary tumours and metastatic tumour foci. Int. J. Exp. Pathol. 2007, 88, 351–360.
17. Aslakson, C.J.; Miller, F.R. Selective events in the metastatic process defined by analysis of the sequential dissemination of subpopulations of a mouse mammary tumor. Cancer Res. 1992, 52, 1399–1405.
18. Dykxhoorn, D.M.;Wu, Y.; Xie, H.; Yu, F.; Lal, A.; Petrocca, F.; Martinvalet, D.; Song, E.; Lim, B.; Lieberman, J. miR-200 enhances mouse breast cancer cell colonization to form distant metastases. PLoS ONE 2009, 4, e7181.
19. Shishido, S.N.; Varahan, S.; Yuan, K.; Li, X.; Fleming, S.D. Humoral innate immune response and disease. Clin. Immunol. 2012, 144, 142–158.
20. Han, Y.; Mao, F.; Wu, Y.; Fu, X.; Zhu, X.; Zhou, S.; Zhang, W.; Sun, Q.; Zhao, Y. Prognostic role of c-reactive protein in breast cancer: A systematic review and meta-analysis. Int. J. Biol. Markers 2011, 26, 209–215.
21. Róka, B.; Tod, P.; Kaucsár, T.; Vizovišek, M.; Vidmar, R.; Turk, B.; Fonovi´c, M.; Szénási, G.; Hamar, P. The acute phase response is a prominent renal proteome change in sepsis in mice. Int. J. Mol. Sci. 2019, 21, 200.
22. Iwaniec, J.; Robinson, G.P.; Garcia, C.K.; Murray, K.O.; De Carvalho, L.; Clanton, T.L.; Laitano, O. Acute phase response to exertional heat stroke in mice. Exp. Physiol. 2020, 106, 222–232.
23. Roumenina, L.T.; Daugan, M.V.; Petitprez, F.; Sautès-Fridman, C.; Fridman, W.H. Context-dependent roles of complement in cancer. Nat. Rev. Cancer 2019, 19, 698–715.
24. Conrad, D.M.; Hoskin, D.W.; Liwski, R.; Naugler, C. A re-examination of the role of the acute phase protein response in innate cancer defence. Med. Hypotheses 2016, 93, 93–96.
25. Rutkowski, M.J.; Sughrue, M.E.; Kane, A.J.; Mills, S.A.; Parsa, A.T. Cancer and the complement cascade. Mol. Cancer Res. 2010, 8, 1453–1465.

26. Pio, R.; Ajona, D.; Lambris, J.D. Complement inhibition in cancer therapy. Semin. Immunol. 2013, 25, 54–64.
27. Chen, J.; Cheuk, I.W.-Y.; Siu, M.-T.; Yang, W.; Cheng, A.S.; Shin, V.Y.; Kwong, A. Human haptoglobin contributes to breast cancer oncogenesis through glycolytic activity modulation. Am. J. Cancer Res. 2020, 10, 2865–2877.
28. Liu, Y.-L.; Yan, Z.-X.; Xia, Y.; Xie, X.-Y.; Shi, Y.-L.; Zhou, K.; Xu, L.-L.; Cui, C.-X.; Wang, Q.; Bi, J. Ligustrazine reverts anthracycline chemotherapy resistance of human breast cancer by JAK2/STAT3 signaling inhibition and decreased fibrinogen gamma chain (FGG) expression. Am. J. Cancer Res. 2020, 10, 939–952.
29. Serganova, I.; Rizwan, A.; Ni, X.; Thakur, S.B.; Vider, J.; Russell, J.; Blasberg, R.; Koutcher, J.A. Metabolic imaging: A link between lactate dehydrogenase a, lactate, and tumor phenotype. Clin. Cancer Res. 2011, 17, 6250–6261.
30. Tsang, Y.-W.; Chi, K.-H.; Huang, C.-C.; Chi, M.-S.; Chiang, H.-C.; Yang, K.-L.; Li, W.-T.; Wang, Y.-S. Modulated electrohyperthermia-enhanced liposomal drug uptake by cancer cells. Int. J. Nanomed. 2019, 14, 1269–1279.
31. Tsang, Y.-W.; Huang, C.-C.; Yang, K.-L.; Chi, M.-S.; Chiang, H.-C.; Wang, Y.-S.; Andocs, G.; Szasz, A.; Li, W.-T.; Chi, K.-H. Improving immunological tumor microenvironment using electro-hyperthermia followed by dendritic cell immunotherapy. BMCCancer 2015, 15, 708.
32. Qin, W.; Akutsu, Y.; Andocs, G.; Suganami, A.; Hu, X.; Yusup, G.; Komatsu-Akimoto, A.; Hoshino, I.; Hanari, N.; Mori, M.; et al. Modulated electro-hyperthermia enhances dendritic cell therapy through an abscopal effect in mice. Oncol. Rep. 2014, 32, 2373–2379.
33. Jeon, T.-W.; Yang, H.; Lee, C.G.; Oh, S.T.; Seo, D.; Baik, I.H.; Lee, E.H.; Yun, I.; Park, K.R.; Lee, Y.-H. Electro-hyperthermia up-regulates tumour suppressor Septin 4 to induce apoptotic cell death in hepatocellular carcinoma. Int. J. Hyperth. 2016, 32, 648–656.
34. Cha, J.; Jeon, T.-W.; Lee, C.G.; Oh, S.T.; Yang, H.-B.; Choi, K.-J.; Seo, D.; Yun, I.; Baik, I.H.; Park, K.R.; et al. Electro-hyperthermia inhibits glioma tumorigenicity through the induction of E2F1-mediated apoptosis. Int. J. Hyperth. 2015, 31, 784–792.
35. Mold, C.; Baca, R.; Du Clos, T.W. Serum amyloid p component and c-reactive protein opsonize apoptotic cells for phagocytosis through Fc receptors. J. Autoimmun. 2002, 19, 147–154.
36. Rovere, P.; Peri, G.; Fazzini, F.; Bottazzi, B.; Doni, A.; Bondanza, A.; Zimmermann, V.S.; Garlanda, C.; Fascio, U.; Sabbadini, M.G.; et al. The long pentraxin PTX3 binds to apoptotic cells and regulates their clearance by antigen-presenting dendritic cells. Blood 2000, 96, 4300–4306.
37. Merle, N.S.; Noe, R.; Halbwachs-Mecarelli, L.; Fremeaux-Bacchi, V.; Roumenina, L.T. Complement system part II: Role in immunity. Front. Immunol. 2015, 6, 257.
38. Simões, R.V.; Serganova, I.S.; Kruchevsky, N.; Leftin, A.; Shestov, A.A.; Thaler, H.T.; Sukenick, G.; Locasale, J.W.; Blasberg, R.G.; Koutcher, J.A.; et al. Metabolic plasticity of metastatic breast cancer cells: Adaptation to changes in the microenvironment.Neoplasia 2015, 17, 671–684.
39. Xie, B.; Stammes, M.A.; Van Driel, P.B.; Cruz, L.J.; Knol-Blankevoort, V.T.; Löwik, M.A.; Mezzanotte, L.; Que, I.; Chan, A.; van den Wijngaard, J.P.; et al. Necrosis avid near infrared fluorescent cyanines for imaging cell death and their use to monitor therapeutic efficacy in mouse tumor models. Oncotarget 2015, 6, 39036–39049.
40. Yang, Y.; Yang, H.H.; Hu, Y.; Watson, P.H.; Liu, H.; Geiger, T.R.; Anver, M.R.; Haines, D.C.; Martin, P.; Green, J.E.; et al. Immunocompetent mouse allograft models for development of therapies to target breast cancer metastasis. Oncotarget 2017, 8, 30621–30643.
41. Tao, K.; Fang, M.; Alroy, J.; Sahagian, G.G. Imagable 4T1 model for the study of late stage breast cancer. BMC Cancer 2008, 8, 228.
42. Bredholt, G.; Mannelqvist, M.; Stefansson, I.M.; Birkeland, E.; Bø, T.H.; Oyan, A.M.; Trovik, J.; Kalland, K.-H.; Jonassen, I.; Salvesen, H.B.; et al. Tumor necrosis is an important hallmark of aggressive endometrial cancer and associates with hypoxia, angiogenesis and inflammation responses. Oncotarget 2015, 6, 39676–39691.
43. Milross, C.G.; Tucker, S.L.; Mason, K.A.; Hunter, N.R.; Peters, L.J.; Las, L.M. the effect of tumor size on necrosis and polarographically measured pO2. Acta Oncol. 1997, 36, 183–189.
44. Lee, S.Y.; Ju, M.K.; Jeon, H.M.; Jeong, E.K.; Lee, Y.J.; Kim, C.H.; Park, H.G.; Han, S.I.; Kang, H.S. Regulation of tumor progression by programmed necrosis. Oxid. Med. Cell. Longev. 2018, 2018, 3537471.
45. Wang, W.; Wu, J.; Zhang, P.; Fei, X.; Zong, Y.; Chen, X.; Huang, O.; He, J.-R.; Chen, W.; Li, Y.; et al. Prognostic and predictive value of Ki-67 in triple-negative breast cancer. Oncotarget 2016, 7, 31079–31087.
46. Soliman, N.A.; Yussif, S.M. Ki-67 as a prognostic marker according to breast cancer molecular subtype. Cancer Biol. Med. 2016, 13, 496–504.
47. Inwald, E.C.; Klinkhammer-Schalke, M.; Hofstädter, F.; Zeman, F.; Koller, M.; Gerstenhauer, M.; Ortmann, O. Ki-67 is a prognostic parameter in breast cancer patients: Results of a large population-based cohort of a cancer registry. Breast Cancer Res. Treat. 2013, 139, 539–552.
48. Gruys, E.; Toussaint, M.; Niewold, T.; Koopmans, S. Acute phase reaction and acute phase proteins. J. Zhejiang Univ. Sci. B 2005, 6, 1045–1056.

49. Aldred, A.R.; Southwell, B.; Schreiber, G. Extrahepatic synthesis of acute phase proteins and their functions. Folia Histochem. Cytobiol. 1992, 30, 223–232.
50. Gabay, C.; Kushner, I. Acute-phase proteins. eLS 2001.
51. Kalmovarin, N.; Friedrichs, W.E.; O'Brien, H.V.; Linehan, L.A.; Bowman, B.H.; Yang, F. Extrahepatic expression of plasma protein genes during inflammation. Inflammation 1991, 15, 369–379.
52. D'Armiento, J.; Dalal, S.S.; Chada, K. Tissue, temporal and inducible expression pattern of haptoglobin in mice. Gene 1997, 195, 19–27.
53. Korbelik, M.; Cecic, I.; Merchant, S.; Sun, J. Acute phase response induction by cancer treatment with photodynamic therapy. Int. J. Cancer 2007, 122, 1411–1417.
54. Pang, W.W.; Abdul-Rahman, P.S.; Wan-Ibrahim, W.I.; Hashim, O.H. Can the acute-phase reactant proteins be used as cancer biomarkers? Int. J. Biol. Markers 2010, 25, 1–11.
55. Prins, A. Proteases and Protease Inhibitors Involved in Plant Stress Response and Acclimation. Ph.D. Thesis, University of Pretoria, Pretoria, South Africa, 2008.
56. Chelbi, S.T.; Wilson, M.L.; Veillard, A.-C.; Ingles, S.A.; Zhang, J.; Mondon, F.; Gascoin-Lachambre, G.; Doridot, L.; Mignot, T.-M.; Rebourcet, R.; et al. Genetic and epigenetic mechanisms collaborate to control SERPINA3 expression and its association with placental diseases. Hum. Mol. Genet. 2012, 21, 1968–1978.
57. Cao, L.-L.; Pei, X.-F.; Qiao, X.; Yu, J.; Ye, H.; Xi, C.-L.;Wang, P.-Y.; Gong, Z.-L. SERPINA3 silencing inhibits the migration, invasion, and liver metastasis of colon cancer cells. Dig. Dis. Sci. 2018, 63, 2309–2319.
58. Yang, G.D.; Yang, X.M.; Lu, H.; Ren, Y.; Ma, M.Z.; Zhu, L.Y.; Wang, J.H.; Song,W.W.; Zhang,W.M.; Zhang, R.; et al. SERPINA3 promotes endometrial cancer cells growth by regulating G2/M cell cycle checkpoint and apoptosis. Int. J. Clin. Exp. Pathol. 2014, 7, 1348–1358.
59. Zhou, J.; Cheng, Y.; Tang, L.; Martinka, M.; Kalia, S. Up-regulation of SERPINA3 correlates with high mortality of melanoma patients and increased migration and invasion of cancer cells. Oncotarget 2017, 8, 18712–18725.
60. Swiderski, R.E.; Nishimura, D.Y.; Mullins, R.F.; Olvera, M.A.; Ross, J.L.; Huang, J.; Stone, E.M.; Sheffield, V.C. Gene expression analysis of photoreceptor cell loss in Bbs4-knockout mice reveals an early stress gene response and photoreceptor cell damage. Investig. Ophthalmol. Vis. Sci. 2007, 48, 3329–3340.
61. Gueugneau, M.; D'Hose, D.; Barbé, C.; De Barsy, M.; Lause, P.; Maiter, D.; Bindels, L.B.; Delzenne, N.M.; Schaeffer, L.; Gangloff, Y.-G.; et al. Increased Serpina3n release into circulation during glucocorticoid-mediated muscle atrophy. J. Cachex-Sarcopenia Muscle 2018, 9, 929–946.
62. Trosseau, A. Phlegmatia alba dolens. In Clinique Médicale de l'Hôtel-Dieu de Paris, 2nd ed.; Librarie J.-B. Billiere et Fils: Paris, France, 1865; Volume 3, pp. 654–712.
63. Vilar, R.; Fish, R.J.; Casini, A.; Neerman-Arbez, M. Fibrin(ogen) in human disease: Both friend and foe. Haematologica 2020, 105, 284–296.
64. Rybarczyk, B.J.; Simpson-Haidaris, P.J. Fibrinogen assembly, secretion, and deposition into extracellular matrix by MCF-7 human breast carcinoma cells. Cancer Res. 2000, 60, 2033–2039.
65. Simpson-Haidaris, P.J.; Rybarczyk, B. Tumors and fibrinogen. The role of fibrinogen as an extracellular matrix protein. Ann. N. Y. Acad. Sci. 2001, 936, 406–425.
66. Rifkind, J.M.; Mohanty, J.G.; Enagababu, E. The pathophysiology of extracellular hemoglobin associated with enhanced oxidative reactions. Front. Physiol. 2014, 5, 500.
67. Lebegge, E.; Arnouk, S.M.; Bardet, P.M.R.; Kiss, M.; Raes, G.; Van Ginderachter, J.A. Innate immune defense mechanisms by myeloid cells that hamper cancer immunotherapy. Front. Immunol. 2020, 11, 1395.
68. Yang, Y.; Chung, E.K.; Zhou, B.; Blanchong, C.A.; Yu, C.Y.; Füst, G.; Kovács, M.; Vatay, Á.; Szalai, C.; Karádi, I.; et al. Diversity in intrinsic strengths of the human complement system: Serum C4 protein concentrations correlate with C4 gene size and polygenic variations, hemolytic activities, and body mass index. J. Immunol. 2003, 171, 2734–2745.
69. Roumenina, L.T.; Rayes, J.; Frimat, M.; Fremeaux-Bacchi, V. Endothelial cells: Source, barrier, and target of defensive mediators. Immunol. Rev. 2016, 274, 307–329.
70. Markiewski, M.M.; DeAngelis, R.A.; Benencia, F.; Ricklin-Lichtsteiner, S.K.; Koutoulaki, A.; Gerard, C.; Coukos, G.; Lambris, J.D. Modulation of the antitumor immune response by complement. Nat. Immunol. 2008, 9, 1225–1235.
71. Zafar, G.I.; Grimm, E.A.; Wei, W.; Johnson, M.M.; Ellerhorst, J.A. Genetic deficiency of complement isoforms C4A or C4B predicts improved survival of metastatic renal cell carcinoma. J. Urol. 2009, 181, 1028–1034.
72. Nishioka, K.; Kawamura, K.; Hirayama, T.; Kawashima, T.; Shimada, K.; Kogure, M. The complement system in tumor immunity: Significance of elevated levels of complement in tumor bearing hosts. Ann. N. Y. Acad. Sci. 1976, 276, 303–315.
73. Wang, H.; Li, Y.; Shi, G.;Wang, Y.; Lin, Y.;Wang, Q.; Zhang, Y.; Yang, Q.; Dai, L.; Cheng, L.; et al. A Novel antitumor strategy: Simultaneously inhibiting angiogenesis and complement by targeting VEGFA/PlGF and C3b/C4b. Mol. Ther. Oncolytics 2020, 16, 20–29.

74. Hwang, N.; Kwon, M.-Y.; Woo, J.M.; Chung, S.W. Oxidative stress-induced pentraxin 3 expression human retinal pigment epithelial cells is involved in the pathogenesis of age-related macular degeneration. Int. J. Mol. Sci. 2019, 20, 6028.
75. Haapasalo, K.; Meri, S. Regulation of the complement system by pentraxins. Front. Immunol. 2019, 10, 1750.
76. Giacomini, A.; Ghedini, G.C.; Presta, M.; Ronca, R. Long pentraxin 3: A novel multifaceted player in cancer. Biochim. Biophys. Acta Rev. Cancer 2018, 1869, 53–63.
77. Song, T.; Wang, C.; Guo, C.; Liu, Q.; Zheng, X. Pentraxin 3 overexpression accelerated tumor metastasis and indicated poor prognosis in hepatocellular carcinoma via driving epithelial-mesenchymal transition. J. Cancer 2018, 9, 2650–2658.
78. Ying, T.-H.; Lee, C.-H.; Chiou, H.-L.; Yang, S.-F.; Lin, C.-L.; Hung, C.-H.; Tsai, J.-P.; Hsieh, Y.-H. Knockdown of Pentraxin 3 suppresses tumorigenicity and metastasis of human cervical cancer cells. Sci. Rep. 2016, 6, 29385.
79. Pulaski, B.A.; Ostrand-Rosenberg, S. Mouse 4T1 breast tumor model. Curr. Protoc. Immunol. 2001, 39, 20.2.1–20.2.16.
80. Dobin, A.; Davis, C.A.; Schlesinger, F.; Drenkow, J.; Zaleski, C.; Jha, S.; Batut, P.; Chaisson, M.; Gingeras, T.R. STAR: Ultrafast universal RNA-seq aligner. Bioinformatics 2013, 29, 15–21.
81. Anders, S.; Pyl, P.T.; Huber,W. HTSeq—A Python framework to work with high-throughput sequencing data. Bioinformatics 2015, 31, 166–169.
82. Robinson, M.D.; McCarthy, D.J.; Smyth, G.K. edgeR: A Bioconductor package for differential expression analysis of digital gene expression data. Bioinformatics 2010, 26, 139–140.
83. Law, C.W.; Chen, Y.; Shi,W.; Smyth, G.K. voom: Precision weights unlock linear model analysis tools for RNA-seq read counts. Genome Biol. 2014, 15, R29.
84. Ritchie, M.E.; Phipson, B.; Wu, D.; Hu, Y.; Law, C.W.; Shi, W.; Smyth, G.K. limma powers differential expression analyses for RNA-sequencing and microarray studies. Nucleic Acids Res. 2015, 43, e47.
85. Babicki, S.; Arndt, D.; Marcu, A.; Liang, Y.; Grant, J.R.; Maciejewski, A.; Wishart, D.S. Heatmapper: Web-enabled heat mapping for all. Nucleic Acids Res. 2016, 44, W147–W153. 86. Cox, J.; Mann, M. MaxQuant enables high peptide identification rates, individualized p.p.b.-range mass accuracies and proteomewide protein quantification. Nat. Biotechnol. 2008, 26, 1367–1372.
87. Deutsch, E.W.; Csordas, A.; Sun, Z.; Jarnuczak, A.; Perez-Riverol, Y.; Ternent, T.; Campbell, D.S.; Bernal-Llinares, M.; Okuda, S.; Kawano, S.; et al. The ProteomeXchange consortium in 2017: Supporting the cultural change in proteomics public data deposition. Nucleic Acids Res. 2017, 45, D1100–D1106.

Clinical study of modulated electro hyperthermia for advanced metastatic breast cancer

Takuya Nagata, Masahiko Kanamori, Shinichi Sekine, Mie Ara, Makoto Moriyamas and Tsutomu Fujii

Department of Surgery, Toho University Ohashi Medical Center, Tokyo 153-8515
Department of Human Science, University of Toyama, Toyama 930-0194
Department of Surgery, Kamiichi General Hospital, Toyama 930-0391
Department of Surgery, Toyama Nishi General Hospital, Toyama 939-2716
Department of Surgery, Tomei Atsugi Hospital, Kanagawa 243-8571
Department of Science and Surgery, University of Toyama, Toyama 930-0194, Japan

Cite this article as:
Nagata T. et al. (2021): Clinical study of modulated electro hyperthermia for advanced metastatic breast cancer, Molecular and Clinical Oncology 14, 2021, Artical number: 103; Pages 1-7.
https://www.spandidos-publications.com/10.3892/mco.2021.2265

Oncothermia Journal 31, 2022 March: 32-41
www.oncotherm.com/sites/oncotherm/files/2022-03/Nagata_Clinical.pdf

Patients and methods

Patients. Ten patients with advanced or recurrent breast cancer participated in the present study since November 2015. All patients had undergone conventional therapies following standard protocols for breast cancer. Patients received hormonal therapy, external irradiation, surgery, various chemotherapies, targeted molecular treatment, and other available state of the art therapies (15). The selected patients were treated with mEHT coupled with adjuvant therapies (chemotherapy, hormone therapy or irradiation) when possible (6 cases); in case of complete failure of conventional methods, monotherapy was used (4 cases). The adjuvant therapies were trastuzumab emtansine (TDM-1; 1 case), mammalian target of rapamycin (mTOR; 3 cases), eribulin (1 case), irradiation (1 case) and fulvestrant (1 case). The study was approved by the local ethics committee of the University of Toyama (approval no. 26-13), and the patients provided written consent for the treatment, as well as for the research and publication of their data and images.

Procedure of mEHT. mEHT was performed twice a week in 7 patients and thrice a week in the other 3. The session lasted for ~60 min, with at least 1 day in between. The treatment was performed using the EHY2000+ device (Oncotherm Kft.). The electrode used was 30 cm in diameter. Patients were placed in the supine position on the water mattress of the treatment bed. A step-up heating protocol was used, starting with 60 W, which was then increased to 140 W. The average number of treatments performed per patient was 48.6 (range, 8-90). The average dose of 374.6 (range, 371-376) kJ was administered.

Procedure and display of the analytical results. The endpoint of the study was local control (response rate). A follow-up examination of local control was conducted via inspection, computed tomography (CT), or magnetic resonance imaging, and was compared with that at baseline before the start of the mEHT treatment process. The age, estrogen receptor (ER)/progesterone receptor (PgR)/human epidermal growth factor receptor type 2 (HER2) status, actual status of metastases, and pretreatment for each patient are shown in Table I. The number and duration of mEHT sessions and the total amount of mEHT energy delivered to each patient are summarized in Table II. The complementary therapies and local responses are shown in Table III. The statistical analysis results are shown in Table IV.

Statistical analysis. The comparison of the distribution between the two groups of partial response (PR)+stable disease (SD) cases and progressive disease (PD) cases was conducted using unpaired t-test for continuous variables [age, total mEHT, mEHT/w, mEHT period, mEHT dose, pre-treatment, pre-CT, pre-carcinoembryonic antigen (CEA) and post-CEA] and the Mann-Whitney test for categorical variables (Stage). $P<0.05$ was considered to indicate a statistically significant difference. All analyses were performed using the JMP15.0 software.

Results

Statistics of mEHT. Out of the 10 cases registered, 5 were stage 3 or 4 preoperatively (Table I). The ER status was positive in all cases, and HER2 was positive in 1 case. In 9/10 cases, some treatments were performed before mEHT; however, due to the lack of a satisfactory antitumor effect, mEHT was performed or combined with other treatments (Table I). Case 2 received the most treatments prior to mEHT, including two types of postoperative adjuvant chemotherapy, 5 types of chemotherapy for tumor recurrence, two types of hormone therapy, and irradiation. In addition, Case 2 received two types of chemotherapy in combination with mEHT (Table III). On the other hand, Case 10 received no treatment prior to mEHT, following the patient's request. The statistics of the mEHT are shown in Table II. As a result, 8-90 mEHTs were performed. The decision to discontinue was entirely based on the request of the patient; the most common reason identified was difficulty in continuing the treatment. Case 7 underwent mEHT only 8 times. The reason for this was that the combined use of irradiation and mEHT reduced the metastatic skin cancer to PR; the patient hoped that mEHT would be terminated at the same time as the termination of irradiation. There were no apparent complications during mEHT.

Clinical estimation of the PD case. A summary of the local responses is presented in Table III. Patients felt comfortable with warming around the targeted area during treatment. The elevated body temperature observed was mild, and some patients presented with sweating without discomfort. In addition, there were no adverse effects, such as skin blisters, erythema, or dermatitis. PR was achieved in 3/10 (30%) patients, and so was SD. A total of 4/10 patients (40%) showed PD. All 3 patients (cases 2, 4 and 6) that were treated with a combination of mEHT and mTOR achieved PD. They had multiple-organ metastases from the breast cancer and had undergone multiple sessions of mEHT (46-90). Only case 2 received anthracycline and taxane for the treatment of breast cancer. Cases 4 and 6 refused chemotherapy and only approved the use of mTOR, which has relatively few side effects, such as hair loss and malaise. Therefore, these cases might have deviated from the usual treatment for advanced breast cancer and do not indicate a low therapeutic effect of the combination of mEHT and mTOR. However, 2/3 PR patients exhibited a re-increase in tumor size after the follow-up period. By contrast, another patient recovered and underwent curative surgery. At the time of writing, she was still alive with no signs of recurrence (9 months after initial mEHT therapy). A total of 4 patients judged as PD exhibited worsening of the local tumor and metastases. Three patients died of cancer during (2 patients) or after the completion of mEHT (1 patient). Case 2 was a 66-year-old woman. Bt+Ax was performed in the right breast. After administering two types of postoperative adjuvant chemotherapy, hormone therapy was performed. Five years after the operation, lung, liver and bone metastases occurred. Following recurrence, seven types of treatment were performed (five types of chemotherapy, one type of hormone therapy, and radiation therapy). In addition, case 2 received two types of chemotherapy in combination with 90 sessions of mEHT for 30 weeks. The tumor did not grow until 24 weeks after the start of treatment, but thereafter, lung metastasis gradually worsened, with the eventual occurrence of pleural effusion. Due to dyspnea, the patient could not visit the hospital; therefore, mEHT was discontinued. Three months later, the patient died of cancerous pleurisy. Case 5 was a 74-year-old woman. Bt+SLN was performed for left breast cancer. She continued hormone therapy following surgery. Three years after the operation, liver, bone and lymph node metastases occurred. Two types of chemotherapy, activated autologous lymphocyte therapy and dendritic cell vaccine therapy were then performed; however, tumor growth was observed. At her request, mEHT alone was performed for 24 weeks and 73 times without chemotherapy. The symptoms of cough and dyspnea gradually worsened, and mEHT was discontinued due to difficulty in visiting the hospital. One month later, the patient died of cancerous pleurisy. Case 7 was a 75-year-old man with skin metastasis, lung. Preoperative chemotherapy was performed for stage IV breast cancer. Although lung metastasis was reduced, skin metastasis did not change. Eight sessions of mEHT+radiation therapy were performed, and a reduction in skin metastasis was observed (PR). Following treatment, he was recommended to undergo surgery but refused. Two months after the follow-up, chest CT revealed an exacerbation of lung metastases. Although anticancer drug treatment was restarted, progressively worsening lung metastases and dyspnea were observed. The patient eventually died of cancerous pleurisy 6 months after the completion of mEHT.

Table I. Patient statistics and metastasis.

Case	Age, years	Surgery	Stage	ER	PgR	HER2	Metastasis	CT	HT	RT	Total
1	58	Bp+Ax	2A	+	+	+	Skin, lung, LN	4	1	1	6
2	66	Bt+Ax	3A	+	+	-	Lung, liver, bone	7	2	1	10
3	63	Bt+Ax	2B	+	+	-	Lung, LN	0	2	0	2
4	45	Bp+Ax	2B	+	+	-	Bone, LN	1	2	2	5
5	74	Bt+SLN	1	+	+	-	Liver, bone, LN	2	1	0	3
6	68	(-)	4	+	-	-	Lung, liver, bone	0	4	2	6
7	75	(-)	4	+	-	-	Skin, lung	3	0	1	4
8	49	Bt+Ax	4	+	+	-	Lung	0	2	0	2
9	66	Bt+Ax	2A	+	-	-	Lung, liver, bone	4	2	1	7
10	71	Bt+Ax	3A	+	+	-	Skin, muscle	0	0	0	0

Bp, partial mastectomy; Bt, total mastectomy; Ax, axillary lymph node dissection; SLN, sentinel lymph-node; ER, estrogen receptor; PgR, progesterone receptor; LN, lymph-node involvement; CT, chemotherapy; HT, hormone therapy; RT, irradiation therapy; HER2, human epidermal growth factor receptor type 2; (-), no surgical treatment; +, positive; -, negative.

Table II. Statistics of the mEHT treatments.

Case	Total mEHT, n	mEHT/w, n	mEHT period, weeks	mEHT dose, kJ
1	36	3	12	13,464
2	90	3	30	33,660
3	47	2	23.5	17,578
4	87	2	43.5	32,538
5	73	3	24.3	27,302
6	46	2	23	17,204
7	8	2	4	2,992
8	40	2	20	14,960
9	15	2	7.5	5,610
10	44	2	22	16,456

Total mEHT, total number of mEHT; mEHT/w, number of mEHT per week; mEHT period, periods of mEHT (weeks); mEHT dose, total doses of mEHT (kj); mEHT, modulated electro-hyperthermia.

mEHT monotherapy. A total of 4 patients were treated with mEHT alone, following their request. As a result, one patient showed PR, two showed SD, and one showed PD. Case 3 had undergone breast cancer surgery and postoperative chemotherapy 22 years ago, and a recurrence of lung metastases was observed 19 years later. Hormone therapy was continued; however, an exacerbation of lung metastases was observed. Nevertheless, this time, the patient refused to receive anticancer drug treatment and only mEHT was performed 47 times. During that time, chest CT revealed no exacerbation of lung metastases; therefore, the patient was judged to be SD. Case 5 had undergone breast cancer surgery 5 years ago; 2 years later, she was diagnosed with liver, bone and lymph node metastases and received chemotherapy, hormone therapy and activated dendritic cell therapy. This time, the patient refused to receive anticancer drug treatment; therefore, only mEHT was performed 73 times. During that time, the level of the tumor marker CEA was elevated and an abdominal CT revealed aggravation of liver metastases; therefore, the patient was judged as PD. Case 8 had multiple lung metastases on preoperative chest CT; however, the patient refused any treatment other than surgery; therefore, only mEHT was performed 40 times after mastectomy. During the treatment period, no obvious subjective symptoms were observed and chest CT revealed no exacerbation of lung metastases. Therefore, the patient was considered to be SD. Details regarding the status of case 10 are provided later.

Table III. Complementary therapies and local responses.

Case	Combination	Response	CEA1, ng/ml	CEA2, ng/ml
1	TDM-1	PR	8.1	5.1
2	mTOR, PTX+BV	PD	292.8	209.8
3	(-)	SD	3.6	4.5
4	mTOR, Erib., PTX+BV	PD	115.1	262.7
5	(-)	PD	12.9	45.1
6	mTOR	PD	145.5	624.8
7	irradiation	PR	3.7	3.8
8	(-)	SD	3.2	3.5
9	AI, Fulvestrant	SD	3.9	4.0
10	(-)	PR	10.6	2.1

mTOR, mammalian target of rapamycin; TDM-1, Trastuzumab emtansine; Erib, Eribulin; PTX, Pacritaxel; BV, Bevasitsuzumab; AI, Aromatase inhibitor; PR, partial remission; SD, stable disease; PD, progressive disease; CEA, Carcinoembryonic antigen; (-), no combination therapy.

Statistical evaluation of mEHT. Univariate analysis of the number of various treatments performed before mEHT and their therapeutic effects are shown in Table IV. PD patients received more types of treatments before mEHT than PR+SD patients. CEA levels before and after mEHT were significantly higher in PD patients than in PR+SD patients (P=0.017, 0.009), and mEHT was performed in patients with more advanced cancer. Statistical analysis of the various parameters of mEHT and their therapeutic effects are shown in Table IV. The average number of treatments for PR+SD patients (6 cases) was 31.6 times, and the treatment period 14.8 weeks, which was significantly less than that for PD cases (number of treatments, 74.0; treatment period, 30.2 weeks; P=0.002). There were many advanced cancer patients with PD, and mEHT was often performed in combination with chemotherapy (75%); however, no clear mEHT-related side effects were observed, and treatment for long periods was possible.

Clinical estimation of the PR cases. Showing the details, 2 PR cases are described. The PR cases 1, 7 and 10 had progression-free survival rates of 2, 7 and 9 months, respectively.

Case 1. Seven years ago, a 58-year-old woman visited our hospital due to left breast cancer recurrence. The TNM classification was T1N1M0 stage IIA at that time. Breast-conserving operation and additional dissection of left axillary lymph nodes were performed. However, the patient (then aged 65 years old) developed lung, skin and lymph node metastases. She was positive for the expression of HER2, ER and PgR. Postoperative radiation therapy (55 Gy) was performed on the left residual breast tumor area, and 50 Gy radiotherapy on the left clavicular region. Hormone therapy (aromatase inhibitor) was continued after the completion of radiation therapy. A fluorodeoxyglucose-positron emission tomography scan revealed left chest wall skin invasion (or metastasis). Left cervical, subclavian and right axillary lymph node metastases were also observed. Although intravenous chemotherapy of trastuzumab was administered, metastatic skin lesions did not respond to these treatments. Combination chemotherapy with trastuzumab, pertuzumab and docetaxel was administered; however, intolerable diarrhea occurred. Since an exacerbation of skin metastasis was observed after this treatment, the drug was changed to TDM-1. However, there was no improvement in the skin lesions (Fig. 1A). Finally, mEHT was used for adjuvant therapy using TDM-1. As a result of the combination of anticancer drug treatment (TDM-1) once every 3 weeks and mEHT thrice a week, a marked improvement in skin invasion and metastases was observed (Fig. 1B). During mEHT, right axillary lymph node metastasis was also reduced without direct intervention. However, the tumor re-increased after 2 months of post-treatment evaluation. The

tumor metastasized to the brachial plexus. The patient was alive with disease 1.2 years after the final mEHT treatment.

Table IV. Results of statistical analysis.

Factor	PR+SD	PD	P-value
Age, years	63.6	63.3	0.953
Stage			0.737
1	0	1	
2	3	1	
3	1	1	
4	2	1	
Total mEHT, n	31.6	74.0	0.006
mEHT/w, n	2.0	2.5	0.312
mEHT period, weeks	14.8	30.2	0.002
mEHT dose, kJ	11,843	27,676	0.002
Pre-treat, total	3.5	6.0	0.199
Pre-CT, n	1.8	2.5	0.689
Pre-CEA, ng/ml	5.51	141.5	0.017
Post-CEA, ng/ml	3.85	285.6	0.009

Total mEHT, total number of mEHT; mEHT/w, number of mEHT per week; mEHT period, periods of mEHT (weeks); mEHT dose, total doses of mEHT (kj); pre-treat, number of treatments before mEHT; pre-CT, number of chemotherapies before mEHT; pre-CEA, CEA before of mEHT; post-CEA, CEA after mEHT; PR, partial remission; SD, stable disease; PD, progressive disease; mEHT, modulated electro-hyperthermia.

Case 10. A 71-year-old woman had observed the presence of a mass in her right breast for >15 years but decided to ignore it. Two years ago, she was referred to our university hospital for the assessment of apparent discharge and bleeding from the protruding right breast mass. The definite diagnosis was breast cancer. The patient was recommended to undergo chemotherapy, hormone therapy and radiation therapy, but she rejected these treatment plans, out of fear of developing adverse effects. Therefore, she was followed up without any treatment. However, after the tumor increased in size with exudation and a foul-smelling odor, she accepted mEHT monotherapy. At the start of mEHT, an initial blood test showed a CEA level of 10.4 ng/ml and cancer antigen 15-3 (CA 15-3) of 132 U/ml. CT and magnetic resonance imaging revealed the presence of a massive tumor measuring 15 cm in diameter in the right breast (Fig. 2A). Swelling of the axillary lymph nodes was also observed; however, distant metastasis to other organs was not detected. mEHT therapy was continued twice a week for 6 months, resulting in tumor shrinkage, as observed by CT; therefore, the patient was judged to have achieved PR (Fig. 2B). The preoperative diagnosis was T4cN3bM0 stage IIIB, which was an indication for right mastectomy (combined resection of the chest skin and partial large pectoral muscle), right axillary dissection, and second-stage skin transplantation. Intraoperative findings revealed that infiltration into the large pectoral muscle was mild and that it was possible to avoid total resection of the chest muscle. The skin with changed color was excised, and the tumor resection margin was histologically negative. The axillary lymph nodes were dissected to level II, and it was evaluated that only level I lymph node was positive for metastasis. The postoperative course was unremarkable, and she was discharged on postoperative day 14. The pathological diagnosis of the resected specimen was pT3N1 (level I, 2/24; level II, 0/14; level III, 0/2) M0 stage IIIA. The tumor was removed at the curative margin, due to the effectiveness of mEHT. After 3 weeks, the artificial dermis was affixed to the mastectomy part and grafting was performed from the thigh part of the patient. Postoperatively, the tumor did not reccur. The CEA level normalized to 2.1 ng/ml 1 month after the surgery. CA15-3 also normalized to 18.6 U/ml 3 months after the surgery. Nine months after the surgery, she showed no evidence of the disease (Fig. 2C).

Discussion

As the general lifestyle of people changes, the type and structure of malignant diseases also changes. The clinical course of cancer and its treatments have diversified. Furthermore, the growing of available open-access information has allowed patients to select their preferred therapies. The widely published adverse effects deter some individuals from receiving conventional therapies and favor conservative treatments with the hope of maintaining a normal life despite the occurrence of cancer. Hyperthermia is considered a less aggressive antitumor treatment strategy and sometimes could be applied even in patients who are unresponsive to conventional treatments (surgery, radiation or chemotherapy), as well as to new cancer immunotherapies, suchas checkpoint inhibitors, cancer-specific cytotoxic T lymphocytes or chimeric antigen receptor-T-cell therapy.

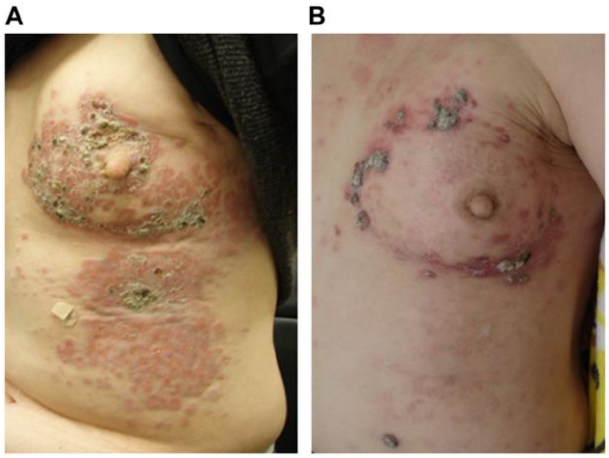

Figure 7. A representative case. (A) Exacerbation of skin metastasis from the breast cancer is presented before mEHT treatment. (B) Skin lesions responded very well to the treatment, whereas the tumor invasively penetrated into the large pectoral muscle.

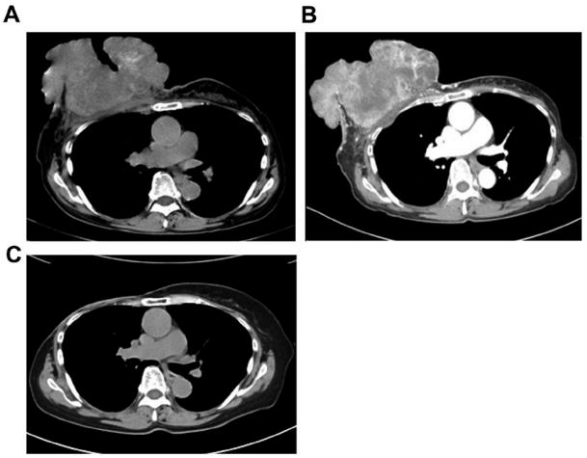

Figure 2. A second representative case. (A) CT showing the presence of a large tumor 15 cm in diameter. (B) Following mEHT treatment (twice a week), the tumor reduced in size after 6 months. (C) The tumor was removed at the curative margin due to the eff

In general, cancer cells proliferate autonomously and randomly. The cytoskeleton and genomic structure of malignant cells have an inherent instability; therefore, they are more sensitive to heat than normal cells (16). Utilizing this feature, the concept of hyperthermia has been established and various therapeutic approaches have been developed (17), including heating the lesion isothermally. Most hyperthermia methods use bio-electromagnetic energy-absorption heating of the cancer tissue of up to 43°C or higher temperatures to kill them, mainly by inducing local necrosis, such as the hyperthermia dose (CEM43°CTx) calibrated in vitro. Moreover, many experimental studies have shown that the obviously heterogenic solid tumors and their blood flow derail the developed temperature distribution, despite the use of iso-dose focusing. The usual vasodilatation that occurs in the vivid part of the tumor and its healthy neighborhood increases blood flow, possibly facilitating the delivery of chemotherapeutic drugs and increasing the reaction rate, as well improving the efficacy of ionization radiation therapies by delivering oxygen (18). Despite the advantages of high blood flow, it has several disadvantages, including delivering nutrients that support tumor growth and helping the dissemination of the malignant cells by the blood stream, thereby increasing the incidence of distant metastases (19). On the other hand, the heavily developed tumors have neo-angiogenetic vessels that form vasocontraction, increasing the severity of hypoxia and assisting rapid temperature growth in that part of the tissue (20,21). This is the reason why local control is significantly good following the use of this method; however, overall survival is decreased due to metastases (22-26).

Due to the complex physiological feedback and the attempt to re-establish thermal homeostasis by increasing blood flow, as well as by other methods, the effects of conventional hyperthermia are not stable and mostly insufficient for a lifetime increase in blood flow. At the end of the 20th day of treatment, the clinical results for

local control following radiation therapy alone vs. treatment with radiation+hyperthermia for advanced, recurrent breast cancer were reported to be 41 vs. 59%, respectively (26). Therefore, many patients and medical doctors who continue to treat various types of cancer, including advanced pancreatic cancer and other advanced cases, without further conventional treatment options are looking for a more effective therapeutic method, including the safe and secure hyperthermia treatment. Based on these backgrounds, mEHT is conducted in accordance with basic and clinical research data, which is based on the cellular selection of tumor cells, inducing programmed cell death (apoptosis), in various cancer cells by causing a temperature gradient and prompting extrinsic pathways to produce damage-associated molecular patterns (27) and immunogenic cell death (28,29), thereby producing tumor-specific immune reactions (30) and an abscopal effect (31). The inhibition of protective autophagy via sublethal hyperthermia in hepatocellular carcinoma has been shown to enhance hyperthermia-induced apoptosis via the ATP/AMPK/mTOR signaling pathway (32). Furthermore, it has been reported that the inhibition of protective autophagy could be a therapeutic strategy for RAS-induced pancreatic cancer (33). Unfortunately, the combination therapy with mTOR inhibitor and mEHT used in the present study resulted in PD in all cases; however, it is possible to continue long-term treatment for advanced breast cancer cases with multiple organ metastases. More studies with more cases are needed to explore the combined treatment of mTOR inhibitor and mEHT. The following clinical advantages have been reported from this therapeutic principle: i) Very high heating efficiency for cancer with a low power (150 W) (34); ii) modulated electromagnetic waves do not result in burns on the skin (35), and (3) these waves adequately reach tumors deep within the body, such as those in the pancreas (36), lung (37), liver (32) and cervix (38).

Due to the lack of awareness and delay in discovery, elderly patients with breast cancer are sometimes at a very progressive stage, with skin invasion or other metastases upon first diagnosis. Therefore, it is essential to consider the risks and benefits of surgery and anticancer drug treatment for these patients. When conventional therapies with standard protocols fail, only palliative care is selected after informed consent. However, mEHT is recommended as a valid option with few adverse effects for patients with advanced cancer.

In conclusion, it was reported in the present study that the use of mEHT is feasible for advanced or recurrent metastatic breast cancer where pretreatment is ineffective. The results suggested that mEHT has no side effects and could be combined with various treatments for a long time.

Acknowledgements

The authors would like to thank Professor Takashi Kondo (Division of Radiation Oncology, Department of Radiology, Faculty of Medicine, University of Toyama, Toyama, Japan) for providing medical advice for this research. The authors would also like to thank Mrs. Nagisa Isobe (Division of Oncothermia, Department of Human Science, Faculty of Medicine, University of Toyama, Toyama, Japan) for technical support in operating the mEHT system.

Funding

The current study was funded by Teteyamma Machine Co. (Toyama, Japan).

Availability of data and materials

The datasets used and/or analyzed during the current study are available from the corresponding author on reasonable request.

Authors' contributions

MK conceived and designed the study. SS, MA and MM acquired the data. TN and TF analyzed and interpreted the data. TN drafted the manuscript. MK, SS and TF performed critical revision of the manuscript. All authors read and approved the final manuscript.

Ethics approval and consent to participate

All experiments were approved by the Ethics Committee of the University of Toyama (Toyama, Japan; approval no. 26-13), and written informed consent was obtained from all participants.

Patient consent for publication

All patients provided written consent for the publication of their data and images.

Competing interests

The authors declare that they have no competing interests.

References

1. Tremont A, Lu J and Cole JT: Endocrine therapy for early breast cancer: Updated review. Ochsner J 17: 405-411, 2017.
2. Balaji K, Subramanian B, Yadav P, Radha CA and Ramasubramanian V: Radiation therapy for breast cancer: Literature review. Med Dosim 41: 253-257, 2016.
3. Cody HS III: Current surgical management of breast cancer. Curr Opin Obstet Gynecol 14: 45-52, 2002.
4. Ito Y: Chemotherapy and hormone therapy for breast cancer: Current status and perspective. JMAJ 45: 424-433, 2002.
5. Munagala R, Aqil F and Gupta RC: Promising molecular targeted therapies in breast cancer. Indian J Pharmacol 43: 236-245, 2011.
6. Vincze G, Szasz O and Szasz A: Generalization of the thermal dose of hyperthermia in oncology. Open J Biophys 5: 97-114, 2015.
7. Roussakow S: The History of Hyperthermia Rise and Decline. Hindawi Publishing Corporation Conference Papers in Medicine. Vol 2013, ID428027, 2013. http://www.hindawi.com/archive/2013/428027/.
8. Szasz A, Iluri N and Szasz O: Local hyperthermia in oncology-to choose or not to choose? In: Hyperthermia. Huilgol N (ed). InTech, Croatia, pp1-82, 2013.
9. Szasz O, Szasz AM, Minnaar C and Szasz A: Heating-trends in modern oncological hyperthermia. Open J Biophys 7: 116-144, 2017.
10. Szasz A: Electromagnetic effects in nanoscale range. In: Cellular Response to Physical Stress and Therapeutic Applications, cheptor 4. Shimizu T and Kondo T (eds). Nova Science Publishers, New York, NY, pp55-81, 2013.
11. Papp E, Vancsik T, Kiss E and Szasz O: Energy absorption by the membrane rafts in the modulated electro-hyperthermia (mEHT). Open J Biophys 7: 216-229, 2017.
12. Szasz A, Szasz N and Szasz O: Oncothermia-principles and practices. Springer Science, Heidelberg, 2010.
13. Lee SY and Lee NR: Positive response of a primary leiomyosarcoma of the breast following salvage hyperthermia and pazopanib. Korean J Intern Med 33: 442-445, 2018.
14. Schirrmacher V, Stücker W, Lulei M, Bihari AS and Sprenger T: Long-term survival of a breast cancer patient with extensive liver metastases upon immune and virotherapy: A case report. Immunotherapy 7: 855-860, 2015.
15. Anjum F, Razvi N and Massod MA: Breast cancer therapy: A mini review. MOJ Drug Des Develop Ther 1: 35-38, 2017.
16. Dewey WC, Hopwood LE, Sapareto SA and Gerweck LE: Cellular responses to combinations of hyperthermia and radiation. Radiology 123: 463-474, 1977.
17. Smythe WR and Mansfield PF: Hyperthermia: Has its time come? Ann Surg Oncol 10: 210-212, 2003.
18. Oleson JR: Eugene robertson special lecture, hyperthermia from the clinic to the laboratory: A hypothesis. Int J Hyperthermia 11: 315-322, 1995.

19. Mitsumori M, Zeng ZF, Oliynychenko P, Park JH, Choi IB, Tatsuzaki H, Tanaka Y and Hiraoka M: Regional hyperthermia combined with radiotherapy for locally advanced non-small cell lung cancers: A multi-institutional prospective randomized trial of the international atomic energy agency. Int J Clin Oncol 12: 192-198, 2007.
20. Reinhold HS and Endrich B: Tumor microcirculation as a target for hyperthermia. Int J Hyperthermia 2: 111-137, 1986.
21. Song CW: Effect of local hyperthermia on blood-flow and microenvironment: A review. Cancer Res 44 (Suppl 10): 4721s-4730s, 1984.
22. Kay CS, Choi IB, Jang JY, Choi BO, Kim A and Shinn KS: Thermoradiotherapy in the treatment of locally advanced nonsmall cell lung cancer. J Korean Soc Ther Radiol Oncol 14: 115-122, 1996.
23. Zolciak-Siwinska A, Piotrkowicz N, Jonska-Gmyrek J, Nicke-Psikuta M, Michalsky W, Kawczyńska M, Bijok M and Bujiko K: HDR brachytherapy combined with interstitial hyperthermia in locally advanced cervical cancer patients initially treated with concomitant radiochemotherapy-a phase III study. Radiother Oncol 109: 194-199, 2013.
24. Jones EL, Oleson JR, Prosnitz LR, Samulski TV, Vujaskovic Z, Yu D, Sanders LL and Dewhirst MW: Randomized trial of hyperthermia and radiation for superficial tumors. J Clin Oncol 23: 3079-3085, 2005.
25. Sherar M, Liu FF, Pintilie M, Levin W, Hunt J, Hill R, Hand J, Vernon C, van Rhoon G, van der Zee J, et al: Relationship between thermal dose and outcome in thermoradiotherapy treatments for superficial recurrences of breast cancer: Data from a phase III trial. Int J Radiat Oncol Biol Phys 39: 371-380, 1997.
26. Vernon CC, Hand JW, Field SB, Machin D, Whaley JB, van der Zee J, van Putten WL, van Rhoon GC, van Dijk JD, González González D, et al: Radiotherapy with or without hyperthermia in the treatment of superficial localized breast cancer: Results from five randomized controlled trials. International collaborative hyperhtermia group. Int J Radiat Oncol Biol Phys 35: 731-744, 1996.
27. Forika G, Balogh A, Vancsik T, Zalatnai A, Petovari G, Benyo Z and Krenacs T: Modulated electro-hyperthermia resolves radioresistance of Panc1 pancreas adenocarcinoma and promotes DNA damage and apoptosis in vitro. Int J Mol Sci 21: 5100, 2020.
28. Hurwitz MD: Hyperthermia and immunotherapy: Clinical opportunities. Int J Hyperthermia 36 (Suppl 1): S4-S9, 2019.
29. Huang L, Li Y, Du Y, Zhang Y, Wang X, Ding Y, Yang Y, Meng F, Tu J, Luo L and Sun C: Mild photothermal therapy potentiates anti-PD-L1 treatment for immunologically cold tumors via an all-in-one and all-in-control strategy. Nat Commun 10: 4871, 2019.
30. You SH and Kim S: Feasibility of modulated electro-hyperthermia in preoperative treatment for locally advanced rectal cancer: Early phase 2 clinical results. Neoplasma 67: 677-683, 2020.
31. Minnaar CA, Kotzen JA, Ayeni OA, VAngu MD and Bawyens A: Potentiation of the abscopal effect by modulated electro-hyperthermia in locally advanced cervical cancer patients. Front Oncol 10: 376, 2020.
32. Jiang J, Chen S, Li K, Zhang C, Tan Y, Deng Q, Chai Y, Wang X, Chen G, Feng K, et al: Targeting autophagy enhances heat stress-induced apoptosis via the ATP-AMPK-mTOR axis for hepatocellular carcinoma. Int J Hyperthermia 36: 499-510, 2019.
33. Kinsey CG, Camolotto SA, Boespflug AM, Gillen KP, Foth M, Truong A, Schuman SS, Shea JE, Seipp MT, Yap JT, et al: Protective autophagy elicited by RAF→MEK→ERK inhibition suggests a treatment strategy for RAS-driven cancers. Nat Med 25: 620-627, 2019.
34. Van Gool SW, Makalowski J, Feyen O, Prix L, Schirrmacher V and Stuecker W: The induction of immunogenic cell death (ICD) during maintenance chemotherapy and subsequent multimodal immunotherapy for glioblastoma (GBM). Austin Oncol Case Rep 3: 1-8, 2018.
35. Szasz AM, Minnaar CA, Szentmártoni G, Szigeti GP and Dank M: Review of the clinical evidences of modulated electro-hyperthermia (mEHT) method: An update for the practicing oncologist. Front Oncol 9: 1012, 2019.
36. Fiorentini G, Sarti D, Casadei V, Milandri C, Dentico P, Mambrini A, Nani R, Fiorentini C and Guadagni S: Modulated electro-hyperthermia as palliative treatment for pancreatic cancer: A retrospective observational study on 106 patients. Integr Cancer Ther 18: 1534735419878505, 2019.
37. Ou J, Zhu X, Chen P, Du Y, Lu Y, Peng X, Bao S, Wang J, Zhang X, Zhang T and Pang CLK: A randomized phase II trial of best supportive care with or without hyperthermia and vitamin C for heavily pretreated, advanced, refractory non-small-cell lung cancer. J Adv Res 24: 175-182, 2020.
38. Minnaar CA, Kotzen JA, Ayeni OA, Naidoo T, Tunmer M, Sharma V, Vangu MD and Baeyens A: The effect of modulated electro-hyperthermia on local disease control in HIV-positive and -negative cervical cancer women in South Africa: Early results from a phase III randomised controlled trial. PLoS One 14: e0217894, 2019.

Modulated electro-hyperthermia with weekly paclitaxel or cisplatin in patients with recurrent or persistent epithelial ovarian, fallopian tube or primary peritoneal carcinoma: The KGOG 3030 trial

Kidong Kim, Jae-Hoon Kim, Seung Cheol Kim, Yong Beom Kim, Byung-Ho Nam, Jae Hong No Hanbyoul Cho, Woong Ju, Dong Hoon Suh and Yun Hwan Kim

Department of Obstetrics and Gynecology, Seoul National University Bundang Hospital, Seongnami, Gyeonggi 13620;
Department of Obstetrics and Gynecology, Gangnam Severance Hospital, Yonsei University College of Medicine, Seoul 06273;
Department of Obstetrics and Gynecology, Ewha Womans University Mokdong Hospital, Seoul 07985;
Department of Obstetrics and Gynecology, College of Medicine, Seoul National University, Seoul 03080;
Herings Co., Ltd., Seoul 06144; 6Department of Obstetrics and Gynecology, College of Medicine, Ewha Womans University, Seoul 03760, Republic of Korea

*Correspondence to: Dr Yong Beom Kim, Department of Obstetrics and Gynecology, College of Medicine, Seoul National University, 103 Daehak-ro, Jongno, Seoul 03080, Republic of Korea
E-mail: ybkimlh@snubh.org

Cite this article as:
Kidong Kim et al. (2021): Modulated electro hyperthermia with weekly paclitaxel or cisplatin in patients with recurrent or persistent epithelial ovarian, fallopian tube or primary peritoneal carcinoma: The KGOG 3030 trial, Experimental and Therapeutic Medicine 22, Artical number: 787; Pages 1-7.
https://www.spandidos-publications.com/10.3892/etm.2021.10219

Oncothermia Journal 31, 2022 March: 42-50
www.oncotherm.com/sites/oncotherm/files/2022-03/Kidong_Modulated.pdf

Abstract. The present study (KGOG 3030) aimed to evaluate the safety of modulated electro-hyperthermia (mEHT) therapy with weekly administration of paclitaxel or cisplatin in female patients with recurrent or persistent epithelial ovarian, fallopian tube or primary peritoneal carcinoma. A total of 12 patients were randomized into the paclitaxel or cisplatin arm at a 1:1 ratio. Patients received weekly administration of paclitaxel (70 mg/m2) or cisplatin (40 mg/m2) intravenously on days 1, 8 and 15, and underwent mEHT therapy for 1 h on days 1, 4, 8, 11, 15, 18, 21 and 24 for each 4-week cycle. The primary endpoint was the occurrence of dose-limiting toxicity (DLT). The secondary endpoints were treatment-emergent adverse events (TEAEs), objective response rate, carbohydrate antigen 125 (CA125) response rate, progression-free survival (PFS) and overall survival (OS). In total, 16 patients were recruited, but four patients dropped out. None of the 12 remaining patients (6 each in the two arms) experienced DLT. Overall, 0 and 4 grade 3 TEAEs (anemia, nausea, neutrophil count decreased and platelet count decreased) occurred in the paclitaxel and cisplatin arm, respectively. Furthermore, one confirmed partial response and two CA125 responses were observed in the cisplatin arm. The median PFS time in the paclitaxel and cisplatin arms was 3.0 months (range, 1.7-4.6 months) and 6.8 months (range, 3.9-11.8 months), respectively, while the median OS time was 11.5 months (range, 8.4-28.8+ months) and not reached (range, 3.9-38.5+ months), respectively. In conclusion, mEHT therapy with weekly paclitaxel or cisplatin appeared safe and warrants further investigation. The present trial was registered with www.clinicaltrials.gov on January 22, 2015 (trial registration no. NCT02344095).

Key words: cisplatin, induced hyperthermia, ovarian epithelial carcinoma, paclitaxel, toxicity

Introduction

Recurrent ovarian cancer is incurable and, accordingly, has poor prognosis. In a study analyzing survival data from clinical trials of ovarian cancer, the median overall survival (OS) after the first, second, third, fourth and fifth recurrence was 17.6, 11.3, 8.9, 6.2 and 5.0 months, respectively (1). Therefore, novel treatment options are urgently required for such patients. Radiofrequency hyperthermia (RFH) therapy involves heating of the body using radiofrequency energy. While it has been applied for the treatment of different cancer types, its efficacy remains conflicting. For instance, in a randomized trial of 73 patients with advanced ovarian cancer, those who received chemotherapy with RFH achieved better tumor remission rates than those who received chemotherapy alone (2). However, in a randomized trial of patients with cervical cancer, there was no significant difference in survival between those who received RFH with radiotherapy and those who received radiotherapy alone. In addition, acute toxicity was significantly worse in the RFH plus radiotherapy arm (3).

Modulated electro-hyperthermia (mEHT) is a type of RFH that uses impedance coupling with amplitude-modulated 13.56 MHz carrier radiofrequency (4). Similar to conventional RFH, mEHT is usually administered for 60 min, 1-3 times per week (3,5-7). However, unlike conventional RFH, the energy of radiofrequency is selectively absorbed by the tumor cells in mEHT (8). In addition, an in vitro study reported that the cellular response to mEHT is different from that to conventional RFH. Specifically, in contrast to conventional RFH, mEHT activates caspase-dependent pathways and induces apoptosis (9). Therefore, it was hypothesized that the oncologic effect of mEHT may be different from that of conventional RFH.

To the best of our knowledge, only 3 trials investigating the effects of mEHT therapy on cancer have been published to date. Although the trials were on different cancers, the results all suggested that the addition of mEHT was beneficial for achieving a higher response rate (5) and better local control (6) than conventional treatments and was highly feasible (7). However, evidence on the usefulness and safety of mEHT combined with chemotherapy in the treatment of ovarian cancer is currently lacking (10). Thus, the present study aimed to evaluate the safety of mEHT therapy with weekly paclitaxel or cisplatin administration in females with recurrent or persistent epithelial ovarian, fallopian tube or primary peritoneal carcinoma.

Materials and methods

Trial design and randomization. The present trial (KGOG 3030) was a phase 1 trial with 1 dose level performed at three tertiary hospitals (Seoul National University Bundang Hospital, Seongnam, Gyeonggi; Gangnam Severance Hospital, Seoul; Ewha Womans University Mokdong Hospital, Seoul) in the Republic of Korea between February 2015 and November 2017. The study was conducted according to the tenets of the Declaration of Helsinki and its later amendments, and the protocol was approved by the Institutional Review Board (IRB) of each hospital (Seoul National University Bundang Hospital IRB, approval no. E-1407/258-001, approval date 17th Sep 2014; Yonsei University Gangnam Severance Hospital IRB, approval no. 3-2014-0272, approval date 14th January 2015; Ewha Womans University Medical Center IRB, approval no. EUMC 2014-09-009, approval date 1st December 2014) and registered at www.clinicaltrials.gov (on January 22, 2015; registration no. NCT02344095). Written informed consent was obtained from all subjects. The present study was reported in line with the Consolidated Standards of Reporting Trials guidelines (11).

There is already a widely used protocol for mEHT therapy and numerous cases in which mEHT therapy was combined with various chemotherapy modalities were encountered in our clinical practice. Therefore, the widely used protocol for mEHT therapy (1 h; 2 sessions per week; maximum energy, 140 W) (10) was adopted. In addition, it was decided not to test several dose levels of chemotherapy and adopt a 3+3 design with only 1 dose level (70 mg/m2 for paclitaxel, 40 mg/m2 for cisplatin). Specifically, 3 patients were enrolled and underwent therapy with a dose level of chemotherapy plus mEHT. If dose-limiting toxicity (DLT) was observed in <2 of 3 patients, 3 more patients were enrolled. If DLT occurred in <2 of 6 patients, it was concluded that the dose was safe enough for use in a further investigation. There was no dose escalation or de-escalation. Therefore, the anticipated number of patients was 12 (6 in each arm).

The optimal chemotherapy drug to be combined with mEHT therapy in recurrent ovarian cancer has remained undetermined. In vitro studies suggested that hyperthermia potentiates the cytotoxic effects of cisplatin (12,13). Furthermore, weekly paclitaxel administration is an effective regimen in recurrent ovarian cancer (14). After a thorough review of the literature and discussion, paclitaxel and cisplatin were selected (12-14). To determine which drug should be selected for further investigation at the completion of the present trial, both the paclitaxel and cisplatin arms were launched and compared using randomization. Patients were randomized into the paclitaxel arm or the cisplatin arm at a 1:1 ratio using block randomization with 'hospital' as a stratification factor. Randomization and notification of results were performed by the independent data center and the randomization result was not concealed.

Eligibility and intervention. The inclusion criteria were as follows: i) Recurrent or persistent epithelial ovarian, fallopian tube or primary peritoneal carcinoma; ii) tumor evaluable with radiologic study or serum carbohydrate antigen (CA)125; and iii) Eastern Cooperative Oncology Group performance status score (15) of 0-2. The exclusion criteria were as follows: i) Tumor located in previously irradiated area; ii) brain metastasis; iii) residual neurotoxicity or history of severe neurotoxicity; iv) hypersensitivity to paclitaxel or cisplatin; and v) pacemaker or metal implants. The number of previous chemotherapy regimens was limited to <3 at initiation. However, due to slow accrual, the limit was changed to <4 in August 2015 and was removed in July 2016.

Patients in the paclitaxel arm received 4 cycles of mEHT therapy with weekly paclitaxel chemotherapy, with each cycle lasting 4 weeks. After steroids and anti-histamines were administered to prevent infusion reactions, 70 mg/m2 of paclitaxel was intravenously infused for 1 h on days 1, 8 and 15 every 4 weeks. Within 3 h of completion of paclitaxel infusion, mEHT therapy was initiated. The mEHT therapy was performed 2 times weekly (days 1, 4, 8, 11, 15, 18, 21 and 24 per cycle) using an EHY 2000 plus device (Oncotherm GmbH) and each mEHT therapy session lasted 60 min. During the mEHT therapy, patients were placed in a supine position and a 30-cm diameter circular mEHT electrode was attached to the abdominal wall over the tumor. No precise targeting of the tumor was performed. Starting from 60 W, energy was gradually increased to 140 W. If the

patient felt hot or had any discomfort, the energy was decreased to the previous level and then maintained at that level throughout the duration of the session. When tumors were present in the abdomen and chest area, mEHT therapy was performed sequentially (starting at the abdomen and then the chest).

Patients in the cisplatin arm received 4 cycles of mEHT therapy plus weekly cisplatin chemotherapy, with each cycle lasting 4 weeks; 40 mg/m2 of cisplatin was intravenously infused for 1 h on days 1, 8 and 15 every 4 weeks. The mEHT therapy protocol was the same as that for the paclitaxel arm.

Endpoints. The primary endpoint was the occurrence of DLT from enrollment to fourth cycle completion in evaluable patients of each arm. DLT was defined as the occurrence of any of the following: i) Neutropenic fever requiring inotropics or intensive care unit admission; ii) hematologic toxicity not recovered to grade 1 or 2 within 3 weeks (except anemia); iii) non-hematologic toxicity not recovered to grade 1 or 2 within 3 weeks (except alopecia); and iv) death. Evaluable patients were defined as patients who completed the second cycle.

The secondary endpoints were safety and preliminary efficacy. Safety was measured according to the type, grade and incidence of treatment-emergent adverse events (TEAEs) evaluated using the Common Terminology Criteria for Adverse Events version 4.0 (16). The efficacy endpoints were objective response rate in patients with measurable disease as evaluated using the Response Evaluation Criteria in Solid Tumors version 1.1 (17), CA125 response rate in patients with elevated baseline CA125, progression-free survival (PFS) and OS.

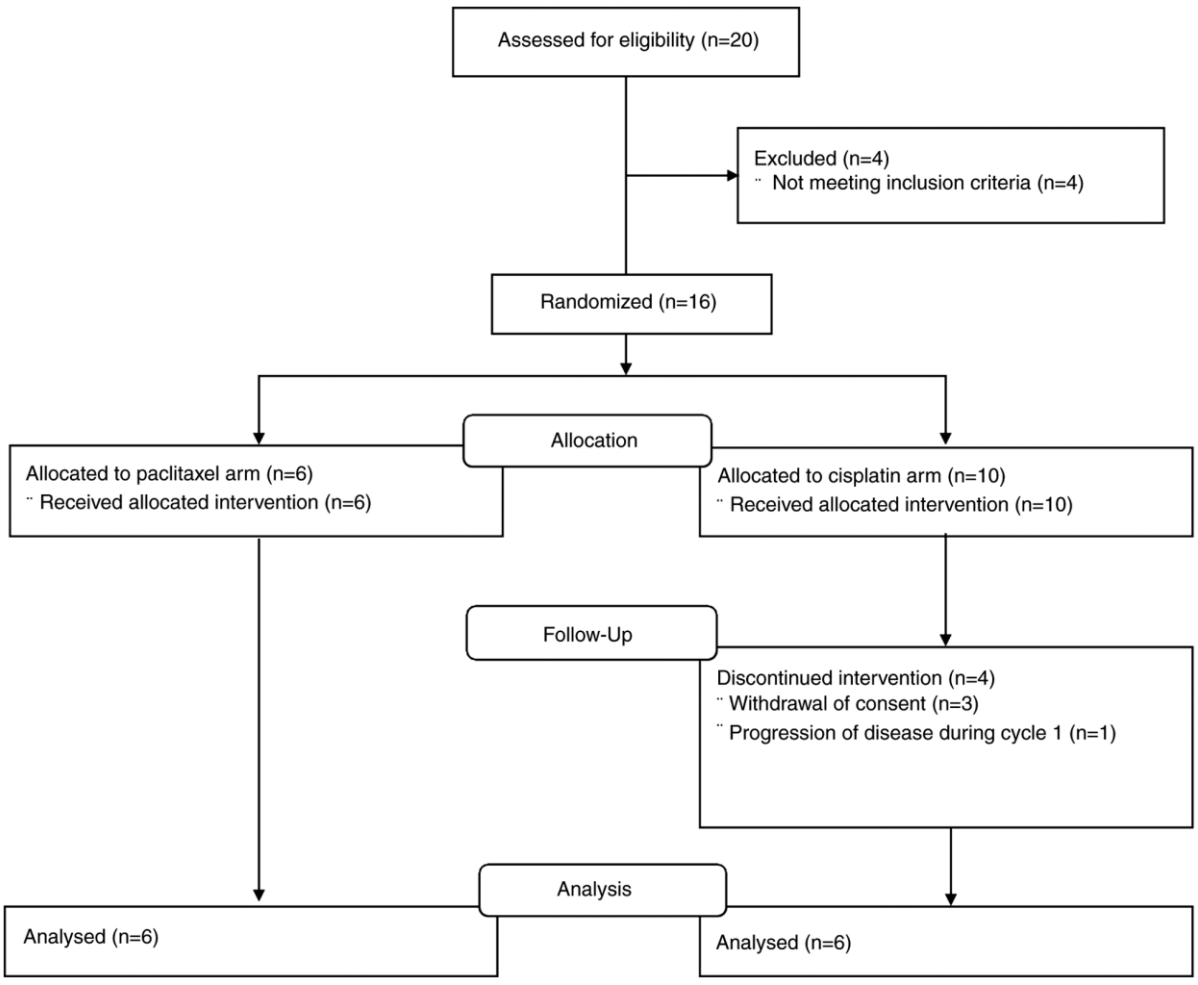

Figure 8. Flowchart depicting the movement of patients throughout the present trial.

The CA125 response was defined as a decrease of >50% from the baseline with confirming repeat test results. During treatment, physical examination and CA125 test were performed every cycle. After treatment was completed, patients were followed up every 3 months until death. CA125 and imaging tests were performed at the discretion of the physician.

Statistical analysis. All statistical analyses were performed using SPSS version 25 (IBM Corp.). Continuous variables were presented as the median and range. Categorical variables were presented as counts and percentages. PFS and OS were estimated using the Kaplan-Meier method.

Results

Baseline characteristics. In total, 16 patients were recruited for the present study. A flowchart depicting the movement of the patients throughout the study is provided in Fig. 1. Of 16 patients, four patients in the cisplatin arm did not complete the first cycle and were not evaluable. The time-point and reasons for treatment discontinuation of the 4 patients were as follows: Patient 1 (prior to cycle 1, withdrawal of consent), patient 2 (cycle 1 day 1, withdrawal of consent), patient 3 (cycle 1 day 15, clinical deterioration due to presumed cancer progression) and patient 4 (cycle 1 day 8, withdrawal of consent). No TEAEs of grade 3 or above were observed in the 4 patients. The 4 patients were excluded from the efficacy and safety analysis according to the protocol.

The baseline characteristics of the 12 evaluable patients are summarized in Table I. The median age was 64 years and the high-grade serous type was the most common histological type. The number of previous chemotherapy regimens ranged from 1 to 5 and most of patients were platinum-resistant or refractory.

Safety. None of the 12 evaluable patients experienced DLT. No severe TEAE occurred in the paclitaxel arm. The common TEAEs were constipation, dyspepsia, headache and neutropenia. A total of, four grade-3 TEAEs occurred in the cisplatin arm. These were grade-3 anemia (n=1), nausea (n=1), neutropenia (n=1) and thrombocytopenia (n=1). The common TEAEs were neutropenia and nausea. TEAEs according to type and grade in the paclitaxel and cisplatin arms are summarized in Tables II and III, respectively.

Table I. Baseline characteristics of the patients.

Variable	Paclitaxel + mEHT (n=6)	Cisplatin + mEHT (n=6)
Age, years	67 (53-71)	61 (56-72)
Body height, cm	155 (143-163)	153 (149-156)
Body weight, kg	60 (50-64)	55 (47-86)
Origin of cancer		
Ovary	5 (83)	4 (67)
Peritoneal	1 (17)	2 (33)
FIGO stage		
3	4 (67)	5 (83)
4	2 (33)	1 (17)
Histologic type		
High-grade serous	4 (67)	5 (83)
Clear cell	1 (17)	0 (0)
Low-grade serous	0 (0)	1 (17)
Carcinosarcoma	1 (17)	0 (0)
Number of previous regimens	2 (1-4)	2 (1-5)
Treatment-free interval from previous treatment, months	5 (1-16)	6 (0-27)
Sensitivity to platinum		
Sensitive	2 (33)	1 (17)
Resistant	2 (33)	4 (67)
Refractory	2 (33)	1 (17)

Values are expressed as the median (range) or n (%). mEHT, modulated electro-hyperthermia; FIGO, International Federation of Gynecology and Obstetrics.

Efficacy. Of the 12 patients, 9 patients (5 in the paclitaxel arm, 4 in the cisplatin arm) had measurable disease at baseline. Of the 9 patients, 1 confirmed partial response was observed in the cisplatin arm

(platinum-resistant, high-grade serous). The duration of response was 4 months. Furthermore, 9 of the 12 patients (4 in the paclitaxel arm, 5 in the cisplatin arm) had elevated baseline CA125 levels. Among them, 2 CA125 responses (2 in the cisplatin arm, both were platinum-resistant, high-grade serous) were observed. The duration of response was 4 and 10 months. Progression was observed in all patients. The median PFS in the paclitaxel and cisplatin arms was 3.0 months (range, 1.7-4.6 months) and 6.8 months (range, 3.9-11.8 months), respectively. At the cut-off of September 12, 2018, 5 of the 12 patients had died (4 in the paclitaxel arm, 1 in the cisplatin arm). The median OS in the paclitaxel and cisplatin arms was 11.5 months (range, 8.4-28.8+ months) and not reached (range, 3.9-38.5+ months), respectively (data not shown).

Discussion

Table II. Treatment-emergent adverse events in the paclitaxel arm.

Type	Grade 1	Grade 2	Sum
Abdominal distension	1	0	1
Abdominal pain	0	1	1
Alopecia	1	0	1
Anorexia	0	1	1
Constipation	1	1	2
Creatinine increased	0	1	1
Dysarthria	0	1	1
Dyspepsia	2	0	2
Dyspnea	0	1	1
Fatigue	1	0	1
Flank pain	0	1	1
Headache	2	1	3
Hyperkalemia	1	0	1
Hypocalcemia	1	0	1
Neutrophil count decreased	0	2	2
Pain	1	0	1
Peripheral sensory neuropathy	0	1	1
Productive cough	1	0	1
Toothache	0	1	1
Tremor	0	1	1
Wound complication	1	0	1
Sum	13	13	26

Patients who experienced multiple treatment-emergent adverse events were counted more than one time.

In a previous study, chemotherapy combined with conventional RFH was reported to be more effective than chemotherapy alone for the treatment of advanced ovarian cancer (2). However, to the best of our knowledge, no previous study has examined the efficacy and safety of chemotherapy combined with mEHT for ovarian cancer. Therefore, the present study is novel and it is the first to examine the safety and efficacy of chemotherapy combined with mEHT for the treatment of ovarian cancer.

The results of the present phase 1 trial indicated that mEHT therapy combined with weekly chemotherapy is safe enough to proceed to be investigated in further clinical trials. Specifically, no DLT occurred in both the paclitaxel and cisplatin arms, and only 4 grade 3 TEAEs were observed. Therefore, both modalities appeared tolerable. The safety of RFH therapy combined with chemotherapy has been reported in previous studies. In a trial on RFH therapy combined with weekly docetaxel in patients with locally advanced non-small cell lung cancer, grade 3 or 4 neutropenia occurred in only 24% of the patients (18). In a randomized trial comparing RFH plus chemotherapy with chemotherapy alone in advanced ovarian cancer, toxicity was similar between arms (2). Collectively, these findings and the results of the current trial indicated that mEHT therapy may be safely combined with chemotherapy.

To the best of our knowledge, no study has reported superiority of RFH with chemotherapy over chemotherapy alone in the treatment of platinum-resistant ovarian cancer. In the present study, mEHT therapy combined with weekly chemotherapy showed intermediate efficacy. Of the 9 patients, only 1 partial response was confirmed (response rate, 11%). Response based on CA125 was observed in 2 of 9 patients (22%). All responses were observed in the cisplatin arm. Specifically, in the cisplatin arm, 1 of 4 patients with measurable disease responded (response rate, 25%), and 2 of 5 patients with elevated baseline CA125 levels exhibited CA125 response (40%). This suggests that when combined with mEHT, while cisplatin appeared to be slightly more toxic, it was also more efficacious than paclitaxel. Supporting the present results, previous cell line studies suggested that hyperthermia enhanced the cytotoxicity of cisplatin but inhibited that of paclitaxel (12,13,19,20). Thus, mEHT therapy combined with weekly cisplatin administration should be considered a regimen for further investigation.

Of note, one radiologically confirmed partial response and two CA125 responses were observed in the present study in platinum-resistant patients in the cisplatin arm. A single-arm trial testing the efficacy of oral etoposide plus weekly cisplatin reported a 46% response rate in platinum-resistant patients and high-dose intensity achieved by weekly dosing was suggested as a mechanism for overcoming platinum resistance (21). Both weekly dosing and synergy between cisplatin and mEHT may be the mechanisms accountable for the responses observed in the present study.

The present study has certain limitations. First, the safety of therapy was determined using data from only 6 patients per group. Therefore, the safety of therapy should be considered preliminary and only be used to make decisions for further investigations. As another limitation, the present trial did not test multiple dose levels and did not investigate the maximum tolerated dose of mEHT. This may have resulted in undertreatment. However, a recent study indicated that the optimal dose of mEHT in the treatment of recurrent ovarian cancer is 150 W for 1 h (7), and that dose is similar to the energy used in the present study (140 W). Nevertheless, a strength of the present study was that it was a multi-center study.

Our group is planning a subsequent phase 2 trial, testing the efficacy and safety of weekly cisplatin plus mEHT for recurrent ovarian cancer, and efficacy will be evaluated in platinum-sensitive and -resistant subgroups separately.

In conclusion, mEHT therapy with weekly paclitaxel or cisplatin appeared safe in female patients with recurrent or persistent epithelial ovarian, fallopian tube, or primary peritoneal carcinoma, thus warranting further investigation in clinical trials.

Acknowledgements

The abstract of this study was previously e-published for presentation at the 2019 Annual Meeting of the American Society of Clinical Oncology (Chicago, USA). The authors would like to thank Ms. EunSun Park (Clinical Research Nurse, Gangnam Severance Hospital) and Ms. Moon Kyoung Bae (Clinical Research Nurse, Ewha Womans University Medical Center) (both Seoul, South Korea) for conducting this trial. Professor Soyeon Ahn (Division of Statistics, Medical Research Collaborating Center, Seoul National University Bundang Hospital, Seongnam, South Korea), Professor Jae Yong Chung (Department of Clinical Pharmacology and Therapeutics, Seoul National University College of Medicine and Bundang Hospital, Seongnam, South Korea) and Professor Seok Ju Seong (Department of Obstetrics and Gynecology, CHA Gangnam Medical Center, CHA University, Seoul, South Korea) contributed to this study as Data Safety Monitoring Board members.

Funding

This work was supported by a grant (grant no. E-1407/258-001) from Hospicare Co. Ltd. (Seoul, Republic of Korea). The funder was not involved in the study design, writing of the manuscript and the decision to submit the manuscript for publication.

Availability of data and materials

The datasets used and/or analyzed during the current study are available from the corresponding author on reasonable request.

Authors' contributions

KK contributed to protocol/project development, follow-up/examination/treatment of the patients, data collection or management, data analysis and manuscript writing/editing. YBK and BHN contributed to protocol/project development, data collection or management and manuscript writing/editing. JHK, SCK, JHN, HC, WJ, DHS and YHK contributed to follow-up/examination/treatment of the patients, data collection or management and manuscript writing/editing. KK and DHS checked and approved the authenticity of the raw data. All authors read and approved the final manuscript.

Ethics approval and consent to participate

The study was performed according to the tenets of the Declaration of Helsinki and its later amendments, and the protocol was approved by the IRB of each hospital [Seoul National University Bundang Hospital IRB (Seongnam, South Korea), approval no. E-1407/258-001, approval date 17th Sep 2014; Yonsei University Gangnam Severance Hospital IRB (Seoul, South Korea), approval no. 3-2014-0272, approval date 14th January 2015; Ewha Womans University Medical Center IRB (Seoul, South Korea), approval no. EUMC 2014-09-009, approval date 1st December 2014]. Written informed consent was obtained from all individual participants included in the study.

Patient consent for publication

Not applicable.

Competing interests

The authors declare that they have no competing interests.

References

1. Hanker LC, Loibl S, Burchardi N, Pfisterer J, Meier W, Pujade-Lauraine E, Ray-Coquard I, Sehouli J, Harter P, du Bois A; AGO and GINECO study group: The impact of second to sixth line therapy on survival of relapsed ovarian cancer after primary taxane/platinum-based therapy. Ann Oncol 23: 2605-2612, 2012.
2. Li Z, Sun Q, Huang X, Zhang J, Hao J, Li Y and Zhang S: The efficacy of radiofrequency hyperthermia combined with chemotherapy in the treatment of advanced ovarian cancer. Open Med (Wars) 13: 83-89, 2018.
3. Vasanthan A, Mitsumori M, Park JH, Zhi-Fan Z, Yu-Bin Z, Oliynychenko P, Tatsuzaki H, Tanaka Y and Hiraoka M: Regional hyperthermia combined with radiotherapy for uterine cervical cancers: A multi-institutional prospective randomized trial of the international atomic energy agency. Int J Radiat Oncol Biol Phys 61: 145-153, 2005.
4. Yang W, Han GH, Shin HY, Lee EJ, Cho H, Chay DB and Kim JH: Combined treatment with modulated electro-hyperthermia and an autophagy inhibitor effectively inhibit ovarian and cervical cancer growth. Int J Hyperthermia 36: 9-20, 2019.
5. Lee SY, Lee NR, Cho DH and Kim JS: Treatment outcome analysis of chemotherapy combined with modulated electro-hyperthermia compared with chemotherapy alone for recurrent cervical cancer, following irradiation. Oncol Lett 14: 73-78, 2017.
6. Minnaar CA, Kotzen JA, Ayeni OA, Naidoo T, Tunmer M, Sharma V, Vangu MDT and Baeyens A: The effect of modulated electro-hyperthermia on local disease control in HIV-positive and -negative cervical cancer women in South Africa: Early results from a phase III randomised controlled trial. PLoS One 14: e0217894, 2019.
7. Yoo HJ, Lim MC, Seo SS, Kang S, Joo J and Park SY: Phase I/II clinical trial of modulated electro-hyperthermia treatment in patients with relapsed, refractory or progressive heavily treated ovarian cancer. Jpn J Clin Oncol 49: 832-838, 2019.
8. Hegyi G, Szigeti GP and Szász A: Hyperthermia versus oncothermia: Cellular effects in complementary cancer therapy. Evid Based Complement Alternat Med 2013: 672873, 2013.
9. Yang KL, Huang CC, Chi MS, Chiang HC, Wang YS, Hsia CC, Andocs G, Wang HE and Chi KH: In vitro comparison of conventional hyperthermia and modulated electro-hyperthermia. Oncotarget 7: 84082-84092, 2016.

Dank M: Review of the clinical evidences of modulated electro-hyperthermia (mEHT) method: An update for the practicing oncologist. Front Oncol 9: 1012, 2019.
11. Schulz KF, Altman DG, Moher D; CONSORT Group: CONSORT 2010 statement: Updated guidelines for reporting parallel group randomized trials. Ann Intern Med 152: 726-732, 2010.
12. Haveman J, Bergs JWJ, Franken NAP, van Bree C and Stalpers LJA: Effect of hyperthermia on uptake and cytotoxicity of cisplatin in cultured murine mammary carcinoma cells. Oncol Rep 14: 561-567, 2005.
13. Raaphorst GP and Yang DP: The evaluation of thermal cisplatin sensitization in normal and XP human cells using mild hyperthermia at 40 and 41 degrees C. Anticancer Res 25: 2649-2653, 2005.
14. Gynecologic Oncology Group; Markman M, Blessing J, Rubin SC, Connor J, Hanjani P and Waggoner S: Phase II trial of weekly paclitaxel (80 mg/m2) in platinum and paclitaxel-resistant ovarian and primary peritoneal cancers: A gynecologic oncology group study. Gynecol Oncol 101: 436-440, 2006.
15. Oken MM, Creech RH, Tormey DC, Horton J, Davis TE, McFadden ET and Carbone PP: Toxicity and response criteria of the eastern cooperative oncology group. Am J Clin Oncol 5: 649-655, 1982.
16. U.S.Department of Health and Human Services: Common Terminology Criteriafor Adverse Events (CTCAE). Version 4.0. https://evs.nci.nih.gov/ftp1/CTCAE/CTCAE_4.03/CTCAE_4.03_2010-06-14_QuickReference_5x7.pdf. Accessed June 14, 2010.
17. Eisenhauer EA, Therasse P, Bogaerts J, Schwartz LH, Sargent D, Ford R, Dancey J, Arbuck S, Gwyther S, Mooney M, et al: New response evaluation criteria in solid tumours: Revised RECIST guideline (version 1.1). Eur J Cancer 45: 228-247, 2009.
18. Jiang Z, Yan W, Ming J and Yu Y: Docetaxel weekly regimen in conjunction with RF hyperthermia for pretreated locally advanced non-small cell lung cancer: A preliminary study. BMC Cancer 7: 189, 2007.
19. Leal BZ, Meltz ML, Mohan N, Kuhn J, Prihoda TJ and Herman TS: Interaction of hyperthermia with taxol in human MCF-7 breast adenocarcinoma cells. Int J Hyperthermia 15: 225-236, 1999.
20. Rietbroek RC, Katschinski DM, Reijers MH, Robins HI, Geerdink A, Tutsch K, d'Oleire F and Haveman J: Lack of thermal enhancement for taxanes in vitro. Int J Hyperthermia 13: 525-533, 1997.
21. van der Burg MEL, de Wit R, Van Putten WL, Logmans A, Kruit WH, Stoter G and Verweij J: Weekly cisplatin and daily oral etoposide is highly effective in platinum pretreated ovarian cancer. Br J Cancer 86: 19-25, 2002.

The Capacitive Coupling Modalities for Oncological Hyperthermia

Andras Szasz

Department of Biotechnics, St. Istvan University, Budaörs, Hungary

* Correspondence: Szasz.Andras@gek.szie.hu

Cite this article as:
Szász, A. (2021): The Capacitive Coupling Modalities for Oncological Hyperthermia Open Journal of Biophysics , 11, 252-313.
https://doi.org/10.4236/ojbiphy.2021.113010

Oncothermia Journal 31, 2022 March: 51-99
www.oncotherm.com/sites/oncotherm/files/2022-03/Szasz_Capacitive.pdf

Abstract
The local-regional oncological hyperthermia has various electromagnetic methods for energy-transfer. The differences involve conceptual considerations and technical solutions. The most frequently applied energy transfer is capacitive coupling, concentrating the electric field to be the active heating component. The realization of the capacitive coupling set-up is divided into two different categories based on their goals for heating: 1) the homogeneous (conventional) heating, using isothermal conditions for dosing, and 2) the selective heterogeneous heating, using cellularly absorbed energy for dosing. The homogeneous heating utilizes plane-wave matching, absorbing the wave for energy transfer. The heterogenic heating uses impedance matching, selecting the malignant cells by their electromagnetic specialties, like their heterogenic impedance, higher membrane-raft density, and different spatio-temporal (pathologic pattern) arrangements. This article's objective is to compare and discuss the details of the two kinds of capacitive coupling techniques.

Keywords
Plane-Wave Matching, Impedance Matching, Apoptosis, DAMP, ICD, Selective Heating, Electromagnetic Heterogeneity, Membrane Raft

1. Introduction

1.1. Strategy in the Fight against Cancer

Life is based on energetically open systems, where environmental conditions determine their equilibrium. The general system's theory [1] was one of the early efforts to show the complexity of open living systems focusing on the deep embedment of its processes in the environmental interactions. Due to the environmental actions, the physical laws work well to explain the evolutionary processes [2]. The energetically open living system intensively interacts with its environment, exchanging molecules and various thermodynamic and electromagnetic parameters. Simply speaking: our focus differs from living motility to the energy-transfer. A. Szent-Gyorgyi described the life-energy relationship using the analogy that it is not important that the monkey goes through the jungle, what is important is how the jungle goes through the monkey, in the form of nutrition, water, and oxygen, keeping the monkey alive using the environmental energy-sources [3]. The living system is complexly controlled, to maintain homeostasis. Diseases, especially cancers, break the relative equilibrium and risk the system's relative instability. The human body tries to re-establish homeostasis in many ways by enhancing the negative feedback controls. Multiple actions of human physiology try to compensate and correct the damage caused by cancer.

Healthy homeostasis struggles to control the malignancy. The first few attempts block the proliferation and start intracellularly controlling the DNA replication. It fails for various reasons, including genetic aberration [4], mitochondrial dysfunction [5], or other intracellular [6], and additionally extracellular [7] hallmarks of malignancy.

The malignancy in this general meaning is a distortion of the healthy cellular network, the rules of a multicellular organization being broken. The breaking of cellular networks is a general behavior of all tumors independent of their locations within the body. In this sense, cancer is an organizing (networking) disease, where the cells unleashed from their networks abandon the living advantages of collectivism, and individualism prevails [8]. Cancerous and bacterial proliferations have a lot in common [9]. The tumor itself has atavism qualities [10], in the sense that the malignant cells act like self-ruled unicellular organisms. The atavism-like process is general, not only with the loss of cellular connections but also with the altered intracellular genetic structures. The unicellular individualism develops the great potential for adaptability to environmental changes, making these cells more vigorous than those in the multicellular network. The modified genetic activity at the active boundary between unicellular and multicellular areas, causes disorganization of the multicellular structure, promoting primitive transcriptional programs [11]. However, the similarity with atavism is only formal. The atavistic development is supported by the environment which is rich in energy-resources needed for the

proliferation. Still, the active use decreases the valuable matter around the bacteria, and only some physical processes (like diffusion, flows in aqueous solution, etc.) may passively replace the missing materials. In cancer conditions, the proliferating cell actively changes its environment, forcing the healthy host to supply the needed materials [12]. The cancer is afforded a friendly environment by the host, which tries to "heal" the abnormality by strengthening angiogenesis, injury current, and numerous other supportive mechanisms. There are telling arguments for the likening of the cancerous process to wound repair [13]. The bio-system falsely recognizes the tumor—as a wound and stimulates its environment to heal the irregularity (meaning to produce cells to heal) [14].

We are in a war against this disease [15]. The end of this war seems to be far away [16]. This war's strategic decision may be borrowed from the military: attack the enemy's weakest point, and avert to direct fight with its strongest forces. The most vital force of the malignancy is its uncontrolled proliferation, while the weakest side is the autonomy of the proliferated cells, and their isolation from the regular cellular network. The cooperation of the healthy cells regulates, controls, and supplies the members of the network. The malignant cells are "individual fighters" competing against all healthy and malignant cells for the energy sources to proliferate. This "loneliness" behavior makes the malignant cells vulnerable. They miss the complex support from the network. The missing network otherwise helps the proliferative development due to the easy motility and forming micro and macro metastases. Following this strategy, the final aim of cancer treatments is to eliminate the cancer cells throughout the body.

1.2. Some Tactical "Weapons"

To follow the strategic goal to attack the malignant cells' individualism, we have multiple "tactical" possibilities to choose from. The lack of coherence and support it in the network modifies the cells and their microenvironment. This modification could be used to select and kill the cells. The most characteristic changes are a result of the cells' autonomy:

• The individual cells are more vulnerable than the cells connected via the network. Healthy cells may share their extra absorbed energy with the neighbors, while the autonomous cells are at risk of being overloaded by the absorbed energy can be overloaded.

• The autonomy means that the cell's microenvironment is like an ocean around it, only with a few, if any, connections. The molecular "bridges" that made the bonds in the network are broken, and numerous transmembrane proteins remain unconnected and free to move along the membrane and form clusters.

• A large part of the homeostatic control is missing due to the autonomy, and the cells live unregulated. This allows the use of metabolic mechanisms which are rare in networked systems. The mitochondrial symbiosis with the cell has less importance and becomes mostly dysfunctional.

• The autonomy promotes cellular motility that uses the transport systems (lymph and blood), and once separated from the group, these cells more vulnerable.

• Consequently, the energy-demand massively increases in malignant cells as the cells require the extra energy to produce the daughter cells and to support the entire division process.

• The basic chemical reactions are out of systemic harmony. The long-range, and broadly scaled fluctuation and constant multiscale entropy is broken by autonomy, producing easily distinguishable fluctuations (noises) in measurable electromagnetic signals.

The above points are interconnected, and the "tactical actions" could affect many of them simultaneously. Some of the popularly applied treatments are as follows:

➢ Change the conditions by special, strict diets (like Gerson's diet), constraining the body back to the previously working equilibrium. However, in many cases, it works against the natural homeostasis; the constrained action induces new negative feedbacks from the living object. The living organism starts to fight against our constraints together with the fight against the disease itself, which unnecessarily overloads the controlling system and could lead to its collapse, causing serious side effects.

➢ An interesting tactic is to put out the fire with fire. This method increases the already significant metabolic rate of the malignant cells without allowing an increased delivery of the supplies. This was the original idea of hyperthermia: to locally heat the malignant tissue, and force the cells' metabolism, without allowing the replacement of the energy. This method is against the general physiological control, which is governed the blood-flow. The higher local temperature increases the blood-flow to cool-down the targeted volume. The extra blood delivers nutrients, and oxygen, so the method could easily turn in the opposite direction.

➢ Some proposed treatments favor fasting or supplying the body with only one kind of nutrient, like blocking carbohydrates' consumption and expecting that the limited supply will starve the malignant cells.

The above treatments do not work, mainly because the living complexity does not isolate one of the other's dynamic characters, so the action easily turns to the opposite. The general problem with these is proposed methods is that the complexity is not accounted for in the applied principles, the principles involve oversimplified mechanisms, due to the lack of complex knowledge. This problem is well formulated by a playwriter Berthold Brecht: "The aim is not to open the door to the infinite wisdom, but to circumscribe the infinite fallacy… The main reason for the poverty in science is the conceited property." [17]. The physicist Stephan Hawking formulated the same: "The greatest enemy of knowledge is not ignorance, it is an illusion of knowledge".

The dark-side of the tactical elements is the multiple quackeries distributed by social media. This approach uses the "formal knowledge" of the complexity, declaring their method as a special secret, which drives the complex processes. This could be characterized by the statement of Frederici Di Trocchio "Swindle was used to art. Nowadays, it became a science too…" [18].

1.3. Oncological Hyperthermia

Hyperthermia in oncology appeared in ancient medicine. Today heating processes for medical purposes have become a vital "home remedy", from the sun-bathing to the hot-bathes, including the Japanese high-temperature bath and Finish sauna. Hippocrates first described the application of heat in oncology in European medicine. The use of heat therapy to cure cancer has since emerged in various settings in the medical field. The appearance of electromagnetism in medicine renewed the heating efforts, and extended the applications for various cancers. Two main categories divide the electromagnetic-based heating applications: the local deep heating which results in local-regional hyperthermia (LRHT), and the whole-body hyperthermia (WBH). Just as the categories of chemotherapy and radiotherapy include many different modes of treatments, "hyperthermia" is also a large category with different technical aspects. Figure 1 maps the main differences between the technical solutions.

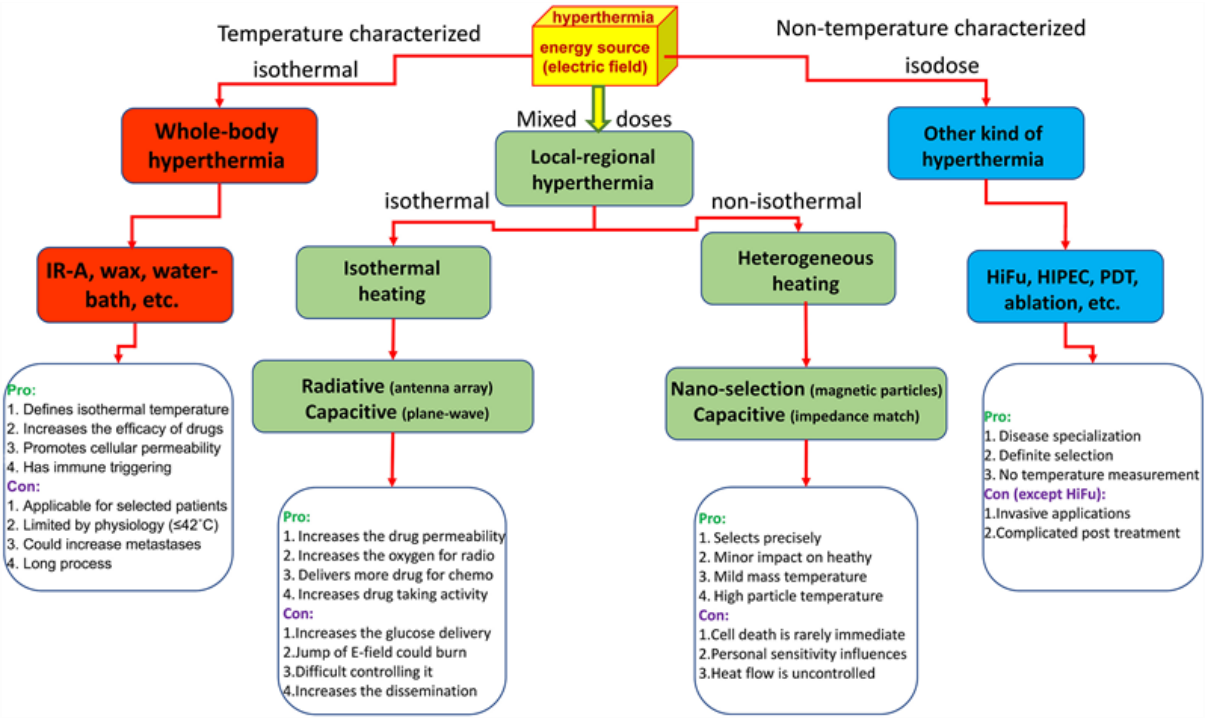

Figure 9. The major categories of hyperthermia methods.

The relatively simple physical-physiological heating concepts do not mean a simple application in humans. The complexity of human physiology, and the non-linear feedbacks of the homeostatic regulation, limits the heating possibilities. Despite the proven in vitro benefits of heating in cancer treatment, the clinical results have strongly demonstrated how the control of treatment is often influenced more by the human body than by the treatment intention. This complication made the development of oncologic hyperthermia non-monotonic, having both great successes and failures [19]. It was clear from the beginning of oncological applications that the real, local cell-distortion must have a high temperature, higher than the physiological limit of 42°C. However, this limit restricts the high temperature application of WBH which has moved towards mild temperature range, promoting the reactivation of the immune system. Contrary to WBH, LRHT does not limit by the temperature in the tumor. When the high temperature targets the healthy host tissues around the tumor, it could produce unintended necrotic burns with serious damage to the treated organ's function.

Consequently, the energy absorption during the heating process significantly depends on the technique applied. No unified protocol for the various technologically determined targets of the heat has currently been described.

The category "hyperthermia" includes various energy-absorption methods, and each individual solution requires its own protocol. It is very similar in this regard to the chemo-variants of oncological therapies. Chemotherapy, depending on the targets of the drug, has different protocols. Mixing these could cause serious adverse effects and even fatal events such as poisoning. Homogeneous targeting in most of these therapies requires very different protocols to the local or cell-sensitive selection. For example, chemotherapy is administered intravenously (i.v.), at different doses to the doses administered with chemoembolization or other types of local administration. Isodose homogeneity, as in radiotherapy, is also not used in most brachytherapies, radiation seed, or nanoparticle administration. We are sure that the hyperthermia variants also have specific differences in their dose and protocol, sharply depending on their technical solution and targeting method. Defining a general dose and protocol for all hyperthermia methods is a misleading request. The methods are not equal. Their effects are different, so the dose and protocol have to fit the specific situation.

The heating techniques determine the result of the clinical treatment. Just as the categories of chemotherapy or radiotherapy, which include many different treatments, "hyperthermia" is also a large category with different technical aspects. We have seen that exposing the tumor to 42°C in whole-body hyperthermia has entirely different results than the same temperature in any local treatment. Characterization of the temperature alone is not enough to categorize the technical solutions.

A water bath is used in many experimental models to achieve hyperthermia, and this models homogeneous heating solutions. The various electromagnetic heating technologies also have their specialties. The bioelectromagnetic action of the technology determines the actions. Evaluating the applied technique, we consider the kind of energy delivery, the method of heat absorption, and handling the target tumor's physiological reactions, together with their inhomogeneities. The target's absorbed energy, and its temperature distribution are not the same [20], and these characteristics are largely determined by the blood-flow. The technical solutions must handle how the provided energy I transformed into the desired temperature.

1.4. The Electromagnetic Coupling Modalities

Variants of energy-transfer realize the absorption in the target. Various "antennas" (sources) couple the energy to the target (Figure 2). The homogeneity of the absorption defines the main character of the actual coupling. The inductive arrangements have two heating forms. One is the Eddy-current (induced current loop in the body) and the other uses magnetic materials for heating. In living objects, both the Eddy-current and magnetic approaches are applied. Life does not have natural inherent magnetic properties. Artificial magnetic materials (like nanoparticles, seeds, rods, etc.) orient the energy for heating. Internal Eddy-current induction needs an extra high magnetic field, and the induced current has no specified orientation but is sensitive for inhomogeneities inside the body. Consequently, both induction methods heat in a heterogenic way. The conventional relative antenna solution radiates the electromagnetic energy, which is absorbed by the target. It is less sensitive to heterogenic structures, so is usually applied for homogeneous heating to use the dosing of isothermal volumes. The capacitive coupling has two major kinds of energy transfers: 1) the plane-wave antenna process, which aims to achieve similar isothermal absorption of the electromagnetic waves as the radiative applications; 2) the impedance coupling process, which uses the precise impedance-matching of the target. The isothermal kind of capacitive coupling requires high energy transferred via the plane-wave, while the impedance matching (mimics the galvanic match), uses less energy provided the heterogenic absorption processes are exploited and dominate. The galvanic coupling firmly touches the actual target. In non-living applications, this is the simple discrete resistor situation. The galvanic coupling in the case of living items applies tightly connected electrodes invasively with direct solid contact with the body's surface.

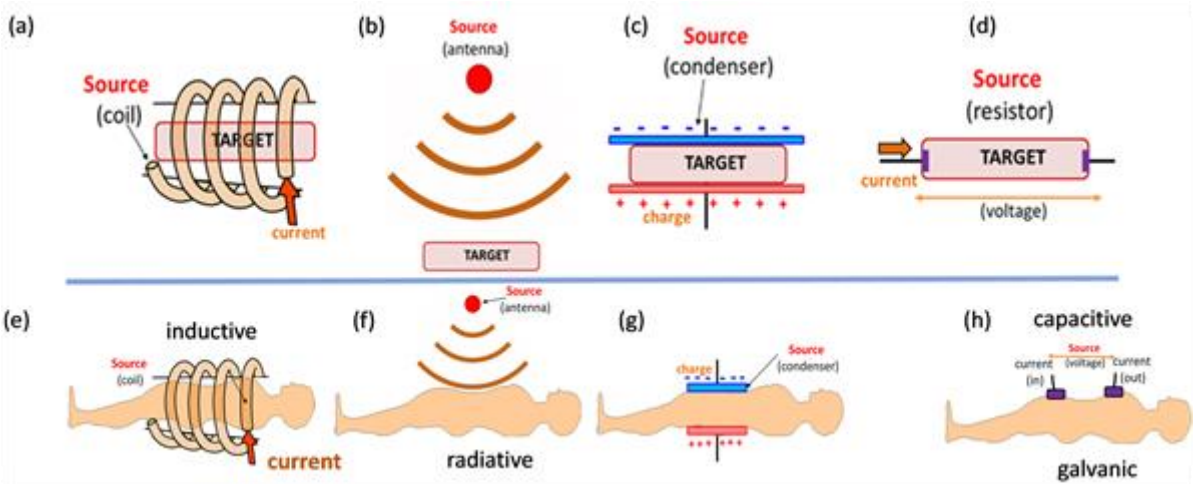

Figure 10. The major coupling methods for local-regional heating. (a)-(d) Homogeneous (non-living) targets; (e)-

(h) Heterogeneous (living) target. The energy-absorption induces different effect in various couplings.

Applications using capacitive and radiative (microwave) solutions are the most popular methods used in the technical realization of the treatments; however, due to the sharp decrease of penetration depth with the increase of frequency, microwave solutions are mainly applied for surface lesions (see later). Capacitive coupling of energy delivery has become the most frequently applied technique, and the frequency of choice for the technique is the so-called "free-frequency" of 13.56 MHz, approved for industrial, scientific, and medical use (ISM frequency) [21]. Different effects in the human applications are observed, based on the coupling effects of the applied technique, Figure 3 .

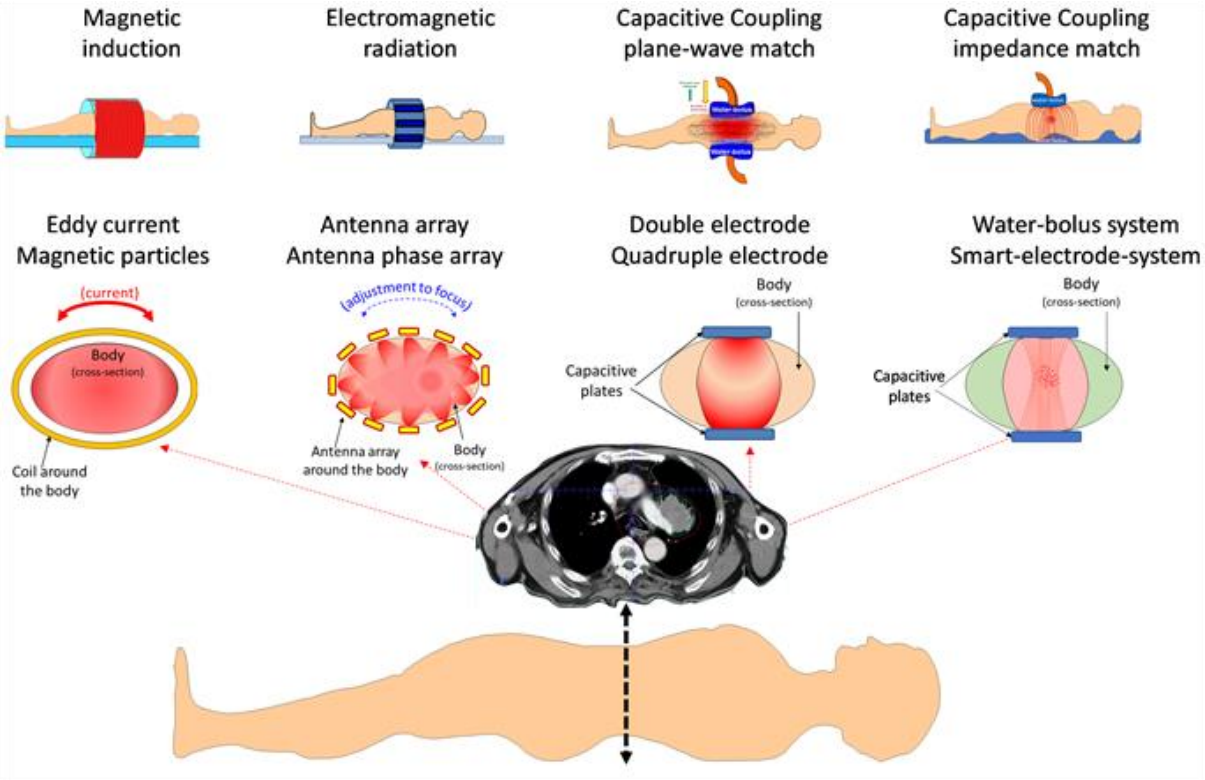

Figure 11. The local-regional treatment intends to select the cross-section of the body for energy absorption.

2. The Capacitive Coupling

Two kinds of capacitive couplings exist, depending on how the matching tunes the antenna, how the antenna structure's method and the electronical environment incorporates the tumor in the body as part of the regulated electric circuit. The concept of the complete electric circuit defines the matching method. The complete system, not only the capacitive arrangement of the electrodes, defines the coupling.

2.1. Plane-Wave Matching

The conventional solution involves plane-wave matching, in which the antenna's plane-parallel plates are tuned as per the standard antenna-tuning method. This solution does not consider the energy losses by various electric circuit elements and their interactions with the environment. In this case, the increased power (P) compensates for the lost energy. Due to the relatively high complex impedance, the voltage (V) is high, while the current (I) is low. The product of voltage and current defines the useful power, $P_{real} = V \cdot I \cdot \cos(\varphi)$, while the reactance (the power refused by the load) is $P_{react} = V \cdot I \cdot \sin(\varphi)$. The possible timing delay of the complex fit of the voltage with current is characterized by the cosine of the phase angle $(\cos(\varphi))$ of the complex values. In case of dielectric losses and/or radiations $0 < \varphi < 90^0$. Due to the losses, the impedance of the system (Z_{sys})

from the radiofrequency (RF) source to the target is large. The capacitance (C) describes the dielectric (isolating) resistivity, and the conductive part (defined by the real resistivity (R) defines the reaction time of the system (time-constant, $\tau = R \cdot C$). The circuit for the hyperthermia plane-wave system has many various capacitances and resistivities additional to the target in the human body, and then we have to calculate the time-constant in a more complicated way (open-circuit time constant method [22]).

The time constant, in the case of plane wave solution, is relatively high, limiting the tuning's reaction time. This delay could cause a challenge when the physiological changes (breathing, heart-rate, etc.) are quicker than the reaction time. The plane wave method applies conventional antenna tuning where the antenna is fixed, so the reaction time has no relevance.

The plane-wave matching radiates RF-waves for energy-absorption, and direct heating, and necrotic cell-death ($CEM43^0CT_x$ dose) is expected. This matching technology aims to reach at least 43°C temperature in the Tx effective percentages of the temperature measurement in the tumor.

The wave matching induces extensive radiation, due to the wave-transmission adding a significant factor to the energy-loss, and this could produce safety issues for operating staff. An important phenomenon of this coupling is that it could tune on the air without a patient in the active radiation zone.

2.2. Impedance Matching

The impedance matching of capacitive coupling does not use the wave concept. The system construction approaches the galvanic touch of the electrodes. The normal resistor has the maximal power in the galvanic coupling: $P_{\max} = U \cdot I$,, where U is the galvanic potential (voltage), and I is the current (Amps). In the case of a patient's complex impedance (Z_{pat}) the imaginary part limits the effective power. When Z_{pat} coupled galvanically, it modifies the maximal efficient power to: $P_{\mathrm{Pat}} = U \cdot I \cdot cos(\varphi)$. A resonance solution of the components approaches the minimal imaginary part of the Zpat impedance [23], and maximizes the power on the patient. The resonance uses a near-zero phase angle $\varphi \cong 0$consequently $\cos(\varphi) \cong 1$ [24]. The low imaginary part decreases the voltage

and increases on the same ratio the RF-current, [25] [26]; because $I_{Pat}^2 = \frac{P_{\mathrm{Pat}}}{Z_{pat}}$, and $U_{Pat}^2 = P_{\mathrm{Pat}} \cdot Z_{pat}$.

Approaching the proper impedance matching, the solution has negligible reflected power (order of 1 W), mimicking the skin's galvanic contact as much as possible. When the electrodes directly touch the targeted volume's surface, the galvanic situation, without any isolating materials, offers the most amount of available current. The impedance matching aims to mimic the galvanic situation as much as possible. This solution minimizes the reactive part and maximizes the real power on the load.

The main principle of impedance matching is to approach the "galvanic-like-touching" that would be the best available non-invasive electromagnetic energy-delivery. The invasive method (when electrodes are inserted into the body) is also "galvanic", but its invasivity has multiple medical complications, such as bleeding, a high risk of infections, ulcer formation, and inflammation. One of the invasive "galvanic" methods is ablation technology, which has remarkable successes in local, small tumors [27]. With minimal energy loss, impedance matching allows the concentration of the energy on the malignant volume [28]. Due to the selection, this solution has better efficacy and offers a safer treatment because the voltage could be less than in higher resistivity isolation cases, at the same power application, while the current is increased.

The full arrangement of impedance matching minimizes the losses in the circuit ($Z_{loss} = Z_{sys} - Z_{pat} \Rightarrow min.$). The minimal loss allows optimization of the reaction time with a low time-constant. The small delay of the reaction to the physiological changes allows prompt adaptation to alterations during the treatment; even small animals in preclinical experiments have a significantly higher heartbeat and breathing frequency than humans [29].

The impedance matching needs a conductive media between the electrodes, and the RF-current flows through it. Consequently, the system cannot tune on the situation when a patient does not present in the active radiation zone. The technique therefore induces minimal radiation to the environment, and it is safe.

Due to the forced RF-current, the patient becomes an electric component of the real-time adaptive tuned electric circuit, representing active electrical impedance. In this matching, the patient is not simply an "energy absorbent" but an active electric element of the serial circuit.

2.3. Comparison of Capacitive Couplings

In general, all capacitive couplings are equal based on the formal capacitive arrangement level, however their technical details differentiate them. The variation could be so significant that it produces—either homogeneous or heterogeneous heating in the target.

Comparing the variants of capacitive couplings requires a detailed study of the electronic, structural, and material design differences of the circuits. All capacitive couplings involve a capacitor used for energy transmission to the target, emphasizing the electromagnetic interactions' electric field component, using electrodes with the target volume placed between them.

The plane wave capacitive coupling transmits the radiofrequency by the plane antenna, and some of the radiofrequency is even transmitted through the air, Figure 4 . A popular hyperthermia technique applies a typical radiative plane-wave solution [30], but the high voltage for radiation necessitates enormous power (600 W for a mouse with tumors weighing 2 g) [31] [32]. However, the plane-wave solution could work with a lower power when the distance (space in the air) between the electrode and the body surface is small, or negligible, or the matching parameters allow high voltage and low current for the applied power.

Importantly, impedance matching of capacitive coupling does not work when isolated (i.e. when there is a space or air between the electrode and body surface), Figure 5.

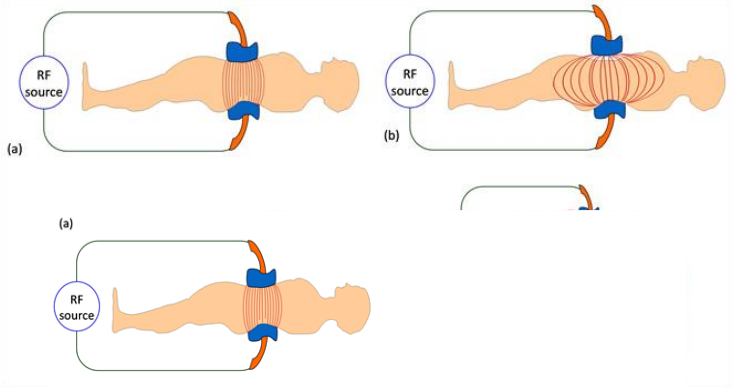

Figure 12. The plane-wave radiation works through the air, and so it is not sensitive for electrode fixing.

Figure 13. The impedance matching uses the RF-current-flow through the body and does not work when an air slit exists between the electrode and the body.

All capacitive couplings have an engineering control point to optimize and maximize the provided power from the RF source and, using the power-supply safely, to avoid its overheating. The measuring points fit the circuit's impedance to the source's internal resistivity, using the conventional standard 50 Ω. However, this engineering control does not take into account the medical control. The medical control or reference point refers to the point at which there is minimal loss of energy to the environment and maximal absorption in the patient while ensuring the safety of the patient and minimizing unwanted hot spots.

The optimal engineering settings do not necessarily align with the optimal requirements for the patient safety and treatment, Figure 6 .

Figure 14. All losses are minimized by proper geometry, material-selection, careful design of specialized electronics, super-low imaginary (reflected) power, ($\varphi \cong 0 \varphi \cong 0$) etc.

There are decisional differences between the realization of capacitive coupling methods at the level of simple measuring observations. The two major categories are the plane-wave and impedance matching techniques Figure 7 , and other solutions combine these two categories.

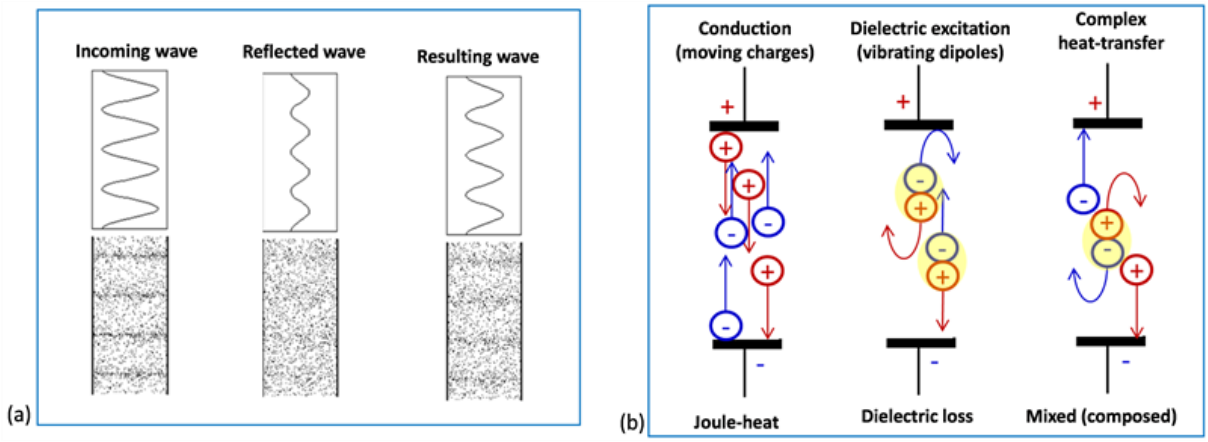

Figure 15. The matching arrangements. (a) The plane-wave matching uses a forwarded power and measures the reflected one to deduct and calculate the resulting radiative power; (b) The impedance (quasi-galvanic) matching uses the current-flow of the free charges (ionic species in aqueous electrolytes on the body) and the rotational or gradient-induced linear movements of dipoles in the tissues.

The observed differences could be technically detected by measuring the engineering reference point (optimal engineering set-up), and the medical reference-request point. The inequality between the reference points is due to the losses in the circuit, including the matching tuner, cables, radiation processes, used materials, and structures, as well as the capacitive coupling with the environmental objects (like walls, other types of equipment nearby, or the operating personnel). At this point, the engineering control and the medical control could significantly differ from each other, Figure 8 .

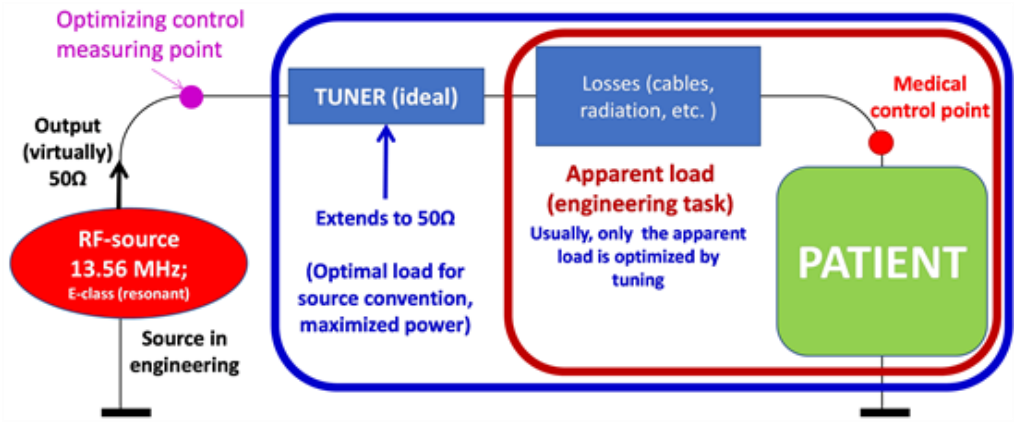

Figure 16. All losses are minimized by proper geometry, material-selection, careful design of specialized electronics, super-low imaginary (reflected) power, ($\varphi \cong 0 \varphi \cong 0$) etc. The matching has to accurately control the medical point shown in the figure.
The tuner electronically compensates for the overall losses, and the power- supply increases the power to replace the missing, lost energy. This type of matching procedure favors plane-waves on the patient, which uses wave-absorption, with a particular exponential decrease from the surface incident energy in the body, and is intended to create homogeneous heating in an actual depth.

The compensation of the general losses by the circuit components and environmental interactions do not optimize the patient-power from a medical point of view. After the medical point (which begins at the electrode), the initial RF-current enters the "coupling complex," including the patient's targeted volume. After this point, new unwanted losses challenge the optimization of the treatment. These include the electrode structure, electrode material, the bolus system, the patient's surface adipose tissue, the healthy impedance, etc. This extra impedance is the vital target: the impedance of the tumor. Hence the optimization of the treatment point is crucial in order to successfully heat the tumor. How this is optimised defines the type of capacitive coupling (Figure 9).

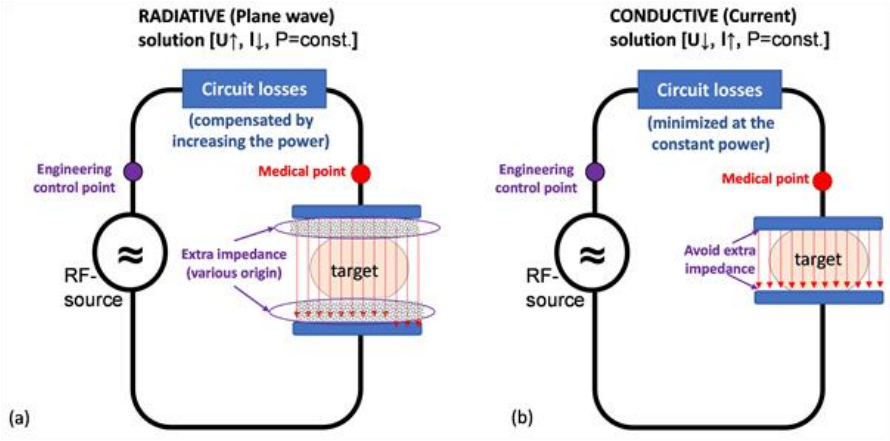

Figure 17. (a) The plane-wave matching allows a lazy connection of the electrode for various reasons; (b) The

impedance (quasi-galvanic) matching does not work with improper impedance between the “medical point” and the body surface.
The impedance matching focuses on the medical control-point, minimizing the impedance of components that derail the primary target’s energy, the tumor. Without taking into account the medical point, the RF-current flows through two different impedance categories: the objects’ impedance, which fits the current transfer to the body, and the body impedance.

The various components of object impedance challenge the conductive approach (Figure 10).

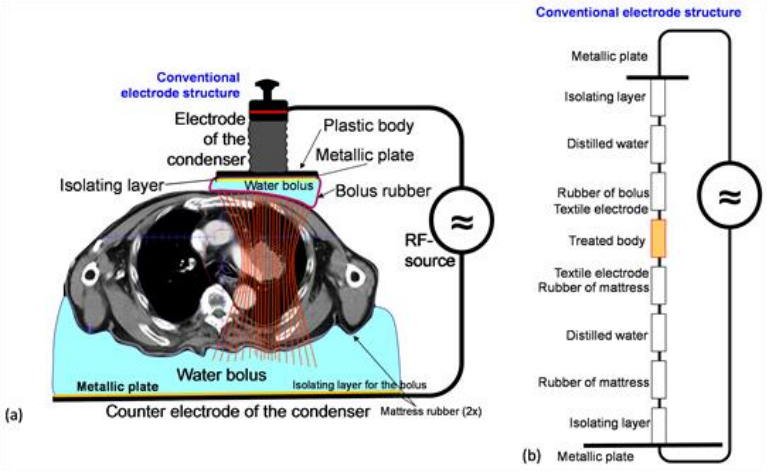

Figure 18. Numerous serial impedances modify the energy-distribution in capacitive coupling. (a) The main structure of the conventional capacitive coupling with water-bolus; (b) The draft of the impedance of the conventional electrode structure.

The best solution would be the galvanic contact of electrodes (Figure 11), which may be approached by the electrode design accompanied with the resonant compensation.

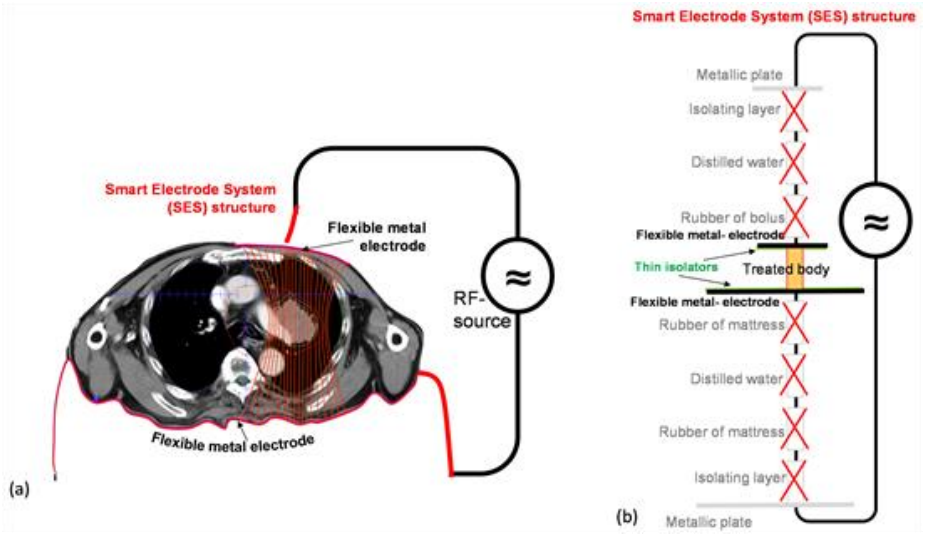

Figure 19. The draft of the design of impedance matching, which is (a) quasi-galvanic, or (b) the solution mimics the galvanic touching with a precise resonant compensation.
The body impedance contains a very heterogenic structure. Each of which represents a resistor and a serial capacitor (the inductive parts are missing) (Figure 12).

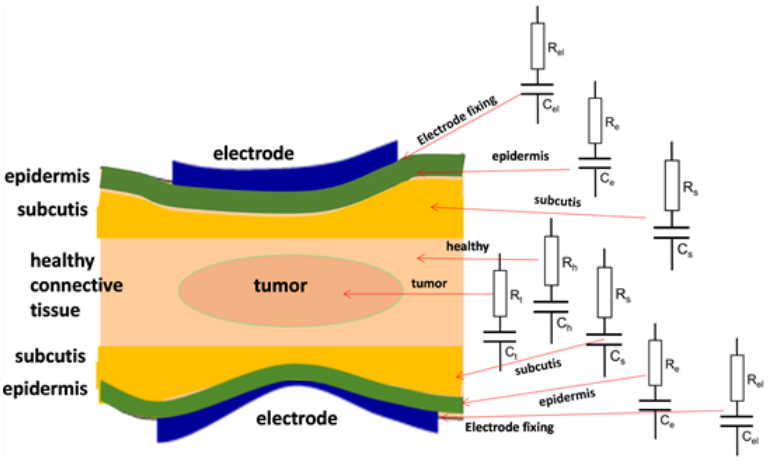

Figure 20. The major layers of the human body's targeted volume show the serial RC parts in every layer.

The compensation procedure in impedance matching minimizes the capacitive (imaginary reactance) factor, and the resistive part remains in focus. A particular category of impedance matching is the modulated electro-hyperthermia (mEHT) which selects the malignant cells in this heterogeneity, and the tumor-cells concentrate the primary energy absorption (see later text below). Consequently, the dominant resistivity part is the set of the tumor-cells in the targeted volume. On this basis, we approximate the effect of the different resistivities and the resistivity of the healthy tissues is negligible in the first attempt (Figure 13).

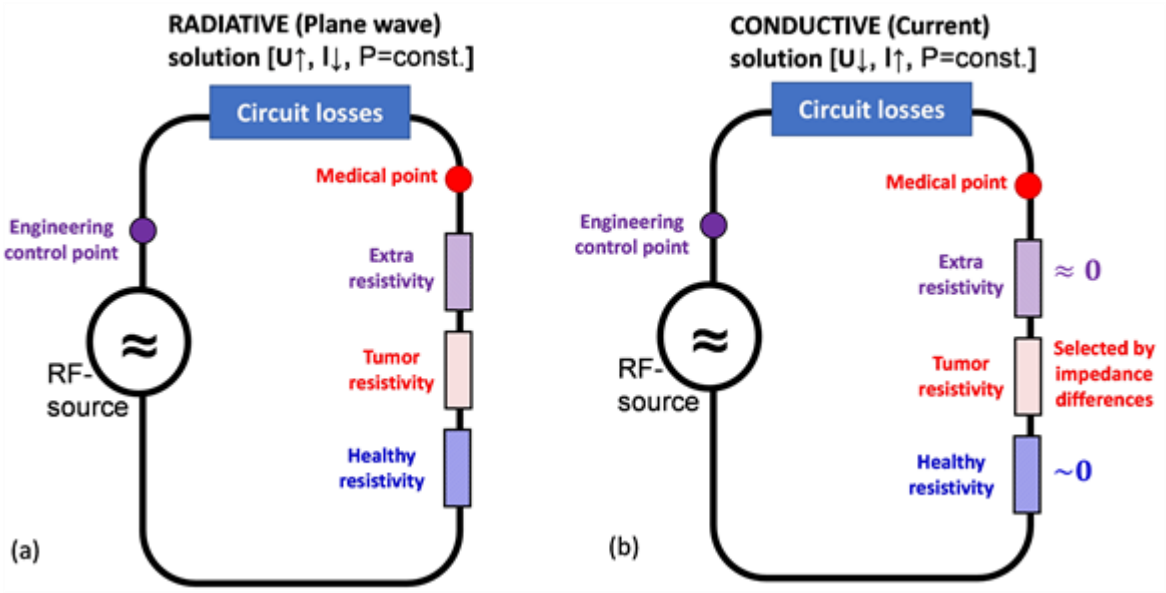

Figure 21. The voltage and current generation with the same value of power in plane-wave matching (a), and in impedance (quasi-galvanic) matching solutions (b).

All of these considerations involve a resonant matching method. AC/RF circuits imply a certain frequency determined by the values of the resistance, capacitance, and inductance of the serial circuit (Figure 14).

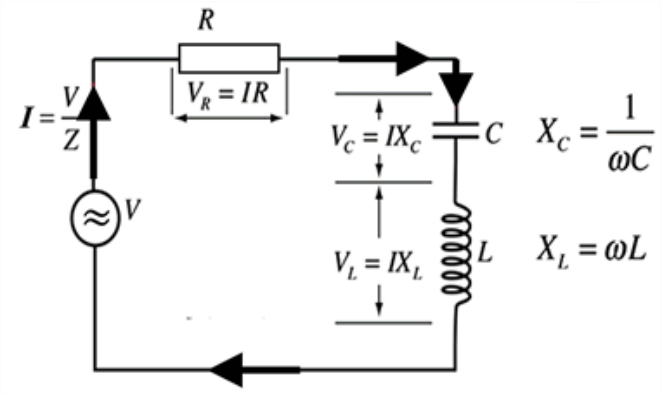

Figure 22. The discrete representation of the circuit describing the impedance matching. V_R, V_C and V_L are the voltage drop on the discrete elements. The resonant compensation produces the V_L.

The dielectric permittivity and the conductivity affect the RF-current differently, and the result is called impedance. Mathematics using complex numbers describe the two independent effects showing the conduction on the real conductor while the dielectric permittivity defines the isolators, where the conduction of the RF-current is imaginary. The patient's impedance represents the real part (R_{pat}), and the reactive part (Y_{pat}), and $Z_{pat} = R_{pat} + iY_{pat}$, where $i = \sqrt{-1}$ denotes the imaginary part. In geometrical representation, it shows a vector (Figure 15).

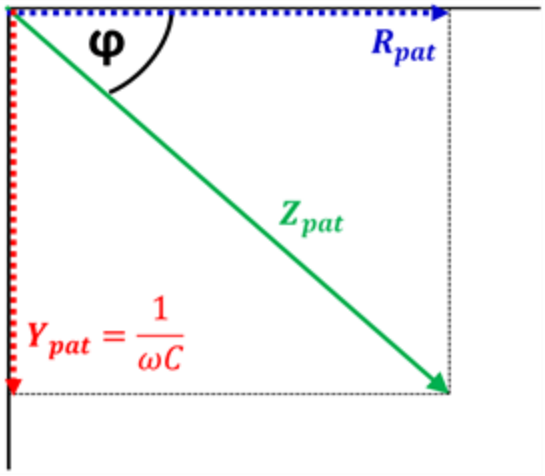

Figure 23. The vector picture of the impedance in living objects. The R_{pat}real resistance and Y_{pat}imaginary reactance produces the Z_{pat}impedance with the φ phase angle. Due to the only capacitive part (no inductive element exists in the living orga

The impedance minimum characterizes the serial resonance. The impedance from the imaginary parts of capacity (C), and inductivity (L) are $Y_C = \frac{1}{\omega C}$,, and $Y_L = \omega L$, respectively, and the impedance is $Z = \sqrt{R^2 + (Y_L - Y_C)^2}$. Hence, when $\omega_0 = \frac{1}{\sqrt{L \cdot C}}$then $Y_L = Y_C$, and the resulting minimal impedance is $Z = R$ with zero phases. The selectivity of a circuit depends on the circuit's serial resistance.

The Y_{pat} depends on the applied frequency (f), while the real conductor does not depend on f. The living matter has a negligible inductive (coil-like) component in Y_{pat}. Mostly the membranes, and the other isolation layers form Y_{pat}, which act as a C capacitor, $Y_{pat} = \frac{1}{2\pi f C} = \frac{1}{\omega C}$Where $\omega = 2\pi f$. Applying the vector representation of the impedances (Figure 15), the variation of the major layers in the target volume of a human body gives a resultant impedance $R_{pat} = \sum_{i=1}^{N} R_i$i, and $YY_{pat} = \frac{1}{\omega}\sum_{i=1}^{N}\frac{1}{C_i}$. Using the resonance frequency $\omega_0 = \frac{1}{\sqrt{L \cdot C}}$, an additional inductive factor would compensate the Y_{pat} to minimize the impedance of the target. The necessary inductivity for resonance is $L = \frac{\omega_0^2}{C} = \omega_0^2 \sum_{i=1}^{N}\frac{1}{C_i}$ (Figure 16).

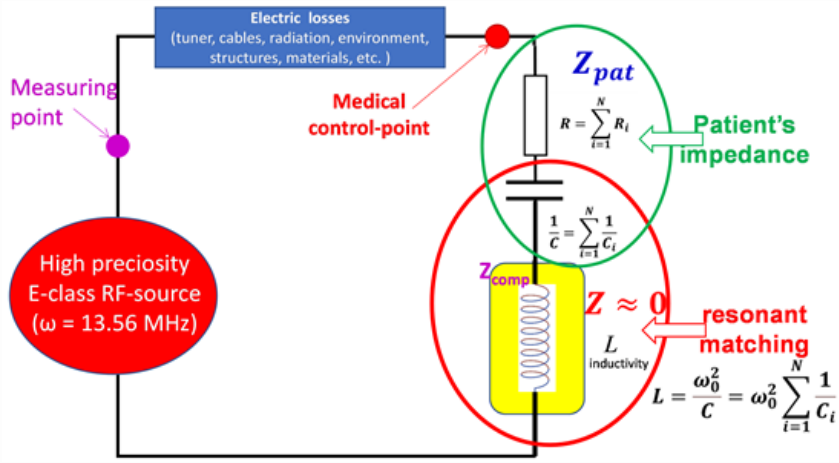

Figure 24. The patient is an electric component of a precisely tuned resonant circuit. The compensation clears the target impedance minimizing its reactance.

The compensation transforms the impedance near a real resistance value as shown in vectorial representation (Figure 17). The vectors show the complex impedances of some critical layers in the body during the RF-current flow. The horizontal axis is the real part (the real conduction), while the perpendicular one is the imaginary part, representing the isolation. All tissues have isolation also due to the various membranes. The electrode isolations are neglected, so the resulting impedance vector shows a decline, which a single inductive resonance could easily compensate for.

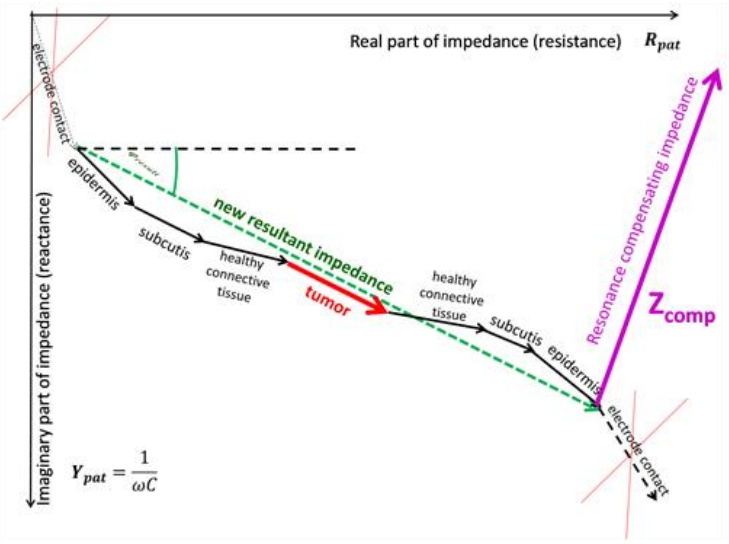

Figure 25. The vector diagram of the cross-sectional impedances in the average human body. Only the major components are shown, and for clarity, they are regarded as a discrete element.

The original current was $I_{orig} = \frac{V}{Z} = \frac{V}{\sqrt{R^2 + \left(\omega L - \frac{1}{\omega C}\right)^2}}$, the new current in resonance is higher $I_{orig} < I_{res} = \frac{V}{R}$, and in resonance depends only on the real resistivity. The current changes by resonance. The RF-current flowing through the target depends on the values of the components of the circuit. The well-selected situation filters a relatively small part of the targeted volume, the malignant cells, so their resistivity is small compared to the complete targeted volume. The small resistivity increases the peak of the current in resonance, Figure 18 .

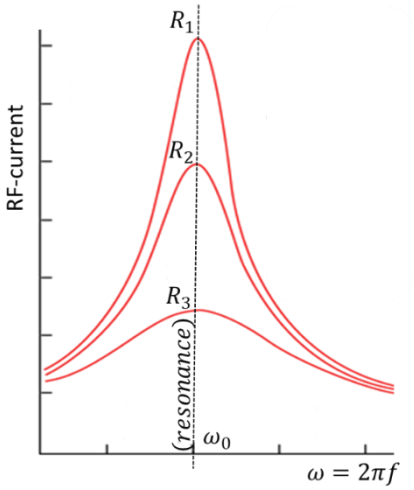

Figure 18. The RF-current distribution in the resonant conditions. The resistivity is decisional; when it is low, the peak is sharper ($R_1 < R_2 < R_3$). The $f_0 = \frac{\omega_0}{2\pi}$ is the resonant frequency.

Since this power depends on the square of the current the resonant curves appear steeper and narrower in the presence of lower resistivity. The quality factor Q is defined by $Q = \frac{\omega_0}{\Delta\omega}$where Δω is the width of the resonant power curve at half maximum (Figure 19).

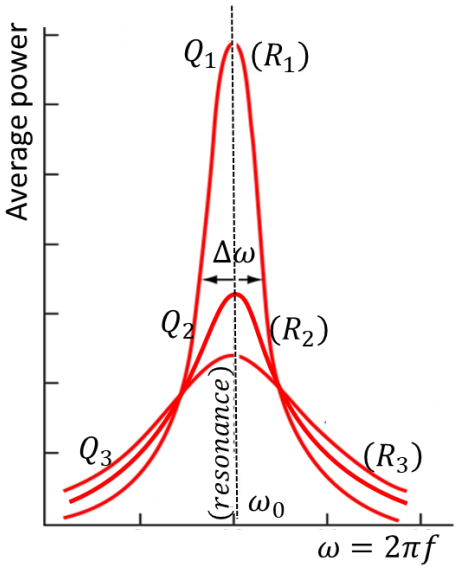

Figure 19. The resonance quality factor (Q) defines the average power in resonance. $R_1 < R_2 < R_3$, and so $Q_1 > Q_2 > Q_3$. The $f_0 = \frac{\omega_0}{2\pi}$is the resonant frequency.

Since that width turns out to be $\Delta\omega = \frac{R}{L}$, the value of Q can also be expressed as $Q = \frac{\omega_0 L}{R}$. The Q is a commonly used parameter in electronics, with values are usually in the range of Q = 10 to Q = 100 for circuit applications. The smaller the resistance, the higher the "Q" for given values of L and C. The power, of course, depends on the product of actual current and voltage. When the current increases due to the resonance, the voltage decreases, while maintaining the same power.

The resonant approach uses the minimizing of the reactance (imaginary part) of impedance. Physiological regulation also has a vital role in the process. One of the reasons for using the plane-wave capacitive coupling is the surface adipose tissue challenge, forming an isolator-like layer at the skin. In a plane-wave situation, the

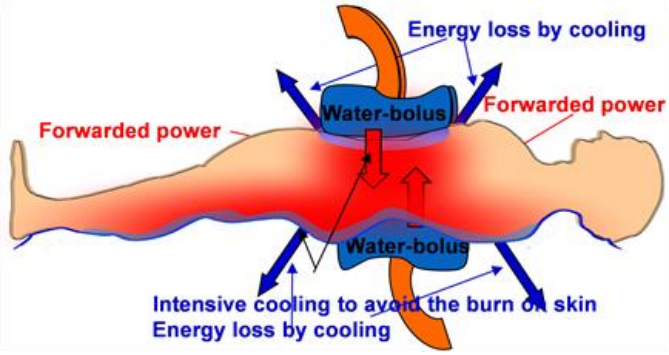

Figure 20. The cooling of the bolus produces uncontrolled energy-loss and induces a positive-feedback physiological regulation. (see the text)

voltage is increased to surmount the gap by the isolator of the adipose layer. However, this way, the energy-absorption in this layer is extremely large, so the risk of burn increases. In order to avoid this risk, the plane-wave method uses intensive cooling of the skin by using the bolus system, Figure 20 .

However, this cooling has unexpected positive feedback reactions from the physiological control of the body homeostasis: the cooled skin lowers the blood- flow in the subcutis, which increases the layer's isolation towards RF-current. This induces a higher voltage request, which increases the risk of burn, so a further increase of the cooling is necessary. It further increases the isolation, and so on, the situation would be hard to control. Furthermore, the intensive cooling absorbs a large part of unmeasured energy, which makes the therapy dosing with incident energy impossible, as is similar in the case of ionizing radiation. Consequently, the impedance matching takes attention to the cooling process and keeps the homeostatic control stable in the subcutis layer under the electrodes.

In summary, the strategy of impedance matching concentrates on increasing the current as much as possible. The major factors to maximize the current are:

- the resonance approach,

- the design, structure, materials of the electrode system,

- the grounding optimization to lower the radiation, and coupling to environmental objects,

- the regulation of the homeostatic status of the skin blood-flow (which regulates the imaginary part of the skin-structure of the patient),

- eliminating the losses in an electric circuit as much as possible,

- the high current value (in the unchanged power conditions) makes a more effective selection,

- the high current accompanied with low voltage at the constant power, increasing the safety of the treatment.

3. The Modulated Electrohyperthermia (mEHT)

3.1. The Challenge of Homogeneous Heating

The classical heating concept applies a mass-heating of the entire tumor. The mass heating tries to be homogeneous in temperature (isotherm), and uses the temperature as the only control parameter.

The control of homogeneous (conventional) heating is problematic because

1) the local blood-flow is enhanced, which increases the risk of dissemination and metastases,

2) colossal power is necessary to ensure quasi homogeneity, which again involves many safety issues,

3) due to the heterogeneity of the target, the control of homogeneity is very complicated, in most cases it could not be achieved,

4) the homogeneous hyperthermia thermally kills the cells and occasionally triggers immunogenic effects in the area,

5) the challenge of measuring temperatures at has not been solved; MRI thermometry is promising but still has challenges,

6) the only homogenous (and large CEM43T100) solution is the whole body treatment (WBH), which does not show the expected success.

The invasive measurement of the tumor's temperature has multiple problems, as a result the temperature is typically measured in the nearby lumina or cavities of the body. So the mass heating must be regional, having comparable temperature in the nearby lumen (like oesophagus, bronchus, colon, vagina). The same isotherm heating appears in the plane-wave concept of capacitive coupling. The modulated electro-hyperthermia (mEHT) method uses impedance matching of capacitive coupling with some unique features, which have been developed over the past 32 years, and documented and patented. The mEHT method harnesses the impedance matching shown above with additional elements, improving its efficacy.

The present technical challenges are:

1) The energy selection ensures the local place of energy absorption. It has major complications due to the normal physiological movements caused by breathing; and the technical solution has limitations when attempting to heat deep-seated tumors without considerable heating of other tissues.

2) The dose determination, which controls the medical application, is a mandatory parameter, but the heating techniques determine the clinical results. We have seen that exposing the tumor isothermally to 42°C in whole-body hyperthermia, has entirely different results than the same temperature in any local treatment. The technical solutions based on the temperature alone do not characterize the applied method.

3) The role and measurement of temperature in the treatment efficacy are challenging. The value of the temperature in the target supposes an isothermal mass-heating, which never happens in LRHT. The temperature measurement approximates the tumor's value, checking the temperature in the nearby lumen (like esophagus, bronchus, colon, vagina). This method assumes that the heating does not focus on the tumor-mass, but equally heats its healthy environment.

Due to the above challenges, temperature measurement is mandatory to approximate the absorbed energy, which differs from the technically provided value. The high energy losses (like various electric losses, losses from cooling water, etc.), and the need to control safety (avoid burns) are fundamental reasons to measure the temperature.

3.2. Heterogeneous Heating

The mEHT chooses a new paradigm, it heats the cancer-cells selectively in the tumor, using the malignant cells' unique thermal and electromagnetic characteristics. The structural change of the local heat-capacities, heat-conduction differences, heat transfer by blood, and lymph electrolytes cause the thermal heterogeneity. Significant differences in the electric behavior of micro-states of living matter determine the electromagnetic heterogeneity. The variation of electric conductivity and dielectric permittivity by the living processes and the differences of lipid-protein structures in the cell-membranes and the cells' cooperative differences appear to be the most influential factors for electric heterogeneity. Further differences between the malignant cells and

their healthy counterparts develop as a result of the heat-resistance, motility of the cells, and cellular and extracellular mechanical properties.

Some other significant differences are present at a molecular level, but these are less effective in distinguishing the malignant cells from their healthy counterparts. Using heterogeneity offers a valuable tool to select the malignant cells in the heterogenic tissue. The RF-current presents a possible tool for clear recognizing of the heterogeneities. The current-flow changes based on the electric heterogeneities and its heating effects connect the current to the thermal properties. An essential component of tissue heterogeneity involves molecular reactions, which differ depending on the tissue and cells. For example, the apoptotic control, a well-known regulation in healthy tissues, is almost entirely missing in malignant tissue, as described in the hallmarks of apoptosis could happen through multiple molecular mechanisms, which do not work in cancer.

3.3. Considering the Homeostatic Regulation

From the beginning of human medicine, physicians recognized the equilibrium of the living organisms, which defines the healthy state, and has multiple dynamic components which are finely balanced. This was the first recognition of homeostasis, which has definite lower and upper limits of the interactions and conditions. The body homeostasis is stable within a certain interval of the parameters; the level of any interactions is determined and measured by the harm caused at the extreme limits. However, the harm is a relative notion: the safety and the harmless categories are not identical. The "no action" treatment can be safe but harmful because the uncontrolled disease harms, which we can stop by action. The acceptable changes in medical actions attempt to reestablish the normal, healthy homeostasis; or if it is not possible anymore, then it attempts to approach it as close as possible. The Hippocrates-phrase, "Nil nocere" also has to be understood in this way. Otherwise, the meaning is "Do nothing".

The internal transports, like the blood-stream, have a central role in keeping homeostasis. The blood circulation regulates multiple vital processes, including the heat exchange, to ensure the body's proper functional conditions. The blood-stream tries to compensate for the overheating by intensive perfusion and regulation of the vessels' flow-capacity. However, the regulation process of the blood-stream is non-linear. The quantitative analysis [33] shows the non-linear changes of the blood-flow in characteristic tissues varying by the temperature. The deviation (selection) of the tumor blood-flow starts just above 38°C, Figure 21 .

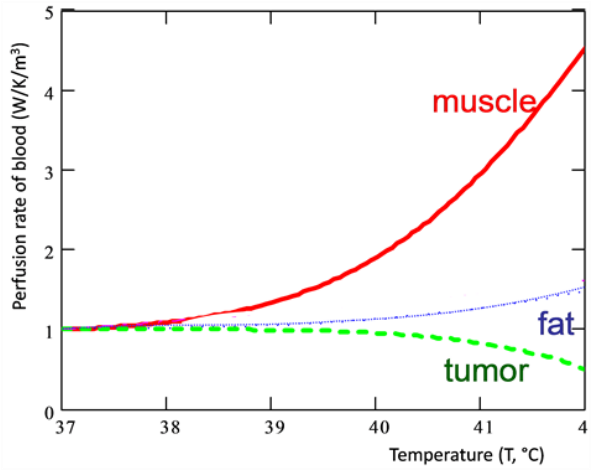

Figure 21. Relative quantitative changes of the blood-flow by a temperature increase in muscle, adipose tissue, and tumor lesion.

Due to the variation of the blood-flow, the necessary energy in a mass unit (specific absorption rate; SAR [W/kg]) non-linearly changes in the range between 39°C - 42.5°C [34] by the actual temperature, Figure 22 .

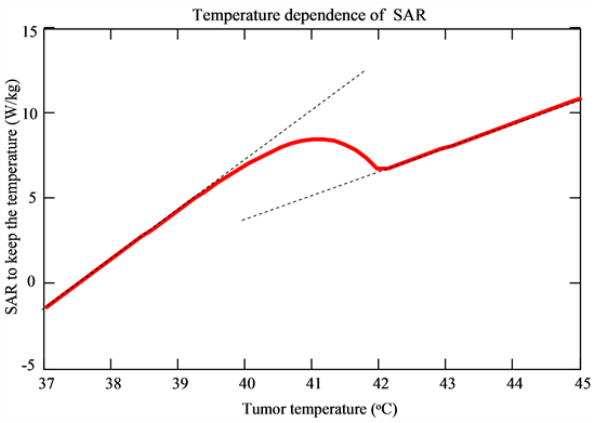

Figure 22. Variation of the requested specific absorption rate (SAR) to keep the given temperature in the tissue.

The non-linear regulation is general, using physiologic control by negative feedbacks. The promoter-suppressor action realizes the contraction of the feedbacks, which has a broad response-time for intervention.

3.3.1. The Selection Mode

The classical heating concept applies mass-heating of the entire tumor. The mass heating tries to be homogeneous in temperature (isotherm) and uses the temperature as the only control parameter. As previously discussed the temperature is usually measured in the nearby lumina or cavity and the same temperature must therefore be achieved in the lumina/cavity. The mEHT method uses a different paradigm, its heats the cancer-cells selectively in the tumor (Figure 23), using the malignant cells' unique thermal and electromagnetic characteristics.

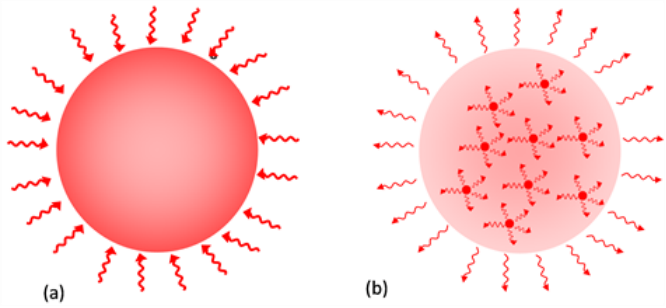

Figure 23. The differences between the heating paradigms: (a) Plane wave matching homogeneous heating causes energy-absorption in the complete target, while (b) impedance matching could be selective, heats only selected parts in a heterogenic manner, heating up the surrounded tissue by heat conduction (mEHT principle).

The selection uses the natural heterogeneity. The RF-current recognizes the electrical heterogeneity, and its heat effect results in thermal heterogeneity, resulting in the complex synergy of electric, and thermal processes [35], induces molecular changes driven by mEHT. The malignant differences make it possible to distinguish malignant cells from healthy cell structures [36]. The amount and composition of the extracellular aqueous electrolyte in the micro-environment of tumor cells massively differs from healthy tissues.

The malignant cells need a significantly higher energy amount than the healthy cells due to the intensive metabolism required to supply their proliferation [37]. The metabolic rate in most of the tumors is higher than their healthy counterpart (at least 15%, [38]), which selectively increases their temperature. The process has positive feedback because the higher temperature decreases the tissue's impedance [39]. Their metabolism requests a robust amount of nutrients which in the simplest way demands glucose. Due to the high level of necessary ATP production, the tumor cells predominantly perform simple anaerobic glycolysis instead of mitochondrial phosphorylation. The positron emission tomography (PET [40] [41]) identifies the extreme glucose intake in cancer cells. The rapid, intense fermentative process produces lactate, increasing the electrolyte's ionic conductivity in the cellular microenvironment, jointly with the higher in- and outflux transport

of other ionic species. The increased ionic concentration means higher conductivity [42] of the microenvironment of tumor-cells, so it lowers the whole tumor's resistivity. This can be used to distinguish between healthy and malignant situations [43]. The RF-current selectively flows through the low resistance (highly conductive) tumor rather than the more resistive healthy environment.

Malignant cells are autonomic, independently fighting for the energy against all other cells irrespective of healthy or fellow cancer-cells. For autonomy, they break their networking bonds and stop direct intercellular communications. The bonds formed by adherent proteins and junctions mostly vanish. Due to the missing cellular network, the extracellular matrix of malignant cells has high dielectric permittivity, which can be used for selection [43]. The structure of the microenvironment rearranges due to the missing bonds [44]. The altered structure allows the recognition of the malignant cells by their dielectric properties, which modifies the applied RF current [45] [46]. A well-developed diagnostic method uses this phenomenon [47], and it is applied in mammography [48].

The permittivity and the conduction modify the complete impedance in the microenvironment of the malignant cells [5], allowing their selection in an automatic way, while the RF-current flows in the direction of low electric impedance. The RF-current-density (specially chosen frequency and modulation) self-selectively flows toward the malignant cells, which is measurable by MRI current density imaging, [49] [50] [51]. This effect is completely automatic, it follows all movements of the cells in real-time, actually solving the challenge of focusing. The direct MRI electrical impedance tomography confirms the feasibility of using the impedance differences for selection [52].

The broken bonds between the cells leave the transmembrane proteins unconnected. These transmembrane proteins group by lipid-protein interaction in the membrane. The concentration of lipid rafts on malignant cells' membranes is significantly higher than on the membrane of non-malignant cells. The impedance-selected malignant cells' dense lipid rafts become an easy target of energy absorption. The rafts' clusters absorb the energy from the RF-current selectively [53] because the rafts have significantly lower electric impedance than the surrounding isolating lipid membrane. The selective energy-absorption promoted by a characteristic frequency dispersion in the applied 13.56 MHz frequency range (β/δ dispersion [54]), and the Schwan effect [55]), targets the lipid-protein interactions and selects water-bound states [56] at the membrane, effectively focusing the energy on the target [57]. This way, the natural electric heterogeneities drive the selection for energy absorption automatically, constructing an "autofocusing" process.

Further selection could be realized by the structural differences of the malignant tissue from their healthy counterpart. Usually, the pathological investigation of biopsies utilizes these differences by image pattern recognition in the samples. The pathological pattern naturally affects the RF-current in-situ, allowing additional selection of cancer tissue in the body. The alterations of the pattern modify the cells' spatiotemporal interactions, which dynamically act via intercellular interactions. The well-chosen noise could transduce free energy for the cellular reactions [58]. The dynamic relations produce a noise of homeostatic equilibrium, which is measured as a peculiar signal [59] [60]. This noise differs in malignancy versus healthy tissue and is measurable by the RF current [61]. The noise difference is the basis for the applied modulation on the RF carrier in the mEHT method [62]. The modulation is an information delivery to the malignant lesion. The applied time-fractal has such autocorrelation time-lags that well fit the apoptotic excitation processes and may also act in enzymatic catalysis [58]. The spectrum of the reaction-times and rates appears in the modulation frequencies. The mEHT method applies such modulation, which is in harmony with the homeostatic collective network.

The collective excitations comprise the non-local waves and activate the energy-flow in the homeostatic networks. These excitations are mostly in a low-frequency range, and the expected frequency spectrum follows the natural 1/f fluctuations. Simply speaking, the modulation acts in harmony with the natural collective

processes, promoting them, like keeping the swing in motion using harmonic push. Both the multicellular networked and the unicellular autonomic states of cells maintain a balance which is probably realized by an electromagnetic route [63]. The FDA-approved TTF also uses this kind of interaction to arrest malignant cell-division [64]. The method of mEHT uses an electrical field to modify the polymerization processes in the mitotic phase of the cellular division [65] with fractal noise modulation for a complex effect.

Furthermore, the applied noise is an active harmonizing factor [66], which has an emerging physiological application [67]. The fluctuations of electrical properties have unique information related to cell-membrane processes [68]. The monitoring of the noise as fluctuations in the complex system could be a factor in its surveillance [69]. Forcing harmony reconstructs the broken E-cadherin-beta- catenin cellular connections [70], which as was effectively and repeatedly demonstrated in an independent study [71]. The malignant cells' membrane is more rigid [72], while the cells themselves are softer than their neighboring healthy cells. The adherent connections and junctions could be formed only when the reactive ligands are close to each other.

As a result, the cellular connections have a geometric requirement to be re-established. The fermentative way of metabolism of malignant cells develops a strongly negative glycocalyx shell, which works against the proper geometric order, blocking bonding between the appropriate ligands. However, the extremely high fluctuating cataphoretic forces from the pink-noise modulation compensate the repulsion, and make the adherent connections possible.

The modulated carrier signal targets the selected malignant cells, and the cells rectify (demodulate) the received signal. The demodulation process uses two factors:

normal rectification by the highly polarized cell-membrane, [73] [74] [75].

stochastic resonance that makes the rectification, [76]

The non-temperature dependent rectification (non-linearity) was a question-mark for a long time because only linear attenuation was measured through the living object. The double membrane effect causes this apparent linearity. The challenge is to measure the rectification in a tissue in which every cell with its opposite positions of the entry and exit points on the cell membrane acts like two diodes connected oppositely. So no rectification could be detected by measuring the tissue alone, Figure 24 .

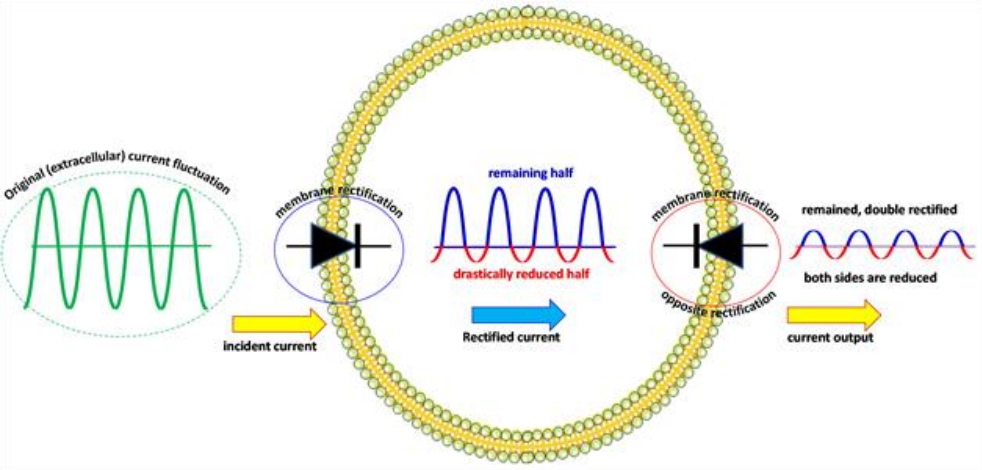

Figure 24. The symmetric but opposite rectification of the cell-membrane when the current goes through the cell makes the measured material linear, the rectification is not visible.

The mEHT impedance-matched capacitive coupling has four interconnected mechanisms for selection: the heterogeneities in conductivity and dielectric permittivity select the tumor, and its independent, while the membrane rafts absorb the energy in selected cells (the hyperthermia step), and the spatiotemporally distinguishable tumor-pattern provides an additional factor for selectivity, and isolation of the malignant cells, Figure 25 .

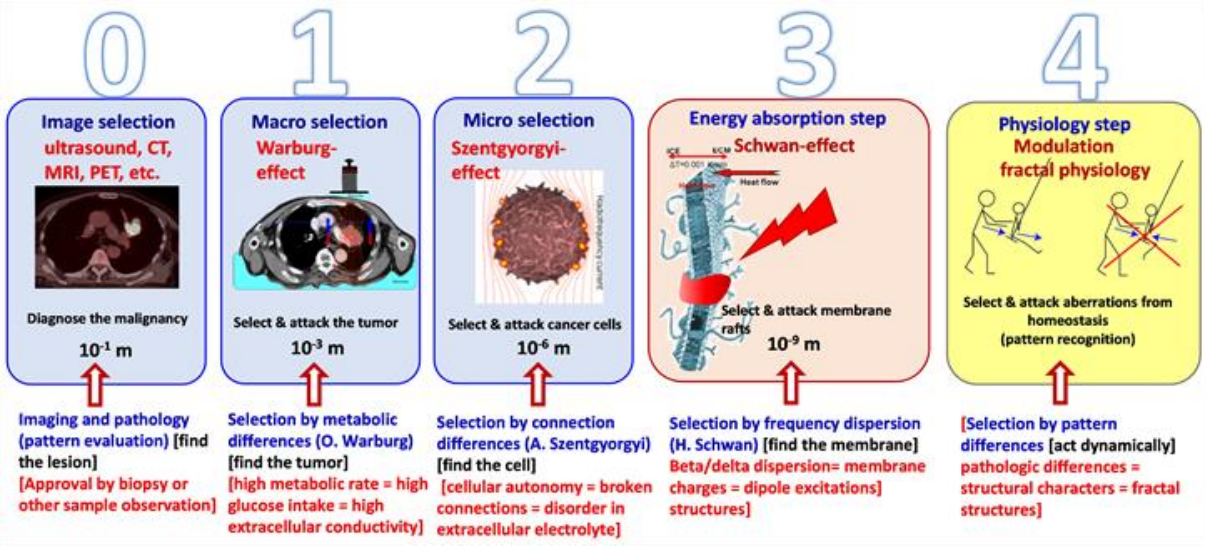

Figure 25. The steps of the mEHT action. (0) The conventional imaging supports the diagnosis; (1) The macro selection by conductive heterogeneities; (2) The micro-selection by the permittivity heterogeneities; (3) The energy absorption (the hyperthermia step) on the nano-range membrane raft; (4) A broad time-fractal spectrum recognizes and corrects the spatiotemporal pattern irregularities in the body.

Contrary to the above complex focusing (selection) mechanisms of mEHT, the plane-wave capacitive coupling methods regulate their approximate focussing of the energy by the size of the electrodes. The appropriately chosen electrode size is their focusing mechanism and their homogeneous mass-heating does not select on the cellular level.

The homogeneous heating has to balance the higher temperature and the increased blood-flow, induced by the intensive heating. The bloodstreams are a promising sensitizer of chemo- and radiotherapies, but are also a potential promoter of metastases resulting from the massive transport possibility of the cancer-cells. This process risks increase the metastases by forming circulating tumor cells (CTC). The CTCs could produce micrometastases throughout the entire body, which are not observable by the present imaging techniques. Heterogenic heating with microscopic (cellular) selection does not have such a challenge: the targeted particles can be supposed to have equal absorbed energy-doses, so the absorbed energy is the measured parameter. While the homogeneous heating method heats all parts of the target from outside, the heterogenic heating heats only the selected particles, and those heat the tumor where they are located. The selected particles are heated up intensively to have a higher temperature than their environment. The RF current at the <15 MHz frequency predominantly flows in the extracellular electrolyte. Its energy-absorption creates an active temperature gradient through the membrane [77], converting the electric heterogeneity to a thermal one. The mEHT heating does not make a massive general temperature increase of the targeted volume, macroscopically it presents a moderate temperature increase, but microscopically mEHT could produce extreme hyperthermia [78] [79]. The gradient causes the complete target's heating to the level of mild hyperthermia [80], which complements the applied chemo- and radiotherapies [81], but reduces the risk of metastases by CTCs. Notably, the pharmacokinetics of drugs are promoted by mEHT selective heating [82] [83].

The mEHT limits the increase of the SAR, which forces the development of the temperature. At a high temperature, the microscopic selection disappears, and an average temperature characterizes the target, like in plane-wave energy absorption Figure 26 . For mEHT, the limited energy-absorption is mandatory.

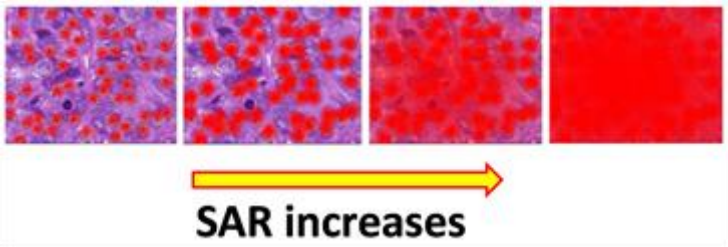

Figure 26. When the energy is too high, then everything is heated up, no selection could be seen. The selection factors became negligible. The selectivity has been lost, like the difference between the medicament and poison.

The electromagnetic selection mechanisms are general, and valid to all electromagnetic absorption methods treating cancer. However, the careful design with focus on the precise selection emphasizes the anyway small effect. The emphasis of the selection over the thermal averaging needs the above factors, which consistently exceed the selection effects over the massive trend to homogeneous temperature averaging. On average, the relatively small SAR is high in the rafts, similar to the nanoparticle selective heating. However, the nanoparticles in mEHT are molecular clusters, which are sensitive to overheating. When the absorbed energy destroys the rafts by overheating them then the mEHT loses its largest advantage: the excitation of signal-transports for apoptosis and immunogenic cell-death.

A natural question arises: without the modulation is the effect of mEHT the same as other capacitive plane wave techniques applied at a lower power? The answer is yes, if their technical solutions fit the low energy, then they could form such complex situations as the modulation and the low-energy selection does.

However, it is not enough to have low energy alone; it must be that the energy is there where we need it, inside. For this, absolute fine-tuning (resonance to kill all imaginary part of the impedance), in order to promote the high current instead of the high voltage at the coupling, and the well-controlled radiation losses. An example for this fine tuning is how: the same Otto engine works in the high and low category cars. However, the same petrol makes different values for dynamism, the fuel consumption of the cars or the same electromotor principle gives different “output” efficiency in the electric car.

In summary, the specialization operates with precise electromagnetic impedance selection [84], using the heat on membrane rafts [53], and makes harmony by applying thermal [85], and non-thermal effects [86] [87]. The applied modulation well supports the precise selection of the malignant cells [85]. The mEHT breaks the paradigm that the physical conditions do not allow the proper biological effects, as researchers show from Charite University [88]. The electric concept in sequential magnification summarizes the main principle, Figure 27 .

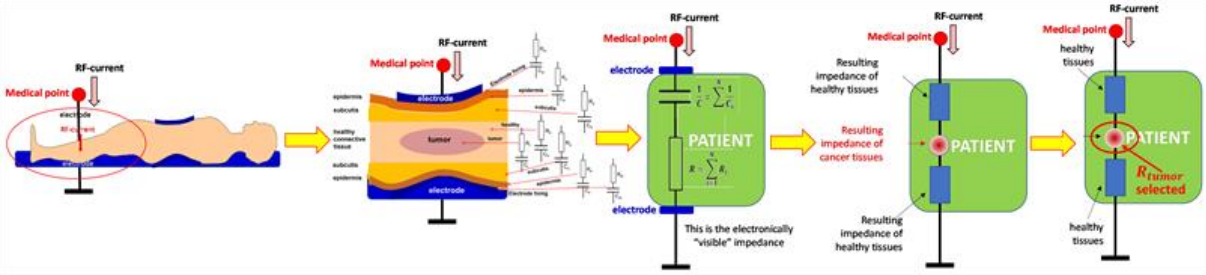

Figure 27. The series of the action of mEHT shows how it matches the focus on the tumor.

3.3.2. Penetration Depth

The penetration depth in the case of wave-absorption is the radiative penetration depth defined by the planar-wave absorption [89] [90], which is a loss of the absorbed specific energy or field in the body. The definition of the penetration depth of energy-absorption is the distance in the body when the initial 100% of energy from the surface decreases by 1/e (remains only 37% of the energy). This does not mean blocking the beam deeper. It is an exponential function. We have practical knowledge about the X-ray diagnosis, which sees the deep lesions in the body. However, these X-rays have less penetration depth than 10 cm, Figure 28 [91].

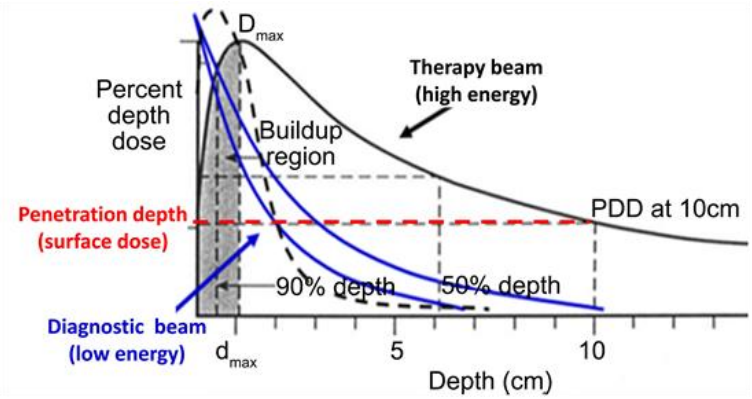

Figure 28. Diagnostic and therapeutical photon beams in X-ray radio diagnosis and therapy. Typical dose curves by photon (X-ray, γ-ray) radiation with typical penetration into dense tissues.

The beam continues its way in the body with 37% intensity, reaching the doubling of the penetration depth with 13.7% intensity, and so on, Figure 29 .

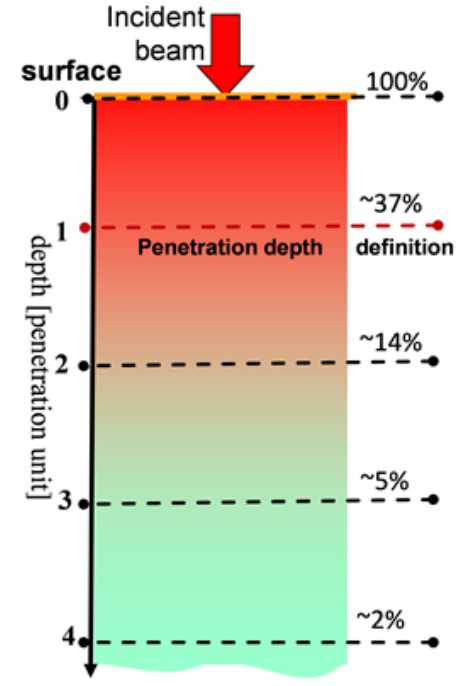

Figure 29. The principle of the definition of penetration depth: when the energy loss is 63% (remains 37%). Four times of penetration-depth, about 2% of the energy of the incident beam remains. This is the basis of X-ray diagnostic detection.

Assuming a patient with 20 cm thickness, the X-ray detection has less than 2% of the initial 100% beam intensity, but this is enough to construct an image, Figure 30 [92].

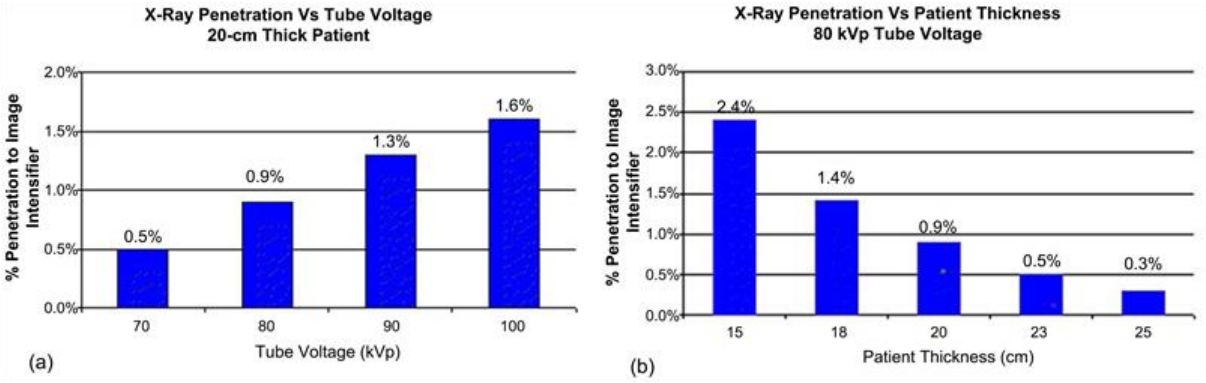

Figure 30. Typical intensities (percentage of the incident 100% beam) can be detected for X-ray images through the patient. In this case, and this tube voltage, the 20 cm patient thickness is approx. four times larger than the penetration depth. (a) Dependence of the voltage of the tube; (b) Dependence of the thickness of the patient at 80 kVp tube voltage.

In the case of electron-beam, the exponential loss is sharper, decreasing quickly, Figure 31 [93].

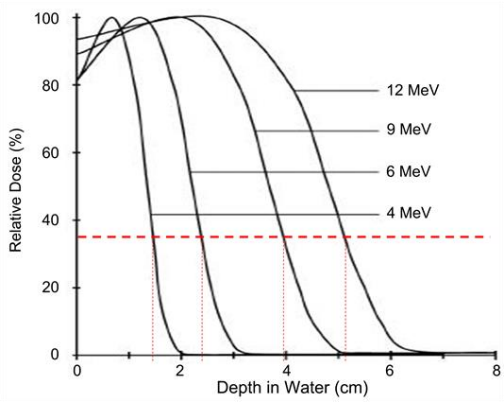

Figure 31. Penetration of electron-beam has a sharper decrease by depth. The definitive penetration depth is a few cm, shown with a dashed line.

In the case of non-ionizing radiation, the penetration is longer depending on the applied frequency (Figure 32) [94] and conductivity of the tissue (Figure 33) [94].

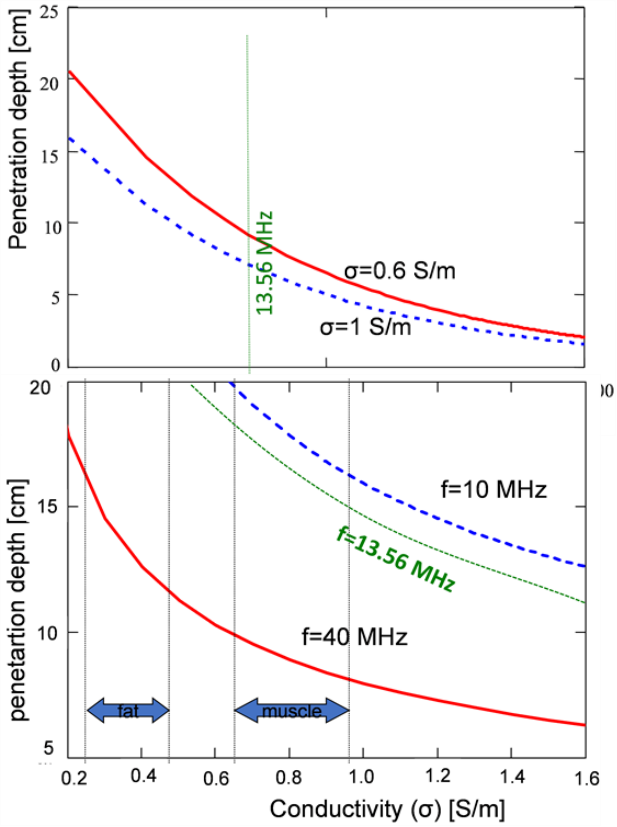

Figure 32. The penetration depth (37%) depends on the conductivity of the tissue. The average conductivity of muscle is approximately 0.5 S/m, so the penetration depth at 13.56 MHz frequency is about 17 cm. (at 8 MHz, it is approx. 20 cm.)

Figure 33. While the penetration depth is high in the fat, that absorbs a high energy value, leading to adipose burn. The apparent contradiction is the constrained increased voltage of the electrode required to push through the fatty tissue.

The jump of the electric field vector on the surface layer causes energy-absorption.

Measurements of the frequency dependence of the penetration depth in ex-vivo tissues show the correctness of the above considerations, Figure 34 [95].

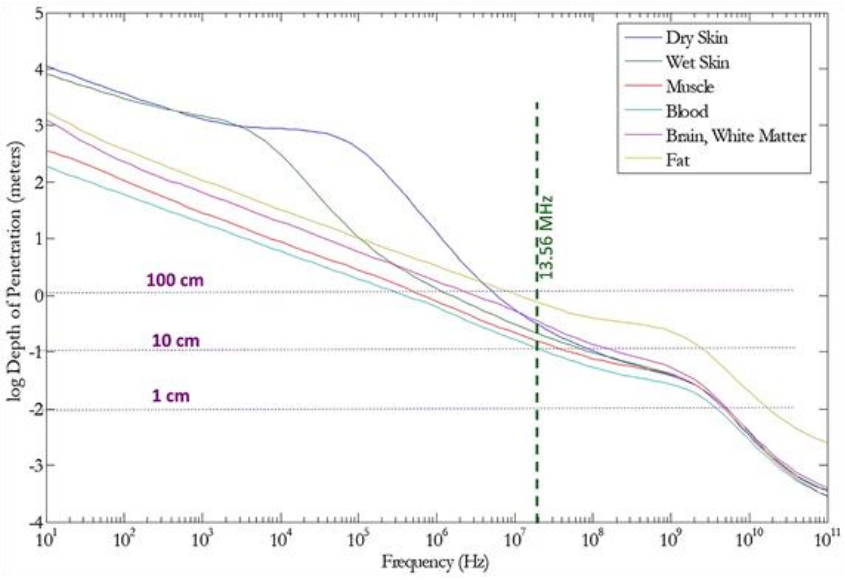

Figure 34. The penetration depth in various tissues vs. applied frequency. The 13.56 MHz is over 10 cm in all of the cases (the lowest is for blood, which is very good for selection). The penetration is rapidly decreasing by increasing frequency.

It is clear that the same forwarded energy exposition with identical energy-flow [W/m^2] can cause different energy-absorptions depending on the given conditions [96] [97], the actual organ [98], and the actual frequency [99]. The penetration depends on the electromagnetic parameters but does not depend on the patients' thickness. The impedance matching increases the penetration depth in homogeneous media by an additional 38%. (Note that the measurements and calculations assume homogeneous media.) The impedance matching selection focuses on the tumor-cells. The mEHT maximizes the RF-current, and only the focusing and the original energy deposit has importance [28]. The selection means that the real penetration is much more, and crosses the entire body.

3.3.3. Action Depth

Plane-wave capacitive coupling and all the homogeneous heating methods use only the heat to destroy the cancer-cells. The mEHT in its selective (heterogenic) heating combines the heat effect with the excitation of cellular signals. This fact modifies the induced processes' action depth as mEHT does not need such a massive energy-absorption as homogeneous heating needs in order to heat for the entire tumor-mass. We know very well that the real depth where the action is effective is an interval. For example, the effects of X-ray for apoptosis do not follow the decreasing energy-curve at the penetration. Even oppositely, it increases when the energy drops below a specific level, Figure 35 [100]. This is because the smaller energy can generate bystander effects and so it can trigger apoptotic signals. This makes a complete interval for the apoptosis, which does not correlate with the penetration depth.

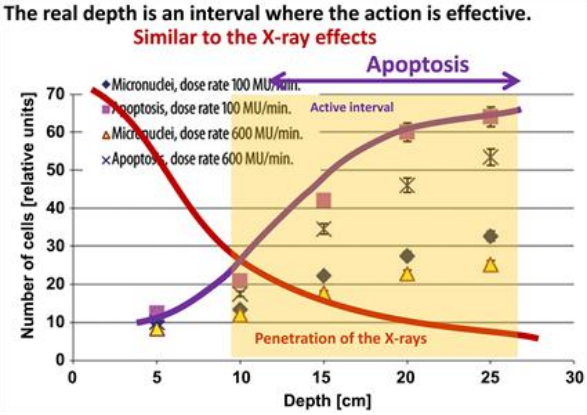

Figure 35. The number of cells with micronuclei, apoptosis as a medium depth function for 100 MU/min, and 600 MU/min dose rates, $p < 0.05$. Each point represents the mean value of three experiments; MU—Monitor Units (arbitrary).

The mEHT method also kills the malignant cells with apoptosis [101]. The apoptotic signal needs much less energy (and field) than the necrotic process [102], shown in the strict synergy of the heat and field effects [35]. The selection and initialization of the process are essential for this, which could happen by a few watts in-depth only. This is even more trivial when we see the immune effects, which are generated, act at distant sites [103], and have no real boundary with the observed abscopal effect [104]. In this meaning, instead of the penetration depth, we have to use the "depth of action," which defines the depth when the mEHT is active, even when the energy is less than the 37% of the incident beam, Figure 36 .

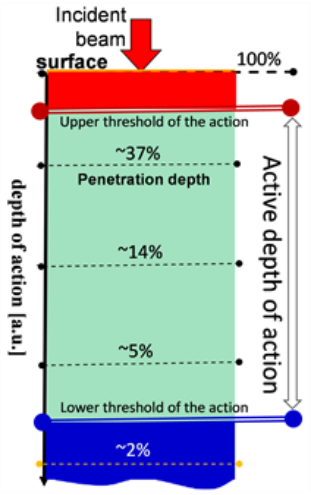

Figure 36. The active depth of mEHT is deeper than the average penetration depth because even 5 W could cause lethal apoptotic signals in selected cells. When the incident beam has 100 W energy, the depth when the mEHT is active could be three times the definitive (37 W) penetration depth.

The increased drug penetration and intensified pharmacokinetics by mEHT [82] [83] promote further elongation of the action depth.

In summary, the action depth for mEHT is deeper than the thickness of the patient's treated cross-sectional distance up to 60 cm (~200 cm circumflex of the cross-section).

3.3.4. The Dosing

Oncological hyperthermia presently faces multiple problems [19], where the most challenging is the lack of a clearly defined and measurable dose for clinical and research applications. The correct dose-definition of hyperthermia therapy is a critical issue in research and is crucial to the future of hyperthermia in oncology [105].

In a homogeneous heating approach, the dose considerations concentrate on the volume percentage, which could be considered having isothermal status. Complete homogeneity of heating of living objects could be achieved only in the WBH process, as LRHT has huge anatomical, physiological, bio-electromagnetic, and thermal heterogeneities, limiting the isodose-type approach. In the WBH process, the temperature was easily measurable and could be used for dosing the therapy. The proposed dose at present is the cumulative equivalent minutes referring to 43°C: CEM43T$_x$ (measured in minutes) [106] [107] [108]; referring to necrotic cell killing at 43°C. Due to the natural inhomogeneities, this dose contains the percentage of the target which has an approximately isothermal condition, denoted by T_x at the end of the practical applications [107]. For example, when the measured temperature is actually T_{90} in 90% of the monitored sites (referred to as the thermal isoeffect dose in 90% of the area).

In LRHT, the absorbed energy creates heat, but due to the non-linear feedback by transport properties (intensified blood and lymph flow), the situation is far from a state of equilibrium [109]. The blood-flow increases more in the healthy host tissues, causing a certain gradient of the flow intensity to heat the tumor's boundary. The most vivid, mostly proliferative layer of the tumor is near its border, so the cells which need the most heat-treatment remain at a lower temperature than the internal part of the tumor lesion, so the basic homogenous requirement is less realizable in the vivid tumor part than inside of its volume, which is often necrotic, without transport activity. The temperature dosing is problematic not only by the missing the isotherm condition but also because of its very complicated measurement.

Moreover, CEM43Tx is controversial, it failed to show the local control characterization of clinical results in soft tissue sarcomas, [110], but was correlated with clinical results for superficial tumors [111]. When administering a dose of CEM43T90 for local hyperthermia, it did not show a correlation between dose and clinical outcomes (like local remissions, local disease-free survival, and overall survival) [112]. It is calibrated by in vitro experiments [110], which are far from the reality of human medicine. Its necrotic reference at 43°C makes this dose unrealistic because in most human hyperthermia treatments, such a temperature is not reachable in the whole tumor. While the high temperature is realized in the ablation-like locality, the dosing by $CEM43T_x$ was false [113]. The inapplicability of this in-vitro calibrated dose is echoed in the whole-body hyperthermia (WBH) application, in which CEM43T100 is very high (T100 means the complete isothermal heating of the tumor by the whole-body heating), but the results are very different from the same dose provided by local hyperthermia of the tumor lesion [114].

However, the challenge is that due to the considerable energy-loss in homogeneous heating processes, the temperature measurement is mandatory because otherwise there is no idea about the actual absorbed power in the target. In the method of mEHT, the measurement is not necessary in order to determine the absorbed power. The technique is able to accurately measure the absorbed energy by the incident beam [84]. Due to the high efficiency of current matching [115], the dosing of the treatment is simply calculable by the absorbed energy [64] [116] instead of by the complicated, inaccurate, and mostly invasive measurement of local temperature.

3.3.5. Heating Process

The homeostatic concept allows adaptation time for the physiological regulations to stabilize the actual homeostatic status. This complex approach requests a non-constant power during the treatment [117]. The simplest realization of the complex process involves step-up heating. The step-up heating is crucial. It has multiple additions to the success of mEHT:

● At electromagnetic heating, the stress is considerably focused on the cells which develop stress-proteins (HSPs) (chaperons to defend their status). The healthy cells rapidly develop 10-times more protective intracellular HSPs than the base level, while the stressful malignant cells only develop a maximum of 30% - 50% more of these intracellular proteins. This makes the healthy cells more protected compared to their malignant counterparts.

● The gradually increased HSP chaperones in malignant cells have time to go to the membrane and be liberated from the cell when the rafts are excited and the signals force their release (such selection does not occur in healthy cells). This liberation process is one of the factors of immunogenic cell death.

● The step-up heating supports the heating periods and upregulates the power when it starts to be saturated, which is optimal for the mEHT selection system.

● The step-up fits the homeostatic equilibrium, and so mEHT remains within the well-controllable quasi-linear physiological reactions.

● The sudden heating causes non-linear, non-controllable conditions, and the power shoots over the burning limit, and in most of the cases causes blisters (as is frequently reported by radiate heating methods). So the step-up method allows the control of homeostasis and helps the patient adapt to the actual energy-increase (I quote a famous experiment when a frog is in the water, which is slowly but gradually heated-up, the animal remains in hot water, even to its death, however, when you try to put a frog in hot water directly, it immediately tries to escape).

When the mEHT is applied strictly as a monotherapy, then step-down heating is necessary to block the neoangiogenic vessels. Due to the missing radio- or chemotherapy effect, the serious cases' metastatic spread has a higher probability, so blocking the vessels' immediately is crucial. But of course, the operating control in these cases has to be more strict.

Even in the step-up approach, the longer heating time tends to the homogenic temperature distribution due to the thermal equalization processes. To keep the non-homogeneous selection, periodic heating is also applicable, but it was only shown in preclinical applications [118].

3.4. Molecular Differences between the Effects of Impedance, and Plane-Wave Matching

The high energy absorption excites the rafts to trigger a signal transmission [78] [79]. The extrinsic signal transfer ignites apoptosis [101] [119] [120], Figure 37 .

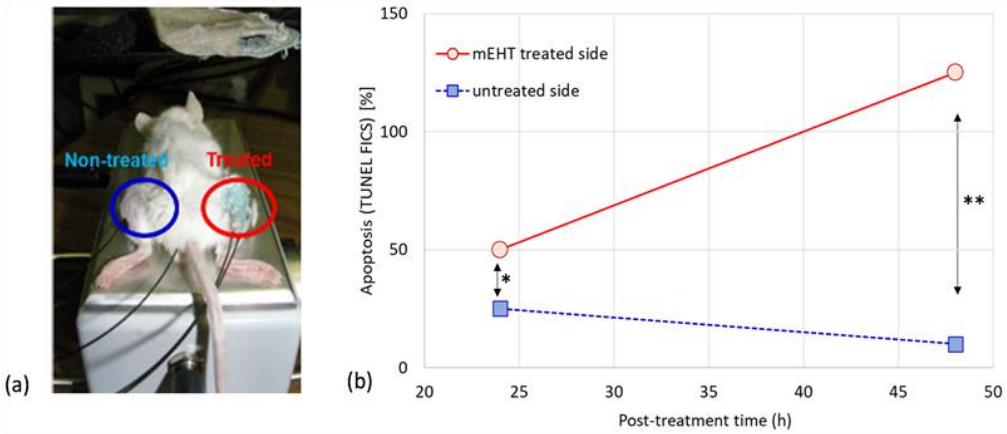

Figure 37. Late apoptosis measurement with TUNEL FICT method (Annexin V positive cells %) in HT29 cells (in vivo) 42°C 30 min treatment parameters, two tumor animal models (a), results show a significant increase of apoptosis in the treated side.

The difference between the molecular effect of the two matching methods of capacitive coupling techniques has been effectively demonstrated in vitro [71]. The plane-wave capacitive hyperthermia (PWCHT) gives the same results as the naturally homogeneous water-bath hyperthermia (WBHT), as seen by the apoptotic processes including the reactive oxygen species (ROS) and calreticulin (Figure 38) [121].

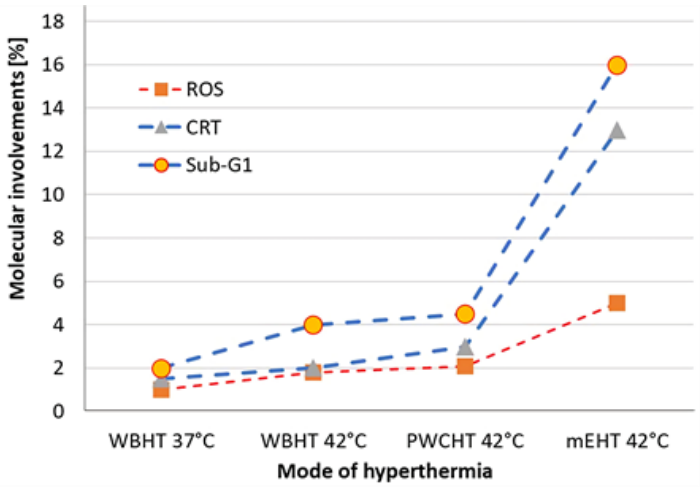

Figure 38. Molecular changes in Hepatoma (HepG2) cell-line in vitro. Apoptosis final state TUNEL (Annexin V positive cells %). WBHT—water bath hyperthermia (homogeneous heating reference at 37°C and 42°C); PWCHT—plane-wave capacitive hyperthermia at 42°C, mEHT at 42°C.

It is important to note that the purely homogeneous heating resulting from the water-bath hyperthermia (WBHT) produces comparable results to the plane-wave matching, indicating that plane-wave matching techniques also favour homogeneous heating, while mEHT differs significantly in the effects and outcomes. The apoptotic process involves a change in the potential of the mitochondria's membrane and the Ca^{2+} influx into the cell, Figure 39 [122].

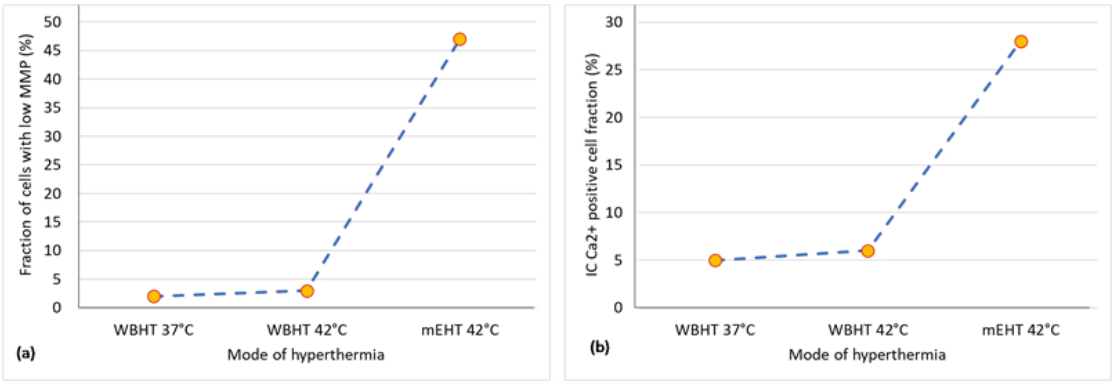

Figure 39. Comparison of heterogeneous heating caused by mEHT with homogeneous heating. (a) Fraction of cells with lowered mitochondrial membrane potential; (b) The calcium influx and intracellular ionic concentration (homogeneous (WBHT) heating reference at 37°C and 42°C, mEHT at 42°C). Abb: WBHT—water bath hyperthermia, mEHT: modulated electro-hyperthermia.

The caspase developments' variants during the apoptosis require the extrinsic and intrinsic pathways (involving Caspases 8 and 9 Figure 40), and the caspase-independent signal routs [101]. Additionally, Septin4 blocks the XIAP, which makes free the extrinsic pathway from this suppressor [123]. All of these factors combined ensure apoptosis is the final result.

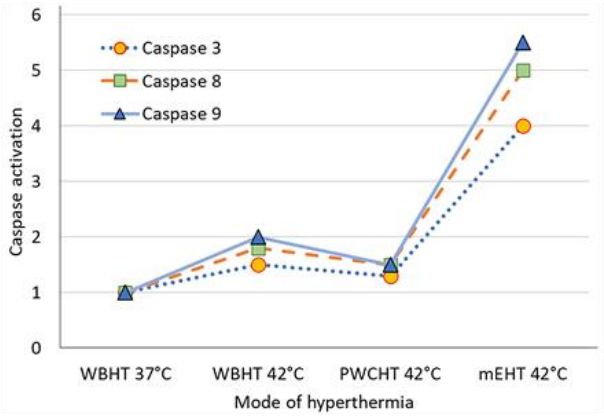

Figure 40. Caspase activation shows Caspase 8 and Caspase 9 for extrinsic and intrinsic pathways, respectively. WBHT—water bath hyperthermia (homogeneous heating reference at 37°C and 42°C); PWCHT—plane-wave capacitive hyperthermia at 42°C, mEHT—modulated electro-hyperthermia at 42°C.

The homogeneous heating results in energy-absorption in the tumor-mass, in an attempt to realize an isothermal situation. However, mEHT focuses the energy absorption on membrane rafts (nanoscopic size). The excess energy makes the extrinsic excitation of the apoptotic pathways (TRAIL-FAS-FADD complex), and makes the gradients through the cell-membrane, producing various thermal effects [79]. It increases the extracellular and the raft temperature to a level much higher than their environment. In consequence the calibration curves by measuring the apoptotic intensity significantly differ, Figure 41 [35] [79]. It is clear that mEHT produces the same 25% relative cell-death as homogeneous heating in ≈3°C lower temperature, which is an approximate difference between the local nano-temperature (at the membrane rafts) and the tumor-average temperature.

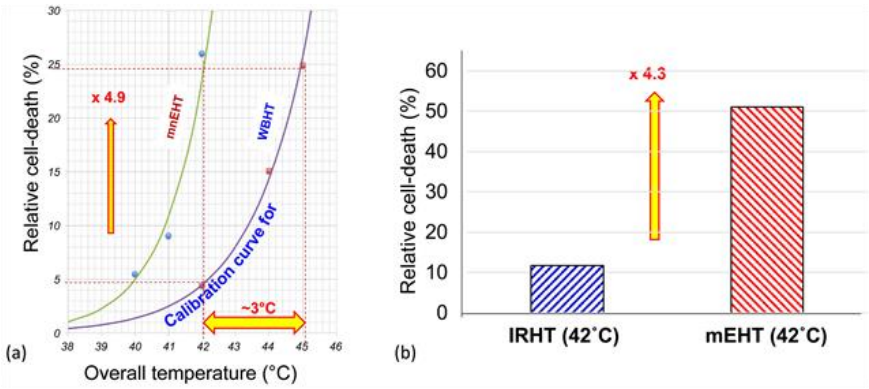

Figure 41. The relative cell-death (%) (a) invitro [U937 cell-line] and (b) in vivo [HT-29 cell-line, xenograft]. The mEHT heterogeneous heating is >4 times more effective than the homogeneous technique at the 42°C reference temperature. (IRHT—infrared, homogeneous heating technics).

In another experiment, a rough calibration comparison between mEHT and water-bath homogeneous heating shows even higher differences between the nano-scale and macro-average temperature, Figure 42 .

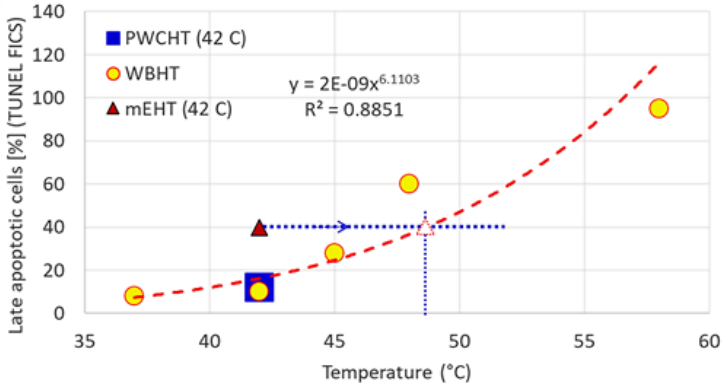

Figure 42. The temperature dependence of the apoptosis. The mEHT at 42°C produces such apoptotic level, like homogeneopus heating does at >45°C (WBHT—water bath hyperthermia (homogeneous heating reference); PWCHT—plane-wave capacitive hyperthermia at 42°C, mEHT at 42°C). (Apoptosis final state TUNEL (Annexin V positive cells %))

A direct temperature measurement of membrane rafts also shows a significant difference in a pilot experiment, Figure 43 [124].

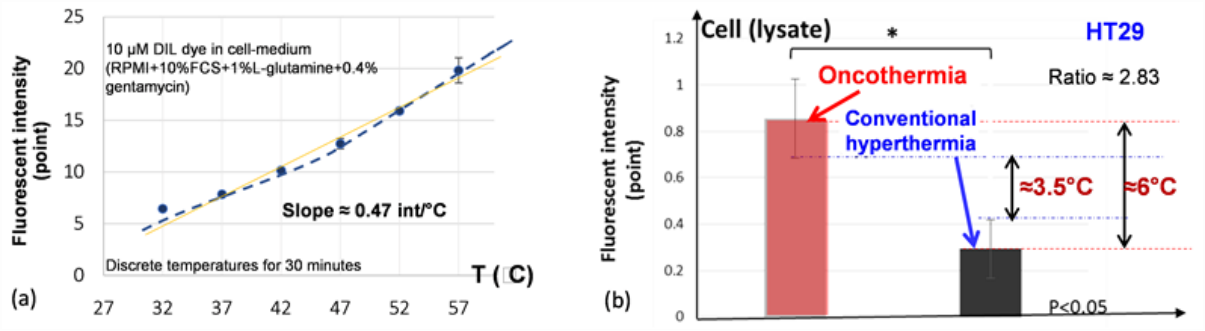

Figure 43. Membrane temperature measurement in vivo (mice, HT29 cells) 42°C, 30 min. (a) DIL (Dilatometry)temperature calibration; (b) Fluorescent measurement, show the much higher temperature on the membrane of mEHT treated sample than on the membrane of the homogeneously (WBHT) heated one.

The heating certainly causes stress, producing chaperone proteins. The most characteristic protein family of chaperons is the heat shock protein 70 (HSP70). This protein has a double edge sword reaction: intracellularly it tries to avoid the cell's apoptosis, extracellularly it acts oppositely: it promotes the cellular apoptosis. Any kind of hyperthermia results in the expression of HSP70, but at different levels. Due to the large electromagnetic load that accompanies the heating processes, mEHT trigger the expression of more HSP70 than homogeneous heating, Figure 44 . This difference is most significant 48 hours after treatment.

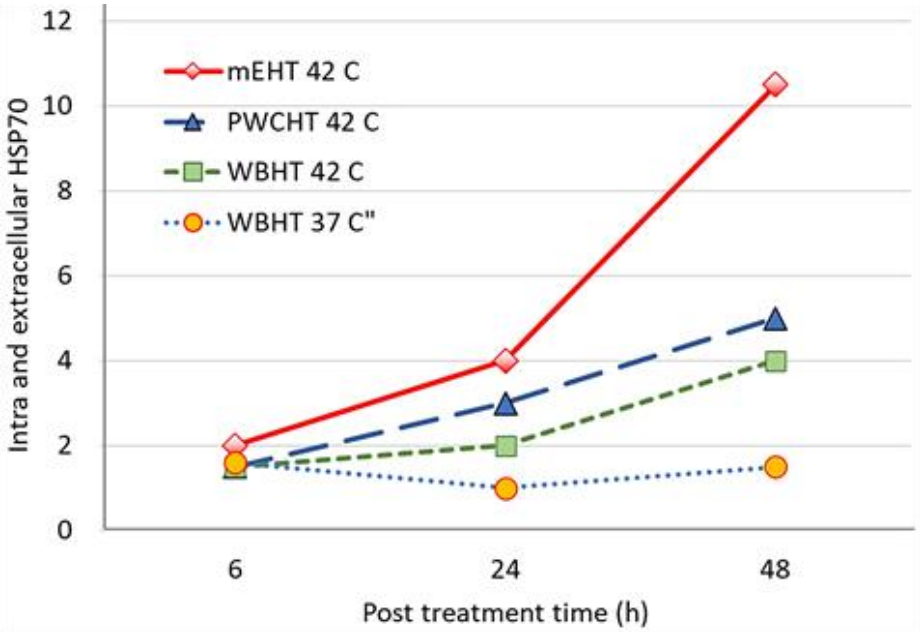

Figure 44. Comparison of the cleaved Caspase CD3+ expression. (WBHT—water bath hyperthermia (homogeneous heating reference); PWCHT—plane-wave capacitive hyperthermia at 42°C, mEHT at 42°C).

However, the location of the measured HSP70 is different. After 48 hours the concentration of the intracellular HSP70 returns to the level it was before the heating, but the extracellular levels increase, Figure 45 [125].

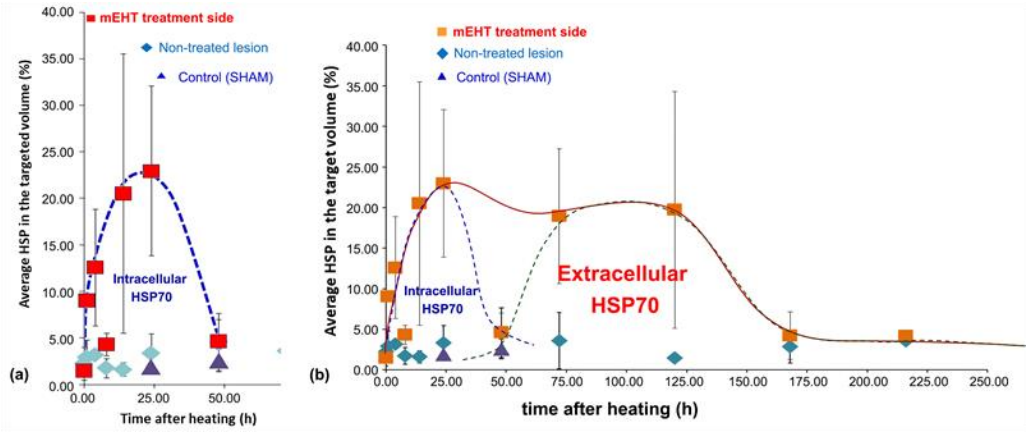

Figure 45. Development of HSP70 after mEHT treatment of in vivo xenograft mouse model (HT29 cell-line, at 42°C, 30 min). (a) The level of HSP70 returned to the baseline level at 48 h post-treatment; (b) The development of the extracellular HSP70 only returns to the baseline level after a week.

A detailed review of cancer models describes the molecular mechanisms of mEHT [126].

3.4.1. Immunogenic Cell-Death

The apoptosic process caused by mEHT causes special immunogenic type of changes, allowing the genetic information to form antigen-presenting cell (APC) by the maturation of the dendritic cells (DCs) or the macrophages. The excitation of the actual membrane rafts initiates immunogenic cell death (ICD). This process starts by producing a particular damage-associated molecular pattern (DAMP) (Figure 46) [127].

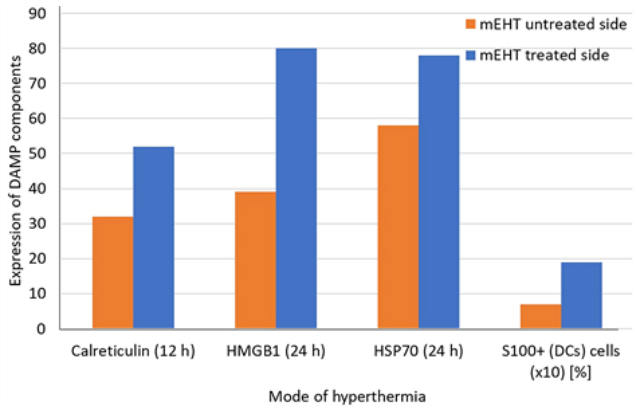

Figure 46. The DAMP development in vivo in an allograft mouse model (CT26 cells).

The proper signal transfer, and DAMP production could be limited or blocked by too much energy absorption on the rafts, which destroys it instead of exciting the transmembrane proteins, and receptors. The high energy-absorption may ignite phase transition mechanisms. For example, the kink in the Arrhenius plot at ~42.5°C is probably a lipid-associated phase transition [128] [129] [130], which could lower the activation energy needed to facilitate the desired changes [131]. The change in the kink is expected to be influenced by the blood flow [33]. Among such conditions, the immunogenic cell-death is seldom, and also the APC and the immune actions will not be produced, because the temperature is high, and the membrane phase-transition makes hard producing apoptotic bodies. Well-defined sequences and spatio-temporal actions are necessary for the DAMP, which high energy technologies are not able to do. The possible small amount of proper DAMP production by high energy technologies would be disrupted, resulting in a mixture of effects, as is often observed many hyperthermia studies. This causes inconsistent results as there is no control of the processes in the complex dynamical network seen at a nanoscopic level.

3.4.2. Tumor-Specific Immune Effect

The main effect of mEHT is the energy absorption, like in all hyperthermia treatments, but it is further enhanced by the selection mechanisms, which makes it heterogenic, targeting, and energy-focused. The bio-electromagnetic and structural differences of malignancies appear in their spatial and temporal self-organized fractal structure, harnessed by the modulation effect. The DAMP-ICD associated tumor-specific immune effect is active in the entire body and therefore acts as vaccination. The re-challenge of the body with the same malignancy therefore be expected to be unsuccessful [121]. It is an excellent advantage that without any invasive sampling and extra laboratory preparation, the immune effect is in situ and real-time.

Studies with DC, Figure 47 [121]; and Marsdenia Tenacissima (MTE), Figure 48 [127] as an immune-support suggest that when the patient's immune system is weak, due to tumor-development and the side effects of the previous treatments, additional immune support could help for complete action.

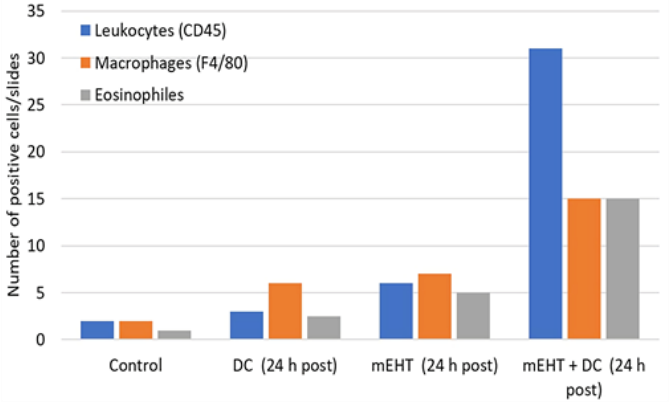

Figure 47. Immune invasion at the tumor 24 h post-treatment (DC—dendritic cell injection).

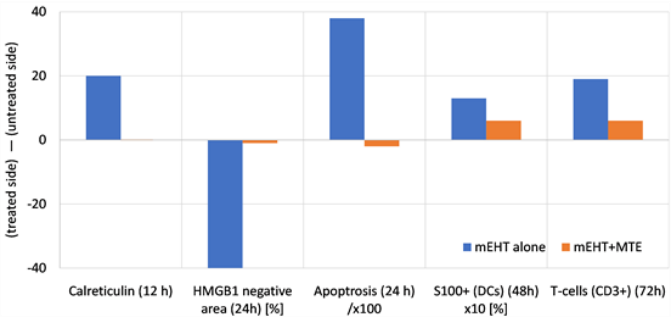

Figure 48. Effect of the immune-support Marsdenia Tenacissima (MTE).

This way, mEHT can create a favorable tumor microenvironment for an immunological chain reaction, improving the success rate of intratumoral dendritic cell immunotherapy [104] [121]. The applied paradigm's strategic point is that our task is to help the body recognize and destroy the malignancy. Targeting a product (such as weak points of tumor growth or simple destruction of the cell by thermal necrosis) could not repair the complex system. The entire process has to be targeted in order to re-establish the healthy state [132]. Developing a tumor-specific immune reaction directly drives the immune system to reparation. The mEHT method recognizes the tumor by its biophysical, mainly electric impedance parameters, which at the same time has diagnostic value, Figure 49 [104] [133] [134].

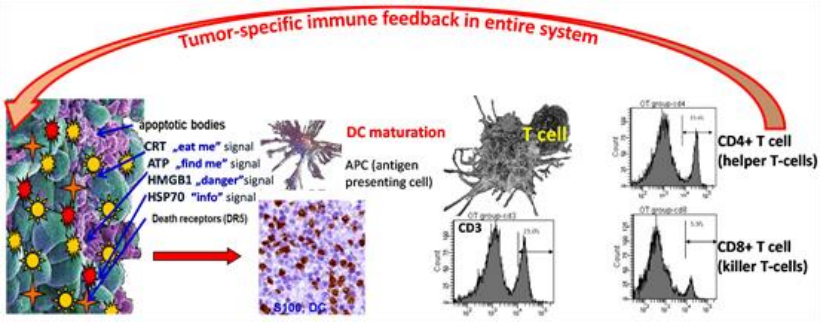

Figure 49. Producing the tumor-specific immune reaction. The gentle apoptosis produces DAMP and ICD presenting genetic information to antigen-presenting cells (APCs) which produces killer T-cells which are active in the entire body. (Works like a tumor-vaccination.)

The mEHT in this combination is a typical theranostic [135] therapy, which could be applied in combination with other standard tumor therapies like chemotherapies [136] [137], radiotherapies [138] [139], or check-point inhibitors [140]. A promising immunological approach is the combination of mEHT with viral therapies [141] [142].

3.5. Clinical Applications

A review of the clinical pieces of evidence of mEHT summarized essential clinical evidence [143]. The clinical trials are summarized in Table 1.

No.	Tumor site	Number of patients	Treatment used	Results	Reference
1	Relapsed high-grade gliomas	15	mEHT + alkylating chemotherapy	Tolerable and safe for patients with relapses by high escalation of the dose too.	Wismeth, et al. 2010 [144]
2	Advanced gliomas	12	Chemotherapy, radiotherapy + mEHT	CR = 1, PR = 2, RR = 25%. Median duration of response = 10 m. Median survival = 9 m, 25% survival rate at 1 year.	Fiorentini, Giovanis, et al. 2006 [145]
3	Relapsed malignant gliomas	24	mEHT	Median survival = 19.5 months, 55% survival rate at 1 year, 15% at 2 years.	Fiorentini, Sarti, et al. 2018 [146]
4	Advanced glioblastoma	60	mEHT + immunotherapy	No added toxicity by immunotherapy. Median progression-free survival (PFS) = 13 m. Median follow up 17 m, median OS was not reached. Estimated OS at 30 m was 58%.	Van Gool, et al. 2018 [142]
5	Various brain-gliomas	140	Chemotherapy + radiotherapy + mEHT	OS = 20.4 m. mEHT was safe and well tolerated.	Sahinbas, et al. 2007 [147]
6	High-grade gliomas	179	mEHT + radiotherapy + chemotherapy	Longstanding complete and partial remissions after recurrence in both groups.	Hager, Groenemeyer, et al. 2008 [148]

Table 1. Clinical trials that used mEHT in combination with other treatments.

4. Conclusions

The two variants of capacitive coupling, the plane-wave, and impedance matching, make different treatment applications in preclinical experiments and human medical applications. Technically the difference between these capacitive methods is the design for homogeneous or heterogeneous heating. The homogeneous heating needs to measure the target's temperature, obtaining information about the amount of absorbed energy, while the impedance matching gets direct information about the energy-absorption. This results in a difference in the dosing method because, in the homogeneous approach, the temperature is the mandatory part of the heating dose, while in the heterogeneous case, the absorbed energy characterizes the process. The heterogeneous heating without artificial nanoparticles is realized in the mEHT method. This method has special qualities which improve the conventional hyperthermia results:

1) Excites apoptotic signals by extrinsic pathways.
2) Though the selected membrane rafts, mEHT excites the TRAIL DR5 death-receptor (with FADD and FAS complex), and this extrinsic excitation triggers the ICD.
3) The raft excitation triggers the DAMP and ICD, crucial for the immunogenic (abscopal) effect. This turns the local treatment into a systemic treatment, shown in the elongation of the survival time, without being limited to local control.
4) The immunogenic effect is vital for the cases with far advanced, relapsed, metastatic disease, and not only locally advanced cases.

Acknowledgements

This work was supported by the Hungarian National Research Development and Innovation Office PIACI KFI grant: 2019-1.1.1-PIACI-KFI-2019-00011.

Conflicts of Interest

The author declares no conflicts of interest regarding the publication of this paper.

References

[1] von Bertalanffy, K.L. (1934) Untersuchungen über die Gesetzlichkeit des Wachstums: I. Teil: Allgemeine Grundlagen der Theorie; Mathematische und physiologische Gesetzlichkeiten des Wachstums bei Wassertieren. Wilhelm Roux' Archiv für Entwicklungsmechanik der Organismen, 131, 613-652. https://doi.org/10.1007/BF00650112

[2] Green, D.M. (1991) Chaos, Fractals and Nonlinear Dynamics in Evolution and Phylogeny. Trends in Ecology & Evolution, 6, 334-337. https://doi.org/10.1016/0169-5347(91)90042-V

[3] Szentgyorgyi, A. (1978) The Living State and Cancer. Marcel Dekker Inc., New York.

[4] Balmain, A., Gray, J. and Ponder, B. (2014) The Genetics and Genomics of Cancer. Nature Genetics, 33, 238-244. https://doi.org/10.1038/ng1107

[5] Szigeti, G.P., Szasz, O. and Hegyi, G. (2017) Connections between Warburg's and Szentgyorgyi's Approach about the Causes of Cancer. Journal of Neoplasm, 1, 1-13. http://neoplasm.imedpub.com/connections-between-warburgs-and-szentgyorgyis-approach-about-thecauses-of-cancer.pdf

[6] Hanahan, D. and Weinberg, R.A. (2000) The Hallmarks of Cancer. Cell, 100, 57-70. https://doi.org/10.1016/S0092-8674(00)81683-9

[7] Hanahan, D. and Weinberg, R.A. (2011) Hallmarks of Cancer: The Next Generation. Cell, 144, 646-674. https://doi.org/10.1016/j.cell.2011.02.013

[8] Aktipis, C.A., Bobby, A.M., Jansen, G., et al. (2015) Cancer across the Tree of Life: Cooperation and Cheating in Multicellularity. Philosophical Transactions of the Royal Society B, 370, Article ID: 20140219. https://doi.org/10.1098/rstb.2014.0219

[9] Popkin, G. (2011) Physics Sheds Light on Cancer and Bacteria Evolution. APC News, 20. https://www.aps.org/publications/apsnews/201105/cancerbacteria.cfm .

[10] Trigos, A.S., Pearson, R.B., Paenfuss, A.T., et al. (2018) How the Evolution of Multicellularity Set the Stage for Cancer. British Journal of Cancer, 118, 145-152. https://doi.org/10.1038/bjc.2017.398

[11] Trigos, A.S., Pearson, R.B., Papenfuss, A.T., et al. (2016) Altered Interactions between Unicellular and Multicellular Genes Drive Hallmarks of Transformation in a Diverse Range of Solid Tumors. Proceedings of the National Academy of Sciences of the United States of America, 114, 6406-6411. https://doi.org/10.1073/pnas.1617743114

[12] Davidson, C.D., Wang, W.Y., Zaimi, I., et al. (2019) Cell Force-Mediated Matrix Reorganization Underlies Multicellular Network Assembly. Scientific Reports, 9, Article No. 12. https://doi.org/10.1038/s41598-018-37044-1

[13] Meng, X., Riordan, N.H. (2006) Cancer Is a Functional Repair Tissue. Medical Hypotheses, 66, 486-490. https://doi.org/10.1016/j.mehy.2005.09.041

[14] Dvorak, H.F. (1986) Tumors: Wounds That Do Not Heal, Similarities between Tumor Stroma Generation and Wound Healing. The New England Journal of Medicine, 315, 1650-1659. https://doi.org/10.1056/NEJM198612253152606

[15] National Cancer Institute. National Cancer Act of 1971. https://www.cancer.gov/about-nci/overview/history/national-cancer-act-1971

[16] Spector, R. (2010) The War on Cancer A Progress Report for Skeptics. Skeptical Inquirer, 34, 25-31.

[17] Brecht, B. (1935) Leben des Galilei. In: Losey, J. (1975), Galileo, Grove Press, New York.

[18] DiTrocchio, F. (1994) Der grosse schwindel: Betrug und falschung in der wissenschaft. Campus Verlag, Frankfurt.

[19] Roussakow, S. (2013) The History of Hyperthermia Rise and Decline. Conference of the International Clinical Hyperthermia Society 2012, 2013, Article ID: 428027. https://doi.org/10.1155/2013/428027

[20] Van der Zee, J. (2005) Radiotherapy and Hyperthermia in Cervical Cancer. ESTRO/TMH Presentation, Mumbai, 2 March 2005. http://www.docstoc.com/docs/73493260/Welcome-to-Tata-Memorial-Centre

[21] ITU Radio Regulations, CHAPTER II—Frequencies, ARTICLE 5 Frequency Allocations, Section IV—Table of Frequency Allocations.

[22] Hajimiri, A. (2010) Generalized Time- and Transfer-Constant Circuit Analysis. IEEE Transactions on Circuits and Systems I: Regular Papers, 57, 1105-1121. https://doi.org/10.1109/TCSI.2009.2030092

[23] Szasz, A. (2014) Oncothermia: Complex Therapy by EM and Fractal Physiology. 2014 XXXIth URSI General Assembly and Scientific Symposium (URSI GASS), Beijing, 16-23 August 2014, 1-4. https://doi.org/10.1109/URSIGASS.2014.6930100

[24] Rao, N.N. (1994) Elements of Engineering Electromagnetics, Prentice Hall, Englewood Cliffs, NJ.

[25] Szasz, A. (2015) Bioelectromagnetic Paradigm of Cancer Treatment Oncothermia. In: Rosch, P.J., Ed., Bioelectromagnetic and Subtle Energy Medicine, CRC Press, Taylor & Francis Group, 323-336.

[26] Fiorentini, G. and Szasz, A. (2006) Hyperthermia Today: Electric Energy, a New Opportunity in Cancer Treatment. Journal of Cancer Research and Therapeutics, 2, 41-46. https://doi.org/10.4103/0973-1482.25848

[27] Keisari, Y. (2013) Tumor Ablation, Effects on Systemic and Local Anti-Tumor Immunity and on Other Tumor-Microenvironment Interactions. Springer Science + Business Media, Dordrecht. https://doi.org/10.1007/978-94-007-4694-7

[28] Szasz, O., Szigeti, G.P., Vancsik, T. and Szasz, A. (2018) Hyperthermia Dosing and Depth of Effect. Open Journal of Biophysics, 8, 31-48. https://doi.org/10.4236/ojbiphy.2018.81004

[29] Szasz, A., Szasz, N. and Szasz, O. (2010) Experimental Condition in Vivo. In: Oncothermia: Principles and Practices, Springer Science, Heidelberg, 476-477. https://doi.org/10.1007/978-90-481-9498-8

[30] Moran, C.H., Wainerdi, S.M., Cherukuri, T.K., et al. (2009) Size-Dependent Joule Heating of Gold Nanoparticles Using Capacitively Coupled Radiofrequency Fields. Nano Research, 2, 400-405. https://doi.org/10.1007/s12274-009-9048-1

[31] Raoof, M., Cisneros, B.T., Corr, S.J., et al. (2013) Tumor Selective Hyperthermia Induced by Short-Wave Capacitively-Coupled RF Electric-Fields. PLoS ONE, 8, e68506. https://doi.org/10.1371/journal.pone.0068506

[32] Raoof, M. and Curley, S.A. (2011) Non-Invasive Radiofrequency-Induced Targeted Hyperthermia for the Treatment of Hepatocellular Carcinoma. International Journal of Hepatology, 2011, Article ID: 676957. https://doi.org/10.4061/2011/676957

[33] Erdmann, B., Lang, J. and Seebass, M. (1998) Optimization of Temperature Distributions for Regional Hyperthermia Based on a Nonlinear Heat Transfer Model. Annals of the New York Academy of Sciences, 858, 36-46.
https://doi.org/10.1111/j.1749-6632.1998.tb10138.x

[34] Szasz, O., Szigeti, G.P. and Szasz, A. (2016) Connections between the Specific Absorption Rate and the Local Temperature. Open Journal of Biophysics, 6, 53-74. http://file.scirp.org/pdf/OJBIPHY_2016063014260548.pdf
https://doi.org/10.4236/ojbiphy.2016.63007

[35] Andocs, G., Renner, H., Balogh, L., Fonyad, L., Jakab, C. and Szasz, A. (2009) Strong Synergy of Heat and Modulated Electro-Magnetic Field in Tumor Cell Killing. Strahlentherapie und Onkologie, 185, 120-126. http://www.ncbi.nlm.nih.gov/pubmed/19240999
https://doi.org/10.1007/s00066-009-1903-1

[36] Warburg, O. (1956) On the Origin of Cancer Cells. Science, 123, 309-314. https://doi.org/10.1126/science.123.3191.309

[37] Semenza, G.L. (2008) Tumor Metabolism: Cancer Cells Give and Take Lactate. The Journal of Clinical Investigation, 118, 3835-3837. https://doi.org/10.1172/JCI37373

[38] Stoy, R.D., Foster, K.R. and Schwan, H.P. (1982) Dielectric Properties of Mammalian Tissues form 0.1 to 100 MHz: A Summary of Recent Data. Physics in Medicine & Biology, 27, 501-513. https://doi.org/10.1088/0031-9155/27/4/002

[39] Gershing, E. (1999) Monitoring Temperature-Induced Changes in Tissue during Hyperthermia by Impedance Methods. Annals of the New York Academy of Sciences, 873, 13-20. https://doi.org/10.1111/j.1749-6632.1999.tb09444.x

[40] Oehr, P., Biersack, H.J., Coleman, R.E., Eds. (2004) PET and PET-CT in Oncology. Springer Verlag, Berlin-Heidelberg.
https://doi.org/10.1007/978-3-642-18803-9

[41] Larson, S.M. (2004) Positron Emission Tomography-Based Molecular Imaging in Human Cancer: Exploring the Link between Hypoxia and Accelerated Glucose Metabolism. Clinical Cancer Research, 10, 2203-2204. https://doi.org/10.1158/1078-0432.CCR-0002-4

[42] Sha, L., Ward, E.R. and Story, B. (2002) A Review of Dielectric Properties of Normal and Malignant Breast Tissue. Proceedings IEEE SoutheastCon 2002, Columbia, SC, 5-7 April 2002, 457-462.

[43] Blad, B., Wendel, P., Jönsson, M., et al. (1999) An Electrical Impedance Index to Distinguish between Normal and Cancerous Tissues. Journal of Medical Engineering & Technology, 23, 57-62. https://doi.org/10.1080/030919099294294

[44] Szentgyorgyi, A. (1968) Bioelectronics: A Study on Cellular Regulations, Defense, and Cancer. Academic Press, New York, London.

[45] Foster, K.R. and Schepps, J.L. (1981) Dielectric Properties of Tumor and Normal Tissues at Radio through Microwave Frequencies. Journal of Microwave Power, 16, 107-119. https://doi.org/10.1080/16070658.1981.11689230

[46] Blad, B. and Baldetorp, B. (1996) Impedance Spectra of Tumour Tissue in Comparison with Normal Tissue: A Possible Clinical Application for Electric Impedance Tomography. Physiological Measurement, 17, A105-A115. https://doi.org/10.1088/0967-3334/17/4A/015

[47] Babaeizadeh, S. (2007) 3-D Electrical Impedance Tomography of Piecewise Constant Domains with Known Internal Boundaries. IEEE Transactions on Biomedical Engineering, 54, 2-10. https://doi.org/10.1109/TBME.2006.886839

[48] TransCan TS: Transcan Medical Ltd. Migdal Ha'Emek, Israel, distributed by Siemens AG, Germany, 2000.

[49] Joy, M.L.G. (2004) MR Current Density and Conductivity Imaging: The State of the Art. IEMBS 26th Annual International Conference of the IEEE, 2, 5315-5319.

[50] Suk, H.O. (2003) Conductivity and Current Density Image Reconstruction Using Harmonic Bz Algorithm in Magnetic Resonance Electrical Impedance Tomography. Physics in Medicine & Biology, 48, 3101-3116. https://doi.org/10.1088/0031-9155/48/19/001

[51] Mikac, U., Demsar, F., Beravs, K. and Sersa, I. (2001) Magnetic Resonance Imaging of Alternating Electric Currents. Magnetic Resonance Imaging, 19, 845-856. https://doi.org/10.1016/S0730-725X(01)00393-9

[52] Muftuler, T.L., Hamamura, M.J., Birgul, O. and Nalcioglu, O. (2006) In Vivo MRI Electrical Impedance Tomography (MREIT) of Tumors. Technology in Cancer Research & Treatment, 5, 381-387.

[53] Papp, E., Vancsik, T., Kiss, E. and Szasz, O. (2017) Energy Absorption by the Membrane Rafts in the Modulated Electro-Hyperthermia (mEHT). Open Journal of Biophysics, 7, 216-229. https://doi.org/10.4236/ojbiphy.2017.74016

[54] Caduff, A., Talary, M.S. and Zakharov, P. (2010) Cutaneous Blood Perfusion as a Perturbing Factor for Noninvasive Glucose Monitoring. Diabetes Technology & Therapeutics, 12, 1-9. https://doi.org/10.1089/dia.2009.0095

[55] Schwan, H.P. (1982) Nonthermal Cellular Effects of Electromagnetic Fields: AC-Field Induced Ponderomotoric Forces. British Journal of Cancer, 45, 220-224.

[56] Pething, R. (1979) Dielectric and Electronic Properties of Biological Materials. John Wiley & Sons, New York.

[57] Szasz, O., Andocs, G., Kondo, T., Rehman, M.U., Papp E, Vancsik T. (2015) Heating of Membrane Raft of Cancer-Cells. Journal of Clinical Oncology, 33, e22176. https://doi.org/10.1200/jco.2015.33.15_suppl.e22176

[58] Astumian, R.D. and Chock, P.B. (1989) Effects of Oscillations and Energy-Driven Fluctuations on the Dynamics of Enzyme Catalysis and Free-Energy Transduction. Physical Review A, 39, 6416-6435. https://doi.org/10.1103/PhysRevA.39.6416

[59] Musha, T. and Sawada, Y. (1994) Physics of the Living State. IOS Press, Amsterdam.

[60] West, B.J. (1990) Fractal Physiology and Chaos in Medicine. World Scientific, Singapore, London.

[61] Lovelady, D.C., Richmond, T.C., Maggi, A.N., Lo, C.M. and Rabson, D.A. (2007) Distinguishing Cancerous from Noncancerous Cells through Analysis of Electrical Noise. Physical Review E, 76, Article ID: 041908. https://doi.org/10.1103/PhysRevE.76.041908

[62] Szasz, O., Andocs, G. and Meggyeshazi, N. (2013) Modulation Effect in Oncothermia. Conference of the International Clinical Hyperthermia Society 2012, 2013, Article ID: 395678. http://www.hindawi.com/archive/2013/398678/ https://doi.org/10.1155/2013/398678

[63] Szentgyorgyi, A. (1998) Electronic Biology and Cancer. Marcel Dekker, New York.

[64] Kirson, E.D., Gurvich, Z., Schneiderman, R., et al. (2004) Disruption of Cancer Cell Replication by Alternating Electric Fields. Cancer Research, 64, 3288-3295. https://doi.org/10.1158/0008-5472.CAN-04-0083

[65] Vincze, G. and Sziget, G.P. (2016) Reorganization of the Cytoskeleton. Journal of Advances in Biology, 9, 1872-1882. https://cirworld.com/index.php/jab/article/view/4059

[66] Springer, M. and Paulsson, J. (2006) Harmonies from Noise. Nature, 439, 27-28. https://doi.org/10.1038/439027a

[67] West, J.B. (2013) Fractal Physiology and Chaos in Medicine. World Scientific, Singapore. https://doi.org/10.1142/8577

[68] Hoop, B. and Peng, C.-K. (2000) Fluctiations and Fractal Noise in Biological Membranes. The Journal of Membrane Biology, 177, 177-185. https://doi.org/10.1007/s002320010001

[69] Szasz, O., Vincze, G., Szigeti, G.P. and Szasz, A. (2017) Intrinsic Noise Monitoring of Complex Systems. Open Journal of Biophysics, 7, 197-215. https://doi.org/10.4236/ojbiphy.2017.74015

[70] Szasz, A., Szasz, N. and Szasz, O. (2010) Oncothermia—Principles and Practices. Springer Science, Heidelberg. (Ch 4.1, pp. 220, Fig. 4.52)

[71] Yang, K.-L., Huang, C.-C., Chi, M.-S., Chiang, H.-C., Wang, Y.-S., Andocs, G., et al. (2016) In Vitro Comparison of Conventional Hyperthermia and Modulated Electro-Hyperthermia. Oncotarget, 7, 84082-84092. https://doi.org/10.18632/oncotarget.11444

[72] Shinitzky, M. (1984) Membrane Fluidity in Malignancy Adversative and Recuperative. Biochimica et Biophysica Acta, 738, 251-261. https://doi.org/10.1016/0304-419X(83)90007-0

[73] Goldman, D.E. (1943) Potential, Impedance, and Rectification in Membranes. Journal of General Physiology, 27, 37-60. https://doi.org/10.1085/jgp.27.1.37

[74] Ramachandran, S., Blick, R.H. and van der Weide, DW. (2010) Radio Frequency Rectification on Membrane Bound Pores. Nanotechnology, 21, Article ID: 075201. https://doi.org/10.1088/0957-4484/21/7/075201

[75] Tanaka, A. and Tokimasa, T. (1999) Theoretical Background for Inward Rectification. The Tokai Journal of Experimental and Clinical Medicine, 24, 147-153.

[76] Astumian, R.D., Weaver, J.C. and Adair, R.K. (1995) Rectification and Signal Averaging of Weak Electric Fields by Biological Cells. Proceedings of the National Academy of Sciences of the United States of America, 92, 3740-3743.
https://doi.org/10.1073/pnas.92.9.3740

[77] Szasz, A., Vincze, G., Szasz, O. and Szasz, N. (2003) An Energy Analysis of Extracellular Hyperthermia. Electromagnetic Biology and Medicine, 22, 103-115.
https://doi.org/10.1081/JBC-120024620

[78] Vincze, G., Szigeti, G., Andocs, G. and Szasz, A. (2015) Nanoheating without Artificial Nanoparticles. Biology and Medicine, 7, Article Number 1000249.
http://www.omicsonline.com/open-access/nanoheating-without-artificial-nanoparticles-0974-8369-1000249.php?aid=61783

[79] Andocs, G., Rehman, M.U., Zhao, Q.L., Papp, E., Kondo, T. and Szasz, A. (2015) Nanoheating without Artificial Nanoparticles Part II. Experimental Support of the Nanoheating Concept of the Modulated Electro-Hyperthermia Method, Using U937 Cell Suspension Model. Biology and Medicine, 7, 1-9.
https://www.omicsonline.org/open-access/nanoheating-without-artificial-nanoparticles-part-ii-experimental-support-of-the-nanoheating-concept-of-the-modulated-electrohyperthermiamethod-0974-8369-1000247.php?aid=60362
https://doi.org/10.4172/0974-8369.1000247

[80] Lee, S.-Y, Kim, J.-H, Han, Y.-H., et al. (2018) The Effect of Modulated Electro-Hyperthermia on Temperature and Blood Flow in Human Cervical Carcinoma. International Journal of Hyperthermia, 34, 953-960.
https://doi.org/10.1080/02656736.2018.1423709

[81] Lee, S.-Y. (2020) Concurrent Chemo-Hyperthermia for Recurrent Cervical Cancer after Previous CCRT. In: Szasz, A., Ed., Challenges and Solutions of Oncological Hyperthermia, Ch. 9, Cambridge Scholars Publishing, Newcastle upon Tyne, 163-186.
https://www.cambridgescholars.com/challenges-and-solutions-of-oncological-hyperthermia

[82] Lee, S.-Y. and Kim, M.-G. (2015) The Effect of Modulated Electro-Hyperthermia on the Pharmacokinetic Properties of Nefopam in Healthy Volunteers: A Randomised, Single-Dose, Crossover Open-Label Study. International Journal of Hyperthermia, 31, 869-874.
http://www.ncbi.nlm.nih.gov/pubmed/26507458
https://doi.org/10.3109/02656736.2015.1095358

[83] Lee, S.-Y. and Kim, M.-G. (2016) Effect of Modulated Electrohyperthermia on the Pharmacokinetics of Oral Transmucosal Fentanyl Citrate in Healthy Volunteers. Clinical Therapeutics, 38, 2548-2554.
https://www.ncbi.nlm.nih.gov/pubmed/27866658
https://doi.org/10.1016/j.clinthera.2016.10.012

[84] Lee, S.-Y., Szigeti, G.P. and Szasz, A.M. (2019) Oncological Hyperthermia: The Correct Dosing in Clinical Applications. International Journal of Oncology, 54, 627-643.
https://www.spandidos-publications.com/10.3892/ijo.2018.4645#
https://doi.org/10.3892/ijo.2018.4645

[85] Wust, P., Ghadjar, P., Nadobny, J., et al. (2019) Physical Analysis of Temperature-Dependent Effects of Amplitude-Modulated Electromagnetic Hyperthermia. International Journal of Hyperthermia, 36, 1246-1254.
https://www.ncbi.nlm.nih.gov/pubmed/31818170
https://doi.org/10.1080/02656736.2019.1692376

[86] Szasz, A. (2019) Thermal and Nonthermal Effects of Radiofrequency on Living State and Applications as an Adjuvant with Radiation Therapy. Journal of Radiation and Cancer Research, 10, 1-17.
http://www.journalrcr.org/article.asp?issn=2588-9273;year=2019;volume=10;issue=1;spage=1;epage=17;aulast=Szasz
https://doi.org/10.4103/jrcr.jrcr_25_18

[87] Wust, P., Kortum, B., Strauss, U., Nadobny, J., Zschaeck, S., Beck, M., et al. (2020) Non-Thermal Effects of Radiofrequency Electromagnetic Fields. Scientific Reports, 10, Article No. 13488.
https://www.nature.com/articles/s41598-020-69561-3
https://doi.org/10.1038/s41598-020-69561-3

[88] Wust, P., Nadobny, J., Zschaeck, S. and Ghadjar, P. (2020) Physics of Hyperthermia—Is Physics Really against Us? In: Szasz, A., Ed., Challenges and Solutions of Oncological Hyperthermia, Ch. 16, Cambridge Scholars Publishing, Newcastle upon Tyne, 346-376.
https://www.cambridgescholars.com/challenges-and-solutions-of-oncological-hyperthermia

[89] Rao, N.N. (2004) Elements of Engineering Electromagnetics. Pearson-Prentice Hall International, Pearson Education Inc., London UK.

[90] Szasz, A., Szasz, O. and Szasz, N. (2006) Physical Background and Technical Realization of Hyperthermia. In: Baronzio, G.F. and Hager, E.D., Eds., Hyperthermia in Cancer Treatment: A Primer, Springer, Boston, MA, 27-59.
https://doi.org/10.1007/978-0-387-33441-7_3

[91] http://www.nist.gov/pml/div682/grp02/upload/FT11Bourland.pdf

[92] Fluoroscopy Radiation Safety Training Manual (FDA Involved). https://www.case.edu/ehs/Training/RadSafety/fluoro.htm

[93] Beddar, A.S. and Krishnan, S. (2005) Intraoperative Radiotherapy Using a Mobile Electron LINAC: A Retroperitoneal Sarcoma Case. Journal of Applied Clinical Medical Physics, 6, 95-107. http://www.jacmp.org/index.php/jacmp/rt/printerFriendly/2109/1220
https://doi.org/10.1120/jacmp.v6i3.2109

[94] Szasz, A. (2006) Physical Background, and Technical Realization of Hyperthermia. In: Baronzio, G.F. and Hager, E.D., Eds., Hyperthermia in Cancer Treatment: A Primer. Springer Science, Berlin.

[95] Gabriel, C. and Gabriel, S. (1996) Compilation of the Dielectric Properties of Body Tissues at RF and Microwave Frequencies.
http://niremf.ifac.cnr.it/docs/DIELECTRIC/Report.html

[96] Findlay, R.P. and Dimbylow, P.J. (2005) Effects of Posture on FDTD Calculations of Specific Absorption Rate in a Voxel Model of the Human Body. Physics in Medicine & Biology, 50, 3825-3835. https://doi.org/10.1088/0031-9155/50/16/011

[97] Joo, E., Szasz, A. and Szendro, P. (2005) Metal-Framed Spectacles and Implants and Specific Absorption Rate among Adults and Children Using Mobile Phones at 900/1800/2100 MHz. Electromagnetic Biology and Medicine, 25, 103-112. https://doi.org/10.1080/15368370600719042

[98] Jianging, W., Mukaide, N. and Fujiwara, O. (2003) FTDT Calculation of Organ Resonance Characteristics in an Anatomically Based Human Model for Plane-Wave Exposure. Proceedings of the Asia-Pacific Conference on Environmental Electromagnetics, Hangzhou, 4-7 November 2003, 126-129.

[99] Armstron Laboratory, USAF School of Aerospace Medicine, AFSC (1997) Radiofrequency Radiation Dosimetry Handbook.
http://niremf.ifac.cnr.it/docs/HANDBOOK/chp1.htm

[100] Slosarek, K., Konopacka, M., Rogoliński, J., Latocha, M. and Sochanik, A. (2005) Effect of Depth on Radiation-Induced Cell Damage in a Water Phantom. Reports of Practical Oncology and Radiotherapy, 10, 37-41. https://doi.org/10.1016/S1507-1367(05)71080-4

[101] Meggyeshazi, N., Andocs, G., Balogh, L., Balla, P., Kiszner, G., Teleki, I., et al. (2014) DNA Fragmentation and Caspase-Independent Programmed Cell Death by Modulated Electrohyperthermia. Strahlentherapie und Onkologie, 190, 815-822. https://doi.org/10.1007/s00066-014-0617-1

[102] Vincze, G., Szasz, O. and Szasz, A. (2015) Generalization of the Thermal Dose of Hyperthermia in Oncology. Open Journal of Biophysics, 5, 97-114. https://doi.org/10.4236/ojbiphy.2015.54009

[103] Andocs, G., Meggyeshazi, N., Balogh, L., et al. (2015) Up-Regulation of Heat Shock Proteins and the Promotion of Damage-Associated Molecular Pattern Signals in a Colorectal Cancer Model by Modulated Electrohyperthermia. Cell Stress and Chaperones, 20, 37-46. https://doi.org/10.1007/s12192-014-0523-6

[104] Qin, W., Akutsu, Y., Andocs, G., Suganami, A., Hu, X., Yusup, G., et al. (2014) Modulated Electro-Hyperthermia Enhances Dendritic Cell Therapy through an Abscopal Effect in Mice. Oncology Reports, 32, 2373-2379. https://doi.org/10.3892/or.2014.3500

[105] Jones, E., Thrall, D., Dewhirst, M.W. and Vujaskovic, Z. (2006) Prospective Thermal Dosimetry: The Key to Hyperthermia's Future. International Journal of Hyperthermia, 22, 247-253. https://doi.org/10.1080/02656730600765072

[106] Dewhirst, M.W., Viglianti, B.L., Lora-Michiels, M., Hanson, M. and Hoopes, P.J. (2003) Basic Principles of Thermal Dosimetry and Thermal Thresholds for Tissue Damage from Hyperthermia. International Journal of Hyperthermia, 19, 267-294. https://doi.org/10.1080/0265673031000119006

[107] Dewey, W.C. (1994) Arrhenius Relationships from the Molecule and Cell to the Clinic. International Journal of Hyperthermia, 10, 457-483. https://doi.org/10.3109/02656739409009351

[108] Perez, C.A. and Sapareto, S.A. (1984) Thermal Dose Expression in Clinical Hyperthermia and Correlation with Tumor Response/Control. Cancer Research, 44, 4818-4825.

[109] Hegyi, G., Vincze, G. and Szasz, A. (2012) On the Dynamic Equilibrium in Homeostasis. Open Journal of Biophysics, 2, 64-71. http://file.scirp.org/pdf/OJBIPHY20120300001_81525786.pdf https://doi.org/10.4236/ojbiphy.2012.23009

[110] Maguire, P.D., Samulski, T.V., Prosnitz, L.R., Jones, E.L., Rosnre, G.L., Powers, B., Layfield, L.W., Brizel, D.M., Scully, S.P., Herrelson, M., et al. (2001) A Phase II Trial Testing the Thermal Dose Parameter CEM43oCT90 as a Predictor of Response in Soft Tissue Sarcomas Treated with Pre-Operative Thermoradiotherapy. International Journal of Hyperthermia, 17, 283-290. https://doi.org/10.1080/02656730110039449

[111] Dewhirst, M.W., Vujaskovic, Z., Jones, E. and Thrall, D. (2005) Re-Setting the Biologic Rationale for Thermal Therapy. International Journal of Hyperthermia, 21, 779-790. https://doi.org/10.1080/02656730500271668

[112] de Bruijne, M., van der Holt, B., van Rhoon, G.C. and van der Zee, J. (2010) Evaluation of CEM43°CT90 Thermal Dose in Superficial Hyperthermia: A Retrospective Analysis. Strahlentherapie und Onkologie, 186, 436-443. https://doi.org/10.1007/s00066-010-2146-x

[113] Assi, H. (2009) A New CEM43 Thermal Dose Model Based on Vogel-Tammann-Fulcher Behaviour in Thermal Damage Processes. Ryerson University, Toronto, Ontario.

[114] Thrall, D.E., Prescott, D.M., Samulski, T.V., Rosner, G.L., Denman, D.L., Legorreta, R.L., Dodge, R.K., Page, R.L., Cline, J.M., Lee, J., Case, B.C., Evans, S.M., Oleson, J.R. and Dewhirst, M.W. (1996) Radiation plus Local Hyperthermia versus Radiation plus the Combination of Local and Whole-Body Hyperthermia in Canine Sarcomas. International Journal of Radiation Oncology · Biology · Physics, 34, 1087-1096.

[115] Szasz, O. and Szasz, A. (2016) Heating, Efficacy and Dose of Local Hyperthermia. Open Journal of Biophysics, 6, 10-18. https://doi.org/10.4236/ojbiphy.2016.61002

[116] Szasz, O. (2019) Bioelectromagnetic Paradigm of Cancer Treatment—Modulated Electro-Hyperthermia (mEHT). Open Journal of Biophysics, 9, 98-109. https://doi.org/10.4236/ojbiphy.2019.92008

[117] Szasz, O. and Szasz, A. (2021) Approaching Complexity: Hyperthermia Dose and Its Possible Measurement in Oncology. Open Journal of Biophysics, 11, 68-132. https://doi.org/10.4236/ojbiphy.2021.111002

[118] Kao, P.H.-J., Chen, C.-H., Chang, Y.-W., et al. (2020) Relationship between Energy Dosage and Apoptotic Cell Death by Modulated Electro-Hyperthermia. Scientific Reports, 10, Article No. 8936. https://www.nature.com/articles/s41598-020-65823-2 https://doi.org/10.1038/s41598-020-65823-2

[119] Meggyeshazi, N., Andocs, G. and Krenacs, T. (2013) Programmed Cell Death Induced by Modulated Electro-Hyperthermia. Conference of the International Clinical Hyperthermia Society 2012, 2013, Article ID: 187835, http://www.hindawi.com/archive/2013/187835/

[120] Danics, L., Schvarcz, C.A.., Viana, P., et al. (2020) Exhaustion of Protective Heat Shock Response Induces Significant Tumor Damage by Apoptosis after Modulated Electro-Hyperthermia Treatment of Triple Negative Breast Cancer Isografts in Mice. Cancers, 12, 2581. https://pubmed.ncbi.nlm.nih.gov/32927720/ https://doi.org/10.3390/cancers12092581

[121] Tsang, Y.-W., Huang, C.-C., Yang, K.-L., et al. (2015) Improving Immunological Tumor Microenvironment Using Electro-Hyperthermia Followed by Dendritic Cell Immunotherapy. BMC Cancer, 15, Article No. 708. http://www.ncbi.nlm.nih.gov/pubmed/26472466 https://doi.org/10.1186/s12885-015-1690-2

[122] Andocs, G., Rehman, M.U., Zhao, Q.-L., Tabuchi, Y., Kanamori, M. and Kondo, T. (2016) Comparison of Biological Effects of Modulated Electro-Hyperthermia and Conventional Heat Treatment in Human Lymphoma U937 Cell. Cell Death Discovery, 2, Article No. 16039. http://www.nature.com/articles/cddiscovery201639 https://doi.org/10.1038/cddiscovery.2016.39

[123] Jeon, T.-W., Yang, H., Lee, C.G., Oh, S.T., et al. (2016) Electro-Hyperthermia Up-Regulates Tumour Suppressor Septin 4 to Induce Apoptotic Cell Death in Hepatocellular Carcinoma. International Journal of Hyperthermia, 32, 648-656. https://doi.org/10.1080/02656736.2016.1186290

[124] Vancsik, T., Andocs, G., Kovago, C., et al. (2015) Electro-Hyperthermia May Target Tumor-Cell Membranes. 33rd Annual Conference of International Clinical Hyperthermia Society (ICHS), Nidda, Germany, 11-13 July 2015.

[125] Meggyeshazi, N. (2015) Studies on Modulated Electrohyperthermia Induced Tumor Cell Death in a Colorectal Carcinoma Model. PhD Thesis, Semmelweis University, Budapest. http://repo.lib.semmelweis.hu/handle/123456789/3956

[126] Krenacs, T., Meggyeshazi, N., Forika, G., Kiss, E., et al. (2020) Modulated Electro-Hyperthermia-Induced Tumor Damage Mechanisms Revealed in Cancer Models. International Journal of Molecular Sciences, 21, 6270. https://www.mdpi.com/1422-0067/21/17/6270 https://doi.org/10.3390/ijms21176270

[127] Vancsik, T., Kovago, C., Kiss, E., et al. (2018) Modulated Electro-Hyperthermia Induced Loco-Regional and Systemic Tumor Destruction in Colorectal Cancer Allografts. Journal of Cancer, 9, 41-53. https://www.ncbi.nlm.nih.gov/pmc/articles/PMC5743710/pdf/jcav09p0041.pdf https://doi.org/10.7150/jca.21520

[128] Biosca, J.A., Travers, F. and Barman, T.E. (1983) A Jump in an Arrhenius Plot Can Be the Consequence of a Phase Transition. The Binding of ATP to Myosin Subfragment 1. FEBS Letters, 153, 217-220. https://doi.org/10.1016/0014-5793(83)80151-3

[129] Hasegawa, T., Gu, Y.H., Takahashi, T., Hasegawa, T. and Yamamoto, I. (2001) Enhancement of Hyperthermic Effects Using Rapid Heating. In: Kosaka, M., Sugahara, T., Schmidt, K.L., et al., Eds., Thermotherapy for Neoplasia, Inflammation, and Pain, Springer Verlag, Tokyo, 439-444. https://doi.org/10.1007/978-4-431-67035-3_49

[130] Watson, K., Bertoli, E. and Griffiths, D.E. (1975) Phase Transitions in Yeast Mitochondrial Membranes. The Effect of Temperature on the Energies of Activation of the Respiratory Enzymes of Saccharomyces cerevisiae. Biochemical Journal, 146, 401-407. https://doi.org/10.1042/bj1460401

[131] Szigeti, G.P., Szasz, O. and Hegyi, G. (2016) Personalised Dosing of Hyperthermia. Journal of Cancer Diagnosis, 1, 107. https://doi.org/10.4172/2476-2253.1000107

[132] Rosenberg, S.M. and Queitsch, C. (2014) Combacting Evolution to Fight Disease. Science, 343, 1088-1089. https://doi.org/10.1126/science.1247472

[133] Szasz, A. (2020) Towards the Immunogenic Hyperthermic Action: Modulated Electro-Hyperthermia. Clinical Oncology and Research, 3, 1-6. https://www.sciencerepository.org/towards-the-immunogenic-hyperthermic-action-modulated-electro-hyperthermia_COR-2020-9-107 https://doi.org/10.31487/j.COR.2020.09.07

[134] Szasz, O. (2020) Local Treatment with Systemic Effect: Abscopal Outcome. In: Szasz, A., Ed., Challenges and Solutions of Oncological Hyperthermia, Ch. 11, Cambridge Scholars Publishing, Newcastle upon Tyne, 192-205. https://www.cambridgescholars.com/challenges-and-solutions-of-oncological-hyperthermia

[135] Palekar-Shanbhag, P., Jog, S.V., Chogale, M.M. and Gaikwad, S.S. (2013) Theranostics for Cancer Therapy. Current Drug Delivery, 10, 357-362. https://doi.org/10.2174/1567201811310030013

[136] Lee, S.-Y., Lee, N.-R., Cho, D.-H., et al. (2017) Treatment Outcome Analysis of Chemotherapy Combined with Modulated Electro-Hyperthermia Compared with Chemotherapy Alone for Recurrent Cervical Cancer, Following Irradiation. Oncology Letters, 14, 73-78. https://doi.org/10.3892/ol.2017.6117

[137] Iyikesici, M.S., Slocum, A.K., Slocum, A., et al. (2017) Efficacy of Metabolically Supported Chemotherapy Combined with Ketogenic Diet, Hyperthermia, and Hyperbaric Oxygen Therapy for Stage IV Triple-Negative Breast Cancer. Cureus, 9, e1445. https://doi.org/10.7759/cureus.1445

[138] Yeo, S.-G. (2015) Definitive Radiotherapy with Concurrent Oncothermia for Stage IIIB Non-Small-Cell Lung Cancer: A Case Report. Experimental and Therapeutic Medicine, 10, 769-772. https://doi.org/10.3892/etm.2015.2567

[139] Pesti, L., Dankovics, Z., Lorencz, P., et al. (2013) Treatment of Advanced Cervical Cancer with Complex Chemoradio-Hyperthermia. Conference of the International Clinical Hyperthermia Society 2012, 2013, Article ID: 192435. https://doi.org/10.1155/2013/192435

[140] Kleef, R., Kekic, S. and Ludwig, N. (2012) Successful Treatment of Advanced Ovarian Cancer with Thermochemotherapy and Adjuvant Immune Therapy. Case Reports in Oncology, 5, 212-215. https://doi.org/10.1159/000338617

[141] Schirrmacher, V., Bihari, A.-S., Stücker, W., et al. (2014) Long-Term Remission of Prostate Cancer with Extensive Bone Metastases upon Immuno- and Virotherapy: A Case Report. Oncology Letters, 8, 2403-2406. https://doi.org/10.3892/ol.2014.2588

[142] Van Gool, S.W., Makalowski, J., Feyen, O., Prix, L., Schirrmacher, V. and Stuecker, W. (2018) The Induction of Immunogenic Cell Death (ICD) during Maintenance Chemotherapy and Subsequent Multimodal Immunotherapy for Glioblastoma (GBM). Austin Oncology Case Reports, 3, 1010.

[143] Szasz, A.M., Minnaar, C.A., Szentmartoni, G., et al. (2019) Review of the Clinical Evidences of Modulated Electro-Hyperthermia (mEHT) Method: An Update for the Practicing Oncologist. Frontiers in Oncology, 9, Article 1012. https://www.frontiersin.org/articles/10.3389/fonc.2019.01012/full https://doi.org/10.3389/fonc.2019.01012

[144] Wismeth, C., Dudel, C., Pascher, C., et al. (2010) Transcranial Electro-Hyperthermia Combined with Alkylating Chemotherapy in Patients with Relapsed High-Grade Gliomas—Phase I Clinical Results. Journal of Neuro-Oncology, 98, 395-405. http://www.ncbi.nlm.nih.gov/pubmed/?term=Transcranial+electro-hyperthermia+combined+with+alkylating+chemotherapy+in+patients+with+relapsed+high-grade+gliomas+%E2%80%93+Phase+I+clinical+results https://doi.org/10.1007/s11060-009-0093-0

[145] Fiorentini, G., Giovanis, P., Rossi, S., et al. (2006) A Phase II Clinical Study on Relapsed Malignant Gliomas Treated with Electro-Hyperthermia. In Vivo, 20, 721-724. https://www.ncbi.nlm.nih.gov/pubmed/17203754

[146] Fiorentini, G. and Casadei, V. (2018) Modulated Electro-Hyperthermia (mEHT) in Integrative Cancer Treatment for Relapased Malignant Gliobastroma and Astrocytoma: A Retrospective Multicenter Controlled Study. Oncothermia Journal, 24, 464-481. https://oncotherm.com/sites/oncotherm/files/2018-10/Modulated_electro_hyperthermia_%28mEHT%29_in_integrative_cancer_treatment.pdf

[147] Sahinbas, H., Groenemeyer, D.H.W., Boecher, E. and Szasz, A. (2007) Retrospective Clinical Study of Adjuvant Electro-Hyperthermia Treatment for Advanced Brain-Gliomas. Deutsche Zeitschrift für Onkologie, 39, 154-160. https://www.thieme-connect.com/products/ejournals/abstract/10.1055/s-2007-986020 https://doi.org/10.1055/s-2007-986020

[148] Hager, E.D., Sahinbas, H., Groenemeyer, D.H., et al. (2008) Prospective Phase II Trial for Recurrent High-Grade Malignant Gliomas with Capacitive Coupled Low Radiofrequency (LRF) Deep Hyperthermia. Journal of Clinical Oncology, 26, 2047. https://ascopubs.org/doi/abs/10.1200/jco.2008.26.15_suppl.2047 https://doi.org/10.1200/jco.2008.26.15_suppl.2047

[149] Fiorentini, G., Sarti, D., Milandri, C., et al. (2018) Modulated Electrohyperthermia in Integrative Cancer Treatment for Relapsed Malignant Glioblastoma and Astrocytoma: Retrospective Multicenter Controlled Study. Integrative Cancer Therapies, 18. https://www.ncbi.nlm.nih.gov/pubmed/30580645 https://doi.org/10.1177/1534735418812691

[150] Gadaleta-Caldarola, G., Infusino, S., Galise, I., et al. (2014) Sorafenib and Locoregional Deep Electro-Hyperthermia in Advanced Hepatocellular Carcinoma. A Phase II Study. Oncology Letters, 8, 1783-1787. http://www.ncbi.nlm.nih.gov/pmc/articles/PMC4156230/ https://doi.org/10.3892/ol.2014.2376

[151] Ferrari, V.D., De Ponti, S., Valcamonico, F., et al. (2007) Deep Electro-Hyperthermia (EHY) with or without Thermo-Active Agents in Patients with Advanced Hepatic Cell Carcinoma: Phase II Study. Journal of Clinical Oncology, 25, Article ID: 15168. http://ascopubs.org/doi/abs/10.1200/jco.2007.25.18_suppl.15168 https://doi.org/10.1200/jco.2007.25.18_suppl.15168

[152] Lee, D.-J., Haam, S.-J., Kim, T.-H., et al. (2013) Oncothermia with Chemotherapy in the Patients with Small-Cell Lung Cancer. Conference of the International Clinical Hyperthermia Society 2012, 2013, Article ID: 910363. http://www.hindawi.com/archive/2013/910363/ https://doi.org/10.1155/2013/910363

[153] Minnaar, C., Baeyens, A. and Kotzen, J. (2016) Update on Phase III Randomized Clinical Trial Investigating the Effects of the Addition of Electro-Hyperthermia to Chemoradiotherapy for Cervical Cancer Patients in South Africa. Physica Medica, 32, 151-152.

http://www.physicamedica.com/article/S1120-1797(16)30175-2/abstract
https://doi.org/10.1016/j.ejmp.2016.07.042

[154] Lee, S.-Y., Kim, J.-H., Han, Y.-H., et al. (2018) The Effect of Modulated Electro-Hyperthermia on Temperature and Blood Flow in Human Cervical Carcinoma. International Journal of Hyperthermia, 34, 953-960. https://doi.org/10.1080/02656736.2018.1423709

[155] Minnaar, C.A., Kotzen, J.A., Ayeni, O.A., et al. (2020) Potentiation of the Abscopal Effect by Modulated Electro-Hyperthermia in Locally Advanced Cervical Cancer Patients. Frontiers in Oncology, 10, 376. https://www.ncbi.nlm.nih.gov/pmc/articles/PMC7105641/
https://doi.org/10.3389/fonc.2020.00376

[156] Minnaar, C.A., Kotzen, J.A., Naidoo, T., et al. (2020) Analysis of the Effects of mEHT on the Treatment-Related Toxicity and Quality of Life of HIV-Positive Cervical Cancer Patients. International Journal of Hyperthermia 37, 263-227.
https://www.ncbi.nlm.nih.gov/pubmed/32180481
https://doi.org/10.1080/02656736.2020.1737253

[157] Minnaar, C.A., Kotzen, J.A., Ayeni, O.A., et al. (2019) The Effect of Modulated Electro-Hyperthermia on Local Disease Control in HIV-Positive and -Negative Cervical Cancer Women in South Africa: Early Results from a Phase III Randomized Controlled Trial. PLoS ONE, 14, e0217894. https://www.ncbi.nlm.nih.gov/pmc/articles/PMC6584021/
https://doi.org/10.1371/journal.pone.0217894

[158] Ou, J., Zhu, X., Lu, Y., et al. (2017) The Safety and Pharmacokinetics of High Dose Intravenous Ascorbic Acid Synergy with Modulated Electrohyperthermia in Chinese Patients with Stage III-IV Non-Small Cell Lung Cancer. European Journal of Pharmaceutical Sciences, 109, 412-418. http://www.sciencedirect.com/science/article/pii/S0928098717304554?via%3Dihub
https://doi.org/10.1016/j.ejps.2017.08.011

[159] Ou, J., Zhu, X., Chen, P., et al. (2020) A Randomized Phase II Trial of Best Supportive Care with or without Hyperthermia and Vitamin C for Heavily Pretreated, Advanced, Refractory Non-Small-Cell Lung Cancer. Journal of Advanced Research, 24, 175-182. https://www.ncbi.nlm.nih.gov/pubmed/32368355
https://doi.org/10.1016/j.jare.2020.03.004

[160] Szasz, A. (2014) Current Status of Oncothermia Therapy for Lung Cancer. Korean Journal of Thoracic and Cardiovascular Surgery, 47, 77-93. http://www.ncbi.nlm.nih.gov/pmc/articles/PMC4000888
https://doi.org/10.5090/kjtcs.2014.47.2.77

[161] Iyikesici, M.S. (2019) Feasibility Study of Metabolically Supported Chemotherapy with Weekly Carboplatin/Paclitaxel Combined with Ketogenic Diet, Hyperthermia and Hyperbaric Oxygen Therapy in Metastatic Non-Small Cell Lung Cancer. International Journal of Hyperthermia, 36, 445-454. https://www.ncbi.nlm.nih.gov/pubmed/30931666
https://doi.org/10.1080/02656736.2019.1589584

[162] Pang, C.L.K., Zhang, X., Wang, Z., Ou, J.W., et al. (2017) Local Modulated Electro-Hyperthermia in Combination with Traditional Chinese Medicine vs. Intraperitoneal Chemoinfusion for the Treatment of Peritoneal Carcinomatosis with Malignant Ascites: A Phase II Randomized Trial. Molecular and Clinical Oncology, 6, 723-732.
https://pubmed.ncbi.nlm.nih.gov/28529748/
https://doi.org/10.3892/mco.2017.1221

[163] You, S.H. and Kim, S. (2019) Feasibility of Modulated Electro-Hyperthermia in Preoperative Treatment for Locally-Advanced Rectal Cancer: Early Phase 2 Clinical Results. Neoplasma, 67, 677-683. https://www.ncbi.nlm.nih.gov/pubmed/32039629
https://doi.org/10.4149/neo_2020_190623N538

[164] Hager, E.D., Dziambor, H., Höhmann, D., et al. (1999) Deep Hyperthermia with Radiofrequencies in Patients with Liver Metastases from Colorectal Cancer. Anticancer Research, 19, 3403-3408. http://www.ncbi.nlm.nih.gov/pubmed/10629627

[165] Jeung, T.-S., Ma, S.-Y., Choi, J., et al. (2015) Results of Oncothermia Combined with Operation, Chemotherapy and Radiation Therapy for Primary, Recurrent and Metastatic Sarcoma. Case Reports in Clinical Medicine, 4, 157-168.
http://www.scirp.org/journal/PaperInformation.aspx?PaperID=56280
https://doi.org/10.4236/crcm.2015.45033

[166] Volovat, C., Volovat, S.R., Scripcaru, V., et al. (2014) The Results of Combination of Ifosfamid and Locoregional Hyperthermia (EHY 2000) in Patients with Advanced Abdominal Soft-Tissue Sarcoma after Relapse of First Line Chemotherapy. Romanian Reports in Physics, 66, 175-181. http://www.rrp.infim.ro/2014_66_1/A19.pdf

[167] Iyikesici, M.S. (2020) Long-Term Survival Outcomes of Metabolically Supported Chemotherapy with Gemcitabine-Based or FOLFIRINOX Regimen Combined with Ketogenic Diet, Hyperthermia, and Hyperbaric Oxygen Therapy in Metastatic Pancreatic Cancer. Complementary Medicine Research, 27, 31-39. https://www.ncbi.nlm.nih.gov/pubmed/31527373, https://doi.org/10.1159/000502135

[168] Volovat, C., Volovat, S.R., Scripcaru, V., et al. (2014) Second-Line Chemotherapy with Gemcitabine and Oxaliplatin in Combination with Loco-Regional Hyperthermia (EHY-2000) in Patients with Refractory Metastatic Pancreatic Cancer—Preliminary Results of a Prospective Trial. Romanian Reports in Physics, 66, 166-174. http://www.rrp.infim.ro/2014_66_1/A18.pdf

[169] Fiorentini, G., Sarti, D., Casadei, V., et al. (2019) Modulated Electro-Hyperthermia as Palliative Treatment for Pancreas Cancer: A Retrospective Observational Study on 106 Patients. Integrative Cancer Therapies, 18, 1-8. https://journals.sagepub.com/doi/pdf/10.1177/1534735419878505 https://doi.org/10.1177/1534735419878505

[170] Hager, E.D., Süsse, B., Popa, C., et al. (1994) Complex Therapy of the Not in Sano Resectable Carcinoma of the Pancreas—A Pilot Study. Journal of Cancer Research and Clinical Oncology, 120, R47.

[171] Dani, A., Varkonyi, A., Magyar, T. and Szasz, A. (2008) Clinical Study for Advanced Pancreas Cancer Treated by Oncothermia. Forum Hyperthermie, 1, 13-20. http://www.pyatthealth.com/wp-content/uploads/2015/03/Hyperthermia-Pancreatic-Cancer.pdf

[172] Ranieri, G., Ferrari, C., Di Palo, A., et al. (2017) Bevacizumab-Based Chemotherapy Combined with, Regional Deep Capacitive Hyperthermia in Metastatic Cancer Patients: A Pilot Study. International Journal of Molecular Sciences, 18, 1458. https://www.ncbi.nlm.nih.gov/pubmed/28684680 https://doi.org/10.3390/ijms18071458

[173] Chi, M.-S., Mehta, M.P., Yang, K.-L., et al. (2020) Putative Abscopal Effect in Three Patients Treated by Combined Radiotherapy and Modulated Electrohyperthermia. Frontiers in Oncology, 10, 254. https://www.frontiersin.org/articles/10.3389/fonc.2020.00254/full https://doi.org/10.3389/fonc.2020.00254

[174] Iyikesici, M.S. (2020) Survival Outcomes of Metabolically Supported Chemotherapy Combined with Ketogenic Diet, Hyperthermia, and Hyperbaric Oxygen Therapy in Advanced Gastric Cancer. Nigerian Journal of Clinical Practice, 23, 734-740. https://www.ncbi.nlm.nih.gov/pubmed/32367884 https://doi.org/10.25000/acem.650341

[175] Fiorentini, G., Sarti, D., Gadaleta, C.D., et al. (2020) A Narrative Review of Regional Hyperthermia: Updates from 2010-2019. Integrative Cancer Therapies, 19, 1-13. https://pubmed.ncbi.nlm.nih.gov/33054425/ https://doi.org/10.1177/1534735420932648

[176] Van Gool, S.W., Makalowski, J., Fiore, S., et al. (2021) Randomized Controlled Immunotherapy Clinical Trials for GBM Challenged. Cancers, 13, 32. https://pubmed.ncbi.nlm.nih.gov/33374196/ https://doi.org/10.3390/cancers13010032

[177] Kim, S., Lee, J.H., Cha, J. and You, S.H. (2021) Beneficial Effects of Modulated Electro-Hyperthermia during Neoadjuvant Treatment for Locally Advanced Rectal Cancer. International Journal of Hyperthermia, 38, 144-151. https://pubmed.ncbi.nlm.nih.gov/33557636/ https://doi.org/10.1080/02656736.2021.1877837

[178] Fiorentini, G., Sarti, D., Casadei, V., et al. (2020) Modulated Electro-Hyperthermia for the Treatment of Relapsed Brain Gliomas. In: Szasz, A., Ed., Challenges and Solutions of Oncological Hyperthermia, Ch. 6, Cambridge Scholars Publishing, Newcastle upon Tyne, 110-125. https://www.cambridgescholars.com/challenges-and-solutions-of-oncological-hyperthermia

[179] Garay, T., Kiss, E., Szentmartoni, G., et al. (2020) Gastrointestinal Cancer Series Treated with Modulated Electro-Hyperthermia (mEHT)—A Single Centre Experience In: Szasz, A., Ed., Challenges and Solutions of Oncological Hyperthermia, Ch. 8, Cambridge Scholars Publishing, Newcastle upon Tyne, 159-162. https://www.cambridgescholars.com/challenges-and-solutions-of-oncological-hyperthermia

[180] Wookyeom, Y., Han, G.H., Shin, H.-Y., et al. (2018) Combined Treatment with Modulated Electro-Hyperthermia and an Autophagy Inhibitor Effectively Inhibit Ovarian and Cervical Cancer Growth. International Journal of Hyperthermia, 36, 9-20. https://doi.org/10.1080/02656736.2018.1528390

[181] Szasz, A.M., Szentmartoni, G., Garay, T., et al. (2020) Breast Cancer Series Treated with Modulated Electro-Hyperthermia (mEHT)—A Single Centre Experience. In: Szasz, A., Ed., Challenges and Solutions of Oncological Hyperthermia, Ch. 5, Cambridge Scholars Publishing, Newcastle upon Tyne, 105-109, https://www.cambridgescholars.com/challenges-and-solutions-of-oncological-hyperthermia

[182] Lee, Y. (2013) Oncothermia Application for Various Malignant Diseases. Conference of the International Clinical Hyperthermia Society 2012, 2013, Article ID: 245156. http://www.hindawi.com/archive/2013/245156/ https://doi.org/10.1155/2013/245156

[183] Parmar, G., Rurak, E., Elderfield, M., et al. (2020) 8-Year Observational Study on Naturopathic Treatment with Modulated Electro-Hyperthermia (mEHT): A Single-Centre Experience. In: Szasz, A., Ed., Challenges and Solutions of Oncological Hyperthermia, Ch. 13, Cambridge Scholars Publishing, Newcastle upon Tyne, 227-266. https://www.cambridgescholars.com/challenges-and-solutions-of-oncological-hyperthermia

[184] Arrojo, E.E. (2020) The Position of Modulated Electro-Hyperthermia (Oncothermia) in Combination with Standard Chemo- and Radiotherapy in Clinical Practice—Highlights of Upcoming Phase III Clinical Studies in Hospital Universitario Marqués de Valdecilla (HUMV). In: Szasz, A., Ed., Challenges and Solutions of Oncological Hyperthermia, Ch. 4, Cambridge Scholars Publishing, Newcastle upon Tyne, 91-104. https://www.cambridgescholars.com/challenges-and-solutions-of-oncological-hyperthermia

[185] Roussakow, S. (2017) Clinical and Economic Evaluation of Modulated Electrohyperthermia Concurrent to Dose-Dense Temozolomide 21/28 Days Regimen in the Treatment of Recurrent Glioblastoma: A Retrospective Analysis of a Two-Centre German Cohort Trial with Systematic Comparison and Effect-to-Treatment Analysis. BMJ Open, 7, e017387. http://bmjopen.bmj.com/content/bmjopen/7/11/e017387.full.pdf; https://doi.org/10.1136/bmjopen-2017-017387

Therapeutic Basis of Electromagnetic Resonances and Signal-Modulation

Andras Szasz

Department of Biotechnics, St. Istvan University, Budaörs, Hungary

* Correspondence: Szasz.Andras@gek.szie.hu

Cite this article as:
Szász, A. (2021): Therapeutic Basis of Electromagnetic Resonances and Signal-Modulation, Open Journal of Biophysics , 11, 314-350.
https://doi.org/10.4236/ojbiphy.2021.113011

Oncothermia Journal 31, 2022 March: 100-130
www.oncotherm.com/sites/oncotherm/files/2022-03/Szasz_Therapeutic.pdf

Abstract
The medical application of electromagnetic resonances is a controversial area of knowledge. Numerous unproven statements and some medical quackeries were published and distributed in informal channels among suffering patients. The fake information is hazardous in such severe diseases as cancer. The optimal, high efficacy energy transport by resonances attracts the interest of the experts and the public. The focus of the attention is technical and concentrates on the careful selection and excitation of the target compounds or cells, expecting helpful modifications. The complication is the complexity of the living systems. The targets are interconnected with an extensive network in the tissues where homeostasis, a dynamic equilibrium, regulates and controls changes. The broad range of energy-transfer variants could cause resonant effects, but the necessary criteria for the selection and proper action have numerous limits. The modulated high-frequency carrier may solve a part of the problem. This mixed solution uses the carrier and modulation's particular properties to solve some of the obstacles of selection and excitation processes. One of the advantages of modulation is its adaptive ability to the living complexity. The modulated signal uses the homeostatic time-fractal pattern ($1/f$ noise). The task involves finding and providing the best available mode to support the healthy state of the body. The body's reaction to the therapy remains natural; the modulation boosts the body's ability for the homeostatic regulation to reestablish the healthy state.

Keywords
ElectricImpedance, Coherency, Complexity, MolecularExcitations, Collectivity, Homeostasis, Entropy, $1/f$ - Noise, Time-Fractal

1. Introduction

The bioelectromagnetic effects attracted the significant attention of various researchers and laypersons in the last couple of centuries. The observation shows that the electric and magnetic fields influence the biological processes. However, the therapeutic applications of bioelectromagnetics cause heated debates from its start described it as "humbug" [1] and "utter idiocy" [2]. The weak proofs well support the medical skepticism nowadays too [3] [4]. Many patented ideas like Lakhovsky's radio-cellular-oscillator [5] [6], the Priore's electromagnetic therapy [7] [8] [9], deal with the bioelectromagnetic therapy, without any proof, creditable systematic studies, only some positive case-reports were published. Others, like Gurvich's mitotic wave in mitosis and some enzymatic reactions [10], have no tools, which are sensitive enough to measure the supposed effects [11]. Even such genius giant as Nikola Tesla had patented a method about the high-frequency oscillators for electro-therapeutics, using "ultraviolet rays", [12] presently also out of convincing data.

One of the most influential ideas in the bioresonance field was developed by Royal Raymond Rife. The "resonance topic" started with a revolutionary step of optical microscopy [13]. The Rife-microscope had the ultimate resolution in that time [14], able to record time-lapse movies of microbes [15]. Various pathogen organisms show cellular damages at "resonant frequencies". The phenomenon was described with "mortal oscillatory rate" (MOR) [16] [17] [18] [19]. The cancer-cells had showed also mortality by resonances [19] [20]. Strong critical opinions appeared about the method [21] [22], and the electronic devices for cancer management [23]. The lack of pieces of evidence, the selected favorable cases formed the "pseudomedicine" supported by electronics [24]. The fraudulent activities were punished [25] [26].

The role of bioelectromagnetics and especially the resonance phenomena became the "battlefield" of science with multiple quackeries and unscientific theories. The serious doubts make this topic an impossible research venture. Notwithstanding the importance of this great challenge, this work aims to study the possible application of electromagnetic resonances and modulation in cancer therapies.

2. Challenge of Complexity

The living systems are complex, well self-regulated, and controlled. The molecular biology's deterministic approach, about the completeness of the molecular development, strictly follows the stored model of the whole system in the DNA. However, the living processes are more complex than enough computer capacity could describe the system. Reducing life to a simple deterministic approach (reductionism) loses the system as an interconnected and complexly regulated unit. The proper consideration is to handle the living system as a whole (holism).

The biological systems have the same complementary duality as the particles in quantum mechanics have. Nested and overlapping levels of the observation depend on the scale of the studied part of the system [27], an inspection of the same living feature from different points of view. This phenomenon is similar to the quantum duality, the observation depends on the observer also: "A living thing cannot be explained in terms of its parts but only in terms of the organization of these parts" [28].

It is more challenging that the living complexity involves a logical incompleteness [29], discovered by Gödel almost a century ago [30]. The incomplete, complex situation means that we may address valid questions which have no answer in a deterministic way. These questions have a loop with a self-reference: first, the hen or the egg? The answer goes to the evolutionary field; and necessarily leaves the deterministic thinking. Similarly, the answer to the question "what existed first: the promoter or the suppressor" has no direct answer. A loop also needs a developmental, non-deterministic consideration. The complex system is regulated and controlled by primarily negative feedback loops, having the Gödelian incompleteness. Theoretical biology faces these challenges, which builds a "tragicomic" situation [31].

2.1. Homeostasis of Life

Biological systems and their macro- and micro-parts are energetically open, operate on various in- and outputs, causing a specified event. The product's reaction could amplify/promote the further shift or inhibit/block it, suppressing the change. The promoter-suppressor pairs work in sensitive order, modified by the feedback loops, the processes maintain the dynamic equilibrium of the living system, forming homeostasis. The homeostasis is far from the static equilibrium, but in normal conditions, it has a self-adjusted stationery state, regulated by the negative feedback. The feedback control mechanism regulates the promoter-suppressor balance in a relatively narrow predetermined range around the set-point value. The dynamic homeostatic equilibrium keeps the system stable but constantly changing. The dynamic equilibrium approaches to count "degrees of truth" rather than the usual "true or false" decisions [32]. Numerous negative feedback loops control the homeostasis [33] [34] in the micro and macro-structures levels.

The system's open character needs positive feedback processes too, which are one-promoting/accelerating the started process. Positive feedback results in more of a product or accelerates the progress.

The homeostasis governs the equilibria in all living ranges of space and time.

It is tuned by the intertwining of processes, which at each step seeks to have a dynamic and interconnected balance of suppressor-promoter pairs of the regulatory process [35].

The dynamic behavior of the interacting complexity guarantees robust stability. The regulation and controlling process are essentially inherently dynamical, so the term "homeodynamics" describes it better than "homeostasis" [36].

2.2. Self-Organizing

The living system exchanges energy with its environment, and every part, like the cells, tissues, and organs, has open energy trade with other parts of the system. The spatiotemporal arrangement of the living organisms and their parts are self-organized [37] [38]. The self-organized feedbacks secure the stability against a relatively wide range of perturbations. The structures' self-similar building simplifies their construction by deterministically or statistically repeating the same template and connecting them with the same structure [39], building a self-similar harmony.

The systematically built structures are fractals, which commonly appear in natural forms [40]. The fractal description of living objects' spatial irregularities allows for an objective comparison of complex morphogenetic differences [41], and provides a useful tool to follow the physiological changes in pathologic processes [42]. Fractal models explain the structural developments of life processes [43]. The collectivity of the organization also could be monitored by the fractal concept [44].

The structural fractals complete the dynamic properties of life. The dynamical structures develop a complex spatiotemporal approach of biology, the fractal physiology [45] [46] [47], dealing with random stationary stochastic self-organizing processes in physiologic phenomena. Fractal physiology offers practical applications recognizing the diseases [48]. The self-similarity allows modeling cancer tissues by fractals [49], described by a generalized model [50]. The fractal geometry helps to evaluate the various images in oncology [51], describes the pathological architecture of tumors and their growth mechanisms accompanying time-dependent processes [52], and prognostic value [53].

The self-similar self-organizing process is collective [54] and relates to the allometric scaling of living species [55] [56]. The collectivity subordinates the individual needs to the groups and optimizes the energy distribution for the best survival with the lowest energy consumption. This energy-share works like some kind of democracy [57].

2.3. Stochastic Processes

The well-organized complex dynamic equilibrium characterizes the regulative activities of the living systems from genomic to global adaptation of the organisms to the environmental challenges [41]. The time-dependent processes realize the observed signal with a probability of requesting a stochastic approach instead of conventional thinking based on deterministic changes [58]. The homeostasis is often ignored and used as a static framework for effects [59]. The stochastic approach is fundamental in biological dynamism [60]. Deterministic reductionism can mislead the research.

Diagnostic parameters (signals) characterize the living organism. The average in time represents the measurement of signals, which fluctuate around the average value in a controlled band. The fluctuation sets various actual microstates in the body, only for a short time regarded as a signal's noise. The homeostatic control of the body regulates the fluctuations. The homeostasis needs "order" in noise structure parameters like frequencies, intensities, phases. The minimal number of diagnostic signals describing in a state is defined by the quasi-independent, weakly overlapping regulation intervals. The number of these quasi-independent diagnostic signals does not change during the system meets the conditions of the healthy dynamical equilibrium. However, together with the relative constant averages with a standard deviation in the fluctuation band, the distribution of the signal frequencies varies. The variation depends on the adaptation to internal and environmental conditions. The measured quantities appear an average $\langle D_i \rangle$ of microscopic diagnostic states $\langle D_i \rangle$. If the change of D_i remains within a tolerance band l_{D_i} around $\langle D_i \rangle$, the homeostasis is considered faultless, the subject is declared healthy.

The fluctuation of the signals around the actual average $f_{D_i} = D_i - \langle D_i \rangle$ opens a new possibility to study the living processes. The change in the fluctuation of the signal occurs sooner than the variation of the average value. However, the changing of the regulative processes could drastically modify the signal's fluctuation without changing their average value. The alterations in the noise spectrum can predict reorganizations of the regulative feedback, which could point a healthy adaptive process to the environmental challenges but could indicate disease as well. The various curative processes could reestablish the signal averages. Although the new reestablished average is the same as was the previous, the fluctuations around the average could differ from the previous dynamism. The interacting connections and regulating signal loops could vary the fluctuations from earlier. This variation happens for example, when the immune system develops new functions by "learning" the fight against pathogens. The systemic control is modified, and the system reflects it in the regulative fluctuations. Nevertheless, it could happen that the therapy reestablishes the proper average of the diagnosis signal, but the patient remains ill. The noise spectrum examination may recognize such incompatibilities, when the problem does not appear immediately in the averages. The opportunity of noise analysis is an accurate novel approach to diagnose and follow the illness in its early stages.

The power spectrum $S(f)$characterizes the stochastic signal with the f frequency. The other important functional character of the signal is the autocorrelation ($R_{XX}(t_1, t_2)$)), which measures how the signal correlates with itself with a delayed copy of itself. The correlation is displayed as a function of time-lag ($\tau = t_2 - t_1$)in X position. The $R_{XX}(t_1, t_2)$ is the similarity of the signal-parts having time delay between them. The autocorrelation evaluation is a mathematical tool for finding repeating patterns, looking for periodicity in the signal. It is a useful tool also to find a missing periodic signal, which we regard as an important component when a set of repeated interactions form the investigated fluctuation.

The simplest complex noise is Gaussian (the amplitudes have normal distribution), and its power function $S(f)$ is self-similar through many orders of magnitudes. The $S(f)$ is characterized with α in a simple form, like in(1)

$$S(f) = \frac{A}{f^{\alpha}} \tag{1}$$

The α exponent is usually formally referred to on optics, noted as the "color" of the noise. The white-noise is flat ($\alpha = 0$), the pink-noise has $\alpha = 1$, and other colors are described by various other numbers up to $\alpha = 2$, the brown-noise. The $S(f)$ of pink-noise inversely depends on f frequency, noted as $1/f$ noise. The self-similar processes produce $1/f$ (pink) noise covering the time-fractal of life's dynamism [61] [62]. This dynamical fractal structure marks the self-organizing both in structural and time arrangements [63] and dynamically regulates the living matter [64]. The $1/f$ fluctuations [65] define time-fractal structure in a stochastic way of the living systems [66]. The physiological control shows $1/f$ spectrum [67]. One of the most studied such spectra is the heart rate variability (HRV).

Each octave interval (halving or doubling in frequency) carries an equal amount of noise energy in the $1/f$ noise. The self-organized symmetry of living system transforms the white noise to pink [68], forming the most common signal in biological systems [69].

3. Electromagnetic Effect

Biology fundamentally depends on the water. The electromagnetic forces act on various aqueous electrolytes and some solids (like bones) in the systems. The external application of electromagnetic fields on living bodies has four basic categories:

1) displacements of free charges, causing electric current in the system;

2) vibrations of charges in chemical or physical bonds (electrons in atoms, atoms in molecules, surface adhesions, collective-networks);

3) reorientation (torque, rotation, structural change) of dipoles (like water molecules proteins, complex structures);

4) displacement and reorientation of complete cells.

These above effects could make notable changes in the living object:

- heat (temperature growth) by energy absorption,

- ignite molecular and systemic excitation,

- modify some suppressor-promoter loops directly by altering the feedback set-point.

These changes could trigger physiologic and biophysical changes of the homeostatic regulation and rearrange of the control. Electromagnetic resonance phenomena attract extensive attention, especially connected to the cells as the integrated carrier and "building blocks" of the living organisms. The Rife resonances appear as a part of these efforts. The critical point is how the electromagnetic forces make an active selection and distort the targeted cells.

The most trivial connection to how electromagnetism transformed to an obvious direct cellular effector is the heating by energy absorption. When the absorbed energy heats the target homogeneously, we may define the average energy-absorption measurable with the temperature. When the absorption is heterogeneous, the temperature as an average cannot be defined.

The temperature can be replaced by electric fields using their similarities in the absorbed energy [70]. The similarity emphasizes the possibility of the non-temperature changing but due to the energy exchange thermal processes involving the $\sum_i \mathcal{E}_i d\, P_i$ in the internal energy of electromagnetically heterogeneous media, Figure 1 .

Less obvious and more complicated effects are "nonthermal", meaning that the temperature change is not observable. Low-level, non-stationary magnetic fields have been observed [71] and adopted [72] as the nonthermal electromagnetic effect. One of the most important nonthermal processes is the so-called "window" effects [73], having an optimum both frequency and amplitude to interact with cellular membrane [74]. The window effects have some resonance characters. The measured frequency dependence sensitively varies on the experimental conditions and could be in synergy with chemical effects [75].

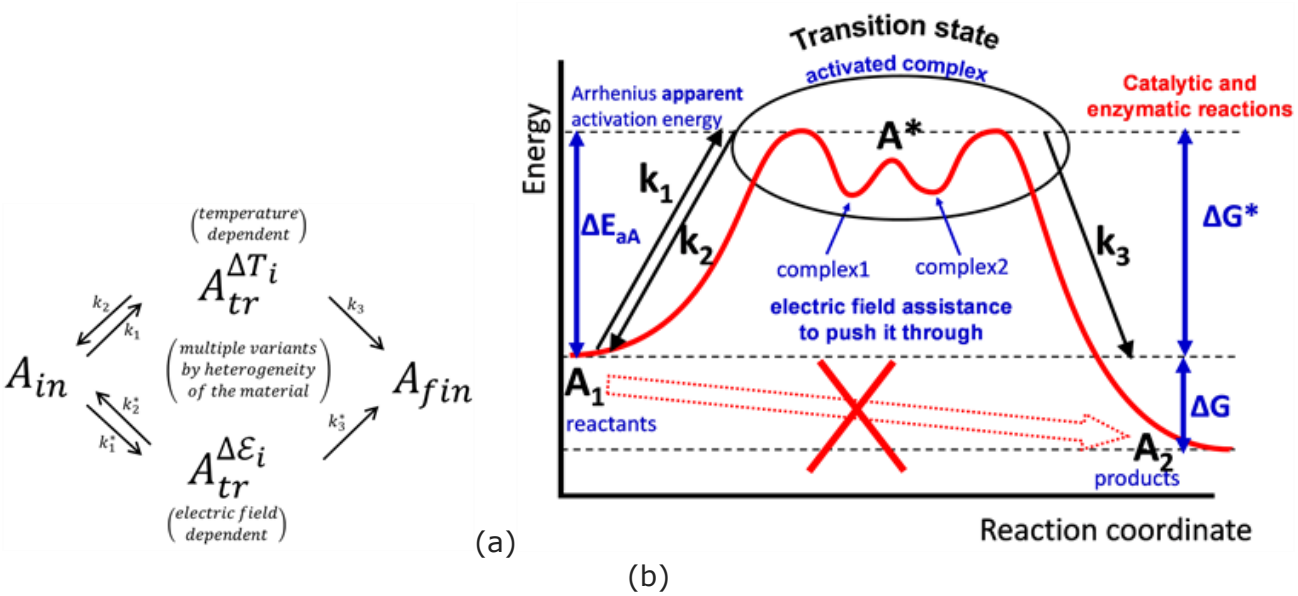

Figure 1. The direct transition between A_1 and A_2 is impossible due to the energy barrier. Enzymatic reactions could lower the height of the barrier by a chemical transition state. (a) The electric field-assisted transition works in a similar way, excites the targeted molecules, and forms a transitional state as enzymes do; (b) The transition state A* is a complex molecular reaction, and the electric field pushes it to the point of no return to finish the transition process.

The "window" was measured in multiple power ranges [76], depending on the applied power (amplitude of the signal at the same impedance load), with such small energy, which categorized these experiments definitely as nonthermal. (They used max. $5\mu W/g$ energy). The active Na^+ flux pumping was observed as the maximum between $0.1 - 10\ MHz$ [77], which "window" effect could be well explained by the active transport system model in the membrane [78]. The "window" to increase DNA concentration in the specimen was measured at 10 Hz between $0.03 - 0.06\ V/m$ and $4 - 5\ \mu A/cm^2$ electric field and current density, respectively. These low frequencies differ from the Rife-declared ones.

The inherent heterogeneity of the living objects varies the electromagnetic processes in constituting parts of the target. The heterogenic electromagnetic effects sharply divide depending on the aqueous electrolytes or lipid substances (like membranes or adipose cells) or solids (like bones). The actions are frequency-dependent, which form dispersion relations.

Schwan [79] measured the electrical properties of tissue and cell suspension over a broad frequency range. He observed three major frequency dispersions, introduced three dispersion mechanisms (α, β, γ) to characterize the anomalous electric properties of biomaterials. The high heterogeneity of the living tissue differentiation was since low-frequency, radiofrequency, and microwave effects have multiple relaxational processes in their interval [80], Figure 2 . They are considering different mechanisms at low frequency (α), radio frequency (β), and microwave frequency (γ) processes.

The low frequency (approx. 10 Hz to 10 kHz) α-dispersion. This frequency-range acts mainly in muscle tissue [81], and so it is connected to the tubular system [82]. The vanishing of the α-dispersion frequencies indicates first the dying process of the tissue [83].

The β-dispersion is superimposed to the high-frequency end of α-dispersion. It has a link to the cellular structure of biological materials [84]. The β-dispersion occurs at the interface of membrane-electrolyte structures, using Maxwell-Wagner relaxation [85]. Interfacial polarization of the cell membranes appears in this frequency range [86], connected to the charge distribution at the cellular of interfacial boundaries [87].

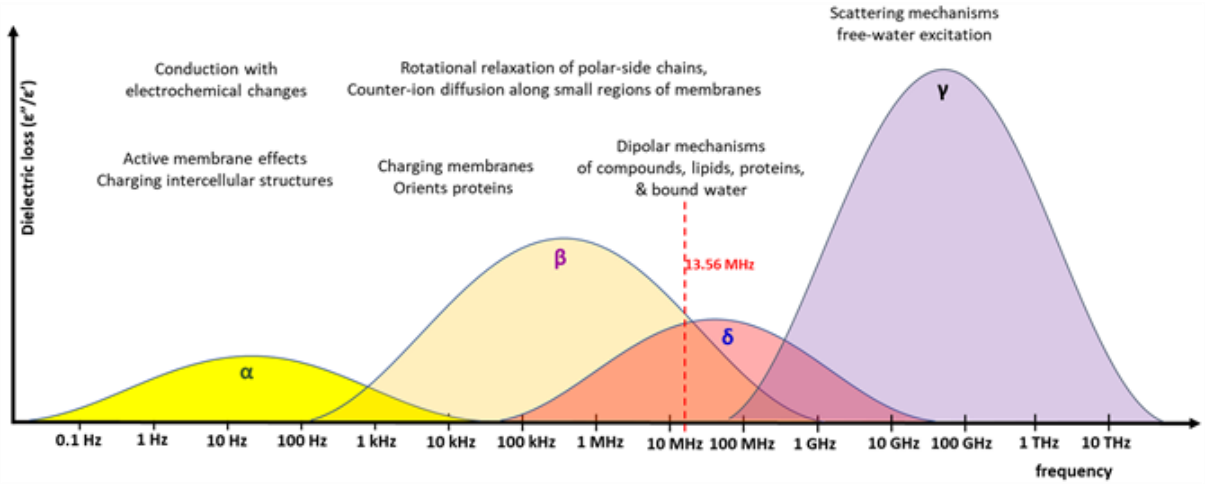

Figure 2. The various frequency intervals of the dispersion phenomena. The overlapping of β and intermediate band between β and γ form a biologically important range. The protein-lipid interaction and the bound water could react in this frequency interval.

The upper tail of the β-dispersion continues to the δ-dispersion [88]. The dipolar moments of proteins and other large molecules (like cellular organelles, biopolymers) cause this frequency spectrum [89]. This second Maxwell-Wagner dispersion (δ) also depends on the suspended particles surrounded by cells [90], as well as the protein-bound water, and cell organelles such as mitochondria [91] [92] appear in the range. Furthermore, other relaxation processes like molecular side chains, bound water molecules, diffusion of charged molecules, and near membrane bounds change the δ-dispersion. The most frequently used ISM-frequency (spectrum reserved internationally for industrial, scientific, and medical use) is 13.56 MHz in the overlapped region β- and δ-dispersion range. The model calculation also shows the importance of the 13.56 MHz [93].

The plentiful tissue water causes the high-frequency dispersion (γ) at microwave frequencies [94]. The excitation of various electrolytes' water content in the cytoplasm and extracellular matrix (ECM) is responsible for this high-frequency end. The time constant is proportional to the third power of the molecules' radius, and typical characteristic frequencies are, e.g., 15 - 20 GHz for associated with the polarization of water molecules and 400 - 500 MHz for simple amino acids. The gamma range locates the molecular resonance of proteins [95].

The dispersion effects overlap and depend on the target material and their environmental connections, so the electromagnetic fields could influence many parts simultaneously, even with constant frequency.

4. Challenge of Resonant Energy-Absorption

The resonances appear in various thermal, electrical, and mechanical properties of the cells, tissues, and organs. The well-tuned resonance minimizes the energy loss during its transfer, which is in harmony with nature's general thermodynamic rules. The application of the resonance phenomena for the living systems has two fundamental challenges:

Which mechanism transfers the resonant energy to the cells?

How can the cancer cells be selected to be destroyed by resonance, and how is it harmless for healthy cells?

Rife's original idea initialized the resonant phenomena to eliminate the "unhealthy living cells" with the frequencies used for cellular resonances around kHz. The energies of these waves (in order of pico eV) are certainly less than the temperature background's thermal energy ~300 K of the human body (250 meV). His experiments were completed in vitro on cell cultures, where the challenge of selection does not appear; all cells were malignant. His observations did not give any clue for the energy transfer mechanism, and the MOR investigation misses the statistical evaluation. Only the visually observed cell distortion was measured; no other parameters are available. So, these early observations were indicative only.

4.1. Deterministic Resonance

Rife declared a mechanical "blow up" of the cellular structures, investigating in vitro. The cavity may work as a resonator which could cause resonant energy absorption. There are plenty of cavities by a membrane with surfaces of lipid-constructed boundaries like cells, mitochondria, intracellular organelles (like tubes of tubulin, and various intracellular structures with cavities). However, cavity resonance would require a wavelength comparable to its size. The mechanical effect depends on the size and the actual form of the cells, which are well unified in bacteria culture but not unified in a tumor, where heterogeneity is a fundamental inherent behavior. The Rife frequencies' wavelengths are many magnitudes longer than the cell sizes, so the direct mechanical cavity resonance does not fit.

Additionally to the heterogenic form of the cellular cavities of malignancy, their electromagnetic and mechanical parameters (like dielectric constant, conductivity, density) change by their present activity depending on their functions in the system's structure. Other resonance possibilities are represented by the different molecules, including the water. These molecular components have notable resonance bands, but their frequencies are too high to compare them to Rife declarations.

A kind of mechanical resonance induced by ultrasound could exist [96] in the kHz-MHz region [97]. It could select the cancer cells [98], because they are softer than their healthy counterparts [99] [100], so the waves could interfere with the soft and individual cells. Nonthermal cellular resonant mechanisms which convert electromagnetic radiation to such mechanical frequency have no proof yet.

One of the most proven resonance phenomena in living objects is the ion cyclotron resonance (ICR). The method has strong theoretical [101] [102], and experimental pieces of evidence [103]. We shall assume a long impact time at ionic cyclotron resonance so that the trajectories should form and endure for a long time. However, the ICR and the connected phenomena need a magnetic field's assistance, and the resonances happen in low frequencies, on the order of a few times ten Hz. This does not fit to Rife's assumptions.

4.2. Stochastic Resonance

A mixture of deterministic signals and noise could produce stochastic resonance output in a nonlinear system. Its autocorrelation function $R_{XX}(t_1, t_2)$or power density spectrum $S(f)$could characterize the output noise.

One of the origins of the stochastic (probability) behavior of the living matter is the intrinsic bifurcation in all the levels of the living organization [104]. The basic bifurcation mechanism could be introduced by a simple nonlinearity of the potential wells of chemical reactions [105] [106] showing nonlinear behavior by double-well potential (non-harmonic potential, chaotic arrangement). The simplest bifurcative phenomenon is when the active forces $F_a(x)$ are not linear with the displacements x (or generally with the deformations):

$$F_a(x) = ax + bx^3 \tag{2}$$

where a and b are characteristic parameters of the interaction. The potential energy $E_{pot}(x)$of this force

$$E_{pot}(x) = ax^2 + bx^4 \quad (3)$$

which shows the bifurcative double potential well when $a < 0$ and $b > 0$. This potential offers equal probability for the particle involved in the $F_a(x)$ being in both wells, so the particle bifurcates between the two positions x_1 and x_2 Figure 3 . There are particles in the potential valleys that perform a harmonic oscillation. The noise constrains the particle to oscillate between the wells randomly.

An additional factor cx^3 (3) breaks the equal probability, Figure 4 , and the bifurcation (or multifurcation), the probability distribution biases the jumps.

The system's noise adds an anharmonic factor to the potential, so the wells' equivalence disappears. The change modifies the optimal energy situation and constrains the bifurcation, which could direct the particle movement in the series of jumps into one direction. The noise modifies the depth of the wells. When the force is periodical, the wells periodically fluctuate accordingly up and down in opposite directions. When the amplitude A of periodic force is small to compare $\Delta E_{pot}(x)$ the equality of the two wells of the potential periodically is oppositely broken, but in a long-time average remains equal (Figure 5).

At the start in the time $t = 0$ the jump from right to left is more probable than a half period later, at time $t = \pi/2\Omega$, and opposite in the time of $t = \pi/\Omega$.

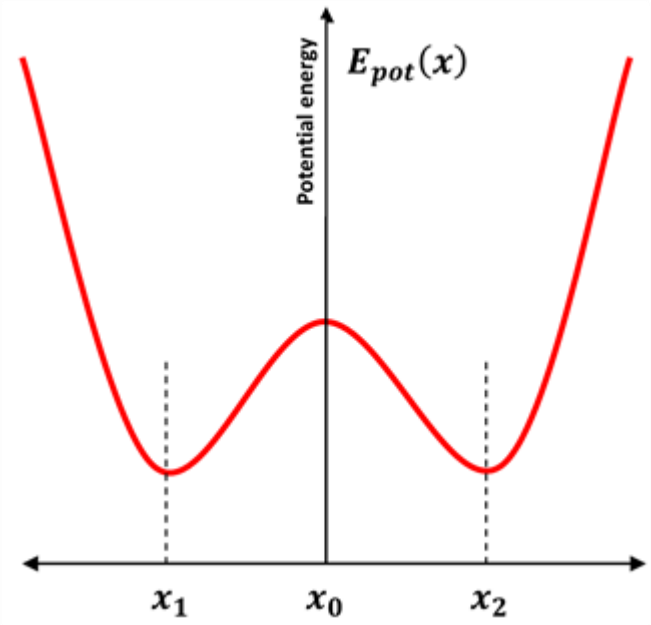

Figure 3. The bistable potential-well. The system has two stable positions (two energy minima), and it is in dynamic equilibrium when the two states are occupied with equal probability by oscillation. When one state becomes fixed in one well, the system is "frozen", the equilibrium is broken.

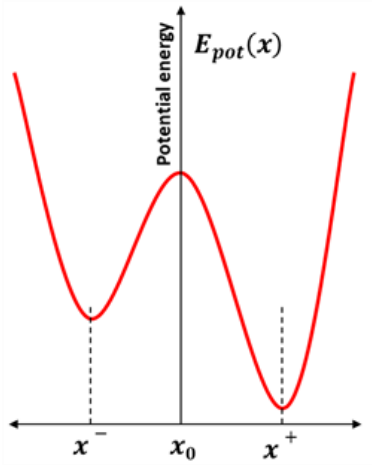

Figure 4. The characterization parameters of the unbalanced bistable potential-well, $E'_{pot}(x) = ax^2 + cx^3 + bx^4, \ \ (a < 0, b > 0, c > 0)$. The oscillation is unbalanced, the probability being in the well at x^+ is higher than at x^-.

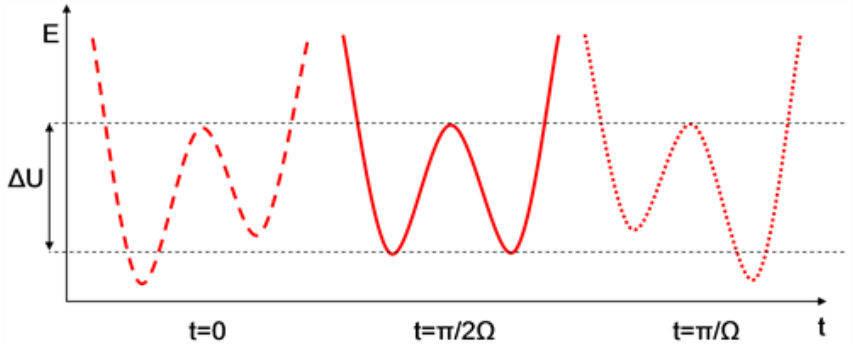

Figure 5. Changes of the bistable potential-well by elapsed time (one time period of the exciting signal is $T = 2\pi/\Omega$, where $\Omega = 2\pi f$ is the conventionally used circular frequency).

In this way, the weak periodic signal compared to the activation energy $\Delta E_{pot}(x)$ synchronizes the jumps in a stochastic (not deterministic) way. Consequently, the jumping time's distribution function through the barrier from the potential well in the noise, which is modulated with a weak periodic signal, will not be rigorously monotonic. A considerable amplification of the weak periodic signal could be observed depending on the strength of the noise. The amplification also increases by the decreasing frequencies at a constant amplitude of the periodic carrying signal. The amplification also increases by the decreasing amplitude of the periodic carrier on the same signal frequency, and suddenly (at a threshold), the resonance disappears (window phenomenon). Probably this is the reason for the observed Adey-window, [77]; and some other detected resonance phenomena with an application of outside periodic electric field.

The resonance-like maximum depends on D noise energy or at $D = const.$ the frequency determines the maximum. This is the typical frequency-amplitude window formulated before the experiments [84]. The amplitude has a resonance-like behavior, Figure 6 . White noise induces the resonance when $D = k_B T$ (thermal noise) and so the noise intensity is temperature dependent.

A particularly notable application of this stochastic resonance is the possibility of using electrically generated subthreshold stimuli in various biological processes [107]. The stochastic resonance works, and it remains a vivid possibility to explain Rife frequencies. The entry of a molecule to the cell through gating membrane channels has Poisson distribution in the stochastic resonance study for single-cell [108]. The response to very weak external electric fields could be far below the thermal noise limit. We had shown for zero-order of the noise that thermal limitation does not exist [109].

4.3. Enzymatic Resonance

Enzymatic assistance boost most of the chemical reactions in living processes. The cellular machinery requests various and numerous catalytic reactions. The living systems have tremendous enzymatic processes (so-called "catalytic wheels" [110]). The wheels model describes a cyclic catalytic reaction having two conformation states of the enzyme governing the actual process's speed. This classical model (Michaelis-Menten enzyme model, [111], MME) well describes the enzymatic procedures steady-state [112]. The simple mathematical description involves an enzyme (E) starting the formation of the product (P) from a substrate material (S) through a transition state (E^*):

$$E + S \underset{C_{forv}}{\overset{C_{rev}}{\rightleftarrows}} E^* \xrightarrow[C_{fin}]{} A + P \tag{4}$$

where the reaction rates characterize the reverse, forward, and final conversions (C_{rev}, C_{forv} and C_{fin}), respectively. At first, the enzyme in conformal state E connected to S substrate state and form E^*complex: $E + S \rightarrow E^*$. The E^* state is highly complex because it has two states (E_1^* and E_2^*) in the reaction: the $E_1^* = (ES)$ complex transforms to P product, via $E_2^* = (EP)$ complex, while the enzyme transforms back to E state at the end of the process, Figure 7 .

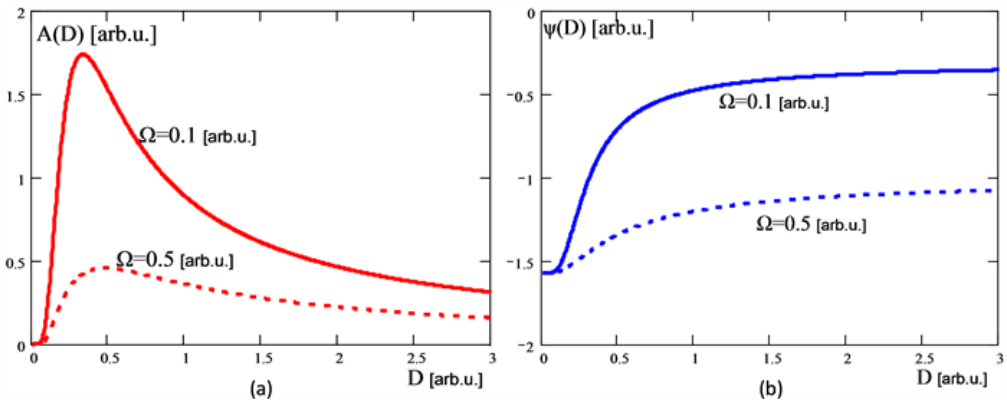

Figure 6. The stochastic resonance depends on the noise-density D. (a) Amplitude $A(D)$; (b) Phase-shift $\psi(D)$ of the noisy carrier. The resonance depends on $\Omega = 2\pi f$ circular frequency in stochastic processes.

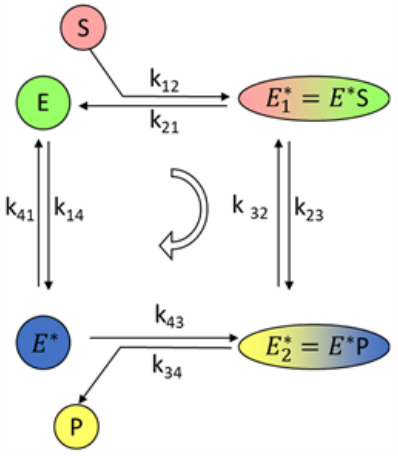

Figure 7. The enzymatic "wheel". In practice $k_{14} < k_{41}$, $k_{21} < k_{12}$, $k_{32} < k_{23}$ and $k_{43} < k_{34}$, so the "wheel" works in one direction, by Michaelis-Menten process

To understand the complex enzymatic transition state, let us assume two certainly distinguishable confirmation state of an actual enzymatic reaction: E_1^* and E_2^*, with concentrations $[E_1^*]$ and $[E_2^*]$ respectively. These two states are the result of chemical reactions, hence

$$E_1^* \underset{\alpha=\mathrm{k}_{23}}{\overset{\beta=\mathrm{k}_{32}}{\rightleftarrows}} E_2^* \tag{5}$$

An external electric field could modify the catalytic/enzymatic wheel. This process is the electro-conformational coupling (ECC, [113] [114]), it activates the energy over the barrier by oscillatory stimulation [115]. The outside periodic field modifies the activation energies with $\Omega = 2\pi f$ circular frequency. Stochastic resonance determines the final catalysed state's probability in the dynamic equilibrium of homeostasis [116]. The thermal white noise energy $D = k_B T$, pumps the resonance, so enzymes get the energy from the environmental conditions. Significantly the lower frequencies (smaller Ω) increase the resonant peak, but the effect vanishes at the too low frequency when the acting noise washes out the signal. This threshold depends on the processes and conditions when the process is applied. The optimal (peak) resonance depends on the D noise-density. Due to the thermal noise depends on the temperature. Consequently, the excitation process has an optimal temperature, but the temperature dependence less effective when a colored noise forces the resonance.

The number of resonance frequencies as many as catalytic reactions exist. It is a large number indeed. All cells have mostly identical enzymatic reactions, hindering the selection of cancer cells by stochastic resonances. All small amplitude modulation with the carrier stochastic resonance frequency makes certain resonant effects with enzymatic processes but also excites other two-state situations (like voltage-gated ionic channels), which further complicates the selection. Due to the ordered reaction lines in cellular processes, the microscopic effects have a macroscopic result when the autocorrelation of the excitatory signal forces the order of the signal pathway in the cell. Consequently, the selection of malignant cells could be possible by well-chosen signal modulation, a time-set of frequencies, and not only a single one.

A weak periodic perturbation promotes transport activities by stochastic resonance near the membrane. The thermal noise plays a vital role in pumping the energy to this process by Brownian engine [117] [118]. The enzymatic resonance fundamentally depends on the thermal conditions of the tumor and cellular microenvironment, the extracellular matrix. The thermal noise activates the Brownian motor, which drives the enzymatic wheel. The ECC situation rectifies the thermal fluctuations, producing directed motion in one direction only [119] [120]; forming a "ratchet", excluding the swivel's opposite turn. The free energy can be obtained from the inherent fluctuations and outside electric noises [121], by the stochastic concept. The "ratchet" idea was originally proposed by Feynman [122], but it was incomplete and cleared later [123]. The ECC realizes a direct coupling between the outside electric field and the enzymatic processes at the membrane. The alternating electric field impacts enzyme activity [124] and modifies the extrinsic signal-transduction [125].

The stochastic resonance excites any catalytic wheel reaction or voltage-controlled ion channel. Consequently, shifting of the ionic composition and pH could destroy the microbes. However, the stochastic resonance has frequency windows. Below and over an amplitude or noise energy, it does not work. Subsequently, in principle, the explanation of the resonant frequencies measured by Rife and others is possible, or at least it is not excluded in this way, but as numerous as enzymatic reactions exist in the system. This involves a dense spectrum of

resonances, and the real destroying process needs a set of resonances that are adequate to the signal-transduction line in the cells. With these resonances, we do not expect prompt necrotic cell-death.

The stochastic resonance may amplify the signals. In a simple model, the wheel is energized by ATP hydrolysis with 10-16-10-17 W, while the molecular scattering due to the thermal effects provides 10-8 W [126]. The stochastic resonance conditions promote the ATP hydrolysis as a periodic process, producing the given reaction's direct stimulation. The same could happen by excitation with a periodic outside field using the EEC effect and supporting the stochastic resonance. However, the fluctuation-driven directional flow described by ECC needs more effort to clear the ion-pump processes in detail [127].

An appropriate regularly oscillating electric field may convert the free energy-producing transports or chemical reactions coupled through enzymatic processes [123]. The translational symmetry can be broken in one direction by the periodic signal superimposed on the double-well symmetric enzyme-potential, Figure 8 . A Brownian motor drives this process, enforced by an electric field pushing through the ligand on the membrane from one side to the other, differs from the MME.

These processes excellently demonstrate the irreversible thermodynamics in the presence of an external periodic perturbation [128]. The transduction of

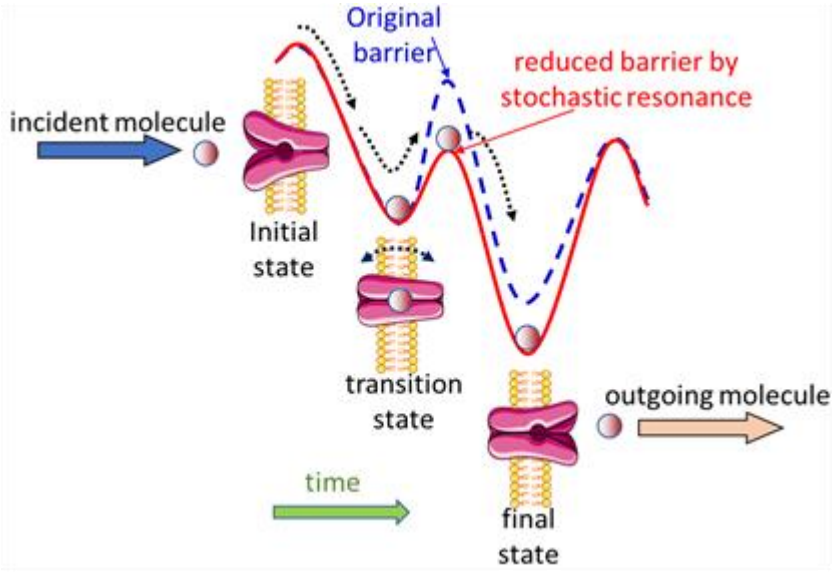

Figure 8. Stochastic resonance promotes the ion transfer through the membrane.

low-level signals can be resonant [117], acting on the enzyme's oscillating barrier involved in the studied reaction. The energy barrier of $APT \rightarrow ADP$ reaction is $\approx 30k_BT$ and the maximal energy oscillation by the external field is $\sim 2.5k_BT$. This oscillatory activation was observed as low as $5\frac{mV}{cm} = 5 \cdot 10^{-7}\frac{mV}{nm}$ with AC (10 kHz). The reactions involve a synergy of the enzyme with excitation with extremely low levels of electromagnetic fields.

4.4. Collective Excitations

The living system has chain reactions (like the Krebs cycle) using the transient states to go over the energy barriers' sequences. The Brownian-ratchet might be involved in all the barriers, reducing the height of the barrier by ECC pumped by environmental noise, Figure 9 . The reactions follow Markovian sequences and develop conditions for the next step of the series in the chain. The various steps have different energy consumption and chemical reaction rates, far from a simple staircase process. The well-definite set of the chain fixes a certain time-series required by the setting of the ongoing reactions. The characteristic time-sets appear in the time lag of the measured signals' autocorrelation function.

The reaction avalanche on this way has an energy-wave "sliding" through the chain, energized by the $APT \rightarrow ADP$ conversion and promoted by the ECC process. One form of the sliding energy-bag through a system is the biosolitons [129] [130]. The solitons (solitary waves) maintain their shape by self-reinforcing wave packets (energy-bags) propagating constant velocity. The dispersion in nonlinear conditions produces permanent and localized waveforms in a region. The solitons remain unchanged by their mutual interactions, only their phase-shift changes. The energy-transfer by solitons has negligible energy loss [131]. One of the most practical simple soliton presentations led to its discovery, seeing a bump-shaped sliding single wave of water through a canal. The sliding energy bag is easily presented with a falling domino-row when the actual energy outside the energy source (the gravitation) subsequently plunges the single dominos in the row, and a wave runs with unchanged shape generating energy delivery. The

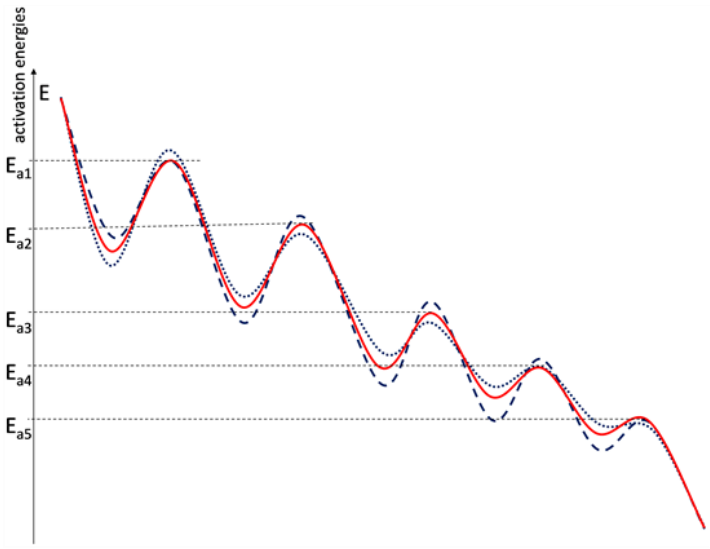

Figure 9. Cascade of activation energies. Time series of sequentially happening reactions going over the actual activation energy. The well chosen autocorrelation time-lag promotes this series.

phenomenon is collective [132] and has broad applicability in neuron signal propagation [133], and has a role of membrane dynamics [134]. Excitation of individual large complex molecules like DNA [135] and proteins [136] also show collectivity. The thermal noise background influences the solitons, but the biosolitons are stable in the living temperature range [137] [138].

The formation and decay of solitons explain the unidirectional enzymatic cycle of ECC [139]. In molecular chains triggered by periodic external electromagnetic fields, solitons create a ratchet directed [140], sliding stability bag, Figure 10. The experiments show soliton-coupling of K^+, Na^+, Rb+ through membranes [124] [141] [142].

The nonlinear, systemic collective harmony of macroscopic phenomena characterizes the biosolitons. The collectivity driven by the energy-transfer is well shown in large molecules like alpha-helix of proteins [143] in THz frequency region but also appears mass-movement at lower frequencies [144]. The soliton harmonization of the collective movements emerges when the cells starve and need collective efforts to survive, sharing the available energy as optimally as possible [145].

The hydrogen ion can be transported by the hydrogen bridges, which is crucial in living systems [146]. The Grotthuss-mechanism describes the high-speed and low dissipation of the transport propagation [147] [148]. Here the proton tunnels (jumps) from one water cluster to another bridged by hydrogen bonds, Figure 11. A "frustrated bifurcative" proton dynamically connects the neighboring water molecules, producing a chain reaction.

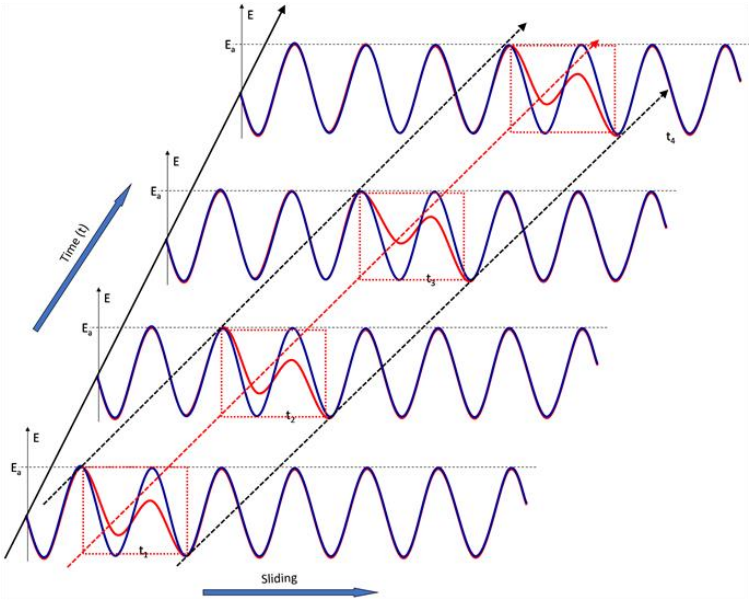

Figure 10. The "siding" bistability by the enzymatic processes.

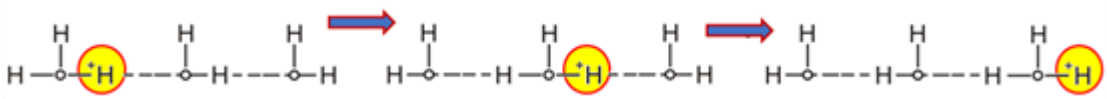

Figure 11. The Grotthuss mechanism of proton-jumping in a chain. (Three subsequent steps of the process are shown.)

$$H_2O + H_2O \rightleftharpoons OH^- + H_3O^+ \tag{6}$$

The lifetime of H3O+ (hydronium ion) in (7) is relatively small (~3 × 10−12 s) so the speed of proton transport by Grotthuss-mechanism is approximately ten times higher than the diffusion, so it is decisional. The Grotthuss-mechanism propagates the ionizing chain of a water molecule. The dissociation and recombination steps are altering in the "traveling". The recombination-dissipation is a quantum-mechanical process, in principle almost free of dissipation [149]. The process works like quantum wiring [150], having temperature dependence. The vector potential can modify the quantum-states of the water [151] [152] [153], which could modify the complete chain processes. The water order selects between the ionic flows preferring the proton against all the other reaction-product. The outside electric field's effect could conduct the hydroxyl (OH−) and hydronium (H3O+) ions by the same Grotthuss mechanism going through the chain like a stability bag.

4.5. Modulation of the Electromagnetic Signal

The concept of modulation is centered on the stochastic dynamics (time-dependent events) in the biosystems. The chosen frequency spectrum is devoted to direct actions promoting healthy controls and suppressing the cancerous processes. The carrier frequency is in the RF range, which delivers an audio range ($< 20\ kHz$) to the place of use, Figure 12.

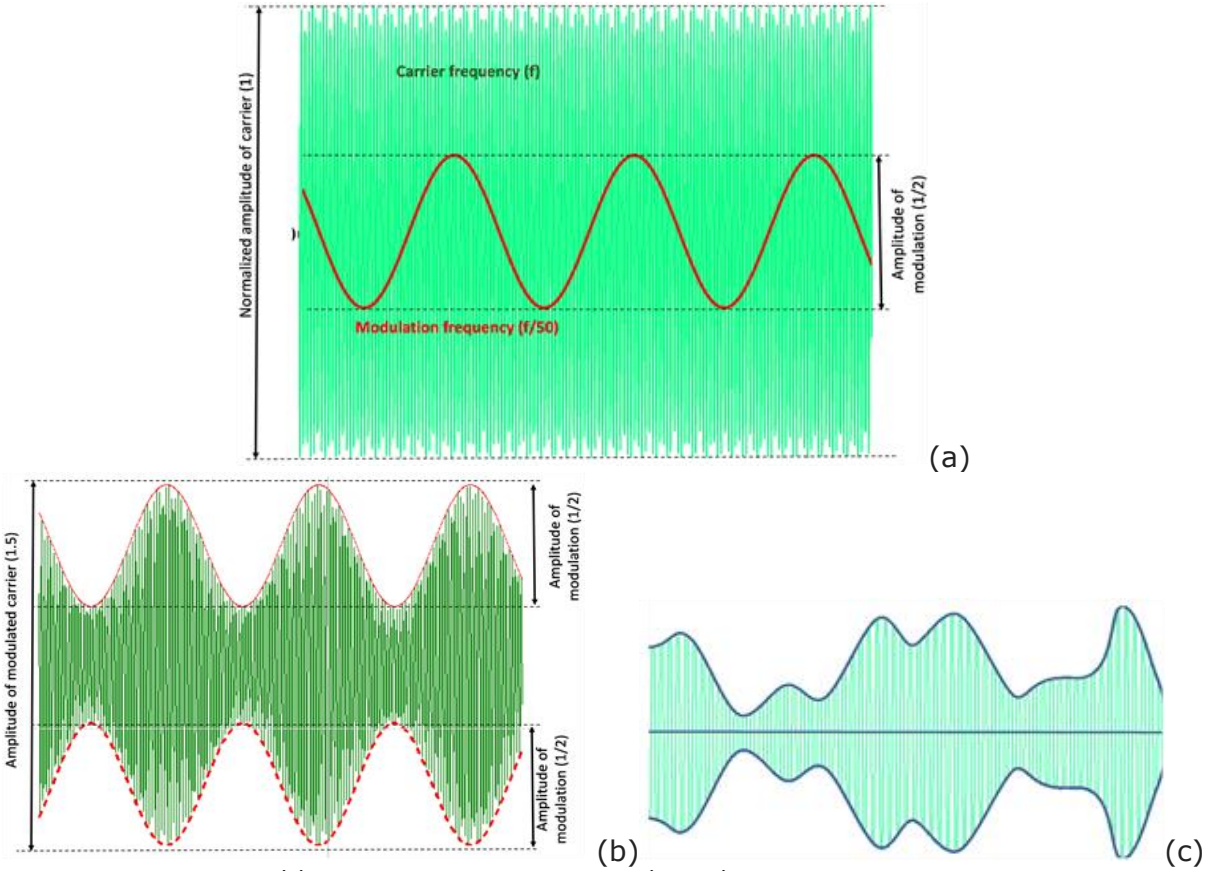

Figure 12. The modulation. (a) The high carrier frequency (green) modulated with the periodic low-frequency signal; (b) The modulated signal shows the importance of the much higher frequency of carrier than the carried modulation; due to follow the shape point-by-point; (c) Modulated transmission of a non-periodic signal.

The expected actions mark out the following basic goals:

1) Support the healthy network against the out-network, autonomic cells in the selected target.

2) Support the immune system, boost the homeostatic chains of reactions.

3) Excite the selected molecules in cancer cells for particular damage-associated molecular patterns (DAMP) and immunogenic cell death.

Due to the complex interconnection of the living objects, these effects overlap and support each other. The question naturally arises: when the modulation frequencies have such an advantage, why does the complication with carrier frequency be involved, and why not applied the modulation frequency directly, without a carrier? Deliver the low frequency into the body and focus it on the selected places is a challenging issue. The adipose tissue in the skin layer, the various membranes, and isolation compartments block the low-frequency penetration deeply into the body. The electric impedance of these heterogenic isolating (capacitive) factors inversely depends on the frequency. This resistivity became too high in low frequencies, and no deep targeting is possible. Invasive application may surmount the adipose layer, but the electrochemical Warburg impedance [154] [155] is high in low frequencies, preventing penetration. The proper solution of the deep penetration needs a high frequency in β/δ-dispersion range. The modulation of a high-frequency carrier with a low frequency solves the apparent contradiction. The well-chosen carrier makes the selection of excitations, and the low-frequency modulation excites. The advantage of the energy absorption compared to conventional heating has significant approval [156].

4.6. Demodulation of Electromagnetic Signal

Theoretical [157] and experimental researches [158] show that at high frequencies only thermal energy-dissipation happen. Low frequency is requested for electric excitation of molecules ("nonthermal" effects). The signal needs demodulation, separate the low-frequency from the carrier. The demodulation is a rectification process, which extracts the information from the carrier wave.

The cells demodulate the received signal by two ways:

- normal rectification by the highly polarized cell-membrane, [159] [160] [161]

- stochastic resonance makes the rectification, [162].

The existence of nonlinearity in cellular biological objects had intensive research, but at the beginning, only linear attenuation of the amplitude of the alternating current through the living object was measured. The double membrane effect causes this apparent linearity, Figure 13.

The excitation process acts on the transmembrane proteins, so the single membrane demodulation perfectly satisfies the demands. The nonlinearity through the membrane can be measured [163], and the harmonics make dissipative terms [164].

The noise threshold complicates the rectification of the applied signal. In principle, the modulated signal must be larger than the thermal noise. The requested

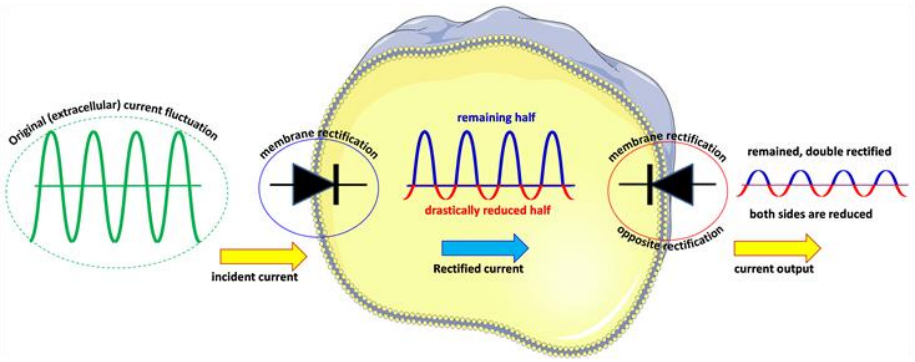

Figure 13. The symmetric but opposite rectification of the cell-membrane when the current goes through the cell makes the measured material linear, the rectification disappears. (The ⊣▶ sign symbolizes the rectifier (diode).)

signal intensity would have such high electric field, which impossible to apply in the living system without fatal damage. In the early model it had been shown this strict thermal noise limit at low frequencies [165], but in a revision it had been shown that the zero mode currents have no thermal limit of the electric rectification [109]. The low frequency (the $1/f$ signal) of the AM modulation is intensively active in its demodulated form [166]. The demodulation of the AM modulated signal by stochastic process is an option too [167], which is applicable also for other forms of modulation [168].

4.7. Excitation Processes

The special autonomy and high metabolic activity of the malignant cells allow their recognition and selection, and attack. In consequence of the higher metabolic rate of malignant cells than their normal hosts, the microenvironment's electric conductivity grows for a detectable range. Furthermore, malignant cells' autonomic behavior rearranges the microstructure of the ECM, which changes their dielectric permittivity [169] [170], and the order-disorder transition of the aqueous electrolyte also has a role in the changes [171]. The conductivity and permittivity allow the selection of these cells [172]. The amplitude modulation intensifies the tumor-specific energy absorption as a part of the selection mechanism [173]. The electromagnetic selection of the malignant cells guides the energy delivery. The small energy absorption could cause damages in the cytosol [174], or trigger apoptotic signals and destroy the cell [175]. The nonthermal processes result from the change of the chemical or structural situation in the targeted assembly [176]. The transition does not use heat from the field but directly uses the electric field's work for the actual changes by absorption. Besides, the β/δ-dispersion of the carrier frequency orients the attack on the membrane reaction of the impedance selected cells [177] [178], primarily for the transmembrane groups (rafts) of proteins [179]. The rafts of the plasma-membrane of malignant cells are denser in rafts than their healthy counterparts [180], allowing intensive excitation of the transmembrane proteins [181]. A new kind of treatment applies to these facilities [182].

4.7.1. Boost the Healthy Network

The malignant development avoids the healthy homeostatic regulation, "defrauds" the controls for their intensive, unhealthy proliferation. Cancer, in general, is the missing of homeostatic control over malignant cells. The cancerous lesions develop the strength to proliferate as intensively as possible, ignoring the healthy regulations and exploiting the host tissue's collectivity. The proliferation subordinates all malignant features. The cancer cells became gradually autonomic, break the connections. Here is their weakness: the cancer cells are individual and not networked like the regulated healthy host. Their collectivity satisfies the individual demands to use energy as much as possible for the cellular division.

The modulation frequency spectrum follows the natural dynamism of the $1/f$ time-fractal fluctuations and forces to reestablish the harmony with the homeostatic collective network. Simply speaking, the modulation acts in harmony with the natural collective processes, promoting them, like keeping the swing in move using harmonic push, Figure 14.

4.7.2. Support the Immune System

Homeostatic dynamic equilibrium is too complex for external constraints to be effective in repairing it. Tightly connected feedback mechanisms regulate the system, and the reaction of homeostatic control will be against any simple constraints. Consequently, any winning strategy must work in conjunction with homeostatic controls, utilizing natural processes and supporting the immune system to recognize and destroy malignant cells throughout the body. The immune system's preparation could be a perfect target instead of cancer's main strength, its proliferation. The lack of adaptive immunity to tumors can be revised and form tumor-specific immune action to eliminate the malignancy in healthy regulation by the host system itself.

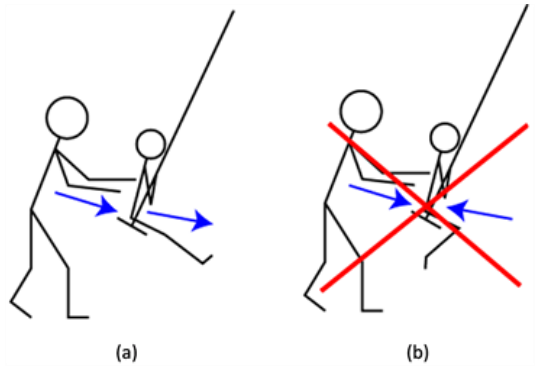

Figure 14. A simple swing example of harmonic and non-harmonic excitation. (a) The swing is harmonically (resonantly) pushed, the energy transfer is optimal; (b) In case of an unharmonic push, the system does not follow the resonant rules. The efficacy is low with tremendous efficacy loss.

Numerous variants aim to activate personal immune defenses against cancer. The key point of these is the immunological recognition of the malignancy. The immune system needs recognizable signs to direct its actions. However, the highly adaptive hiding strategy of malignant cells protects them from being identified by immune cells. The innate antitumor immune action of NK cells [183] [184] offers one of the effective possibilities against cancer invasion. NK does not need information through the host's MCH-I molecules and also acts in the absence of priming. The cytotoxic activity of NK potentially controls tumor growth [185]. Intensive low-frequency components in the modulated treatment spectrum may trigger the NK activity and enrich NK cells in the targeted, selected tumor [186].

The modulation also effectively supports the healthy adaptive immune effects with tumor-specific CD8+ killer T-cells. The destruction of the malignant cells is dominantly apoptotic by the signal excitations of modulated RF-current [187], developing damage-associated molecular pattern (DAMP); as important genetic information for the immunogenic cell-death (ICD) [188] [189]. Immune-stimulators, which have no anticancer effects alone, have synergy with the modulated field. One in vivo study showed the synergy with a herb extract from Marsdenia tenacissima (MTE), producing systemic effects from local application of modulated field [190]. With dendritic cell (DC) inoculation to mouse, which anyway does not cause antitumor effect, the field application showed a significant effect of immune reactions, measured the high value of tumor-specific adaptive response [191]. The DC addition not only effectively develops tumor-specific killer and helper T-cells but also works like a vaccination against the rechallenging of the same tumor to the previously cured animal [192]. Significantly the additional administering dendritic cells may boost the overall immune effects, and also, independent immune-stimulator work in harmony with modulated treatment. In this way, the local treatment became a systemic fight with the malignancy in the entire body [193] [194]. The clinical applications well correspond with preclinical experiments, had shown the same results, using other synergic immune-stimuli [195] [196]. Recent reviews of preclinical [197] and clinical results [198] show efficacy in oncology of this bioelectrodynamical resonant approach.

5. Conclusions

The modulated electric field is an emerging new direction of cancer therapies [154]. The treatment uses stochastic processes, including resonances, "nonthermal" effects, and collective excitations. It could selectively deliver energy to the tumor cells to ignite antitumor-effect by producing DAMP and ICD and liberating the malignant cells' genetic information. The remarkable advantage of this method is that no ex-vivo laboratory manipulation is necessary for the perfect antigen production and cellular reactions.

The proper electromagnetic resonance therapy adopts the natural heterogeneity of the dynamic properties of the living system. The modulated field application chooses a new paradigm of resonances: it heats heterogeneously instead of the homogenous (isothermal) approach of conventional hyperthermia. The selection uses the tumor, malignant cells' thermal, and electromagnetic behaviors. The heterogeneity is presented by cell-specific electric conductivity, dielectric permittivity, the structural differences of the cell membranes, and the variation of the cooperative harmony of the malignancy. The natural heterogeneity allows producing a synergy of electric and thermal processes [199]. The specialization operates with precise electromagnetic impedance selection [200], using the heat on membrane rafts [201], and makes harmony by thermal and nonthermal effects, too [202].

The structural and time fractals of the living organisms with malignancies offer a special use of fractal physiology. The applied time-fractal amplitude-modulated RF carrier frequency forces proper healthy resonance utilizing the homeostasis's dynamism is followed and modified by time-fractals. A collective resonance occurs, exciting the biosolitons in large molecules. The $1/f$ modulation approach differs from the direct resonance, acting on the collective harmony, setting harmony within the reactions by the modulated signal's autocorrelation. The resonances mostly happen in a stochastic way, modifying the enzymatic

processes. A large number of enzymatic reactions fit the stochastic resonance frequencies. Consequently, the number of resonant frequencies is as many as the enzymatic reactions in the target.

The above considerations allowed to develop new method called modulated

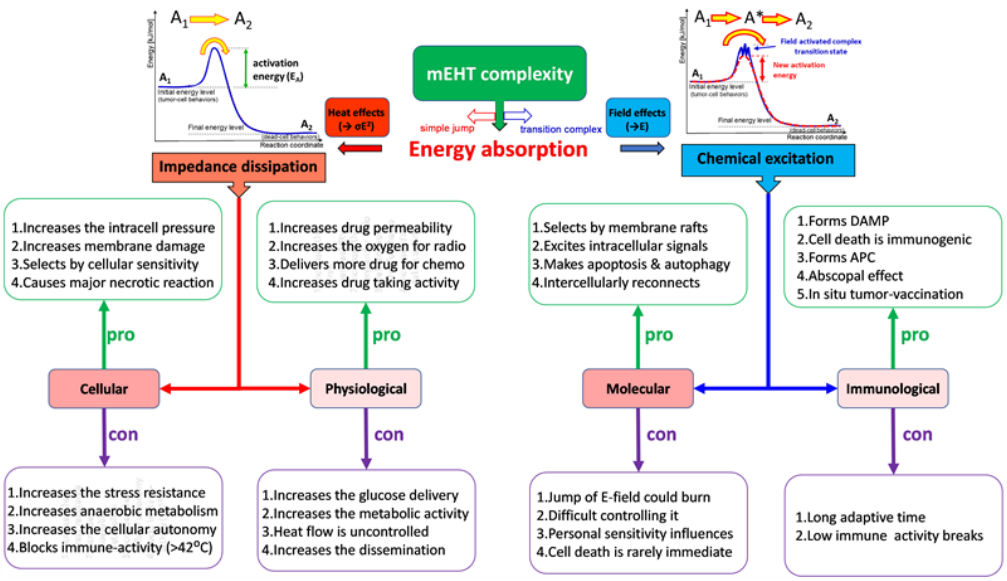

Figure 15. The complex system of the mEHT effect

electrohyperthermia (mEHT, trade name oncothermia®) specialized on the electromagnetic resonances with time-fractal modulation. The mEHT is a kind of specialized hyperthermia, where the electric field has a double role. The thermal energy dissipation is proportional to the electric field's square, while the molecular actions depend on the field linearly. The two parts of the complex impedance are equally applied in this method, Figure 15 [203]:

1) The square (the absolute value) of the field is responsible for the heating. This process depends on the conductivity of the target.

2) The field vector makes the excitation, working resonantly like an enzymatic action, lowers the energy barrier (the activation energy) through a transition state. This process depends mostly on the dielectric properties of the target.

The modulated electro-hyperthermia (mEHT) applies to these researches in preclinical experiments [197] and clinical applications [198].

Acknowledgements

This work was supported by the Hungarian National Research Development and Innovation Office PIACI KFI grant: 2019-1.1.1-PIACI-KFI-2019-00011.

Conflicts of Interest

The author declares no conflicts of interest regarding the publication of this paper.

References

[1] Bolton, H.C. (1898) Iatro-Chemistry in 1897. Science, 7, 397-402. https://doi.org/10.1126/science.7.169.397

[2] Kempf, E.J. (1906) European Medicine: A Résumé of Medical Progress during the Eighteenth and Nineteenth Centuries. Journal of the Medical Library Association, 3, 231-248.

[3] Basford, J.R. (2001) A Historical Perspective of the Popular Use of Electric and Magnetic Therapy. Archives of Physical Medicine and Rehabilitation, 82, 1261-1269. https://doi.org/10.1053/apmr.2001.25905

[4] Barrett, S. (2008/2019) Magnet Therapy: A Skeptical View. Quackwatch. https://quackwatch.org/consumer-education/qa/magnet

[5] Lakhovsky, G. (1925) Curing Cancer with Ultra Radio Frequencies. Radio News, February, 1282-1283.

[6] Lakhovsky, G. (1988) Secret of Life: Electricity Radiation & Your Body. 4th Revised Edition, Noontide Press, Los Angeles.

[7] Bearden, T.E. (1995) Vacuum Engines and Priore's Methodology: The True Science of Energy Medicine. Explore More, #10:16.

[8] Bateman, J.B. (1978) A Biologically Active Combination of Modulated Magnetic and Microwave Fields: The Prioré Machine. Office of Naval Research, London, Report R-5-78, Aug. 16.

[9] Camp, J. (1973) Magic, Myth and Medicine. Priory Press Ltd., Dunstable.

[10] Manning, C.A. and Vanrenen, L.J. (1989) Bioenergetic Medicines East and West. North Atlantic Books, Berkeley.

[11] Volodiaev, I. and Belousssov, L.V. (2015) Revisiting the Mitogenetic Effect of Ultra-Weak Photon Emission. Frontiers in Physiology, 6, 241. https://doi.org/10.3389/fphys.2015.00241

[12] Tesla, N. (1898) High Frequency Oscillators for ElectroTherapeutic and Other Purposes. The Electrical Engineer, Vol. 26, No. 550.

[13] A Brief History of Dr. Royal Raymond Rife. https://www.nationallibertyalliance.org/files/NaturalHealing/Rife/History%20of%20Dr%20Rife.pdf

[14] Bird, C. (1976) What Has Become of the Rife Microscope? New Age Journal, March 1976, 41-47.

[15] Kendall, A.I. and Rife, R.R. (1931) Observations on Bacillus Typhosus in Its Filterable State: A Preliminary Communication. California and Western Medicine, 35, 409-411.

[16] Line, B. (2017) Rife's Great Discovery: Why "Resonant Frequency" Therapy Is Kept Hidden from Public Awareness. Biomed Publishing Group, South Lake Tahoe.

[17] Lynes, B. (1997) The Cancer Cure That Worked: 50 Years of Suppression. Marcus Publishing, Santo Domingo Este.

[18] Allegretti, M. (2018) The Frequencies of Rifing—From the First Frequencies Discovered by Royal Rife to Today: Guide to Selection and Use of Spooky2 Frequencies. Independently Published.

[19] Silver, N. (2001) The Handbook of Rife Frequency Healing: Holistic Technology for Cancer and Other Diseases. The Center for Frequency Education Publishing, New York.

[20] Rife, R.R. (1953) History of the Development of a Successful Treatment for Cancer and Other Virus, Bacteria and Fungi. Rife Virus Microscope Institute, San Diego.

[21] Humbug Is Rife: Cancer Quackery, 1892 and 2015. Evidence Bytes, 2015. https://evidence-bytes.com/2015/09/16/humbug-is-rife-cancer-quackery-1892-and-2015

[22] Frost, J. (2017) A Skeptical Look at the Spooky2 Rife System. Quackwatch. https://quackwatch.org/device/reports/spooky2

[23] (1994) Questionable Methods about Cancer Management: Electronic Devices. CA: A Cancer Journal for Clinicians, 44, 115-127. https://doi.org/10.3322/canjclin.44.2.115

[24] Energy Medicine—Radionics Rife Machine. http://www.skepdic.com/radionics.html

[25] Barrett, S. (2010) Device Watch—Rife Device Marketer Sentenced to Prison. https://quackwatch.org/device/reports/rife/folsom

[26] Barrett, S. (2012) Quackwatch—Rife Machine Operator Sued. Based on Investigators' Reports, FDA Consumer. U.S. Food and Drug Administration, Silver Spring. https://quackwatch.org/consumer-education/News/rife https://web.archive.org/web/20071214170405/https://www.fda.gov/fdac/departs/796_irs.html

[27] Theise, N.D. and Kafatos, M.C. (2013) Complementarity in Biological Systems—A Complexity View. Complexity, 18, 11-20. https://doi.org/10.1002/cplx.21453
[28] Mohr, H. (1977) Structure and Significance of Science. Springer, New York, 102.
[29] Brandas, E.J. (2010) Gödelian Structures and Self-Organization in Biological Systems. International Journal of Quantum Chemistry, 111, 1321-1332. https://doi.org/10.1002/qua.22616
[30] Gödel, K. (1931) über formal unentscheidbare Sätze der Principia Mathematica und verwandter Systeme, I. Monatshefte für Mathematik und Physik, 38, 173-198. https://doi.org/10.1007/BF01700692
[31] Seel, M. and Ladik, J. (2019) The Tragicomedy of Modern Theoretical Biology. In: Advances in Quantum Chemistry, Elsevier, Amsterdam, 1-13. https://doi.org/10.1016/bs.aiq.2019.11.001
[32] Wierman, M.J. (2010) An Introduction to Mathematics of Uncertainty. Hoors Program, Creighton University, College of Arts and Sciences, Omaha. http://typo3.creighton.edu/fileadmin/user/CCAS/programs/fuzzy_math/docs/MOU.pdf
[33] Sneppen, K., Krisna, S. and Semsey, S. (2010) Simplified Models of Biological Networks. Annual Review of Biophysics, 39, 43-59. https://doi.org/10.1146/annurev.biophys.093008.131241
[34] Turrigiano, G. (2017) Homeostatic Signaling: The Positive Side of Negative Feedback. Current Opinion in Neurobiology, 17, 318-324. https://doi.org/10.1016/j.conb.2007.04.004
[35] Modell, H., Cliff, W., Michael, J., et al. (2015) A Physiologist's View of Homeostasis. Advances in Physiology Education, 39, 259-266. https://doi.org/10.1152/advan.00107.2015
[36] Lloyd, D., Aon, M.A. and Cortassa, S. (2001) Why Homeodynamics, Not Homeostasis? The Scientific World, 1, 133-145. https://doi.org/10.1100/tsw.2001.20
[37] Walleczek, J. (2000) Self-Organized Biological Dynamics & Nonlinear Control. Cambridge University Press, Cambridge. https://doi.org/10.1017/CBO9780511535338
[38] Kurakin, A. (2011) Self-Organizing Fractal Theory as a Universal Discovery Method: The Phenomenon of Life. Theoretical Biology and Medical Modelling, 8, Article No. 4. https://doi.org/10.1186/1742-4682-8-4
[39] Anteneodo, C. and da Luz, M.G.E. (2010) Complex Dynamics of Life at Different Scales: From Genomic to Global Environmental Issues. Philosophical Transactions of the Royal Society A, 368, 5561-5568. https://doi.org/10.1098/rsta.2010.0286
[40] Mandelbrot, B.B. (1977) The Fractal Geometry of Nature. Times Books, New York.
[41] Losa, G.A. (2014) The Fractal Geometry of Life. Rivista di Biologia, 102, 29-60.
[42] Losa, G.A. (2012) Fractals and Their Contribution to Biology and Medicine. Medicographia, 34, 365-374.
[43] Weibel, E.R. (1991) Fractal Geometry: A Design Principle for Living Organisms. American Journal of Physiology, 261, L361-L369. https://doi.org/10.1152/ajplung.1991.261.6.L361
[44] Waliszewski, P., Molski, M. and Konarski, J. (2011) Self-Similarity, Collectivity, and Evolution of Fractal Dynamics during Retinoid-Induced Differentiation of Cancer Cell Population. Fractals, 7, 139-149. https://doi.org/10.1142/S0218348X99000165
[45] Deering, W. and West, B.J. (1992) Fractal Physiology. IEEE Engineering in Medicine and Biology, 11, 40-46. https://doi.org/10.1109/51.139035
[46] West, B.J. (1990) Fractal Physiology and Chaos in Medicine. World Scientific, Singapore, London.
[47] Bassingthwaighte, J.B., Leibovitch, L.S. and West, B.J. (1994) Fractal Physiology. Oxford University Press, New York, Oxford. https://doi.org/10.1007/978-1-4614-7572-9
[48] Goldberger, A.L., Amaral, L.A., Hausdorff, J.M., et al. (2002) Fractal Dynamics in Physiology: Alterations with Disease and Aging. PNAS Colloquium, 99, 2466-2472. https://doi.org/10.1073/pnas.012579499
[49] Stehlik, M., Hermann, P. and Nicolis, O. (2016) Fractal Based Cancer Modelling. REVSTAT—Statistical Journal, 14, 139-155.

[50] Deisboeck, T.S., Guiot, C., Delsanto, P.P., et al. (2006) Does Cancer Growth Depend on Surface Extension? Medical Hypotheses, 67, 1338-1341. https://doi.org/10.1016/j.mehy.2006.05.029
[51] Stehlik, M., Wartner, F. and Minarova, M. (2013) Fractal Analysis for Cancer Research: Case Study and Simulation of Fractals. Pliska Studia Mathematica Bulgarica, 22, 195-206.
[52] Baish, J.W. and Jain, R.K. (2000) Fractals and Cancer. Cancer Research, 60, 3683-3688.
[53] Liu, S., Wang, Y., Xu, K., Wang, Z., Fan, X., Zhang, C., Li, S., Qiu, X. and Jiang, T. (2017) Relationship between Necrotic Patterns in Glioblastoma and Patient Survival: Fractal Dimension and Lacunarity Analyses Using Magnetic Resonance Imaging. Scientific Reports, 7, Article No. 8302. https://doi.org/10.1038/s41598-017-08862-6
[54] Goldenfeld, N. and Woese, C. (2010) Life Is Physics: Evolution as a Collective Phenomenon Far from Equilibrium. Annual Review of Condensed Matter Physics, 2, 375-399. https://doi.org/10.1146/annurev-conmatphys-062910-140509
[55] West, B.J. and West, D. (2011) Are Allometry and Macroevolution Related? Physica A: Statistical Mechanics and Its Applications, 390, 733-1736. https://doi.org/10.1016/j.physa.2010.11.031
[56] Camazine, S., Deneubourg, J.L., Franks, N.R., et al. (2003) Self-Organization in Biological Systems. Princeton Studies in Complexity, Princeton University Press, Princeton, Oxford.
[57] West, G.B. and Brown, J.H. (2005) The Origin of Allometric Scaling Laws in Biology from Genomes to Ecosystems: Towards a Quantitative Unifying Theory of Biological Structure and Organization. Journal of Experimental Biology, 208, 1575-1592. https://doi.org/10.1242/jeb.01589
[58] Eskov, V.M., Filatova, O.E., Eskov, V.V., et al. (2017) The Evolution of the Idea of Homeostasis: Determinism, Stochastics, and Chaos—Self-Organization. Biophysics, 62, 809-820. https://doi.org/10.1134/S0006350917050074
[59] Billman, G.E. (2020) Homeostasis: The Underappreciated and Far Too Often Ignored Central Organizing Principle of Physiology. Frontiers in Physiology, 11, Article No. 200. https://doi.org/10.3389/fphys.2020.00200
[60] Mode, C.J., Durrett, R., Klebaner, F., et al. (2013) Applications of Stochastic Processes in Biology and Medicine. International Journal of Stochastic Analysis, 2013, Article ID: 576381. https://doi.org/10.1155/2013/790625
[61] Cramer, F. (1995) Chaos and Order (The Complex Structure of Living Systems). VCH, Weinheim, New York, Cambridge.
[62] Peng, C.K., Buldyrev, S.V., Hausdorff, J.M., et al. (1994) Fractals in Biology and Medicine: From DNA to the Heartbeat. In: Bunde, A. and Havlin, S., Eds., Fractals in Science, Springer-Verlag, Berlin, 49-87. https://doi.org/10.1007/978-3-662-11777-4_3
[63] Bak, P., Tang, C. and Wieserfeld, K. (1988) Self-Organized Criticality. Physical Review A, 38, 364. https://doi.org/10.1103/PhysRevA.38.364
[64] Musha, T. and Sawada, Y. (1994) Physics of the Living State. IOS Press, Amsterdam.
[65] Schlesinger, M.S. (1987) Fractal Time and 1/f Noise in Complex Systems. Annals of the New York Academy of Sciences, 504, 214-228. https://doi.org/10.1111/j.1749-6632.1987.tb48734.x
[66] Wentian, L. (1989) Spatial 1/f Spectra in Open Dynamical Systems. Europhysics Letters, 10, 395-400. https://doi.org/10.1209/0295-5075/10/5/001
[67] Kim, J.J., Parker, S., Henderson, T. and Kirby, J.N. (2020) Physiological Fractals: Visual and Statistical Evidence across Timescales and Experimental States. Journal of the Royal Society Interface, 17, 1-8. https://doi.org/10.1098/rsif.2020.0334
[68] Szendro, P., Vincze, G. and Szasz, A. (2001) Bio-Response on White-Noise Excitation. Electromagnetic Biology and Medicine, 20, 215-229. https://doi.org/10.1081/JBC-100104145
[69] Szendro, P., Vincze, G. and Szasz, A. (2001) Pink-Noise Behaviour of Biosystems. European Biophysics Journal, 30, 227-231. https://doi.org/10.1007/s002490100143
[70] Vincze, Gy. and Szasz, A. (2018) Similarities of Modulation by Temperature and by Electric Field. OJBIPHY, 8, 95-103. https://doi.org/10.4236/ojbiphy.2018.83008

[71] Lin, J.C. (1989) Electromagnetic Interaction with Biological Systems. Pergamon Press, New York. https://doi.org/10.1007/978-1-4684-8059-7

[72] Bersani, F. (1999) Electricity and Magnetism in Biology and Medicine. Kluwer Academic Plenum Publishers, New York. https://doi.org/10.1007/978-1-4615-4867-6

[73] Marko, M. (2005) "Biological Windows": A Tribute to WR Adey. The Environmentalist, 25, 67-74. https://doi.org/10.1007/s10669-005-4268-8

[74] Adey, W.R. (1984) Nonlinear, Nonequilibrium Aspects of Electromagnetic Field Interactions at Cell Membranes. In: Adey, W.R. and Lawrence, A.F., Eds., Nonlinear Electrodynamics in Biological Systems, Plenum Press, New York, 3-22. https://doi.org/10.1007/978-1-4613-2789-9_1

[75] Adey, W.R. (1990) Joint Actions of Environmental Nonionizing Electromagnetic Fields and Chemical Pollution in Cancer Promotion. Environmental Health Perspectives, 86, 297-305. https://doi.org/10.1289/ehp.9086297

[76] Blackman, C.F., Kinney, L.S., House, D.E., et al. (1989) Multiple Power-Density Windows and Their Possible Origin. Bioelectromagnetics, 10, 115-128. https://doi.org/10.1002/bem.2250100202

[77] Liu, D.-S., Astumian, R.D. and Tsong, T.Y. (1990) Activation of Na+ and K+ Pumping Modes of (Na,K)-ATPase by an Oscillating Electric Field. The Journal of Biological Chemistry, 265, 7260-7267. https://doi.org/10.1016/S0021-9258(19)39108-2

[78] Markin, V.S. and Tsong, T.Y. (1991) Frequency and Concentration Windows for the Electric Activation of a Membrane Active Transport System. Biophysical Journal, 59, 1308-1316. https://doi.org/10.1016/S0006-3495(91)82345-1

[79] Schwan, H.P. (1957) Electrical Properties of Tissue and Cell Suspensions. In: Lawrence, J.H. and Tobias, C.A., Eds., Advances in Biological and Medical Physics, Academic Press, New York, Vol. V, 147-209. https://doi.org/10.1016/B978-1-4832-3111-2.50008-0

[80] Schwan, H.P. (1993) Mechanism Responsible for Electrical Properties of Tissues and Cell Suspensions. Medical Progress through Technology, 19, 163-165.

[81] Schwan, H.P. (1954) Electrical Properties of Muscle Tissue at Low Frequencies. Zeitschrift für Naturforschung, 9B, 245.

[82] Falk, G. and Fatt, P. (1964) Linear Electrical Properties of Striated Muscle Fibers Observed with Intracellular Electrodes. Proceedings of the Royal Society of London, Series B, 160, 69-123. https://doi.org/10.1098/rspb.1964.0030

[83] Martinsen, Ø.G., Grimnes, S. and Mirtaheri, P. (2000) Non-Invasive Measurements of Post Mortem Changes in Dielectric Properties of Haddock Muscle—A Pilot Study. Journal of Food Engineering, 43, 189-192. https://doi.org/10.1016/S0260-8774(99)00151-X

[84] Schwan, H.P. and Takashima, S. (1991) Dielectric Behavior of Biological Cells and Membranes. Bulletin of the Institute for Chemical Research, Kyoto University, 69, 459-475.

[85] Cole, K.S. (1972) Membranes, Ions and Impulses. University of California Press, Berkeley.

[86] Anderson, J.C. (1964) Dielectrics. Chapman & Hall, London.

[87] Pethig, R.R. (1979) Dielectric and Electronic Properties of Biological Materials. Wiley, Hoboken.

[88] Pethig, R.R. (2017) Dielectrophoresis: Theory, Methodology and Biological Applications. John Wiley & Sons, Hoboken. https://doi.org/10.1002/9781118671443

[89] Asami, K. (2002) Characterization of Biological Cells by Dielectric Spectroscopy. Journal of Non-Crystalline Solids, 305, 268-277. https://doi.org/10.1016/S0022-3093(02)01110-9

[90] Pauly, H. and Schwan, H.P. (1959) Uber die Impedanz einer Suspension von Kugelformigen Teilchen mit einer Schale. Zeitschrift für Naturforschung, 14B, 125-131. https://doi.org/10.1515/znb-1959-0213

[91] Stoy, R.D., Foster, K.R. and Schwan, H.P. (1982) Dielectric Properties of Mammalian Tissues from 0.1 to 100 MHz: A Summary of Recent Data. Physics in Medicine & Biology, 27, 501-513. https://doi.org/10.1088/0031-9155/27/4/002

[92] Gotz, M., Karsch, L. and Pawelke, J. (2017) A New Model for Volume Recombination in Plane-Parallel Chambers in Pulsed Fields of High Dose-per-Pulse. Physics in Medicine & Biology, 62, 8634-8654. https://doi.org/10.1088/1361-6560/aa8985

[93] Stubbe, M. and Gimsa, J. (2015) Maxwell's Mixing Equation Revisited: Characteristic Impedance Equations for Ellipsoidal Cells. Biophysical Journal, 109, 194-208. https://doi.org/10.1016/j.bpj.2015.06.021

[94] Rajewsky, B. and Schwan, H.P. (1948) The Dielectric Constant and Conductivity of Blood at Ultrahigh Frequencies. Naturwissenschaften, 35, 315. https://doi.org/10.1007/BF00626639

[95] Calabro, E. and Magazu, S. (2018) Resonant Interaction between Electromagnetic Fields and Proteins: A Possible Starting Point for the Treatment of Cancer. Electromagnetic Biology and Medicine, 37, 155-158. https://doi.org/10.1080/15368378.2018.1499031

[96] Johns, L.D. (2002) Nonthermal Effects of Therapeutic Ultrasound: The Frequency Resonance Hypothesis. Journal of Athletic Training, 37, 293-299.

[97] Cross, S.E., Jin, Y.-S., Rao, J. and Gimzewski, J.K. (2007) Nanomechanical Analysis of Cells from Cancer Patients. Nature Nanotechnology, 2, 780-783. https://doi.org/10.1038/nnano.2007.388

[98] Fraldi, M., Cugno, A., Deseri, L., et al. (2015) A Frequency-Based Hypothesis for Mechanically Targeting and Selectively Attacking Cancer Cells. Journal of the Royal Society Interface, 12, Article ID: 2015656. https://doi.org/10.1098/rsif.2015.0656

[99] Cross, S., Jin, Y.-S., Tondre, J., Wong, R., Rao, J. and Gimzewski, J. (2008) AFM-Based Analysis of Human Metastatic Cancer Cells. Nanotechnology, 19, Article ID: 384003. https://doi.org/10.1088/0957-4484/19/38/384003

[100] Lekka, M., et al. (2012) Cancer Cell Detection in Tissue Sections Using AFM. Archives of Biochemistry and Biophysics, 518, 151-156. https://doi.org/10.1016/j.abb.2011.12.013

[101] Liboff, A.R. (1985) Geomagnetic Cyclotron Resonance in Living Cells. Journal of Biological Physics, 13, 99-102. https://doi.org/10.1007/BF01878387

[102] McLoad, B.R. and Liboff, A.R. (1986) Dynamic Characteristic of Membrane Ions in Multifield Configurations of Low-Frequency Electromagnetic Readiation. Bioelectromagnetics, 7, 177-189. https://doi.org/10.1002/bem.2250070208

[103] Liboff, A.R. (2003) Ion Cyclotron Resonance in Biological Systems: Experimental Evidence. In: Stavroulakis, P., Ed., Biological Effects of Electromagnetic Fields, Springer Verlag, Berlin, 76-113.

[104] Szasz, A. (1991) An Electronically Driven Instability: The Living State. Physiological Chemistry and Physics and Medical NMR, 23, 43-50.

[105] Frohlich, H. (1983) Coherence in Biology. In: Frohlich, H. and Kremer, F., Eds., Coherent Excitations in Biological Systems, Springer Verlag, Berlin, 1-5. https://doi.org/10.1007/978-3-642-69186-7_1

[106] Frohlich, H. (1988) Biological Coherence and Response to External Stimuli. Springer Verlag, Berlin. https://doi.org/10.1007/978-3-642-73309-3

[107] McDonnell, M. and Abbott, D. (2009) What Is Stochastic Resonance? Definitions, Misconceptions, Debates, and Its Relevance to Biology. PLOS Computational Biology, 5, e1000348. https://doi.org/10.1371/journal.pcbi.1000348

[108] Bezrukov, S.M. and Vodyanoy, I. (1997) Stochastic Resonance at the Single-Cell Level. Nature, 388, 632-633. https://doi.org/10.1038/41684

[109] Vincze, Gy., Szász, A. and Szasz, N. (2005) On the Thermal Noise Limit of Cellular Membranes. Bioelectromagnetics, 26, 28-35. https://doi.org/10.1002/bem.20051

[110] Tsong, T.Y. and Chang, C.-H. (2007) A Markovian Engine for a Biological Energy Transducer: The Catalytic Wheel. Bio Systems, 88, 323-333. https://doi.org/10.1016/j.biosystems.2006.08.014

[111] Michaelis, L. and Menten, M.L. (1913) Die Kinetik der Invertinwirkung. Biochemische Zeitschrift, 49, 333-369. (In German) Translation to English: Goody, R.S. and Johnson, K.A. (2011) The Original Michaelis Constant: Translation of the 1913 Michaelis-Menten Paper. Biochemistry, 50, 8264-8269. https://doi.org/10.1021/bi201284u

[112] Savageau, M.A. (1998) Development of Fractal Kinetic Theory for Enzyme-Catalysed Reactions and Implications for the Design of Biochemical Pathways. Biosystems, 47, 9-36. https://doi.org/10.1016/S0303-2647(98)00020-3

[113] Tsong, T.Y. and Astumian, R.D. (1988) Electroconformational Coupling: How Membrane-Bound ATPase Transduces Energy from Dynamic Electric Fields. Annual Review of Physiology, 50, 273-290. https://doi.org/10.1146/annurev.ph.50.030188.001421

[114] Astumian, R.D. (1994) Electroconformational Coupling of Membrane Proteins. Annals of the New York Academy of Sciences, 720, 136-140. https://doi.org/10.1111/j.1749-6632.1994.tb30441.x

[115] Markin, V.S., Liu, D., Rosenberg, M.D., et al. (1992) Resonance Transduction of Low Level Periodic Signals by an Enzyme: An Oscillatory Activation Barrier Model. Biophysical Journal, 61, 1045-1049. https://doi.org/10.1016/S0006-3495(92)81913-6

[116] McNamara, B. and Wiesenfeld, K. (1989) Theory of Stochastic Resonance. Physical Review A, 39, 4854-4869. https://doi.org/10.1103/PhysRevA.39.4854

[117] Astumian, R.D. (1997) Thermodynamics and Kinetics of a Brownian Motor. Science, 276, 917-922. https://doi.org/10.1126/science.276.5314.917

[118] Astumian, R.D. and Bier, M. (1994) Fluctuation Driven Ratchets: Molecular Motors. Physical Review Letters, 72, 1766-1769. https://doi.org/10.1103/PhysRevLett.72.1766

[119] Astumian, R.D. and Derényi, I. (1998) Fluctuation Driven Transport and Models of Molecular Motors and Pumps. European Biophysics Journal, 27, 474-489. https://doi.org/10.1007/s002490050158

[120] Linke, H., Downton, M.T. and Zuckermann, M.J. (2005) Performance Characteristics of Brownian Motors. Chaos, 15, Article ID: 026111. https://doi.org/10.1063/1.1871432

[121] Astumian, R.D., Chock, P.B., Tsong, T.Y., et al. (1987) Can Free Energy Be Transduced from Electric Noise? Proceedings of the National Academy of Sciences of the United States of America, 84, 434-438. https://doi.org/10.1073/pnas.84.2.434

[122] Feynman, R.P., Leighton, R.B. and Sands, M. (1966) The Feynman Lectures on Physics. Adison-Wesley, California Institute of Technology, Reading.

[123] Vincze, Gy., Szigeti, Gy.P. and Szasz, A. (2018) On the Feynman Ratchet and the Brownian Motor. Open Journal of Biophysics, 2, 22-30. https://doi.org/10.4236/ojbiphy.2018.81003

[124] Westerhoff, H.V., Tsong, T.Y., Chock, P.B., et al. (1986) How Enzymes Can Capture and Transmit Free Energy from an Oscillating Electric Field. Proceedings of the National Academy of Sciences of the United States of America, 83, 4734-4738. https://doi.org/10.1073/pnas.83.13.4734

[125] Seegers, J.C., Engelbrecht, C.A. and Papendorp van, D.H. (2001) Activation of Signal-Transduction Mechanisms May Underlie the Therapeutic Effects of an Applied Electric Field. Medical Hypotheses, 57, 224-230. https://doi.org/10.1054/mehy.2001.1292

[126] Tinoco, I., Sauer, K., Wang, J.C., et al. (2002) Physical Chemistry. Principles and Applications in Biological Sciences. 4th Edition, Prentice-Hall Inc., Hoboken.

[127] Xie, T.D., Chen, Y., Marszalek, P., et al. (1997) Fluctuation-Driven Directional Flow in Biochemical Cycle: Further Study of Electric Activation of Na,K Pumps. Biophysical Journal, 72, 2496-2502. https://doi.org/10.1016/S0006-3495(97)78894-5

[128] Astumian, R.D. and Chock, P.B. (1989) Effects of Oscillations and Energy-Driven Fluctuations on the Dynamics of Enzyme Catalsysis and Free-Energy Transduction. Physical Review A, 39, 6416-6435. https://doi.org/10.1103/PhysRevA.39.6416

[129] Davydov, A.S. (1982) Biology and Quantum Mechanics. Pergamon Press Ltd., Oxford.

[130] Scott, A.C. (1982) Dynamics of Davydov Solitons. Physical Review A, 26, 578-595. https://doi.org/10.1103/PhysRevA.26.578

[131] Hameroff, S. (1987) Ultimate Computing: Biomolecular Consciousness and Nanotechnology. Elsevier Science Publishers B.V., Amsterdam, 18.

[132] Sinkala, Z. (2006) Soliton/Exciton Transport in Proteins. Journal of Theoretical Biology, 241, 919-927. https://doi.org/10.1016/j.jtbi.2006.01.028

[133] Andersen, S.S.L., Jackson, A.D. and Heimburg, T. (2009) Towards a Thermodynamic Theory of Nerve Pulse Propagation. Progress in Neurobiology, 88, 104-113. https://doi.org/10.1016/j.pneurobio.2009.03.002

[134] Heimburg, T. and Jackson, A.D. (2005) On Soliton Propagation in Biomembranes and Nerves. Proceedings of the National Academy of Sciences of the United States of America, 102, 9790-9795. https://doi.org/10.1073/pnas.0503823102

[135] Yakushevich, L.V. (2004) Nonlinear Physics of DNA. 2nd Revised Edition, Wiley-VCH, Hoboken. https://doi.org/10.1002/3527603700

[136] Davydov, A.S. (1991) Solitons in Molecular Systems. Mathematics and Its Applications (Soviet Series), Vol. 61, 2nd Edition, Kluwer Academic Publishers, Dordrecht. https://doi.org/10.1007/978-94-011-3340-1

[137] Cruzeiro, L., Halding, J., Shristiansen, P.L. and Skovgaard, O. (1988) Temperature Effects on the Davydov Soliton. Physical Review A, 37, 880-887. https://doi.org/10.1103/PhysRevA.37.880

[138] Cruzeiro-Hansson, L. (1992) Mechanism of Thermal Destabilization of the Davydov Soliton. Physical Review A, 45, 4111-4115. https://doi.org/10.1103/PhysRevA.45.4111

[139] Careri, G. and Wyman, J. (1984) Soliton-Assisted Unidirectional Circulation in a Biochemical Cycle. PNAS, 81, 4386-4388. https://doi.org/10.1073/pnas.81.14.4386

[140] Brizhik, L.S., Eremko, A., Piette, B. and Zakrzewski, W. (2004) Solitons in Alpha-Helical Proteins. Physical Review E, 70, Article ID: 031914. https://doi.org/10.1103/PhysRevE.70.031914

[141] Xie, T.D., Marszalek, P., Chen, Y.D., et al. (1994) Recognition and Processing of Randomly Fluctuating Electric Signals by Na,K-ATPase. Biophysical Journal, 67, 1247-1251. https://doi.org/10.1016/S0006-3495(94)80594-6

[142] Tsong, T.Y. and Xie, T.D. (2002) Ion Pump as Molecular Ratchet and Effects of Noise: Electric Activation of Cation Pumping by Na,K-ATPase. Applied Physics A, 75, 345-352. https://doi.org/10.1007/s003390201407

[143] Kadanttsev, V.N. and Goltsov, A. (2019) Collective Excitations in Alpha-Helical Protein Structures Interacting with Environment. https://doi.org/10.1101/457580

[144] Kuwayama, H. and Ishida, S. (2013) Biological Soliton in Multicellular Movement. Scientific Reports, 3, Article No. 2272. https://doi.org/10.1038/srep02272

[145] Bonner, J.T. (2009) The Social Amoebae: The Biology of Cellular Slime Molds. Princeton University Press, Princeton. https://doi.org/10.1515/9781400833283

[146] Szasz, A., van Noort, D., Scheller, A., et al. (1994) Water States in Living Systems. I. Structural Aspects. Physiological Chemistry and Physics and Medical NMR, 26, 299-322. http://www.ncbi.nlm.nih.gov/pubmed/7700980

[147] Agmon, N. (1995) The Grotthuss Mechanism. Chemical Physics Letters, 244, 456-462. https://doi.org/10.1016/0009-2614(95)00905-J

[148] Markovitch, O. and Agmon, N. (2007) Structure and Energetics of the Hydronium Hydration Shells. The Journal of Physical Chemistry A, 111, 2253-2256. https://doi.org/10.1021/jp068960g

[149] Maryan, M.I., Kikineshy, A., Szendrö, P., et al. (2001) Modeling of the Dissipative Structure of Water. Acta Technologica Agriculturae Slovaca Universitas Agriculturae Nitriae, 3, 77-80.

[150] Pavlenko, N. (2004) Proton Wires in an Electric Field: The Impact of Grotthuss Mechanism on Charge Translocation.

[151] Szendro, P., Koltay, J., Szasz, A., et al. (1999) Is the Structure of the Water Convertible in Physical Way? Hungarian Agricultural Engineering, 12, 43-45.

[152] Andocs, G., Vincze, Gy., Szasz, O., Szendro, P. and Szasz, A. (2009) Effect of Curl-Free Potentials on Water. Electromagnetic Biology and Medicine, 28, 166-181. http://www.ncbi.nlm.nih.gov/pubmed/19811398 https://doi.org/10.1080/15368370902724724

[153] Tao, F.-M. (2003) Solvent Effects of Individual Water Molecules. In: Buch, V. and Devilin, J.P., Eds., Water in Confining Geometries, Cluster Physics, Springer Verlag. Berlin, 79-99. https://doi.org/10.1007/978-3-662-05231-0_5

[154] Szasz, A., Szasz, N. and Szasz, O. (2010) Oncothermia—Principles and Practices. Springer Science, Heidelberg. https://doi.org/10.1007/978-90-481-9498-8

[155] Varma, R. and Selman, J.S. (1991) Techniques for Characterisation of Electrodes and Electrochemical Processes. John Wiley & Sons, New York.
[156] Yang, K.-L., Huang, C.-C., Chi, M.-S., Chiang H.-C., Wang, Y.-S. andocs, G., et al. (2016) In Vitro Comparison of Conventional Hyperthermia and Modulated Electro-Hyperthermia. Oncotarget, 7, 84082-84092. http://www.ncbi.nlm.nih.gov/pubmed/27556507 https://doi.org/10.18632/oncotarget.11444
[157] Pickard, W.F. and Rosenbaum, F.J. (1978) Biological Effects of Microwaves at the Membrane Level: Two Possible Athermal Electrophysiological Mechanisms and a Proposed Experimental Test. Mathematical Biosciences, 39, 235-253. https://doi.org/10.1016/0025-5564(78)90055-X
[158] Barsoum, Y.H. and Pickard, W.F. (1982) Radio-Frequency Rectification in Electrogenic and Nonelectrogenic Cells of Chara and Nitella. The Journal of Membrane Biology, 65, 81-87. https://doi.org/10.1007/BF01870471
[159] Goldman, D.E. (1943) Potential, Impedance, and Rectification in Membranes. The Journal of General Physiology, 27, 37-60. https://doi.org/10.1085/jgp.27.1.37
[160] Ramachandran, S., Blick, R.H. and van der Weide, D. (2010) Radio Frequency Rectification on Membrane Bound Pores. Nanothechnology, 21, Article ID: 075201. https://iopscience.iop.org/article/10.1088/0957-4484/21/7/075201 https://doi.org/10.1088/0957-4484/21/7/075201
[161] Tanaka, A. and Tokimasa, T. (1999) Theoretical Background for Inward Rectification. The Tokai Journal of Experimental and Clinical Medicine, 24, 147-153.
[162] Astumian, R.D., Weaver, J.C. and Adair, R.K. (1995) Rectification and Signal Averaging of Weak Electric Fields by Biological Cells. Proceedings of the National Academy of Sciences of the United States of America, 92, 3740-3743. https://doi.org/10.1073/pnas.92.9.3740
[163] Balzano, Q. (2002) Proposed Test for Detection of Nonlinear Responses in Biological Preparations Exposed to RF Energy. Bioelectromagnetics, 23, 278-287. https://doi.org/10.1002/bem.10017
[164] Balzano, Q. and Sheppard, A.R. (2003) RF Nonlinear Interactions in Living Cells—I: Nonequilibrium Thermodynamic Theory. Bioelectromagnetics, 24, 473-482. https://doi.org/10.1002/bem.10126
[165] Weaver, J.C. and Astumian, R.D. (1990) The Response of Living Cells to Very Week Electric Fields: The Thermal Noise Limit. Science, 247, 459-462. https://doi.org/10.1126/science.2300806
[166] Bier, M. (2006) How to Evaluate the Electric Noise in a Cell Membrane? Acta Physica Polonica B, 37, 1409-1424.
[167] Yesufu, T.K. and Atijosan, A.O. (2015) Weak Amplitude Modulated (AM) Signal Detection Algorithm for Software-Defined Radio Receivers. International Journal of Intelligent Information Systems, 4, 79-83. https://doi.org/10.11648/j.ijiis.20150404.12
[168] Pinto, R.P., Reboul, J.M.Q., Vega-Leal, A.P. and Tombs, J. (2008) Stochastic Resonance as a Null Distortion Demodulation. IEEE International Instrumentation and Measurement Technology Conference, Victoria, 12-15 May 2008, 2120-2125. https://doi.org/10.1109/IMTC.2008.4547398
[169] Szentgyorgyi, A. (1978) The Living State and Cancer. Marcel Dekker Inc., New York.
[170] Szentgyorgyi, A. (1998) Electronic Biology and Cancer. Marcel Dekkerm, New York.
[171] Szentgyorgyi, A. (1968) Bioelectronics, a Study on Cellular Regulations, Defense and Cancer. Academic Press, New York.
[172] Szasz, O., Szasz, A.M., Minnaar, C. and Szasz, A. (2017) Heating Preciosity—Trends in Modern Oncological Hyperthermia. Open Journal of Biophysics, 7, 116-144. https://doi.org/10.4236/ojbiphy.2017.73010
[173] Wust, P., Kortum, B., Strauss, U., Nadobny, J., Zschaeck, S., Beck, M., et al. (2020) Nonthermal Effects of Radiofrequency Electromagnetic Fields. Scientific Reports, 10, Article ID: 13488. https://doi.org/10.1038/s41598-020-69561-3
[174] Wust, P., Nadobny, J., Zschaeck, S. and Ghadjar, P. (2020) Physics of Hyperthermia—Is Physics Really against Us? In: Szasz, A., Ed., Challenges and Solutions of Oncological Hyperthermia, Cambridge Scholars, Cambridge, Ch. 16, 346-376.

[175] Meggyeshazi, N., Andocs, G., Balogh, L., Balla, P., Kiszner, G., Teleki, I., Jeney, A. and Krenacs, T. (2014) DNA Fragmentation and Caspase-Independent Programmed Cell Death by Modulated Electrohyperthermia. Strahlentherapie und Onkologie, 190, 815-822. https://doi.org/10.1007/s00066-014-0617-1

[176] Wust, P., Ghadjar, P., Nadobny, J., et al. (2019) Physical Analysis of Temperature-Dependent Effects of Amplitude-Modulated Electromagnetic Hyperthermia. International Journal of Hypertension, 36, 1246-1254. https://doi.org/10.1080/02656736.2019.1692376

[177] Pethig, R. (1984) Dielectric Properties of Biological Materials: Biophysical and Medical Application. IEEE Transactions on Electrical Insulation, EI-19, 453-474. https://doi.org/10.1109/TEI.1984.298769

[178] Schwan, H.P. (1963) Determination of Biological Impedances. In: Physical Techniques in Biological Research, Vol. 6, Academic Press, New York, 323-406. https://doi.org/10.1016/B978-1-4831-6743-5.50013-7

[179] Szasz, A. (2013) Electromagnetic Effects in Nanoscale Range. In: Shimizu, T. and Kondo, T., Eds., Cellular Response to Physical Stress and Therapeutic Applications, Chapter 4, Nova Science Publishers, Inc., Hauppauge, 55-81.

[180] Staunton, J.R., et al. (2008) The Physical Sciences—Oncology Centers Network; a Physical Sciences Network Characterization of Non-Tumorigenic and Metastatic Cells. Scientific Reports, 3, Article No. 1449.

[181] Vincze, Gy., Szigeti, Gy. andocs, G. and Szasz, A. (2015) Nanoheating without Artificial Nanoparticles. Biology and Medicine, 7, 249.

[182] Szasz, O. and Szasz, A. (2014) Oncothermia Nano-Heating Paradigm. Journal of Cancer Science and Therapy, 6, 4. https://doi.org/10.4172/1948-5956.1000259

[183] Waldhauer, I. and Steinle, A. (2008) NK Cells and Cancer Immunosurveillance. Oncogene, 27, 5932-5943. https://doi.org/10.1038/onc.2008.267

[184] Zamai, L., Ponti, C., Mirandola, P., et al. (2007) NK Cells and Cancer. The Journal of Immunology, 178, 4011-4016. https://doi.org/10.4049/jimmunol.178.7.4011

[185] Hu, W., Wang, G., Huang, D., et al. (2019) Cancer Immunotherapy Based on Natural Cell Killer Cells: Current Progress and New Opportunities. Frontiers in Immunology, 10, Article No. 1205. https://doi.org/10.3389/fimmu.2019.01205

[186] Vancsik, T., Mathe, D., Horvath, I., Varallyaly, A.A., et al. (2021) Modulated Electro-Hyperthermia Facilitates NK-Cell Infiltration and Growth Arrest of Human A2058 Melanoma in a Xenograft Model. Frontiers in Oncology, 11, Article ID: 590764. https://doi.org/10.3389/fonc.2021.590764

[187] Megyesshazi, N. (2015) Studies on Modulated Electrohyperthermia Induced Tumor Cell Death in a Colorectal Carcinoma Model. PhD Theses, Pathological Sciences Doctoral School, Semmelweis University, Budapest.

[188] Andocs, G., Meggyeshazi, N., Balogh, L., Spisak, S., Maros, M.E., Balla, P., Kiszner, G., Teleki, I., Kovago, Cs. and Krenacs, T. (2014) Upregulation of Heat Shock Proteins and the Promotion of Damage-Associated Molecular Pattern Signals in a Colorectal Cancer Model by Modualted Electrohyperthermia. Cell Stress and Chaperones, 20, 37-46. https://doi.org/10.1007/s12192-014-0523-6

[189] Szasz, A. (2020) Towards the Immunogenic Hyperthermic Action: Modulated Electro-Hyperthermia, Clinical Oncology and Research. Science Repository, 3, 5-6. https://doi.org/10.31487/j.COR.2020.09.07

[190] Vancsik, T., Kovago, Cs., Kiss, E., et al. (2018) Modulated Electro-Hyperthermia Induced Loco-Regional and Systemic Tumor Destruction in Colorectal Cancer Allografts. Journal of Cancer, 9, 41-53. https://doi.org/10.7150/jca.21520

[191] Qin, W., Akutsu, Y., Andocs, G., et al. (2014) Modulated Electro-Hyperthermia Enhances Dendritic Cell Therapy through an Abscopal Effect in Mice. Oncology Reports, 32, 2373-2379. http://www.ncbi.nlm.nih.gov/pubmed/25242303 https://doi.org/10.3892/or.2014.3500

[192] Tsang, Y.-W., Huang, C.-C., Yang, K.-L., et al. (2015) Improving Immunological Tumor Microenvironment Using Electro-Hyperthermia Followed by Dendritic Cell Immunotherapy. BMC Cancer, 15, 708. http://www.ncbi.nlm.nih.gov/pubmed/26472466

[193] Szasz, A. (2019) Immune-Effects with Local Hyperthermia. Oncothermia Journal, 26, 139-148. https://doi.org/10.1186/s12885-015-1690-2

[194] Szasz, O. (2020) Local Treatment with Systemic Effect: Abscopal Outcome. In: Szasz, A., Ed., Challenges and Solutions of Oncological Hyperthermia, Ch. 11, Cambridge Scholars, Cambridge, 192-205.

[195] Van Gool, S.W., Makalowski, J., Feyen, O., Prix, L., Schirrmacher, V. and Stuecker, W. (2018) The Induction of Immunogenic Cell Death (ICD) during Maintenance Chemotherapy and Subsequent Multimodal Immunotherapy for Glioblastoma (GBM). Austin Oncology Case Reports, 3, 1-8.

[196] Van Gool, S., Makalowski, J. and Feyen, O. (2019) Can We Monitor Immunogenic Cell Death (ICD) Induced with Modulated Electrohyperthermia and Oncolytivc Virus Injections? Oncothermia Journal, 26, 120-125.

[197] Krenacs, T., Meggyeshazi, N., Forika, G., et al. (2020) Modulated Electro-Hyperthermia-Induced Tumor Damage Mechanisms Revealed in Cancer Models. International Journal of Molecular Sciences, 21, 6270. https://www.mdpi.com/1422-0067/21/17/6270
https://doi.org/10.3390/ijms21176270

[198] Szasz, A.M., Minnaar, C.A., Szentmartoni, Gy., et al. (2019) Review of the Clinical Evidences of Modulated Electro-Hyperthermia (mEHT) Method: An Update for the Practicing Oncologist. Frontiers in Oncology, 9, Article No. 1012. https://www.frontiersin.org/articles/10.3389/fonc.2019.01012/full
https://doi.org/10.3389/fonc.2019.01012

[199] Andocs, G., Renner, H., Balogh, L., Fonyad, L., Jakab, C. and Szasz, A. (2009) Strong Synergy of Heat, and Modulated Electro-Magnetic Field in Tumor Cell Killing, Study of HT29 Xenograft Tumors in a Nude Mice Model. Strahlentherapie und Onkologie, 185, 120-126. http://www.ncbi.nlm.nih.gov/pubmed/19240999
https://doi.org/10.1007/s00066-009-1903-1

[200] Lee, S.-Y., Szigeti, G.P. and Szasz, A.M. (2019) Oncological Hyperthermia: The Correct Dosing in Clinical Applications. International Journal of Oncology, 54, 627-643. https://www.spandidos-publications.com/10.3892/ijo.2018.4645#
https://doi.org/10.3892/ijo.2018.4645

[201] Papp, E., Vancsik, T., Kiss, E. and Szasz, O. (2017) Energy Absorption by the Membrane Rafts in the Modulated Electro-Hyperthermia (mEHT). Open Journal of Biophysics, 7, 216-229. https://file.scirp.org/pdf/OJBIPHY_2017102715065328.pdf
https://doi.org/10.4236/ojbiphy.2017.74016

[202] Szasz, A. (2019) Thermal, and Nonthermal Effects of Radiofrequency on Living State, and Applications as an Adjuvant with Radiation Therapy. Journal of Radiation, and Cancer Research, 10, 1-17. https://doi.org/10.4103/jrcr.jrcr_25_18
http://www.journalrcr.org/article.asp?issn=2588-9273;year=2019;volume=10;issue=1;spage=1;epage=17;aulast=Szasz

[203] Szasz, A. (2020) Preface. In: Szasz A., Ed., Challenges and Solutions of Oncological Hyperthermia, Cambridge Scholars, Cambridge, 8-13. https://www.cambridgescholars.com/challenges-and-solutions-of-oncological-hyperthermia

Vascular Fractality and Alimentation of Cancer

Andras Szasz

Department of Biotechnics, St. Istvan University, Budaörs, Hungary

* Correspondence: Szasz.Andras@gek.szie.hu

Cite this article as:
Szasz, A. (2021): Vascular Fractality and Alimentation of Cancer.
International Journal of Clinical Medicine , 12, 279-296.
https://doi.org/10.4236/ijcm.2021.127025

Oncothermia Journal 31, 2022 March: 131-146
www.oncotherm.com/sites/oncotherm/files/2022-03/Szasz_Vascular.pdf

Abstract
Background: The basal metabolic rate has a scaling by tumor mass on the exponent of 3/4, while a simple surface-supplied volume of the mass would have a lower exponent, 2/3. The higher exponent can be explained by optimizing the overall energy distribution in the tumor, assuming that the target is four-dimensional. There are two possible ways of approximating the metabolic rate of the malignant tumor: 1) the volume blood-supply remains, but the surface and the length of the vessel network are modified; or 2) assuming that the malignant cell clusters try to maximize their metabolic rate to energize their proliferation by the longer length of the vessels. Our objective is to study how vascular fractality changes due to the greater demand for nutrients due to the proliferation of cancerous tissue. **Results:** It is shown that when a malignant tumor remains in expected four-dimensional volumetric conditions, it has a lower metabolic rate than the maximal metabolic potential in the actual demand of the proliferating cancer tissue. By maximizing the metabolic rate in malignant conditions, the allometric exponent will be smaller than 3/4, so the observed "dimensionality" of the metabolic rate versus mass becomes greater than four. The first growing period is exponential and keeps the "four-dimensional volume", but the growth process turns to the sigmoidal phase in higher metabolic demand, and the tumor uses other optimizing strategies, further lowering the scaling exponent of metabolic rate. **Conclusion:** It is shown that a malignant cellular cluster changes its metabolic scaling exponent when maximizing its energy intake in various alimentary conditions.

Keywords
Allometry, Metabolism, Fractal Dimensions, Optimization, Cancer, Vascularity

1. Introduction

The highly organized living systems are energetically open and far from thermal equilibrium [1]. Its physical phenomena are collective and have strong physical roots [2]. Structures built up by anabolism and store information in the open system [3]. The living matter is heterogeneous, having numerous different electrolytes engulfed by specialized tissues or lipids enveloping isolated aqueous electrolytes in definite structures. The isolating layers control the chemical and physical reactions between the electrolytes and regulate the complex interactions. The fundamental division of electrolytes is between the cytosol (the intracellular electrolyte) and the Extracellular Matrix (ECM). The membrane is a complexly organized multifunctioning part. This double lipid layer regulates the information and ionic exchange between the intra and extracellular reagents, having a vital role in the energy distribution and production of the entire system. The mass of the living object is volume dependent (scaling by 3), while the surface is scaled only by 2. Consequently, we expect an exponent for mass-dependence of

energy exchange (metabolism) as ⅔, the ratio of the cell surface to the cell volume (($\propto \frac{r^2}{r^3} = r^{2/3}$). So the expected metabolic power (P_{met}) in rest state (Basal Metabolic Power, BMP) dependence vs. mass (M) is expected:

$$P_{met} = BMP \propto M^{\frac{2}{3}} = M^{\alpha} \tag{1}$$

However, the experiments show a variation of exponents, the $\alpha = ⅔$ is not shared. When the metabolism is concentrated on surfaces, the $\alpha \approx ⅔$. well approaches reality. On the other hand, when it is centered on the energy resources, the exponent is close to $\alpha \approx ¾$. When the whole mass of the organism is involved in the metabolic energy exchange, the exponent is near to $\alpha \approx 1$. In complete demand, the actual body-part (organ or whole-body) needs maximally available energy supply, proportional to its mass, so the scaling exponent is $\alpha = 1$ in this case [4]. In this case, the actual demand decides about the metabolic power and not the geometry. Of course, both the extremes are not ideal for the living object and could not follow evolutional requests. What is

optimal? Despite the different exponential power, one feature is strictly common, all the experiments show power-scale (called scaling) in a few orders of magnitudes of the parameters, which is linear in the double logarithmic plot:

$$ln(P_{met}) \propto \alpha \cdot ln(M) \quad (2)$$

The scaling behavior is the consequence of the self-similarity of the living objects [5] [6]. The fundamental phenomenon behind it is the relative proportional change of the parameters [7]. The fundamental principle was oriented on the changes of the same organism, which has to grow in collective harmony, so the relative growth of parts must have balanced growth [8]. The structure and regulation of biosystems are complex. Various modern approaches have been developed in the last few decades to describe this complexity. The description of statistics of complex systems is far from the normal (Gaussian) distribution. Usually, power-law-tailed distributions (with a general exponent α) are applied:

$$f(x) = x^{\alpha} \quad (3)$$

There are various phenomena, including social, economic, physical, chemical, and biological, to be described by this function [9] [10] [11] [12] [13]. Despite the somewhat different fields of applications of the power law, it has a common root in complex systems: self-organization. The simplest fingerprint of the self-organized complexity is the self-similar or scale-free structures characterized by a power function. This power-function relation magnifies the $f(x)$ by a constant only, m-dependent $\Xi = m^{\alpha}$ value at any m magnification of x:

$$f(mx) = (mx)^{\alpha} = m^{\alpha}x^{\alpha} = \Xi x^{\alpha} = \Xi f(x) \quad (4)$$

Self-organization explains the evolution of the system [14], expressed in non-linear dynamics [15].

The objective of this present article focuses on analyzing the metabolic alimentation of the healthy tissues in normal conditions and the developing tumors in two different conditions:

1) When the tumor metabolizes as a homeostatic organized unit, the theoretically expected allometric exponent corresponds with the optimal healthy allometry;

2) When the tumor metabolism is not in such an "ideal" optimization of the metabolic supply, its alimentation is suboptimal, using the observed fractal behavior of its angio-structure.

2. Method

Fractal physiology describes the structural and dynamical properties of living organisms and their parts [16] [17], based on physical principles [18]. The self-similar behavior could be described by the normalized relative change of the magnitudes, similarly to the Weber-Fechner law [19] in psychophysics like:

$$\frac{\Delta f}{f} = \alpha \frac{\Delta x}{x} \quad (5)$$

where α is a constant fitting factor. By integration, we get the (3):

$$\ln(f) = \alpha \ln(x) \quad \rightarrow \quad f(x) = x^{\alpha} \tag{6}$$

The self-similar functional relation makes a "scale-invariance" feature due to the independence of the magnification, which is the fundamental behavior of the fractal structures, too [20].

The power function is the central description of the scaling in (1), which bases the allometry of living organisms [21]. The original allometry idea was recognized almost a hundred years ago [22], but the exciting question of the energizing of the life phenomena explained in connection of allometry is a half-century-old knowledge [23]. The connection between the homeostatic energizing level and the basal metabolic rate (B_0) as a self-similar function of mass (m) of living objects is [24]:

$$B_0 = am^{\alpha} \tag{7}$$

where the two parameters are determined experimentally; a is the allometric coefficient, and α is the allometric exponent, and (7) is usually called bioscaling [25]. The usual regression analysis uses the logarithmic transformation of (7):

$$lnB_0 = \alpha\, ln(m) + ln(a) \tag{8}$$

which allows high linear accuracy and fits both parameters a and α well [26]. The literature has numerous debates about the theoretical allometric relation based on fractal calculus and the empirical fits based on probability calculus [27]. The B_0 of living objects shows allometric scaling to its mass, which refers to the energy supply of the living mass of the volume. The (7) function gives a correct mathematical and biological framework for the complex bio-systems fractal studies [28]. The scaling power function of the mass describes it, and it has been shown valid in a broad category of living structures and processes [29]. The scaling considerations are applied not only in biology but broader, in the complete biosystem as well [30]. The importance of understanding the challenges of the complexity of human medicine was recognized on this basis [31] [32].

In a simple formulation, metabolic processes are surface-dependent, while the mass is proportional to the volume. Therefore, the exponent of their ratio mirrors their dimensionality, and consequently, the exponent is ⅔ [33]. Complex living allometry most likely shows the exponent as ¾instead of ⅔ in a broad spectrum of living objects [34], or at least have no linearity in a double-logarithmic plot [35]. However, the large data-mining does not show an overall validity of the ¾ exponent over ⅔ [36]. The curvature could be size-dependent in developing clusters by their size [37]. The ¾ exponent could be described as a relation between the three-dimensional surface and the four-dimensional volume [38]. The explanation of the fourth dimension is based on the fractal structure of microcirculation [39], which supplies the energy demand according to a homeostatic equilibrium (B_0) in the living complexity. Life in this meaning is "four-dimensional". Its metabolic exchange processes proceed on fractal surfaces, maximizing the available energy consumption, scaling even the fluctuation of the metabolic power in the universal scaling law as well [40].

The optimization of energy consumption was formulated rigorously by the scaling idea and discussed in a universal frame, even on the energy-consumption subcellular level, including the mitochondria and respiratory complexes [41]. The allometry shows a structural, geometrical constraint for living organisms in homeostatic equilibrium.

The metabolic scaling in cancer development is critical [42]. Contrary to the homeostatic homogeneity of the healthy tissue [43]; the functional heterogeneity of the solid tumor allows an abnormal organ self-possession of multiple cell-types and electrolytes like the Extracellular Matrix (ECM) lymph and blood-transports [44]. The tumor metabolism is based on the blood transport to the tumor. The logarithm of wet-weight of the tumor (m_{wet}) and the tumor blood-flow (B_t) have linear dependence [45], which was observed in model xenografts of ovarian cancer, so they have a bioscaling relation:

$$\log(B_t) = -0.808\log(m_{wet}) - 0.436 \quad r^2 = 0.79 \quad p < 0.001 \qquad (9)$$
$$[\, B_t = 0.6466 \cdot m_{wet}^{-0.808}]$$

where the exponent is close to ¾.

The allometric scaling supposes three geometrical variables to define the optimization of the circulatory system in living objects:

· The average length of the blood circulatory network (l);

· The surface of the relevant material exchange of the blood circulation system (s);

· The volume of the blood (v).

Furthermore, we suppose that these parameters are represented by the self-similar, self-organized functions of the L value, which is characteristic of a given organ. Hence:

$$l \propto L^{a_l}, \;\; s \propto L^{a_s}, \;\; v \propto L^{a_v} \qquad (10)$$

Using the theoretical fractal explanation, the conditions are: $a_l \geq 1$, $a_s \geq 2$ and $a_v \geq 3$, from where:

$$l \propto {L_0}^{1+\varepsilon_l}, \;\; s \propto {L_0}^{2+\varepsilon_s}, \;\; v \propto {L_0}^{3+\varepsilon_v} \qquad (11)$$

where $0 \leq \varepsilon_l \leq 1$, $0 \leq \varepsilon_s \leq 1$, and L_0 is the characteristic length. The first relation limits the pattern of the circulatory system to the maximum that could be planar, while the second is limited to a maximum, filling up a three-dimensional space. The third exponent ε_v could be calculated because the exponents are not independent. The volume is proportional to the product of the surface and length:

$$v \propto s \times l \qquad (12)$$

consequently

$$\varepsilon_v = \varepsilon_l + \varepsilon_s \qquad (13)$$

Using these conditions, we obtain from (11):

$$L_0 \propto v^{\frac{1}{3+\varepsilon_v}} \rightarrow s \propto v^{\frac{2+\varepsilon_s}{3+\varepsilon_v}} \qquad (14)$$

Furthermore, the actual volume of the blood is proportional to the actual mass of the given system or organ:

$$v \propto {L_0}^{3+\varepsilon_v} \propto m^1 \qquad (15)$$

Considering (14) and (15), now we have:

$$s \propto m^{\frac{2+\varepsilon_s}{3+\varepsilon_l+\varepsilon_s}} \tag{16}$$

The metabolism is a surface-controlled mechanism, so $(BMR) \propto s$, consequently:

$$B_0 \propto m^{\frac{2+\varepsilon_s}{3+\varepsilon_l+\varepsilon_s}} \tag{17}$$

If the living structure is geometric in conventional Euclidean meaning, then $\varepsilon_l = \varepsilon_s = \varepsilon_v = 0$ and therefore $a_l = a_s = a_v$; consequently, the scaling is $(BMR) \propto m^{\alpha}$, where $\alpha = \frac{2+\varepsilon_s}{3+\varepsilon_l+\varepsilon_s} = ⅔$. When at least one of the $\varepsilon_l \neq 0$, $\alpha \neq ⅔$, which modifies the common simple dimensional approach of the metabolic processes.

3. Results

The allometry gives a possibility to describe the development of the tumor [46]. It is valid for the primary cancer lesions but not always applicable in metastases [47]. We are dealing with primary tumors only. There are two ways of approximating the allometric metabolic rate of a tumor:
1) The theoretical approach accepts that a healthy life has a four-dimensional behavior connected to the highly self-organized, consequently self-similar hierarchic order [48], we fix the exponent to ¾.

2) The experimental approach assumes that the cell cluster tries to maximize its metabolic rate [49], and this way, it modifies the scaling exponent from the value of ¾.

Both approaches depend on the environmental conditions of the tumor, mainly on the nourishment of the cells.

3.1. Optimal Alimentation to Maximum Metabolic Rate

Evolution maximized the surface where the nutrients are transferred from the blood to the cells, ensuring the best conditions of the living object, so:

$$s(\varepsilon_l, \varepsilon_s) = max \tag{18}$$

This task is equivalent to the minimizing of the reciprocal value of the exponent in (16):

$$\frac{3+\varepsilon_l+\varepsilon_s}{2+\varepsilon_s} = min \tag{19}$$

with constraint conditions of:

$$0 \leq \varepsilon_l \leq 1, \qquad 0 \leq \varepsilon_s \leq 1 \tag{20}$$

(19) can be transformed into

$$\frac{3+\varepsilon_l+\varepsilon_s}{2+\varepsilon_s} = 1 + \frac{1+\varepsilon_l}{2+\varepsilon_s} = min \tag{21}$$

Hence, considering (20), the minimum condition demands that:

$$\varepsilon_l = 0, \qquad \varepsilon_s = 1 \tag{22}$$

Substituting (22) into (11), the exponents of the self-similar structures are:

$$l \propto {L_0}^1, \qquad s \propto {L_0}^3, \qquad v \propto {L_0}^4 \tag{23}$$

Consequently, in cases of ideal alimentation, these exponents are the fractal dimensions of the parameters of the network, and while the length is one dimensional, the surface is three, and the volume is four [38]. Because metabolism is a surface-regulated process, $s \propto (BMR)$, the scaling exponent of the metabolic rate versus mass using (16) is ¾:

$$B_0 \propto s \propto m^{\frac{2+\varepsilon_S}{3+\varepsilon_l+\varepsilon_S}} = m^{\frac{3}{4}} \tag{24}$$

and so B_0 in the unit mass:

$$\frac{B_0}{m} \propto m^{-\frac{1}{4}} \tag{25}$$

Primarily the blood stream provides the metabolic supply, so the fractality of the vascular network could be decisional in its allometric evaluation. The condition of (24) maximizes the blood flow energizing all the parts of the volume for their optimum, providing a maximum metabolic rate.

In consequence of (24), the life prefers the large masses as more effective energy-consumers in a unit volume shown in (25). However, on another side this process could lead to the loss of complex information, developing higher instability of the system, arguing that this is a negative tendency manifest the "aging of life's algorithm as a whole" [50]. The model could be applied by guessing when the energy supply is optimal, so the developed active surface cannot supply the actual demands. Two different sources are possible to create such a situation (1) the length of the supplier system changes (the constructional template differs), or (2) the volume of transport exchange is limited despite the growing demands. Various irregularities originate both challenges could be a symptom of disease, like cancer [51].

3.2. Suboptimal Alimentation for Tumor

The malignancy usually demands a higher energy input from its healthy environment than the available. The tumor supply is suboptimal. The higher energy demand (usually exponential in starting phase [52]) forces to increase the length of the vessel network. In cancerous clusters, contrary to (22), the vascular fractal dimension (D_v) of the supplying blood-vessel network ($l \propto {L_0}^{D_v}$) is larger than 1, ($D_v \geq 1$) [51]; consequently $\varepsilon_l \neq 0$ in the relation of (11). D_v could be measured by the box-counting method [51].

According to (11), the actual active surface is evolutionary normal for self-organizing of healthy tissues ($s \propto {L_0}^3$). The extra energy demand of the intensive proliferation changes the exponents of parameters in (11). In this case, the surface of the supply follows the evolution-requested exponent of 3 ($\varepsilon_s = 1$ from (22)) in the self-similar conditions, but the requested length changes:

$$l \propto {L_0}^{1+\varepsilon_l} = {L_0}^{D_v} \qquad s \propto {L_0}^3 \tag{26}$$

where εl>0εl>0 modifies the power of the transport measures, so the fractal organization of the transport lines is different. This type of change could be formed by neoangiogenesis satisfying the higher energy demand in cancerous tissues and could cause abnormalities as inflammation, thrombosis, varicose veins modification of the arteries, etc. The corresponding power-law for the actual metabolic rate at the longer length of vessels, so the suboptimal metabolic rate in this phase (B_{so1}) from (24) is:

$$B_{so1} \propto m^{\frac{2+\varepsilon_S}{3+\varepsilon_l+\varepsilon_S}} = m^{\frac{3}{4+\varepsilon_l}} = m^{\frac{3}{3+D_v}} \tag{27}$$

The apparent "dimension" of the reaction request for volume is $(4 + \varepsilon_l) > 4$, the dimension increases. According to $l \propto {L_0}^{1+\varepsilon_l}$ the measurable fractal dimension of the blood vessel network is $D_v = 1 + \varepsilon_l$. In this way the ε_l is

measurable by the fractal dimension of the vessel structures [53], for example, with the box-counting method [51]. When $D_v = 1.3$ [53], $\varepsilon_l = 0.3$, and the scaling exponent is $\alpha \cong 0.7 > 2/3$. The Microvessel Fractal Dimension (MFD) (which is equivalent with $(1 + \varepsilon_l)$ for renal cell carcinoma ranges between $1.30 - 1.66$ [54], and correlates well with the tumor Microvessel Density (MVD) [54]. From (27) we know, when $\varepsilon_l = 0.478$, the scaling exponent describes a non-fractal-like structure, $\alpha = 2/3$.

When the tumor growth is so intensive that the available length of the vessel network cannot deliver appropriate energy, then another possible deviation from the homeostatic self-organization happens. In this case, the volume of the delivered energy remains constant, which limits the energy supply. The tumor-growth turns to sigmoidal this stage [55], usually follows Weibull distribution due to the self-similar development [6]. This could happen in severe hypoxia, low oxygen saturation in blood, anemia, various hematological diseases. In this case, the volume of the supply follows the evolution-requested exponent of 4 ($\varepsilon_v = 1$) (23), in the self-similar conditions in [53], but the requested length and surface is not enough for the proper work, so $\varepsilon_l' > 1$ and $\varepsilon_s < 1$. The self-similar conditions differ from (22) due to (13):

$$\begin{matrix} l \propto {L_0}^{1+\varepsilon_l'} & s \\ \propto {L_0}^{3-\varepsilon_l'} & v \propto {L_0}^4 \end{matrix} \tag{28}$$

Consequently, at fixed four-dimensional volume, the metabolic surface reactions behave by power-law of suboptimal metabolic rate in this phase:

$$B_{so2} \propto m^{\frac{2+\varepsilon_S}{3+\varepsilon_l'+\varepsilon_S}} = m^{\frac{3-\varepsilon_l'}{4}} = m^{\frac{4-D_v'}{4}} \tag{29}$$

Here the volume "dimension" of the reaction request is 4, but the actual conditions are worse than optimal. The ε_l' again here also is measurable by the fractal dimension of the structures [56], in this case, the fractal dimension of the vessel system is $D_v' = 1 + \varepsilon_l'$. For example, measuring the vascular fractal dimension in one disease as $D_v' = 1.41$ [51], we use $\varepsilon_l' = 0.41$, so the scaling exponent is $\alpha = 0.65$. When $\varepsilon_l' = 0.28$ [56], the scaling exponent is $p = 0.68$. At $\varepsilon_l' = 0.33$, the scaling exponent is the well-known $\alpha = 2/3$.

The exponents of the active transport surface in the two suboptimal supplies

$$\alpha = \frac{3}{4+\varepsilon_l} = \frac{3}{3+D_v} \quad \text{and} \quad \alpha' = \frac{3-\varepsilon_l'}{4} = \frac{4-D_v'}{4} \tag{30}$$

Both these exponents are smaller than the optimal, and the exponent in the second phase of growth is the smallest (Figure 1).

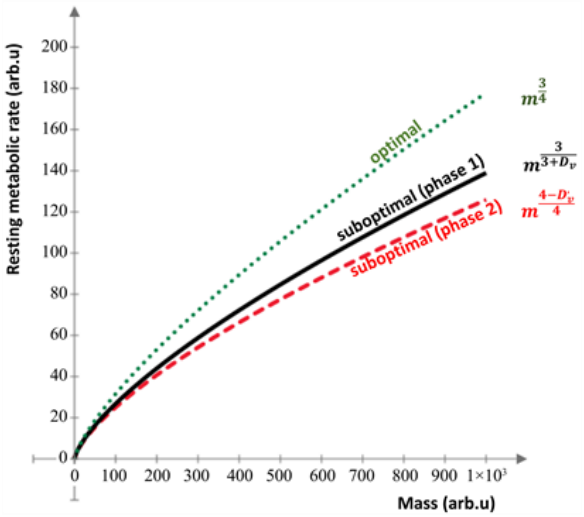

Figure 1. The allometric development with the various exponents. The initial phase of tumor growth is exponential, and the allometric scale follows the phase1 curve, while the intensive development further decreases the exponent, which turns to a sigmoid phase in a tumor-specific time.

Following the idea of "4-dimensionality", the volume dimension changes in α, while the active surface in α'. Both exponents are $\leq$ ¾because of the length fractal dimension > 1. The mechanisms which cause this modification are different. The same exponent could be only in Euclidean non-fractal case, when $D_v = D_v' = 1$. Due to $D_v < 3 \ and \ D_v' < 3$, hence $\alpha > 0.5 \ \ and \ \ \alpha' > 0.25$. The Mandelbrot calculated 2.7 for the fractal dimension of the arterial tree of the lung [57], which was supported by experiments later [58], the relevant changes are $\alpha \approx 0.526 \ \ and \ \ \alpha' \approx 0.325$. Both values are smaller than $\alpha = ⅔$.

Both non-optimal situations (defect of the length of transport way or limited transport against the demands) make the tissue under-energized, and the exponent of the power-relation scaling down-regulated. In such a way, measuring the scaling exponent of metabolism and the fractal dimension of the supplying microvessels have a diagnostic value about the actual deviations from normal.

4. Discussion

The optimal alimentation in a healthy system makes the energy distribution balanced, supplying all requirements of the homeostatic state. The exponent ¾ has a strong predominance on a theoretical and empirical basis [59] in healthy homeostatic basal metabolic activity. The ideal nutrition supply supports ontogenic growth. However, at least at larger sizes, the cancer growth never happens with an optimal nutrition supply; the cells compete intensively for the available energy sources.

The cancer is out of the overall homeostatic balance. The tumor development certainly has a higher energy supply due to its proliferation than its healthy counterpart needs. Due to the extra-large energy demand, the tumor development's alimentation in most cases is far from optimal, so the tumor is in a permanent energy deficiency. When the oxygen supply is limited, the first attempt to produce more ATP is the massive fermentative use of glucose, a simple and quick production mechanism. The cell extends its ATP production to fermentation by non-mitochondrial respiration, abandoning the more complicated Kerbs-cycle in the mitochondria [60].

While the mitochondrial metabolism is always aerobic, its scaling exponent is nearly $\alpha = ¾$ [30]. However, the scaling of metabolic activity is also different in mitochondrial and non-mitochondrial processes [61]. The metabolic power not only depends on the active surface of the transport but also on the transport rate at the same active surface size. Due to the transport modifications at the changed metabolic pathway, the deviation from the ¾ exponent could be remarkable. The allometric scaling exponent of fermentative processes decreases to nearly ⅔. This last scaling exponent shows that the cell-membrane directly regulates the

fermentation, and the surface/volume ratio controls the complete process, which could be anticipated from the direct linear dependence of the lactate production (V_L) on the glucose-intake ((V_G) with a slope of $\cong 1$ [45]:

$$\log(V_L) = +0.977 \log(V_G) + 0.108 \quad r^2 = 0.72 \quad p < 0.001 \tag{31}$$

while the bioscaling of the oxygen (V_{O_2}) and glucose (V_G) intake [45] are even lower than ⅔, −0.570, and −0.523, respectively.

Not only does the malignancy need an intensive extra metabolism. For example, the benthic invertebrates (n = 215) have the lowest average scaling exponent ($\alpha_{mean} = 0.63$, [near to ⅔], $CI_{mean} = 0.18$), which metabolizes in an anaerobic way [62]. No regulative factor exists when the cells are entirely independent, and the available alimentation is unlimited (like in most in vitro experiments). The metabolic rate is linearly proportional to the mass, so the exponent is $\alpha \cong 1$ [30].

The metabolic transformation of the cells [63] is one of the well-recognized hallmarks of malignancy [64] that has an emerging intensive interest in the field of oncology [65], as the core hallmark of cancer [66]. The adaptation of mitochondria in energy-limited conditions is the focus of the research [67]. The tumor forces the development of the angiogenetic processes [68] and overcomes the energy limitations. The vascularity is promoted [69], and the rapid development by intensive proliferation supports the changes of the scaling behavior [70]. Without extra angiogenesis (starting clusters), only the ready-made capacity of the delivery is available, so the tumor has a suboptimal alimentation. In the beginning, its fractal structure was developed, which is similar to the healthy structure, so the four-dimensional scaling remains valid (28).

When the tumor develops, the fractal structure of vascularity changes. Consequently, its fractal dimension changes too. The forced angiogenesis [68] tries to provide a sufficient supply to the hypoxic (insufficiently supported) tumor, and the structure changes rapidly, broadening the scaling exponent in a wide range [71]. The missing supply suppresses the scaling exponent, shown in (27). Still, the angiogenetic pool changes the trend, approaching linearity. The unlimited availability of nutrients for every cell realizes the linearity measured in vitro [48], limited to ~0.9 in vivo by insufficient oxygen transport [72]. However, the angiogenesis is usually not fast enough to supply the faster-growing larger tumors, so the inner part of the tumor becomes necrotic, forming a smaller living mass to supply, easing the energy distribution [68]. The essential message of the cases of insufficient alimentation from the calculations above is that when the fractal dimension of the supplying network grows, the scaling exponent decreases. The four-dimensionality and the allometry with the evolutional optimizing request are not the same approaches: further evolution conditions have a higher than four-dimensional allometric scaling. The tumor mass is a somewhat indefinite parameter because the whole environment of the tumor suffers from suboptimal alimentation. Consequently, we tried to find a more fundamental networking condition parameter published elsewhere [73].

There is a vast number of researches about the vascular development of the tumor progression, calculating the fractal dimension of the vascularity. The in silico modeling of the growing tumor vessel architecture in high-grade gliomas [74] shows that the fractal dimension is less than 1 in the avascular state and growing linearly by time, reaching $D_{t=2760h} \cong 1.2$ at $t = 2760h$, by slope approximately $\cong 6.2 \cdot 10^{-4}$. In a longer time, the development of the fractal dimension drastically changes, follows a less rapid development ($\text{slope} \cong 2.5 \cdot 10^{-4}$) until $D_{t=4000h} \cong 1.48$. We may assume that the fractal dimension 1.2 characterizes the finally developed vessel structure inside the tumor, followed by neo-angiogenetic processes reaching the tumor-surface, changing the vascular architecture, growing slower to the higher values of the fractal dimension.

In optimal alimentation, the allometric scaling shows exponent ¾ (24); which supposes the $l \propto {L_0}^1$, so the vascular fractal dimension in this case is $D_{va} = 1$. However $D_{va} > 1$ by the growing vessel network, so $\alpha <$

3/4 in the allometric scaling of tumor-vascularity due to the suboptimal energy supply, which triggers the angiogenesis. Using the results from in silico model-calculations, the internal

growth of the vessels have $(B_0)_{i1} \propto m^{\frac{2.8}{4}} = m^{0.700}$, or $(B_0)_{i2} \propto m^{\frac{3}{4.2}} = m^{0.714}$, according to the assumption of suboptimal alimentation by maximal metabolic rate (case 1) or by the metabolic rate forced four-dimensional "optimizing" concept (case 2). When the external angiogenesis is developing, the allometry changes: $(B_0)_{e1} \propto m^{\frac{2.52}{4}} = m^{0.63}$, and $(B_0)_{e2} \propto m^{\frac{3}{4.48}} = m^{0.67}$. So, the optimizing of the suboptimal energy availability in extended angiogenetic cases realizes the allometry, which fits the simple geometrical expectations $\alpha = 2/3$ well.

The measurements of vascular fractal dimensions in various tumors show a lower scaling exponent than the ideal ¾, depending on the conditions of the tumor-angiogenesis development. For example, when the epithelial-connective tissue interfaces with a malignant tumor in the oral mucosa, it is $D_{va} \geq 1.41$ [75], the scaling exponent in suboptimal alimentation situations in cases 1 and 2 are $\alpha \cong 0.64$ and $\alpha = 0.68$. The last one (optimal distribution of the suboptimally available energy) is near the "conventional" ⅔. Another microscopic evaluation of angio-structures [76] shows lower values of α, like the fractal dimension of the normal and malignant tissues are $D_{healthy} \cong 1.65$ and $D_{malignant} \cong 1.74$, respectively [77]; resulting in low α values. In other evaluations, the vascular structure's dimensionality grows to 1.9, which provides the maximal energy usage of the suboptimal alimentation, and the exponent became as low as $\alpha = 0.525$.

It is interesting to see the effect of various anti-tumor treatments on the vascular fractal dimension. The treatment changes the vascularization and suppresses the fractal dimension forms 1.135 1.037, 0.933, 0.982 by Photodynamic Therapy (PDT); Cysteine Proteases Inhibitors (CPI), combined therapy, PDT and CPI [78]; which corresponds in cases when the maximalizing of the energy-supply is equivalent to the allometric exponents of 0.716, 0.741, 0.767 and 0.755, respectively (the optimal distribution of the suboptimal availability would be 0.726, 0.743, 0.763, and 0.753). By treating VEGF165, the fractal dimension increases from 1.65 to 1.69, decreasing the allometric exponent [79] [80]. In matrigel inoculated human umbilical vein endothelial cells (HUVEC) treated by docetaxel, the fractal dimension of the vascular structure has decreased from 1.2 to 1.09, corresponding in case 1 $\alpha_{control} \cong 0.70$; $\alpha_{treated} \cong 0.73$,, and in case 2 $\alpha_{control} \cong 0.71$; $\alpha_{treated} \cong 0.73$ [81]. The fractal analysis is a successful and rather accurate method for monitoring the efficacy of angiogenic consequences of therapies [82].

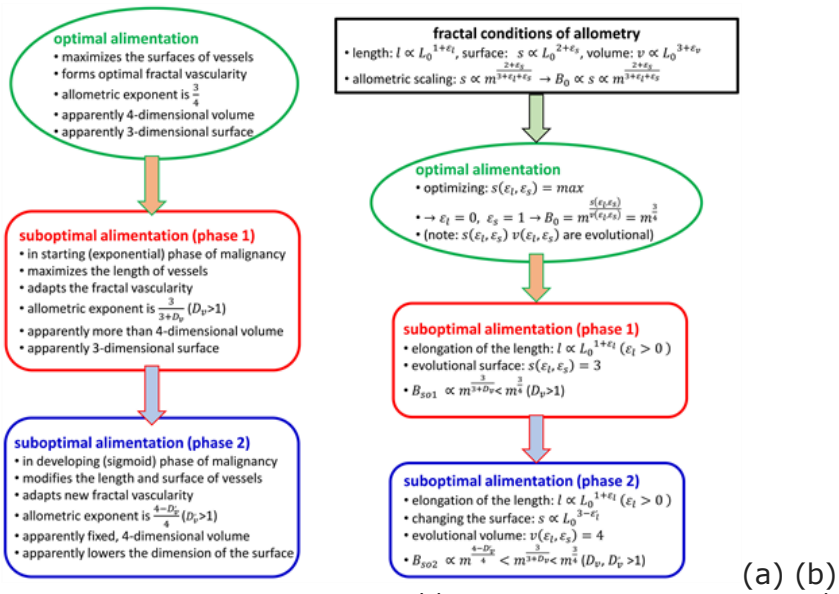

Figure 2. The summary of the structure of calculation. (a) The biophysical considerations (b) The mathematical description.

5. Summary

We had shown that the allometric relation of basal metabolic rate and the tumor mass depends on the fractal dimension of the vascular structure. Due to the desperate need for energy supply and the intensive proliferation of the malignant tumor, cancer does not have an optimal alimentation. Two strategies could distribute the available (not sufficient) energy by the main transport of it, the vascular network:

1) Assuming that the cell cluster tries to maximize its metabolic rate by the surface transports and lowers the scaling exponent from the value of ¾;

2) Accepting that in the case of a four-dimensional volumetric behavior limits the energy supply. The tumor optimizes the energy distribution in its volume in among these conditions.

The structure of the biophysical considerations and their mathematical steps are summarized in Figure 2 .

The two strategies in consequent phases of tumor growth optimize the available energy by different allometric scalings. The organized optimum of the suboptimal availability of energy gives lowered allometric scaling exponents.

Acknowledgements

This work was supported by the Hungarian National Research Development and Innovation Office PIACI KFI grant: 2019-1.1.1-PIACI-KFI-2019-00011.

Conflicts of Interest

The author declares no conflicts of interest regarding the publication of this paper.

References

[1] Barge, L.M., Branscomb, E., Brucato, J.R., Cardoso, S.S.S., Cartwright, J.H.E., Danielache, S.O., et al. (2017) Thermodynamics, Disequilibrium, Evolution: Far-From-Equilibrium Geological and Chemical Considerations for Origin-Of-Life Research. Origins of Life and Evolution of the Biospheres. The journal of the International Society for the Study of the Origin of Life, 47, 39-56. https://doi.org/10.1007/s11084-016-9508-z

[2] Goldenfeld, N. and Woese, C. (2011) Life Is Physics: Evolution as a Collective Phenomenon Far from Equilibrium. Annual Review of Condensed Matter Physics, 2, 375-399. https://doi.org/10.1146/annurev-conmatphys-062910-140509

[3] Schrodinger, E. (1944) What Is Life? The Physical Aspect of the Living Cell. Cambridge University Press, Cambridge.

[4] Glazier, D.S. (2008) Effects of Metabolic Level on the Body Size Scaling of Metabolic Rate in Birds and Mammals. Proceedings of the Royal Society B: Biological Sciences, 275, 1405-1410. https://doi.org/10.1098/rspb.2008.0118

[5] Szasz, O., Szigeti, G.P. and Szasz, A. (2017) On the Self-Similarity in Biologyical Processes. Open Journal of Biophysics, 7, 183-196. https://doi.org/10.4236/ojbiphy.2017.74014

[6] Szasz, O. and Szasz, A. (2020) Parametrization of Survival Measures, Part I: Consequences of Self-Organizing. International Journal of Clinical Medicine, 11, 316-347. https://doi.org/10.4236/ijcm.2020.115031

[7] Huxley, J.S. and Teissier, G. (1936) Terminology of Relative Growth. Nature, 137, 780-781. https://doi.org/10.1038/137780b0
[8] Huxley, J.S. (1932) Problems of Relative Growth. Book Review by C.H.K. in Gahan: New Parasitic Ilymenoplera, Lincoln Mac Veagh—The Dial Press, New York, 757.
[9] Newman, M.E.J. (2005) Power Laws, Pareto Distributions and Zipf's Law. Contemporary Physics, 46, 323-351. https://doi.org/10.1080/00107510500052444
[10] Mitzenmacher, M. (2004) A Brief History of Generative Models for Power Law and Lognormal Distributions. Internet Mathematics, 1, 226-251. https://doi.org/10.1080/15427951.2004.10129088
[11] Fisher, M.E. (1998) Renormalization Group Theory: Its Basis and Formulation in Statistical Physics. Reviews of Modern Physics, 70, 653-681. https://doi.org/10.1103/RevModPhys.70.653
[12] Barabasi, A. and Albert, R. (1999) Emergence of Scaling in Random Networks. Science, 286, 509-512. https://doi.org/10.1126/science.286.5439.509
[13] Chignola, R., Sega, M., Stella, S., Vyshemirsky, V. and Milotti, E. (2014) From Single-Cell Dynamics to Scaling Laws in Oncology. Biophysical Reviews and Letters, 9, 273-284. https://doi.org/10.1142/S1793048014300035
[14] Kauffman, S.A. (1992) The Origins of Order: Self-Organization and Selection. In: Varela, F.J. and Dupuy, J.P., Eds., Understanding Origin, Vol. 130, Springer, Dordrecht, 153-181. https://doi.org/10.1007/978-94-015-8054-0_8
[15] Walleczek, J. (Ed.) (2000) Self-Organized Biological Dynamics & Nonlinear Control. Cambridge Univesity Press, Cambridge.
https://doi.org/10.1017/CBO9780511535338
[16] Bassingthwaighte, J.B., Leibovitch, L.S. and West, B.J. (1994) Fractal Physiology. Springer, New York. https://doi.org/10.1007/978-1-4614-7572-9
[17] Deering, W. and West, B.J. (1992) Fractal physiology. IEEE Engineering in Medicine and Biology, 11, 40-46. https://doi.org/10.1109/51.139035
[18] Musha, T. and Sawada, Y., Eds. (1994) Physics of the Living State. IOS Press, Amsterdam.
[19] Fechner, G.T., Howes, D.H. and Boring, E.G., Eds. (1966) Elements of Psychophysics. Volume 1, Adler, H.E., Trans., Holt, Rinehart and Winston, New York.
[20] Mandelbrot, B.B. (1967) How Long Is the Coast of Britain? Statistical Self-Similarity and Fractional Dimension. Science, 156, 636-638. https://doi.org/10.1126/science.156.3775.636
[21] West, B.J. and West, D. (2012) Fractional Dynamics of Allometry. Fractional Calculus & Applied Analysis, 15, 70-96.
https://doi.org/10.2478/s13540-012-0006-3
[22] Huxley, J.S. (1932) Problems of Relative Growth. Johns Hopkins University Press, Methuen, London, 273.
[23] Kleiber, M. (1961) The Fire of Life: An Introduction to Animal Energetics. Wiley, New York.
[24] Savage, Van M., Allen, A.P., Brown, J.H., Gillooly, J.F., Herman, A.B., Woodruff, W.H. and West, G.B. (2007) Scaling of Number, Size, and Metabolic Rate of Cells with Body Size in Mammals. Proceedings of the National Academy of Sciences of the United States of America, 104, 4718-4723. https://doi.org/10.1073/pnas.0611235104
[25] Brown, J.H. and West, G.B., Eds. (2000) Scaling in Biology. Oxford University Press, Oxford.
[26] Mascaro, J., Litton, C.M., Hughes, R.F., Uowolo, A. and Schnitzer, S.A. (2014) Is Logarithmic Transformation Necessary in Allometry? Ten, One-Hundred, One-Thousand-Times Yes. Biological Journal of the Linnean Society, 111, 230-233. https://doi.org/10.1111/bij.12177
[27] West, D. and West, B.J. (2012) On Allometry Relations. International Journal of Modern Physics B, 26, Article ID: 1230010.
https://doi.org/10.1142/S0217979212300101
[28] Brown, J.H., West, G.B. and Enquis, B.J. (2005) Yes, West, Brown and Enquist's Model of Allometric Scaling Is Both Mathematically Correct and Biologically Relevant. Functional Ecology, 19, 735-738. https://doi.org/10.1142/S0217979212300101
[29] Calder III, W.A. (1984) Size, Function and Life History. Dover Publications Inc., Mineola, New York.
[30] West, G.B. and Brown, J.H. (2005) The Origin of Allometric Scaling Laws in Biology from Genomes to Ecosystems: Towards a Quantitative Unifying Theory of Biological Structure and Organization. Journal of Experimental Biology,

208, 1575-1592. https://doi.org/10.1242/jeb.01589
[31] West, B.J. (2006) Where Medicine Went Wrong: Rediscovering the Path to Complexity. Vol. 11, World Scientific Publishing Co. Pte. Ltd., New Jersey, London. https://doi.org/10.1142/6175
[32] West, B.J. (1990) Fractal Physiology and Chaos in Medicine. World Scientific, Singapore, London.
[33] White, C.R. and Seymour, R.S. (2003) Mammalian Basal Metabolic Rate Is Proportional to Body Mass2/3. Proceedings of the National Academy of Sciences of the United States of America, 100, 4046-4049. https://doi.org/10.1073/pnas.0436428100
[34] Moses, M.E., Hou, C., Woodruff, W.H., West, G.B., Nekola, J.C., Wenyun Zuo, et al. (2008) Revisiting a Model of Ontogenic Growth: Estimating Model Parameters from Theory and Data. American Naturalist, 171, 632-645. https://doi.org/10.1086/587073
[35] Kolokotrones, T., Savage, Van M., Deeds, E.J. and Fontana, W. (2010) Curvature in Metabolic Scaling. Nature, 464, 753-755. https://doi.org/10.1086/587073
[36] Dodds, P.S., Rothman, D.H. and Weitz, J.S. (2001) Re-Examination of the "3/4-Law" of Metabolism. Journal of Theoretical Biology, 209, 9-27. https://doi.org/10.1006/jtbi.2000.2238
[37] Milotti, E., Vyshemirsky, V., Stella, S., Dogo, F. and Chignola, R. (2017) Analysis of the Fluctuations of the Tumour/Host Interface. Physica A. Statistical Mechanics and its Applications, 486, 587-594. https://doi.org/10.1016/j.physa.2017.06.005
[38] West, G.B., Brown, J.H. and Enquist, B.J. (1999) The Four Dimension of Life: Fractal Geometry and Allometric Scaling of Organisms. Science, 284, 1677-1679. https://doi.org/10.1126/science.284.5420.1677
[39] West, G.B., Brown, J.H. and Enquist, B.J. (1997) A General Model for the Origin of Allometric Scaling Laws in Biology. Science, 276, 122-126. https://doi.org/10.1126/science.276.5309.122
[40] Labra, F.A., Marquet, P.A. and Bozinovic, F. (2007) Scaling Metabolic Rate Fluctuations. Proceedings of the National Academy of Sciences of the United States of America, 104, 10900-10903. https://doi.org/10.1073/pnas.0704108104
[41] West, G.B., Woodruff, W.H. and Brown, J.H. (2002) Allometric Scaling of Metabolic Rate from Molecules and Mitochondria to Cells and Mammals. Proceedings of the National Academy of Sciences of the United States of America, 99, 2473-2478. https://doi.org/10.1073/pnas.012579799
[42] Guiot, C., Delsanto, P.P.P., Carpinteri, A., Pugno, N., Mansury, Y. and Deisboeck, T.S. (2006) The Dynamic Evolution of the Power Exponent in a Universal Growth Model of Tumors. Journal of Theoretical Biology, 240, 459-463. https://doi.org/10.1016/j.jtbi.2005.10.006
[43] Puliafito, A., Primo, L. and Celani, A. (2017) Cell-Size Distribution in Epithelial Tissue Formation and Homeostasis. Journal of The Royal Society Interface, 14, Article ID: 20170032. https://doi.org/10.1098/rsif.2017.0032
[44] Egeblad, M., Nakasone, E.S. and Werb, Z. (2010) Tumors as Organs: Complex Tissues That Interface with the Entire Organism. Developmental Cell, 18, 884-901. https://doi.org/10.1016/j.devcel.2010.05.012
[45] Kallinowski, F., Schlenger, K.H., Runkel, S., Kloes, M., Stohrer, M., Okunieff, P. and Vaupel, P. (1989) Blood Flow, Metabolism, Cellular Microenvironment, and Growth Rate of Human Tumor Xenografts. Cancer Research, 49, 3759-3764.
[46] Guiot, C., Degiorgis, P.G, Delsanto, P.P., Gabriele, P. and Deisboeck, T.S. (2003) Does Tumor Growth Follow a "Universal Law"? Journal of Theoretical Biology, 225, 147-151. https://doi.org/10.1016/S0022-5193(03)00221-2
[47] Moatemed, F., Sahimi, M. and Naeim, F. (1998) Fractal Dimension of the Bone Marrow in Metastatic Lesions. Human Pathology, 29, 1299-1303. https://doi.org/10.1016/S0046-8177(98)90261-1
[48] West, G.B. and Brown, J.H. (2004) Life's Universal Scaling Laws. Physics Today, 57, 36-44. https://doi.org/10.1063/1.1809090
[49] West, G.B., Brown, J.H. and Enquist, B.J. (2001) A General Model for Ontogenic Groth. Nature, 413, 628-631. https://doi.org/10.1038/35098076

[50] Makarieva, A.M., Nefiodov, A.V. and Li, B.-L. (2020) Life's Energy and Information: Contrasting Evolution of Volume versus Surface-Specific Rates of Energy Consumption. Entropy, 22, Article No. 1025. https://doi.org/10.3390/e22091025
[51] Baish, J.W. and Jain, R.K. (2000) Fractals and Cancer. Cancer Research, 60, 3683-3688.
[52] Tubiana, M. (1989) Tumor Cell Proliferation Kinetics and Tumor Growth Rate. Acta Oncologica, 28, 113-121. https://doi.org/10.3109/02841868909111193
[53] Gazit, Y. (1996) Fractal Vasculature and Vascular Network Growth Modeling in Normal and Tumor Tissue. PhD Thesis, Massachusetts Institute of Technology, Cambridge, MA.
[54] Sabo, E., Boltenko, A., Sova, Y., Stein, A., Kleinhaus, S. and Resnick, M.B. (2001) Microscopic Analysis and Significance of Vascular Architectural Complexity in Renal Cell Carcinoma. Clinical Cancer Research, 7, 533-537.
[55] Herman, A.B., Savage, V.M. and West, G.B. (2011) A Quantitative Theory of Solid Tumor Growth, Metabolic Rate and Vascularization. PLoS ONE, 6, e22973. https://doi.org/10.1371/journal.pone.0022973
[56] Bauer, W. and Mackenzie, C.D. (1995) Cancer Detection via Determination of Fractal Cell Dimension. arXiv:patt-sol/9506003.
[57] Mandelbrot, B.B. and Wheeler, J.A. (1983) The Fractal Geometry of Nature. American Journal of Physics, 51, 286-287.
https://doi.org/10.1119/1.13295
[58] Huang, W., Yen, R.T., McLaurine, M. and Bledsoe, G. (1996) Morphometry of the Human Pulmonary Vasculature. Journal of Applied Physiology, 81, 2123-2133. https://doi.org/10.1152/jappl.1996.81.5.2123
[59] Savage, Van M., Gillooly, J.F., Woodruff, W.H., West, G.B., Allen, A.P., Enquist, B.J. and Brown, J.H. (2014) The Predominance of Quarter-Power Scaling in Biology. Functional Ecology, 18, 257-282. https://doi.org/10.1111/j.0269-8463.2004.00856.x
[60] Szigeti, G.P., Szasz, O. and Hegyi, G. (2017) Connections between Warburg's and Szentgyorgyi's Approach about the Causes of Cancer. Journal of Neoplasm, 1, 1-13.
[61] Voet, D., Voet, J.G. and Pratt, C.W. (2006) Fundamentals of Biochemistry. 2nd Edition, John Wiley and Sons, Inc., Hoboken, 547, 556.
[62] Pamatmat, M.M. (2005) Measuring Aerobic and Anaerobic Metabolism of Benthic Infauna under Natural Conditions. Journal of Experimental Zoology, 228, 405-413. https://doi.org/10.1002/jez.1402280303
[63] Costello, L.C. and Franklin, R.B. (2006) Tumor Cell Metabolism: The Marriage of Molecular Genetics and Proteomics with Cellular Intermediary Metabolism; Proceed with Caution! Molecular Cancer, 5, Aticle No. 59. https://doi.org/10.1186/1476-4598-5-59
[64] Warburg, O. (1956) On the Origin of Cancer Cells. Science, 123, 309-314. https://doi.org/10.1126/science.123.3191.309
[65] Jeon, S.-M. and Hay, N. (2018) Expanding the Concepts of Cancer Metabolism. Experimental & Molecular Medicine, 50, 1-3.
https://doi.org/10.1038/s12276-018-0070-9
[66] Ward, P.S. and Thompson, C.B. (2012) Metabolic Reprogramming: A Cancer Hallmark Even Warburg Did Not Anticipate. Cancer Cell, 21, 297-308. https://doi.org/10.1016/j.ccr.2012.02.014
[67] Hand, S.V. and Menze, M.A. (2008) Commentary Mitochondria in Energy-Limited States: Mechanisms That Blunt the Signaling of Cell Death. The Journal of Experimental Biology, 211, 1829-1840. https://doi.org/10.1242/jeb.000299
[68] Szasz, O., Vincze, G., Szigeti, G.P., Benyo, Z. and Szasz, A. (2018) An Allometric Approach of Tumor-Angiogenesis. Medical Hypotheses, 116, 74-78. https://doi.org/10.1016/j.mehy.2018.03.015
[69] Tannock, I.F. (1968) The Relation between Cell Proliferation and the Vascular System in a Transplanted Mouse Mammary Tumour. British Journal of Cancer, 22, 258-273. https://doi.org/10.1038/bjc.1968.34
[70] Milotti, E., Vyshemirsky, V., Sega, M. and Chignola, R. (2012) Interplay between Distribution of Live Cells and Growth Dynamics of Solid Tumours. Scientific Reports, 2, Article No. 990. https://doi.org/10.1038/srep00990
[71] Milotti, E., Vyshemirsky, V., Sega, M. and Chignola, R. (2013) Metabolic Scaling in Solid Tumours. Scientific Reports, 3, Article No. 1938. https://doi.org/10.1038/srep01938

[72] Painter, P.R. (2005) Allometric Scaling of the Maximum Metabolic Rate of Mammals: Oxygen Transport from the Lungs to the Heart Is a Limiting Step. Theoretical Biology and Medical Modelling, 2, Article No. 31. https://doi.org/10.1186/1742-4682-2-31

[73] Szasz, O. and Szigeti, Gy.P. (2020) Allometric Scaling by the Length of the Circulatory Network. Frontiers in Physiology Fractal and Network Physiology. (Under Review)

[74] Shim, E.B., Kim, Y.S. and Deisboeck, T.S. (2007) 2D FEM Tumor Angiogenesis Model 1 Analyzing the Dynamic Relationship between Tumor Growth and Angiogenesis in a Two Dimensional Finite Element Model. https://arxiv.org/ftp/q-bio/papers/0703/0703015.pdf

[75] Landini, G. and Rippin, J.W. (1993) Fractal Dimensions of the Epithelial-Connective Tissue Interfaces in Premalignant and Malignant Epithelial Lesions of the Floor of the Mouth. Analytical and Quantitative Cytology and Histology, 15, 144-149.

[76] McDonald, M.D. and Choyke, P.L. (2003) Imaging of Angiogenesis from Microscope to Clinic. Nature Medicine, 9, 713-725.
https://doi.org/10.1038/nm0603-713

[77] Ichim, L. and Dobrescu, R. (2013) Characterization of Tumor Angiogenesis Using Fractal Measures. 19th International Conference on Control Systems and Computer Science, Bucharest, 29-31 May 2013, 345-349. https://doi.org/10.1109/CSCS.2013.18
https://www.researchgate.net/publication/261092279

[78] Jurczyszyn, K., Osiecka, B.J. and Ziolkowski, P. (2012) The Use of Fractal Dimension Analysis in Estimation of Blood Vessels Shape in Transplantable Mammary Adenocarcinoma inWistar Rats after Photodynamic Therapy Combined with Cysteine Protease Inhibitors. Computational and Mathematical Methods in Medicine, 2012, Article ID: 793291. https://doi.org/10.1155/2012/793291

[79] Avakian, A., Kalina, R.E., Sage, E.H., Rambhia, A.H., Elliott, K.E., Chuang, E.L., Clark, J.I., Hwang, J.N. and Parsons-Wingerter, P. (200) Fractal Analysis of Region-Based Vascular Change in the Normal and Non-Proliferative Diabetic retina. Current Eye Research, 24, 274-280. https://doi.org/10.1076/ceyr.24.4.274.8411

[80] Parsons-Wingerter, P., Chandrasekharan, U.M., McKay, T.L., Radhakrishnan, K., DiCorleto, P.E., Albarran, B. and Farr, A.G. (2006) A VEGF165-Induced Phenotypic Switch from Increased Vessel Density to Increased Vessel Diameter and Increased Endothelial NOS Activity. Microvascular Research, 72, 91-100. https://doi.org/10.1016/j.mvr.2006.05.008

[81] Guidolin, D., Vacca, A., Nussdorfer, G.G. and Ribatti, D. (2004) A New Image Analysis Method Based on Topological and Fractal Parameters to Evaluate the Angiostatic Activity of Docetaxel by Using the Matrigel Assay in Vitro. Microvascular Research, 67, 117-124. https://doi.org/10.1016/j.mvr.2003.11.002

[82] Mancardi, D., Varetto, G., Bucci, E., Maniero, F. and Guiot, C. (2008) Fractal Parameters and Vascular Networks: Facts & Artifacts. Theoretical Biology and Medical Modelling, 5, Article No. 12. https://doi.org/10.1186/1742-4682-5-12

Allometric Scaling by the Length of the Circulatory Network

Andras Szasz

Department of Biotechnics, St. Istvan University, Budaörs, Hungary

* Correspondence: Szasz.Andras@gek.szie.hu

Cite this article as:
Szasz, A. (2021): Allometric Scaling by the Length of the Circulatory Network. Open Journal of Biophysics, 11, 359-370.
https://doi.org/10.4236/ojbiphy.2021.114013

Oncothermia Journal 31, 2022 March: 147-158
www.oncotherm.com/sites/oncotherm/files/2022-03/Szasz_Allometric.pdf
.

Abstract
Background: Allometric scaling is a well-known research tool used for the metabolic rates of organisms. It measures the living systems with fractal physiology. The metabolic rate versus the mass of the living species has a definite scaling and behaves like a four-dimensional phenomenon. The extended investigations focus on the mass-dependence of the various physiological parameters. **Objective:** Proving the length of vascularization is the scaling parameter instead of mass in allometric relation. **Method:** The description of the energy balance of the ontogenic growth of the tumor is an extended cell-death parameter for studying the mass balance at the cellular level. **Results:** It is shown that when a malignant cellular cluster tries to maximize its metabolic rate, it changes its allometric scaling exponent. A growth description could follow the heterogenic development of the tumor. The mass in the allometric scaling could be replaced by the average length of the circulatory system in each case. **Conclusion:** According to this concept, the dependence of the mass in allometric scaling is replaced with a more fundamental parameter, the length character of the circulatory system. The introduced scaling parameter has primary importance in cancer development, where the elongation of the circulatory length by angiogenesis is in significant demand.

Keywords
Allometry, Metabolism, Four-Dimension, Optimization, Cancer, Circulatory System, Characteristic Length

1. Introduction

The spatiotemporal organization of biosystems is complex. The complexity is driven by self-organization ([1] [2] [3]), and validated by new science: fractal physiology ([4] [5]), including the bioscaling processes ([6] [7]). Understanding the challenges of the complexity of human medicine requires the development of a new paradigm [8].

The Basal Metabolic Rate (BMR) shows allometric scaling of the mass of the organism [9], describes as the power function of the mass ($\mathcal{M}$) [10]:

$$BMR \propto \mathcal{M}^{\alpha} \tag{1}$$

The allometric relation connects the surface-controlled metabolic processes with the geometry of the given material, which uses the available energy. In the simple formulation, metabolic processes are surface-dependent, while the mass is proportional to the volume. Therefore, the exponent of their ratio mirrors the dimensionality, and consequently, the exponent is $\alpha = ⅔$. On the other hand, the complex living allometry shows the exponent as $\alpha = ¾$ instead of $\alpha = ⅔$ [11], explaining the relationship between the three-dimensional surface and the four-dimensional volume. Metabolic scaling in solid tumors is significant, but its heterogeneity and its rapid development by intensive proliferation and the supporting vascularity [12] change the scaling behavior [13], and this is described as dynamic evolution [14].

Life in this context is "four-dimensional" based on its metabolic exchange processes [15]. The self-organized multicellular structure creates fractal arrangements, and their metabolic energy-exchange proceeds on fractal surfaces, maximizing the available energy-consumption, scaling the fluctuation of the metabolic power by the universal scaling law [16]. This optimization of energy consumption was rigorously tested in the context of the scaling idea and can be extended to broader mechanisms [17], such as the energy-consumption's subcellular level, including the mitochondria and respiratory complexes [17].

The scaling model has been shown to be valid in a broad category of living structures and processes. The primary physiological parameters exponentially depend on the mass of the body [18]. The allometry shows a structural, geometrical constraint for living organisms. Nevertheless, life is more complex than what can be determined by its geometrical structure. A self-similar spatial-temporal-fractal structure defines the self-organizing procedure both in space and time [19]. A particular noise (temporal fractal noise)—like a fingerprint of the self-organizing [20] —is a typical and general behavior of the living biomaterial [21]. The stochastic fluctuations have a characteristic effect on malignant development [22], acting in the apoptotic threshold of cancer [23], and is well observable in the growth process [24].

The measured structural patterns could be applied to evaluate the cancer development [25] [26], an example of this is the use of image analysis is done by a pathologist. The metabolic power not only depends on the size of the surface involved in active transport, but also on the flow-rate of the same active surface size. This dependence could modify the transport. In the case of Benthic invertebrates (n=215), they have the lowest average scaling exponent because they metabolize in an anaerobic way. This can be written as: ($\alpha_{mean} = 0.63$, [near to ⅔], $CI_{mean} = 0.18$), where α is the scaling exponent, and CI is the Confidence Interval [27]. However, the other studied animals (n=496) have ($\alpha_{mean} = 0.74$, [near to $\alpha_{mean} = ¾$], $CI_{mean} = 0.18$) [28]. The scaling of the metabolic activity is also different in mitochondrial and non-mitochondrial processes [29]. Mitochondrial metabolism is always aerobic, and its scaling exponent is nearly $\alpha = ¾$ [30] [31]. When the oxygen supply is limited, the cell extends its ATP production to fermentation by non-mitochondrial respiration, where the allometric scaling exponent lowers to nearly $\alpha = ⅔$.

Based on the scaling theory, a general model for ontogenic growth has been proposed [32] [33] [34]. Allometry is a consequence of the evolution process [35]. The variation of the personal sizes of the organs and the whole body of the individuals can be addressed in the frame of the power-law. The high fractal dimension could be used as a significant prognostic factor in diseased tissues [36]. There is research on tumor growth evaluated from an ontogenic basis [14] [37] [38] in which the tumor is successfully described, despite the substantial heterogeneity of the blood-supply [39] and the cellular structures differing from their regular counterparts. If the whole tumor mass differs from the mass of the viable part of the tumor, and the viable part has a scaling by the complete tumor mass with a high confidence scaling exponent $\alpha = 0.78$ then the inadequate metabolic supply causes an extension of the nectrotic tissue inside advanced tumors [40].

2. Method

The general model for ontogenic growth described tumor-cell growth needs to calculate the cell-production considering also the vanished cells in the energy balance [40]. We learned, however, how vital programmed cell-death (apoptosis) is in the development of the fetus of mammals [41], and we considered it as a basic biological phenomenon [42]. The concept of cell-death is crucial in cancer development, considering one of the hallmarks of the malignancy is its escape from apoptosis [43], and is instead more susceptible to a more drastic kind of death: necrosis [44]. Following the line and extensive discussion of numerous other authors [28] [30] [32] [33] [34], who adapted the death-free energy balance from the original [45] publication, we extended this view with the changes caused by the perished cells. This approach became even more relevant with the study of malignancies, where a large mass of the tumor could well involve non-living necrotic tissue, so the ontogenic calculations [37] [40] need modification based on their energy-balance.

The number of cancerous cells (N_c) is the difference between the newly produced cells (P), and the perished (due to apoptosis or necrosis) drop off cells (D) at the unit time, basically follow the method of [40]:

$$\frac{dN_c}{dt} = P - D \qquad (2)$$

The value of the changing cells is zero, while production just equal to the perished cells (P=DP=D). It is a realistic assumption that the perished cells are proportional to the complete cell number in unit time:

$$D = \lambda N_c \tag{3}$$

where λ is the cell death-rate in a tumor. Note, at the beginning of the tumor-growth the P is also proportional with N_c, $(P = \xi N_c)$ and in this case, the tumor growth exponentially: $N_{c(0)}(t) = \exp(\xi - \lambda)t$. When P is constant during the development, the balance of the cell number by the time:

$$\frac{dN_c}{dt} = P - \lambda N_c \tag{4}$$

The $P = const$ deviates from the assumption of [40]. Our consideration concentrates on the fact that the cellular production after the initial period of growth became constant due to the stabilized balance of the resources and the autonomic growth of cells in a supporting healthy host environment by resources. The situation in this phase is well similar to the in-vitro experiments of the monoculture system when the allometric exponent is zero [31]. The energy balance is determined by the transported energy-flux delivered by the bloodstream. The energy-transport current intensity, the metabolic rate (B), is divided into two parts: one produces new cells, while the other keeps the living set alive. Hence:

$$B = N_c B_c + E_c P = N_c B_c + E_c \left(\frac{dN_c}{dt} + \lambda N_c\right) = \\ = N_c B_c + E_c \left(\frac{dN_c}{dt} + \frac{N_c}{T_c}\right) \tag{5}$$

where B_c is the metabolic rate of a cell, and E_c is the necessary metabolic energy to create a new cell and $\lambda^{-1} = T_c$ c is the average lifespan of a cell in the tumor. Consequently:

$$E_c \frac{dN_c}{dt} = B - N_c(B_c + \lambda E_c) \tag{6}$$

Metabolic energy can be scaled by exponent α,

$$B = B_0 N_c^{\propto}, \tag{7}$$

where B_0 is a normalizing factor that shows the metabolic rate in the unity of N_c. Therefore, we obtain:

$$E_c \frac{dN_c}{dt} = B_0 N_c^{\propto} - N_c(B_c + \lambda E_c) \tag{8}$$

Hence:

$$\frac{dN_c}{dt} = a_c {N_c}^{\propto} - b_c N_c \tag{9}$$

$$a_c = \frac{B_0}{E_c}; \qquad b_c = \frac{B_c}{E_c} + \lambda$$

By multiplying N_c by the average mass of a single cell (m_c) we now obtain the energy-balance for the full tumor-mass (m):

$$\frac{dm}{dt} = am^{\propto} - bm \tag{10}$$

where:

$$a = \frac{B_0 {m_c}^{1-\propto}}{E_c} \tag{11}$$

and

$$b = \frac{B_c}{E_c} + \lambda = \frac{B_c}{E_c} + \frac{1}{T_c}$$

This balance was previously similarly formulated [46]. The mass has a maximum limit M, asymptotic value, a saturation when no more real changes of the mass can be observed, so:

$$0 = \frac{dM}{dt} = aM^{\propto} - bM \tag{12}$$

Consequently:

$$M = \left(\frac{a}{b}\right)^{\frac{1}{1-\propto}} = \left(\frac{B_0 {m_c}^{1-\propto}}{B_c + \lambda E_c}\right)^{\frac{1}{1-\propto}} \tag{13}$$

3. Results

A death parameter of the single-cell characteristically appears in the energy-balance of the ontogenic growth of the tumor. The nutrients supply profoundly determines the death of cancer-cells. At least at larger tumor sizes, the cell growth never happens with optimal nutrition supply; the cells intensively compete for the available energy sources.

The exponent α is located in the interval $⅔ \leq \alpha \leq 1$, and it is $\alpha = ¾$ at ideal basal conditions [15] [45]. The ideal nutrition supply supports ontogenic growth. The "ideal" asymptotic mass (M_{id}) from (13) is: $M_{id} = \left(\frac{a}{b}\right)^4$, hence the BMR* in non-ideal conditions:

$$M = \left(\frac{a}{b}\right)^{\frac{1}{1-\propto}} = (M_{id})^{\frac{1}{4(1-\propto)}} \implies BMR^* = M^{\alpha} = (M_{id})^{\frac{\alpha}{4(1-\propto)}} \tag{14}$$

Substituting (14) into (10):

$$\frac{dm}{dt} = am^{\propto}\left(1 - \left(\frac{m}{M}\right)^{1-\propto}\right) \tag{15}$$

So:

$$\frac{d\left(\frac{m}{M}\right)^{1-\propto}}{dt} = \frac{a(1-\propto)}{M^{1-\propto}}\left(1 - \left(\frac{m}{M}\right)^{1-\propto}\right) \tag{16}$$

which has a sigmoidal solution:

$$\left(\frac{m}{M}\right)^{1-\propto} = 1 - \left(1 - \left(\frac{m_0}{M}\right)^{1-\propto}\right) e^{-\frac{a(1-\propto)t}{M^{1-\propto}}} = 1 - exp\left(-\frac{at(1-\propto)}{M^{1-\propto}} + ln\left(1 - \left(\frac{m_0}{M}\right)^{1-\propto}\right)\right) = 1 - e^{-\tau} \quad (17)$$

where

$$\tau = \frac{at(1-\propto)}{M^{1-\propto}} - ln\left(1 - \left(\frac{m_0}{M}\right)^{1-\propto}\right) \quad (18)$$

and m_0 is the mass at the start of a tumor (probably a few times m_c), the initial (just born) mass. The ratio (r) of the energy spent on keeping cells alive ($\lambda = 0$) from (13) is:

$$r(\tau) = \frac{N_c B_c}{B} = \frac{B_c m}{m_c B_0 m^{\propto}} = \frac{b}{a} m^{1-\propto} = \left(\frac{m}{M}\right)^{1-\propto} = 1 - e^{-\tau} \quad (19)$$

Using α = ¾ for the ideal four-dimensional case, the solution is:

$$\left(\frac{m}{M}\right)^{\frac{1}{4}} = 1 - e^{-\tau}, \qquad \tau = \frac{at}{4M^{\frac{1}{4}}} - ln\left(1 - \left(\frac{m_0}{M}\right)^{\frac{1}{4}}\right) \quad (20)$$

This is formally the universal growth law [45], but has a difference in the values of b (see (11)) and M (see (13)), including the average life-time of the malignant cells (death rate λ) in ontology description. The M value became smaller by shortening the average life-time of the cells and elongating τ time approaching the saturatin of the mass.

4. Discussion

The four-dimensionality and the allometry with evolutional optimization require different approaches: as the evolutionary conditions have a higher than a four-dimensional allometric scaling. The tumor mass is a somewhat indefinite parameter because the whole environment of the tumor suffers from sub-optimal alimentation. Consequently, the mass does not describe the allometry well. A more fundamental parameter of the networking conditions is requested.

From the original "four-dimensional life" fractal concept, we get scaling of the characteristic volume (v) with a characteristic length (l) [15] [45]:

$$v = kl^4 \quad (21)$$

where k is a constant.

When the mass density of the tumor is relatively homogeneous, we assume proportional relation between the mass and volume:

$$m \propto v \quad (22)$$

When l_0 is the average asymptotic length of the circulatory network of the organ, and M is the asymptotic mass, from (21) and (22) with other K constant:

$$M = K{l_0}^4 \tag{23}$$

Consequently, from (23) and (21), we obtain:

$$r = \left(\frac{m}{M}\right)^{\frac{1}{4}} = \left(\frac{Kl^4}{Kl_0^4}\right)^{\frac{1}{4}} = \frac{l}{l_0} \tag{24}$$

The fourths-root of the relative mass growth to the asymptotic value (the relative basal metabolic rate) corresponds to the relative ratio of the length of the circulatory network. The geometrical parameter of the vascularity offers a more evident intrinsic factor than the mass. The length looks essential in the allometric relations.

From (20) and (24) the geometric growth rate is obtained, where a universal law can describe the average relative length of the circulatory network:

$$r(\tau) = 1 - e^{-\tau} \qquad \tau = \frac{at}{4M^{\frac{1}{4}}} - ln(1 - r_0) \tag{25}$$

where $r_0 = \left(\frac{m_0}{M}\right)^{1/4}$. The ratio of the energy maintaining new cells is $R(\tau) = (1 - r(\tau)) = e^{\tau}$. Assuming the average density of the cancerous cell colony in the experiments of Bru et al. [47], the scaling law could be determined by the characteristic lengths, which are (at $\alpha = ¾$, [45]), $m \propto \mathrm{L}^4$ in ideal cases, consequently:

$$r(\tau) = \left(\frac{m}{M}\right)^{1-\propto} = \left(\frac{L^4}{L_0^4}\right)^{\frac{1}{4}} = \frac{L}{L_0} = 1 - e^{-\tau} \tag{26}$$

where L_0 is the asymptotic size of the cancer-cell cluster. It is naturally assumed that $L_0 \gg L$, then from equation (17) the Taylor expansion of τ could be truncated at its second term, so (26) will be the linear dependence as measured:

$$L(t) \cong \frac{a}{4K}t - L_0\, ln\left(1 - \frac{L(\tau=0)}{L_0}\right) \tag{27}$$

However, if the energy supply is not ideal (which is the case in almost all the developed tumors in-vivo), the results do not support the ideal scaling by $\alpha = ¾$ [38]. It is shown in a generalized model that the fractal surface and the covered volume are scaled rigorously [48].

In cases of sub-optimal alimentation (there is an energy-deficiency for optimal growth), the scaling-exponent changes, and it depends on the fractal dimension of the vascular network (D_v) [48]. The shortage of energy for adequate alimentation is a usual condition for the rapidly proliferating structures. Two strategies can be followed to distribute the available (sub-optimal) energy resources: maximizing the metabolism on the surface of the cells. The elongation of the vascular network (angiogenesis) is the optimal strategy in this growing phase of the tumor ($\alpha_1 = \frac{3}{3+D_{v1}}$) [49]. The optimizing strategy could change in the advanced stages when the blood volume is limited despite the elongated vascular possibilities. In the advanced cases, the energy-distribution

request a $\alpha_2 = \frac{4-D_{v2}}{4}$ exponent ($\alpha_2 < \alpha_1,\ D_v > 1$) [49]. The growth of the mass would be in these cases (as described by (16)):

$$\frac{dm_{max}^{(1)}}{dt} = \frac{aD_{v1}}{(3+D_{v1})M^{\frac{D_{v1}}{3+D_{v1}}}}\left(1-\left(\frac{m}{M}\right)^{\frac{D_{v1}}{3+D_{v1}}}\right) \tag{28}$$

and

$$\frac{dm_{max}^{(2)}}{dt} = \frac{aD_{v2}}{4M^{\frac{4-D_{v2}}{4}}}\left(1-\left(\frac{m}{M}\right)^{\frac{4-D_{v2}}{4}}\right) \tag{29}$$

The generalized form of relation (25) could be used in $\alpha_2 < \alpha_1,\ (D_{v1},\ D_{v2} > 1)$exponents, when the allometry exponent is α. The phase 1 and phase 2 stages of tumors had been studied by various publications [49] [50] [51]. We choose two characteristic values to demonstrate the differences, D_{v1} =1.28 and D_{v2} =1.52.

The time development well shows the different saturation time of the processes with various exponents (Figure 1).

The mass and the characteristic length are strictly connected:

$$m_{max}^{(1)} = Kl^{\frac{3+D_v}{D_v}} \quad and \quad m_{max}^{(2)} = Kl^{\frac{4-D_v}{4}} \tag{30}$$

In general:

$$M = Kl_0^{\frac{1}{1-\alpha}} \tag{31}$$

and therefore:

$$r = \left(\frac{m_{max}}{M}\right)^{1-\alpha} = \frac{l}{l_0} \tag{32}$$

For optimal distribution, we get the exact same result:

$$r = \left(\frac{m_{opt}}{M}\right)^{1-\alpha} = \frac{l}{l_0} \tag{33}$$

The limited nutrition, the energetic control of the tumor could be considered as a part of the controlled therapy [52]. If the cell culture were to be placed on the tumour region, and the cell culture had the same or higher demands as the tumour tissue, then it could successfully compete against the cancer cells supplied from the same sources of energy. These in-silico results have not yet been verified experimentally, they are expected in the future.

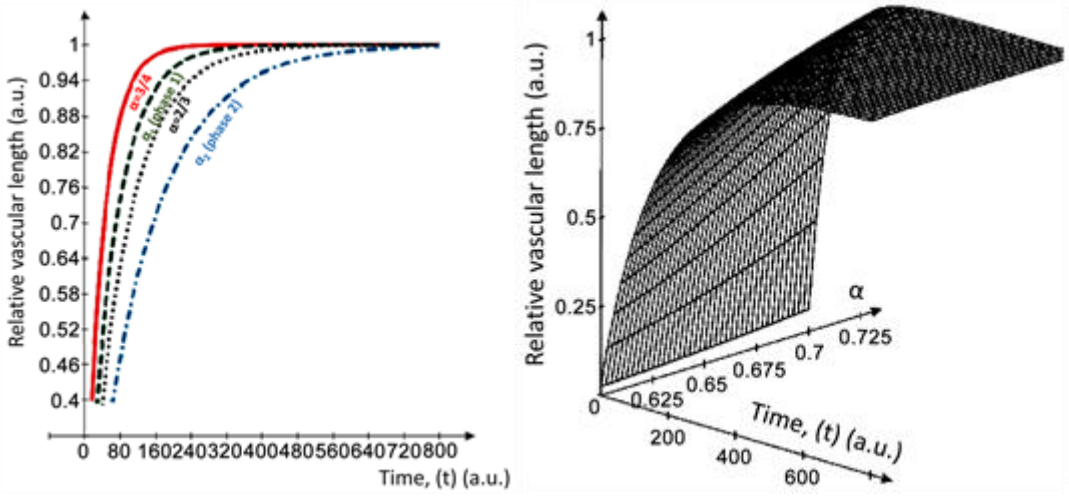

Figure 1. Development of the relative length in time of vascular structure in a tumor at various allometric exponents: the normal, tumor-free tissue $\alpha = ¾$ (solid line) and in the Euclidean geometrical construction $\alpha = ⅔$ (dotted line). The saturation time to reach the final length increases by the decreasing of the vascular fractal-dimension, ($\propto_1 = 0.701$, dashed line; and $\propto_2 = 0.62$, dash-dotted line). The chosen sample parameters: $m_0 = 1\ a.u.$. and $M = 1000\ a.u.$

5. Conclusions

The mass change to the more fundamental length of the vascular network in allometric scaling is generally proven in optimal metabolic conditions. We had shown the application in two basic kinds of non-optimal alimentation processes, too.

We proved that allometric scaling could eliminate the mass and an entirely intrinsic parameter, the average relative length of the circulatory network. The allometric model by the length directly connects the metabolic energy intake of the tumor with the length of the vascular system, as a supplier of energy. The derivation of the equations is rather general because the obtained fractal dimensions are model-independent. We regard the vascular length as more fundamental than the mass because the tumor volume is usually indefinitely smeared out, having a gradient formed by the mix of the precancerous and host cells. Hence, the fractal determination of the vascular network gives a more precise solution for allometric relations.

Acknowledgements

This work was supported by the Hungarian National Research Development and Innovation Office PIACI KFI grant: 2019-1.1.1-PIACI-KFI-2019-00011.

Conflicts of Interest

The author declares no conflicts of interest regarding the publication of this paper.

References

[1] Sornette, D. (2000) Chaos, Fractals, Self-Organization and Disorder: Concepts and Tools. Springer Verlag, Berlin.

[2] Walleczek, J. (2000) Self-Organized Biological Dynamics & Nonlinear Control. Cambridge University Press, Cambridge. https://doi.org/10.1017/CBO9780511535338

[3] Kauffman, S.A. (1993) The Origins of Order: Self-Organization and Selection in Evolution. Oxford University Press, New York https://doi.org/10.1007/978-94-015-8054-0_8

[4] West, B.J. (1990) Fractal Physiology and Chaos in Medicine. World Scientific, Singapore.

[5] Bassingthwaighte, J.B., Leibovitch, L.S. and West, B.J. (1994) Fractal Physiology. Oxford University Press, New York. https://doi.org/10.1007/978-1-4614-7572-9

[6] Brown, J.H. and West, G.B. (2000) Scaling in Biology. Oxford University Press, Oxford.

[7] Brown, J.H., West, G.B. and Enquis, B.J. (2005) Yes, West, Brown and Enquist's Model of Allometric Scaling Is Both Mathematically Correct and Biologically Relevant. Functional Ecology, 19, 735-738 https://doi.org/10.1111/j.1365-2435.2005.01022.x

[8] West, B.J. (2006) Where Medicine Went Wrong: Rediscovering the Path to Complexity. World Scientific London. https://doi.org/10.1142/6175

[9] West, D. and West, B.J. (2012) On Allometry Relations. International Journal of Modern Physics B, 26, 116-171 https://doi.org/10.1142/S0217979212300101

[10] Deering, W. and West, B.J. (1992) Fractal Physiology. IEEE Engineering in Medicine and Biology, 11, 40-46 https://doi.org/10.1109/51.139035

[11] Kleiber, M. (1961) The Fire of Life: An Introduction to Animal Energetics. Wiley, Hoboken.

[12] Tannock, I.F. (1968) The Relation Between Cell Proliferation and the Vascular System in a Transplanted Mouse Mammary Tumour. British Journal of Cancer, 22, 258-273 https://doi.org/10.1038/bjc.1968.34

[13] Milotti, E., Vyshemirsky, V., Sega, M. and Chignola, R. (2012) Interplay between Distribution of Live Cells and Growth Dynamics of Solid Tumours. Scientific Reports, 2, Article No. 990 https://doi.org/10.1038/srep00990

[14] Guiot, C., Delsanto, P.P.P., Carpinteri, A., et al. (2006) The Dynamic Evolution of the Power Exponent in a Universal Growth Model of Tumors. Journal of Theoretical Biology, 240, 459-463 https://doi.org/10.1016/j.jtbi.2005.10.006

[15] West, G.B., Brown, J.H. and Enquist, B.J. (1990) The Four Dimension of Life: Fractal Geometry and Allometric Scaling of Organisms. Science, 284, 1677-1679 https://doi.org/10.1126/science.284.5420.1677

[16] Labra, F.A., Marquet, P.A. and Bozinovic, F. (2007) Scaling Metabolic Rate Fluctuations. Proceedings of the National Academy of Sciences of the United States of America, 104, 10900-10903 https://doi.org/10.1073/pnas.0704108104

[17] West, G.B. and Brown, J.H. (2000) Scaling in Biology. Oxford University Press, Oxford.

[18] Calder, W.A. III (1996) Size, Function and Life History. Dover Publications Inc., Mineola.

[19] Schlesinger, M.S. (1987) Fractal Time and 1/f Noise in Complex Systems. Annals of the New York Academy of Sciences, 504, 214-228 https://doi.org/10.1111/j.1749-6632.1987.tb48734.x

[20] Bak, P., Tang, C. and Wieserfeld, K. (1988) Self-Organized Criticality. Physical Review A, 38, 364-373 https://doi.org/10.1103/PhysRevA.38.364

[21] Musha, T. and Sawada, Y. (1994) Physics of the Living State. IOS Press, Amsterdam.

[22] Berryman, M.J., Spencer, S.L., Allison, A. and Abbott, D. (2004) Fluctuations and Noise in Cancer Development Proceedings of SPIE—The International Society for Optical Engineering, 5471 https://doi.org/10.1117/12.546641

[23] Qui, B., Zhou, T. and Zhang, J. (2020) Stochastic Fluctuations in Apoptotic Threshold of Tumor Cells Can Enhance Apoptosis and Combat Fractional Killing. Royal Society Open Science, 7, Article ID: 190462 https://doi.org/10.1098/rsos.190462

[24] Fiasconaro, A., Ochab-Marcinek, A., Spagnolo, B. and Gudowska-Nowak, E. (2008) Monitoring Noise-Resonant Effects in Cancer Growth Influenced by External Fluctuations and Periodic Treatment. Physics of Condensed Matter, 65, 435-442 https://doi.org/10.1140/epjb/e2008-00246-2

[25] Chan, A. and Tuszynski, J.A. (2016) Automatic Prediction of Tumour Malignancy in Breast Cancer with Fractal Dimension. Royal Society Open Science, 3, Article ID: 160558 https://doi.org/10.1098/rsos.160558

[26] Tambasco, M. and Magliocco, A.M. (2008) Relation between Tumor-Grade and Computed Architectural Complexity in Breast Cancer Specimens. Human Pathology, 39, 740-746 https://doi.org/10.1016/j.humpath.2007.10.001

[27] Pamatmat, M.M. (1983) Measuring Aerobic and Anaerobic Metabolism of Benthic Infauna under Natural Conditions. Journal of Experimental Zoology, 228, 405-413 https://doi.org/10.1002/jez.1402280303

[28] Moses, M.E., Hou, C., Woodruff, W.H., et al. (2008) Revisiting a Model of Ontogenic Growth: Estimating Model Parameters from Theory and Data. The American Naturalist, 171, 632-645 https://doi.org/10.1086/587073

[29] Voet, D., Voet, J.G. and Pratt, C.W. (2006) Fundamentals of Biochemistry. 2nd Edition, John Wiley and Sons, Inc., Hoboken.

[30] West, G.B. and Brown, J.H. (2005) The Origin of Allometric Scaling Laws in Biology from Genomes to Ecosystems: Towards a Quantitative Unifying Theory of Biological Structure and Organization. Journal of Experimental Biology, 208, 1575-1592 https://doi.org/10.1242/jeb.01589

[31] West, G.B., Woodruf, W.H. and Born, J.H. (2002) Allometric Scaling of Metabolic Rate from Molecules and Mitochondria to Cells and Mammals. Proceedings of the National Academy of Sciences of the United States of America, 99, 2473-2478 https://doi.org/10.1073/pnas.012579799

[32] West, G.B., Brown, J.H. and Enquist, B.J. (2004) Growth Models Based on First Principles or Phenomenology? Functional Ecology, 18, 188-196 https://doi.org/10.1111/j.0269-8463.2004.00857.x

[33] Banavar, J.R., Damuth, J., Maritan, A., et al. (2002) Modelling Universality and Scaling. Nature, 420, 626 https://doi.org/10.1038/420626a

[34] West, G.B., Enquist, B.J. and Brown, J.H. (2002) Modelling Universality and Scaling—REPLY. Nature, 420, 626-627. https://doi.org/10.1038/420626b

[35] Stevens, C.F. (2009) Darwin and Huxley Revisited: The Origin of Allometry. Journal of Biology, 8, Article No 14. https://doi.org/10.1186/jbiol119

[36] Delides, A., Panayiotides, I., Alegakis, A., et al. (2005) Fractal Dimension as a Prognostic Factor for Laryngeal Carcinoma. Anticancer Research, 25, 2141-2144.

[37] Guiot, C., Degiorgis, P.G., Delsanto, P.P., et al. (2003) Does Tumor Growth Follow a "Universal Law"? Journal of Theoretical Biology, 225, 147-151 https://doi.org/10.1016/S0022-5193(03)00221-2

[38] Deisboeck, T.S., Guiot, C., Delsanto, P.P., et al. (2006) Does Cancer Growth Depend on Surface Extension? Medical Hypotheses, 67, 1338-1341 https://doi.org/10.1016/j.mehy.2006.05.029

[39] Nagy, J.A., Chang, S.-H., Shih, S.-C., Dvorak, A.M. and Dvorak, H.F. (2010) Heterogeneity of the Tumor Vasculature. Seminars in Thrombosis and Hemostasis, 36, 321-331 https://doi.org/10.1055/s-0030-1253454

[40] Herman, A.B., van Savage, M. and West, G.B. (2011) A Quantitative Theory of Solid Tumor Growth, Metabolic Rate and Vascularization. PLoS ONE, 6, e22973 https://doi.org/10.1371/journal.pone.0022973

[41] Haanen, C. and Vermes, I. (1996) Apoptosis: Programmed Cell Death in Fetal Development. European Journal of Obstetrics & Gynecology and Reproductive Biology, 64, 129-133 https://doi.org/10.1016/0301-2115(95)02261-9

[42] Kerr, J.F.R., Wyllie, A.H. and Currie, A.R. (1972) Apoptosis: A Basic Biological Phenomenon with Wide-Ranging Implications in Tissue Kinetics. British Journal of Cancer, 26, 239-257 https://doi.org/10.1038/bjc.1972.33

[43] Lowe, S.W. and Lin, A.W. (2000) Apoptosis in Cancer. Carcinogenesis, 21, 485-495 https://doi.org/10.1093/carcin/21.3.485

[44] Karsch-Bluman, A., Feiglin, A., Arbib, E., Stern, T., Shoval, H., Schwob, O., Berger, M. and Benny, O. (2018) Tissue Necrosis and Its Role in Cancer Progression. Oncogene, 38, 1920-1935 https://doi.org/10.1038/s41388-018-0555-y

[45] West, G.B., Brown, J.H. and Enquist, B.J. (2001) A General Model for Ontogenetic Growth. Nature, 413, 628-631 https://doi.org/10.1038/35098076

[46] von Bertalanffy, L. (1957) Quantitative Laws of Metabolism and Growth. The Quarterly Review of Biology, 32, 217-231. https://doi.org/10.1086/401873

[47] Bru, A., Albertos, S., Subiza, J.L., Asenjo, J.L.G. and Bru, I. (2003) The Universal Dynamics of Tumor Growth. Biophysical Journal, 85, 2948-2961 https://doi.org/10.1016/S0006-3495(03)74715-8

[48] Szasz, A. (2021) Vascular Fractality and Alimentation of Cancer. International Journal of Clinical Medicine, 12, 279-296.

[49] di Leva, A., Bruner, E., Widhalm, G., Michev, G., Tschabitscher, M. and Grizzi, F. (2012) Computer-Assisted and Fractal-Based Morphometric Assessment of Microvascularity in Histological Specimens of Gliomas. Scientific Reports, 2, Article No. 429 https://doi.org/10.1038/srep00429

[50] Grizzi, F., Russo, C., Colombo, P., Franceschini, B., Frezza, E.E., et al. (2005) Quantitative Evaluation and Modeling of Two-Dimensional Neovascular Network Complexity: The Surface Fractal Dimension. BMC Cancer 5, 14 https://doi.org/10.1186/1471-2407-5-14

[51] Ceelen, W., Boterberg, T., Smeets, P., Van Damme, N., et al. (2007) Recombinant Human Erythropoietin d Modulates the Effects of Radiotherapy on Colorectal Cancer Microvessels. British Journal of Cancer, 96, 692-700. https://doi.org/10.1038/sj.bjc.6603568

[52] Deisboeck, T.S. and Wang, Z. (2008) A New Concept for Cancer Therapy: Out-Competing the Aggressor. Cancer Cell International, 8, 19 https://doi.org/10.1186/1475-2867-8-19

Time-Fractal in Living Objects

Andras Szasz

Department of Biotechnics, St. Istvan University, Budaörs, Hungary

* Correspondence: Szasz.Andras@gek.szie.hu

Cite this article as:
Szasz, A. (2022): Time-Fractal in Living Objects. Open Journal of Biophysics, 12, 1-26.
https://doi.org/10.4236/ojbiphy.2022.121001

Oncothermia Journal 31, 2022 March: 159-183
www.oncotherm.com/sites/oncotherm/files/2022-03/Szasz_LivingObjects.pdf

Abstract

Homeostasis creates self-organized synchrony of the body's reactions, and despite the energetically open system with intensive external and internal interactions, it is robustly stable. Importantly the self-organized system has scaling behaviors in its allometry, internal structures, and dynamic processes. The system works stochastically. Deterministic reductionism has validity only by the great average of the probabilistic processes. The system's dynamics have a characteristic distribution of signals, which may be characterized by their frequency distribution, creating a particular "noise" $1/f$ of the power density. The stochastic processes produce resonances pumped by various noise spectra. The chemical processes are mostly driven by enzymatic processes, which also have noise-dependent resonant optimizing. The resonance frequencies are as many as many enzymatic reactions exist in the target.

Keywords

Homeostasis, Self-Organizing, Feedbacks, Complexity, Resonance, Stochastic Processes, $1/f$ Noise, Dissipation, Enzymatic Reactions

1. Introduction

All parts of the biosystems are energetically open. The micro and macro environment have a decisional influence on their processes. The system exchanges energy and information with its environment. According to a well-defined balance, the processes are dynamic and interconnected with each other, the homeostasis [1]. This dynamic stability is self-organized [2], and despite the intensive interactions, it is robustly stable at large order of magnitudes [3]. The dynamic stability is regulated and controlled by the homeostatic feedback mechanisms [4], keeping the balance between promoters and suppressors in the complete system [5]. The living network is undoubtedly not a simple addition of its parts [6]. It forms a complex structure [7]. Theoretical biology faces a severe challenge of complexity [8].

Regardless of its living of lifeless state build forms, the natural structures are far from the possibility to describe them in the frame of Euclidean geometry with straight lines and circles. The natural structures are self-organized and mostly form fractal structures [9]. The fractal geometry in life makes it possible to categorize the living species by their allometric comparison [10] comparison of complex morphogenetic differences [11]. This type of universality of the complex feedback mechanisms controls the dynamic equilibrium maintaining the homeostasis [12]. Fractal models represent an excellent approach to explaining the living processes' structural development [13], even for the genetic code structure [14].

The genetic code construction uses Kronecker products (KP) of matrixes with binary numbers. The construction of KP sequences the same template and so represents fractals too [15] [16]. The generated nucleotide sequences characteristic of various living systems form a fractal pattern. An extension of KP construction introduces blocks and a multifractal approach [17], which fits the living complexity [18].

The fractal description is suitable for extending the dynamic physiological processes and analyzing the fractal properties in time [19]. The time-fractal studies are based on the research of the structure of various signals [20] [21]. The dynamism of the energetically open living systems dominantly involves self-organizing processes allowing their fractal description [22]. The time fractals reflect the complex space-time approach developed a new discipline, fractal physiology [23] [24], expressing the collectivity of the processes [25].

The modulation of the external bioelectromagnetic signals has well-explained principles. The carrier frequency helps in the selection mechanisms, while its modulation supports homeostasis by its time fractal ($1/f$)

frequency distribution [26]. The modulation could have multiple effects locally and systematically. The local force for the homeostatic control acts as a further selection factor regarding the lost control of the tumorous cells. Furthermore, the modulation forces the healthy dynamical order providing a compulsory process for apoptosis of the out-of-control cells. *HRV* may characterize the homeostasis [27], presenting the complexity of the system.

The well applied time-fractal current flow may activate the structural fractals in the living systems, and the personal fractal structure could modify the time-fractal pattern, too [28]. The fundamentally nonlinear physiological system dynamics work on the edge of chaos, a border of order and disorder showing a constant dynamic interplay between these states [29]. The challenge of the homeostatic equilibrium is the apparent chaos. The chaos looks complete randomness only. However, the chaos in biosystems results from the stochastic self-organizing and the energetically open system, which directly and permanently interacts with the environment. Its structural and temporal structure is fractal, which appears in the fundamental arrangements of the self-similar building and dynamism of the energy exchanges internally and externally. The living processes are complex. They are in self-organized criticality (*SOC*) [30], which is formulated, as the "life at the edge of chaos" [31]. This chaos is the realization of a well-organized stochastic (probabilistic) system [32]. The chaos is only an ostensible complete disorder [33].

2. Methods

2.1. Fluctuations

An organism has a finite number of possible states. These states could be characterized in terms of operational quality utilizing a diagnostic parameter (signals). All signals have an average in time, and the signals fluctuate around this value in a controlled band. The random fluctuation sets various states (microstates) of the body, which exist only briefly and appear as fluctuation. The temporal fluctuation is regarded as a noise of the signal. The noise of living processes usually does not fluctuate randomly. The homeostatic control of the body regulates them. The minimal number of diagnostic signals is defined by the quasi-independent, weakly overlapping regulation intervals. The number of these quasi-independent diagnostic signals does not change during the system meets the conditions of the healthy dynamical equilibrium, the homeostasis. The average values, the fluctuation band, and the distribution of the frequencies may vary, depending on age and adaptation to changing environmental conditions. These quantities are called macroscopic diagnostic determinants and the status vector with D_i diagnostic states:

$$D_i = D_i\left(\boldsymbol{X},\boldsymbol{Y}\right) \quad \left(i=1,2,\cdots,n\right) \tag{1}$$

where $\boldsymbol{X}$ and $\boldsymbol{Y}$ are the signals of the system and outside environment, respectively. Due to the short time realized microstates, the number of diagnostic states is significantly less than the numberof its determinant signals D_i, consequently, the microstates appear as statistical statements. The same homeostatic macrostate has a wide variety of microstates that change rapidly over time, fluctuating around the averages. The probability that the microstate falls in the interval $\left(\boldsymbol{X},\boldsymbol{X}+\mathrm{d}\boldsymbol{X}\right)$ at time *t, i.e.,* the probability density $w\left(\boldsymbol{X},t\right)$ with:

$$P_{\boldsymbol{X}}\left(\boldsymbol{X}<\boldsymbol{\xi}\le\boldsymbol{X}+\mathrm{d}\boldsymbol{X}\right)=w\left(\boldsymbol{X},t\right)\mathrm{d}X \tag{2}$$

Consequently D_i is given by $w\left(\boldsymbol{X},t\right)$ it is a stochastic determinant which primarily we characterize with its average (mean value)

$$\left\langle D_i\right\rangle=\int_{(X)}D_i\left(\boldsymbol{X},\boldsymbol{Y}\right)w\left(X,t\right)\mathrm{d}X \quad \left(i=1,2,\cdots,n\right) \tag{3}$$

and its variance

$$\sigma_{D_i} = \left\langle \left(D_i - \langle D_i \rangle \right)^2 \right\rangle \quad (i = 1, 2, \cdots, n) \tag{4}$$

where $\langle\ \rangle$ denotes the average of the values. The failure of the dynamic equilibrium when $\left| D_i - \langle D_i \rangle \right|$ is larger than a predetermined threshold with a limiting value (l_{D_i}). According to the Chebyshev theorem [34] the probability that $\left| D_i - \langle D_i \rangle \right| > l_{D_i}$ (so the system is out from the healthy homeostasis) is:

$$P_{fail}\left(\left| D_i - \langle D_i \rangle \right| > l_{D_i} \right) \le \frac{\sigma_{D_i}^2}{l_{D_i}^2} = \frac{\left(D_i - \langle D_i \rangle \right)^2}{l_{D_i}^2} \tag{5}$$

In a healthy state the P_{fail} is small. The $\langle D_i \rangle$ average characterizes this state. The conventional diagnostics controls $\langle D_i \rangle$ values only, regarding the patient healthy when the fluctuations $f_{D_i} = D_i - \langle D_i \rangle$ remain within a tolerance band l_{D_i} . However, the fluctuation carries essential information about the microstates. Changes in the regulative processes could drastically modify the fluctuation of the signal without changing its average value. Study the noise spectrum may predict modifications of the regulative feedbacks, so it has diagnostic value.

The living, dynamic equilibrium is well-regulated but in a probabilistic way. The time-dependent processes realize the observed signal with a probability, as the actual exposition from the possibilities of the fluctuations of the measured signal.

The vital principle is the feedback mechanism, which controls the balance within a predetermined range around the reference value. It is usually well modeled with fuzzy logic, an approach to counting "degrees of truth" rather than the usual "true or false" decisions [35]. This logic governs homeostatic equilibria in all ranges of space and time in living systems. This uncertain value is undoubtedly in a controlled reference interval, were strongly interconnected negative feedback loops regulate the balance in the micro and macro ranges, forming the system's dynamic stability.

These phenomena request a stochastic approach (probability of events dependent on time) instead of conventional thinking based on deterministic changes [36]. Deterministic reductionism can mislead the research. The homeostasis is often ignored and used as a static framework for effects [37]. The stochastic approach is fundamental in biological dynamism [38]. The dynamic homeostatic equilibrium keeps the system in a stable but constantly changing state.

2.2. Stochastic and Deterministic Approach

A model calculation of tumor growth shows the strength of the stochastic approach. In a simple example, the growth of a tumor can be described deterministically. The deterministic change of tumor mass (ΔM_t) by observation time (Δt) is proportional with its actual mass (M_t):

$$\Delta M_t(t) = k M_t(t) \Delta t \tag{6}$$

where k is a constant. A well-known exponential solution uses the mass of the tumor at the start of its observation (M_0):

$$\frac{\mathrm{d}M_t(t)}{\mathrm{d}t} = k M_t(t) \quad \Rightarrow \quad M_t(t) = M_0 \mathrm{e}^{kt} \tag{7}$$

In a deterministic way, the prognostic task of oncology would be simple regarding exponential growth. However, the process is stochastic, requesting the step-by-step analysis of the development of the tumor. We follow the additional or disappearing individual cells producing the mass growth. The probability P_{M_t} to add a cell to the tumor at t time during Δt interval is proportional with $kM_t(t)\Delta t$, as we assumed initially been in (6). Then the probability equation with the added and eliminated cells in time interval Δt is:

$$P_{M_t}(t+\Delta t) = P_{M_t}(t) + k(M_t - 1)\Delta t P_{M_t-1}(t) - kM_t \Delta t P_{M_t}(t) \tag{8}$$

It depends on the added cells to the tumor from the previous time interval ($P_{M_t}(t+\Delta t)$) and the eliminated cells in the actual time ($-kM_t\Delta t P_{M_t}(t)$) considering the process in one step before ($k(M_t-1)\Delta t P_{M_t-1}(t)$). In a differential equation form:

$$\frac{\mathrm{d}P_{M_t}(t)}{\mathrm{d}t} = k(M_t - 1)P_{M_t-1}(t) - kM_t P_{M_t} \tag{9}$$

When we start from a single cell ($P_{M_t}(0) = 1$ if $M_0 = 1$, $P_{M_t}(0) = 0$ in every other case), the solution of (9) at $M_t \geq M_0$ cases:

$$P_{M_t}(t) = \begin{pmatrix} M_t - 1 \\ M_t - M_0 \end{pmatrix} \mathrm{e}^{-kM_0 t}\left(1 - \mathrm{e}^{-kt}\right)^{M_t - M_0} \tag{10}$$

Compare (7) and (10) how they are different! The deterministic approach (7) is continuous in time, running in real values, while the stochastic, probability-based approach (10) jumps on integers, building up the tumor-mass step by step. The deterministic equation gives a fixed result, while the stochastic shows "only" probability. It is interesting to see that the deterministic result is the particular case of the stochastic one, the deterministic $P_{M_t}(t) = \langle M_t(t) \rangle$ condition does not depend of the actual number of steps. Consequently, the averaging of the stochastic probability results provide the deterministic solution:

$$P_{M_t}(t) = \langle M_t(t) \rangle = \sum_{M_t = M_0}^{\infty} M_t P_{M_t}(t) = M_0 \mathrm{e}^{kt} \tag{11}$$

2.3. The Fluctuation Phenomena

The signals follow the living, dynamic interactions, the molecular changes, and the chemical and physical excitations give a structured noise. The power spectral density of a signal ($S(f)$), is the power of the noise (fluctuation) per unit of bandwidth. Define the work of the $x(t)$ stochastic process:

$$W := \int_{-\infty}^{\infty} x^2(t)\,\mathrm{d}t \tag{12}$$

The (12) with the Parseval's formula may be evaluated

$$W = \int_{-\infty}^{\infty} x^2(t)\,\mathrm{d}t = \int_{-\infty}^{\infty} S(f)\,\mathrm{d}f \tag{13}$$

where $S(f)$ is the spectral power density in any random stationary case. The Fourier transform of $x(t)$ stochastic process is the primary step to study the phenomena [39],

$$X(f)=\frac{1}{\sqrt{2\pi}}\int_{-\infty}^{\infty}x(t)\mathrm{e}^{-j2\pi ft}\mathrm{d}t:=F\{x(t)\} \tag{14}$$

where the spectral density function $S(f)$ is:

$$S(f)=\frac{|X(f)|^2}{2\pi} \tag{15}$$

The even function of the frequency, i.e., $S(f)=S(-f)$.

The $S(f)$ gives the intensity of noise as a function of spatial frequency, measured in $\frac{W}{Hz}=J$, characterizing the stochastic signal with the f frequency.

The most straightforward complex noise follows normal (Gaussian) distribution (the amplitudes have normal distribution), and its power function $S(f)$ is self-similar through many orders of magnitudes. In this simple case, the $S(f)$:

$$S(f)=\frac{A}{f^{\alpha}} \tag{16}$$

The α exponent in (16) formally refers to optics, noted as the "color" of the noise. The white-noise is flat ($\alpha=0$), the pink-noise has $\alpha=1$, and other colors are described by various other numbers up to $\alpha=2$, the brown-noise. So, the $S(f)$ of pink-noise inversely depends on f frequency, noted as $1/f$ noise. The $1/f$ noise carries the self-similar structure of living processes having a time-fractal covering the life's dynamism [40] [41]. The dynamical fractal structure of living systems marks the self-organizing both in geometric and time structures and dynamically regulates the living matter [42], defines time-fractal structure in stochastic way of the living systems [43], a $1/f$ fluctuation. The physiological control shows $1/f$ spectrum [44]. One of the most studied such spectra is the heart rate variability (HRV).

This $1/f$ noise has a particular behaviour. Each octave interval (halving or doubling in frequency) carries an equal amount of noise energy. The living system makes special signal processing due to its self-organized symmetry, so it transforms the white noise to pink [45], forming the most common signal in biological systems [46].

Stochastic signals additionally to $S(f)$ are usually characterized by their autocorrelation function $R_{XX}(t_1,t_2)$. The autocorrelation measures how the signal correlates with a delayed copy of itself in the function of time-lag $(\tau=t_2-t_1)$, measuring the signal in t_1 and subsequent t_2 in X position. The autocorrelation evaluation is a mathematical tool for finding repeating patterns, looking for periodicity in the signal. It allows identifying the existence of the biological chain processes. The $S(f)$ and $R_{XX}(t_1,t_2)$ functions are not independent, they could be converted to each other by Fourier transformation. Measuring the power density $S(f)$ of a signal is easier than its autocorrelation, so usually the studies concentrate on the power density function.

3. Results

3.1. White Noise

All frequencies in the entire interval have the same A amplitude in the white noise spectrum:

$$S(f) = A \propto \frac{1}{f^{\alpha}} \tag{17}$$

i.e., from (16), $\alpha = 0$. Consequently, the autocorrelation function is completely uncorrelated:

$$\begin{aligned} R_{XX}(\tau) &= \frac{1}{2\pi}\int_{-\infty}^{\infty} S(f)\cos(2\pi f\tau)\mathrm{d}\pi f = \int_{0}^{\infty} S(f)\cos(2\pi f\tau)\mathrm{d}f \\ &= \frac{A}{2}\int_{0}^{\infty} 2\cos(2\pi f\tau)\mathrm{d}f = \frac{A}{2}\delta(\tau) \end{aligned} \tag{18}$$

The band constraint in a limited interval, up to $f_{\max}$ upper-frequency limit affects a longer-term correlation:

$$\begin{aligned} R_{XX}(\tau) &= \frac{1}{2\pi}\int_{-\omega_0}^{\omega_0} S(f)\cos(2\pi f\tau)\mathrm{d}\pi f = \int_{0}^{f_{\max}} S(f)\cos(2\pi f\tau)\mathrm{d}f \\ &= \frac{A}{2}\int_{0}^{f_{\max}} 2\cos(2\pi f\tau)\mathrm{d}f = A\frac{\sin(2\pi f_{\max}\tau)}{2\pi f_{\max}\tau} \end{aligned} \tag{19}$$

For example, the completely flat $S(f)$ limited to the frequency-band [−10 - 10] has well-defined autocorrelation Figure 1:

The correlation function oscillates, so the correlation length does not monotonically decrease in band-limited white noise.

3.2. The 1/f Noise

A stationary random process has an indefinite duration. To introduce a modified density spectrum, consider a finite segment of the random process $x(t)$ of duration $2T$, defined by:

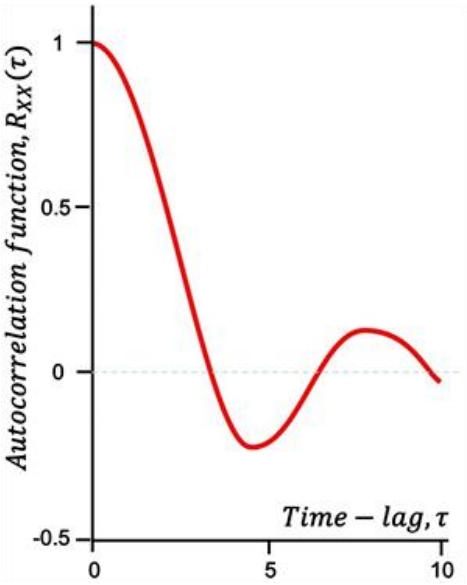

Figure 1. The correlation function $R_{XX}(\tau)$ of band-limited white noise than the $S(f) = f^{0} = \cos t$.

$$x_T = \begin{cases} x(t), & -T \le t \le T \\ 0, & \text{otherwise} \end{cases} \quad \text{and} \quad \lim_{T\to\infty} x_T(t) = x(t) \tag{20}$$

According to (14), the Fourier transform of $x_T(t)$ has the form of

$$X(f,T)=\frac{1}{\sqrt{2\pi}}\int_{-T}^{T}x_T(t)\mathrm{e}^{-j2\pi ft}\mathrm{d}t \tag{21}$$

The Fourier transform of the function $x(a\cdot t)$, where a is an arbitrary complex number, and f is the frequency:

$$F\{x(a\cdot t)\}=\frac{1}{a}X\left(\frac{f}{a}\right) \tag{22}$$

Use (21) and (22) we get:

$$F\{x_T(at)\}=\frac{1}{a}X\left(\frac{f}{a},T\right) \tag{23}$$

Using Parseval's formula and (15):

$$\lim_{T\to\infty}\frac{1}{2T}\int_{-T}^{T}x^2(t)\mathrm{d}t=\int_{-\infty}^{\infty}S(f)\mathrm{d}f \quad \left\{S(f)=\frac{1}{2\pi}\lim_{T\to\infty}\frac{|X(f,T)|^2}{2T}\right\} \tag{24}$$

The living processes are basically self-similar, so it is convenient to define the self-similarity of a stochastic process. A stochastic process is said to be self-similar if the effective power of the stochastic process representation $x(t)$ equals the effective power of the representation $x(at)$ defined over time scale [at], for every a positive scalar, i.e.:

$$\lim_{T\to\infty}\frac{1}{2T}\int_{-T}^{T}x^2(t)\mathrm{d}t=\lim_{T\to\infty}\frac{1}{2T}\int_{-T}^{T}x^2(at)\mathrm{d}(at) \tag{25}$$

And so from (22) and (20), we get

$$a\int_{-\infty}^{\infty}\frac{1}{a^2}S\left(\frac{f}{a}\right)\mathrm{d}f=\int_{-\infty}^{\infty}S(f)\mathrm{d}f \tag{26}$$

Also, for the power spectral density function, the functional equation may be expressed:

$$S\left(\frac{f}{a}\right)=aS(f) \tag{27}$$

for every positive scalar a and every scalar f. To solve this equation, we assume that $f>0$ and set for a the value $a=f$:

$$S(f)=\frac{S(1)}{f} \tag{28}$$

On the other hand, if $f<0$ then $f=-|f|$, and

$$\frac{1}{a}S\left(\frac{f}{a}\right)=\frac{1}{a}S\left(-\frac{|f|}{a}\right)=S(f) \tag{29}$$

Let us set for a the value $a=|f|$ and take into account that the power density function is even, so we obtain the $1/f$ spectrum, or "pink-noise":

$$S(f)=\frac{S(1)}{|f|} \tag{30}$$

The autocorrelation function of $S(f)\propto\frac{1}{f^1}$ pink noise with Fourier transformation has a singular result:

$$\begin{aligned} R_{XX}(\tau) &= \frac{1}{2\pi}\int_{-\infty}^{\infty} S(f)\cos(2\pi f\tau)\mathrm{d}\pi f \\ &= \int_0^{\infty}\frac{1}{f}\cos(2\pi f\tau)\mathrm{d}f \\ &= \int_0^{\infty}\frac{\cos(2\pi f\tau)}{2\pi f\tau}\mathrm{d}(2\pi f\tau) \end{aligned} \tag{31}$$

follows the $Ci(x)$ function:

$$Ci(x)=-\int_x^{\infty}\frac{\cos(2\pi f\tau)}{2\pi f\tau}\frac{\cos x'}{x'}\mathrm{d}x' \tag{32}$$

Due to $Ci(\infty)=0$, the autocorrelation of $1/f$ noise in long time-lag is zero Figure 2.

By the ergodic hypothesis [47], the autocorrelation function of a stationary random process $x(t)$ can be defined as

$$R_{xx}(\tau)=\lim_{T\to\infty}\frac{1}{2T}\int_{-T}^{T}x(t)x(t+\tau)\mathrm{d}t \quad \left\{R_{xx}(\tau)=R_{xx}(-\tau)\right\} \tag{33}$$

where τ is the time-lag. The relation between autocorrelation function and the power density spectrum can be expressed by the Fourier transform of the autocorrelation function (Wiener-Khinchine theorem), namely:

$$\begin{aligned} R_{xx}(f) &= \frac{1}{\sqrt{2\pi}}\int_{-\infty}^{\infty}R_{xx}(\tau)\mathrm{e}^{-j2\pi f\tau}\mathrm{d}\tau \\ R_{xx}(\tau) &= \frac{1}{\sqrt{2\pi}}\int_{-\infty}^{\infty}R_{xx}(f)\mathrm{e}^{j2\pi f\tau}\mathrm{d}f \end{aligned} \tag{34}$$

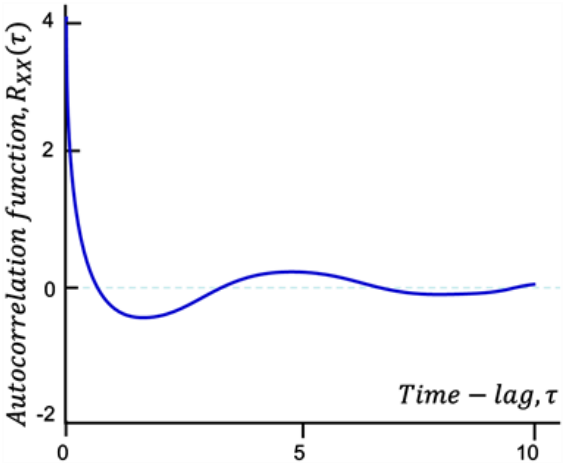

Figure 2. Autocorrelation function of $1/f$ noise (negative integral cosine function, $-Ci(x)$).

From these (considering [36] and [48]), we may conclude

$$R_{xx}(\tau)=\int_{-\infty}^{\infty}S(f)\mathrm{e}^{j2\pi f\tau}\mathrm{d}f=\int_{-\infty}^{\infty}\frac{S(1)}{|f|}\mathrm{e}^{j2\pi f\tau}\mathrm{d}f=\frac{\sqrt{2\pi}S(1)}{|\tau|} \tag{35}$$

Assuming the lower cutoff frequency $f_{\min}$, the function of such an approximate $1/f$ noise correlation from(31)

$$\phi(\tau)=\int_{f_{\min}}^{\infty}\frac{1}{f}\cos(2\pi f\tau)\mathrm{d}f=\int_{f_{\min}}^{\infty}\frac{\cos(2\pi f\tau)}{2\pi f\tau}\mathrm{d}(2\pi f\tau)=-Ci(2\pi f_{\min}\tau) \tag{36}$$

The procedure is also shown in Figure 2.

It can be seen from the figure that here too, there is a problem with the introduction of the correlation length since the correlation function oscillates.

In the case where the lower cutoff frequency is minimal, the argument of the *Ci*--function is small even at significant offset times. Then the correlation function is as shown in Figure 3.

It appears that this case can be approximated by the sum of white noise and a virtually constant correlation function. More precisely, the can be asymptotically approximated by

$$\varphi(\tau)=-\left(\gamma+\ln(2\pi f_0\tau)\right) \tag{37}$$

with a function where $\gamma\cong 5772$ is the Euler-Mascheroni constant.

The autocorrelation function of $1/f^{\alpha}$ ($\alpha\neq 0$ and $\alpha\neq 1$):

$$R_{XX}(\tau)=\int_{0}^{\infty}\frac{1}{f^{\alpha}}\cos(2\pi f\tau)\mathrm{d}f=\frac{1}{\tau^{1-\alpha}}\frac{\sqrt{\pi}}{\sqrt{2}\sin\left(\frac{\alpha\pi}{2}\right)\Gamma(1-\alpha)} \tag{38}$$

Note that colored noises do not fit the white and pink noises, so the basic noises have no common expression.

The pink noise cannot be described with the classical apparatus of non-equilibrium thermodynamics. Macroscopic fluctuation characterizes the thermodynamic processes. The range of space in which the fluctuation occurs is not uniform concerning the fluctuating quantity (s) but is thermodynamically in equilibrium at all points. The latter means that the exchange of extensive amounts characteristic of fluctuation between spatial domains during the relaxation period of equilibrium is negligible. A further feature of thermodynamic fluctuations is that the fluctuation persists for a finite time and that the rate of change of each ai(i=1,2,⋯,n)ai(i=1,2,⋯,n) extensive can be expressed in terms of the extensive amounts involved in the fluctuation, i.e.

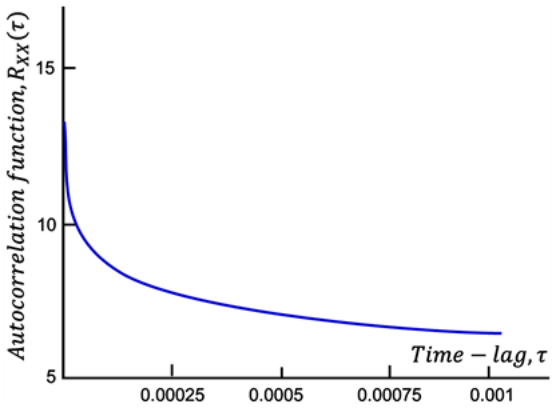

Figure 3. Autocorrelation function $1/f$ noise for very low cutoff frequency (negative, integral cosine function, $-Ci(x)$).

$$\frac{\mathrm{d}a_i}{\mathrm{d}t} = f\left(a_1, a_2, \cdots, a_n\right) \quad (i = 1, 2, \cdots, n) \tag{39}$$

Let be an extensive one whose relaxation time is much longer than the others. Then the fluctuation can be described by this single extensive one. When (39) is linear and returns to the equilibrium position of the system, then the equation is a one-sided fluctuation process, completely deterministic, with no noise in it:

$$\frac{\mathrm{d}a}{\mathrm{d}t} = -\lambda a \tag{40}$$

Solving (41):

$$a(t) = a(0)\mathrm{e}^{-\lambda t} \tag{41}$$

Then the correlation function is:

$$R_{aa}(\tau) = \langle a(\tau)a(0)\rangle = \left[a(0)\right]^2 \mathrm{e}^{-\lambda|\tau|} \tag{42}$$

and its power spectrum:

$$S(i\omega) = \int_{-\infty}^{\infty} R_{aa}(\tau)\mathrm{e}^{-i\omega\tau}\mathrm{d}\tau = \left[a(0)\right]^2 \frac{\lambda}{\lambda^2 + \omega^2} \tag{43}$$

For stochasticity, the necessary noise appears in the fluctuation and spectrum for the whole, but the considerations lead to (43) are deterministic. Therefore, it is assumed that this deterministic signal is repeated randomly, forming a noise of a series of randomly repeated deterministic signals. Introducing a white noise function into the deterministic equation (like is in the Langevin equation) applies the amplitudes of the white noise spectrum that corresponds to the noise spectrum given by the deterministic random fluctuation and accordingly with the correlation function too. This is white noise ($\frac{1}{\omega}$) for small ω values, while Brown noise ($\frac{1}{\omega^2}$) for large values.

In the case of pink-noise, these considerations do not work. The Fourier transform connects the $S(f)$ power function and the R_{xx} autocirreklation function:

$$S(i\omega) \Leftrightarrow R_{aa}(\tau) \;\Rightarrow\; \frac{1}{|b|} S\left(\frac{i\omega}{b}\right) \Leftrightarrow R_{aa}(b\tau) \tag{44}$$

Because

$$S(i\omega) = \frac{1}{|\omega|} \tag{45}$$

because of this

$$\frac{1}{|b|} S\left(\frac{i\omega}{b}\right) = \frac{1}{|\omega|} \tag{46}$$

so it follows that

$$R_{aa}(\tau) = R_{aa}(b\tau) \tag{47}$$

The correlation function is constant in this case, so the pink noise correlated in the same way for each shift, so there can be no thermodynamic fluctuation!

Starting with such randomized deterministic fluctuations, we get equivalents to form of (40), like:

$$\frac{\mathrm{d}a}{\mathrm{d}t} = -\lambda a = -\frac{1}{\tau} a \tag{48}$$

In this case, instead of (41), we get the following spectrum:

$$S(i\omega) = \int_{-\infty}^{\infty} f_{aa}(\tau) \mathrm{e}^{-i\omega\tau} \mathrm{d}\tau = \left[a(0)\right]^2 \frac{\tau}{1+(\tau\omega)^2} \tag{49}$$

Assuming that the temporal correlation length probability density function is lognormal, the resulting noise spectrum is: $1/f^{\alpha}$. It is the same as the originally white-noise pumped stochastic case. It is confusing, of course, that this process started from deterministic distribution, but it was overcome by assuming that there is a random series of such deterministic fluctuations.

Two stochastic processes can be considered equivalent if their noise spectrum is the same. Based on this, we introduce a stochastic excitation term $q(t)$ to (48):

$$\frac{\mathrm{d}a}{\mathrm{d}t} = -\frac{1}{\tau} a + q(t) \tag{50}$$

The $q(t)$ spectrum is chosen of the signal resulting from the solution of the equation is equal to the power spectrum of the fluctuation (49). This can always be done. To prove this, Fourier transforms Equation (50), then we get that

$$\left(i\omega + \frac{1}{\tau}\right) a = q(\omega) \rightarrow a(\omega) = \frac{\tau}{1+(i\omega\tau)} q(\omega) \tag{51}$$

Hence the power spectrum

$$S(\omega)=\frac{\tau^2}{1+(\omega\tau)^2}\left|q(\omega)\right|^2 \tag{52}$$

The following choice leads to the desired result:

$$q(\omega)=\frac{a(0)}{\sqrt{\tau}} \tag{53}$$

Consequently, if $q(t)$ is a white noise with $\frac{a(0)}{\sqrt{\tau}}$ amplitude, then the noise spectrum of the signal is the same as the noise spectrum of the fluctuation.

3.3. Orstein-Uhlenbeck Process

The power spectrum of a random series of such deterministic fluctuations differs from the white-noise pumped Langevin solution only in a proportionality factor. We approach the fluctuation by decomposing it into the sum of quasi-periodic stochastic processes of different statistically independent time scales. The quasi-periodic stochastic processes with different time scales also have different frequency scales. All such component processes are assumed to be statistically similar. Note the increase of a stochastic $X(t)$ process $X(t+\mathrm{d}t)-X(t)$ without memory with Θ-function:

$$X(t+\mathrm{d}t)-X(t)=\Theta\left[X(t),t,\mathrm{d}t\right]. \tag{54}$$

Assume that $\Theta\left[X(t),t,\mathrm{d}t\right]$ is a smooth function of the $X,t,\mathrm{d}t$ variables and that $X(t)$ is continuous:

$$\lim_{\mathrm{d}t\to 0} X(t+\mathrm{d}t)=X(t). \tag{55}$$

The approach that the observed noise by the emission of subsequent process-chains in statistical mechanics, the Markov process [49] describes the chain reaction, which is used in biology too [50]. The Markovian recursive successive building the $X(t+\mathrm{d}t)$, while the function $X(t)$ from where it was derived depends only from t in memory-less construction, using:

$$\begin{aligned}\Theta\left[X(t),t,\mathrm{d}t\right]&=\sum_{i=1}^{n}X\left(t+i\frac{\mathrm{d}t}{n}\right)-X\left(t+(i-1)\frac{\mathrm{d}t}{n}\right)\\&=\sum_{i=1}^{n}\Theta\left[X\left(t+(i-1)\frac{\mathrm{d}t}{n}\right),t+(i-1)\frac{\mathrm{d}t}{n},\frac{\mathrm{d}t}{n}\right]\end{aligned} \tag{56}$$

Since dt can be chosen to be arbitrarily small, the $t_{i-1}=t+(i-1)\frac{\mathrm{d}t}{n}$ can be placed in any proximity of the *t* times by choosing *n* large enough. Exploiting the continuity, in this case:

$$\begin{aligned}&t_{i-1}\to t,\quad X(t_{i-1})=X(t)\\&\Theta\left[X(t),t,\mathrm{d}t\right]=\textstyle\sum_{i=1}^{n}\Theta_i\left[X(t),t,\frac{\mathrm{d}t}{n}\right]\end{aligned} \tag{57}$$

Here, the $\Theta_i\left[X(t),t,\frac{\mathrm{d}t}{n}\right]$ terms can be considered as representations of the $\Theta\left[X(t),t,\frac{\mathrm{d}t}{n}\right]$ variable that is statistically independent due to being the memory free of the process. Since n is arbitrarily large, it follows from the central limit theorem that $\Theta\left[X(t),t,\mathrm{d}t\right]$ is the sum of n statistically independent $\Theta_i\left[X(t),t,\frac{\mathrm{d}t}{n}\right]$ probability variables. Hence, this probability variable distributes normally. The following properties follow from the property of normally distributed random variables:

$$\begin{aligned}\left\langle\Theta\left[X(t),t,\mathrm{d}t\right]\right\rangle &= n\cdot\left\langle\Theta\left[X(t),t,\frac{\mathrm{d}t}{n}\right]\right\rangle\\ \left\langle\left\langle\Theta\left[X(t),t,\mathrm{d}t\right]\right\rangle\right\rangle &= n\cdot\left\langle\left\langle\Theta\left[X(t),t,\frac{\mathrm{d}t}{n}\right]\right\rangle\right\rangle\end{aligned} \tag{58}$$

Where $\langle\ \rangle$ notes the mean, and $\langle\langle\ \rangle\rangle$ is the standard deviation. Solving function equations

$$\begin{aligned}\left\langle\Theta\left[X(t),t,\mathrm{d}t\right]\right\rangle &= A\left[X(t),t\right]\mathrm{d}t\\ \left\langle\left\langle\Theta\left[X(t),t,\mathrm{d}t\right]\right\rangle\right\rangle &= D\left[X(t),t\right]\mathrm{d}t\end{aligned} \tag{59}$$

where A and D are smooth functions of X and t, and $D>0$. Considering the normality of (55) and (60):

$$\begin{aligned}X(t+\mathrm{d}t)-X(t) &= \Theta\left[X(t),t,\mathrm{d}t\right]\\ &= \boldsymbol{N}\left[A(X,t)\mathrm{d}t, D(X,t)\mathrm{d}t\right]\\ &= A(X,t)\mathrm{d}t + D^{\frac{1}{2}}\boldsymbol{N}(0,1)\mathrm{d}t^{\frac{1}{2}}\end{aligned} \tag{60}$$

where $\boldsymbol{N}(0,1)$ is the unit standard deviation squared normal distribution stochastic process with zero means. Turning to a differential equation, we get the following nonlinear generalized Langevin equation

$$\frac{\mathrm{d}X}{\mathrm{d}t} = A(X,t) + D^{\frac{1}{2}}(X,t)\Gamma(t) \tag{61}$$

driven by normally distributed white noise:

$$\Gamma(t) = \lim_{\mathrm{d}t\to 0}\boldsymbol{N}\left(0,\mathrm{d}t^{-1}\right) \tag{62}$$

In the Gillespie sense [51], the stochastic process is self-similar, resolved to a sum of statistically independent terms normally distributed within the studied interval. Consider the simplest of the self-similar stochastic processes in (61):

$$\frac{\mathrm{d}X}{\mathrm{d}t} = -\frac{1}{\tau}X + D^{\frac{1}{2}}\Gamma(t) \tag{63}$$

where τ is the time constant of the process.

The describes an Ornstein-Uhlenbeck process (OUP), which is stochastic and follows a normal (Gaussian) distribution. The OUP is homogeneous in time. Its homogeneity in time allows the OUP to describe it simply with the stochastic interaction of an energy source and the connected energy-consuming system Figure 4, allowing linear transformations of space and time variables [52].

The central value is exponentially decreasing, and a white noise drives it. The exponential decay should be uniformly distributed rather than lognormal, the maximum entropy belongs to $1/f$, and then the equation and distribution of the distribution should lead to $1/f$.

If we use a lognormal distribution in the interval [53], modifying (63) by $D=\frac{D_0}{\sqrt{\tau}}$ [54]:

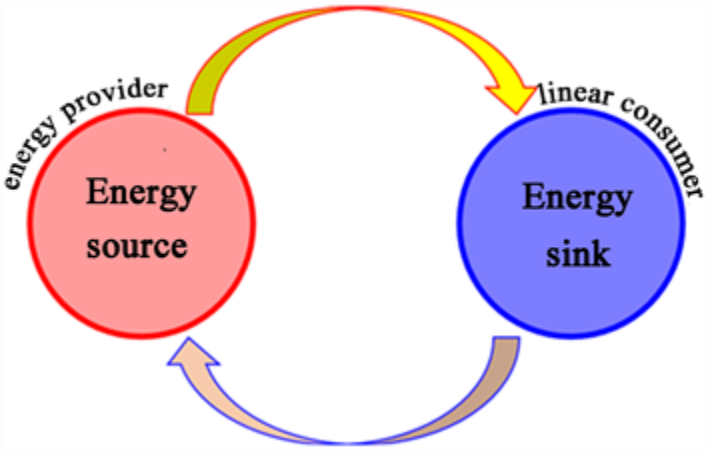

Figure 4. The simplest relation of the energy source (reservoir, mechanical, electronic, etc.) and the linear consumer (energy-sink mechanical electronic, etc.)

$$\frac{\mathrm{d}X}{\mathrm{d}t}=-\frac{1}{\tau}X+\frac{D_0^{\frac{1}{2}}}{\sqrt{\tau}}\Gamma(t) \tag{64}$$

Thus, the power spectrum of this is distributed by the lognormal of the time domain, asymptotically $1/\tau$. The equation describes the noise of a system excited by white noise consisting of an energy store (e.g., mass, rotating mass, capacitor, inductance) and a linear attenuation (e.g., fluid resistance, ohmic resistance).The power spectrum of the process:

$$S(\omega,\tau)=\frac{D_0\tau_s^2}{1+(\omega\tau_s)^2} \tag{65}$$

Here τ_s is the time constant of the system, which can also be considered the natural time scale of the stochastic process. Let's define

$$\lambda=\frac{1}{\tau_s} \tag{66}$$

a frequency scale at which we want to characterize stochastic processes. Let $G(\lambda)\mathrm{d}\lambda$ a be the number of stochastic processes in the frequency interval $(\lambda,\lambda+\mathrm{d}\lambda)$, then the energy spectrum of the stochastic processes in the interval between the frequency scales (λ_2,λ_1):

$$S(\omega,\lambda_1,\lambda_2)=\int_{\lambda_1}^{\lambda_2}\frac{D\cdot G(\lambda)}{\lambda^2+\omega^2}\mathrm{d}\lambda \tag{67}$$

If the distribution is uniform, that is, if,

$$G(\lambda)\mathrm{d}\lambda=\frac{\mathrm{d}\lambda}{\lambda_2-\lambda_1} \tag{68}$$

then we get that

$$S(f,\lambda_1,\lambda_2)=\int_{\lambda_1}^{\lambda_2}\frac{D\cdot G(\lambda)}{\lambda^2+\omega^2}\mathrm{d}\lambda=\begin{cases}D & \text{if } 0<\omega\leq\lambda_1\leq\lambda_2\\ \dfrac{D\pi}{2\omega(\lambda_2-\lambda_1)} & \text{if } \lambda_1\leq\omega\leq\lambda_2\\ \dfrac{D}{\omega^2} & \text{if } \lambda_1\leq\lambda_2\leq\omega\end{cases} \tag{69}$$

a well-known result gives white noise in the first interval, pink in the second, and brown (Wiener noise) in the third.

When the relaxation rate is uniform in an interval $[f_1, f_2]$ and the applied amplitude doesn't change. Hence the spectrum of OUP, $S(f)=\frac{1}{f^{\alpha}}$ has three well distinguishable frequency parts Figure 5.

3.4. Importance of the Self-Similarity

The τ_s the time constant of the system in (65) generates the stochastic signal. The τ_s can be considered as the natural time scale of the stochastic process that characterizes the two-point correlation function of the stochastic process. Indeed, the two-point correlation function from (65) shows the degree of correlation decreases exponentially with τ time constant:

$$\phi_{XX}(\vartheta)=F^{-1}\left[S(\omega,\tau_s)\right]=F^{-1}\left[\frac{D_0\tau_s}{1+(\omega\tau_s)^2}\right]=D_0\mathrm{e}^{-\frac{\vartheta}{\tau_s}} \tag{70}$$

This feature of τsτs is the temporal correlation length.

The complexity of the system involves a $G(\tau_s)\mathrm{d}\tau_s$ number of statistically independent stochastic processes in the temporal correlation length interval $(\tau_s,\tau_s+\mathrm{d}\tau_s)$, then the resulting energy spectrum of the stochastic processes in the $(0,\infty)$ interval is:

$$S(\omega)=\int_0^{\infty}\frac{D_0\tau_s G(\tau_s)}{1+(\tau_s\omega)^2}\mathrm{d}\tau_s \tag{71}$$

when the distribution is scale variant, i.e.:

$$G(\tau_s)\mathrm{d}\tau_s=\frac{\mathrm{d}\tau_s}{\tau_s} \tag{72}$$

form, then using Equation (70) a

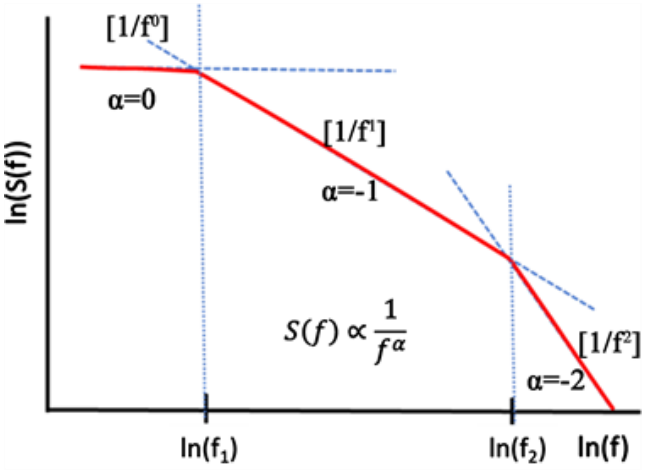

Figure 5. The power density function is divided into three distinguishable parts in Ornstein-Uhlenbeck process. The $\{f_1, f_2\}$ interval, when the probability of realization of the f frequencies are equal.

$$\int_0^\infty \frac{1}{1+(\tau_s\omega)^2}\mathrm{d}\tau_s = \frac{\pi}{2}\frac{1}{\omega} \tag{73}$$

improper integrated, we get the desired result:

$$S(\omega) = \int_0^\infty \frac{D_0\tau_s G(\tau_s)}{1+(\tau_s\omega)^2}\mathrm{d}\tau_s = D_0\int_0^\infty \frac{\tau_s\frac{1}{\tau_s}}{1+(\tau_s\omega)^2}\mathrm{d}\tau = \frac{D_0\pi}{2}\frac{1}{\omega} \propto \frac{1}{f} \tag{74}$$

The scale invariance means that the probability scale is independent,

$$G(\tau_s)\mathrm{d}\tau_s = G(\alpha\tau_s)\mathrm{d}\alpha\tau_s \Rightarrow \frac{\mathrm{d}\alpha\tau_s}{\alpha\tau_s} = \frac{\mathrm{d}\tau_s}{\tau_s} \tag{75}$$

In the case where only self-similarity is required, e.g., as a function of density. That is

$$G(\alpha\tau_s) = \alpha^\beta G(\tau_s) \tag{76}$$

then we get that

$$G(\tau_s) = \tau_s^\beta \tag{77}$$

In this case $\beta = -1$, it provides $1/f$ noise. If we require only self-similarity, we get from (71) and (77) that the noise spectrum of signals in the interval $(0,\infty)$ is:

$$S(\omega) = \int_0^\infty \frac{D_0\tau_s G(\tau_s)}{1+(\tau_s\omega)^2}\mathrm{d}\tau_s = \int_0^\infty \frac{D_0\tau_s^{\beta+1}}{1+(\tau_s\omega)^2}\mathrm{d}\tau_s \tag{78}$$

Due to the physical image, the integrated a

$$S(\omega) = \int_0^\infty \frac{D_0\tau_s^{\beta+1}}{1+(\tau_s\omega)^2}\mathrm{d}\tau_s = \frac{D_0}{\omega^{\beta+2}}\int_0^\infty \frac{(\omega\tau_s)^{\beta+1}}{1+(\tau_s\omega)^2}\mathrm{d}(\omega\tau_s) \tag{79}$$

to shape.

The integral is generally unpredictable. Fortunately, in the case of interest to us, if $0<\beta<2$ the impropriety integral can be given in the closed-form:

$$\int_0^\infty \frac{(\omega\tau_s)^{\beta+1}}{1+(\tau_s\omega)^2}\mathrm{d}(\omega\tau_s)=\frac{\pi}{2\sin\left(\frac{(\beta+2)\pi}{2}\right)}=A \tag{80}$$

This gives (79) that

$$S(\omega)=\frac{D_0}{\omega^{\beta+2}}\int_0^\infty \frac{(\omega\tau_s)^{\beta+1}}{1+(\tau_s\omega)^2}\mathrm{d}(\omega\tau_s)=\frac{D_0 A}{\omega^{\beta+2}} \tag{81}$$

The self-similar distribution function is thus the condition a shaped power spectrum:

$$S(\omega)\propto\frac{1}{\omega^\alpha} \tag{82}$$

The above considerations can be generalized to a large extent.

Namely, if instead of $D=\frac{D_0}{\sqrt{\tau}}$ in (64) use

$$D=\frac{D_0}{\tau^\gamma} \tag{83}$$

We start from the stochastic process described by the equation, using normally distributed white noise as before in (62). Then the power spectrum will be:

$$S(\omega,\tau)=\frac{D_0\tau^{2-\gamma}}{1+(\omega\tau)^2} \tag{84}$$

If we require only self-similarity, we get from (84) and (59) the noise spectrum of signals in the interval $(0,\infty)$:

$$S(\omega)=\int_0^\infty \frac{D_0\tau^{2-\gamma}G(\tau)}{1+(\tau\omega)^2}\mathrm{d}\tau=\int_0^\infty \frac{D_0\tau^{\beta-\gamma+2}}{1+(\tau\omega)^2}\mathrm{d}\tau \tag{85}$$

Due to the physical image, the integral is arranged into a form:

$$S(\omega)=\int_0^\infty \frac{D_0\tau^{\beta-\gamma+2}}{1+(\tau\omega)^2}\mathrm{d}\tau=\frac{D_0}{\omega^{\beta-\gamma+3}}\int_0^\infty \frac{(\omega\tau)^{\beta-\gamma+2}}{1+(\tau\omega)^2}\mathrm{d}(\omega\tau) \tag{86}$$

In the case of interest to us, if the $0<\beta-\gamma+3<2$ the impropriety integral can be given again in closed form:

$$\int_0^{\infty} \frac{(\omega\tau)^{\beta-\gamma+2}}{1+(\tau\omega)^2} \mathrm{d}(\omega\tau) = \frac{\pi}{2\sin\left(\frac{(\beta-\gamma+3)\pi}{2}\right)} = A \tag{87}$$

which gives from (78):

$$S(\omega) = \frac{D_0}{\omega^{\beta-\gamma+3}} \int_0^{\infty} \frac{(\omega\tau)^{\beta-\gamma+2}}{1+(\tau\omega)^2} \mathrm{d}(\omega\tau) = \frac{D_0 A}{\omega^{\beta-\gamma+3}} \tag{88}$$

The self-similarity is again desired the power spectrum:

$$S(\omega) \propto \frac{1}{\omega^{\alpha}} \tag{89}$$

This result concludes to an important note: the self-similarity is a more fundamental feature of the noise than its $1/f$ shape. Support this we derive instead of the $1/f^{\alpha}$ the noise spectrum from thermodynamic fluctuations, [55].

3.5. Energy Dissipation

Considering that the quantum theory of the dissipative systems is not adequately worked out, we stay within the range of the classical theory. We suppose that the pieces of information necessary for the communication are carried by the analog signals describing the physicochemical state of the individual cells. Furthermore, we are going to suppose that the self-similar Markov processes can represent the state of coaching biological subsystems. Gillespie could show that from this assumption, the equation describing the dynamics of processes can be concluded. This is the generalized Langevin equation [56]:

$$\frac{\mathrm{d}X_i}{\mathrm{d}t} = A_i\left(X_j, t\right) + D_i^{\frac{1}{2}}\left(X_j, t\right)\Gamma(t), \ \ (i = 0,1,2,\cdots,N-1) \tag{90}$$

where

$$\Gamma(t) = \lim_{\mathrm{d}t\to 0} \boldsymbol{N}\left(0, \mathrm{d}t^{-1}\right) \tag{91}$$

is the white-noise with zero mean value, infinite dispersion, and normal distribution. Let us decompose the $A_i\left(X_j, t\right)$ function into three parts:

$$A_i\left(X_j, t\right) = f_i(t) + A_i\left(X_i\right) + \sum_{k=0}^{N-1} c_{ik} X_k \tag{92}$$

where the c_{ik} elements form a cyclic matrix.

$$\bar{C} = \begin{bmatrix} c_0 & c_1 & \cdots & c_{N-1} \\ c_{N-1} & c_0 & \cdots & c_{N-2} \\ \vdots & \vdots & \ddots & \vdots \\ c_1 & c_2 & \cdots & c_0 \end{bmatrix} \tag{93}$$

$A_i\left(X_i\right)$ can be nonlinear and the $f_i(t)$ is the time function generated by the internal active processes of the cell. It is reasonable to assume that $A_i\left(X_i\right)$ is identical for each cell, and at the same way, we may suppose that D_i is constant for each cell. This latter can be justified because each cellis to be found in the same heat conditions. We did not assumed any confinement for the $f_i(t)$ function. The proposed equation is the generalization of the

model of the coupled damped oscillators, which showed [57] that the stochastic resonance is included in the forms of motion. We are going to examine a case where the social signal has low amplitude; therefore, the nonlinear members can be neglected. Then (91):

$$\frac{\mathrm{d}X_i}{\mathrm{d}t} = f_i(t) + \sum_{k=0}^{N-1} c_{ik} X_k + D^{\frac{1}{2}} \Psi(t), \ (i = 0, 2, \cdots, N-1) \tag{94}$$

3.6. Cellular Communication in a Noisy Environment

The effective field strength of thermal noise was first calculated by Weaver and Astumian [58]. The Weaver & Astumian model (W-A model) assumed changes in the field strength result from fluctuations of space charges on both sides of the cellular membrane and further showed a thermal noise limit at low frequencies. Kaune [59] revisited the W-A model and showed that the field strengths typical of thermal noise converge to zero at low frequencies. Therefore, the W-A model does not describe this region appropriately. However, thermal noise in Kaune's model [19] is assumed to be synchronized (coherent) over the entire cell membrane. This assumption is called the coherence condition. Unfortunately, thermal noise is unlikely to be coherent over a large structure such as a cell. Therefore, the calculation that followed is limited to a highly unlikely special case. Kaune set all noise-generators to be equipotential based on the coherence condition by assuming parallel connectivity and the equivalent electrical circuit. As the coherence condition does not hold in the general case, the equipotential assumption also does not hold in the general case. We generalized the problem and developed a solution [60]. Our results proved when there are only zero-mode currents present. The limit does not exist. However, at non-zero currents, the thermal noise does limit the efficacy of electromagnetic effects in low frequencies. The zero mode is the action by central symmetry for all individual cells instead of the translation symmetry of the usually applied outside field effects.

The topological construction is an essential factor of the cellular organization, [61], irrespective it is alive or not. The cellular structure, because of some topological reasons, develops preferring special coordination arrangements [62] and could arrange a self-organized collectivity [63] [64]. It was discovered that the division tendency is very low in the cell population, small in number [65]. For the start of a significant cell division, a critical cell density is necessary. This was later observed on a self-synchronization of chemical oscillators [66]. The topological importance was assumed in living cellular cultures also, [67], declaring that not the cell density but the position (coordination number) of cells related to each other determines what is favorable or not favorable from the point of view of division. This hypothesis was later justified experimentally [68].

The cells in developed multicellular living objects are grouped into organs to perform certain tasks in a network together. This network extends inside the cells and has suitable connection points outside the cell wall, ensuring with this to involve the cellular mechanisms in the tasks of the network. The cytoskeleton of the cells provides the basic cellular information-transfers intracellularly. The internal cytoskeleton network has transmembrane bridges (e.g., adherent connections, junctions) connecting the matrix structure on the outer side of the cell through the polar protein molecules [69]. The network develops by polymerization [70], where the water structures of aqueous electrolyte arrange the extracellular matrix partially. For example, the formed "intercellular filaments" in epithelial tissues implements the mechanical coupling of individual cells [71] [72]. Ordered water creates efficient proton conduction mechanisms [73] that disordered water does not have. The hydrogen bridges transport the protons, which is crucial in living systems [74]. This high-speed and low dissipation of the transport propagation is based on Grotthuss-mechanism [75].

The healthy cells are under the control of others in the network ("social" signaling [76], a collective action). Social information should spread within the body without loss of information. However, the environment is noisy, and the living information exchange faces this challenge. Now, we are going to prove that among the modes

belonging to the eigenvectors of the matrix (93) of equation (91), there are modes of zero noise spectrum. It is well known that any cyclic matrix can be diagonalized by the transformation matrix [77], that is

$$T=\frac{1}{\sqrt{N}}\begin{bmatrix}1 & 1 & \cdots & 1 & \cdots & 1\\ 1 & a & \cdots & a^{i} & \cdots & a^{N-1}\\ 1 & a^{j} & \cdots & a^{ji} & \cdots & a^{j(N-1)}\\ \vdots & \vdots & \ddots & \vdots & \ddots & \vdots\\ 1 & a^{N-1} & \cdots & a^{(N-1)i} & \cdots & a^{(N-1)^2}\end{bmatrix}, \tag{95}$$

where $a=\mathrm{e}^{i2\pi/N}$. Applying this transformation to the Equation (94), we obtain:

$$\frac{\mathrm{d}x_{si}}{\mathrm{d}t}=\lambda_i x_{si}+f_{si}(t)+\Gamma_{si}(t)\ (i=0,\cdots,N-1). \tag{96}$$

Here the new coordinates and the eigenvalues of the cyclic matrix are

$$\begin{aligned} x_{si}&=\frac{1}{\sqrt{N}}\sum_{k=0}^{N-1}a^{-ik}x_k',\quad \Gamma_{si}(t)=D^{\frac{1}{2}}\frac{1}{\sqrt{N}}\sum_{k=0}^{N-1}a^{-ik}\Gamma(t),\\ \lambda_j&=\sum_{k=0}^{N-1}a^{jk}c_k,\quad f_{si}(t)=\frac{1}{\sqrt{N}}\sum_{k=0}^{N-1}a^{-ik}f_i(t),\ (j=0,\cdots,N-1)\end{aligned} \tag{97}$$

Let us consider any one of the new

$$\Gamma_{si}(t)=D^{\frac{1}{2}}\frac{1}{\sqrt{N}}\sum_{k=0}^{N-1}a^{-ik}\Gamma(t) \tag{98}$$

noise components for which $k\neq 0$ (non-zero order component). Let us take the Fourier to transform thereof and consider that the amplitudes are unitary in the white-noise spectrum. Then we get that

$$\Gamma_{si}(t)=D^{\frac{1}{2}}\frac{1}{\sqrt{N}}\sum_{k=0}^{N-1}a^{-ik},\ k\neq 0 \tag{99}$$

On the other hand, we know that

$$\sum_{k=0}^{N-1}a^{-ik}=0 \tag{100}$$

In consequence, every non-zero order mode is noiseless because:

$$\Gamma_{si}(t)=0,\ k\neq 0 \tag{101}$$

So the zero-order noises are not only limitless by thermal noises, but the signal exchange in such a way is noiseless.

4. Conclusion

The stochastic processes drive the homeostatic harmony, synchronizes the processes by environmental noises, while the system performs the important internal signal communications noiselessly. The dynamic stochastic living systems involve characteristic resonances. Particular resonant frequencies differentiate and describe the various enzymatic processes.

Acknowledgements

This work was supported by the Hungarian National Research Development and Innovation Office PIACI KFI grant: 2019-1.1.1-PIACI-KFI-2019-00011.

Conflicts of Interest

The author declares no conflicts of interest regarding the publication of this paper.

References

[1] Modell, H., Cliff, W., Michael, J., et al. (2015) A Physiologist's View of Homeostasis. Advances in Physiology Education, 39, 259-266. https://doi.org/10.1152/advan.00107.2015

[2] Walleczek, J. (2000) Self-Organized Biological Dynamics & Nonlinear Control. Cambridge Univ. Press, Cambridge. https://doi.org/10.1017/CBO9780511535338

[3] Anteneodo, C. and da Luz, M.G.E. (2010) Complex Dynamics of Life at Different Scales: From Genomic to Global Environmental Issues. Philosophical Transactions of the Royal Society A, 368, 5561-5568. https://doi.org/10.1098/rsta.2010.0286

[4] Turrigiano, G. (2007) Homeostatic Signaling: The Positive Side of Negative Feedback. Current Opinion in Neurobiology, 17, 318-324. https://doi.org/10.1016/j.conb.2007.04.004

[5] Lloyd, D., Aon, M.A. and Cortassa, S. (2001) Why Homeodynamics, Not Homeostasis? The Scientific World, 1, 133-145. https://doi.org/10.1100/tsw.2001.20

[6] Mohr, H. (1977) Structure and Significance of Science. Springer, New York, 102.

[7] Theise, N.D. and Kafatos, M.C. (2013) Complementarity in Biological Systems—A Complexity View. Periodicals, 18, 11-20. https://doi.org/10.1002/cplx.21453

[8] Seel, M. and Ladik, J. (2019) Chapter 1. The Tragicomedy of Modern Theoretical Biology. In: Advances in Quantum Chemistry, Elsevier, Amsterdam, Vol. 81, 1-13. https://doi.org/10.1016/bs.aiq.2019.11.001

[9] Mandelbrot, B.B. (1977) The Fractal Geometry of Nature. Times Books, New York.

[10] Camazine, S., Deneubourg, J.L., Franks, N.R., et al. (2003) Self-Organization in Biological Systems. Princeton Studies in Complexity. Princeton Univ. Press, Princeton.

[11] Losa, G.A. (2009) The Fractal Geometry of Life. Rivista di Biologia, 102, 29-59.

[12] Losa, G.A. (2012) Fractals and Their Contribution to Biology and Medicine. Medicographia, 34, 365-374.

[13] Weibel, E.R. (1991). Fractal Geometry: A Design Principle for Living Organisms. American Journal of Physiology, 261, L361-L369. https://doi.org/10.1152/ajplung.1991.261.6.L361

[14] Petoukhov, S.V. (2008) The Degeneracy of the Genetic Code and Hadamard Matrices. https://arxiv.org/ftp/arxiv/papers/0802/0802.3366.pdf

[15] Voevudko, A.E. (2018) Fractal Dimension of the Kronecker Product. Mathematics.

[16] Voevudko, A.E. (2017) Generating Kronecker Product Based Fractals. CodeProject. https://www.codeproject.com/Articles/1189288/Generating-Kronecker-Product-Based-Fractals

[17] Moreno, S., Robles-Granda, P. and Neville, J. (2013) Block Kronecker Product Graph Model. https://www.semanticscholar.org/paper/Block-Kronecker-Product-Graph-Model-Moreno-Robles-Granda/ad35b967418cd01f2899b507ae008b816b4b1d82

[18] Leskovec, J., Chakrabarti, D., Kleinber, J., Faloutsos, C., et al. (2010) Kronecker Graphs: An Approach to Modeling Networks. Journal of Machine Learning Research, 11, 985-1042.

[19] Roca, J.L. (2018) Fractal-Based Techniques for Physiological Time Series: An Updated Approach. De Gruyter, Berlin.

[20] Vrobel, S. (2011) Fractal Time, Studies of Nonlinear Phenomena in Life Science. Vol. 14, World Scientific, Singapore. https://doi.org/10.1142/7659

[21] Wornell, G.W. (1996) Signal Processing with Fractals, a Wavelet-Based Approach. Prentice Hall Signal Processing Series, Prentice Hall, Upper Saddle River.

[22] Sturmberg, J. and West, B.J. (2013) Fractals in Physiology and Medicine. In: Sturmberg, J. and Martin, C., Eds., Handbook of Systems and Complexity in Health, Springer, Berlin, 171-192. https://doi.org/10.1007/978-1-4614-4998-0
[23] Deering, W. and West, B.J. (1992) Fractal Physiology. IEEE Engineering in Medicine and Biology, 11, 40-46. https://doi.org/10.1109/51.139035
[24] Bassingthwaighte, J.B., Leibovitch, L.S. and West, B.J. (1994) Fractal Physiology. Oxford Univ. Press, New York. https://doi.org/10.1007/978-1-4614-7572-9
[25] Goldenfeld, N. and Woese, C. (2010) Life Is Physics: Evolution as a Collective Phenomenon Far from Equilibrium.
[26] Szasz, A. and Szasz, O. (2020) Ch. 17. Time-Fractal Modulation of Modulated Electro-Hyperthermia (mEHT). In: Szasz, A., Ed., Challenges and Solutions of Oncological Hyperthermia, Cambridge Scholars, Newcastle upon Tyne, 377-415.
[27] Scheff, J.D., Griffel, B., Corbett, S.A., Calvano, S.E. and Androulakis, I.A. (2014) On Heart Rate Variability and Autonomic Activity in Homeostasis and in Systemic Inflammation. Mathematical Biosciences, 252, 36-44. https://doi.org/10.1016/j.mbs.2014.03.010
[28] Goldberger, A.L., Bhargava, V., West, B.J. and Mandell, A.J. (1985) On a Mechanism of Cardiac Electrical Stability—The Fractal Hypothesis. Biophysics Journal, 48, 525-528. https://doi.org/10.1016/S0006-3495(85)83808-X
[29] Kauffman, S.A. and Johnsen, S. (1991) Coevolution to the Edge of Chaos: Coupled Fitness Landscapes, Poised States, and Coevolutionary Avalanches. Journal of Theoretical Biology, 149, 467-505. https://doi.org/10.1016/S0022-5193(05)80094-3
[30] Bak, P., Tang, C. and Wiesenfeld, K. (1988) Self-Organized Criticality. Physical Review A, 38, 364-374. https://doi.org/10.1103/PhysRevA.38.364
[31] Lewin, R. (1992) Complexity, Life at the Edge of Chaos. University of Chicago Press, Chicago.
[32] Ito, K. and Gunji, Y.P. (1994) Self-Organisation of Living Systems towards Criticality at the Edge of Chaos. Biosystems, 33, 17-24. https://doi.org/10.1016/0303-2647(94)90057-4
[33] Prigogine, I. and Stengers, I. (1985) Order out of Chaos. Flamingo, London. https://doi.org/10.1063/1.2813716
[34] Chernick, M.R. (2011) The Essentials of Biostatistics for Physicians, Nurses, and Clinicians. John Wiley & Sons, Hoboken, 49-50. https://doi.org/10.1002/9781118071953
[35] Wierman, M.J. (2010) An Introduction to Mathematics of Uncertainty. Hoors Program. http://typo3.creighton.edu/fileadmin/user/CCAS/programs/fuzzy_math/docs/MOU.pdf
[36] Eskov, V.M., Filatova, O.E., Eskov, V.V., et al. (2017) The Evolution of the Idea of Homeostasis: Determinism, Stochastics, and Chaos—Self-Organization. Biophysics, 62, 809-820. https://doi.org/10.1134/S0006350917050074
[37] Billman, G.E. (2020) Homeostasis: The Underappreciated and Far Too Often Ignored Central Organizing Principle of Physiology. Frontiers in Physiology, 11, 200. https://doi.org/10.3389/fphys.2020.00200
[38] Mode, C.J., Durrett, R., Klebaner, F., et al. (2013) Applications of Stochastic Processes in Biology and Medicine. International Journal of Stochastic Analysis, 2013, Article ID: 790625. https://doi.org/10.1155/2013/790625
[39] Nigam, N.C. (1983) Introduction to Random Vibrations. The MIT Press, Cambridge.
[40] Cramer, F. (1995) Chaos and Order (The Complex Structure of Living Systems). VCH, Weinheim.
[41] Peng, C.K., Buldyrev, S.V., Hausdorff, J.M., et al. (1994) Fractals in Biology and Medicine: From DNA to the Heartbeat. In: Bunde, A. and Havlin, S., Eds., Fractals in Science, Springer-Verlag, Berlin, 49-87. https://doi.org/10.1007/978-3-662-11777-4_3
[42] Musha, T. and Sawada, Y. (1994) Physics of the Living State. IOS Press, Amsterdam.
[43] Wentian, L. (1989) Spatial 1/f Spectra in Open Dynamical Systems. Europhysics Letters, 10, 395-400. https://doi.org/10.1209/0295-5075/10/5/001
[44] Kim, J.J., Parker, S., Henderson, T. and Kirby, J.N. (2020) Physiological Fractals: Visual and Statistical Evidence across Timescales and Experimental States. Journal of the Royal Society Interface, 17, Article ID: 20200334. https://doi.org/10.1098/rsif.2020.0334
[45] Szendro, P., Vincze, G. and Szasz, A. (2001) Bio-Response on White-Noise Excitation. Electromagnetic Biology and Medicine, 20, 215-229. https://doi.org/10.1081/JBC-100104145

[46] Szendro, P., Vincze, G. and Szasz, A. (2001) Pink-Noise Behaviour of Biosystems. European Biophysics Journal, 30, 227-231.
https://doi.org/10.1007/s002490100143
[47] Szasz, D. (1994) Boltzmann's Ergodic Hypothesis, a Conjecture for Centuries? The International Symposium in Honour of Boltzmann's 150th Birthday, Vienna, 24-26 February 1994, 1-23.
[48] Sneddon, I. (1955) Handbuch der Physik Bd. II. Springer Verlag, Berlin.
[49] Seneta, E. (2016) Markov Chains as Models in Statistical Mechanics. Statistical Science, 31, 399-414. https://doi.org/10.1214/16-STS568
[50] Tsong, T.Y. and Chang, C.-H. (2007) A Markovian Engine for a Biological Energy Transducer: A Catalitic Wheel. Biosystems, 88, 323-333. https://doi.org/10.1016/j.biosystems.2006.08.014
[51] Gillespie, D.T. (1977) Exact Stochastic Simulation of Coupled Chemical Reactions. The Journal of Physical Chemistry, 81, 2340-2361. https://doi.org/10.1021/j100540a008
[52] Doob, J.L. (1942) The Brownian Movement and Stochastic Equations. Annals of Mathematics, 43, 351-369. https://doi.org/10.2307/1968873
[53] Schlesinger, M.S. (1987) Fractal Time and 1/f Noise in Complex Systems. Annals of the New York Academy of Sciences, 504, 214-228. https://doi.org/10.1111/j.1749-6632.1987.tb48734.x
[54] Shesinger, M. and West, B.J. (1988) Versus Noise. In: Stanly, H.E. and Ostrowsky, N., Eds., Random Fluctuations and Pattern Growth. Experiments and Models, Kluwer Academic Publishers, Dordrecht, 320-324.
[55] Milotti, E. (2002) 1/f Noise: A Pedagogical Review. Classical Physics. https://arxiv.org/abs/physics/0204033
[56] Gillespie, D.T. (1992) Markov Processes. Academic Press, San Diego.
[57] White, D.C. and Woodson, H.H. (1959) Electromechanical Energy Conversion. John Wiley and Sons, Inc., New York.
[58] Weaver, J.C. and Astumian, R.D. (1990) The Response of Living Cells to Very Week Electric Fields: The Thermal Noise Limit. Science, 247, 459-462. https://doi.org/10.1126/science.2300806
[59] Kaune, W.T. (2002) Thermal Noises Limit on the Sensitivity of Cellular Membranes to Power Frequency Electric and Magnetic Fields. Bioelectromagnetics, 23, 622-628. https://doi.org/10.1002/bem.10060
[60] Vincze, G., Szász, A. and Szasz, N. (2005) On the Thermal Noise Limit of Cellular Membranes. Bioelectromagnetics, 26, 28-35. https://doi.org/10.1002/bem.20051
[61] Zsoldos, I., Szendro, P., Watson, L., et al. (2001) Topological Correlation in Amorphous Structures. Computational Materials Science, 20, 28-36. https://doi.org/10.1016/S0927-0256(00)00120-8
[62] Vincze, G., Zsoldos, I. and Szasz, A. (2004) On the Aboav-Weaire Law. Journal of Geometry and Physics, 51, 1-12. https://doi.org/10.1016/j.geomphys.2003.08.003
[63] Zsoldos, I. and Szasz, A. (1999) Appearance of Collectivity in Two-Dimensional Cellular Structures. Computational Materials Science, 15, 441-448. https://doi.org/10.1016/S0927-0256(99)00031-2
[64] Maryan, M.I., Kikineshi, A.A. and Szasz, A. (2001) Self-Organizing Processes and Dissipative Structure Formation in the Non-Crystalline Materials. Physics and Chemie Status Solidi, 2, 585-593.
[65] Puck, T.T., Marcus, P.I. and Cieciura, S.J. (1956) Clonal Growth of Mammalian Cells in Vitro: Growth Characteristics of Colonies from Single HeLa Cells with and without a "Feeder" Layer. Journal of Experimental Medicine, 103, 273-283.
https://doi.org/10.1084/jem.103.2.273
[66] Taylor, A.F., Tinsley, M.R., Wang, F., et al. (2009) Dynamical Quorum Sensing and Synchronization in Large Populations of Chemical Oscillators. Science, 323, 614-617. https://doi.org/10.1126/science.1166253
[67] Caer, G.L. (1991) Topological Models of Cellular Structures. Journal of Physics A: Mathematical and General, 24, 1307-1317.
https://doi.org/10.1088/0305-4470/24/6/022
[68] Puck, T.T. and Marcus, P.I. (1955) A Rapid Method for Viable Cell Titration and Clone Production with HeLa Cells in Tissue Culture: The Use of X-Irradiated Cells to Supply Conditioning Factors. Proceedings of the National Academy

of Sciences of the United States of America, 41, 432-437. https://doi.org/10.1073/pnas.41.7.432

[69] Hamerof, S.R. (1988) Coherence in the Cytoskeleton: Implications for Biological Information Processing. In: Froelich, H., Ed., Biological Coherence and Response to External Stimuli, Springer Verlag, Berlin, 242-265. https://doi.org/10.1007/978-3-642-73309-3_14

[70] Del, G., et al. (1988) Structures, Correlations and Electromagnetic Interactions in the Living Matter. In: Froelich, H., Ed., Biological Coherence and Response to External Stimuli, Springer Verlag, Berlin, 49-64. https://doi.org/10.1007/978-3-642-73309-3_3

[71] Janmey, P. (1995) Cell Membranes and the Cytoskeleton. In: Lipowsky, R. and Sackman, E., Eds., Handbook of Biological Physics, Vol. I, Elsevier Science, Amsterdam, 805-849. https://doi.org/10.1016/S1383-8121(06)80010-2

[72] Vincze, Gy. and Szasz, A. (2015) Reorganization of Actin Filaments and Microtubules by Outside Electric Field. Journal of Advances in Biology, 8, 1514-1518.

[73] Markovitch, O. and Agmon, N. (2007) Structure and Energetics of the Hydronium Hydration Shells. The Journal of Physical Chemistry A, 111, 2253-2256. https://doi.org/10.1021/jp068960g

[74] Szasz, A., van Noort, D., Scheller, A., et al. (1994) Water States in Living Systems. I. Structural Aspects. Physiological Chemistry and Physics, 26, 299-322. http://www.ncbi.nlm.nih.gov/pubmed/7700980

[75] Agmon, N. (1995) The Grotthuss Mechanism. Chemical Physics Letters, 244, 456-462. https://doi.org/10.1016/0009-2614(95)00905-J

[76] Raff, M.C. (1992) Social Controls on Cell Survival and Death. Nature, 356, 397-400. https://doi.org/10.1038/356397a0

[77] Lanouette, W. (1992) Genius in the Shadows. Macmillan Publishing Co., New York, 350-361.

Time-Fractal Modulation—Possible Modulation Effects in Human Therapy

Andras Szasz

Department of Biotechnics, St. Istvan University, Budaörs, Hungary

* Correspondence: Szasz.Andras@gek.szie.hu

Cite this article as:
Szasz, A. (2022): Time-Fractal Modulation—Possible Modulation Effects in Human Therapy. Open Journal of Biophysics , 12, 38-87.
https://doi.org/10.4236/ojbiphy.2022.121003

Oncothermia Journal 31, 2022 March: 184-227
www.oncotherm.com/sites/oncotherm/files/2022-03/Szasz_Modulation.pdf

Abstract
The malignant processes deviate from the healthy homeostatic control, and various "tricks" enable malignant cells to avoid the healthy regulation. Consequently, the malignant structures miss the apoptosis and proliferate without restriction, and without the formation of communication networks in the newly formed cells. The modulation supports the homeostatic control to rearrange the health regulation processes in various ways. The modulation acts with stochastic processes, using stochastic resonances for molecular excitations, supporting the regulative enzymatic processes. The number of stochastic resonant frequencies is as many as the number of enzymatic reactions. The malignant cells differ structurally and dynamically in their connections and interactions from their healthy host tissues. The radiofrequency carrier is modulated with an appropriate time-fractal $(1/f)$ noise to select the autonomic cancer-cells, destroy them, or force the precancerous, semi-individual cells to participate in the networking connections. The modulation in this way limits the cellular autonomy of malignant cells and boosts the healthy control. The resonant energy triggers apoptotic processes and helps immunogenic actions deliver extracellular genetic information for antigen-presentation. The modulation is applied in clinical practice. The therapy (modulated electro-hyperthermia, $mEHT$) is intensively used in oncology in complementary applications and for palliative stages, and occasionally even as a monotherapy.

Keywords
Pink-Noise, Homeostasis, Amplitude-Modulation, Cellular-Communication, Antigen-Presentation, Stochastic Resonances, Resonance Frequencies, Cellular Networking

1. Introduction

Healthy homeostasis controls the dynamic balance in the organism, ensuring the harmony of complex micro- and macro-interactions. Cancer destroys this harmony. The modulation goal is to find and force the malignant cells into apoptosis and to restore the healthy synchrony between cells and their communication.

The malignant processes are driven by the unicellular behavior and the individualism of the involved cells. The result is the breakdown of the integrity of the multicellular organization (which normally has a healthy networking structure). Cells with autonomy behavior have potential to better adapt to environmental changes. The transformation from the organized multicellular structure seen in healthy tissues to the structure seen in tumors is driven by the primitive transcriptional programs active in malignant cells [1]. The reorganization of the tumors structure supports the unicellular behavior and autonomy of the malignant cells, promoting the survival of the "colony" of malignant cells [2]. In an attempt to correct the abnormality, the healthy host initiates processes, such as angiogenesis, nerve healing, and numerous other supports, which instead provide essential conditions for the development of the malignancy. This regulation follows the general homeostatic control of the body. From the time that the malignancy appears in the tissue, cancer becomes a systemic disease. The dynamic control mechanisms of the healthy host are not able to repair the malignant lesion due to various reasons: genetic aberrations [3], mitochondrial dysfunction [4], and other intra- [5] and extracellular [6] hallmarks of cancer. Additional challenges which the host must face are the permanent uncontrolled stress on the system exerted by the malignancy [7], the recognition of the lesion as an unhealed wound [8], inflammation [9], and the blocking of apoptotic activity in malignant cells [10].

Cancer is an organizing (networking) disease, where the cells abandon the cooperative advantages [11]. The application of a tool that can help the homeostasis mechanisms to correct the cellular disorder of the malignant lesion and induce apoptosis, could allow for the cancerous cells, which are acting autonomously, to return to a healthy network by forcing cooperative harmony. Our objective is to show the possible effects of the modulated radiofrequency (RF) carrier, and its preclinical and clinical applications, in order to achieve this goal.

2. Methods—The Modulationphenomena

The concept of modulation applied in physiology is centered on the stochastic dynamics (time-dependent events) in the biosystems. The chosen frequency spectrum is devoted to promoting healthy controls and intended to suppress cancerous processes. The carrier frequency is in the radiofrequency (RF) range which delivers an audio range $< 20\ kHz$) to the target. This method is well known and intensively applied by the various telecommunication networks (radio, TV, phone, GPS, etc.) to transfer information between the source and the distant targets.

The masking of the carrier can be achieved using different features of the RF wave, like its amplitude, frequency, or phase. The amplitude modulation was historically the first form of modulation, and it is the easiest to decode the delivered information (demodulation). The resulting shape of the signal follows the shape of modulation (Figure 1); mirroring the modulation signal at both the positive and negative side of the delivery. This amplitude modulation is very vulnerable to environmental noises and absorbents.

2.1. Why Modulation and not Direct Excitations?

The question naturally arises: while the advantages of frequency modulation include better stability over distance, less vulnerability to interferences, better selectivity, why then do we not propose applying directly the modulation frequencies in order to transmit information in biological systems without carrier frequency?

The challenge is to deliver the low frequency to the body and the selected places. The low frequencies are blocked by the heterogenic isolating (capacitive) factors in the application. The adipose tissue in the layer at the skin, the various membranes, and isolation compartments block the low-frequency current because their electric impedance inversely depends on the frequency. This resistivity becomes too high in low frequencies, and no deep targeting of structures is possible. In order to overcome the adipose layer, invasive application could be introduced, but other isolations remain.

The proper solution for the direct effect would be the invasive application of low-frequency, electrodes in the tumor itself, where the low-frequency effect of isolators is negligible. However, the inserted electrodes develop a layer on the surface of electrodes in the tumor, which produces a complex impedance effect (Warburg impedance, Z_W) [12] and has an inverse-square-root dependence on the frequency (f). In a case of planar-electrode and sinusoidal supply, the Warburg impedance is [13]:

$$Z_W(f) = A\frac{(1-i)}{\sqrt{f}} \tag{1}$$

where A is a constant and $i = \sqrt{-1}$. To avoid the Warburg impedance, a high

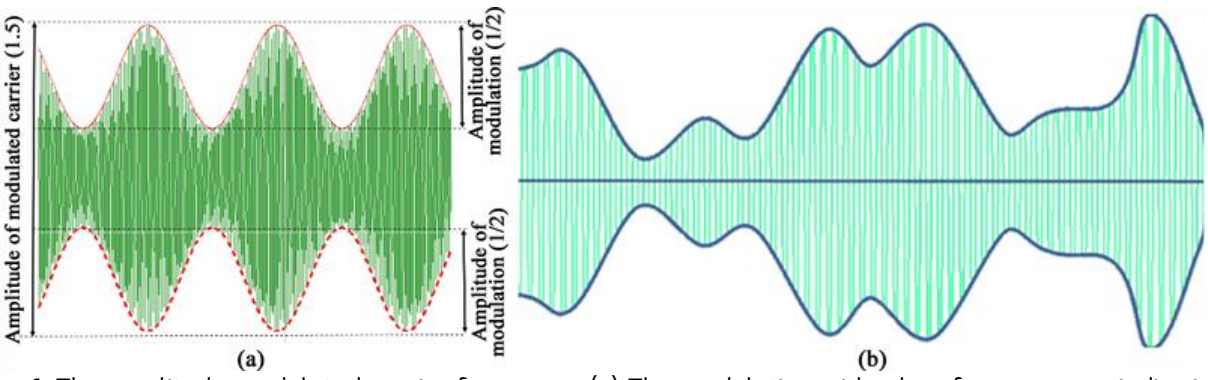

Figure 1. The amplitude modulated carrier frequency. (a) The modulation with a low-frequency periodic signal, (b) the modulation with a non-periodic signal with frequency variants.

frequency is necessary. This noise could limit the accuracy of the measurements. However, in low frequencies, the large Warburg resistance also produces large electric noise because the electric noise of the resistance is proportional to the value of the actual resistivity [14].

The other advantage of the high frequency carrier is its impedance selection, which focuses the effects on the malignant cells, with the dispersion relation to attack the membrane rafts for exciting extrinsic signal pathways to apoptosis.

2.2. The Modulation Process

The electromagnetic interactions with real biological systems are faced with a heterogeneous, non-linear, and complexly regulated target. The in vitro (cell lines), the ex-vivo (tissue samples), the in-vivo (animal experiments), and human applications differ from each other due to the heterogeneity and organization of the biological target. The active regulation processes in the targets, which are complex, could change the electrolytes in the tissue, varying the inhomogeneities, causing further complications in the evaluation of the interactions. The heterogeneity of the targets influences the results; however the structure and function of the cellular membranes have strong similarities, which allows for the use of some unified considerations.

The average isolation of the various membranes in the tissues is enormous $\approx 10^{13}\,\frac{\Omega}{m}$ [15]. It is so large that it can keep $\approx 70\,mV$ at a distance of $\approx 7\,nm$, which is equivalent to ten million volts at a distance of one meter ($\approx 10^{7}\ V/m$), and its capacity is $\approx 10^{-2}\,\frac{A\cdot s}{V\cdot m^2} = \frac{\mathrm{F}}{m^2}$.

The cellular membrane, regulating the ionic transport of selected ionic species in and out of the cells. The idea corresponds to the triode or transistor when the current that flows through the device is non-linearly regulated with an intermediate action (net of base), which could amplify the time-dependent signal. The membrane is also a non-linear element [16]. Applying an RF signal on the membrane, it increases non-linearly Figure 2. The rectification is not ideal because a small amount of the opposite current also exists.

Measurement of the non-temperature dependent rectification (non-linearity) is not simple because it is not measurable through the living object when the integrity of the cells is intact. The current traveling through the cell meets twice with the transmitted signal, first from outside to inside the cell, and the second meeting is in the opposite direction. The two effects eliminate each other. The lipid bilayer, together with the ionic exchanges, completes the rectification phenomena [17] [18].

We had shown [19] the white noise excited linear system with infinite freedom, and cyclic symmetry emits pink noise. It works like a special filter creating $1/f$ noise from the non-correlated white noise spectrum, which was measured [20].

The Fourier transformation of $x(t)$ pink noise is:

$$F(f) = \frac{A}{i2\pi\sqrt{|f|}} \tag{2}$$

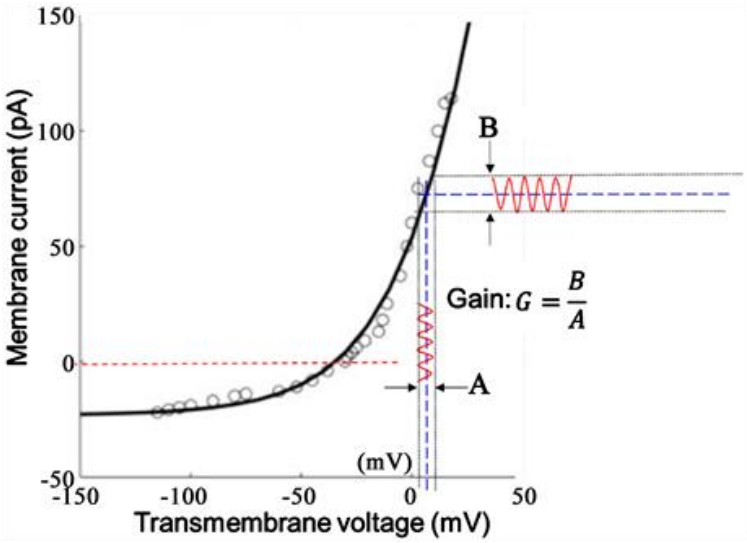

Figure 2. The membranes of cells have enormously large polarization potential ($\approx \frac{70\ mV}{5\ nm} = 1.4 \cdot 10^7\ V/m$), which non-linearity rectifies the RF current. Due to the non-linearity, the rectification increases the signal amplitude A to B (gain: $G = B/A$).

where A is the amplitude. The noise power spectrum:

$$S(f) = F^*(f)F(f) = -i\frac{A}{2\pi\sqrt{|f|}}i\frac{A}{2\pi\sqrt{|f|}} = \left(\frac{A}{2\pi}\right)^2\frac{1}{|f|} \tag{3}$$

where the star is a sign of conjugation. Let be the signal function $v(t)$ of the carrier signal

$$v(t) = U_0\, cos\, 2\,\pi f_v t \tag{4}$$

where $f_v = 13.56\text{MHz}$ is the frequency of the carrier, U_0 is its amplitude (voltage in electric signal). The f_v carrier

$$Y(f) = \frac{1}{2}F(f - f_v) + \frac{1}{2}F(f + f_v) \tag{5}$$

frequency is in the overlapping range of β/δ -dispersions. The Fourier transform of the $y(t) = x(t)\, cos\, 2\,\pi f_v t$ modulated signal:

The Fourier transform of the pink noise modulated carrier is:

$$Y(f) = \frac{1}{2}\frac{AU_0}{i2\pi}\frac{1}{\sqrt{|f - f_v|}} + \frac{1}{2}\frac{AU_0}{i2\pi}\frac{1}{\sqrt{|f + f_v|}} \tag{6}$$

Physically, only positive frequencies can be realized, so the power spectrum is:

$$S(f) = -i\frac{1}{2}\frac{AU_0}{2\pi}\frac{1}{\sqrt{|f - f_v|}}i\frac{1}{2}\frac{AU_0}{2\pi}\frac{1}{\sqrt{|f - f_v|}} = \\ = \left(\frac{AU_0}{4\pi}\right)^2\frac{1}{|f - f_v|} \tag{7}$$

The power spectra of pink noise and pink noise embedded in the carrier are shown in Figure 3. The noise power spectrum shifts to the $\omega_0 = 2\pi f_0$ circular frequency of the periodic carrier.

2.2.1. Amplitude Modulation-Stochastic Resonance

Many chemical reactions have a coordinated subsequent chain, having a series of reactions in a definite order. This set is called the Markov process, a chain-like stochastic reaction-line. When the sequence of the realized states is such, each step depends solely on the state realized in the previous event Figure 4.

The biological processes have well-organized and controlled Markovian chain reactions, avoiding the sudden single-step liberation of energy during the catabolism. The series of effects in the time dynamics are Markovian. A two-state Markov process in which we assume that the coefficients can be influenced by an external electric field are described as follows:

$$\begin{aligned} \frac{dp_1}{dt} &= -\alpha p_1 + \beta p_2 \\ \frac{dp_2}{dt} &= \alpha p_1 - \beta p_2, \\ p_1 + p_2 &= 1 \end{aligned} \tag{8}$$

where p_i $(i = 1,2)$ is the probability of the actual state, and α and β depend on the external electric field. This is the master equation of a Brownian particle bouncing back and forth in a potential well with two minima, excited by a force of an external periodic field.

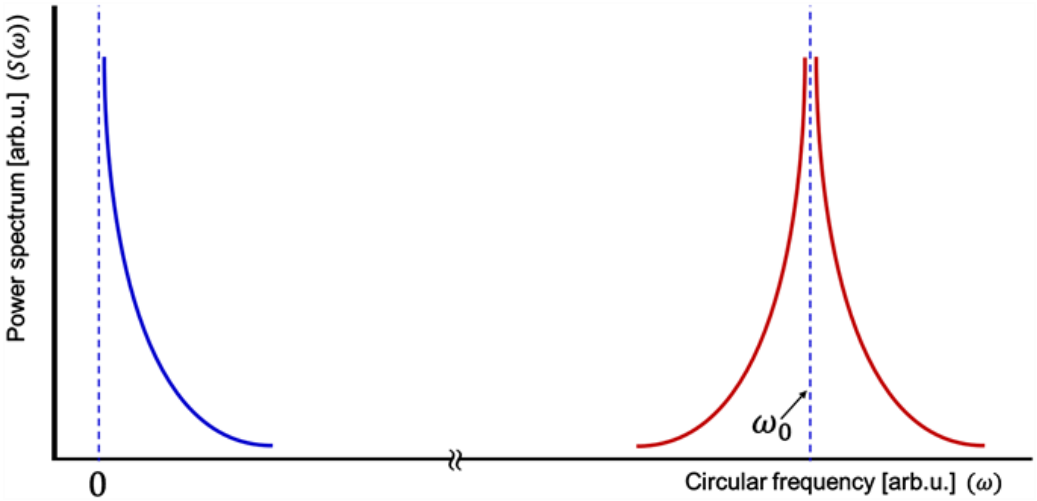

Figure 3. Power spectrum of pink-noise voltage amplitude modulated signal. The shifted pink-noise signal modifies the one-sided distribution towards symmetry around ω_0.

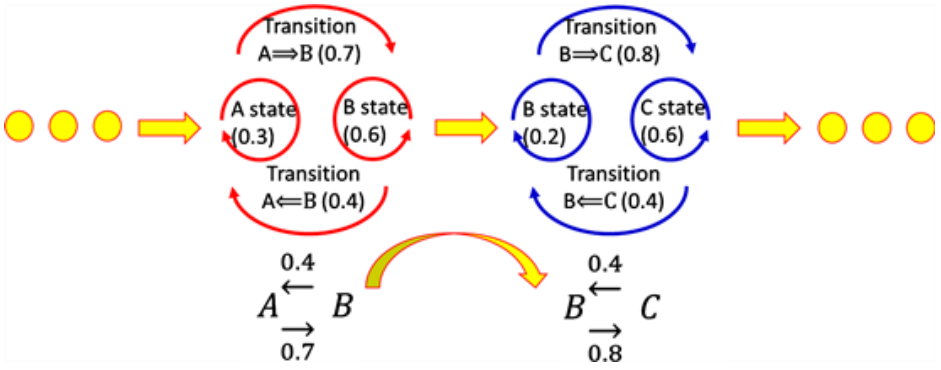

Figure 4. The Markov process is a sequential series of stochastic processes with individual reaction probabilities.

The cell works appropriately as long as the catalyst enzymes are not poisoned and, obviously, as long as the catalyst has something to catalyze. More specifically, although coenzymes provide a high degree of enzyme

selectivity, there may be substances which have suppressor functions (enzyme poisons) that react in an opposite enzymatic way, or the coenzymes act to support the enzyme reaction (promoter function). On the other hand, when the cell actually does not have molecules to catalyze, the chemical reactions are terminated. We assume that the two states of the enzyme, A, and B, are stable but interchanging. The two states are the result of chemical reactions, with α forward, and β backward reaction rate:

$$A \underset{\leftarrow}{\overset{\rightarrow}{}} B \tag{9}$$

The concentration of the enzyme by $[A]$ and $[B]$ in confirmation states A and B. Then, the kinetic equations of the reaction in (9):

$$\begin{aligned} \frac{d[A]}{dt} &= -\alpha[A] + \beta[B] \\ \frac{d[B]}{dt} &= \alpha[A] - \beta[B] \end{aligned} \tag{10}$$

Enter the quantities in (10): $[T] = [A] + [B],\ p_1 = \frac{[A]}{[T]},\ \ p_2 = \frac{[B]}{[T]}$, the equation has the same form as the master Equation (8).

The study of a voltage-gated ion channel defines $A \equiv O$, and $B \equiv C$, where O is the open state and C is the closed state. In this way, the kinetic equation of the ion channel is again the master Equation (8).

To determine the mathematical form of transient probabilities, we examine the stationary state of (8). Then, $\frac{dp_i}{dt} = 0$

$$\frac{p_1}{p_2} = \frac{\beta}{\alpha} \tag{11}$$

The energy of the two states $\pm\Delta E$ deviates from the reference level and assumes a Boltzmann distribution:

$$\frac{p_1}{p_2} = \frac{\beta}{\alpha} = \frac{e^{-\frac{E_0+\Delta E}{kT}}}{e^{-\frac{E_0-\Delta E}{kT}}} \tag{12}$$

We obtain the Arrhenius law for reaction rates from (12):

$$\alpha = Ce^{-\frac{E_0-\Delta E}{kT}},\ \ \beta = Ce^{-\frac{E_0+\Delta E}{kT}} \tag{13}$$

With this, from (8), we get a differential equation; e.g., for p_1

$$\begin{aligned} 2\tau\frac{dp_1}{dt} &= -(e^{\frac{\Delta E}{kT}} + e^{-\frac{\Delta E}{kT}})p_1 + e^{-\frac{\Delta E}{kT}}, \\ 2\tau &= \left(Ce^{-\frac{E_0}{kT}}\right)^{-1} \end{aligned} \tag{14}$$

Apply Taylor series and stop at the first term, then

$$\frac{dp_1}{dt} = -\frac{1}{\tau}p_1 + \frac{1}{2\tau} - \frac{1}{2\tau}\frac{\Delta E}{kT}, \quad 2\tau = \left(Ce^{-\frac{E_0}{kT}}\right)^{-1} \tag{15}$$

When the field strength is a harmonic function of time, the energy depends on it linearly:

$$\Delta E = a \sin \omega t \tag{16}$$

From (15) and (16), we get

$$\frac{dp_1}{dt} = -\frac{1}{\tau}p_1 + \frac{1}{2\tau} - \frac{1}{2\tau}\frac{a}{kT}\sin \omega t \tag{17}$$

To find the form of the excitation, the stationary solution of the following inhomogeneous differential equation has to be determined:

$$\frac{dp}{dt} + \frac{1}{\tau}p = -\frac{1}{2\tau}\frac{a}{kT}\sin \omega t \tag{18}$$

which is

$$\hat{p}(kT) = \frac{a}{2kT}\frac{1}{\sqrt{\tau^2\omega^2 + 1}} = \frac{a}{2kT}\frac{1}{\sqrt{1 + \left(\frac{e^{\frac{E_0}{kT}}}{2C}\omega\right)^2}} \tag{19}$$

The solution shows that the probability associated with such an excitation varies according to a harmonic function with time, regarding the noise intensity of the thermal background kT It follows a sharp maximum at a given f frequency as a function of kT noise intensity Figure 5. Formulate this result oppositely: this also means that there is a frequency where the amplitude is maximum for a given noise level. The stochastic resonance rules also such microscopic molecular structural changes like the protein folding phenomenon [21].

2.2.2. Demodulation Stochastic Resonance

The modulated carrier signal targets the selected malignant cells, and the cells rectify (demodulate) the received signal. The demodulation is basically a rectification process, which uses stochastic resonance [22]. The decomposition of (14):

$$2\tau\frac{dp_1}{dt} = -(2 + \left(\frac{\Delta E}{kT}\right)^2)p_1 + 1 - \frac{\Delta E}{kT} + \frac{1}{2}\left(\frac{\Delta E}{kT}\right)^2, \quad 2\tau = \left(Ce^{-\frac{E_0}{kT}}\right)^{-1} \tag{20}$$

Assume the field strength of the modulated signal is a harmonic function of time and let the energy depend linearly on it

$$\Delta E = a(1 + m\cos\Omega t)\sin\omega t \tag{21}$$

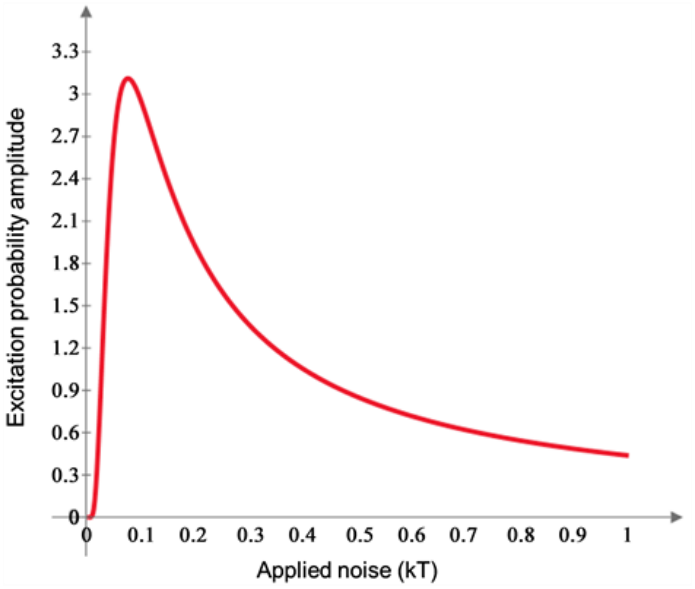

Figure 5. The change in the amplitude of the stochastic resonance probability as a function of the kT noise intensity (Calculated by PTC MathCad).

where $m < 1$, the modulation depth Ω is the modulator and the ω carrier frequency.

Substituting this into our previous equation, we get that

$$\begin{aligned} & 2\tau\frac{dp_1}{dt} \\ & = -(2 + \left(\frac{a}{kT}\right)^2 (1 \\ & + m\cos\Omega t)^2 \sin^2\omega t)p_1 + \\ & +1 - \frac{a}{kT}(1 + m\cos\Omega t)\sin\omega t \\ & + \frac{1}{2}\left(\frac{a}{kT}\right)^2 (1 + m\cos\Omega t)^2 \sin^2\omega t, \\ & 2\tau = \left(Ce^{-\frac{E_0}{kT}}\right)^{-1} \end{aligned} \tag{22}$$

As a function of probability over time, there is a slow change and a rapid fluctuation. The first is from the modulation, and the second is from the carrier.

We are only interested in slow change now. To filter this out of the above equation, we average it over the time of the carrier period. In this case, the slow signal can be considered constant for the time functions, and the time average can be replaced by the fast one.

Under this rule, the slow change is

$$2\tau\frac{dp_1}{dt} = -(2+\left(\frac{a}{\sqrt{2}kT}\right)^2(1 + m\cos\Omega\, t)^2)p_1 + \\ +1+\frac{1}{2}\left(\frac{a}{\sqrt{2}kT}\right)^2(1+m\cos\Omega\, t)^2 \\ 2\tau = \left(Ce^{-\frac{E_0}{kT}}\right)^{-1} \tag{23}$$

equation describes.

Suppose the modulation depth is small. Then our above equation can be further simplified:

$$2\tau\frac{dp_1}{dt} \\ = -(2+\left(\frac{a}{\sqrt{2}kT}\right)^2(1 \\ + 2m\cos\Omega\, t))p_1 + \\ +1+\frac{1}{2}\left(\frac{a}{\sqrt{2}kT}\right)^2(1 \\ + 2m\cos\Omega\, t) \tag{24}$$

This is now a linear differential equation with variable coefficients.

Although there is a general solution to this, we are not going anywhere with it, so we will apply the method of successive approximation to the solution.

Since we are looking for resonance, we only study the effect of the harmonic excitation function:

$$2\tau\frac{dp}{dt} + [2+\left(\frac{a}{\sqrt{2}kT}\right)^2 \\ +\left(\frac{a}{kT}\right)^2 m\cos\Omega\, t]p = \\ =\left(\frac{a}{\sqrt{2}kT}\right)^2 m\cos\Omega\, t \tag{25}$$

Introduce the

$$F(p) := 2\tau\frac{dp}{dt} + [2+\left(\frac{a}{\sqrt{2}kT}\right)^2 +]p, \\ f(p) := p\left(\frac{a}{kT}\right)^2 m\cos\Omega\, t \tag{26}$$

expressions that are continuous functions of p.

Steps of successive approximation:

$$F(p_1) = \left(\frac{a}{\sqrt{2}kT}\right)^2 m \cos \Omega\, t, \tag{27}$$
$$F(p_2) = f(p_1),$$
$$F(p_i) = f(p_{i-1})$$

Now it's true that

$$F(p_1) + F(p_2) + \ldots + F(p_i) = F(p_1 + p_2 + \ldots + p_i) = \left(\frac{a}{\sqrt{2}kT}\right)^2 m \cos \Omega\, t + f(p_1) + f(p_2) + \ldots + f(p_{i-1}) = \left(\frac{a}{\sqrt{2}kT}\right)^2 m \cos \Omega\, t + f(p_1 + p_2 + \ldots + p_{i-1}) \tag{28}$$

If the procedure is convergent, then if $i \to \infty$,, the line proceeds to the solution, and due to the required continuity the above expression reduces to the simple equation:

$$F(p) = \left(\frac{a}{\sqrt{2}kT}\right)^2 m \cos \Omega\, t + f(p) \tag{29}$$

Now let's look at the first approximation! This gives a solution of a smooth diff equation.

$$2\tau \frac{dp_1}{dt} + [2 + \left(\frac{a}{\sqrt{2}kT}\right)^2 +]p_1 = \left(\frac{a\sqrt{m}}{\sqrt{2}kT}\right)^2 \cos \Omega\, t \tag{30}$$

The amplitude of the variable probability according to the harmonic function with modulating frequency can now be determined as follows:

$$\hat{p_1}(RT) = \left(\frac{a\sqrt{m}}{\sqrt{2}kT}\right)^2 \frac{1}{\sqrt{4\tau^2\Omega^2 + \left[2 + \left(\frac{a}{\sqrt{2}kT}\right)^2\right]^2}} = \left(\frac{a\sqrt{m}}{\sqrt{2}kT}\right)^2 \frac{1}{\sqrt{\left[2 + \left(\frac{a}{\sqrt{2}kT}\right)^2\right]^2 + \left(e^{\frac{E_0}{kT}}\frac{\Omega}{C}\right)^2}} \tag{31}$$

It is a resonance again Figure 6.

2.3. Effects of Modulation in Human Therapy

The expected actions mark out the following basic goals:

1) Supports the healthy network over the unhealthy network.

2) Selectively targets the cancer.

3) Supports the immune system, boosts the homeostatic harmony and chains of reactions.

4) Excites the selected molecules in selected cells for special molecular and immunogenic changes.

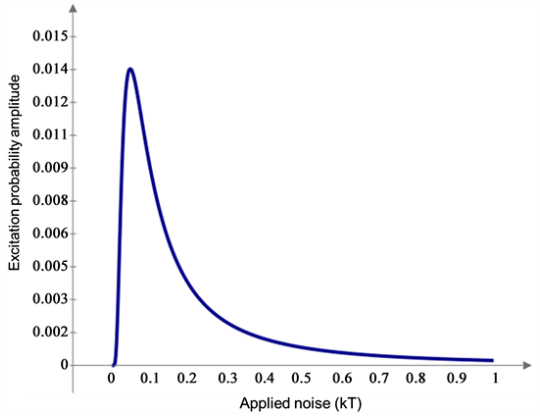

Figure 6. The amplitude of the demodulation stochastic probability depends on the noise intensity too (Calculated by PTC Math Cad).

Due to the complex interconnection of the living objects, these effects are overlapping and are supporting each other.

In the following sections, we focus on emphasizing the features of modulation for fighting against cancer, which is a disease of the dynamic equilibrium breaking the multicellular cooperative network into unicellular individualism of the autonomic "selfish" cells. The task is twofold:

1) find and destroy the malignant cells. The intention is to act with the local treatment systemically, extend the task to the entire body;

2) force cellular homeostasis harmony with a homeostatic synchronization signal.

2.3.1. Boost the Healthy Network

The role of each cell supports each other in the cellular network in a tissue, there must be an interaction between them to realize this. One such possibility is the cyclic interaction in which the thermal noise is eliminated and instead a noiseless mode of information exchange appears [23]. When an abnormality occurs in cellular functions the cyclic symmetry locally brakes. The networked communication between the cells develops disturbances and that became noisy resulting in a break in the communication between cells. The thermal noise at least locally overtakes the healthy harmony. This is a change in the physiological information and is accompanied by broken psychological harmony causing a malaise state.

The social inclination is encoded by evolution into DNA. It is capable of creating a form of movement in which only noiseless modes are realized. As a result, two effects are realized, the noiseless communication, and harmony of physiochemical processes with stress and hormone dependent psychochemical ones. This later is a brain-controlled systemic process, fixing the well-being.

1) One of the crucial steps to re-establish the cyclic symmetry is the synchrony between the cellular activities. The self-synchronization of the chemical processes was observed in the famous Belousov-Zhabotinsky (BZ) reaction [24]. The BZ reactions are far from thermal equilibrium and evolve chaotic features [25], providing a chemical model of self-organized, synchronized but non-equilibrium biological processes and noise-assisted ordering [26]. The self-synchronization of chemical oscillators is also a known phenomenon [27]. An interesting example of neurological harmony is the synchrony promoted by the music affecting neuronal interactions merging the γ, β, and θ EEG signals as electrical synchrony [28]. Recognition of the harmony in 1/f noise fluctuations in music [29], connected to the short-range autocorrelation of rhythms [30]. The synchrony between the living components and the connected, synchronized coupling in living organisms is essential, and the resonance is a highly effective way to achieve it [31]. When the living system functions normally, there are noiseless modes of internal communications. The environment is however noisy, and the living information exchange faces this challenge. This means that the system must work among various external noises and must be perfectly controlled, even in changing thermal white-noise resulting from temperature in a physiologic interval. This ensures the dynamic equilibrium, the homeostasis.

2) The physiological state includes a dynamic chemically driven psychological state in the living organism corresponding to well-being. The relationship between physiological and conscious processes has puzzled many researchers, including Schrödinger [32]. Apparently, the physicochemical processes that take place in each cell are the same, but the healthy cells are under the control of others in the network ("social" signaling [33]) which is a collective action. Social information should spread within the body without loss of information. This accompanied psychological process corrects the well-being. The realization of stochastic resonance indicates that the states of well-being are discrete. Their change is like a "resonance". Based on a finite number of distinguishable states of well-being, it is also likely that the number of modes of communication or modes of disintegration is finite.

The stored information passed down to the new cells through the individual DNA molecules regulates the organ's function, but cannot be designated as controllers of the described self-organized communication. Despite their ability to store all the information about the body in the nucleic DNA, the cells, due to the organ collectivity, use only those pieces of information appropriate to their tasks in the organ. The intranuclear DNA is a blueprint for the production of the new cell. This condition provides amazingly high safety in the functioning of the organ. The "social" communication allows the organ to function even when a part of it is damaged. This is essentially Neumann's concept of realizing a high-reliability system from low-reliability ones [34].

As the network becomes extensive, the communication signal goes over greater distances in an intensively noisy environment, so more and more information is being lost by distance. In the end, the cell cannot recover the received information. Beyond a limit, noise wins, no matter how good the noise-suppressing ability of the communication network of cells is. It can be assumed that the disintegration of the information network is a process similar to the phenomenon of stochastic resonance, i.e., the addition of a small amount of noise leads to the emergence of novel, primarily chaotic behavior. It is reasonable to assume that with stochastic resonance, that cell that lost its communication commits suicide, i.e., ends up with apoptosis.

The collective excitations comprise the non-local waves and activate the energy flow in the homeostatic networks. These excitations are mainly in the low-frequency range, and the expected frequency spectrum follows the natural 1/f fluctuations [35].

The self-similar self-organizing process is collective [36] and relates to the scale-independent phenomena [37]. Terminals of a circulatory system to supply an organ adjacent to the cells are equivalent and supply the cells with the same functions equally. The collectivity subordinates the individual needs to the groups and optimizes the energy distribution for the best survival with the lowest energy consumption. This energy-share works like some kind of democracy [38].

One of the fundamental ordering principles for healthy living subjects is a characteristic "democratic" energy supply in their organisms for optimal energy consumption. The "democratic" idea is more general than just the energy supply. It characterizes the information distribution, as well [39].

This "democracy" is regulated by general biophysical rules, governed by the competition for resources in micro- and macro-phenomena, having intensive interaction with their environment. The goal of the multicellular living object is forming cooperation, optimizing the energy intake. Due to its energetically openness, the individual living object needs internal cooperative distribution of the incoming energy. The survival of its parts determines the overall survival of the object, so the optimization of energy distribution is crucial.

In healthy multicellular systems, numerous mitochondria help the individual cellular functions. Even the otherwise similar cells may vary substantially in their mitochondrial content, together with their size and membrane potential [40]. The variation arises from uneven partitioning at cell division, producing extrinsic differences in energy demand and supplied cellular processes [41]. The cells which have considerable energy demand for their normal function have a higher number of mitochondria. For example, the mitochondria fill up ~20% of the entire cell volume of human liver cells, and they work cooperatively to serve the extreme hepatocellular ATP demand [42]. The uneven mitochondrial density in different kinds of cells shows the energy distribution problem between the cells. The cells use different energies depending on their function, so the "democratic" distribution of energy between all cells equally obviously does not work. However, another kind of "democracy" works: the cells have well-controlled and balanced energy parts depending on their function in the collective. The structure of the entire system optimizes the energy distribution. The energy balance realizes a variation of the transport network supplying the variations of the demand. This directly requires that the fractal structure of transport is not unified as structure in the system, but of the formed or homeostatic demands.

The balancing of autocracy and democracy characterizes the evolution when the "selfish gene" [43] attempting to dominate all processes, but the environment-dependent self-organization requests democratic decisions; otherwise, the process blocks the system's complexity. The game with two actions to cooperate or defect well approaches the biological interactions [44]. The relevance of the strategies of such alternating games is sometimes more appropriate than synchronous games [45].

Moreover, the complex homeostatic control shows the balancing of feedback mechanisms. The negative-feedback interaction tunes to keep the actual state as close to the accurate value, determined by the self-organizing system. Nevertheless, the system is energetically open, which is the mandatory condition for life, so the positive feedback mechanisms force some reactions, determining the metabolic processes in both directions (catabolism and anabolism). This obligatory constraint derives a certainly autocratic line when the probability of reactions drives the defined direction so the processes. Such necessary autocratic strategies can be beneficial for exerting control over asymmetric interactions [46]. The regulatory networks have many similarities, from microbes to humans [47]. The regulation of collaboration and cooperation massively boosts the democratic character with overall genomic complexity. The regulatory effects in complexity have a propensity to a partnership supporting the democratic structure, whereas others regulate primarily in isolation, in a more autocratic fashion [48]. The degree of collaboration forming autocratic, in opposition to democratic, behavior is a specific character of the complexity in the open living systems.

Considering the complexity, the compulsory synchronization attempt by external modulated electric forces looks like a promising strategy in the cases when the collective harmony (the homeostatic regulation) is lost.

2.3.2. Selecting Mechanisms

The biochemically masked, hidden tumor cells show biophysical peculiarities. This biophysical evidence is not enough to turn the immune attention on the tumors but could select them and force the selected cells to show their factual genetic errors.

The first recognizable feature is their enlarged metabolic rate. Due to the intensive proliferation, the energy demand of these cells exceeds the rate of their healthy hosts. The ion transports in their environment increase the conductivity as a result of the higher ionic concentrations. So the adequately chosen RF current has a higher current density in the tumor region, where the electric conductivity is higher than in the healthy host. The high current density in tumor allows for the use of the RF energy to act selectively on cancer and host tissues.

The impedance measurements on Erlich solid tumors [49] identifies the particular fractal structure of malignancy. As the above discussions explained, the malignant specialties dynamically lower the conductivity of the tumor and the definite percolative self-similarity, with a lower impedance than the healthy host [50].

The biophysical selectivity has another distinguishing phenomenon due to the cellular autonomy of cancer cells [51] [52]. The intensive proliferation forms the autonomic feature of the cancer cell. The cytoskeleton of the cells frequently collapses and re-polymerises due to frequent fission. The intercellular connection is connected to the mitotic spindle [53], so the dividing cell breaks its connections with the neighbors during the division process [54]. Autonomy is a perfect concept as a hallmark of malignant cells. However, this hallmark formulates a more uncomplicated situation than the complex process works in reality [5].

Nevertheless, one factor of this phenomenon offers a selection possibility, the weakening or complete loss of the networking connections of these cells to their neighbors. The loss of the cadherin intercellular links promotes tumor growth [55], and allows increased motility of the cells [56], and changes the microenvironment around it. The rearrangement of the structure in this region, due to the autonomic behavior, changes the dielectric permittivity, distinguishing these cells' changed impedance from the healthy cells [57]. The modified environment makes the cell recognizable by the RF-current, which flows through the selected tumor.

The third selective factor uses the modified structure of the tissue's pattern, which is a usual experience of the pathologists to identify the stage and prognosis of the malignancy. The pattern changes the impedance for the RF-current, and also its reaction to the modulation of the carrier frequency fundamentally differs when it forces healthy harmony. The well-chosen modulation delivers such a time pattern, which corresponds with the homeostatic dynamism, and is synchronized with some basic phenomena. But, the cancer is out from this harmony, and the modulation drastically differs from their dynamic properties. There is a simple analogy to represent this process with the pushing of the swing in the playground. When the push is in harmony with the swing's pendulum, it keeps moving with a small amount of energy; however, when the energizing push is out of harmony, considerable energy is lost, and the swing loses its kinetic energy. The applied modulation (synchronization) strategy has to be harmonized with the homeostatic regulation of individual systems.

2.3.3. Control the Autonomy of Cells

Distinguishing the networked, and individual cells was studied in detail by the Nobel Laureate A. Szent-Gyorgyi. He applied an etiological approach: how does the cellular collectivity disappear [53] ? He focused on the pyruvate metabolic pathways for ATP production. He termed the cell which uses the pyruvate dominantly on fermentative way α-state, which characterized the start of cellular evolution when no free oxygen was available [58]. This developmental period was unicellular, with the simple operation of life and replicated as much as possible. These individual cells compete for their demands; acting autonomously, without any cooperative communication. The appearance of free oxygen changed the game of life and made it possible to develop cooperative multicellular units, called β-state. The energy production was taken by a "power plant" in the cell, the mitochondria. Intensive diversity of life was available. The cooperatively connected cells in β-state share the tasks of living processes, to optimize the efficacy of the life.

The evolution on the cellular level is explained by an interplay of α- and β-stages [53]. The regular cooperative system in β-stages interrupted by the reproduction process when the cell breaks its collective functions, became an individual (α-state) to produce its daughter cells, and after this, integrates with the new cells into the system forming β-states. So the α-state locally terminates the multicellular cooperative complexity. The cooperative living complexity easily and naturally transforms into a basic, dividing α-state. When the network is broken, the system becomes unstable, parallel with stable, independent cells in α-state form [59]. The cells in β-state are cooperative, energizing themselves with oxidative metabolism provided by their mitochondria. Their division should be strictly controlled by the networking cells and dynamic processes.

Normal cellular division transforms locally the β-state to α-state, which is a normal process in the multicellular system, although it hurts the systemic collectivity in that local volume. Irregularity happens when the dividing cell remains in α-state, because the individual local conditions prefer autonomy, which ensures a high amount of energy intake to the cell. The long-time optimal collective demand overcame the individual interest of the cell. This state develops cancer which is regarded as "dismantling of multicellularity" [60].

The embryonic cellular organization could be a model of how the cancerous cluster can be stabilized. The "renegade" single-cell [61] is the cell born with a genetic deviation allowing its further development to remain individual. This behavior could be the starting step of forming a malignancy. The driving principle is the mass-dependent allometry of tumor mass [62]. The observed scaling follows from the linear dependence of the relative changes of the parameters. In general, when c is a constant and a and b are the parameters, then:

$$\frac{db}{b} = \mathrm{c}\frac{da}{a} \tag{32}$$

The (32) scaling is observed in the allometric comparison of the various living masses and their metabolic rates [63], where the basal metabolic rate of tumor (B_c) is proportional with $3/4^{th}$ of the M mass of the tumor: $B_c \propto M^{3/4}$, so the metabolic rate for unit volume:

$$\frac{B_c}{M} \propto M^{-1/4} \tag{33}$$

On the other the lifespan T of the tumor also has approximately the same dependence from the mass [64]:

$$T \propto M^{1/4} \tag{34}$$

Note that the universality of the values of exponents has intensive debates [65] [66] [67]. However, there is a consensus that the exponent α<1α<1. This also means that as the final mass increases, the metabolism of unit mass decreases, and at the same time, the mortality rate of the cells lowers. Compare the approximated lifespan of tumor (T_{tumor}) and the healthy part of the body ($T_{healthy}$), using the estimate in (34):

$$\frac{T_{tumor}}{T_{healthy}} = \left(\frac{M_{tumor}}{M_{healthy}}\right)^{\alpha} \tag{35}$$

where $\alpha < 1$ (most frequently it is $\alpha \cong 1/4$) and M_{tumor} and $M_{healthy}$ are the mass of tumor and the healthy body part which is affected by the tumor, respectively. It is obvious, that $M_{tumor} < M_{healthy}$, so from(35)

$$\frac{T_{tumor}}{T_{healthy}} < 1 \tag{36}$$

We assume that the regulators of complete homeostatic control (proliferation, morphogenesis, physiology, immune system, etc.) have an intervention time varying according to (34). As a result of (36), the regulation time of the tumor is shorter than the healthy reaction. Hence, the tumor reacts quicker than the healthy regulation system, so its growth escapes from the standard supervision. The consequence of this is that the regulators in the body are unable to control an activated cancerous cellular cluster.

Since the embryonic cell must be connected to the food network of the adult body, it must develop and increase in its direction by a known mechanism of vascularization. But in the adult body, it is also slow as it has adapted to the adult body. The process goes through the genetic instability of cancer [68] [69]. The p53 gene is the guardian of the genome. It ensures that the genome is stable for the long term. This requires that the p53 gene maintains the appropriate level of p53 protein in the intracellular space. A change in environmental conditions is a stress effect. When it persists for a long time, permanent stress is created. Inflammation and hypoxia are lasting stress effects, reducing the level of p53 protein in the cell. The weakened stability of the genome is observed by inflammation [70], and hypoxia [71], and so increased likelihood of mutations appears. The bystander effect produces precancerous cells in the neighborhood of the cells with intensive permanent stress and the consequent genetic instability [72]. The control needs re-regulation of the tumorous area locally and also systemically [73].

2.3.4. Excite Selected Molecules

The special autonomy and high metabolic activity of the malignant cells allow recognition, and the selection and attack of them. The energy provided with the carefully chosen RF current targets the selected cells and excites a few chemical changes in the selected malignant cells.

Electromagnetic selection of the malignant cells guides the energy delivery. The living targets are inherently heterogenic in thermal and electric properties, so the structural selection at the cellular level needs additional selection to target the chosen heterogeneity of the malignant cells. For this, we have to choose the carrier frequency, acting on different parts of the tissue structure. The applied RF current triggers various processes, which are often grouped in dispersion regions by frequency, defined by the main character of the bio-electromagnetic exchanges.

The β-dispersion ($\sim 1\ kHz - \sim 100\ MHz$ broad spectrum) is linked to the cellular structure of biological materials [74]. It occurs at the interface of membrane-electrolyte structures, using Maxwell-Wagner relaxation

[75]. The effect is an interfacial polarization of the cell membranes [76], resulting in the charge distribution at the cellular of interfacial boundaries [77]. The time dependence of the charge accumulation causes the characteristics of the β-dispersion [78]. In an experiment with sacrificed haddock muscle [79], the β-dispersion increases after a few hours of the sacrifice of the animal, showing the mechanism more connected to the cells than to the intact tissues. The high end of β-dispersion differs from the main effects of the range, called β1-dispersion caused from the torque of biological macro-molecules representing significant dipole moments, like proteins, orienting these against the disordering force of the thermal background [80]. However, the large molecules have limited possibility to follow the applied frequency and to grow further. Due to the massive heterogeneity of the biological tissues, this dispersion could have multiple effects, depending on the excited molecules. The conformational change of the present polymers [81], and macro-molecular relaxation with the exchange of the ionic effect in the vicinity of them [82]. The relaxation of amino-acid chains [83] and the proton fluctuations [84] also could have a role, which has no significant importance [85].

The upper tail of the β-dispersion continues to the δ-dispersion ($\sim 1\ MHz - \sim 1\ GHz$), which represents another mechanism. The δ-dispersion occurs at a distinguished frequency range above the main β-dispersion [86] and is connected to the dipolar moments of proteins and other large molecules (like cellular organelles, biopolymers) [87]. This second Maxwell-Wagner dispersion (δ) is characteristic of suspended particles surrounded by a cell [88]. Proteins also cause these effects, protein-bound water and cell organelles such as mitochondria [89] [90].

Other relaxation processes like those of molecular side chains, bound water molecules, diffusion of charged molecules, and near membrane bonds, could be added to the δ-dispersion.

In addition, the β/δ-dispersion of the chosen carrier frequency orients the attack on the membrane reaction of the impedance selected cells [91] [92]. The optimally chosen carrier frequency is in the interval of intensive overlap of β and δ dispersion and using in a practical point of view is an ISM-frequency 13.56 MHz. (The ISM spectrum is reserved internationally for industrial, scientific, and medical use.) The model calculation also shows the importance of the 13.56 MHz [93]. The chosen modulation enhances the selection. The RF energy dominantly absorbs on the clustered transmembrane proteins (rafts) [94], exciting their receptors [95]. The excitation destructs the malignant cells dominantly in an apoptotic way [96] Figure 7.

2.3.5. Support the Immune System

Homeostatic dynamic equilibrium is too complex for external constraints to be effective in repairing it. Tightly connected feedback mechanisms regulate the system, and the reaction of homeostatic control is against any simple constraints. An excellent example of this is the response to conventional hyperthermia, which aims to kill the tumor by the thermal effect of the absorbed energy. The heating is a valid objective, but unfortunately, homeostatic control mechanisms begin to correct this heating through various actions to maintain thermal balance. The most effective reaction is increased blood flow and perfusion, which aims to cool the heated lesion.However, this feedback carries a danger, as it increases the delivery of nutrients to the tumor and promotes metastasis by cell invasion into the bloodstream.

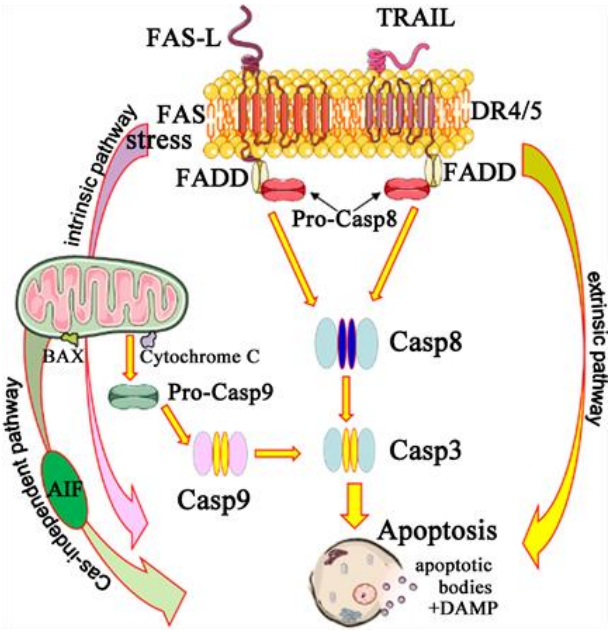

Figure 7. The extrinsic energy absorption excites the TRAIL death receptor and induces extrinsic, caspase-dependent signal transduction to apoptosis. The stress induces double intrinsic signals going on caspase-dependent and independent pathways.

Consequently, any winning strategy to influence the dynamic equilibrium must work in conjunction with homeostatic controls, utilizing natural processes and supporting the immune system to recognize and destroy malignant cells throughout the body. The preparation of the immune system could be a perfect target for oncology treatments, instead of targeting cancer's main strength, its proliferation. In this case, the lack of adaptive immunity to tumors can be revised, and the malignancy can be attacked by the host system itself.

The malignancy lacks the homeostatic complexity, turning the structural and dynamic conditions out of the healthy homeostatic network. Consequently, the challenging general tasks are fighting against cancer and the immune surveillance to support healthy homeostasis. The situation is complicated because the tumor cells hide their genetic information from the immune surveillance. They are well masked to avoid any systemic action against then, even the opposite: their demands are met as the system attempts to correct the irregularities. These "cheats" mislead the regulative actions and start to support the malignant cluster. Due to this falsely presented tumor status, the regular immune system does not act against it. The primary task is to present the signs of danger and stimulate the immune action to target and destroy the dangerous, highly proliferation cells.

The critical point is the immunological recognition of the malignancy. The immune system needs recognizable signs to direct its actions. However, the highly adaptive hiding strategy of malignant cells protects them from being identified by immune cells. A practical possibility for cancer invasion is the innate antitumor immune action of NK cells [97] [98]. Natural Killer (NK) cells do not need information through the host's histocompatibility complex 1 (MHC-I) molecules and act in the absence of priming. The cytotoxic activity of NK potentially controls tumor growth [99]. To complicate the complement of the available positive effect of NK cells, it could also promote tumor progression and angiogenesis [100] by inducing Reactive Oxygen Species (ROS) dysfunction [101]. The NK-cell activation could be achieved with a low-frequency electric field [102] as well as by electroporation [103]. Intensive low-frequency components in the spectrum of the modulated treatment may trigger the NK activity, enriching the NK cells in the targeted, selected tumor [104].

As a standard in immune homeostatic regulation, all processes have promoters and suppressors, so in complexity, every effect maybe a friend or foe, which appears for NK cell activity as well [105].

The modulation also may effectively support the healthy additive immune effects with developing tumor-specific immune reactions. The challenge is how to present the genetic information of the malignancy in order

to ignite the immune system. One of the possible solutions would be immunogenic cell death (ICD). The main point is the particular apoptosis starting with an external signal with the electric field, exciting the Trail R2 (DR5) death receptor with FADD-FAS complex, and the external signal through caspase (Cas) pathway goes to Cas8 and Cas3 finishing in apoptosis [106]. The external signal pathway connects to the internal mitochondrial apoptotic path as well, and forms Bax and cytochrome-c (point of no return) through Cas9, and Cas3 [107] finishing in apoptosis again [108]. The internally excited apoptosis also can follow the caspase-independent pathway through apoptosis-inducing factor (AIF) [104], so the apoptotic end can be reached by three different signal pathways. The XIAP protein could block the main external signal path, but the modulated RF blocks this XIAP activity with Septin4 [109], and with the same function, the SMAC/Diabolo [106].

All of the above processes develop damage-associated molecular patterns (DAMP) [106]; as a factor of the immunogenic cell death (ICD) [108]. The cancer cells, during its apoptosis, in addition to apoptotic bodies, liberates calreticulin (CRT, "eat me" signal), HMGB1 ("danger" signal), and heat-shock protein 70 (HSP70, "info" signal). These processes prepare antigen recognition producing antigen-presenting cells (APCs), which trigger the presence of helper (CD4+) and killer (CD8+) T-cells with explicit recognition of the malignant cells over the body [110]. This process allows the attack of distant micro- and macro-metastases in the system (abscopal effect), turning the local treatment to systemic [111] [73]. Noteworthy, the addition of dendritic cell medication may boost the overall immune effects [112] [113], and also an independent immune-stimulator works in harmony with modulated treatment [110]. Figure 8 shows the schematic summary of the immune processes.

2.3.6. Use Non-Thermal Effects

The amplitude modulation (AM, <20 kHz) of the RF carrier frequency can

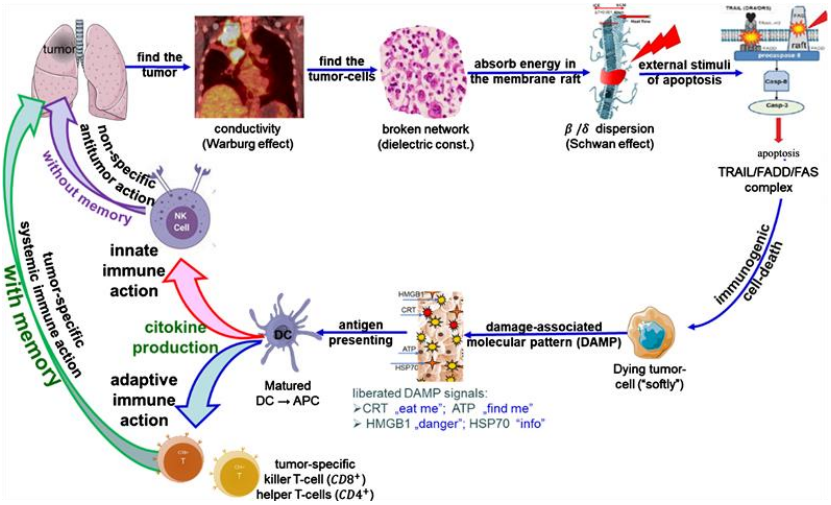

Figure 8. The modulated electromagnetic carrier selects the tumor cells and excites the membrane rafts inducing apoptosis. The special process is immunogenic, and the dying tumor-cell produces damage-associated molecular pattern with calreticulin (CRT), ATP, HMGB1 and HSP70; which generate antigen presentations in lymph-nodes and develops adaptive and innate immune reactions to attack the tumor.

intensify the tumor-specific absorption as a part of the selection mechanism [114]. Despite that, by a theoretical approach of the little energy absorption [115], the membrane demodulation effect could cause damages in the cytosol [116], or trigger apoptotic signals and destroy the cell [106]. The result of the non-thermal processes is the change of the chemical or structural situation in the targeted (investigated) compound assembly [117]. The non-thermal processes form a new phase (structural or chemical), which is a phase transition. The transition does not use heat from the field but directly uses the work of the electric field for the actual changes by absorption. The energy from the applied electric field is absorbed by the electrons or any other particles in a compound. It could be done without temperature change, but the phase of the material alters and the entropy changes without adjusting the temperature.

This phenomenon, however, has two connections to the temperature:

1) We know that 100% energy efficacy does not exist (entropy law), so the "lost" energy (which is kept as internal energy of the system) produces heat as well.

2) We know that the changing temperature changes the conditions of the "non-thermal" processes, which are in this way sharply dependent on the temperature. In other words, the reaction rate changes in the simplest case by the Arrhenius law. This complex process, which contains the thermal dependence of the "non-thermal" effect (transition effect), is described by Eyring transition state theory, which is proposed to describe the hyperthermia where this complexity appears. In Eyring's description, the thermal part is the same as in the Arrhenius law. Still, it has a part, which is a structural dependent factor, which could change without any temperature change, describing the "non-thermal effect" in complex systems.

The DNA damage is non-thermal. It is a phase transition, which has to be fixed by oxygen or by blocking the repairing enzymes. It does not need a temperature change at all. However, we know that both the oxygen-related or enzymatic fixing reactions (which conserves the break as it is) are temperature-dependent. The oxygen and enzyme reactions rapidly change according to temperature, mostly with Arrhenius law. The radiotherapy result has two parts: a temperature-independent and a temperature-dependent part, in the same way as this model describes the modulated electro-hyperthermia (mEHT) effect. This is why the same dose (Gray) is proposed for both the radiation processes (radiotherapy: ionizing; and mEHT: non-ionizing radiation).

3. Results—Applications

The dynamic structures, performing random stationary stochastic self-organizing processes, have practical applications in recognizing the diseases [118] [119]. The self-similarity used modeling of cancer by fractals [120], described by a generalized model [121]; helping to evaluate the various images in oncology [122]. The collectivity of the organization of the biological systems could be monitored by the fractal concept [123]. The fractal geometry describes the pathological architecture of tumors and their growth mechanisms accompanying time-dependent processes [124], and prognostic value [125].

The pink-noise modulation applies the fractal knowledge to support the harmonization efforts of homeostatic regulation and induce stochastic resonance near the frequency of the carrier, to demodulate and excite the desired signal pathways. The intensive backing of the heathy influence on the cancer is mandatory because the tumors are out from the structural and dynamic coordination of the natural organizing control.

Technically a high frequency (RF) carrier delivers the well-chosen time pattern of the modulation, which transports the modulated signal to the body with a carefully fitted applicator [126]. The applicator is driven by a voltage signal formed, as shown in Figure 9.

The spectrum and the power density of the signal which drives the applicator are studied by decomposing the applicator voltage into a signal s(t)s(t) and a noise component n(t)n(t) :

$$\begin{aligned} u(t) &= s(t) + n(t), \\ s(t) &:= U_0 \sin \omega_0 t, \\ n(t) &:= mz(t) U_0 \sin \Omega t \end{aligned} \tag{37}$$

To calculate the power spectrum, we need to construct the autocorrelation

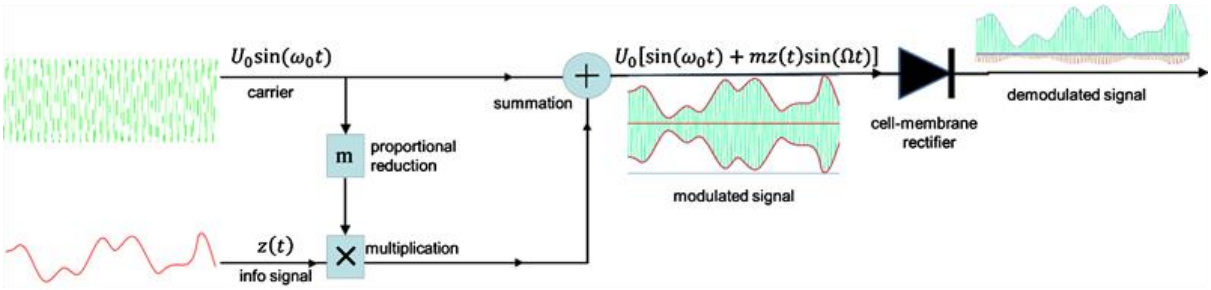

Figure 9. Principle of amplitude modulation with pink noise the Ω is the carrier circular frequency, UOUO the carrier amplitude, m is the modulation depth, and z(t)z(t) is the pink noise.

function $u(t)$::

$$u(t) \otimes u(t+\tau) := \lim_{T\to\infty} \frac{1}{T} \int_{-T}^{T} u(t)u(t+\tau)dt \tag{38}$$

where the sign ⊗ notes the necessary time integration of the signal with self in τ time-lag, and where we have taken into account a sufficiently sizeable averaging time. Considering the signal and noise components, we get:

$$\begin{aligned} &u(t) \otimes u(t+\tau): \\ &= s(t) \otimes s(t+\tau) \\ &+ n(t) \otimes n(t+\tau) \end{aligned} \tag{39}$$

where the average of the function formed by the product of signal and noise approaches zero. First, the properties of the $F\{f(t)\}$ Fourier transformation of the correlation function has to be calculated:

$$\begin{aligned} &F\{f(t) \otimes g(t \\ &+ \tau)\} \\ &= F(\omega)G^*(\omega), \\ &F\{f(t)\} = F(\omega), \\ &F\{g(t)\} = G(\omega) \end{aligned} \tag{40}$$

where the $*$ star notation is a sign of conjugation. The Fourier transform is the pink noise in this approximation, so:

$$\begin{aligned} &F\{z(t)\} = Z(\Omega) \\ &= \frac{1}{i\sqrt{\Omega}} \end{aligned} \tag{41}$$

thus the Fourier transform of noise:

$$\begin{aligned} F\{n(t)\} &:= \frac{i}{2} mU_0[Z(|\omega_0 - \Omega|)] \\ &= \frac{i}{2} mU_0 \left[\frac{1}{i\sqrt{|\omega_0 - \Omega|}}\right] \end{aligned} \tag{42}$$

consequently, the voltage power spectrum of the applicator:

$$\Phi_{uu}(\omega_0) := F\{u(t) \otimes u(t+\tau)\}: \\ = U_0^2 \delta(\omega_0 - \Omega) + \frac{m^2 U_0^2}{4} \frac{1}{|\omega_0 - \Omega|} \tag{43}$$

Figure 10 shows the modulated signal spectrum.

According to the Wiener-Khinchin theorem [127], the square of the voltage amplitude in the frequency interval is:

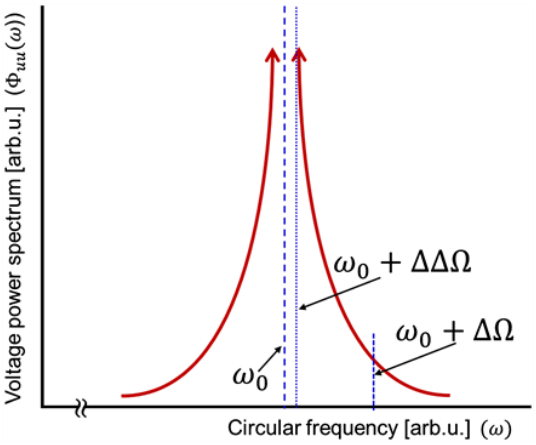

Figure 10. The power spectrum of the voltage where the distribution of the amplitude modulating noise makes a specific symmetric form.

$$\begin{aligned} &\Delta U^2 \\ &= \int_{\omega}^{\omega+\Delta\Omega} R_{uu}(\Omega)\, d\Omega \\ &= \int_{\omega+\Delta\Delta\Omega}^{\omega+\Delta\Omega} \left(U_0^2 \delta(\omega \\ &- \Omega) \\ &+ \frac{m^2 U_0^2}{4} \frac{1}{|\omega - \Omega|} \right) d\Omega \\ &= U_0^2 + \frac{m^2 U_0^2}{4} \ln \frac{\Delta\Omega}{\Delta\Delta\Omega} \end{aligned} \tag{44}$$

The second term of (44) shows that the square of the voltage amplitude can be extremely large near the carrier frequency, where the term tends to be infinite when $\Delta\Delta\Omega \to 0$. It follows that the average potential:

$$\Delta U_{ee} := \sqrt{\Delta U^2} = \sqrt{U_0^2 + \frac{m^2 U_0^2}{4} \ln \frac{\Delta\Omega}{\Delta\Delta\Omega}} \tag{45}$$

And the field strength is represented as:

$$\Delta E_{eff} = \frac{\Delta U_{eff}}{d} = \frac{1}{d} \sqrt{U_0^2 + \frac{m^2 U_0^2}{4} \ln \frac{\Delta\Omega}{\Delta\Delta\Omega}} \tag{46}$$

where d is the distance between the electrodes. Of course, arbitrarily high performance cannot be physically realized. In practice, due to fast Fourier transformation, only a point spectrum is realized. Nevertheless, the field strength amplitude can be large enough, and so the modulation does not demand a high power for appropriate effect. In conclusion, the modulation effect transmits the low-frequency power spectrum of the pink noise near the 13.56 MHz carrier, highly efficiently, and forms two sidebands. The modulation results in very high amplitude field strength peaks near the carrier frequency.

3.1. Modulation for Adherent Bonds

The E-cadherin-β-catenin complex plays a crucial role in cellular adhesion [128]. The suppression of E-cadherin expression leads to dysfunction in cell-cell adhesion, which can cause local invasion following tumor development [53]. Loss of adhesion has been associated with increased invasiveness and metastasis of tumors [129]. On the other hand, the appropriate expression of E-cadherins has a vital role in tumor suppression [130]. The changes in cadherin expression may affect signal transduction leading to the cancer cells growing uncontrollably [131]. This challenge also appears in the bioelectric considerations [132] of cancer development. The junctions as intercellular connections, exchanging molecules in the same was as cadherins exchange molecules [133]. Importantly the adhesive connections have a vital role in tissue repairing [134].

Together with the collective and individual states, a third entity exists too: the pluripotent embryonic resting state (δ), stem cells that adapt themselves to their actual micro-environment [135]. Healthy cells are in a communicative network, maintaining the complexity of a well-controlled system, but the δ cells could form malignant transformations [133]. The malignant cells are mostly autonomic, having lost their "social" connections with other cells, and fighting for nutrients with every other cell, irrespective of their health status. The network state categorizes cells as connected or non-connected [136]. The non-connected cells also have a network but not by cell-cell bonds. The connections are formed by clusters of fighting cells trying to trigger the healthy neighbors to supply them (forced angiogenesis) [137].

The collective activity of cells emits pink noise, which is the noise of self-organization, and so it is the noise originated from the function of homeostasis. The essence of the pink noise of homeostasis is that the function of the organ-specific networked cells is regulated actively in their energy exchange in the harmony of the complex surveillance. Consequently, the variance of physiological signals remains constant over time.

The glycocalyx shell and cell membrane of a cancer cell are also different from those of a healthy cell. Because of this, the movement of proteins in the cell membrane by lateral diffusion is also more limited. Adherents are particular protein formulas that can move in the cell membrane by lateral diffusion. Contact between two cells can occur when two such proteins meet and chemically bond with each other by lateral diffusion Figure 11. The re-established intercellular connections following mEHT have been were experimentally demonstrated [107] [138].

The glycocalyx shell of cancer cells is known to be charged highly negatively. This results in repulsion, so the attraction, which is one of the preconditions for cell recognition and the start of the adhesion process, cannot prevail. Consequently, the bond-formation is hampered by the strong negative charge of the cancer cell glycocalyx shell, so the formation of intercellular bonds and networking in malignancy is unlikely.

The condition for the formation of cellular collectivity is that the cell must be fixed with adherent bonds and junctions, which is largely missing in malignant tumors. The modulation/demodulation stochastic resonance of noise contains signals of very high amplitude, forcing the cell clusters to intercellular bonding, manifested in communication between cells, forming functional collectivity. The self-organizing signal transformed around a carrier produces large fields. The formed gradient promotes the adhesion bonding of neighboring cells. The pink-noise modulated electric field with a very high field strength which the amplitude is transformed near 13.56 MHz, helps build the bonds of adherent proteins Figure 12.

The pink noise modulation transformed around 13.56 MHz creates a field strength gradient towards the cell contact site. Attraction by a gradient of field strength towards the point of contact occurs between the cells. Proteins are normally dipolar with polarization vector pp. Therefore, a cataphoretic force $F=(p\nabla)E$ $F=(p\nabla)E$ acts to move the proteins toward the point of contact. The gradient

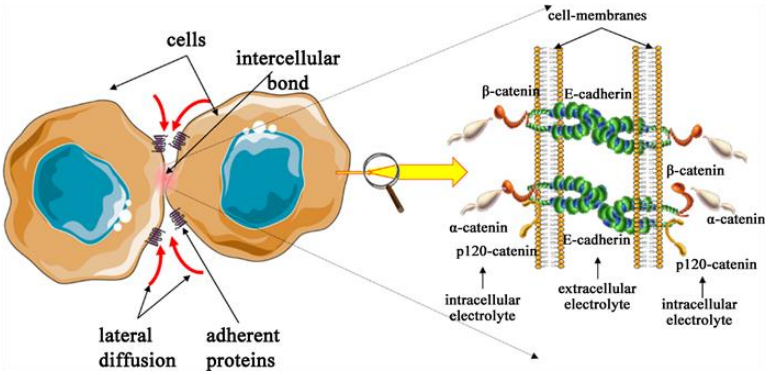

Figure 11. The movement of adherent proteins in the cell membrane promotes the reconnection of broken E-cadherin intercellular bonds.

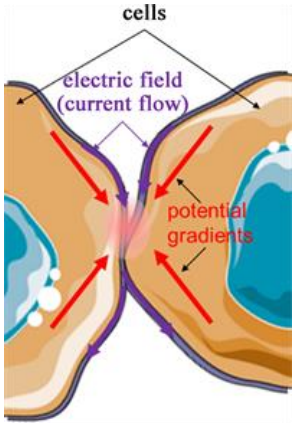

Figure 12. Evolution of field strength for two contact cells. The sizeable potential gradient actively promotes cellular contacts.

generates a high cataphoretic force Figure 13 which promotes the contact of the cells. The process increases the likelihood of forming intercellular bonding by the connection of adherent proteins.
Due to the increased temperature in the contact point, the barrier between the protein electronic states could be easier overcome, so the moderate temperature helps the bonding. So it is expected that the thermal effect of mEHT helps the process. However, when the temperature is high, the break of bonds is more likely.

3.2. Modulation for HSP

The heat-shock proteins (HSPs) are chaperons to help in stabilizing the dynamic equilibrium of the cells. They are named according to their molecular weight. The first observations have connected these proteins to the heat-stress [139], but later their expression for many other stresses was discovered [140] and intensive research into their role in health and diseases began [141]. The extreme stress effect promote HSP translocation to the cellular membrane [142] and liberation to the extracellular matrix. The HSP70 has dual function [143]: inside the cell protects it (chaperone function) and outside it is a danger signal to trigger immune reactions [144]. This feature makes these proteins possible therapeutic targets in various diseases [145] [146], and especially in oncology [147].

We elaborate on a theory that pink noise mEHT is suitable for enhanced HSP expression in the membrane and extracellular electrolyte. There are two important arguments for triggering the effect:

1. The carrier frequency is chosen in the range of the β/δ-dispersion, acting on lipid/protein bonds in the cell membrane.

2. The existence of high power amplitudes produced by the pink noise shifted to the carrier-frequency location.

The selection ensures that we excite the intended targeted cells with the high power pink-noise fluctuation near the carrier frequency. The RF-current density is increased at the cell membrane due to the β/δ-dispersion. The carrier would shift the pink noise into the β/δ-dispersion range, and there we expose the membrane to the pink noise. Streamlines pass from one cell to another at the points of contact of the cells. Electric fields with very high field strengths and gradients are generated in these places Figure 14.

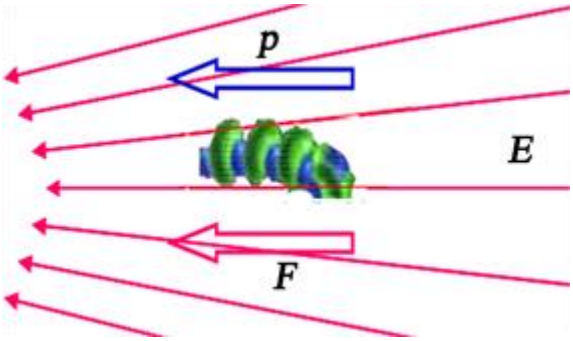

Figure 13. Formation of cataphoretic force. The inhomogeneous electric field turns the proteins in extracellular electrolyte.

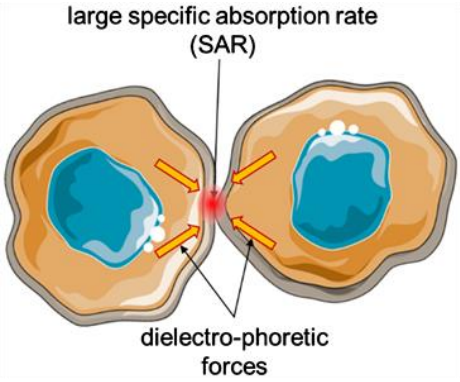

Figure 14. The field gradients are shown in Figure 12 promote the dielectric forces and induces large SAR at the contact point and reconnects the transmembrane proteins as well as provides mild heating for the cells [94] [148].

The connection points have high local SAR. However, due to the high field strength gradient enhanced by pink noise, a dielectrophoretic force also occurs, which moves half of this high SAR location to the micro-domains of the membrane thermo-sensor. The micro-domains are exposed to increased stress due to high power amplitudes. On the one hand, the stress effect is heat stress due to the high SAR and, on the other hand, mechanical deformation stress due to the high field strength gradient.

The β/δ-dispersion is used to produce HSP, and the selected target triggers the production of HSP70 for immune stimuli [149]. The immunomodulation of extracellular HSP70 makes it a promising candidate for vaccination of cancerous diseases by presenting malignant cells' antigens [150]. The danger signal of extracellular HSP is an essential mediator for intercellular signaling and transport [151]. The molecule is part of the damage-associated molecular patternformed by immunogenic cell death, making a perfect way to produce CD8+ killer T-cells for a systemic fight against cancer.

3.3. Modulation for Cellular Communication

The biological transformation of normal (β) to cancerous (α) is a communication phase transition which is explained on the level of individual cells [136]. The starting point of Szent-Gyorgyi is an etiological approach: the disappearance of cellular collectivity [53]. The β→αβ→α state change driven by changes of the micro-environment of the malignant cells [4].

The division naturally needs higher energy income than the regular life of the cells. The cytoskeleton polymerization during the cell division breaks the networking connections, allowing the free formation of the new cytoskeleton and intensifying support of the microenvironment of the dividing cells by higher diffusion in the free electrolyte. After finishing the division, the cells are reconnected, the network control activates again. The internal energy resources promote the appropriate, satisfactory amount of energy. Together with the environmental sources, the cells build up the daughter cells with the healthy cellular division [152]. However,

the malignant cells have no reserves for the extreme energy demand to proliferate [153]. The usual healthy process does not work in malignant proliferation. The tumor cells do not return to the network. They remain as individuals and continue the proliferation. One explanation concentrates on the dielectric changes in the cell microenvironment [154], which is high in the cancerous process in vivid form [155]. Noisy communication can also cause cancer. This can occur when the relative arrangement of the cells does not allow for an interaction leading to cyclic symmetry, like requested [34]. From our perspective, this can be interpreted, meaning that if the symmetry is not cyclic, it is divisible. Otherwise, it is not, which supports the idea, that the cellular position has a vital role in favoring the malignant proliferation [156].

4. Discussion—Cancer Therapy

The strategy to eliminate the cancerous processes focuses on the weakest point of the tumor: individualism. The missing overall network makes them vulnerable, as they are alone in fighting the stress.

The malignant development misses the healthy homeostatic regulation. The systemic controls do not work. Their extreme energy demand drives their systemic effect. The cancerous process concentrates on intensive proliferation and uses healthy hosts to support it. This complex process misleads the healthy host, presenting their actions as normal energy-demand for healing the lesion like a wound (as was described shown 25 years ago [88]). Cancer presents itself as trying to heat, and the system cannot recognize the "cheating" due to the hidden identification signs. This shows that the entire malignant process is essentially a wound repair process [157]. The idea has been investigated more recently, with comparisons between the hallmarks of the two processes [158], demonstrating the role of this mechanism in the formation of metastases [159]. The bio-system falsely recognizes the tumor-like wound [160] and stimulates its environment to heal the irregularity (meaning to produce cells to heal).

The permanent reparation demand depletes the available stem cells, [161] [162], and is emphasizes a different repair pathway: the proto-oncogenes are activated, and malignant transformation could happen, inducing the clinical manifestation of cancer [163]. The malignant transformation of the wound results in the secretion of proto-oncogenes [164] [165] [166], and intensive capture and stimulation of the stem-cells from other places [167] [168].

Ignoring the healthy regulations and the collectivity of the host tissue has some structural and temporal signs to recognize it. The structure of the individual cells is more disordered than the networked healthy tissue, and the intensive individual metabolic demand changes the structure of extracellular electrolyte. The permanent cellular division periodically collapses the cell's actual cytoskeleton and builds up new ones again, decomposed by the subsequent fission and repolymerization. This changes the cellular form individually, and the active dynamism, which differs from the healthy regulated one, is expressed in the noise of the tumor processes. The noisy difference is measurable by electric impedance [169], detecting the "color" of the noise. As shown above, the "color" is determined by the self-similarity scaling exponent of power density by frequency. The measured exponent decreases from the near-1 (pink noise), depending on the weakened cellular interactions, and so the autonomy is field. The same change was observed in the autocorrelation [170], lowering the function value at 1/e, so the correlation was decreasing, which characterizes the trend towards autonomy. The weakness of the malignant process is this autonomy when the cells are alone to fight against any external stresses. So the weakness, which we have to use [171], is the missing network, the missing collective harmony. The individualism of the cells is similar to atavistic reverse development in the evolutionary meaning. The atavistic model could be used as a starting point, but this model does not consider all the crucial details (hallmarks) that keep the single-celled units of cancer development alive [172]. The wound healing support of the host tissue is missing from the atavistic model, and so it is not applicable. However, the proper noise application places the theranostic key in the hand of the therapist. The noise spectrum is measurable for diagnosis [171], and the pink noise as a homeostatic harmony character could make a forceful selected harmonization factor, which harmonizes the

precancerous cells, rebinding their broken intercellular connections [107] [173], forcing back the healthy order. When the rebinding is impossible, the harmonizing force "softly" destroys the cells, exposing their genetic content for antigen presentation, and igniting the normal immune reaction against the malignancy. In other words, the mask falls off.

The practice of modulated electromagnetic applications connects the knowledge of hyperthermia with electromagnetic effects. The modulated electro-hyperthermia (mEHT, trade name oncothermia®) has used this method for years in a broad application for various tumors. Below we summarize the most crucial information-set about its processes and results, showing publications.

Numerous practical applications proved the feasibility of the mEHT treatments. Based on some principal considerations, the method uses the thermal and non-thermal effects [116] in a synergy. The non-thermal effects are connected to the cellular membranes [114] [115], emphasizing the physical potential of the amplitude modulation [174]. The strong connection between the thermal-factors and electric effects involves the similarities between their actions [175], and the strong synergy was indeed observed in vivo [176]. The absorbed power develops the temperature [177] which has a selective heating possibility [178] by electric inhomogeneities and depends on the technical solution of the coupling [179].

The temperature development is a complex process [180], and connected to the dosing in treatment practice [181] [182].

The extracellular action complexly interconnects the electric field with the thermal effects [183]. The thermal noise influences the electric field effect [22] [184], but it does not block the intracellular processes [185]. The modulation technology has been described in oncology [186].

The RF energy is predominantly absorbed on the clustered transmembrane proteins (rafts) [94], exciting their receptors [94] [187] [188]. The excitation damages the malignant cells dominantly in an apoptotic way [105] [149]. The mEHT promoted extracellular HSP70 supports the apoptotic processes [108]. The membrane rafts are the key elements of energy absorption [189], which is an energy intake in the nano-range [148]. The whole mEHT process is immunogenic [190]. The method may be applied complementary to radiotherapy [191] [192]; an example is the resensitization of the radioresistant pancreatic cells for further treatment [193]. The complementary application of mEHT with chemotherapy has also been successful [194] [195].

A recent review summarizes the molecular biology background of the tumor damage mechanisms revealed in cancer models [196].

In the clinical application, the safety of the method was investigated in one of the most sensitive organs, the brain. The prospective safety study involved the dose-expansion for non-invasive transcranial therapy in 3rd and 4th line, advanced; relapsed high-grade gliomas and proved the safety even in the daily applications [197]. Efficacy studies validated the feasibility of this method for such a short survival, high-mortality stage of the disease, [198] [199] [200]. The special safety [201] and efficacy [202] studies in advanced non-small cell lung cancer patients justified the use of mEHT in this type of malignancy as well. The analyses of brain [203] and lung [204] studies support the economic advantage of mEHT. The applications in gastrointestinal tracts like colon, [205], rectum [206], liver [207], and pancreas [208] [209] demonstrated the versatile functions of the mEHT method. The relapsed, refractory, or progressive heavily treated ovarian cancer [210], and the advanced, recurrent cervix uteri [211] [212] were also successfully treated with complementary combinations of conventional chemoradiotherapy and mEHT, obtaining low toxicity and longer survival, with improved quality of life [213]. The applicability for sarcomas in complementary therapy protocols was also proven [214] [215]. The

immunogenic influence in combination with other immune supports is also remarkable [216] and realizes tumor-specific immune reactions for distant metastases (abscopal effect) [217] [218]. These observations orient the treatment to tumor-directed immunotherapy [219] and could be a basis of the personalized medicine [220]. Remarkable application of mEHT for the peritoneal carcinomatosis with malignant ascites, [221], which extends the study focus to ascites cases.

Recently a review had summarized the clinical evidence of mEHT for the practicing oncologists [222], and an application guideline was published by an international collective [223].

Notably, most studies have single-arm protocols, which have inherent complications in evaluating the mEHT method. The patients involved in these studies are in relapsed advanced stages when the conventional therapies are limited or have failed. Collecting a cohort for reference at this stage is exceptionally challenging and, in most cases, impossible [224]. However, the evaluation of single-arm trials has specialties, which could improve the level of evidence of the results. The simplest one is the comparison of the single-arm results from different studies with the same protocol. For example, the comparison of advanced glioblastoma (Figure 15) [225] [226] [227] [200] [203], and pancreas (Figure 16) [228] [229] [225] [230] [231], studies shows the significant difference of the common median from the historical or database control.

Other analysis of single-arm results uses the self-similarity of living processes [232] [233], building up the reference arm from the parameters of the active single-arm [234] [235].

5. Conclusion

The modulation of radiofrequency carriers causes stochastic resonances, which act mainly on enzymatic processes. The demodulation is also effectively performed by stochastic resonance, which allows the low-frequency modulation information to be delivered selectively to the cancerous cells. There are as many resonant frequencies as there are enzymatic reactions that exist.

The modulation intensively changes the paradigm of cancer treatment. It boosts the healthy network and selectively destroys the malignant cells. The cell-killing process is immunogenic, allowing for the release of genetic information

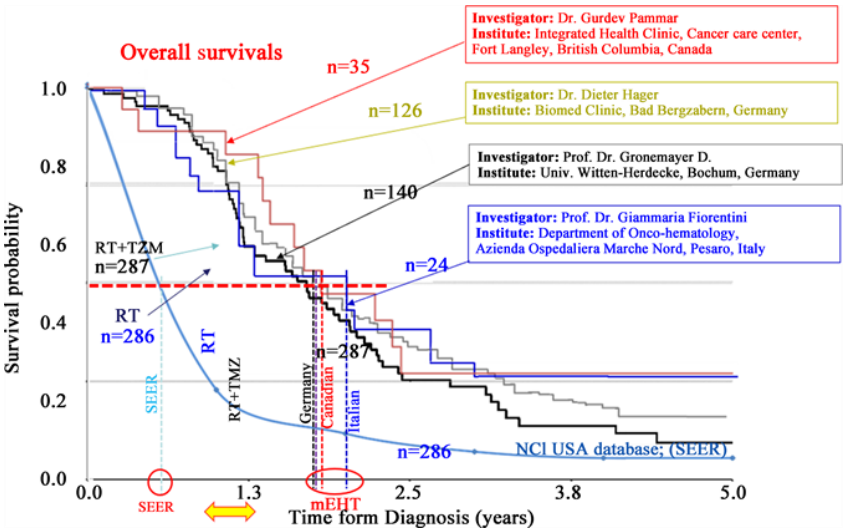

Figure 15. The comparison of the single-arm mEHT studies with the database results for advanced, relapsed glioblastoma multiform. The different groups with different studies based on the same mEHT protocol well correspond with each other and significantly differ from the database.

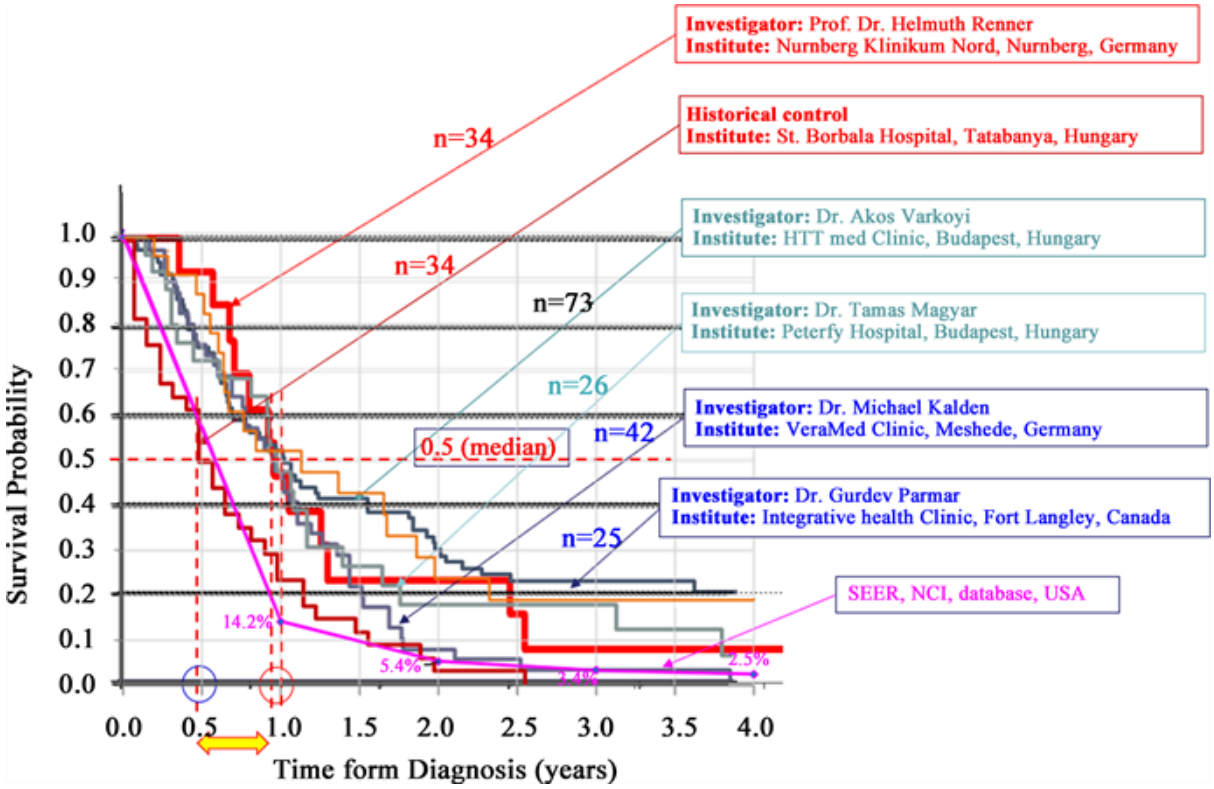

Figure 16. The comparison of the single-arm mEHT studies with the database results for advanced, relapsed inoperable pancreas carcinoma. The database results and the historical arm for the same stage pancreas survivals correspond each other. The different groups with different studies based on the same mEHT protocol well correspond with each other and significantly differ from the database and the historical arm.

in a molecular pattern (DAMP), which could form antigen presenting cells and develop tumor-specific immune reactions. The modulated signal is a complex mixture of non-thermal electron excitation for chemical reactions, and thermal boosting of the enzymatic reactions.

The complex homeostatic network has a cyclic symmetry which controls the balance and the apoptotic processes. The living cellular structures are open to the effects of energy, requiring energy input, followed by the output of waste. This organized transport system is not possible without direct cellular communication (no "social signal"). The cyclic topological order makes the noiseless inter- and intra-cellular communications possible despite the thermal noise background.

The malignant transformation breaks the organized transport system and seeks to build up new structures for the new demands. However, there are fundamental differences: the healthy construction is driven by the collective signal and seeks to optimize the energy-use for highest efficacy, while the malignant construction is only driven by the topology and physics of the mass number of individual, competing cells, irrespective of the efficacy of the energy conversion. The new structure modifies the cell-cell communications and arranges the malignant cellular microenvironment suitable for the autonomic actions. The topology in this meaning has significant diagnostic (pathologic) meaning: the more the pattern of tumor (networking "mesh" and form of the cells) resembles the healthy cells, the less malignant the tumor is.

The modulation affects the malignant construction in various ways:

1) boosts the healthy network;

2) limits the autonomy of the cells;

3) selects the malignant cells and targets them with resonance energy-absorption;

4) excites selected molecules, influencing and promoting the enzymatic processes;

5) supports the immune system and triggers selective antitumor effects;

6) regenerates the lost intercellular adherent bonds, and with this limits the invasion of the malignant cells;

7) frees the HSP70 extracellularly to carry genetic information about the malignant cell to antigen-presenting cells;

8) supports the cellular communications and the synchrony of the cells.

The modulation signal is a time-fractal representing the systemic homeostatic fluctuations. It is self-similar, having 1/f noise of the power density. It might promote the-establishing the lost cellular communications or stimulate apoptosis of the cells which remain individual.

The modulation principles to support the healthy processes have broad feasibility to treat the patients. The therapy is a complex, multi-component clinical process, where one of the factors is the modulated electro-hyperthermia (mEHT). The mEHT has proved its exceptional capability to treat late-stage, relapsed cancerous tumors, complementary to any other conventional therapies. In instances where there are no further treatment options available, mEHT could be applied as monotherapy, or in some cases, could desensitize tumors to the previously ineffective conventional treatment.

Acknowledgments

This work was supported by the Hungarian National Research Development and Innovation Office PIACI KFI grant: 2019-1.1.1-PIACI-KFI-2019-00011.

Conflicts of Interest

The author declares no conflicts of interest regarding the publication of this paper.

References

[1] Trigos, A.S., Pearson, R.B., Papenfuss, A.T., et al. (2016) Altered Interactions between Unicellular and Multicellular Genes Drive Hallmarks of Transformation in a Diverse Range of Solid Tumors. PNAS, 114, 6406-6411. https://doi.org/10.1073/pnas.1617743114

[2] Davidson, C.D., Wang, W.Y., Zaimi, I., et al. (2019) Cell Force-Mediated Matrix Reorganization Underlies Multicellular Network Assembly. Scientific Reports, 9, Article No. 12 https://doi.org/10.1038/s41598-018-37044-1

[3] Balmain, A., Gray, J. and Ponder, B. (2014) The Genetics and Genomics of Cancer. Nature Genetics Supplement 33, 238-244 https://doi.org/10.1038/ng1107

[4] Szigeti, G.P., Szasz, O. and Hegyi, G. (2017) Connections between Warburg's and Szentgyorgyi's Approach about the Causes of Cancer. Journal of Neoplasm, 1, 1-13.

[5] Hanahan, D. and Weinberg, R.A. (2000) The Hallmarks of Cancer. Cell, 100, 57-70 https://doi.org/10.1016/S0092-8674(00)81683-9

[6] Hanahan, D. and Weinberg, R.A. (2011) Hallmarks of Cancer: The Next Generation. Cell, 144, 646-674 https://doi.org/10.1016/j.cell.2011.02.013

[7] Dyas, F.G. (1928) Chronic Irritation as a Cause of Cancer. JAMA, 90, 457 https://doi.org/10.1001/jama.1928.92690330003008c

[8] Dvorak, H.F. (1986) Tumors: Wounds That Do Not Heal, Similarities between Tumor Stroma Generation and Wound Healing. The New England Journal of Medicine, 315, 1650-1659 https://doi.org/10.1056/NEJM198612253152606

[9] Platz, E.A. and Marzo, A.M. (2004) Epidemiology of Inflammation and Prostate Cancer. The Journal of Urology 171, S36-S40 https://doi.org/10.1097/01.ju.0000108131.43160.77

[10] Punyiczki, M. and Fesus, L. (1998) Heat Shock and Apoptosis: The Two Defense Systems of the Organisms May Have Overlapping Molecular Elements. Annals of the New York Academy of Sciences, 951, 67-74 https://doi.org/10.1111/j.1749-6632.1998.tb08978.x

[11] Aktipis, C.A., Bobby, A.M., Jansen, G., et al. (2015) Cancer across the Tree of Life: Cooperation and Cheating in Multicellularity. Philosophical Transactions of the Royal Society B, 370, Article ID: 20140219. https://doi.org/10.1098/rstb.2014.0219

[12] Varma, R. and Selman, J.S., (1991) Techniques for Characterisation of Electrodes and Electrochemical Processes. John Wiley & Sons, New York.

[13] Jacobsen, T. and West, K. (1995) Diffusion Impedance for Planar, Cylindrical, and Spherical Geometry. Electrochimica Acta, 40, 255-262 https://doi.org/10.1016/0013-4686(94)E0192-3

[14] Robinson, F.N.H. (1962) Noise in Electrical Circuits. Oxford Univ. Press, London.

[15] Goldup, A., Ohki, S. and Danielli, J.F. (1970) Black Lipid Films. Recent Progress in Surface Science, 3, 193-261 https://doi.org/10.1016/B978-0-12-571803-5.50013-4

[16] Goldman, D.E. (1943) Potential, Impedance, and Rectification in Membranes. Journal of General Physiology, 27 37-60. https://doi.org/10.1085/jgp.27.1.37

[17] Ramachandran, S., Blick, R.H. and van der Weide, D.W. (2010) Radio-Frequency Rectification on Membrane Bound Pores. Nanotechnology, 1, 75201 https://doi.org/10.1088/0957-4484/21/7/075201

[18] Tanaka, A. and Tokimasa, T. (1999) Theoretical Background for Inward Rectification. Tokai Journal of Experimental and Clinical Medicine, 24, 147-153.
[19] Szendro, P., Vincze, G. and Szasz, A. (2001) Bio-Response to White Noise Excitation. Electro- and Magnetobiology 20, 215-229 https://doi.org/10.1081/JBC-100104145
[20] Kerr, W.T., Anderson, A., Lau, E.P., et al. (2012) Automated Diagnosis of Epilepsy Using EEG Power Spectrum. Epilepsia, 53, e189-e192.
[21] Dave, K., Davtyan, A., Papoian, G.A., et al. (2015) Environmental Fluctuations and Stochastic Resonance in Proteir Folding. ChemPhysChem, 17, 1341-1348 https://doi.org/10.1002/cphc.201501041
[22] Astumian, R.D., Weaver, J.C. and Adair, R.K. (1995) Rectification and Signal Averaging of Weak Electric Fields by Biological Cells. Proceedings of the National Academy of Sciences of the United States of America, 92, 3740-3743. https://doi.org/10.1073/pnas.92.9.3740
[23] Vincze, Gy., Szasz, A. and Szasz, N. (2005) On the Thermal Noise Limit of Cellular Membranes. Bioelectromagnetics, 26, 28-35 https://doi.org/10.1002/bem.20051
[24] Winfree, A.T. (1984) The Prehistory of the Belousov-Zhabotinsky Oscillator. Journal of Chemical Education, 61 661-663. https://doi.org/10.1021/ed061p661
[25] Hudson, J.L. and Mankin, J.C. (1981) Chaos in the Belousov-Zhabotinskii Reaction. The Journal of Chemical Physics 74, 6171-6177 https://doi.org/10.1063/1.441007
[26] Matsumoto, K. and Tsuda, I. (1983) Noise-Induced Order. Journal of Statistical Physics, 31, 87-106 https://doi.org/10.1007/BF01010923
[27] Taylor, A.F., Tinsley, M.R., Wang, F., et al. (2009) Dynamical Quorum Sensing and Synchronization in Large Populations of Chemical Oscillators. Science, 323, 614-617 https://doi.org/10.1126/science.1166253
[28] Hunt, T. and Schooler, J.W. (2019) The Easy Part of the Hard Problem: A Resonance Theory of Consciousness Frontiers in Human Neuroscience, 13, Article No. 378 https://doi.org/10.3389/fnhum.2019.00378
[29] Voss, R.F. and Clarke, J. (1975) "1/f Noise" in Music and Speech, Nature, 28, 317-318 https://doi.org/10.1038/258317a0
[30] Colley, I.D. and Dean, R.T. (2019) Origins of 1/f Noise in Human Music Performance from Short-Range Autocorrelations Related to Rhythmic Structures. PLoS ONE, 1, e0216088 https://doi.org/10.1371/journal.pone.0216088
[31] Chorvatova, A. and Chorvat Jr., D. (2011) Coherent Resonant Properties of Cardiac Cells. In: Min, M., Ed., Cardiac Pacemakers—Biological Aspects, Clinical Applications and Possible Complications, IntechOpen, London, 25-45 https://doi.org/10.5772/23292
[32] Schrödinger, E. (1951) Science and Humanism. Cambridge University Press, Cambridge.
[33] Raff, M.C. (1992) Social Controls on Cell Survival and Death. Nature, 356, 397-400 https://doi.org/10.1038/356397a0
[34] Von Neumann, J. (1959) The Computer and the Brain. Yale University Press, London.
[35] Szendro, P., Vincze, G. and Szasz, A. (2001) Pink Noise Behaviour of the Bio-Systems. European Biophysics Journal, 30, 227-231 https://doi.org/10.1007/s002490100143
[36] Goldenfeld, N. and Woese, C. (2010) Life Is Physics: Evolution as a Collective Phenomenon Far from Equilibrium.
[37] West, B.J. and West, D. (2011) Are Allometry and Macroevolution Related? Physica A: Statistical Mechanics and Its Applications, 390, 1733-1736 https://doi.org/10.1016/j.physa.2010.11.031
[38] West, G.B. and Brown, J.H. (2005) The Origin of Allometric Scaling Laws in Biology from Genomes to Ecosystems: Towards a Quantitative Unifying Theory of Biological Structure and Organization. Journal of Experimental Biology, 208, 1575-1592 https://doi.org/10.1242/jeb.01589
[39] Häusser, M. (2001) Synaptic Function: Dendritic Democracy. Current Biology, 11, R10-R12 https://doi.org/10.1016/S0960-9822(00)00034-8

[40] Das, Neves, R.P., Jones, N.S. andreu, L., Gupta, R., Enver, T. and Iborra, F.J. (2010) Connecting Variability in Global Transcription Rate to Mitochondrial Variability. PLOS Biology, 8, e1000560 https://doi.org/10.1371/journal.pbio.1000560
[41] Johnston, I.G., Gaal, B., das, Neves, R.P., Enver, T., Iborra, F.J. and Jones, N.S. (2012) Mitochondrial Variability as a Source of Extrinsic Cellular Noise. PLOS Computational Biology, 8, e1002416 https://doi.org/10.1371/journal.pcbi.1002416
[42] Alberts, B., Alexander, J., Julian, L., Martin, R., Keith, R. and Peter, W. (1994). Molecular Biology of the Cell. Garland Publishing Inc., New York.
[43] Dawkins, R. (1976) The Selfish Gene. Oxford University Press, Oxford.
[44] McAvoy, A. and Hauert, C. (2016) Autocratic Strategies for Iterated Games with Arbitrary Action Spaces. PNAS, 113, 3573-3578 https://doi.org/10.1073/pnas.1520163113
[45] McAvoy, A. and Hauert, C. (2016) Autocratic Strategies for Alternating Games. Theoretical Population Biology, 113, 13-22 https://doi.org/10.1016/j.tpb.2016.09.004
[46] Nowak, M.A. and Sigmund, K. (1994) The Alternating Prisoner's Dilemma. Journal of Theoretical Biology, 168, 219-226. https://doi.org/10.1006/jtbi.1994.1101
[47] Ross-Gillespie, A. and Kümmerli, R. (2014) Collective Decision-Making in Microbes. Frontiers in Microbiology, 5, Article No. 54 https://doi.org/10.3389/fmicb.2014.00054
[48] Bhardway, N., Yan, K.K. and Gerstein, M.B. (2010) Analysis of Diverse Regulatory Networks in a Hierarchical Context Shows Consistent Tendencies for Collaboration in the Middle Levels. PNAS, 107, 6841-6846 https://doi.org/10.1073/pnas.0910867107
[49] Dissado, L.A. (1990) A Fractal Interpretation of the Dielectric Response of Animal Tissues. Physics in Medicine & Biology, 35, 1487-1503 https://doi.org/10.1088/0031-9155/35/11/005
[50] El-Lakkani, A. (2001) Dielectric Response of Some Biological Tissues. Bioelectromagnetics, 22, 272-279 https://doi.org/10.1002/bem.50
[51] Chigira, M., Noda, K. and Watanabe, H. (1990) Autonomy in Tumor Cell Proliferation. Medical Hypotheses, 32, 249-254. https://doi.org/10.1016/0306-9877(90)90101-J
[52] Ngo, S., Liang, J., Su, Y.H. and O'Brien, L.E. (2020) Tumor Establishment Requires Tumor Autonomous and Non-Autonomous Deregulation of Homeostatic Feedback Control https://doi.org/10.1101/541912
[53] Li, J., Cheng, L. and Jiang, H. (2019) Cell Shape and Intercellular Adhesion Regulate Mitotic Spindle Orientation. Molecular Biology of the Cell, 30, 2458-2468 https://doi.org/10.1091/mbc.E19-04-0227
[54] Szentgyorgyi, A. (1978) The Living State and Cancer. Marcel Dekker Inc., New York.
[55] Jeanes, A., Gottardi, C.J. and Yap, A.S. (2008) Cadherins and Cancer: How Does Cadherin Dysfunction Promote Tumor Progression? Oncogene, 27, 6920-6929 https://doi.org/10.1038/onc.2008.343
[56] Mendonsa, A.M., Na, T.Y. and Gumbiner, B.M. (2018) E-Cadherin in Contact Inhibition and Cancer. Oncogene, 37, 4769-4780. https://doi.org/10.1038/s41388-018-0304-2
[57] Szasz, O., Szasz, A.M., Minnaar, C. and Szasz, A. (2017) Heating Preciosity—Trends in Modern Oncological Hyperthermia. Open Journal of Biophysics, 7, 116-144 https://doi.org/10.4236/ojbiphy.2017.73010
[58] Szentgyorgyi, A. (1960) Introduction to a Submolecular Biology. Academic Press, New York https://doi.org/10.1016/B978-0-12-395612-5.50005-1
[59] Szasz, A. (1991) An Electrically Driven Instability: The Living-State (Does the Room Temperature Superconductivity Exist?). Physiological Chemistry and Physics and Medical NMR, 23, 43-50.
[60] Alfarouk, K.O., Shayoub, M.E.A., Muddathir, A.K., Elhassan, G.O. and Bashir, A.H.H. (2011) Evolution of Tumour Metabolism Might Reflect Carcinogenesis as a Reverse Evolution Process (Dismantling of Multicellularity) Cancers, 3, 3002-3017 https://doi.org/10.3390/cancers3033002
[61] Weinberg, R.A. (1999) One Renegade Cell. How Cancer Begins. Basic Books, New York.

[62] Szigeti, Gy.P., Szasz, A.M. and Szasz, A. (2020) The Growth of Healthy and Cancerous Tissues. Open Journal of Biophysics, 10, 113-128 https://doi.org/10.4236/ojbiphy.2020.103010
[63] Willmer, P. (2009) Environmental Physiology of Animals. Wiley, Hoboken.
[64] West, G.B., Brown, J.H. and Enquist, B.J. (1997) A General Model for the Origin of Allometric Scaling Laws in Biology. Science, 276, 122-126 https://doi.org/10.1126/science.276.5309.122
[65] Dodds, P.S., Rothman, D.H. and Weitz, J.S. (2001) Re-Examination of the "3/4-Law" of Metabolism. Journal of Theoretical Biology, 209, 9-27 https://doi.org/10.1006/jtbi.2000.2238
[66] Rothman, D.H. and Weitz, J.S. (2005) Beyond the "3/4-Power Law": Variation in the Intra- and Interspecific Scaling of Metabolic Rate in Animals. Biological Reviews, 80, 611-662 https://doi.org/10.1017/S1464793105006834
[67] Kozlowski, J. and Konarzewski, M. (2004) Is West, Brown and Enquist's Model of Allometric Scaling Mathematically Correct and Biologically Relevant? Function Ecology, 18, 283-289 https://doi.org/10.1111/j.0269-8463.2004.00830.x
[68] Beckman, R.A. and Loeb, L.A. (2005) Genetic Instability in Cancer: Theory and Experiment. Seminars in Cancer Biology, 15, 423-435 https://doi.org/10.1016/j.semcancer.2005.06.007
[69] Ferguson, L.R., Chen, H., Collins, A.R., Connel, M., Damia, G., Dasgupta, S., et al. (2015) Genomic Instability in Human Cancer: Molecular Insights and Opportunities for Therapeutic Attack and Prevention through Diet and Nutrition. Seminars in Cancer Biology, 35, S5-S24 https://doi.org/10.1016/j.semcancer.2015.03.005
[70] Colotta, F., Allavena, P., Sica, A., Garlanda, C. and Mantovani, A. (2009) Cancer-Related Inflammation, the Seventh Hallmark of Cancer: Links to Genetic Instability. Carcinogenesis, 30, 1073-1081 https://doi.org/10.1093/carcin/bgp127
[71] Luoto, K.R., Kumareswaran, R. and Bristow, R.G. (2013) Tumor Hypoxia as a Driving Force in Genetic Instability. Genome Integrity, 4, 5 https://doi.org/10.1186/2041-9414-4-5
[72] Loewenstein, W.R. (1999) The Touchstone of Life, Molecular Information, Cell Communication and the Foundations of the Life. Oxford University Press, Oxford, New York, 298-304.
[73] Szasz, O. (2020) Ch. 11. Local Treatment with Systemic Effect: Abscopal Outcome. In: Szasz, A., Ed., Challenges and Solutions of Oncological Hyperthermia, Cambridge Scholars Publishing, Newcastle upon Tyne District Publishing, Newcastle upon Tyne District, 192-205.
[74] Schwan, H.P. and Takashima, S. (1991) Dielectric Behavior of Biological Cells and Membranes. Bulletin of the Institute for Chemical Research, Kyoto University, 69, 459-475.
[75] Cole, K.S. (1972) Membranes, Ions and Impulses. University of California Press, Berkeley.
[76] Anderson, J.C. (1964) Dielectrics, Chapman & Hall, London.
[77] Pethig, R.R. (1979) Dielectric and Electronic Properties of Biological Materials. Wiley, Hoboken.
[78] Schwan, H.P. (1957) Electrical Properties of Tissue and Cell Suspensions. Advances in Biological and Medical Physics, 5, 147 https://doi.org/10.1016/B978-1-4832-3111-2.50008-0
[79] Martinsen, O.G., Grimnes, S. and Mirtaheri, P. (2000) Non-Invasive Measurements of Post Mortem Changes in Dielectric Properties of Haddock Muscle—A Pilot Study. Journal of Food Engineering, 43, 189-192 https://doi.org/10.1016/S0260-8774(99)00151-X
[80] Grant, E.H., Sheppard, R.J. and South, S.P. (1978) Dielectric Behavior of Biological Molecules in Solution. Clarendon Press, Oxford.
[81] Schwarz, G. and Seelig, J. (1968) Kinetic Properties and the Electric Field Effect of Life Helix-Coil Transition of Poly(γ-benzyl L-glutamate) Determined from Dielectric Relaxation Measurements. Biopolymers, 6, 1263-1277 https://doi.org/10.1002/bip.1968.360060904
[82] Debye, F. (1928) Dispersion of the Conductivity and Dielectric Constants of Strong Electrolytes. Physikalische Zeitschrift, 29, 121-401.
[83] Pennock, B.E. and Schwan, H.P. (1969) Further Observations on the Electrical Properties of Hemoglobin Bound Water. The Journal of Physical Chemistry, 73, 2600-2610 https://doi.org/10.1021/j100842a024
[84] Kirkwood, J.G. and Shumaker (1952) Forces between Protein Molecules in Solution Arising from Fluctuations in Proton Charge and Configuration. Proceedings of the National Academy of Sciences of the United States of

America, 38, 863-871 https://doi.org/10.1073/pnas.38.10.863
[85] South, G.P. and Grant, E.H. (1972) Dielectric Dispersion and Dipole Moment of Myoglobin in Water. Proceedings of the Royal Society A, 328, 371 https://doi.org/10.1098/rspa.1972.0083
[86] Pethig, R.R. (2017) Dielectrophoresis: Theory, Methodology and Biological Applications. John Wiley & Sons Hoboken. https://doi.org/10.1002/9781118671443
[87] Asami, K. (2002) Characterization of Biological Cells by Dielectric Spectroscopy. Journal of Non-Crystalline Solids, 305, 268-277 https://doi.org/10.1016/S0022-3093(02)01110-9
[88] Pauly, H. and Schwan, H.P. (1959) Uber die Impedanzeiner Suspension von Kugelformigen Teilchenmiteiner Schale. Zeitschrift für Naturforschung B, 14, 125-131 https://doi.org/10.1515/znb-1959-0213
[89] Stoy, R.D., Foster, K.R. and Schwan, H.P. (1982) Dielectric Properties of Mammalian Tissues from 0.1 to 100 MHz A Summary of Recent Data. Physics in Medicine & Biology, 27, 501-513 https://doi.org/10.1088/0031-9155/27/4/002
[90] Gotz, M., Karsch, L. and Pawelke, J. (2017) A New Model for Volume Recombination in Plane-Parallel Chambers in Pulsed Fields of High Dose-per-Pulse. Physics in Medicine & Biology, 62, 8634-8654 https://doi.org/10.1088/1361-6560/aa8985
[91] Pethig, R. (1984) Dielectric Properties of Biological Materials: Biophysical and Medical Application. IEEE Transactions on Electrical Insulation, E1-19, 453-474 https://doi.org/10.1109/TEI.1984.298769
[92] Schwan, H.P. (1963) Determination of Biological Impedances. In: Physical Techniques in Biological Research, Vol. 6, Academic Press, New York, 323-406 https://doi.org/10.1016/B978-1-4831-6743-5.50013-7
[93] Stubbe, M. and Gimsa, J. (2015) Maxwell's Mixing Equation Revisited: Characteristic Impedance Equations for Ellipsoidal Cells. Biophysical Journal, 109, 194-208 https://doi.org/10.1016/j.bpj.2015.06.021
[94] Papp, E., Vancsik, T., Kiss, E. and Szasz, O. (2017) Energy Absorption by the Membrane Rafts in the Modulated Electro-Hyperthermia (mEHT). Open Journal of Biophysics, 7, 216-229 https://doi.org/10.4236/ojbiphy.2017.74016
[95] Vincze, Gy., Szigeti, Gy. andocs, G. and Szasz, A. (2015) Nanoheating without Artificial Nanoparticles. Biology and Medicine, 7, 249.
[96] Megyesshazi, N. (2015) Studies on Modulated Electrohyperthermia Induced Tumor Cell Death in a Colorectal Carcinoma Model. Ph.D. Theses, Pathological Sciences Doctoral School, Semmelweis University, Budapest.
[97] Waldhauer, I. and Steinle, A. (2008) NK Cells and Cancer Immunosurveillance. Oncogene, 27, 5932-5943 https://doi.org/10.1038/onc.2008.267
[98] Zamai, L., Ponti, C., Mirandola, P., et al. (2007) NK Cells and Cancer. The Journal of Immunology, 178, 4011-4016 https://doi.org/10.4049/jimmunol.178.7.4011
[99] Hu, W., Wang, G., Huang, D., et al. (2019) Cancer Immunotherapy Based on Natural Cell Killer Cells: Current Progress and New Opportunities. Frontiers in Immunology, 10, Article No. 1205 https://doi.org/10.3389/fimmu.2019.01205
[100] Bassani, B., Baci, D. and Gallazzi, M. (2019) Natural Killer Cells as Key Players of Tumor Progression and Angiogenesis: Old and Novel Tools to Divert Their Pro-Tumor Activities into Potent Anti-Tumor Effects. Cancers 11, 461 https://doi.org/10.3390/cancers11040461
[101] Betten, A., Dahlgren, C., Mellqvist, U.H., et al. (2004) Oxygen Radical-Induced Natural Killer Cell Dysfunction: Role of Myeloperosicase and Regulation by Serotonin. Journal of Leukocyte Biology, 75, 1111-1115 https://doi.org/10.1189/jlb.1103595
[102] Rosado, M.M., Simko, M., Mattsson, M.O. and Pioli, C. (2018) Immune-Modulating Perspectives for Low Frequency Electromagnetic Fields in Innate Immunity. Frontiers in Public Health, 6, Article No. 85 https://doi.org/10.3389/fpubh.2018.00085
[103] Reindl, L.M., Albinger, N., Bexte, T., et al. (2020) Immunotherapy with NK Cells: Recent Developments in Gene Modification Open Up New Avenues. OncoImmunology, 9, Article ID: 1777651 https://doi.org/10.1080/2162402X.2020.1777651

[104] Vancsik, T., Mathe, D., Horvath, I., et al. (2021) Modulated Electro-Hyperthermia Facilitates NK-Cell Infiltration and Growth Arrest of Human A2058 Melanoma in a Xenograft Model. Frontiers in Oncology, 11, Article ID: 590764.
https://doi.org/10.3389/fonc.2021.590764

[105] Damele, L., Ottonello, S., Mingari, M.C., Pietra, G. and Vitale, C. (2020) Targeted Therapies: Friends or Foes for Patient's NK Cell-Mediated Tumor Immune-Surveillance? Cancers, 12, 774
https://doi.org/10.3390/cancers12040774

[106] Meggyeshazi, N. andocs, G., Balogh, L., Balla, P., Kiszner, G., Teleki, I., Jeney, A. and Krenacs, T. (2014) DNA Fragmentation and Caspase-Independent Programmed Cell Death by Modulated Electrohyperthermia. Strahlentherapie und Onkologie, 190, 815-822
https://doi.org/10.1007/s00066-014-0617-1

[107] Yang, K.L., Huang, C.C., Chi, M.S., Chiang, H.C., Wang, Y.S. andocs, G., et al. (2016) In Vitro Comparison of Conventional Hyperthermia and Modulated Electro-Hyperthermia. Oncotarget, 7, 84082-84092
https://doi.org/10.18632/oncotarget.11444

[108] Andocs, G., Meggyeshazi, N., Balogh, L., Spisak, S., Maros, M.E., Balla, P., Kiszner, G., Teleki, I., Kovago, Cs. and Krenacs, T. (2014) Upregulation of Heat Shock Proteins and the Promotion of Damage-Associated Molecular Pattern Signals in a Colorectal Cancer Model by Modulated Electrohyperthermia. Cell Stress and Chaperones, 20, 37-46
https://doi.org/10.1007/s12192-014-0523-6

[109] Jeon, T.W., Yang, H., Lee, C.G., et al. (2016) Electro-Hyperthermia Up-Regulates Tumour Suppressor Septin 4 to Induce Apoptotic Cell Death in Hepatocellular Carcinoma. International Journal of Hyperthermia, 7, 1-9
https://doi.org/10.1080/02656736.2016.1186290

[110] Vancsik, T., Kovago, Cs., Kiss, E., et al. (2018) Modulated Electro-Hyperthermia Induced Loco-Regional and Systemic Tumor Destruction in Colorectal Cancer Allografts. Journal of Cancer, 9, 41-53
https://doi.org/10.7150/jca.21520

[111] Szasz, A. (2019) Immune-Effects with Local Hyperthermia. Oncothermia Journal, 26, 139-148.

[112] Qin, W., Akutsu, Y. andocs, G., et al. (2014) Modulated Electro-Hyperthermia Enhances Dendritic Cell Therapy through an Abscopal Effect in Mice. Oncology Reports, 32, 2373-2379
https://doi.org/10.3892/or.2014.3500

[113] Tsang, Y.W., Huang, C.C., Yang, K.L., et al. (2015) Improving Immunological Tumor Microenvironment Using Electro-Hyperthermia Followed by Dendritic Cell Immunotherapy. BMC Cancer, 15, Article No. 708.
https://doi.org/10.1186/s12885-015-1690-2

[114] Wust, P., Kortum, B., Strauss, U., Nadobny, J., Zschaeck, S., Beck, M., et al. (2020) Nonthermal Effects of Radiofrequency Electromagnetic Fields. Scientific Reports, 10, Article No. 13488.
https://doi.org/10.1038/s41598-020-69561-3

[115] Wust, P., Ghadjar, P., Nadobny, J., et al. (2019) Physical Analysis of Temperature-Dependent Effects of Amplitude-Modulated Electromagnetic Hyperthermia. International Journal of Hygiene and Environmental Health, 36, 1246-1254
https://doi.org/10.1080/02656736.2019.1692376

[116] Wust, P., Nadobny, J., Zschaeck, S. and Ghadjar, P. (2020) Ch. 16. Physics of Hyperthermia—Is Physics Really against Us? In: Szasz, A., Ed., Challenges and Solutions of Oncological Hyperthermia, Cambridge Scholars Publishing, Newcastle upon Tyne District, 346-376.

[117] Szasz, A. (2019) Thermal and Nonthermal Effects of Radiofrequency on Living State and Applications as an Adjuvant with Radiation Therapy. Journal of Radiation and Cancer Research, 10, 1-17
https://doi.org/10.4103/jrcr.jrcr_25_18

[118] West, B.J. (1990) Fractal Physiology and Chaos in Medicine. World Scientific, Singapore, London
https://doi.org/10.1142/1025

[119] Goldberger, A.L., Amaral, L.A., Hausdorff, J.M., et al. (2002) Fractal Dynamics in Physiology: Alterations with Disease and Aging. PNAS Colloquium, 99, 2466-2472
https://doi.org/10.1073/pnas.012579499

[120] Stehlik, M., Hermann, P. and Nicolis, O. (2016) Fractal Based Cancer Modelling. REVSTAT—Statistical Journal, 14, 139-155.

[121] Deisboeck, T.S., Guiot, C., Delsanto, P.P., et al. (2006) Does Cancer Growth Depend on Surface Extension? Medical Hypotheses, 67, 1338-1341
https://doi.org/10.1016/j.mehy.2006.05.029

[122] Stehlik, M., Wartner, F. and Minarova, M. (2013) Fractal Analysis for Cancer Research: Case Study and Simulation of Fractals. Pliska Studia Mathematica Bulgarica, 22, 195-206.

[123] Waliszewski, P., Molski, M. and Konarski, J. (2011) Self-Similarity, Collectivity, and Evolution of Fractal Dynamics during Retinoid-Induced Differentiation of Cancer Cell Population. Fractals, 7, 139-149 https://doi.org/10.1142/S0218348X99000165

[124] Baish, J.W. and Jain, R.K. (2000) Fractals and Cancer. Cancer Research, 60, 3683-3688.

[125] Liu, S., Wang, Y., Xu, K., Wang, Z., Fan, X., Zhang, C., Li, S., Qiu, X. and Jiang, T. (2017) Relationship between Necrotic Patterns in Glioblastoma and Patient Survival: Fractal Dimension and Lacunarity Analyses Using Magnetic Resonance Imaging. Scientific Reports, 7, Article No. 8302 https://doi.org/10.1038/s41598-017-08862-6

[126] Szasz, A. (2021) The Capacitive Coupling Modalities for Oncological Hyperthermia. Open Journal of Biophysics, 11, 252-313 https://doi.org/10.4236/ojbiphy.2021.113010

[127] Zbilut, J.P. and Marwan, N. (2008) The Wiener-Khinchin Theorem and Recurrence Quantification. Physics Letters A, 372, 6622-6626 https://doi.org/10.1016/j.physleta.2008.09.027

[128] Petrova, Y.I., Schecterson, L. and Gumbiner, B.M. (2016) Roles for E-cadherin Cell Surface Regulation in Cancer. Molecular Biology of the Cell, 27, 3233-3244 https://doi.org/10.1091/mbc.E16-01-0058

[129] Beavon, I.R. (2000) The E-cadherin-catenin Complex in Tumour Metastasis: Structure, Function and Regulation. European Journal of Cancer, 36, 1607-1620 https://doi.org/10.1016/S0959-8049(00)00158-1

[130] Pećina-Šlaus, N. (2003) Tumor Suppressor Gene E-cadherin and Its Role in Normal and Malignant Cells. Cancer Cell International, 3, 17 https://doi.org/10.1186/1475-2867-3-17

[131] Cavallaro, U., Schaffhauser, B. and Christofori, G. (2002) Cadherins and the Tumour Progression: Is It All in a Switch? Cancer Letters, 176, 123-128 https://doi.org/10.1016/S0304-3835(01)00759-5

[132] Szentgyorgyi, A. (1968) Bioelectronics: A Study on Cellular Regulations, Defence and Cancer. Academic Press, New York, London.

[133] Lowenstein, W.R. and Kanno, Y. (1967) Intercellular Communication and Tissue Growth, I. Cancerous Growth. The Journal of Cell Biology, 33, 225-234 https://doi.org/10.1083/jcb.33.2.225

[134] Lowenstein, W.R. and Penn, R.D. (1967) Intercellular Communication and Tissue Growth, II. Tissue Regeneration. The Journal of Cell Biology, 33, 235-242 https://doi.org/10.1083/jcb.33.2.235

[135] Alimperti, S. and Andreadis, S.T. (2015) CDH2 and CDH11 Act as Regulators of Stem Cell Fate Decisions. Stem Cell Research, 14, 270-282 https://doi.org/10.1016/j.scr.2015.02.002

[136] Szentgyorgyi, A. (1965) Cell Division and Cancer. Science, 149, 34-37 https://doi.org/10.1126/science.149.3679.34

[137] Lugano, R., Ramachandran, M. and Dimberg, A. (2020) Tumor Angiogénesis: Causes, Consequences, Challenges and Opportunities. Cellular and Molecular Life Sciences, 77, 1745-1770 https://doi.org/10.1007/s00018-019-03351-7

[138] Szasz, O. and Szasz, A. (2018) Modulated Electro-Hyperthermia, (mEHT) from LAB to Clinic. Oncothermia Journal, 23, 24-61.

[139] Ritossa, F. (1962) A New Puffing Pattern Induced by Temperature Shock and DNP in Drosophila. Experimental 18, 571-573 https://doi.org/10.1007/BF02172188

[140] Csermely, P. (1998) Stress of Life from Molecules to Man. Annals of the New York Academy of Sciences, 851 547. https://doi.org/10.1111/j.1749-6632.1998.tb08965.x

[141] Soti, C. and Csermely, P. (2007) Protein Stress and Stress Proteins: Implications in Aging and Disease. Journal of Biosciences, 32, 511-515 https://doi.org/10.1007/s12038-007-0050-z

[142] Vega, V.L., Rodriguez, Silva, M., Frey, T., Gehrmann, M., Diaz, J.C., et al. (2008) Hsp70 Translocates into the Plasma Membrane after Stress and Is Released into the Extracellular Environment in a Membrane-Associated form That Activates Macrophages. The Journal of Immunology, 180, 4299-4307 https://doi.org/10.4049/jimmunol.180.6.4299

[143] Juhasz, K., Lipp, A.M., Nimmervoll, B., Sonnleitner, A., et al. (2013) The Complex Function of Hsp70 in Metastatic Cancer. Cancers, 6, 42-66 https://doi.org/10.3390/cancers6010042

[144] Ohtsuka, K., Kawashima, D. and Asai, M. (2007) Dual Functions of Heat Shock Proteins: Molecular Chaperones Inside of Cells and Danger Signals Outside of Cells. Thermal Medicine, 23, 11-22 https://doi.org/10.3191/thermalmedicine.23.11

[145] Soti, Cs., Nagy, E., Giricz, Z., Vigh, L., Csermely, P. and Ferdinandy, P. (2005) Heat Shock Proteins as Emerging Therapeutic Targets. British Journal of Pharmacology, 146, 679-780 https://doi.org/10.1038/sj.bjp.0706396

[146] Torok, Z.S., Crul, T., Maresca, B., Schutz, G.J., Viana, F., et al. (2014) Plasma Membranes as Heat Stress Sensors From Lipid-Controlled Molecular Switches to Therapeutic Applications. Biochimica et Biophysica Acta, 1838, 1594-1618. https://doi.org/10.1016/j.bbamem.2013.12.015

[147] Shevtsov, M., Balogi, Z.S., Khachatryan, W., Gao, H., Vigh, L. and Multhof, F.G. (2020) Membrane-Associated Heat Shock Proteins in Oncology: From Basic Research to New Theranostic Targets. Cells, 9, 1263 https://doi.org/10.3390/cells9051263

[148] Andocs, G., Rehman, M.U., Zhao, Q.L., Papp, E., Kondo, T. and Szasz, A. (2015) Nanoheating without Artificial Nanoparticles Part II. Experimental Support of the Nanoheating Concept of the Modulated Electro-Hyperthermia Method, Using U937 Cell Suspension Model. Biology and Medicine, 7, 1-9 https://doi.org/10.4172/0974-8369.1000247

[149] Danics, L., Schvarcz, Cs., Viana, P., et al. (2020) Exhaustion of Protective Heat Shock Response Induces Significant Tumor Damage by Apoptosis after Modulated Electro-Hyperthermia Treatment of Triple Negative Breast Cancer Isografts in Mice. Cancers, 12, 2581 https://doi.org/10.3390/cancers12092581

[150] Wang, X.Y., Li, Y., Yang, G. and Subjeck, J.R. (2005) Current Ideas about Applications of Heat Shock Proteins in Vaccine Design and Immunotherapy. International Journal of Hyperthermia, 21, 717-722 https://doi.org/10.1080/02656730500226407

[151] Calderwood, S.K., Mambula, S.S. and Gray Jr., P.J. (2007) Extracellular Heat Shock Proteins in Cell Signalling and Immunity. Annals of the New York Academy of Sciences, 1113, 28-39 https://doi.org/10.1196/annals.1391.019

[152] Pederson, T. (2003) Historical Review: An Energy Reservoir for Mitosis, and Its Productive Wake. Trends in Biochemical Sciences, 28, 125-129 https://doi.org/10.1016/S0968-0004(03)00030-6

[153] Warburg, O. (1996) Oxygen, The Creator of Differentiation, Biochemical Energetics. Academic Press, New York.

[154] Szentgyorgyi, A. (1998) Electronic Biology and Cancer. Marcel Dekker, New York.

[155] Sengupta, A., Gupta, S., Sharda, A., et al. (2021) Effect of Low Frequency Electrical Current on the Biophysical and Molecular Properties of Cancer Cells. International Journal of Cancer and Clinical Research, 8, 145 https://doi.org/10.23937/2378-3419/1410145

[156] Lanouette, W. and Silard, B. (1992) Genius in the Shadows. Macmillan Publishing Co., New York.

[157] Meng, X. and Riordan, N.H. (2006) Cancer Is a Functional Repair Tissue. Medical Hypotheses, 66, 486-490 https://doi.org/10.1016/j.mehy.2005.09.041

[158] McCarthy-Morrogh, L. and Martin, P. (2020) The Hallmarks of Cancer Are Also Hallmarks of Wound Healing. Science Signaling, 13, eaay8690 https://doi.org/10.1126/scisignal.aay8690

[159] Deyell, M., Garris C.S. and Laughney, A.M. (2021) Cancer Metastasis as a Non-Healing Wound. British Journal of Cancer, 124, 1491-1502 https://doi.org/10.1038/s41416-021-01309-w

[160] Sundaram, G.M., Quah, S. and Sampath, P. (2018) Cancer: The Dark Side of Wound Healing. The FEBS Journal 285, 4516-4534 https://doi.org/10.1111/febs.14586

[161] Shin, B.J. and Ching, S.S. (2003) A Case of Limbal Stem Cell Deficiency in a Patient with Chronic Mucocutaneous Candiddiasis. Investigative Ophthalmology & Visual Science, 44, 1359.

[162] Houghton, J., Stoicov, C., Nomura, S., et al. (2004) Gastric Cancer Originating from Bone Marrow-Derived Cells Science, 306, 1568-1571 https://doi.org/10.1126/science.1099513

[163] Ouahes, N., Phillips, T.J. and Park, H.Y. (1998) Expression of c-fos and c-Ha-ras Protooncogenes Is Induced in Human Chronic Wounds. Dermatologic Surgery, 24, 1354-1357 https://doi.org/10.1111/j.1524-4725.1998.tb00014.x

[164] Huang, S., Trujillo, J.M. and Chakrabarty, S. (1992) Proliferation of Human Colon Cancer Cells: Role of Epidermal Growth Factor and Transforming Growth Factor. International Journal of Cancer, 52, 978-986 https://doi.org/10.1002/ijc.2910520625

[165] Dahiya, R., Lee, C., Haughney, P.C., et al. (1996) Differential Gene Expression of Transforming Growth Factors Alpha and Beta, Epidermal Growth Factor, Keratinocyte Growth Factor, and Their Receptors in Fetal and Adult Human Prostatic Tissues and Cancer Cell Lines. Urology, 48, 963-970 https://doi.org/10.1016/S0090-4295(96)00376-7

[166] Mizuno, K., Sone, S., Orino, E., et al. (1994) Autonomous Expressions of Cytokine Genes by Human Lung Cancer Cells and Their Paracrine Regulation. Japanese Journal of Cancer and Oncology Research, 85, 179-186 https://doi.org/10.1111/j.1349-7006.1994.tb02080.x

[167] Zhang, H., Vutskits, L., Pepper, M.S., et al. (2003) VEGF Is a Chemoattractant for FGF-2-Stimulated Neural Progenitors. Journal of Cell Biology, 163, 1375-1384 https://doi.org/10.1083/jcb.200308040

[168] Cicuttini, F.M., Begley, C.G. and Boyd, A.W. (1992) The Effect of Recombinant Stem Cell Factor (SCF) on Purified CD34-Positive Human Umbilical Cord Blood Progenitor Cells. Growth Factors, 6, 31-39 https://doi.org/10.3109/08977199209008869

[169] Lovelady, D.C., Richmond, T.C., Maggi, A.N., Lo, C.M. and Rabson, D.A. (2007) Distinguishing Cancerous from Non-Cancerous Cells through Analysis of Electrical Noise. Physical Review E, 76, Article ID: 041908 https://doi.org/10.1103/PhysRevE.76.041908

[170] Lovelady, D.C., Friedman, J., Patel, S., et al. (2009) Detecting Effects of Low Levels of Cytochalasin B in 3T3 Fibroblast Cultures by Analysis of Electrical Noise Obtained from Cellular Micromotion. Biosensors and Bioelectronics, 24, 2250-2254 https://doi.org/10.1016/j.bios.2008.09.033

[171] Lineweaver, C.H., Davies, P.C.W. and Vincent, M.D. (2014) Targeting Cancer's Weaknesses (Not Its Strengths): Therapeutic Strategies Suggested by the Atavistic Model. Bioessays, 36, 827-835 https://doi.org/10.1002/bies.201400070

[172] Jezequel, P. and Campone, M. (2018) Comment on "How the Evolution of Multicellularity Set the Stage for Cancer". British Journal of Cancer, 119, 133-134 https://doi.org/10.1038/s41416-018-0091-0

[173] Andocs, G., Szasz, O. and Szasz, A. (2009) Oncothermia Treatment of Cancer: From the Laboratory to Clinic. Electromagnetic Biology and Medicine, 28, 148-165 https://doi.org/10.1080/15368370902724633

[174] Wust, P., Ghadjar, P., Nadobny, J. and Beck, M. (2019) Physical Potentials of Radiofrequency Hyperthermia with Amplitude Modulation. Oncothermia Journal, 26, 128-137.

[175] Vincze, Gy. and Szasz, A. (2018) Similarities of Modulation by Temperature and by Electric Field. Ojbiphy, 8, 95-103.
https://doi.org/10.4236/ojbiphy.2018.83008

[176] Andocs, G., Renner, H., Balogh, L., Fonyad, L., Jakab, C. and Szasz, A. (2009) Strong Synergy of Heat and Modulated Electro-Magnetic Field in Tumor Cell Killing, Study of HT29 Xenograft Tumors in a Nude Mice Model. Strahlentherapie und Onkologie, 185, 120-126 https://doi.org/10.1007/s00066-009-1903-1

[177] Nagy, G., Meggyeshazi, N. and Szasz, O. (2013) Deep Temperature Measurements in Oncothermia Processes. Conference Papers in Medicine, 2013, Article ID: 685264 https://doi.org/10.1155/2013/685264

[178] Hossain, M.T., Prasad, B., Park, K.S., et al. (2016) Simulation and Experimental Evaluation of Selective Heating Characteristics of 13, 56 MHz Radiofrequency Hyperthermia in Phantom Models. International Journal of Precision Engineering and Manufacturing, 17, 253-256 https://doi.org/10.1007/s12541-016-0033-9

[179] Orczy-Timko, B. (2020) Ch. 18. Phantom Measurements with the EHY-2030 Device. In: Szasz, A., Ed., Challenges and Solutions of Oncological Hyperthermia, Cambridge Scholars Publishing, Newcastle upon Tyne District, 416-428.

[180] Szasz, O. and Szasz, A. (2021) Approaching Complexity: Hyperthermia Dose and Its Possible Measurement in Oncology. Ojbiphy, 11, 68-132 https://doi.org/10.4236/ojbiphy.2021.111002

[181] Szasz, A. and Vincze, Gy. (2006) Dose Concept of Oncological Hyperthermia: Heat-Equation Considering the Cell Destruction. Journal of Cancer Research and Therapeutics, 2, 171-181 https://doi.org/10.4103/0973-1482.29827

[182] Lee, S.Y., Szigeti, G.P. and Szasz, A.M. (2019) Oncological Hyperthermia: The Correct Dosing in Clinical Applications. International Journal of Oncology, 54, 627-643 https://doi.org/10.3892/ijo.2018.4645

[183] Szasz, A., Vincze, Gy., Szasz, O. and Szasz, N. (2003) An Energy Analysis of Extracellular Hyperthermia. Magneto- and Electro-Biology, 22, 103-115 https://doi.org/10.1081/JBC-120024620

[184] Vincze, Gy. and Szasz, A. (2015) Effect of Cellular Membrane Resistivity Inhomogeneity on the Thermal Noise-Limit. Journal of Advances in Physics, 11, 3170-3183 https://doi.org/10.24297/jap.v11i3.6859

[185] Vincze, Gy. and Szasz, A. (2015) Reorganization of Actin Filaments and Microtubules by Outside Electric Field. Journal of Advances in Biology, 8, 1514-1518.

[186] Lee, S.Y., Fiorentini, G., Szasz, A.M., Szigeti, Gy., Szasz, A. and Minnaar, C.A. (2020) Quo Vadis Oncological Hyperthermia (2020)? Frontiers in Oncology, 10, Article No. 1690 https://doi.org/10.3389/fonc.2020.01690

[187] Szasz, O. and Szasz, A. (2014) Oncothermia—Nano-Heating Paradigm. Journal of Cancer Science and Therapy, 6 4. https://doi.org/10.4172/1948-5956.1000259

[188] Szasz, A. (2013) Chapter 4. Electromagnetic Effects in Nanoscale Range. In: Shimizu, T. and Kondo, T., Eds. Cellular Response to Physical Stress and Therapeutic Applications, Nova Science Publishers, Hauppauge, 55-81

[189] Andocs, G., Rehman, M.U., Zhao, Q.L., Tabuchi, Y., Kanamori, M. and Kondo, T. (2016) Comparison of Biological Effects of Modulated Electro-Hyperthermia and Conventional Heat Treatment in Human Lymphoma U937 Cell. Cell Death Discovery, 2, 16039 https://doi.org/10.1038/cddiscovery.2016.39

[190] Szasz, A. (2020) Towards the Immunogenic Hyperthermic Action: Modulated Electro-Hyperthermia. Clinical Oncology and Research, Science Repository, 3, 5-6 https://doi.org/10.31487/j.COR.2020.09.07

[191] Kim, J.K., Prasad, B. and Kim, S. (2017) Temperature Mapping and Thermal Dose Calculation in Combined Radiation Therapy and 13.56 MHz Radiofrequency Hyperthermia for Tumor Treatment. Proceedings SPIE 10047, Optical Methods for Tumor Treatment and Detection: Mechanisms and Techniques in Photodynamic Therapy XXVI. Volume 10047, Article ID: 1004718 https://doi.org/10.1117/12.2253163

[192] Prasad, B., Kim, S., Cho, W., et al. (2019) Quantitative Estimation of the Equivalent Radiation Dose Escalation Using Radiofrequency Hyperthermia in Mouse Xenograft Models of Human Lung Cancer. Scientific Reports, 9. Article No. 3942 https://doi.org/10.1038/s41598-019-40595-6

[193] Forika, G., Balogh, A., Vancsik, T., Zalatnai, A., et al. (2020) Modulated Electro-Hyperthermia Resolves Radioresistance of Panc1 Pancreas Adenocarcinoma and Promotes DNA Damage and Apoptosis in Vitro. International Journal of Molecular Sciences, 21, 5100 https://doi.org/10.3390/ijms21145100

[194] Vancsik, T., Forika, G., Balogh, A., et al. (2019) Modulated Electro-Hyperthermia Induced p53 Driven Apoptosis and Cell Cycle Arrest Additively Support Doxorubicin Chemotherapy of Colorectal Cancer in Vitro. Cancer Medicine, 8, 4292-4303 https://doi.org/10.1002/cam4.2330

[195] Tsang, Y.W., Chi, K.H., Huang, C.C., et al. (2019) Modulated Electro-Hyperthermia-Enhanced Liposomal Drug Uptake by Cancer Cells. International Journal of Nanomedicine, 14, 1269-1579 https://doi.org/10.2147/IJN.S188791

[196] Krenacs, T., Meggyeshazi, N., Forika, G., et al. (2020) Modulated Electro-Hyperthermia-Induced Tumor Damage Mechanisms Revealed in Cancer Models. International Journal of Molecular Sciences, 21, 6270. https://doi.org/10.3390/ijms21176270

[197] Wismeth, C., Dudel, C., Pascher, C., et al. (2010) Transcranial Electro-Hyperthermia Combined with Alkylating Chemotherapy in Patients with Relapsed High-Grade Gliomas—Phase I Clinical Results. Journal of Neuro-Oncology, 98, 395-405 https://doi.org/10.1007/s11060-009-0093-0

[198] Sahinbas, H., Groenemeyer, D.H.W., Boecher, E. and Szasz, A. (2007) Retrospective Clinical Study of Adjuvant Electro-Hyperthermia Treatment for Advanced Brain-Gliomas. Deutsche Zeitschriftfuer Onkologie, 39, 154-160 https://doi.org/10.1055/s-2007-986020

[199] Fiorentini, G., Sarti, D., Milandri, C., et al. (2018) Modulated Electrohyperthermia in Integrative Cancer Treatment for Relapsed Malignant Glioblastoma and Astrocytoma: Retrospective Multicenter Controlled Study. Integrative Cancer Therapies, 18, 1-11 https://doi.org/10.1177/1534735418812691

[200] Fiorentini, G., Sarti, D., Casadei, V., et al. (2020) Ch. 6. Modulated Electro-Hyperthermia for the Treatment of Relapsed Brain Gliomas. In: Szasz, A., Ed., Challenges and Solutions of Oncological Hyperthermia, Cambridge Scholars Publishing, Newcastle upon Tyne District, 110-125.

[201] Ou, J., Zhu, X., Lu, Y., et al. (2017) The Safety and Pharmacokinetics of High Dose Intravenous Ascorbic Acid Synergy with Modulated Electrohyperthermia in Chinese Patients with Stage III-IV Non-Small Cell Lung Cancer. European Journal of Pharmaceutical Sciences, 109, 412-418 https://doi.org/10.1016/j.ejps.2017.08.011

[202] Ou, J., Zhu, X., Chen, P., et al. (2020) A Randomized Phase II Trial of Best Supportive Care with or without Hyperthermia and Vitamin C for Heavily Pretreated, Advanced, Refractory Non-Small-Cell Lung Cancer. Journal of Advanced Research, 24, 175-182 https://doi.org/10.1016/j.jare.2020.03.004

[203] Roussakow, S. (2017) Clinical and Economic Evaluation of Modulated Electrohyperthermia Concurrent to Dose-Dense Temozolomide 21/28 Days Regimen in the Treatment of Recurrent Glioblastoma: A Retrospective Analysis of a Two-Centre German Cohort Trial with Systematic Comparison and Effect-to-Treatment Analysis. BMJ Open, 7, e017387 https://doi.org/10.1136/bmjopen-2017-017387

[204] Roussakow, S.V. (2016) Pharmacoeconomic Study of Oncothermia (Modulated Electro-Hyperthermia) in the Treatment of Lung Cancer. Oncothermia Journal, 18, 116-138.

[205] Ranieri, G., Laface, C., Laforgia, M., et al. (2020) Bevacizumab plus FOLFOX-4 Combined with Deep Electro-Hyperthermia as First-Line Therapy in Metastatic Colon Cancer: A Pilot Study. Frontiers in Oncology, 10, Article ID: 590707 https://doi.org/10.3389/fonc.2020.590707

[206] Kim, S., Lee, J.H., Cha, J. and You, S.H. (2021) Beneficial Effects of Modulated Electro-Hyperthermia during Neoadjuvant Treatment for Locally Advanced Rectal Cancer. International Journal of Hyperthermia, 38, 144-151 https://doi.org/10.1080/02656736.2021.1877837

[207] Gadaleta-Caldarola, G., Infusino, S., Galise, I., et al. (2014) Sorafenib and Locoregional Deep Electro-Hyperthermia in Advanced Hepatocellular Carcinoma. A Phase II Study. Oncology Letters, 8, 1783-1787 https://doi.org/10.3892/ol.2014.2376

[208] Fiorentini, G., Sarti, D., Casadei, V., et al. (2019) Modulated Electro-Hyperthermia as Palliative Treatment for Pancreas Cancer: A Retrospective Observational Study on 106 Patients. Integrative Cancer Therapies, 18, 1-8 https://doi.org/10.1177/1534735419878505

[209] Volovat, C., Volovat, S.R., Scripcaru, V., et al. (2014) Second-Line Chemotherapy with Gemcitabine and Oxaliplatin in Combination with Loco-Regional Hyperthermia (EHY-2000) in Patients with Refractory Metastatic Pancreatic Cancer—Preliminary Results of a Prospective Trial. Romanian Reports in Physics, 66, 166-174.

[210] Yoo, H.J., Lim, M.C., Seo, S.S., et al. (2019) Phase I/II Clinical Trial of Modulated Electro-Hyperthermia Treatment in Patients with Relapsed, Refractory or Progressive Heavily Treated Ovarian Cancer. Japanese Journal of Clinical Oncology, 49, 832-838 https://doi.org/10.1093/jjco/hyz071

[211] Lee, S.Y., Lee, N.R., Cho, D.H., et al. (2017) Treatment Outcome Analysis of Chemotherapy Combined with Modulated Electro-Hyperthermia Compared with Chemotherapy Alone for Recurrent Cervical Cancer, Following Irradiation. Oncology Letters, 14, 73-78 https://doi.org/10.3892/ol.2017.6117

[212] Minnaar, C.A., Kotzen, J.A., Ayeni, O.A., et al. (2019) The Effect of Modulated Electro-Hyperthermia on Local Disease Control in HIV-Positive and -Negative Cervical Cancer Women in South Africa: Early Results from a Phase III Randomized Controlled Trial. PLoS ONE, 14, e0217894 https://www.ncbi.nlm.nih.gov/pmc/articles/PMC6584021 https://doi.org/10.1371/journal.pone.0217894

[213] Minnaar, C.A., Kotzen, J.A., Naidoo, T., et al. (2020) Analysis of the Effects of mEHT on the Treatment-Related Toxicity and Quality of Life of HIV-Positive Cervical Cancer Patients. International Journal of Hyperthermia, 37

263-272.
https://doi.org/10.1080/02656736.2020.1737253
[214] Jeung, T.S., Ma, S.Y., Choi, J., et al. (2015) Results of Oncothermia Combined with Operation, Chemotherapy and Radiation Therapy for Primary, Recurrent and Metastatic Sarcoma. Case Reports in Clinical Medicine, 4, 157-168 https://doi.org/10.4236/crcm.2015.45033
[215] Volovat, C., Volovat, S.R., Scripcaru, V., et al. (2014) The Results of Combination of Ifosfamid and Locoregional Hyperthermia (EHY 2000) in Patients with Advanced Abdominal Soft-Tissue Sarcoma after Relapse of First Line Chemotherapy. Romanian Reports in Physics, 66, 175-181.
[216] Van, Gool, S.W., Makalowski, J., Feyen, O., Prix, L., Schirrmacher, V. and Stuecker, W. (2018) The Induction of Immunogenic Cell Death (ICD) during Maintenance Chemotherapy and Subsequent Multimodal Immunotherapy for Glioblastoma (GBM). Austin Oncology Case Reports, 3, 1010.
[217] Chi, M.S., Mehta, M.P., Yang, K.L., et al. (2020) Putative Abscopal Effect in Three Patients Treated by Combined Radiotherapy and Modulated Electrohyperthermia. Frontiers in Oncology, 10, Article No. 254 https://doi.org/10.3389/fonc.2020.00254
[218] Minnaar, C.A., Kotzen, J.A., Ayeni, O.A., et al. (2020) Potentiation of the Abscopal Effect by Modulated Electro-Hyperthermia in Locally Advanced Cervical Cancer Patients. Frontiers in Oncology, 10, Article No. 376 https://doi.org/10.3389/fonc.2020.00376
[219] Chi, K.H. (2020) Ch. 12. Tumour-Directed Immunotherapy: Clinical Results of Radiotherapy with Modulated Electro-Hyperthermia. In: Szasz, A., Ed., Challenges and Solutions of Oncological Hyperthermia, Cambridge Scholars Publishing, Newcastle upon Tyne District, 206-226 https://www.cambridgescholars.com/challenges-and-solutions-of-oncological-hyperthermia
[220] Van, Gool, S.W., Makalowski, J., Domogalla, M.P., et al. (2020) Ch. 7. Personalised Medicine in Glioblastoma Multiforme. In: Szasz, A., Ed., Challenges and Solutions of Oncological Hyperthermia, Cambridge Scholars Publishing, Newcastle upon Tyne District, 126-158.
[221] Pang, C.L.K., Zhang, X., Wang, Z., et al. (2017) Local Modulated Electro-Hyper-thermia in Combination with Traditional Chinese Medicine vs. Intraperitoneal Chemoinfusion for the Treatment of Peritoneal Carcinomatosis with Malignant Ascites: A Phase II Randomized Trial. Molecular and Clinical Oncology, 6, 723-732 https://doi.org/10.3892/mco.2017.1221
[222] Szasz, A.M., Minnaar, C.A., Szentmartoni, Gy., et al. (2019) Review of the Clinical Evidences of Modulated Electro-Hyperthermia (mEHT) Method: An Update for the Practicing Oncologist. Frontiers in Oncology, 9, Article No. 1012.
https://doi.org/10.3389/fonc.2019.01012
[223] Szasz, A.M., Arkosy, P., Arrojo, E.E., et al. (2020) Ch. 2. Guidelines for Local Hyperthermia Treatment in Oncology. In: Szasz, A., Ed., Challenges and Solutions of Oncological Hyperthermia, Cambridge Scholars Publishing, Newcastle upon Tyne District, 32-71.
[224] Van, Gool, S.W., Makalowski, J., Fiore, S., et al. (2021) Randomized Controlled Immunotherapy Clinical Trials for GBM Challenged. Cancers, 13, 32 https://doi.org/10.3390/cancers13010032
[225] Szasz, A., Szasz, N. and Szasz, O. (2010) Oncothermia—Principles and Practices. Springer Science, Heidelberg https://doi.org/10.1007/978-90-481-9498-8
[226] Parmar, G., Rurak, E., Elderfield, M., et al. (2020) Ch. 13. 8-Year Observational Study on Naturopathic Treatment with Modulated Electro-Hyperthermia (mEHT): A Single-Centre Experience. In: Szasz, A., Ed., Challenges and Solutions of Oncological Hyperthermia, Cambridge Scholars Publishing, Newcastle upon Tyne District, 227-266
[227] Hager, E.D., Sahinbas, H., Groenemeyer, D.H., et al. (2008) Prospectivephase II Trial for Recurrent High-Grade Malignant Gliomas with Capacitive Coupled Low Radiofrequency (LRF) Deep Hyperthermia. ASCO, Journal of Clinical Oncology, Annual Meeting Proceedings (Post-Meeting Edition), 26, 2047 https://doi.org/10.1200/jco.2008.26.15_suppl.2047
[228] Renner, H. and Albrecht, I. (2007) Analyseder überlebenszeiten von Patineten mit Pankreastumoren mit erfolgterkapazitativer Hyperthermiebehandlung, (Erstellt: Mr. Mirko Friedrich; May & STM.
[229] Dani, A., Varkonyi, A., Magyar, T. and Szasz, A. (2008) Clinical Study for Advanced Pancreas Cancer Treated by Oncothermia. Forum Hyperthermie, 1, 13-20.
[230] Parmar, G. (2018) Naturopathic Anti-Tumoral Treatment & 8 Year Survival Benefit Statistics: A Single-Centre Experience. 36th Conference of the International Clinical Hyperthermia Society, Budapest, 28-29 September 2018.
[231] SEER (Surveillance, Epidemiology, and End Result Program) Database https://seer.cancer.gov/data

[232] Szasz, O. and Szasz, A. (2020) Parametrization of Survival Measures, Part I: Consequences of Self-Organizing International Journal of Clinical Medicine, 11, 316-347 https://doi.org/10.4236/ijcm.2020.115031

[233] Szasz, O., Szasz, A.M., Szigeti, G.P. and Szasz, A. (2020) Chapter 2. Data Mining and Evaluation of Single Arm Clinical Studies. In: Yong, X., Ed., Recent Developments in Engineering Research, Vol. 3, GAN Publishing, London 15-74.

[234] Szasz, A., Szigeti, G.P. and Szasz, A.M. (2020) Parametrization of Survival Measures, Part II: Single Arm Studies International Journal of Clinical Medicine, 11, 348-373 https://doi.org/10.4236/ijcm.2020.115032

[235] Szasz, A., Szigeti, G.P. and Szasz, A.M. (2020) Parametrization of Survival Measures, Part III: Clinical Evidences in Single Arm Studies with Endpoint of Overall Survival. International Journal of Clinical Medicine, 11, 389-419 https://doi.org/10.4236/ijcm.2020.116034

Updates of the application of Regional Hyperthermia in the treatment of esophageal, colorectal and pancreatic cancers.

Regional Hyperthermia for gastrointestinal cancers treatment

Giammaria Fiorentini, Donatella Sarti, Girolamo Ranieri, Cosmo Damiano Gadaleta, Caterina Fiorentini, Tommaso Carfagno, Carlo Milandri, Andrea Mambrini, Stefano Guadagni

Department of Onco-Hematology, Azienda Ospedaliera "Ospedali Riuniti Marche Nord", Pesaro 61122, Italy
Oncology Service and Unit of Hyperthermia, Private Clinic Ravenna33, Ravenna 48124, Italy
Oncology-Hematology, Azienda Ospedaliera "Ospedali Riuniti Marche Nord", Pesaro 61122, Italy
Interventional and Integrated Medical Oncology, National Cancer Research Centre, IRCCS Istituto Tumori "Giovanni Paolo II", Bari 70124, Italy, Italy
Integrated Section Translational Medical Oncology, Interventional Radiology Unit, National Cancer Institute of Bari, Bari 70124, Italy
Department of Medical Biothecnologies, Division of Cardiology, University of Siena, Siena 53100, Italy
Department of Radiotherapy , University Hospital of Siena, Siena 53100, Italy
Medical Oncology Unit, San Donato Hospital, Arezzo 52100, Italy
Oncology Department, Apuane Hospital, Massa-Carrara 54100, Italy
Applied Clinical Sciences and Biotechnology, Section of General Surgery, University of L'Aquila, L'Aquila 67100, Italy

Cite this article as:
Fiorentini, G.: Updates of the application of Regional Hyperthermia in the treatment of esophageal, colorectal, and pancreatic cancers.

Oncothermia Journal 31, 2022 March: 228-242
www.oncotherm.com/sites/oncotherm/files/2022-03/Fiorentini_Updates.pdf

Author contributions:

Fiorentini G, Sarti D and Guadagni S wrote the paper; Ranieri G, Gadaleta CD and Carfagno T perfomed the data collection, Fiorentini C collected and evaluated the interactions between hyperthermia and heart, Milandri C and Mambrini A reviewed the manuscript.

Corresponding Author:

Giammaria Fiorentini, MD, Adjunct Professor, Chief Doctor, Director, Department of Onco-Hematology, Azienda Ospedaliera "Ospedali Riuniti Marche Nord", via Lombroso 1, Pesaro 61122, Italy. g.fiorentini2020@gmail.com

Abstract

The therapeutic value of regional hyperthermia (RHT) in oncological treatments has been known for years. Several studies report RHT efficacy for tumor response and survival. RHT can also be used in combination with chemotherapy (CHT) and radiotherapy (RT) and chemoradiotherapy (CRT) and immunotherapy, enhancing their benefit, also in the treatment of gastrointestinal tumor: esophageal, colorectal and pancreatic cancer. However, RHT has not yet become a common therapy in everyday clinical practice due to the difficulty in measuring the temperature increase inside the tissues, the long duration of treatment, the need to have dedicated nurses and doctors, adequate equipment and facilities.
Modulated electro-hyperthermia (mEHT) is a recent RHT method that targets malignant cell membranes and the extracellular matrix, allowing deep tumors sensitization, notwithstanding the thickness of the adipose tissue, and overcoming the issue of homogenous heating.
Several studies confirm the advantage of RHT and mEHT association to CRT, CHT and RT as neoadjuvant and palliative settings in esophageal, colorectal and pancreatic cancer. This article summarizes the available data of RHT for these tumors.

Key words: regional hyperthermia, modulated electro-hyperthermia, colorectum cancer, esophageal cancer, pancreatic cancer

Core tip

Regional hyperthermia in association with radiotherapy and/or chemotherapy may increase median OS, PFS and tumor response of patients with esophageal, colon, rectal, anal and locally advanced or metastatic pancreatic cancer. The mEHT is a relatively new method of regional hyperthermia that targets tumor cell membranes and extra matrix tissue, to increase the temperature inside cancer tissue and sensitize it to cancer therapies. This method has relatively few published studies, however, the results are exciting and comparable to those of other RHT, amplifying the benefits of both chemotherapy and radiotherapy in all the considered tumors and is well tolerated.

Introduction

Regional hyperthermia (RHT) efficacy in the remission of malignant tumors has been known for decades. RHT is achieved by increasing the tissue/body temperature with an external electromagnetic field with rapid fields alterations. Technological developments for local/locoregional heat application allowed RHT to be safe and available for clinical application, showing the beneficial effects of mild RHT (39.5–43°C) and optimizing the devices for minimal hot spot occurrence [1, 2]. Temperature rise >43°C, indeed, has potential risks, such as damage of surrounding normal tissues and enhancement of blood flow that can potentially increase malignant cells dissemination and distant metastases [3].

Nowadays, an increasing number of clinical studies show RHT efficacy in the treatment of different types of cancers. However, only a few centers have included this adjuvant treatment in their clinical practice [1].

The basic biological rationale of heat utilization is the enhancement of radiation, chemotherapeutic agents, and immunotherapy effects, allowing radiation dose reduction. Heat triggers changes in tumor perfusion and oxygenation, inhibition of DNA repair mechanisms and immune stimulation by exposing tumor antigens [1, 2]. Indeed, local radiotherapy in association with RHT increases tumor immunogenicity and results in systemic effects through immune-mediated abscopal effects [3]. Modulated electro-hyperthermia (mEHT) is a recent RHT method that targets malignant cell membranes and the extracellular matrix, allowing deep tumors sensitization, notwithstanding the thickness of the adipose tissue, and overcoming the issue of homogenous heating. The association of regional hyperthermia and mEHT with chemo-(CHT) or radiotherapy (RT) is reported to be successful in several types of tumors, including esophageal, pancreatic and colorectal cancers [3-5].

This is a narrative review aiming to update the current knowledge on RHT use in association with RT and/or CHT in treating esophageal, colorectal and pancreatic cancers.

Types of hyperthermia

There are different types of hyperthermia: superficial hyperthermia, deep/regional hyperthermia, whole-body hyperthermia, interstitial hyperthermia and body orifice insertion hyperthermia [6].

Whole-body hyperthermia increases the entire body's temperature up to a maximum of 41.8°C, using thermal conduction or radiant light techniques. Interstitial hyperthermia places heating electromagnetic devices (needles or catheters) directly inside the tumor. Most interstitial hyperthermia has involved the heating technique. The main advantage of this therapy is that the heating occurs directly inside the tumor, enabling it to reach higher local tumor temperatures than in the surrounding host tissues. Similarly, hyperthermia can be achieved by inserting heating devices into natural body orifices with tumors (body orifice insertion hyperthermia) [6]. Deep/regional hyperthermia can increase the temperature of a portion of the body (at the tumor site) up to a depth of > 5 cm with electromagnetic fields, minimizing the heating of the surrounding tissue [6].

Superficial hyperthermia heats tissues <5cm in depth from the body's surface, using electromagnetic fields. The variability of the blood flow within the treated region also contributes to the temperature variation within the tumor region in all types of hyperthermia, [6].

Regional Hyperthermia

Different methods are used for regional hyperthermia, such as using infrared-A, radiative, capacitive or modulated electro-hyperthermia techniques.

Both radiative and capacitive systems are used for superficial hyperthermia to tumors infiltrating up to 4 cm into the tissue, such as melanoma [7]. Two electrodes are positioned on opposite sides of the body and the electric current flowing between them heats the tissues. The electrodes are placed in direct contact with tumor tissue through a water bolus.

There are several types of commercially available radiative superficial systems, including flexible microwave applicators. They all heat with frequencies of 434 to 915 MHz and are positioned directly in contact with the patient's surface over the targeted tumor [7]. Both methods allow homogeneous heating of the target, but the created hot spots could limit the heating. Radiative heating yields more favorable temperature distribution than capacitive heating does, especially within heterogeneous tissues [7].

The water filter infrared-A radiation method uses a light source (halogen lamp at 24 V/150W) and a water filter built-in as a closed cuvette and absorbs the energy, avoiding painful sensations and burns of the skins [8].

Modulated electro-hyperthermia

Tumor blood flow increase is rather limited upon heating; hence, the heat dissipation is slower than in normal tissues. This is the reason why tumor temperature rises higher than that in normal tissue during hyperthermia [3]. However, the homogenous heating of a tumor to a specified temperature is quite challenging due to the heterogeneous distribution of vasculature inside malignant tissue. Indeed, the tumor blood flow varies widely among different tumor types and inside the same tumor, especially in the presence of necrotic areas within the tumor [3].

To improve the results and reduce the adverse effects of thermal therapy, a new method has been recently developed: the modulated electro-hyperthermia (mEHT) [9]. This method targets malignant cell membranes and the extracellular matrix. This allows sensitizing deep tumors, notwithstanding the thickness of the adipose tissue, and overcoming the issue of homogenous heating [9].

mEHT is performed using a 13.56 MHz capacitive coupled device (EHY-2000+, OncoTherm Ltd., Germany) and has comparable benefits to other types of hyperthermia for a variety of tumors: hepatocellular carcinoma, rectal, cervical, brain, lung and pancreatic cancers, improving local disease control and in some cases the survival [9-13]. Hyperthermia is achieved by applying short radio-frequency waves of 13.56 MHz with capacitive coupling to increase tumor temperature to 41.5°C for >90% of treatment duration [10].

Literature search

This narrative review analyses the relevant professional literature searched in prestigious databases as PubMed-MEDLINE, Embase, Cochrane and ClinicalTrials.gov. The chosen search terms: hyperthermia, pancreatic, gastrointestinal, esophageal, colon, rectal, colorectal, anal cancer. The search had collected 934 papers. In further selection, the review includes only full-text manuscripts in the English language, articles reporting results from an observational or experimental trial that had tumor response, survival or progression-free survival or toxicity among their outcomes were registered, and it was published in years 2000 - 2020. The selection did choose 38 manuscripts and was divided according to tumor type. In the further selection, we kept

only the original manuscript (25) and collected with reference tables in three groups of cancers: esophageal, colorectal and pancreatic.

Esophageal Cancer

The prognosis of esophageal cancer remains poor and long-term survival after potentially curative surgery is 5–20% [14, 15]. Several studies on neo-adjuvant chemotherapy alone fail to prove the benefit of this preoperative treatment, however, promising results have been achieved with the combination of heat and chemotherapy in this setting [15-18].

Neoadjuvant chemotherapy (NCHT) or chemoradiotherapy (CRT) in combination with RHT have positive results concerning survival and tumor response of esophageal cancer patients (table 1). Neoadjuvant CRT with docetaxel associated with RHT results in a response rate of 41.7% with a CR of 17.6% after surgery. This treatment has low toxicity and 3- and 5-year survival rates are 56.3% and 50.0%, respectively [18].

A phase II study with chemotherapy (carboplatin and paclitaxel) and radiotherapy associated with RHT as neo-adjuvant treatment provide good locoregional control and overall survival for esophageal cancer patients who have all R0 resection. Tumor response is complete response (CR), partial response (PR) and stable disease (SD) in 19%, 31% and 23% of patients, respectively and survival rates at 1, 2 and 3 years are 79%, 57% and 54% respectively. Quality of life is good for these patients and the toxicity is low [17]. Similar results in survival are reported by another phase I/II study, showing 1- and 2-year survival rates of 69 and 62%, respectively [15].

Intensity-modulated radiotherapy (IMRT) in association with hyperthermia results in a 3-year progression-free survival (PFS) rate and overall survival (OS) rate was 34.9% and 42.5%, respectively, with a low toxicity and excellent local control of esophageal cancer with supraclavicular lymph node metastasis [18].

The results of a meta-analysis comparing the CRT+RHT and RT groups show that RHT increased significantly the 1-, 2-, 3- and 5-year overall survival (OS) of esophageal cancer patients; decreased both recurrence, distant metastases and gastrointestinal reaction rates [14]. These results deliver evidence of CRT+RHT benefits in esophageal cancer neoadjuvant therapy. The pieces of evidence base very hopeful expectations; however, further randomized clinical studies with a more significant number of patients are required to confirm these data.

Colorectal cancer

Colorectal cancer (CRC) is the third most common cause of cancer death in both men and women in the United States and is the second most common cause of cancer death in the United States [19]. In the past decades, neoadjuvant radiotherapy alone or in association with chemotherapy followed by surgery has become a standard treatment for advanced rectal cancer [20]. CHT is used to enhance the RT effects of radiotherapy. RHT is another method to amplify radiotherapy, overcoming the low oxygen concentrations present in large tumors and hamper the effect of radiotherapy. RHT, indeed, increases the tumor blood flow and hence the tissue oxygenation [21].

Neoadjuvant CRT + RHT results in greater 5-year long-term local control (98% vs 87%, p=0.09) and OS (88% versus 76%, p=0.08) than CRT alone in locally advanced non-metastatic rectal cancer [22]. Similar results are reported in other studies on neoadjuvant CRT + RHT in locally advanced non-metastatic rectal cancer, resulting in 5-year OS ranging 60-87.3% (table 2), distant metastases-free survival (DMFS) and local control (LC) of 79.9% and 95.8% respectively [23-25]. In particular, a study compares OS of CRT alone or in association with

RHT and reports that the combined therapy allows longer OS than CRT alone (5 years OS=76% versus 88% p < 0.08) [22]. This improvement in survival is also observed when the neoadjuvant CRT and RHT is performed for anal cancer treatment with five years OS (95.8 vs. 74.5%, P = 0.045), disease-free survival (DFS=89.1 vs. 70.4%, P = 0.027) and local relapse-free survival (LRFS =97.7 vs. 78.7%, P = 0.006) more favorable than CRT alone [26].

As concerning the tumor response, the disease control rates (DCR) of CRT combined to RHT range is 28.5%-94.8% in rectal cancer patients (table 2) [27-31]. The association of RHT to CRT in neoadjuvant treatment of rectal cancer does not increase the toxicity of CRT and the hyperthermia-related adverse events were mainly of mild-moderate intensity and are reported by 26-34% of patients [27-31].

mEHT in association with CHT is used in a study to treat metastatic colon cancer patients with reasonable tumor response rates and survival. Indeed, the DCR is 95% at 90 days and 89.5% at 3 months and PFS is 12.1 months (range 3.5–32.6 months) [32]. Another study applies mEHT in association to CRT for the treatment of rectal cancer patients, reporting minimal, moderate, near-total, and total regression of primary tumor of 15.0%, 51.7%, 18.3% and 15.0%, respectively [33]. The mEHT is well tolerated in both studies, with predominantly mild hyperthermia toxicity [32, 33].

Neoadjuvant CRT in association with RHT and mEHT does not increase toxicity and allows to achieve encouraging results in terms of both tumor response and survival in rectal, colon and anal cancers patients. Further randomized studies are required to confirm these data.

Pancreatic cancer

Pancreatic cancer has a poor prognosis with a 5-year OS < 10%. This may be due to the fact that pancreatic cancer is quite resistant to RT and CHT, because of its hypoxic microenvironment that diminishes sensitivity these therapies [34]. Most used CHT schedules include gemcitabine-based regimes, nab-paclitaxel and for fit patients, the FOLFIRINOX (leucovorin, fluorouracil, irinotecan and oxaliplatin) [35, 36]. These drugs, however, have high toxicity and often low efficacy. For this reason the association of RTH to conventional CHT and RHT has also been introduced for pancreatic cancer treatment, enhancing the drug delivery and diffusion inside the tumor, improving blood flow, reducing hypoxia and inhibiting DNA repair, hence enhancing tumor apoptosis [34].

Three studies compared the survival of locally advanced pancreatic cancer after treatment with the combination CRT and RHT versus CRT alone. Their results show that the addition of RHT increased significantly the survival: OS=8.8 vs. 4.9 months (p = 0.02), OS= 15 vs 11 months (p = 0.025), 1 year OS=80% vs 57% (p=0.021) and PFS=18.6 vs. 9.6 months (p = 0.01) (table 3) [37-39]. The association of CHT to RHT also encourages survival: median OS of 12.9 -17.7 months, 1 year OS=41% and two years OS=15% [40-42]. As concerning the tumor response of locally advanced pancreatic carcinoma, the association of CHT to RHT resulted in a DCR of 50-61% [40, 42]. The treatment is well-tolerated with toxicity of G2 pain and a skin rash and 5% grade III–IV toxicity [38, 42].

A significant increase in survival is also observed when CRT is associated with mEHT than CRT alone as reported by Fiorentini et al. (OS= 18.0 vs. 10.9 months, p<0.001) [10]. The other two studies report similar survivals on mEHT for locally advanced pancreatic carcinoma treatment, OS of 8.9-15.8 months and PFS of 3.9-12.9 months [43, 44]. mEHT also shows a high tumor response in locally advanced pancreatic carcinoma with DCR of 71-96% and safety without grade III-IV toxicity [10, 43, 44]. These better tumor response and survival results of CHT and/or RT in association with mEHT are also observed in aged (>65 years) patients with pancreatic cancer, indeed, a greater DCR, OS and PFS are reported for mEHT group and no-mEHT group in this population (table 3) [45].

These data suggest that RHT increases CRT and CHT benefit both in terms of median OS and in DCR in locally advanced or metastatic pancreatic cancer with low toxicity. Further studies investigating CRT and RHT in locally advanced pancreatic cancer include the HEATPAC trial, a phase II randomized trial (46).

Conclusions

The data presented in this narrative review are from retrospective and prospective studies and suggests that regional hyperthermia in association with radiotherapy and/or chemotherapy may increase median OS, PFS and tumor response of patients with esophageal, colon, rectal, anal and locally advanced or metastatic pancreatic cancer. mEHT is a relatively new method of regional hyperthermia that targets tumor cell membranes and extracellular matrix of the cancerous tissue to increase the temperature inside cancer tissue and sensitize it to cancer therapies. This method has few published studies in gastrointestinal cancers. However, the results are comparable to those of other RHT, amplifying the benefits of both chemotherapy and radiotherapy in all the considered tumors and is well tolerated (47).

The studies presented have heterogeneity concerning the RHT protocols. For this reason it is challenging to compare the results of different studies. Standardized RHT protocols and more randomized clinical trials are needed for each tumor type to address this issue.

REFERENCES

1. Peeken JC, Vaupel P, Combs SE. Integrating Hyperthermia into Modern Radiation Oncology: What Evidence Is Necessary? Front Oncol. 2017;7:132. [doi:10.3389/fonc.2017.00132]
2. Sauer R, Creeze H, Hulshof M, Issels R, Ott O; Interdisciplinary Working Group for Clinical Hyperthermia (Atzelsberg Circle) of the German Cancer Society and the German Society of Radiooncology. Concerning the final report "Hyperthermia: a systematic review" of the Ludwig Boltzmann Institute for Health Technology Assessment, Vienna, March 2010. Strahlenther Onkol. 2012;188(3):209-13. [doi: 10.1007/s00066-012-0072-9]
3. Datta NR, Ordóñez SG, Gaipl US, Paulides MM, Crezee H, Gellermann J, et al. Local hyperthermia combined with radiotherapy and-/or chemotherapy: recent advances and promises for the future. Cancer Treat Rev. 2015;41:742-53. [doi: 10.1016/j.ctrv.2015.05.009]
4. Lee SY, Fiorentini G, Szasz AM, Szigeti G, Szasz A, Minnaar CA. Quo Vadis Oncological Hyperthermia (2020)? Front Oncol. 2020;10:1690. [doi: 10.3389/fonc.2020.01690]
5. Song CW. Effect of local hyperthermia on blood flow and microenvironment: a review. Cancer Res. 1984;44(10):4721s-4730s. [PMID: 6467226]
6. Turner PF, Schaefermeyer T. Technical Aspects of Hyperthermia. In: Issels RD, Wilmanns W. (eds) Application of Hyperthermia in the Treatment of Cancer. Recent Results in Cancer Research. Springer, Berlin, Heidelberg. 1988;107. [https://doi.org/10.1007/978-3-642-83260-4_10]
7. Kok HP, Crezee J. A comparison of the heating characteristics of capacitive and radiative superficial hyperthermia. Int J Hyperthermia. 2017;33(4):378-386. [doi: 10.1080/02656736.2016.1268726]
8. Kelleher DK, Thews O, Rzeznik J, Scherz A, Salomon Y, Vaupel P. Water-filtered infrared-A radiation: a novel technique for localized hyperthermia in combination with bacteriochlorophyll-based photodynamic therapy. Int J Hyperthermia. 1999;15(6):467-74. [doi: 10.1080/026567399285468]
9. Szasz AM, Minnaar CA, Szentmártoni G, Szigeti GP, Dank M. Review of the Clinical Evidences of Modulated Electro-Hyperthermia (mEHT) Method: An Update for the Practicing Oncologist. Front Oncol. 2019;9:1012. [doi: 10.3389/fonc.2019.01012]
10. Fiorentini G, Sarti D, Casadei V, Milandri C, Dentico P, Mambrini A, Nani R, Fiorentini C, Guadagni S. Modulated Electro-Hyperthermia as Palliative Treatment for Pancreatic Cancer: A Retrospective Observational Study on 106 Patients. Integr Cancer Ther. 2019;18:1534735419878505. [doi: 10.1177/1534735419878505].

11. Forika G, Balogh A, Vancsik T, Zalatnai A, Petovari G, Benyo Z, Krenacs T. Modulated Electro-Hyperthermia Resolves Radioresistance of Panc1 Pancreas Adenocarcinoma and Promotes DNA Damage and Apoptosis In Vitro. Int J Mol Sci. 2020; 21(14):5100 [https://doi.org/10.3390/ijms21145100]
12. Vancsik T, Forika G, Balogh A, Kiss E, Krenacs T. Modulated electro-hyperthermia induced p53 driven apoptosis and cell cycle arrest additively support doxorubicin chemotherapy of colorectal cancer in vitro. Cancer Med. 2019;8(9):4292-4303. doi: 10.1002/cam4.2330. Epub 2019 Jun 10. [PMID: 31183995; PMCID: PMC6675742]
13. Nishimura S, Saeki H, Nakanoko T, Kasagi Y, Tsuda Y, Zaitsu Y, Ando K, Nakashima Y, Imamura YU, Ohgaki K, Oki E, Ohga S, Nakamura K, Morita M, Maehara Y. Hyperthermia combined with chemotherapy for patients with residual or recurrent oesophageal cancer after definitive chemoradiotherapy. Anticancer Res. 2015;35(4):2299-303. [PMID: 25862892]
14. Hu Y, Li Z, Mi DH, Cao N, Zu SW, Wen ZZ, Yu XL, Qu Y. Chemoradiation combined with regional hyperthermia for advanced oesophageal cancer: a systematic review and meta-analysis. J Clin Pharm Ther. 2017;42(2):155-164. [doi:10.1111/jcpt.12498]
15. Albregts M, Hulshof MC, Zum Vörde Sive Vörding PJ, van Lanschot JJ, Richel DJ, Crezee H, Fockens P, van Dijk JD, González González D. A feasibility study in oesophageal carcinoma using deep locoregional hyperthermia combined with concurrent chemotherapy followed by surgery. Int J Hyperthermia. 2004;20(6):647-59. [doi: 10.1080/02656730410001714977. PMID: 15370820]
16. Nakajima M, Kato H, Sakai M, Sano A, Miyazaki T, Sohda M, Inose T, Tanaka N, Suzuki S, Masuda N, Fukuchi M, Kuwano H. Planned Esophagectomy after Neoadjuvant Hyperthermo-Chemoradiotherapy using Weekly Low-Dose Docetaxel and Hyperthermia for Advanced Esophageal Carcinomas. Hepatogastroenterology. 2015;62(140):887-91 [PMID: 26902022]
17. Hulshof MC, Van Haaren PM, Van Lanschot JJ, Richel DJ, Fockens P, Oldenborg S, Geijsen ED, Van Berge Henegouwen MI, Crezee J. Preoperative chemoradiation combined with regional hyperthermia for patients with resectable esophageal cancer. Int J Hyperthermia. 2009;25(1):79-85 [doi: 10.1080/02656730802464078]
18. Sheng L, Ji Y, Wu Q, Du X. Regional hyperthermia combined with radiotherapy for esophageal squamous cell carcinoma with supraclavicular lymph node metastasis. Oncotarget. 2017;8(3):5339-5348. [doi:10.18632/oncotarget.14148]
19. Siegel RL, Miller KD, Goding Sauer A, Fedewa SA, Butterly LF, Anderson JC, Cercek A, Smith RA, Jemal A. Colorectal cancer statistics, 2020. CA Cancer J Clin. 2020;70(3):145-164. [doi: 10.3322/caac.21601]
20. De Haas-Kock DFM, Buijsen J, Pijls-Johannesma M, Lutgens L, Lammering G, Mastrigt GAV, et al. Concomitant hyperthermia and radiation therapy for treating locally advanced rectal cancer. Cochrane Database Syst Rev 2009;3:CD006269. [doi: 10.1002/14651858.CD006269.pub2]
21. Elming PB, Sørensen BS, Oei AL, Franken NAP, Crezee J, Overgaard J, Horsman MR. Hyperthermia: The Optimal Treatment to Overcome Radiation Resistant Hypoxia. Cancers (Basel). 2019;11(1):60. [doi:10.3390/cancers11010060]
22. Gani C, Schroeder C, Heinrich V, Spillner P, Lamprecht U, Berger B, Zips D. Long-term local control and survival after preoperative radiochemotherapy in combination with deep regional hyperthermia in locally advanced rectal cancer. Int J Hyperthermia. 2016;32(2):187-92. doi: 10.3109/02656736.2015.1117661. Epub 2016 Jan 11.PMID: 26754458
23. Zwirner K, Bonomo P, Lamprecht U, Zips D, Gani C. External validation of a rectal cancer outcome prediction model with a cohort of patients treated with preoperative radiochemotherapy and deep regional hyperthermia. Int J Hyperthermia. 2018;34(4):455-460. [doi: 10.1080/02656736.2017.1338364]
24. Maluta S, Romano M, Dall'oglio S, Genna M, Oliani C, Pioli F, Gabbani M, Marciai N, Palazzi M. Regional hyperthermia added to intensified preoperative chemo-radiation in locally advanced adenocarcinoma of middle and lower rectum. Int J Hyperthermia. 2010;26(2):108-17. [doi: 10.3109/02656730903333958]
25. Rau B, Wust P, Tilly W, Gellermann J, Harder C, Riess H, Budach V, Felix R, Schlag PM. Preoperative radiochemotherapy in locally advanced or recurrent rectal cancer: regional radiofrequency hyperthermia correlates with clinical parameters. Int J Radiat Oncol Biol Phys. 2000;48(2):381-91. [doi: 10.1016/s0360-3016(00)00650-7]
26. Ott OJ, Schmidt M, Semrau S, Strnad V, Matzel KE, Schneider I, Raptis D, Uter W, Grützmann R, Fietkau R. Chemoradiotherapy with and without deep regional hyperthermia for squamous cell carcinoma of the anus. Strahlenther Onkol. 2019;195(7):607-614. [doi: 10.1007/s00066-018-1396-x]
27. Shoji H, Motegi M, Osawa K, Okonogi N, Okazaki A, Andou Y, Asao T, Kuwano H, Takahashi T, Ogoshi K. A novel strategy of radiofrequency hyperthermia (neothermia) in combination with preoperative chemoradiotherapy for the treatment of advanced rectal cancer: a pilot study. Cancer Med. 2015;4(6):834-43. [doi: 10.1002/cam4.431]
28. Kato T, Fujii T, Ide M, Takada T, Sutoh T, Morita H, Yajima R, Yamaguchi S, Tsutsumi S, Asao T, Oyama T, Kuwano H. Effect of long interval between hyperthermochemoradiation therapy and surgery for rectal cancer on apoptosis, proliferation and tumor response. Anticancer Res. 2014;34(6):3141-6. [PMID: 24922685]
29. Schroeder C, Gani C, Lamprecht U, von Weyhern CH, Weinmann M, Bamberg M, Berger B. Pathological complete response and sphincter-sparing surgery after neoadjuvant radiochemotherapy with regional hyperthermia for locally

advanced rectal cancer compared with radiochemotherapy alone. Int J Hyperthermia. 2012;28(8):707-14. [doi: 10.3109/02656736.2012.722263]
30. Tsutsumi S, Tabe Y, Fujii T, Yamaguchi S, Suto T, Yajima R, Morita H, Kato T, Shioya M, Saito J, Asao T, Nakano T, Kuwano H. Tumor response and negative distal resection margins of rectal cancer after hyperthermochemoradiation therapy. Anticancer Res. 2011;31(11):3963-7. [PMID: 22110227]
31. Kang MK, Kim MS, Kim JH. Clinical outcomes of mild hyperthermia for locally advanced rectal cancer treated with preoperative radiochemotherapy. Int J Hyperthermia. 2011;27(5):482-90. [doi: 10.3109/02656736.2011.563769]
32. You SH, Kim S. Feasibility of modulated electro-hyperthermia in preoperative treatment for locally advanced rectal cancer: Early phase 2 clinical results. Neoplasma. 2020;67(3):677-683. [doi: 10.4149/neo_2020_190623N538]
33. Ranieri G, Laface C, Laforgia M, De Summa S, Porcelli M, Macina F, Ammendola M, Molinari P, Lauletta G, Di Palo A, Rubini G, Ferrari C, Gadaleta CD. Bevacizumab Plus FOLFOX-4 Combined With Deep Electro-Hyperthermia as First-line Therapy in Metastatic Colon Cancer: A Pilot Study. Front Oncol. 2020;10:590707. [doi: 10.3389/fonc.2020.590707]
34. van der Horst A, Versteijne E, Besselink MGH, Daams JG, Bulle EB, Bijlsma MF, Wilmink JW, van Delden OM, van Hooft JE, Franken NAP, van Laarhoven HWM, Crezee J, van Tienhoven G. The clinical benefit of hyperthermia in pancreatic cancer: a systematic review. Int J Hyperthermia. 2018;34:969-979. [doi: 10.1080/02656736.2017.1401126.]
35. Liu X, Yang X, Zhou G, Chen Y, Li C, Wang X. Gemcitabine based regional intra-arterial infusion chemotherapy in patients with advanced pancreatic adenocarcinoma. Medicine (Baltimore). 2016;95:e3098. [doi: 10.1097/MD.0000000000003098]
36. Suker M, Beumer BR, Sadot E, Marthey L, Faris JE, Mellon EA, El-Rayes BF, Wang-Gillam A, Lacy J, Hosein PJ, Moorcraft SY, Conroy T, Hohla F, Allen P, Taieb J, Hong TS, Shridhar R, Chau I, van Eijck CH, Koerkamp BG. A patient-level meta analysis of FOLFIRINOX for locally advanced pancreatic cancer. Lancet Oncol. 2016;17:801-810. [doi: 10.1016/S1470-2045(16)00172-8]
37. Maebayashi T, Ishibashi N, Aizawa T, Sakaguchi M, Sato T, Kawamori J, Tanaka Y. Treatment outcomes of concurrent hyperthermia and chemoradiotherapy for pancreatic cancer: Insights into the significance of hyperthermia treatment. Oncol Lett. 2017;13(6):4959-4964. [doi: 10.3892/ol.2017.6066]
38. Ohguri T, Imada H, Yahara K, Morioka ·T, Nakano K,·Korogi Y. Concurrent chemoradiotherapy with gemcitabine plus regional hyperthermia for locally advanced pancreatic carcinoma: initial experience. Radiat Med. 2008;26:587-596. [DOI 10.1007/s11604-008-0279-y]
39. Maluta S, Schaffer M, Pioli F, Dall'oglio S, Pasetto S, Schaffer PM, Weber B, Giri MG. Regional hyperthermia combined with chemoradiotherapy in primary or recurrent locally advanced pancreatic cancer : an open-label comparative cohort trial. Strahlenther Onkol. 2011;187(10):619-25. [doi: 10.1007/s00066-011-2226-6]
40. Ono E, Yano M, Ohshiro T, Shishida M, Sumitani D,Yuzou ,Okamoto Y, Och M. Effectiveness of hyperthermia in clinical stage IV pancreatic cancer. Oncothermia Journal. 2019;27:88-93 [https://oncotherm.com/sites/oncotherm/files/2019-10/Effectiveness_of_hyperthermia.pdf]
41. Tschoep-Lechner KE, Milani V, Berger F, Dieterle N, Abdel-Rahman S, Salat C, Issels RD. Gemcitabine and cisplatin combined with regional hyperthermia as second-line treatment in patients with gemcitabine-refractory advanced pancreatic cancer. Int J Hyperthermia. 2013;29(1):8-16. [doi: 10.3109/02656736.2012.740764]
42. Ishikawa T, Kokura S, Sakamoto N, Ando T, Imamoto E, Hattori T, Oyamada H, Yoshinami N, Sakamoto M, Kitagawa K, Okumura Y, Yoshida N, Kamada K, Katada K, Uchiyama K, Handa O, Takagi T, Yasuda H, Sakagami J, Konishi H, Yagi N, Naito Y, Yoshikawa T. Phase II trial of combined regional hyperthermia and gemcitabine for locally advanced or metastatic pancreatic cancer. Int J Hyperthermia. 2012;28(7):597-604. [doi: 10.3109/02656736.2012.695428]
43. Volovat C, Volovat SR, Scripcaru V, Miron L. Second-line chemotherapy with gemcitabine and oxaliplatin in combination with locoregional hyperthermia (EHY-2000) in patients with refractory metastatic pancreatic cancer—preliminary results of a prospective trial. Rom Rep Phys. 2014;66:166-174 [http://rrp.infim.ro/2014_66_1/A18.pdf]
44. Iyikesici MS. Long-Term Survival Outcomes of Metabolically Supported Chemotherapy with Gemcitabine-Based or FOLFIRINOX Regimen Combined with Ketogenic Diet, Hyperthermia, and Hyperbaric Oxygen Therapy in Metastatic Pancreatic Cancer. Complement Med Res. 2020;27(1):31-39. [doi: 10.1159/000502135]
45. Sarti D, Milandri C, Fiorentini C, Mambrini A, Fiorentini G Modulated electro-hyperthermia for the treatment of elderly pancreatic cancer patients. Arguments of Geriatric Oncology. 2020;5(1):1 – 7. [https://www.edisciences.org/scheda-d027]
46. Datta NP, Pestalozzi B, Clavien PA, Members of the HEATPAC Trial Group. "HEATPAC"—a phase II randomized study of concurrent thermochemoradiotherapy versus chemoradiotherapy alone in locally advanced pancreatic cancer. Radiat Oncol. 2017;12:183. [DOI 10.1186/s13014-017-0923-8]
47. Minnaar CA, Szasz AM, Arrojo E, Lee S-Y, Fiorentini G, Borbenyi E, Pang CLK, Dank M. Summary and update of the method modulated electrohyperthermia, Oncothermia Journal Special Edition. 2020,2:49-130. [https://oncotherm.com/sites/oncotherm/files/2020-09/specialedition02.pdf]

Conflict-of-interest

The authors have no conflict of interest

Table 1) Esophageal cancer

Author	*Year*	*Treatment*	*Hypertermia protocol*	*Number of patients (n)*	*Survival*	*Tumor Response*	*RHT related toxicity*
Sheng [18]	2017	CRT with cisplatin based regimens+RHT	Radiofrequency capacitive heating device, with microwave spiral strip applicators, HRL-001, within 30 min from RT, or 2h after CHT	50	3-year OS=42.5% PFS= 34.9%	ND	Pain (G1-2)=38.0%
Nishimura [13]	2015	CRT with cisplatin/5- fluorouracil, oral fluoropyrimidine and irinotecan+RHT	8-MHz radiofrequency, capacitive heating system (Thermotron RF-8), at 400-1400 W (median 1200 W) for 50 min once or twice a week	11	1 year OS=72.7% 2 years OS=54.5% 5 years OS=9.1%	CR=27% SD=45%	ND
Nakajima [16]	2015	CRT with docetaxel + RHT	ND	24	3 years OS=56.3% 5 years OS=50.0%	DCR=41.7% CR=17.6%	toxicity G2 occurred in six patients
Hulshof [17]	2009	Neoadjuvant CRT with carboplatin and paclitaxel+ RHT	home-made AMC (academical medical center), phased array of four 70MHz	28	1 year OS=79% 2 years OS=57%	CR=19% PR=31% SD=23%	pain (sternal or shoulder) or general discomfort in seven

			antennas, at a power of 800 W for 1.5 hour		3 years OS= 54%		patients and in two patients
Albregts [15]	2009	Neoadjuvant CHT with cisplatinum and etoposide+HRT	home-made AMC (academical medical center), phased array of four 70MHz antennas, at a power range of 800–1000 W	26	1 year OS=86% 2 years OS=76%	CR=9%	Discomfort in 1 patient and 'sock-like' sensory neuropathy (G2) in 1 patient

RT= radiotherapy, RHT= hyperthermia, OS= overall survival, SR= survival rate, Clinical benefit= complete response+partial response+ stable disease, CHT= chemotherapy, DFS=Disease free survival, CRT= chemoradiotherapy, LRFS= local relapse-free survival, n.s.= not significant. ND= not reported.

Table 2) Colorectal and anal cancer

Author	Year	Type of tumor	Treatment	Hypertermia protocol	Nr of patients (n)	Survival	Tumor Response	RHT related toxicity
Ranieri [33]	2020	Metastatic colon cancer	CHT with Beva+FOLFOX4+mEHT	mEHT with 13.56 MHz (EHY-2000) twice a week (8 times)	40	PFS=12.1 months (range 3.5–32.6 months).	90 days: PR=30% SD=65% PD=5% DCR=95% 3 months: CR=5.3%, PR=26.3%, SD=55%, PD=10%, DCR=89.5 %	mild positional pain in four patients, Erythema in the target area in 3 patients, power-related pain occurred in two cases
You [32]	2020	Rectal cancer	Neoadjuvant CRT with 5-fluorouracil or oral capecitabine+mEHT	mEHT with 13.56 MHz (EHY-2000) twice a week (8 times)	60	ND	minimal, moderate, near total, and total regression of primary tumor was 15.0%, 51.7%, 18.3% and 15.0% respectively.	26.7% developed thermal toxicity, which was mostly G1 (93.8%)
Zwirner [23]	2018	Locally advanced rectal cancer	Neoadjuvant CRT with 5-fluororuracil +RHT	Deep regional hyperthermia once or twice a week	86	5-years OS =87.3% DFS =79.9 LRFS =95.8%	ND	ND
Gani [22]	2016	Rectal cancer	Neoadjuvant 43 CRT with 5-fluororuracil vs 60 CRT with 5-fluororuracil +RHT	RHT with Sigma Eye or Sigma-60 applicator (BSD 2000/3D) once or twice a week	103	5-years OS= 76% vs 88% p < 0.08 DFS= 73% vs 78% LRFS =77% vs 75%	ND	ND
Shoji [27]	2015	Rectal cancer	Neoadjuvant CRT with Capecitabine+RHT 33 were resected 16 non-resected	RHT with 8 MHz RF capacitive heating device (Thermotron RF-8) after RT for 50 minutes (5 weeks)	49	ND	DCR=28.5 %	One grade 3 patient had perianal dermatitis, 29.7% suffered pain, and 2.1% had subcutaneous induration
Kato [28]	2014	Rectal cancer	Neoadjuvant CRT+RHT	RHT with Thermotron RF-8, Once a week (2-5 times)	48	ND	CR=29.2%	No hematological toxicity
Schroeder [29]	2012	Locally advanced rectal cancer	Neoadjuvant 61 CRT with 5-Fluorouracil+RHT vs 45 CRT with 5-Fluorouracil	RHT with BSD-2000 Once or twice a week (1-9 times)	106	ND	pCR rate 16.4% vs 6.7%	34% hyperthermia discontinuation, due to pain or hot-spot phenomena, urinary tract infections, hypertension, tachycardia

								or severe skin toxicity
Kang [31]	2011	Locally advanced rectal cancer	Neoadjuvant CRT with 5-FU, leucovorin and mitomycin C+RHT	RHT with 8-MHz radiofrequency capacitive heating device (Cancermia GHT-RF8) twice a week during RT	214	5 years OS=73.9% DFS=75.1% LRFS=93,9% DMFS= 79.8%	DCR=50.9 %	ND
Maluta [24]	2010	Locally advanced rectal cancer	Neoadjuvant CRT+RHT	RHT with BSD-2000 Once a week (1-5 times)	76	5-years OS= 86,5% DFS= 74,5% LRFS =73,2%	CR=23,6% DCR=94,8 %	G0-2 general or local discomfort in 15%, no G3, G4 Subcutaneous burns in 5.2%
Rau [25]	2000	primary rectal cancer (PRC) recurrent rectal cancer (RRC)	Neoadjuvant CRT with 5-fluororuracil and leucovorin +RHT	RHT with BSD-2000 Once a week (1-5 times)	37 18	5-year OS=60%	DCR=59% DCR=28%	none
Ott [26]	2019	Squamous anal cancer	CRT with 5-fluororuracil and mitomycin C vs CRT with 5-fluororuracil and mitomycin C + RHT	RHT with the BSD 2000-3D- and BSD 2000-3D-MR-Hyperthermia System once or twice weekly (5-10 times)	112	5 years OS= 95.8 vs. 74.5%, P = 0.045DFS=89.1 vs. 70.4%, P = 0.027LRFS =97.7 vs. 78.7%, P = 0.006	ND	Comparable toxicity for Grades 3–4 early side effects: skin reaction, diarrhea, stomatitis, and nausea/emesis, with the only exception of a higher hematotoxicity rate for the CRT+RHT group (66 vs. 43%, P= 0.032).

RT= radiotherapy, RHT= hyperthermia, OS= overall survival, SR= survival rate, Clinical benefit= complete response+partial response+ stable disease, CHT= chemotherapy, DFS=Disease free survival, CRT= chemoradiotherapy, LRFS= local relapse-free survival, ND=not specified.

Table 3) Locally advanced pancreatic cancer

Author	*Year*	*Treatment*	*Hypertermia protocol*	*Nr of patients (n)*	*Survival*	*Tumor Response*	*RHT related toxicity*
Sarti [45]	2020	mEHT+RT or CHT with gemcitabine regimen vs RT or CHT	mEHT with 13.56 MHz (EHY-2000) twice a week (8 times)	32	OS= 18 months (range 10.3-28.6) versus 10.97 months (range 4.00-22.16) PFS=12 months (range 3-28.6) versus 4.53 months (range 1.33-17.57) (p=0.003)	DCR= 85% vs 26% (p=0.0018).	3% of G1-G2 skin pain and burns
Fiorentini [10]	2019	mEHT+RT or CHT with gemcitabine regimen vs RT or CHT	mEHT with 13.56 MHz (EHY-2000) twice a week (8 times)	106	OS= 18.0 months vs 10.9 months (p<0.001)	3 months DCR= 92% vs 66%	no grade III–IV toxicity
Iyikesici [44]	2019	CHT with gemcitabine or FOLFIRINOX regimen +mEHT	mEHT with 13.56 MHz (EHY-3010) at 110-130W power for 60 minutes	25	OS=15.8 months (95% CI, 10.5–21.1) PFS=12.9 months (95% CI, 11.2–14.6)	3 months DCR=96%	None
Ono [40]	2019	CHT with FOLFIRINOX, Gemsitabin plus nab-Pacritaxel or S-1 +RHT	RHT with Thermotron RF-8, for 50 minutes after CHT once a week (5 times)	28	1 year OS=41% 2 years OS=15%	3 months DCR=57% 6 months DCR=45% 12 months DCR=12%	ND

						18 months DCR=6%	
Maebayashi [37]	2017	CRT with 5-fluororuracil or gemcitabine + RHT vs CRT	RHT with Thermotron RF-8, for 50 minutes at 800-1200W power once or twice a week (5 times)	13	1 year OS=80% vs 57% (p=0.021)		Lower hematological and gastrointestinal toxicity than CRT alone
Tschoep-Lechner [41]	2013	CHT with gemcitabine and cisplatin +RHT	RHT with BSD-2000 day 2 and 4, 1 hour twice a week for 4 months	27	PFS = 5.9 months OS 12.9 months	DCR=50%	no grade III–IV toxicity
Maluta [39]	2011	CRT with gemcitabine based regimens+RHT vs CRT	RHT with BSD-2000 Once a week (1-5 times)	68	Median OS= 15 vs 11 months (p = 0.025)		
Volovat [43]	2014	CHT (GEMOX) +mEHT	mEHT with EHY-2000 device at 70-150 W on day 1, 3, 5 of every CHT cycle	26	Median PFS= 3.9 months. Median OS= 8.9 months.	DCR=71%	no grade III–IV toxicity
Ishikawa [42]	2012	CHT with gemcitabine+RHT	RHT with Thermotron RF-8 at 1100 to 1500 W power for 40 minutes once a week	18	Median OS=17.7 months	ORR=11.1% DCR= 61.1%	G2 pain and a skin rash
Ohguri [38]	2008	CRT with gemcitabine+RHT vs CRT	RHT with Thermotron RF-8 at 900W power, once a week 1–3 hours after RT and during CHT	29	Median OS=8.8 vs. 4.9 months, P = 0.02, Median PFS=18.6 vs. 9.6 months, P = 0.01	ND	5% grade III–IV toxicity

RT= radiotherapy, RHT= hyperthermia, OS= overall survival, SR= survival rate, Clinical benefit= complete response+partial response+ stable disease, CHT= chemotherapy, DFS=Disease free survival, CRT= chemoradiotherapy, LRFS= local relapse-free survival, DCR= disease control rate, mEHT= modulated electro hyperthermia, ORR= overall response rate

Marked local and distant response of heavily treated breast cancer with cardiac metastases treated by combined low dose radiotherapy, low dose immunotherapy and hyperthermia: a case report

Mau-Shin Chi, Jen-Hong Wu1, Suzun Shaw, Ching-Jung Wu, Liang-Kuang Chen, Ho-Chi Hsu, Kwan-Hwa Chi

Department of Radiation Therapy and Oncology, Shin Kong Wu Ho-Su Memorial Hospital, Taipei, Taiwan; Department of Radiation Oncology, Cathay General Hospital, Taipei, Taiwan; Department of Diagnostic Radiology, Shin-Kong Wu Ho-Su Memorial Hospital, Taipei, Taiwan; Department of General Surgery, Shin Kong Wu Ho-Su Memorial Hospital, Taipei, Taiwan

Correspondence to: Ho-Chi Hsu. Department of General Surgery, Shin Kong Wu Ho-Su Memorial Hospital, Wenchang Rd., No. 95, Shihlin District, Taipei, Taiwan. Email: M005284@ms.skh.org.tw; Kwan-Hwa Chi. Department of Radiation Therapy and Oncology, Shin Kong Wu Ho-Su Memorial Hospital, Wenchang Rd., No. 95, Shihlin District, Taipei, Taiwan. Email: khchi45@gmail.com

Cite this article as:
Chi M. A. (2021): Marked local and distant response of heavily treated breast cancer with cardiac metastases treated by combined low dose radiotherapy, low dose immunotherapy and hyperthermia: a case report, Ther Radiol Oncol, 5:17.
doi: 10.21037/tro-21-16

Oncothermia Journal 31, 2022 March: 243-250
www.oncotherm.com/sites/oncotherm/files/2022-03/Chi_Marked.pdf

Abstract: Breast cancer (BC) with cardiac metastases (CMs) is often associated with poor prognosis due to late stage of diagnosis. Palliative radiotherapy (RT) for CMs is generally used for symptomatic treatment and to maintain normal cardiac function. Palliative RT with hyperthermia (HT) or immunotherapy have been reported to be effective in prolonging the overall survival and progression-free survival in metastatic patients. In this case report, we present a heavily pretreated 51-year-old lady of metastatic BC presented with recurrent right breast mass with progressive exertional dyspnea caused by symptomatic CM. She received combined palliative low-dose palliative RT [20 Gray (Gy) in 12 fractions], combined with low-dose chemotherapy, biweekly HT treatment course, and low-dose "double blockade" immunotherapy by ipilimumab (0.3 mg/kg) and nivolumab (0.5 mg/kg). The irradiated right chest tumors responded rapidly to treatment. Interestingly, unirradiated metastatic lesions outside the RT and HT treatment field also demonstrated a sustained abscopal response. She continued monthly low-dose immunotherapy in conjunction with HT after RT. The posttreatment cardiac echography disclosed considerably reduced pericardial effusions without cardiac wall motion abnormalities. She remained stable for more than 6 months with no notable treatment-related toxicities. The combination of low-dose RT, low-dose immunotherapy, and HT protocol appears to be a safe method with promising efficacy in metastatic BC patients.

Keywords: Cardiac metastases (CMs); radiotherapy (RT); immunotherapy; hyperthermia (HT); case report

doi: 10.21037/tro-21-16

Introduction

Cardiac metastases (CMs) occur more frequently than is often expected. The incidence of CMs in metastatic cancers is up to 14.2%, and they are most commonly derived from lung cancer (incidence of 36–39%), followed by breast malignancies (incidence of 10–12%) and hematologic malignancies (incidence of 10–21%) (1). CMs are associated with a grave prognosis due to their generally late diagnosis at profound stages (2). CMs are clinically silent in general; nevertheless, they can be lethal when cardiac tamponade or a rapid accumulation of pericardiac effusion occurs (3). CM management strategies are generally aimed at symptomatic control and maintenance of normal cardiac function. The role of palliative radiotherapy (RT) in managing CMs is limited due to concerns over reported cardiac toxicities. The literature discussing RT as palliative treatment for CMs mostly involves case reports with varied radiation doses [6 to 54 Gray (Gy)] and response durations (4-6).

Breast cancer (BC) patients with CMs are often heavily pretreated before diagnosis, which means the remaining therapeutic window is narrow. Combinatory use of immunotherapy and chemotherapy was determined to be effective in prolonging overall survival and progression-free survival in patients with metastatic triple-negative BC (7). Hyperthermia (HT), known for its radio, or chemo-sensitization effect, combined with salvage RT has become an effective treatment method for recurrent BC (8). Modulated electrohyperthermia (mEHT) is a form of HT that transmits radiofrequency energy into the tumor cell membrane to produce an electric field. This field causes lymphocytic and dendritic cells to penetrate the tumor to achieve pronounced immunogenic cell death (9,10). A combination of RT, mEHT, and immunotherapy may enable a rapid and sustained abscopal effect, as discussed in a retrospective study (11).

Herein, we report the case of a patient with metastatic BC with CMs who achieved marked local and distant responses after receiving a combination of low-dose RT, low-dose chemotherapy, mEHT, and low-dose immunotherapy. We present the following case in accordance with the CARE reporting checklist (available at https://dx.doi.org/10.21037/tro-21-16).

Case presentation

In 2012, a 51-year-old woman was diagnosed as having left-sided luminal A subtype BC (cT2N0M0), stage IIA. After receiving 2 cycles of neoadjuvant chemotherapy, the patient refused surgery and received only tamoxifen and naturopathic therapies for over 6 years. In July 2018, the patient finally agreed to undergo salvage left-sided modified radical mastectomy due to local progression by skin invasion and palpable axillary and supraclavicular nodes, she finally agreed for salvage left-sided modified radical mastectomy. Pathology reports revealed invasive ductal BC with chest wall and skin invasion, 11 positive lymphadenopathies, complicated by positive surgical margins, and extranodular extension, which indicated pT4bN3a, stage IIIB. The patient refused adjuvant treatments after surgery. In February 2019, she noticed multiple eruptions of left chest wall tumors that, through biopsy, were confirmed to be metastatic BC and phenotype transformation into triple-negative subtypes. She was salvaged through reoperation and cryotherapy.

In July 2020, the BC recurred with multiple left chest wall indurations and serous discharge as well as an enlarged axillary mass measuring more than 7 cm. The patient was salvaged through RT administered at 50 Gy in 25 fractions to the left chest wall and regional nodes, in addition to a focal boost of 70 Gy administered in 35 fractions to the axillary mass. After 2 months, the patient sought a second medical opinion due to a rapid outburst of a right breast nodule measuring more than 5 cm, as well as progressive exertional dyspnea. A positron emission tomography (PET) scan performed in October 2020 revealed a right breast tumor of more than 7 cm protruding from the skin along with numerous metastatic nodules over the right breast and left chest wall. The scan also revealed multiple metastatic lesions in the regional and distant lymph nodes, ribs, lungs, and adrenal glands; bilateral pleural effusions; and pericardial masses extending from the left to the right atrium. Cardiac echography revealed pericardial metastases and pericardial effusion (*Figure 1*). The patient refused

intravenous chemotherapy but agreed to receive a combination of palliative RT, oral chemotherapy, mEHT, and low-dose immunotherapy.

Treatment began after pericardiocentesis with a low dose of ipilimumab 15 mg (0.3 mg/kg) and nivolumab 30 mg (0.5 mg/kg) given every 4 weeks, in addition to mEHT treatment in 1-hour sessions twice weekly. mEHT was applied using an EHY 2000+ device (OncoThermGmbH, Germany). The mEHT protocol involved a large treatment field implemented using a 30-cm electrode covering the right breast and a small treatment field implemented using a 10-cm electrode applied directly to the protruding mass on the right breast; the 2 electrodes were applied alternately. A radiofrequency of 13.56 MHz was used with an automatic, real-time tuning device to ensure a standard wave ratio was maintained. The intratumoral temperature was not measured because the temperature elevation inside a treatment field measured using a conventional thermocouple is typically <2 °C (12). After 4 sessions of mEHT treatment, palliative RT at 20 Gy in 12 fractions given daily, was administered to the right ulcerative breast tumor, pericardial lesions, and rib metastatic lesions by tomotherapy (Accuray, Sunnyvale, CA, USA) (*Figure 2*). Chemotherapy was given concurrently by using low-dose capecitabine 500 mg t.i.d. and vinorelbine

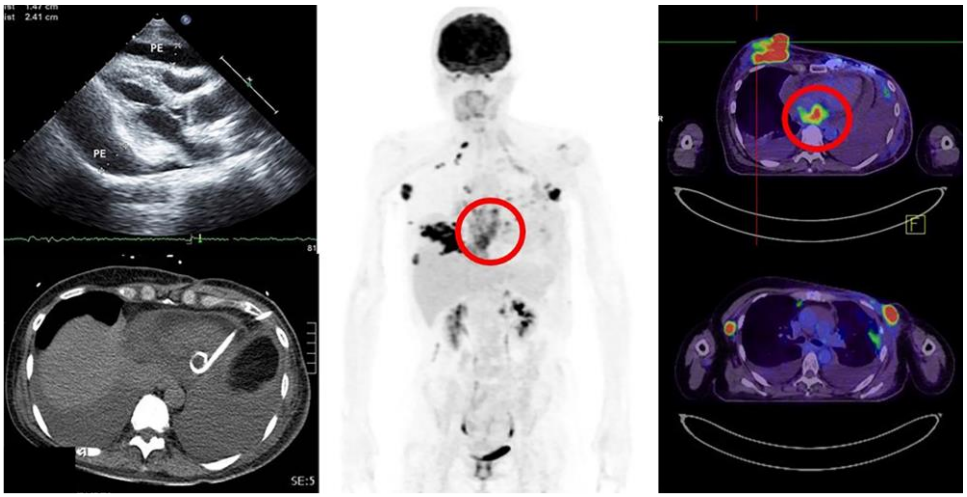

Figure 26. Heavily pretreated metastatic BC with (A) massive pericardial effusions treated through pericardiocentesis and drainage. (B) PET scan revealing multiple lesions involving the bilateral breast, pericardial (red circle), regional, and distant lymp
40 mg weekly. The lesions of the left chest wall were not included in the RT field due to the short retreatment time and high in-field dose in previous treatment.

The patient refused oral chemotherapy 6 weeks after treatment was initiated. The protruding tumor of the right breast was nearly invisible at 3 weeks of treatment, and the patient was free from dyspnea after completing the RT course in December 2020. A PET scan 2 months after treatment revealed marked regression of the irradiated lesions and diminished pleural and pericardial effusions. Notably, the unirradiated left chest wall lesions and adrenal metastases outside the local treatment field demonstrated remote disease control (Figure 3). A posttreatment cardiac echocardiogram revealed diminished pericardium effusions without cardiac wall motion abnormalities. The patient continued the monthly low-dose immunotherapy protocol in conjunction with mEHT without any treatment-related toxicities. The patient's condition has remained stable for more than 6 months at the time of writing.

All procedures performed in studies involving human participants were in accordance with the ethical standards of the institutional and/or national research committee(s) and with the Helsinki Declaration (as revised in 2013).

Written informed consent was obtained from the patient for publication of this case report and accompanying images. A copy of the written consent is available for review by the editorial office of this journal.

Discussion

We present a case of BC with CMs that demonstrated an abscopal response more than 6 months after combination treatment involving low-dose immunotherapy, low-dose chemoradiotherapy, and HT. The prognosis of CMs is generally grave, with a median survival of 3.5 months if untreated (4,5,13). Although patients with CMs typically present with disseminated disease, appropriate management can improve their quality of life and overall survival. Palliative RT is often underused due to the poor prognosis of CMs and the lack of randomized controlled trials (5,6). In our case, we demonstrated that the combinatory treatment was effective and notable in that it produced a rapid and sustained abscopal response, demonstrated a radio- and immune-sensitization effect through HT, and involved of a low-dose immunotherapy protocol.

The patient was heavily pretreated; therefore, the response rate and duration of the response were expected to be low. Nevertheless, the observed local and distant responses to treatment were notably positive. Whether our case was a bona fide abscopal response is debatable because immunotherapy was applied. However, among the millions of patients treated with palliative RT between 1969 and 2014, only 46 cases were identified as abscopal events (14). Accordingly, we hypothesized that a rapid release of extracellular damage-associated molecular secretion patterns (DAMP) through RT and HT would facilitate tumor immunogenicity and enhance the efficacy of immunotherapy. Our patient exhibited a rapid response to treatment at the second week of RT, which supports a previous report that a rapid response may be correlated with abscopal events (11). The prescribed RT dose was low when compared with conventional palliative RT courses administered at 30–35 Gy for 2–4 weeks. Despite the lower fractionated dose, the treatment response was robust and indicated a radiosensitization effect due to the combined HT. A study of metastatic melanoma treated with RT and immunotherapy revealed that, other than HT, an RT fraction size of less than 3 Gy was the only factor associated with a high response rate (15). In our case, the protruding mass, especially the large-sized tumor, exhibited a stronger response than the smaller tumors did when treated with combined RT and mEHT (11). Larger tumors, usually situated near the surface of the body, absorb the radiofrequency energy more effectively. The absorbed energy results in prominent apoptosis, necrosis, and a release of DAMP, which may facilitate abscopal response (7,11,16).

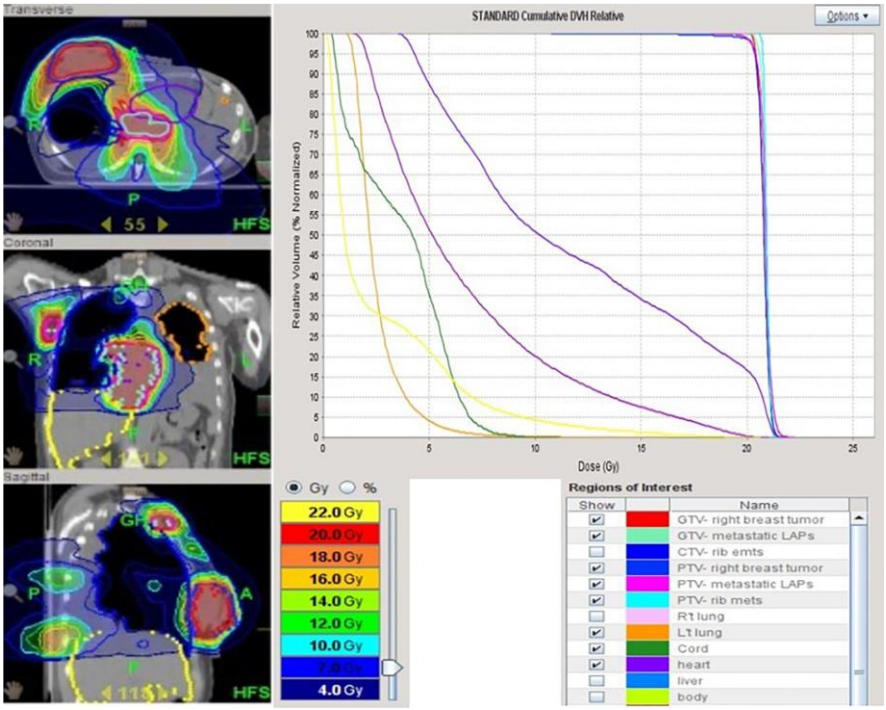

Figure 27. Dose-volume histogram, region of interest, and isodose curve. The RT plan was administered through tomotherapy at 20 Gy in 12 fractions to the right breast tumor, pericardial, and rib metastases. RT, radiotherapy; Gy, Gray.

Immunotherapy along with chemotherapy was observed to prolong the overall survival of patients with metastatic triple-negative BC (7). For patients who refuse chemotherapy, a double checkpoint inhibitor blockade may be a sensible approach. Combination treatment involving an anti-CTLA4 antibody (ipilimumab) and anti-PD-1 antibody (nivolumab) was reported to achieve a 3-year overall survival rate of 63% in metastatic melanoma but at the expense of a 58.5% rate of grade 3 or 4 immune-related adverse events (irAEs) (17). A meta-analysis of 80 clinical trials revealed that a combination of double checkpoint inhibitors (anti-CTLA-4 and anti-PD-1 inhibitors) was associated with the highest rate of irAEs proportional to the prescribed dose (18). The concept of utilizing low-dose double immune checkpoint blockade was analyzed in a retrospective study of 131 metastatic patients who failed all conventional treatments (19). Treatment using low-dose ipilimumab (0.3 mg/kg) with nivolumab (0.5 mg/kg), HT, and interleukin-2 was associated with an objective response rate of 31.3% and a 2-year survival rate of 36.6%. In addition, BC patients (including all phenotypes) demonstrated a 31% response rate, and the documented irAEs were mild (19).

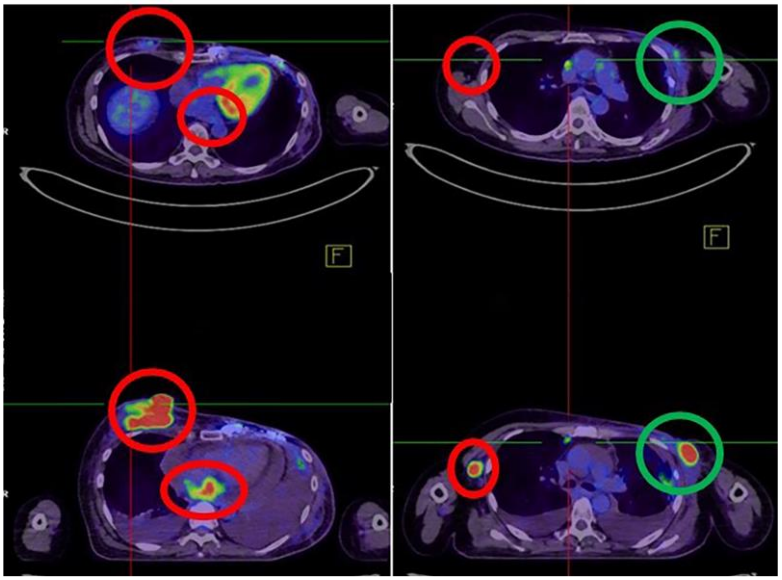

Figure 28. Red circle indicates the irradiated right breast mass and pericardial metastases with almost complete response. Green circle indicates the unirradiated left breast tumor with an abscopal response in the following image with diminished pericardia

The combination of low-dose chemoradiotherapy, low-dose immunotherapy, and HT is a safe option for palliative treatment. The observed rapid and sustained abscopal response renders this combination worthy of further study. An official trial should be launched.

Acknowledgments

The authors thank the staff from the Department of Radiation Therapy and Oncology of Shin Kong Wu Ho-Su Hospital, especially Ms. Yi-Ying Huang and Ms. Yi-Chieh Li for their contributions through hyperthermia treatment. This manuscript was edited by Wallace Academic Editing. Funding: None.

Footnote

Provenance and Peer Review: This article was commissioned by the Guest Editors (Pei-Wei Shueng, Yen-Wen Wu and Long-Sheng Lu) for the series “Cardio-Oncology” published in Therapeutic Radiology and Oncology. The article has undergone external peer review.

Reporting Checklist: The authors have completed the CARE reporting checklist. Available at https://dx.doi.org/10.21037/tro-21-16

Conflicts of Interest: All authors have completed the ICMJE uniform disclosure form (available at https://dx.doi.org/10.21037/tro-21-16). The series "Cardio-Oncology" was commissioned by the editorial office without any funding or sponsorship. CJW serves as an unpaid editorial board member of Therapeutic Radiology and Oncology from May 2020 to Apr 2022. The authors have no other conflicts of interest to declare.

Ethical Statement: The authors are accountable for all aspects of the work in ensuring that questions related to the accuracy or integrity of any part of the work are appropriately investigated and resolved. All procedures performed in studies involving human participants were in accordance with the ethical standards of the institutional and/or national research committee(s) and with the Helsinki Declaration (as revised in 2013). Written informed consent was obtained from the patient for publication of this case report and accompanying images. A copy of the written consent is available for review by the editorial office of this journal.

References

1. Bussani R, De-Giorgio F, Abbate A, et al. Cardiac metastases. J Clin Pathol 2007;60:27-34.
2. Al-Mamgani A, Baartman L, Baaijens M, et al. Cardiac metastases. Int J Clin Oncol 2008;13:369-72.
3. Catton C. The management of malignant cardiac tumors: clinical considerations. Semin Diagn Pathol 2008;25:69-75.
4. Cham WC, Freiman AH, Carstens PH, et al. Radiation therapy of cardiac and pericardial metastases. Radiology 1975;114:701-4.
5. Fotouhi Ghiam A, Dawson LA, Abuzeid W, et al. Role of palliative radiotherapy in the management of mural cardiac metastases: who, when and how to treat? A case series of 10 patients. Cancer Med 2016;5:989-96.
6. Arscott WT, Lal P, Mamtani R, et al. Long-term survival after treating cardiac metastasis with radiation and immune therapy: a case report. Cureus 2018;10:e2607.
7. Schmid P, Adams S, Rugo HS, et al. Atezolizumab and nab-paclitaxel in advanced triple-negative breast cancer. N Engl J Med 2018;379:2108-21.
8. Datta NR, Puric E, Klingbiel D, et al. Hyperthermia and radiation therapy in locoregional recurrent breast cancers: a systematic review and meta-analysis. Int J Radiat Oncol Biol Phys 2016;94:1073-87.
9. Lee SY, Fiorentini G, Szasz AM, et al. Quo Vadis oncological hyperthermia (2020)? Front Oncol 2020;10:1690.
10. Tsang YW, Huang CC, Yang KL, et al. Improving immunological tumor microenvironment using electro-hyperthermia followed by dendritic cell immunotherapy. BMC Cancer 2015;15:708.
11. Chi MS, Mehta MP, Yang KL, et al. Putative abscopal effect in three patients treated by combined radiotherapy and modulated electrohyperthermia. Front Oncol 2020;10:254.
12. Lee SY, Kim JH, Han YH, et al. The effect of modulated electro-hyperthermia on temperature and blood flow in human cervical carcinoma. Int J Hyperthermia 2018;34:953-60.
13. Reynen K, Köckeritz U, Strasser RH. Metastases to the heart. Ann Oncol 2004;15:375-81.
14. Abuodeh Y, Venkat P, Kim S. Systematic review of case reports on the abscopal effect. Curr Probl Cancer 2016;40:25-37.
15. Chandra RA, Wilhite TJ, Balboni TA, et al. A systematic evaluation of abscopal responses following radiotherapy in patients with metastatic melanoma treated with ipilimumab. Oncoimmunology 2015;4:e1046028.
16. Storm FK, Harrison WH, Elliott RS, et al. Normal tissue and solid tumor effects of hyperthermia in animal models and clinical trials. Cancer Res 1979;39:2245-51.
17. Callahan MK, Kluger H, Postow MA, et al. Nivolumab plus ipilimumab in patients with advanced melanoma: updated survival, response, and safety data in a phase I dose-escalation study. J Clin Oncol 2018;36:391-8.
18. Shulgin B, Kosinsky Y, Omelchenko A, et al. Dose dependence of treatment-related adverse events for immune checkpoint inhibitor therapies: a model-based meta-analysis. Oncoimmunology 2020;9:1748982.

19. Kleef R, Nagy R, Baierl A, et al. Low-dose ipilimumab plus nivolumab combined with IL-2 and hyperthermia in cancer patients with advanced disease: exploratory findings of a case series of 131 stage IV cancers - a retrospective study of a single institution. Cancer Immunol Immunother 2021;70:1393-403.

doi: 10.21037/tro-21-16
Cite this article as: Chi MS, Wu JH, Shaw S, Wu CJ, Chen LK,

Hsu HC, Chi KH. Marked local and distant response of heavily treated breast cancer with cardiac metastases treated by combined low dose radiotherapy, low dose immunotherapy and hyperthermia: a case report. Ther Radiol Oncol 2021;5:17.

This work was supported by the

Hungarian National Research Development and Innovation Office

KFI grant: 2019-1.1.1-PIACI-KFI-2019-00011

EHY-2030

A revolutionary new concept

- **New automatic controlled step motor tuning system for rapid impedance matching to achieve faster tuning times**
- **Newly developed RF generator with modified power**
- **Electronically controlled electrode arm to easily and accurately horizontally position the smart electrode**
- **User friendly touch screen display with full system control**
- **New shape and design to ease patient anxiety**
- **Changeable strechy textile electrode fort he smart electrode system and bed**
- **Hand-held emergency stop switch fort he patients**
- **Integrated PMS-100 Patient Management System**

MANUFACTURER

HUNGARY

Oncotherm Kft.
Gyár utca 2.
2040 Budaörs, Hungary

Phone (+36) 23-555-510
Fax (+36) 23-555-515

info@oncotherm.org
www.oncotherm.com

GERMANY

Oncotherm GmbH
Belgische Allee 9
53842 Troisdorf, Germany

Phone (+49) 2241-319920
Fax (+49) 2241-3199211

info@oncotherm.de
www.oncotherm.de